

# CONTRACTOR REPORT

SAND82-8178  
UC-62d  
Unlimited Release

## Molten Salt Receiver Subsystem Research Experiment Phase 1 — Final Report Volume II — Appendices

Babcock & Wilcox Company  
Barberton, Ohio

Prepared by Sandia National Laboratories, Albuquerque, New Mexico 87185  
and Livermore, California 94550 for the United States Department of Energy  
under Contract DE-AC04-76DP00789.

Printed October 1984

***When printing a copy of any digitized SAND  
Report, you are required to update the  
markings to current standards.***

Issued by Sandia National Laboratories, operated for the United States Department of Energy by Sandia Corporation.

**NOTICE:** This report was prepared as an account of work sponsored by an agency of the United States Government. Neither the United States Government nor any agency thereof, nor any of their employees, nor any of the contractors, subcontractors, or their employees, makes any warranty, express or implied, or assumes any legal liability or responsibility for the accuracy, completeness, or usefulness of any information, apparatus, product, or process disclosed, or represents that its use would not infringe privately owned rights. Reference herein to any specific commercial product, process, or service by trade name, trademark, manufacturer, or otherwise, does not necessarily constitute or imply its endorsement, recommendation, or favoring by the United States Government, any agency thereof or any of their contractors or subcontractors. The views and opinions expressed herein do not necessarily state or reflect those of the United States Government, any agency thereof or any of their contractors or subcontractors.

Printed in the United States of America  
Available from  
National Technical Information Service  
5285 Port Royal Road  
Springfield, VA 22161

NTIS price codes  
Printed copy: A19  
Microfiche copy: A01

SAND82-8178  
Unlimited Release  
Printed October 1984

**MOLTEN SALT RECEIVER  
SUBSYSTEM RESEARCH EXPERIMENT**

**FINAL REPORT: Phase I**

**Vol. 2 - Appendices**

**Prepared by:**

**Babcock & Wilcox  
A McDermott Company  
Nuclear Equipment Division  
Barberton, Ohio 44203**

**Submitted by:**

**Babcock & Wilcox  
A McDermott Company  
Contract Research Division  
Barberton, Ohio 44203**

**November 29, 1982**

**Prepared for:**

**Sandia National Laboratories  
Sandia Contract No. 84-2292B  
B&W Contract No. 1081**

**Contractors Technical Report  
Sandia Contract No. 84-2292B  
Sandia Requestor: Dan Dawson 8453  
Sandia Contracting Rep: Jack Hubner 8264  
Sandia Report No: SAND 82-8178**

TABLE OF CONTENTS

<u>APPENDICES</u>	<u>PAGE</u>
A - Receiver Subsystem Requirements and Specifications -----	A-1
B - Elevated Temperature Analysis -----	B-1
C - Control System Design -----	C-1
D - Skewed Heating Analysis -----	D-1
E - Stress Analysis of Full Length Heat Absorption Tubes -----	E-1
F - Cavity Efficiency -----	F-1

## **Appendix A**

# **Receiver Subsystem Requirements and Specifications**

**SYSTEM AND COMPONENTS  
SPECIFICATION AND REQUIREMENTS**

**MOLTEN SALT RECEIVER  
SUBSYSTEM RESEARCH EXPERIMENT**

Prepared By  
Martin Marietta Aerospace  
With Input From  
The Babcock & Wilcox Co.  
Black & Veatch Co.  
Arizona Public Service

Fall, 1982  
B&W Report No. 0012-1 (G)

TABLE OF CONTENTS

	<u>Page</u>
1.0 GENERAL. . . . .	A-3
1.1 Scope. . . . .	A-3
1.2 System Characteristics and Description . . . . .	A-3
1.3 Definition of Terms and Abbreviations. . . . .	A-3
2.0 APPLICABLE DOCUMENTS . . . . .	A-8
2.1 General. . . . .	A-8
2.2 Government Documents . . . . .	A-8
2.3 Non-Government Documents . . . . .	A-8
3.0 REQUIREMENTS . . . . .	A-10
3.1 Receiver Subsystem Design and Performance Requirements . . . . .	A-10
3.2 Environmental Conditions for Design, Operation and Survival. . . . .	A-36
3.3 Molten Salt Compatibility Requirements . . . . .	A-43
3.4 Subcomponent Requirements. . . . .	A-44
4.0 INTERFACE DEFINITIONS AND REQUIREMENTS . . . . .	A-58
4.1 Collector Subsystem. . . . .	A-58
4.2 Energy Storage Subsystem . . . . .	A-60
4.3 Master Control Subsystem . . . . .	A-61
4.4 Electric Power Supply Subsystem. . . . .	A-61
5.0 FABRICATION REQUIREMENTS . . . . .	A-62
6.0 MAINTENANCE. . . . .	A-63
6.1 Dry Layup. . . . .	A-63
6.2 Inspection . . . . .	A-63
6.3 Absorption Panel Repair. . . . .	A-63
6.4 Spare Parts/Tooling. . . . .	A-63
7.0 SPECIAL REQUIREMENTS . . . . .	A-64
7.1 Certification. . . . .	A-64
7.2 Operation and Maintenance Manual . . . . .	A-64
7.3 Safety . . . . .	A-64

1. GENERAL

1.1 Scope - This specification defines the requirements for the design, fabrication, operation, and maintenance of a 320 MWT molten salt receiver subsystem (RS).

1.2 System Characteristics and Description - The function of the Receiver Subsystem (RS) is to transfer the incident radiant energy from a Collector Subsystem into the molten salt working fluid, and transport the hot and cold molten salt to and from the storage subsystem (Figure 1.2-1). The R.S. comprises the following major components:

- a. Quad-Cavity Receiver, including shop-fabricated modular absorbing panels, non-absorbing cavity enclosure, interconnecting piping, structural supports, aperture frames and doors, door supports and actuation mechanisms, instrumentation and controls, valves, an inlet surge tank, an outlet collection tank, insulation and sheathing, radiation shielding of external structures and components, access provisions, and service cranes, etc.

The Quad-Cavity Receiver will intercept reflected solar radiation from a surrounding heliostat field, through its four apertures facing North, South, East and West, respectively.

- b. The Tower, which provides an elevated support for the receiver, and houses the riser, downcomer, elevators, miscellaneous piping and valves, and ancillary equipment.
- c. High-Pressure Booster Pumps, located near the base of the tower;
- d. An energy dissipating system, whose function is to control static head at receiver outlet and to dissipate the potential and kinetic energy of the salt as it leaves the downcomer.

The design of the Receiver Subsystem is to be consistent with the requirements of Repowering/Retrofit systems typified by the Saguaro Power Plant Solar Repowering Project. Its principal design features are to be adaptable to other solar thermal applications as well, including industrial processes.

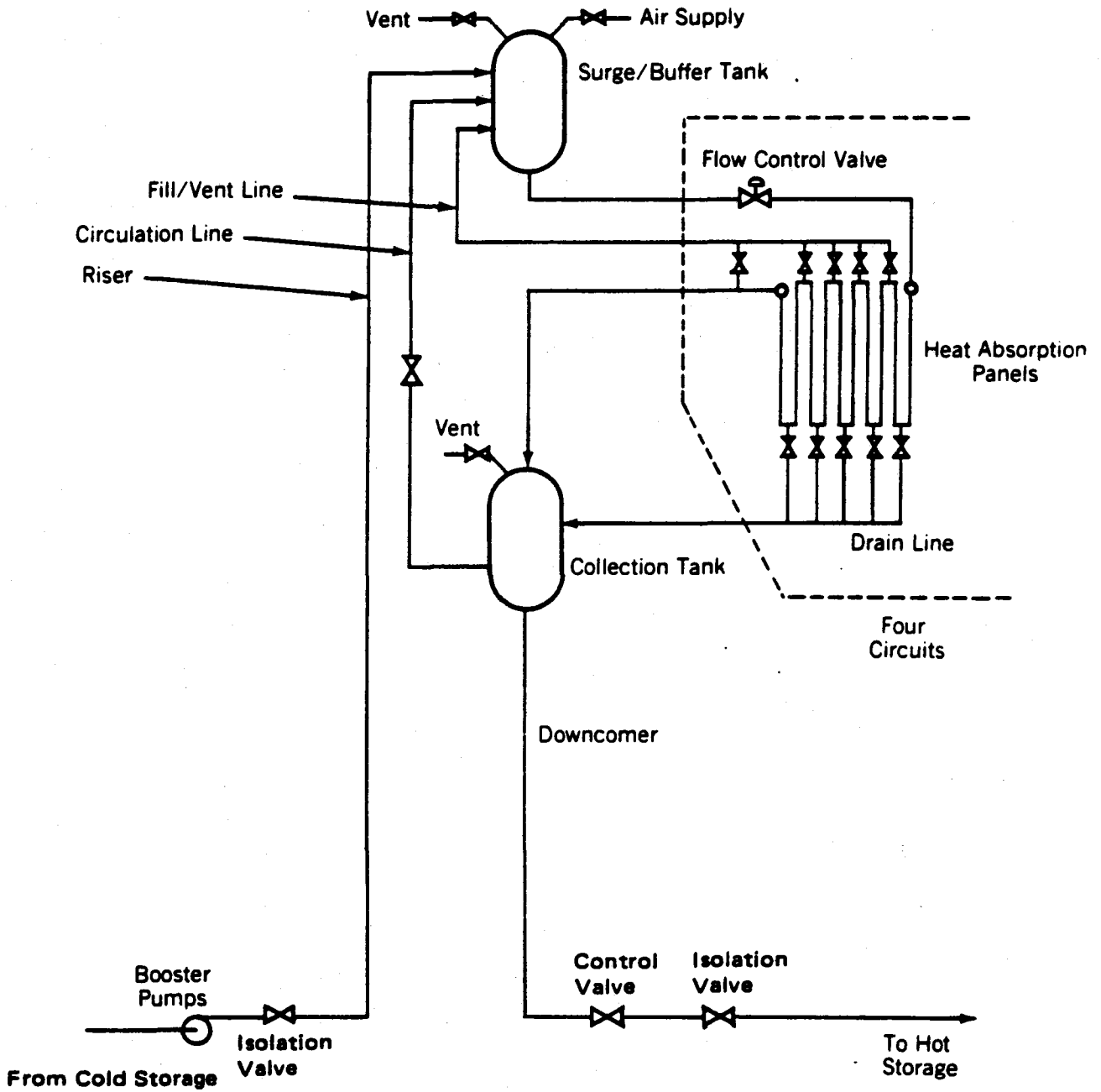
1.3 Definition of Terms and Abbreviations

1.3.1 Definitions

Aim Point - The common centroid of flux patterns produced by several heliostats on a target plane; or the point of intersection of the centerlines of the beams produced by several heliostats.

Aim Point Strategy - The specified distribution of aim points on a target to achieve a desired flux pattern on the receiver absorbing surfaces.





**FIGURE 1.2-1 RECEIVER SUBSYSTEM SCHEMATIC**

Aperture - The opening through which the reflected solar energy from the collector field passes into the receiver cavity.

Availability - Ratio of period of time in operation to the total time when the direct normal solar insolation is above the threshold value. Availability is usually quoted on an annual basis.

$$A = \frac{\text{Number of Hours of Operation}}{\text{Number of Hours of Sufficient Insolation for Operation}}$$

Cold Salt - Molten salt nominally at 288C (550°F).

Collector Subsystem - An array of individually controlled heliostats, including the wiring and controls, that redirects the available solar insolation onto a receiver.

De-focusing (of Heliostats) - The act of moving the aim point of heliostats from the target to the standby point.

Design Point - The time of the day and year for which the system performance is specified.

Direct Insolation - The solar energy incident on a surface that comes from within the solid angle subtended by the solar disk. It is to be distinguished from the diffuse or multidirectional component of solar radiation. Only the direct part of the insolation can be focused by an optical system.

Direct Normal Insolation - The direct insolation on a surface perpendicular to the sun's rays.

Diurnal - Pertaining to the daily cycle.

Distributed Digital Control - Digital control system located at the process (receiver) to be controlled, as opposed to a centrally located control system for several processes.

Downcomer - The pipe carrying the hot molten salt down the tower.

Fail-Over - Automatic or manual switch-over from prime to backup computer in case of failure of the former.

Flux (Radiant) - The time rate of flow of radiant energy.

Flux Density - The radiant flux incident per unit of area.

Focal Length (of Heliostat) - The distance along the centerline of the reflected beam, from the heliostat to the point where the reflected rays from various elements of the heliostat converge. It is achieved by a combination of curvature and canting of the mirror facets comprising the heliostat.

Focusing (of Heliostats) - The act of moving the aim point of heliostats from standby to the target.

Heliostats - A combination of mirrors, support structure, drive mechanism, and mounting foundation that tracks in two axes of motion to continuously reflect the sun's rays onto the receiver.

Hot Salt - Molten salt nominally at 565C (1050°F).

Peak Point - Time of the day and year at which the solar power to a specified cavity (North, South, East or West) is a maximum.

Receiver Control Zone - A flow circuit associated with a controller and a control valve.

Reliability - The probability that an item will perform its required function under specified conditions for a specified time.

Repowering - The retrofitting of existing fossil-fueled electric utility or process heat power plants with solar energy collection systems in order to provide the capability to displace a portion or all of the fossil fuel normally used.

Riser - The pipe carrying the cold molten salt fluid up the tower.

Sacrificial (Material or Structure) - Allowed to be destroyed.

Slant Range - The distance from a heliostat to the target.

Slew Rate - Maximum angular speed of heliostat reflective surface (to be differentiated from "track rate" which refers to angular speed during sun tracking).

Solar Noon - The instant the sun reaches its zenith.

Spillage (Radiation) - Radiation reflected from the collector subsystem which misses the aperture of the receiver.

Standby Point (Heliostats) - Off-target aim point of heliostats from which rapid focusing (or defocusing) onto the target can be achieved.

Stow - A position or act of reaching a position of storage for the heliostats.

Survival - State of damage that may require repairs before returning to operation.

Threshold Insolation - Minimum insolation required for operation at 10% of the rating specified under 3.1.1, or 400 w/m<sup>2</sup>.

Turndown Ratio - Ratio of maximum to minimum operating power.

1.3.2 Abbreviations

DDC - Distributed Digital Control

HC - Heliostat Controller

HFC - Heliostat Field Controller

RS - Receiver Subsystem

TES - Thermal Energy Storage Subsystem

TBD - To Be Determined

## 2.0 APPLICABLE DOCUMENTS

2.1 General - In addition to this specification, the equipment, materials, design, and construction of the receiver subsystem shall comply with all federal, state and local regulations, laws, codes, and ordinances currently applicable at the power plant site. These shall include, but not be limited to, the government and non-government documents listed below. If there is an overlap in, or conflict between, the requirements of these documents and the applicable federal, state, county, or municipal codes, laws, or ordinances, a satisfactory resolution will be formulated on the basis of sound engineering practices.

### 2.2 Government Documents

- a. Specifications
  - Regulations of the Occupational Safety and Health Administration (OSHA)
  - International System of Units, 2nd Revision, NASA SP-7012
- b. Standards
  - Nuclear Regulatory Commission Guides 1.60 and 1.61

### 2.3 Non-Government Documents

- a. Standards and Codes
  - Uniform Building Code, 1979 Edition by International Conference of Building Officials (For tower seismic design, the 1973 Edition shall be used to select the seismic zone in accordance with ACI-307-79)
  - ASME Boiler and Pressure Vessel Codes Section VIII, Div. 1 (Pressure Vessels) and applicable Code Cases.
  - Institute of Electrical and Electronic Engineers (IEEE) Codes, as applicable
  - National Fire Protection Association (NFPA) National Fire Codes - 1975
  - National Electrical Safety Code (NESC) - 1981
  - National Electrical Code (NEC) - 1981
- b. Design, Construction and Fabrication Standards
  - Standards of ACI (American Concrete Institute)
  - Standards of AISC (American Institute of Steel Construction)
  - Standards of ASTM (American Society of Testing Materials)
  - Standards of NEMA (National Electrical Manufacturer's Association)
  - ANSI B31.1-Power Piping
  - ANSI A58.1-Building Code Requirements for Minimum Design Loads in Buildings and Other Structures.
  - ANSI B16.34-Steel Valves, Flanges and Butt welding Ends.
  - ANSI C37.20 Switchgear
  - ANSI C57.12 Power Transformers
  - Standards of AWS (American Welding Society)
- c. Subsystem and Interface Specifications

d. Reference Documents

- "Measurements of Typical Insolation Variation at Daggett, California:, Volumes I and II, Aerospace Report No. ATR-80 (7747)-1, 1 March, 1980
- "Pilot Plant Environmental Conditions"-Aerospace Report No. ATR-78 (7695-05)-05, Revision 1, 15 August, 1978
  
- "Saguaro Power Plant Solar Repowering Project", Final Technical Report, July 1980. Report No. DOE/SF 10739-4.

### 3.0 REQUIREMENTS

#### 3.1 Receiver Subsystem Design and Performance Requirements

Performance requirements are: 320 Mwt with 565C (1050°F) salt outlet temperature, 288C (550°F) salt inlet temperature, at 90.0% receiver thermal efficiency.

##### 3.1.1 Thermal Design and Performance

3.1.1.1 Thermal Rating - The RS shall be designed for 320 Mwt output overall thermal rating at the design point.

3.1.1.2 Insolation Rating - 950 W/M<sup>2</sup> direct normal insolation at the design point. The receiver shall be capable of accepting all reflected energy without heliostat defocus for insolation levels up to 1100 W/M<sup>2</sup>.

3.1.1.3 Efficiency - The thermal efficiency of the receiver -defined as the ratio of thermal output to solar energy passing through the receiver apertures - shall be equal to, or exceed, 90% at the design point.

3.1.1.4 Heat Losses During Hot Standby and Nighttime Shutdown - Thermal losses during hot standby shall be sufficiently low that auxiliary heating will not be required for at least six hours.

3.1.1.5 Radiation Geometry - The geometrical configuration of the receiver cavities shall conform to the following requirements:

- a. Maximum absorbed fluxes on absorbing surfaces shall not exceed those identified on Figure 3.1-1 at the design point.
- b. Incident fluxes on non-absorbing surfaces inside the cavities shall not exceed 2000 BTU/HR-FT<sup>2</sup> on 2 1/4 Cm-LMO surfaces, 10,000 BTU/HR-FT<sup>2</sup> on 304 SS surfaces painted with white pyromark.
- c. The aperture efficiency -defined as the ratio of reflected solar energy that passes through the apertures to the total reflected energy incident on the aperture planes - shall exceed 98% at the design point.

3.1.1.6 Incident Flux Distributions - The thermal design of the RS shall be consistent with the following incident flux distributions derived in accordance with 4.1:

- a. Absorbing Surfaces - Steady State Operation
  - North Cavity - Design Point : Figure 3.1-2a
  - East and West Cavity - Design Point : Figure 3.1-2b, A, and B
  - South Cavity - Design and Peak Points : Figure 3.1-2c
  - North Cavity - Peak Point : Figure 3.1-2d
  - East and West Cavity - Peak Point : Figure 3.1-2e, A, and B
  - North Cavity at East Cavity Peak Point: Figure 3.1-2f
  - East Cavity at North Cavity Peak Point: Figure 3.1-2g
  - South Cavity at East Cavity Peak Point: Figure 3.1-2h
- b. Absorbing Surfaces - Operational Cloud Cover Transients:
  - Figures 3.1-3a through 3.1-3c, with complete loss of insolation to the heat absorbing surfaces during a "100% cloud".
- c. External Non-absorbing Surfaces - Steady State Operation
  - North Aperture Spillage : Figure 3.1-4a
  - East and West Aperture Spillage : Figure 3.1-4b
  - South Aperture Spillage : Figure 3.1-4c
- d. Internal Non-absorbing Surfaces - Steady State Operation
  - North Cavity : Figure 3.1-4d
  - East Cavity : Figure 3.1-4e
  - South Cavity : Figure 3.1-4f

- 3.1.2 Operating Life - The RS components shall be designed for a 30 year operating life.
- 3.1.3 Heat Transfer Fluid - The heat transfer fluid shall be molten salt consisting of 60% sodium nitrate (NaN<sub>3</sub>) and 40% potassium nitrate (KNO<sub>3</sub>) by weight, with thermophysical properties as shown in Table 3.1-1.
- 3.1.4 Molten Salt Temperatures - The RS shall be capable of sustained operation within the temperature ranges and conditions specified below:
- 3.1.4.1 Steady State Operation
- a. Salt inlet to RS :  $288 \pm 15\text{C}$  ( $550 \pm 27\text{F}$ )
  - b. Salt leaving RS :  $565 \pm 5\text{C}$  ( $1050 \pm 10\text{F}$ )
- 3.1.4.2 Operating Cloud Cover Transients - Cloud cover can cause the inlet or outlet salt temperature to go beyond the range specified for steady state operation. For this condition, the operator can continue to operate or go to hot standby. If the salt temperature falls to 288°C (550°F) the system will automatically go to hot standby.
- 3.1.4.3 Hot Standby - With the use of auxiliary heating the plant will be capable of indefinite operation, with salt temperature staying above 246°C (475°F).



A-12

PASS No. 4 FT TYP

	1	2	3	4	5	6	7	8	9	10
60	14.5	28.3	14.3	4.0	7.4	16.5	10.4	1.7	0	0
↑	26.4	34.8	14.0	3.2	6.5	21.4	21.5	5.8	0	0
4 FT TYP	41.5	40.3	14.0	6.5	13.0	30.8	33.2	10.4	0.2	0
	60.6	48.0	19.7	18.4	31.1	46.4	42.5	14.4	0.3	0
40	85.2	66.7	38.8	40.7	57.1	64.7	53.5	20.9	2.7	0
	111.8	92.7	67.2	73.6	84.3	87.3	72.2	38.0	10.4	1.1
	125.0	109.0	92.1	102.9	109.6	111.7	98.9	62.8	24.6	4.9
	122.6	112.3	103.4	119.8	130.7	136.6	125.7	89.4	40.2	10.5
	105.3	101.6	98.8	120.6	139.1	148.5	139.5	103.5	51.8	16.9
20	89.8	90.8	91.6	114.9	136.0	146.2	137.0	103.0	56.2	22.0
	91.7	93.9	92.2	112.5	130.8	139.5	128.9	97.6	58.1	26.5
	115.9	116.3	106.8	121.1	133.1	135.8	123.4	95.5	60.8	31.5
	153.6	150.3	129.2	137.8	142.3	139.3	124.1	97.0	64.3	35.7
	187.5	180.5	148.9	152.6	150.4	141.8	123.5	96.1	65.1	37.4
0	195.5	185.3	149.7	151.3	145.9	133.5	113.7	87.7	59.9	35.1
↓	169.6	159.3	127.1	128.3	122.8	110.8	93.2	71.2	48.3	28.0
	121.3	113.3	90.0	92.0	87.8	78.7	65.4	49.2	33.2	19.1
	71.5	66.4	53.1	54.5	52.8	47.3	38.9	29.6	19.3	10.3
	33.5	30.9	24.9	26.4	25.5	22.9	18.7	13.6	7.9	3.4
-20	9.9	9.1	7.4	8.2	8.1	7.3	5.5	3.3	1.7	0.7

NOTES: Fluxes are in 1000 BTU/HR-FT<sup>2</sup>  
 Day 172, Solar Noon, 950 W/M<sup>2</sup>, Insolation

FIGURE 3.1-2a INCIDENT FLUXES - NORTH CAVITY @ DESIGN POINT

PASS NO:

4 FT TYP

	10	9	8	7	6	5	4	3
60	1.0	8.6	14.0	10.3	5.7	1.6	1.3	6.2
	2.4	16.3	22.8	9.1	15.7	0.9	6.7	17.4
	2.9	22.2	31.4	11.2	0.6	5.0	18.2	30.5
	4.2	27.5	38.8	14.6	4.8	17.3	35.2	37.8
40	7.9	36.6	45.6	22.5	18.9	36.7	51.8	42.2
	14.5	46.6	55.8	41.1	45.3	65.0	68.2	55.0
	22.1	55.8	69.5	69.0	79.0	76.3	94.1	87.3
	29.8	65.5	85.0	93.6	101.9	115.2	117.4	115.2
	38.7	77.8	103.3	111.6	110.4	118.4	121.3	118.5
20	45.8	84.5	111.6	120.2	110.2	111.0	107.0	99.3
	49.1	86.6	114.0	125.5	114.5	113.0	102.7	88.1
	50.9	86.1	116.0	132.6	127.7	131.3	122.4	106.7
	51.3	83.8	115.2	135.8	141.0	155.8	156.8	146.2
	46.5	75.0	103.9	126.0	140.5	166.3	178.9	177.3
0	36.9	58.3	81.2	99.5	116.1	145.1	164.2	169.5
	24.5	38.3	53.1	65.1	77.5	100.4	117.7	124.8
	12.9	20.5	28.2	34.4	40.7	54.3	65.2	69.9
	5.3	8.3	11.3	13.7	15.6	20.6	25.0	27.0
	1.8	2.3	2.3	2.2	2.2	2.8	3.0	2.8
-20	0	0	0	0	0	0	0	0

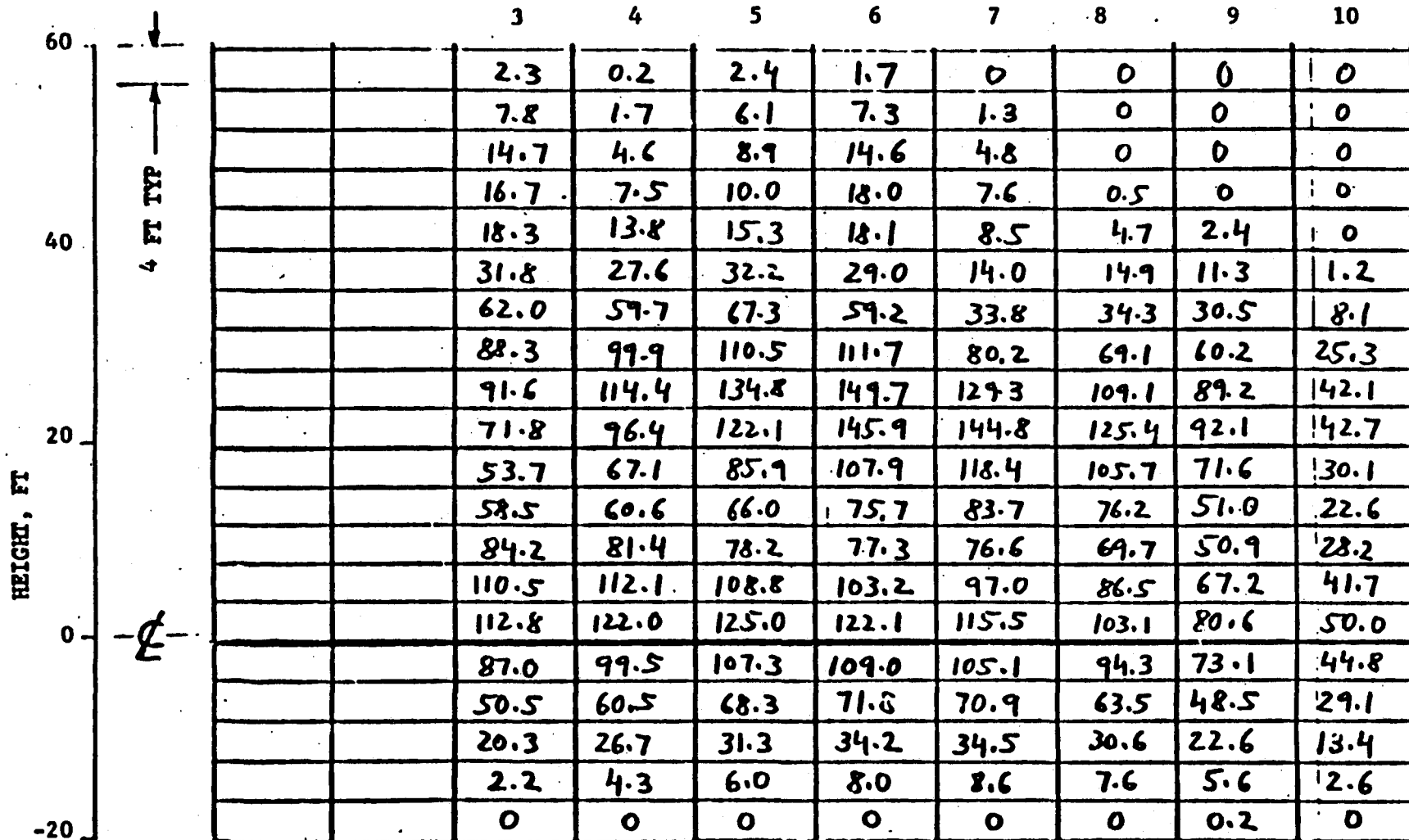
NOTES : Fluxes are in 1000 BTU/HR-FT<sup>2</sup>  
 Day 172, Solar Noon, 950 W/M<sup>2</sup> Insolation

FIGURE 3.1-2b INCIDENT FLUXES - EAST AND WEST CAVITIES @ DESIGN POINT  
 (A) SOUTH AND BACK WALL

PASS NO:

→ 4 FT TYP ←

A-14



NOTES: Fluxes are in 1000 BTU/HR-FT<sup>2</sup>  
 Day 172, Solar Noon, 950 W/M<sup>2</sup> Insolation

FIGURE 3.1-2b INCIDENT FLUXES - EAST AND WEST CAVITIES @ DESIGN POINT  
 (B) NORTH WALL

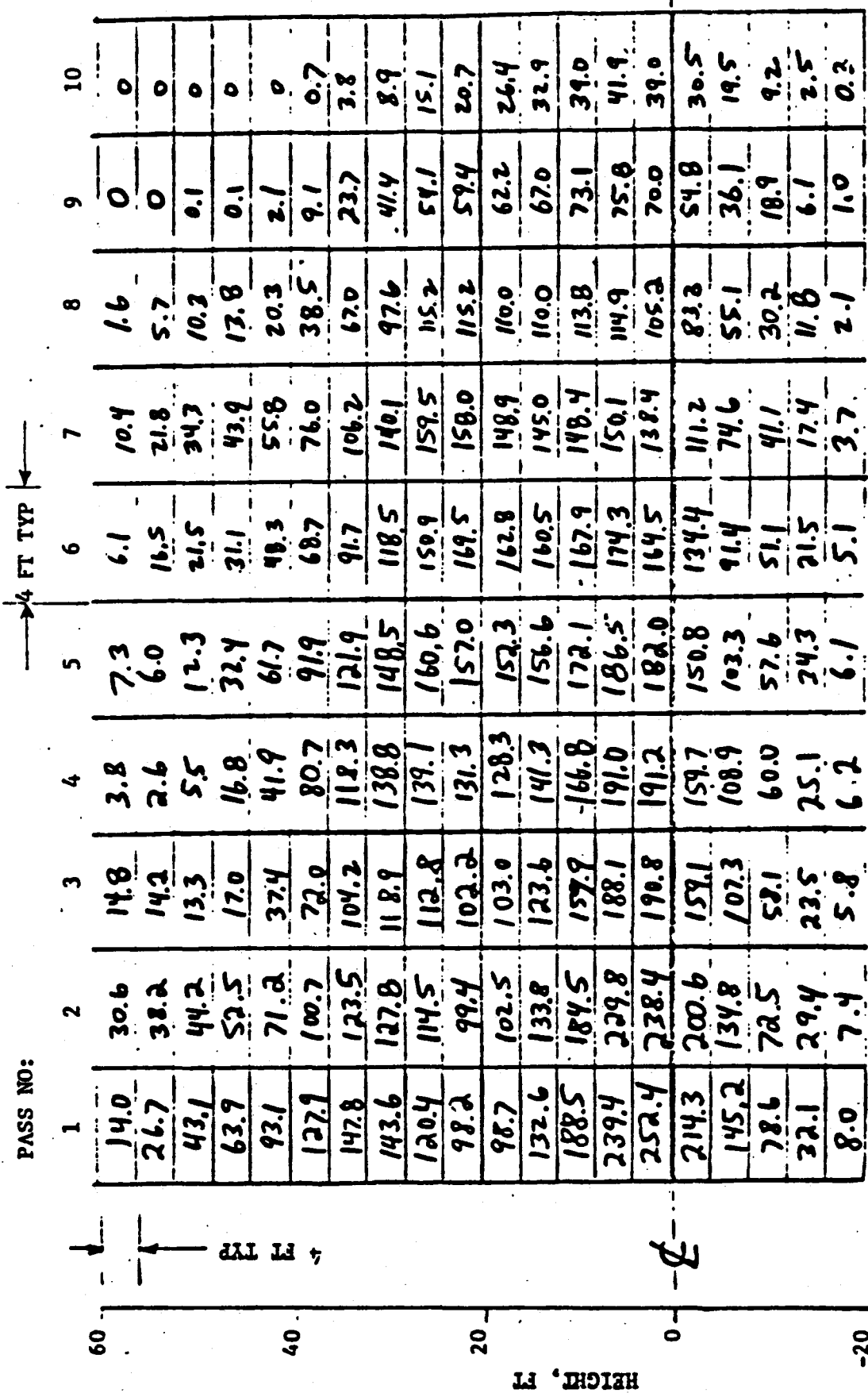
PASS NO:

4 FT TYP

	1	2				7	8	9	10
60	0	0				0	0	0	0
	0	0				0	0	0	0
	0.7	2.2				0.5	0.4	0	0
	3.3	8.2				3.4	3.3	1.6	0
40	6.2	15.2				8.2	8.8	7.3	0.4
	9.4	21.2				14.5	16.7	13.9	1.8
	16.1	27.3				19.4	23.9	20.4	2.8
	41.9	41.9				25.9	32.3	27.0	5.1
	95.5	75.2				50.4	49.6	38.6	9.8
20	145.7	112.2				87.4	81.1	62.6	20.7
	160.0	132.9				123.7	126.2	96.6	41.8
	146.4	133.9				140.6	150.4	120.2	60.4
	140.4	135.8				143.1	150.9	121.9	65.9
	132.5	124.6				123.5	125.8	99.6	55.8
0	95.6	86.0				81.7	81.7	63.4	35.8
	46.5	40.4				38.6	38.6	29.9	16.6
	7.8	6.4				7.1	9.8	8.4	4.1
	0	0				0	0	0.1	0.2
	0	0				0	0	0	0
-20	0	0				0	0	0	0

NOTES: Fluxes are in 1000 BTU/HR-FT<sup>2</sup>  
 Day 172, Solar Noon, 950 W/M<sup>2</sup> Insolation

FIGURE 3.1-2.c INCIDENT FLUXES - SOUTH CAVITY @ DESIGN AND PEAK POINTS

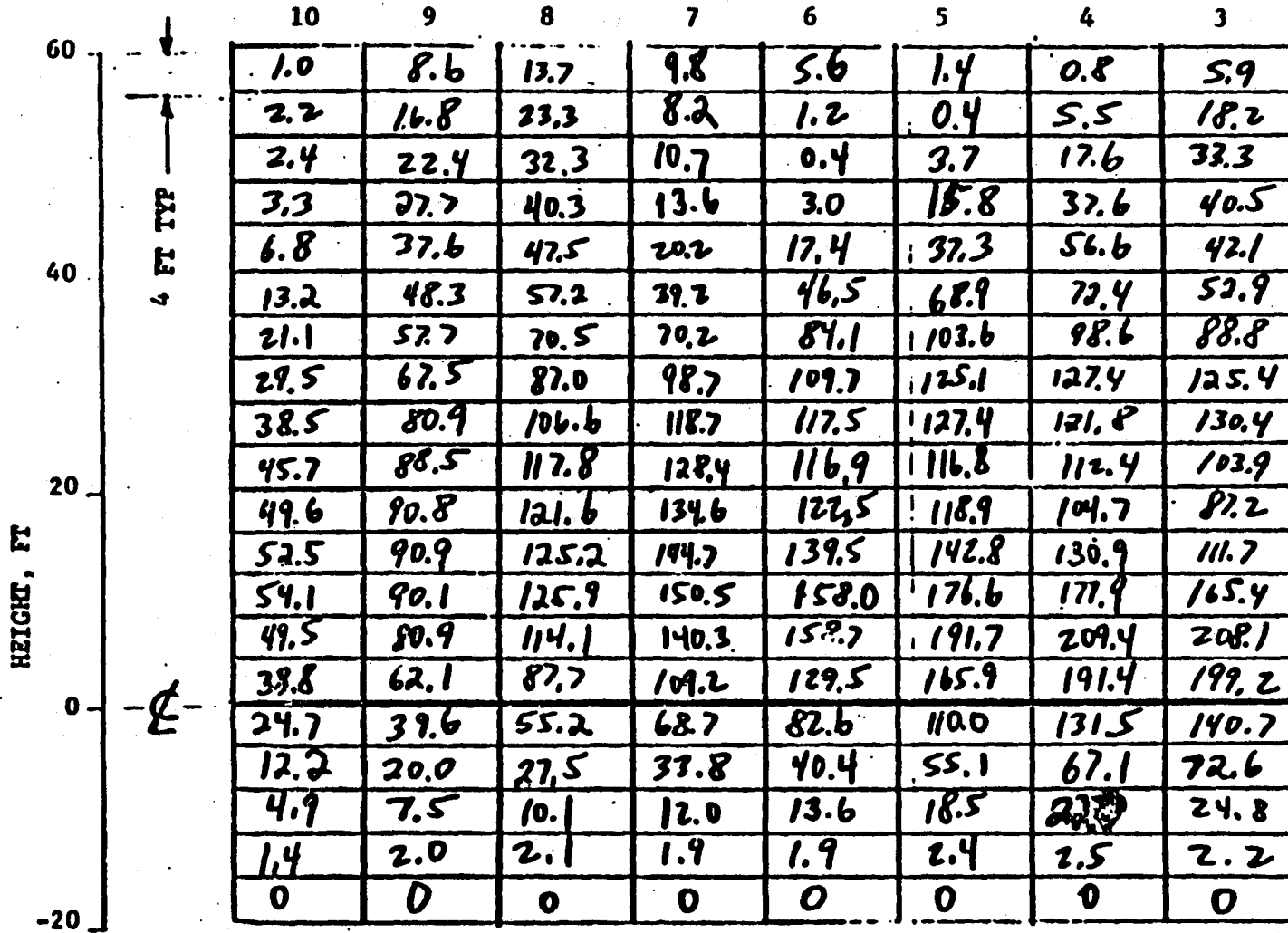


NOTES: Fluxes in 1000 BTU/HR-FT<sup>2</sup>  
Day 356, Solar Noon, 950 W/M<sup>2</sup> Insolation

FIGURE 3.1-2a INCIDENT FLUXES - NORTH CAVITY @ PEAK POINT

PASS NO:

→ 4 FT TYP ←



NOTES: Fluxes are in 1000 BTU/HR-FT<sup>2</sup>

Day 172 at 14:00 Hrs, 950 W/M<sup>2</sup> Insolation for the East Cavity

10:00 Hrs, 950 W/M<sup>2</sup> Insolation for the West Cavity

FIGURE 3.1-2e INCIDENT FLUXES - EAST AND WEST CAVITIES @ PEAK POINTS  
(A) SOUTH AND BACK WALL

A-17

PASS NO:

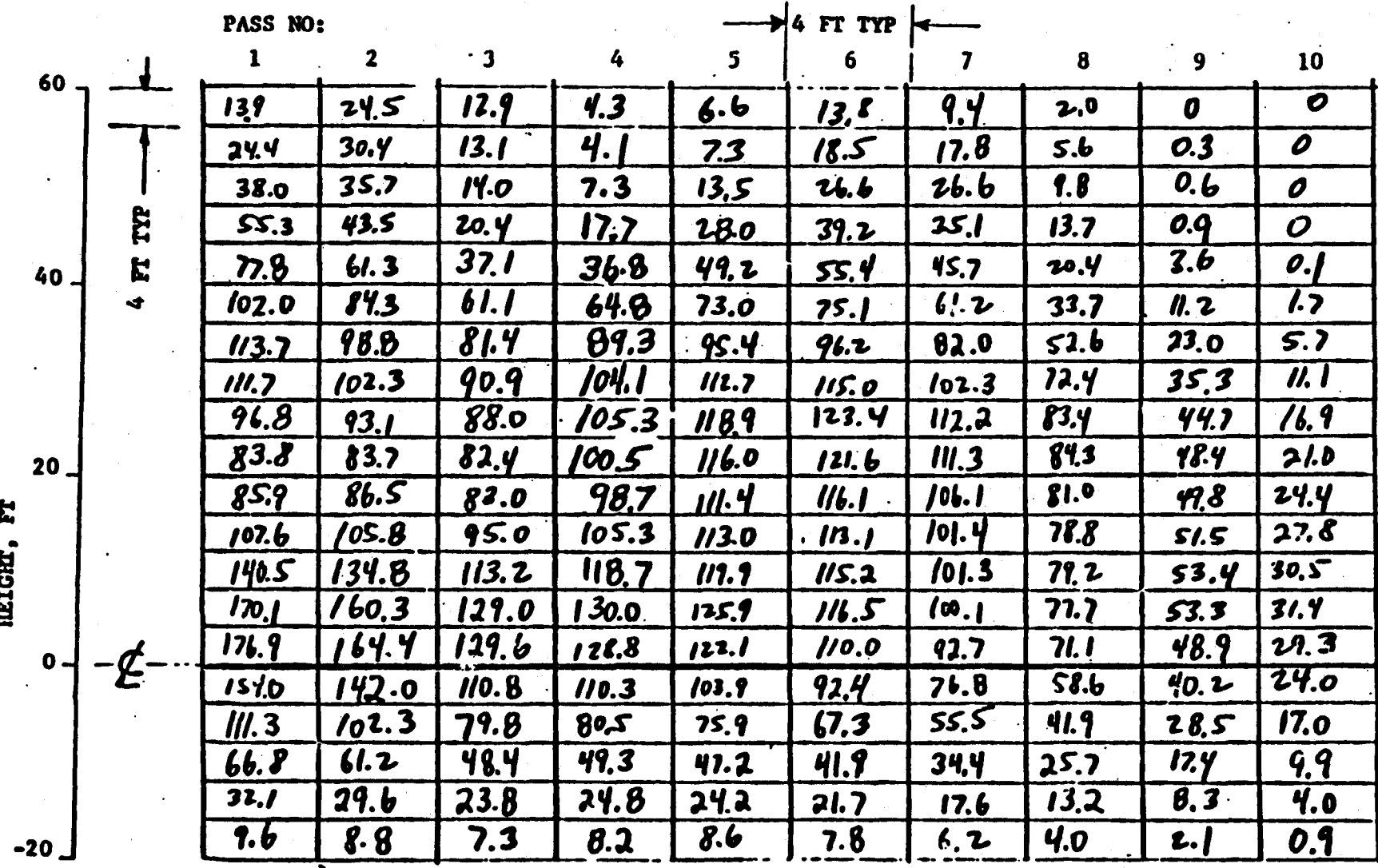
→ 4 FT TYP ←

	3	4	5	6	7	8	9	10
60	1.9	0	2.0	1.5	0	0	0	0
	8.2	1.2	6.0	7.4	1.1	0	0	0
	16.2	4.1	9.3	16.1	4.5	0	0	0
	17.5	6.8	9.3	19.6	7.8	0.1	0	0
40	16.6	113.0	14.1	18.2	7.8	3.9	2.1	0
	30.9	25.9	32.1	29.3	11.2	15.3	11.0	0.9
	67.4	61.2	69.8	63.2	30.7	34.5	31.3	7.1
	99.9	109.4	118.5	121.1	87.0	67.8	63.3	24.7
	102.9	129.0	150.6	169.5	171.1	114.6	97.2	43.4
20	77.2	105.5	135.5	166.0	164.2	138.9	100.7	43.2
	52.1	66.7	89.0	114.6	128.9	115.4	74.8	27.4
	59.1	59.5	63.0	72.5	83.4	77.9	50.4	19.8
	94.8	89.5	82.4	78.2	77.5	71.4	52.3	28.7
	131.4	132.5	126.7	116.9	108.5	97.8	76.1	46.1
0	135.0	146.6	149.1	143.6	134.7	121.3	94.2	56.6
	100.3	116.1	125.4	126.2	121.3	109.2	84.0	49.6
	53.5	65.7	74.3	77.7	76.8	68.7	51.7	30.1
	19.0	25.4	30.0	32.5	32.3	28.7	21.1	12.1
	2.0	3.4	4.7	5.6	5.6	4.9	3.4	1.1
-20	0	0	0	0	0	0	0	0

NOTES: Fluxes in 1000 BTU/HR-FT<sup>2</sup>Day 172 at 14:00 Hrs, 950 W/M<sup>2</sup> Insolation for the East Cavity10:00 Hrs, 950 W/M<sup>2</sup> Insolation for the West Cavity

FIGURE 3.1-2e INCIDENT FLUXES - EAST AND WEST CAVITIES @ PEAK POINTS  
(B) NORTH WALL

A-19

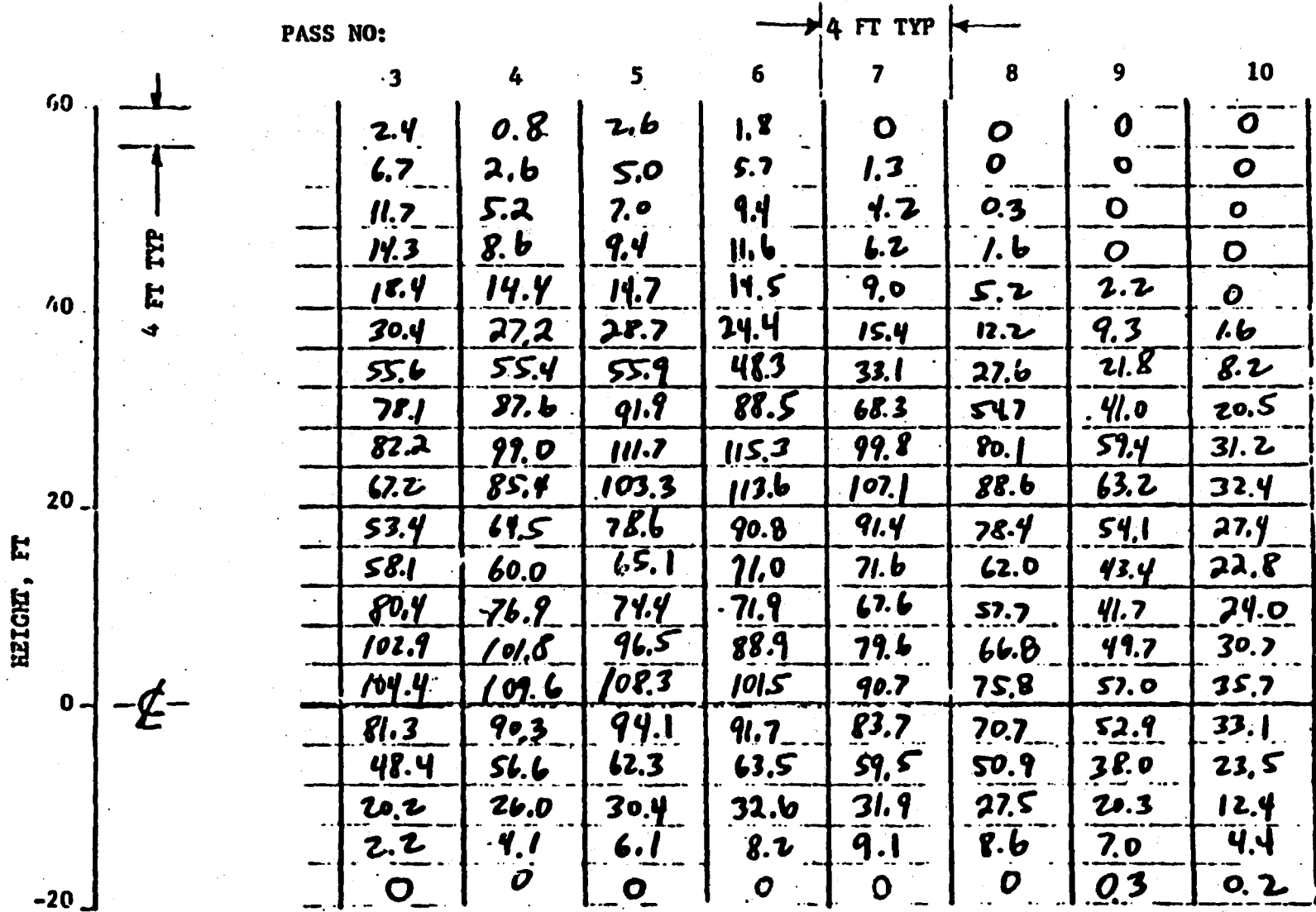


NOTES: Fluxes are in 1000 BTU/HR-FT<sup>2</sup>  
 Day 172, 14:00 Hrs, 950 W/M<sup>2</sup> Insolation

FIGURE 3.1-2f INCIDENT FLUXES - NORTH CAVITY @ EAST CAVITY PEAK POINT



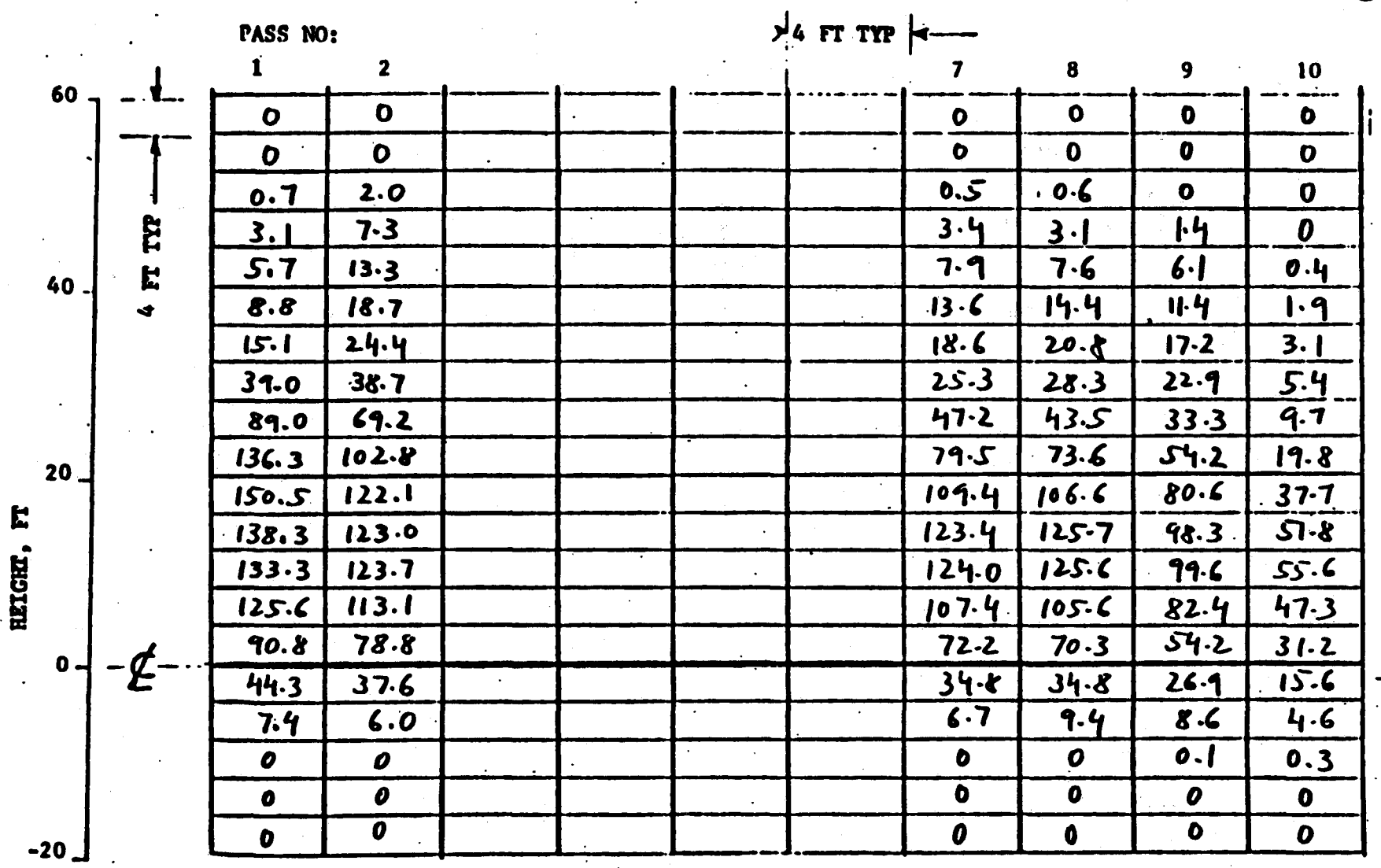
PASS NO:



NOTES: Fluxes are in 1000 BTU/HR-FT<sup>2</sup>  
 Day 356, Solar Noon, 950 W/M<sup>2</sup> Insolation

FIGURE 3.1-2g INCIDENT FLUXES - EAST CAVITY @ NORTH CAVITY PEAK POINT

A-21



NOTES: Fluxes are in 1000 BTU/HR-FT<sup>2</sup>  
 Day 172, 14:00 Hrs, 950 W/M<sup>2</sup> Insolation

FIGURE 3.1-2h INCIDENT FLUXES - SOUTH CAVITY @ EAST CAVITY PEAK POINT

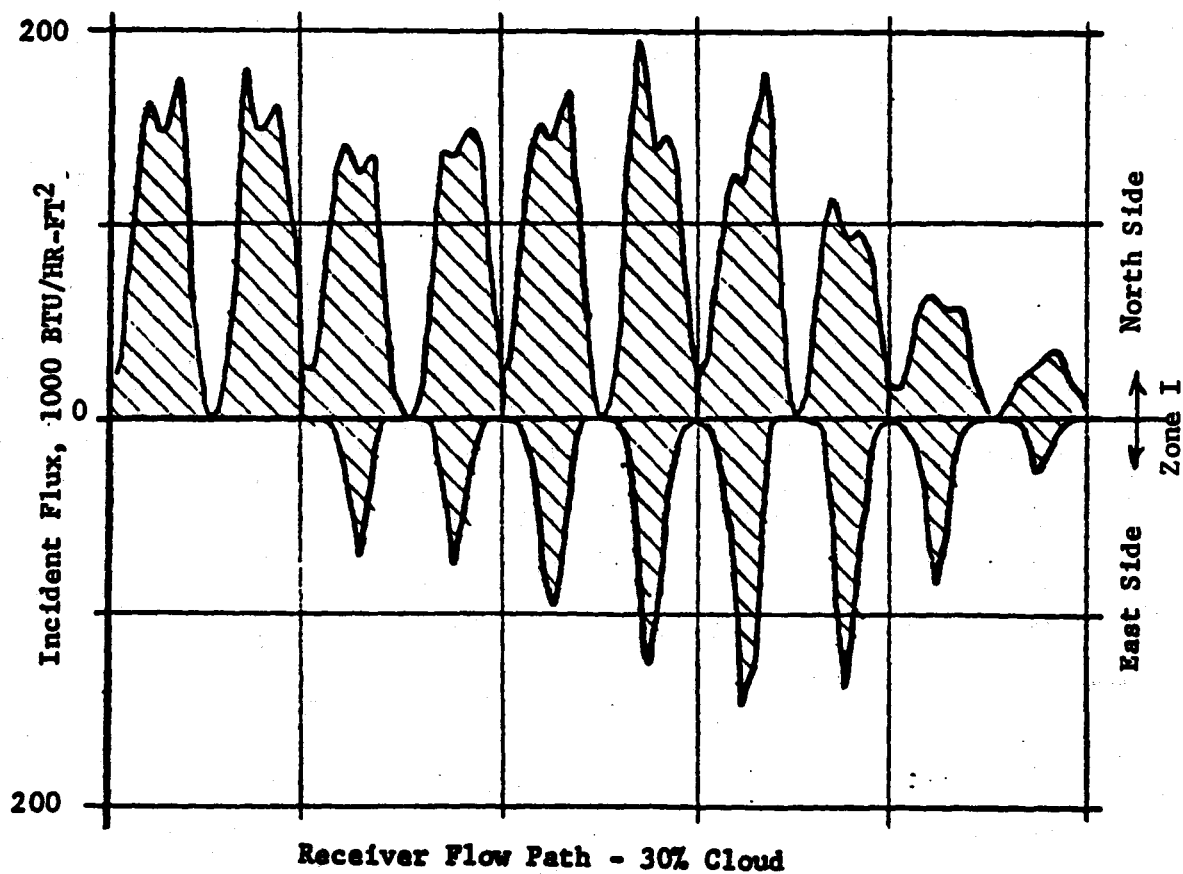
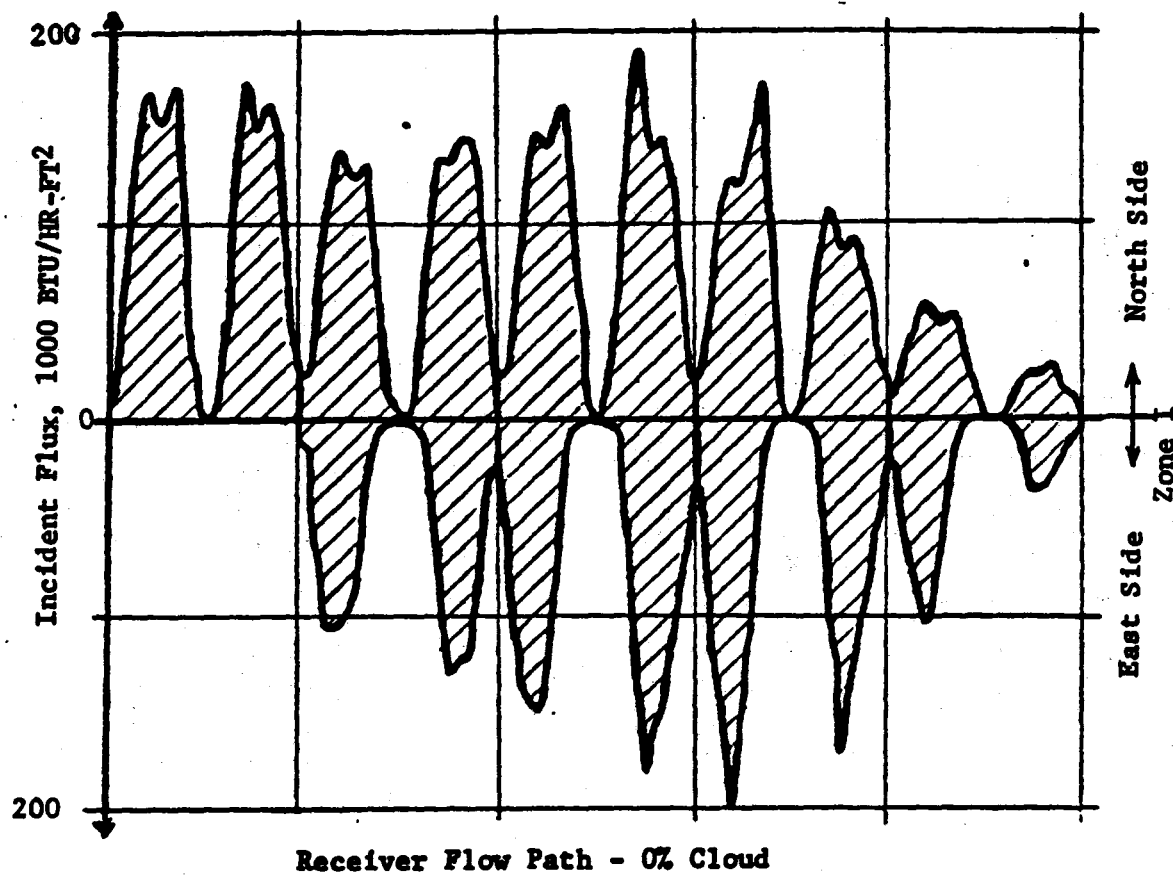
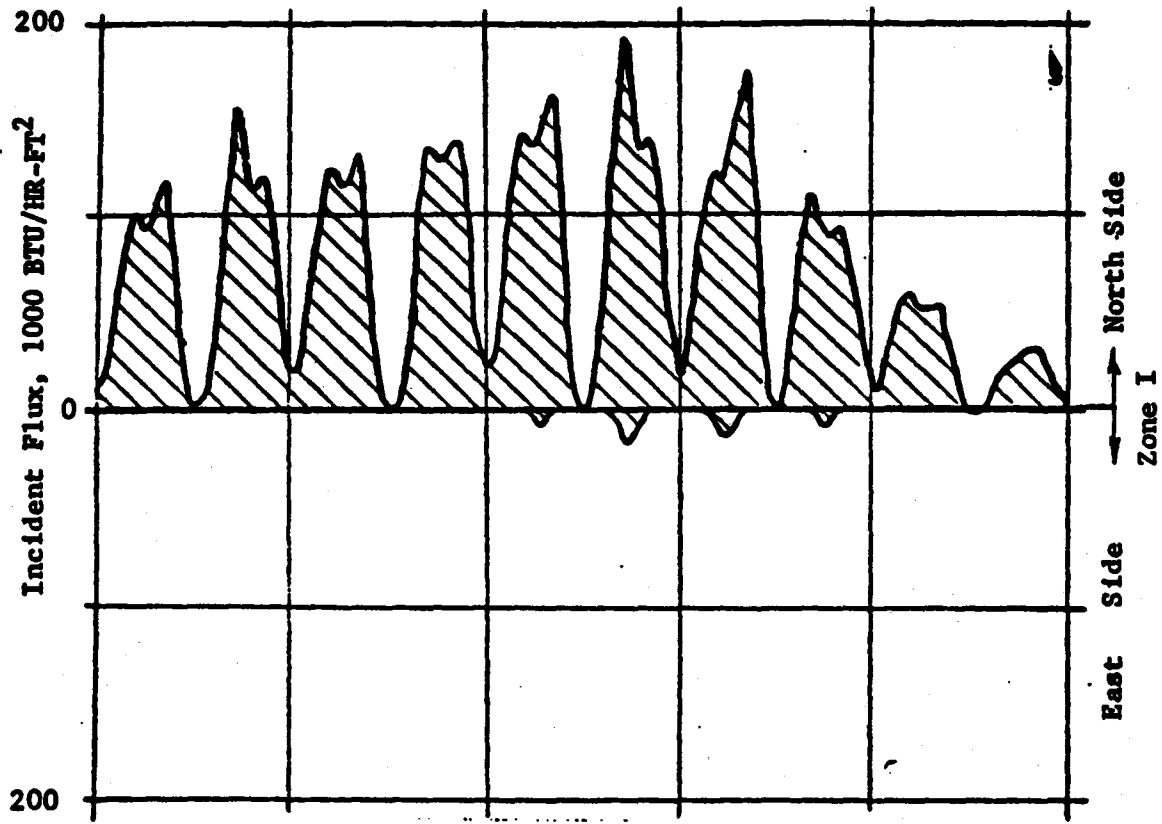
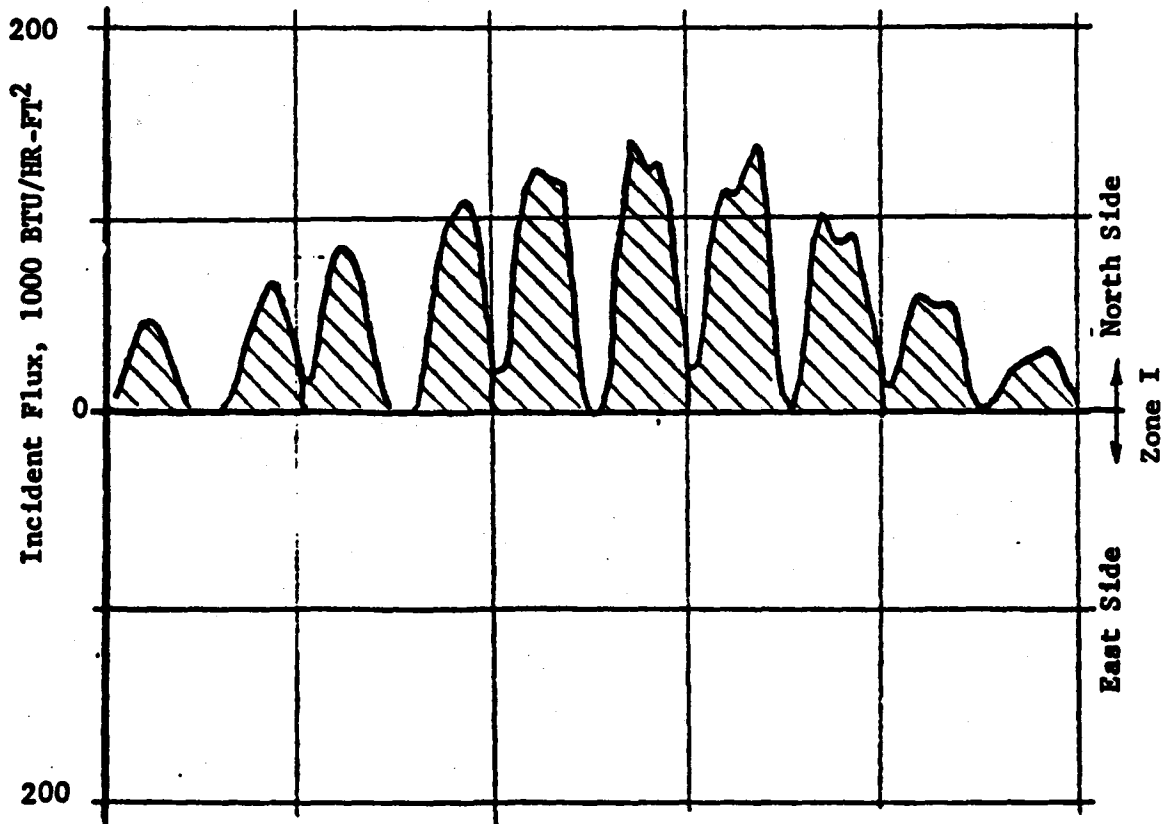


Figure 3.1-3a OPERATIONAL CLOUD COVER TRANSIENTS  
0% and 30% East to West Cloud Cover

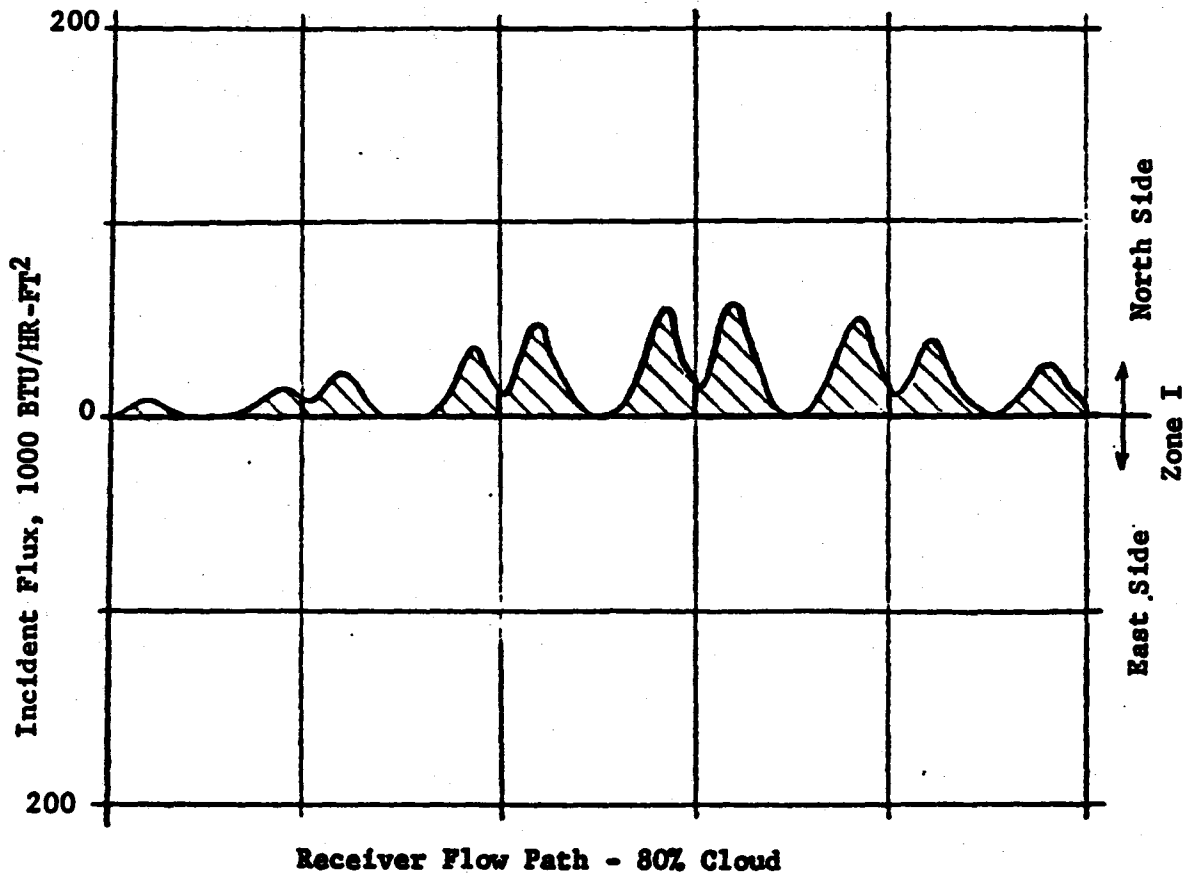


Receiver Flow Path - 50% Cloud

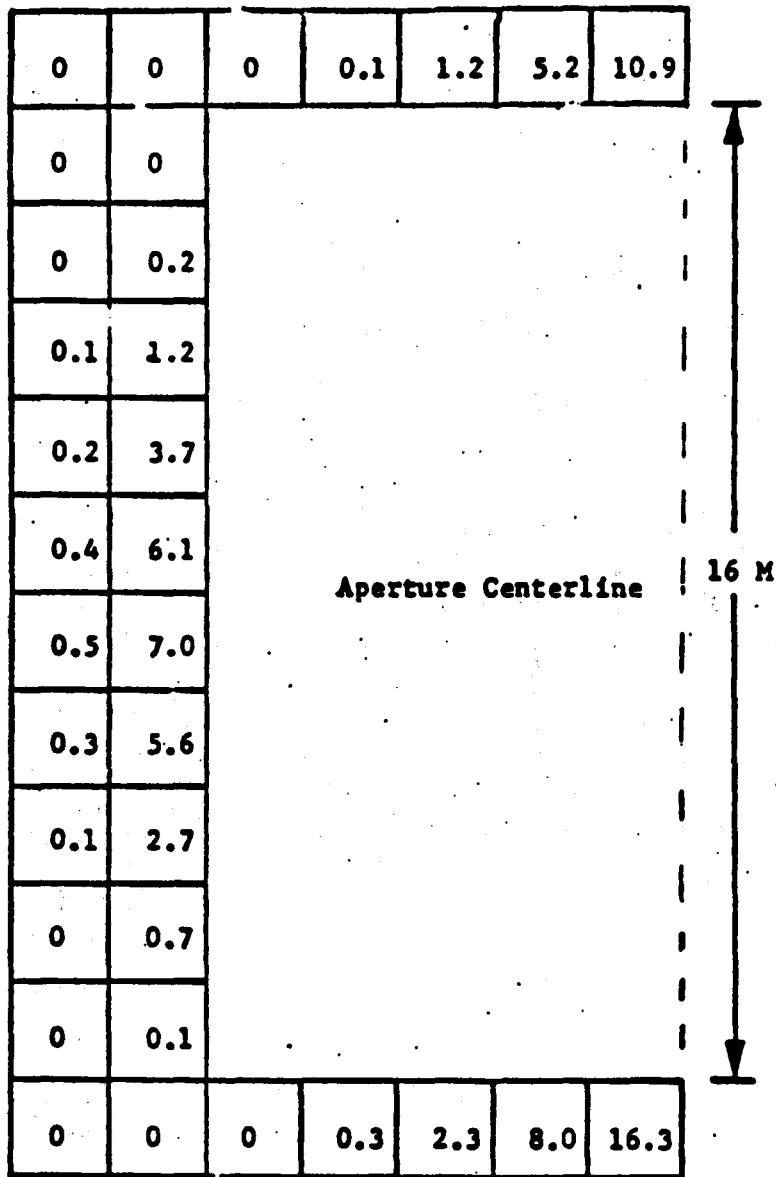


Receiver Flow Path - 60% Cloud

Figure 3.1-3b OPERATIONAL CLOUD COVER TRANSIENTS  
50% and 60% East to West Cloud Cover



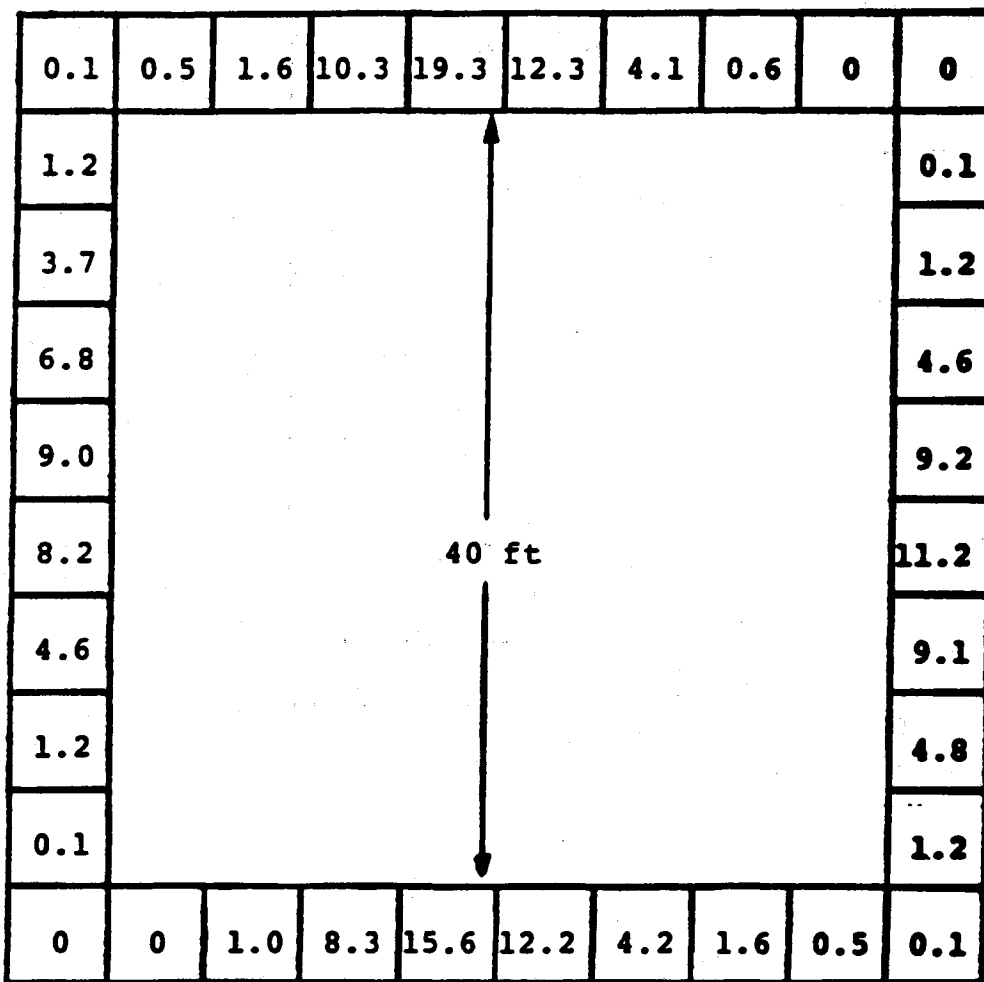
**Figure 3.1-3c OPERATIONAL CLOUD COVER TRANSIENT  
80% East to West Cloud Cover**



**NOTES :** Node Size = 1.6 x 1.6 M (5.25 x 5.25 FT)  
 Fluxes are in 1000 BTU/HR-FT<sup>2</sup> for  
 Day 172, Noon, 1100 W/M<sup>2</sup> Insolation

**FIGURE 3.1-4a NORTH APERTURE SPILLAGE**

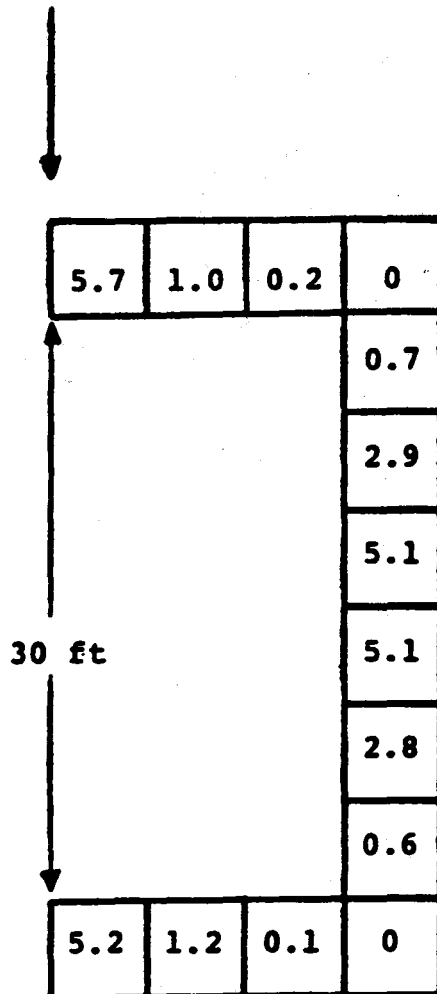
Day 172, Noon  
 1000 BTU/Hr-ft<sup>2</sup>  
 Insolation = 950 W/m<sup>2</sup>



Node Size = 5 x 5 ft<sup>2</sup>

FIGURE 3.1-4b EAST AND WEST APERTURE SPILLAGE

Day 172, Noon  
 1000 BTU/Hr ft<sup>2</sup>  
 Insolation = 950 W/M<sup>2</sup>  
Aperture Center Line

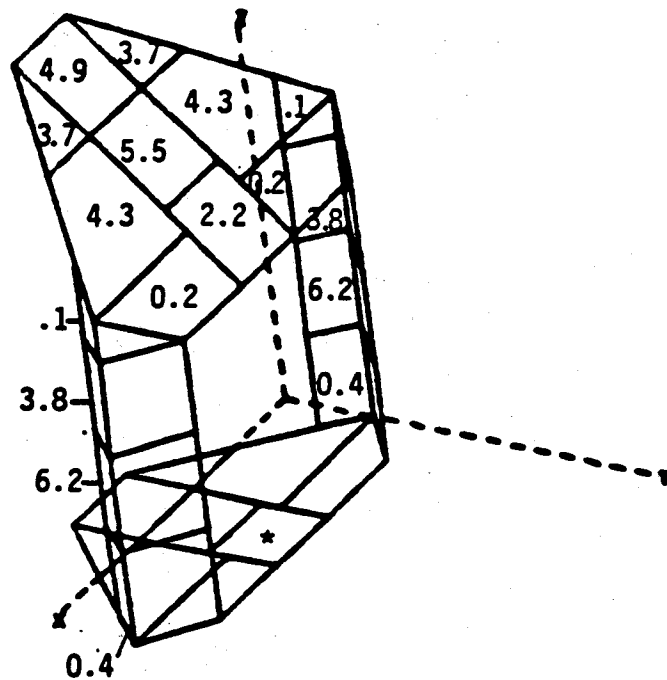


Node Size = 5 x 5 ft<sup>2</sup>

FIGURE 3.1-4c SOUTH APERTURE SPILLAGE



SURFACE FLUXES (1000 Btu/hr-ft<sup>2</sup>)



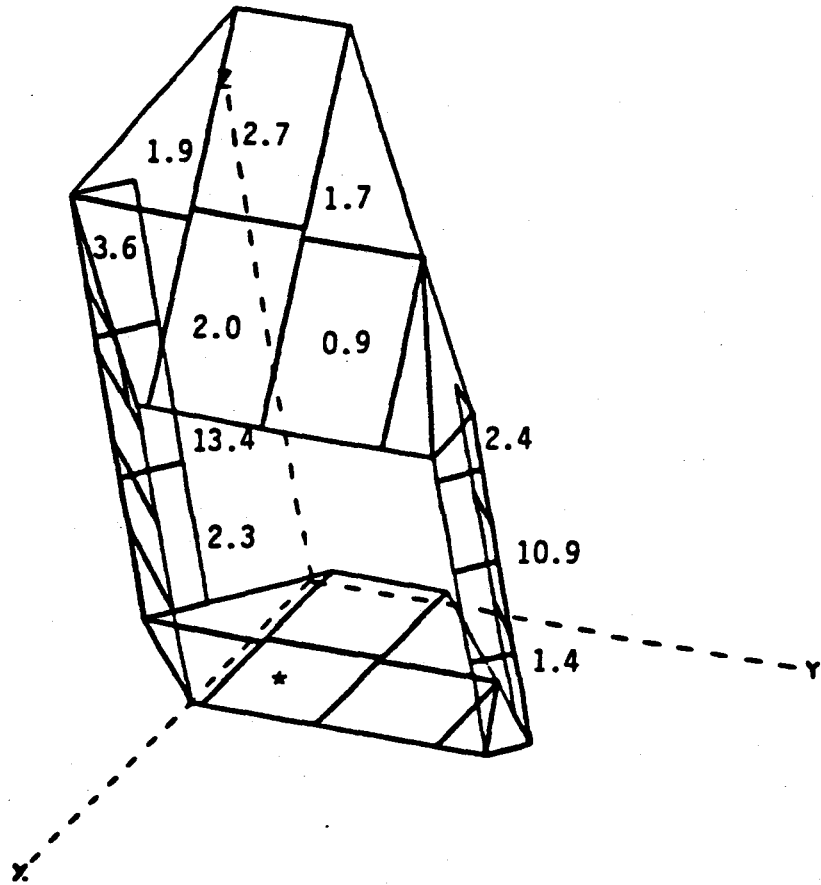
DAY 172, NOON

DESIGN POINT

\*All surfaces unmarked have no direct incident flux.

FIGURE 3.1-4d INCIDENT FLUXES - INTERNAL NONABSORBING SURFACES  
NORTH CAVITY

SURFACE FLUXES (1000 Btu/hr-ft<sup>2</sup>)

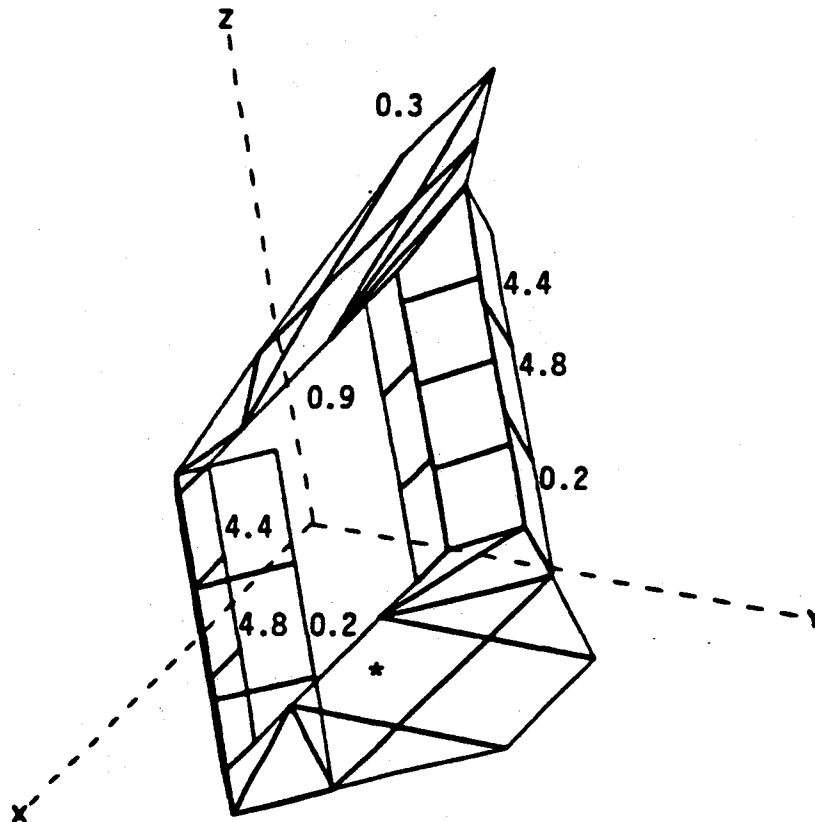


DAY 172, NOON  
DESIGN POINT

\* All unmarked surfaces have no direct incident flux.

FIGURE 3.1-4e INCIDENT FLUXES - INTERNAL NONABSORBING SURFACES  
EAST CAVITY

SURFACE FLUXES (1000 Btu/hr-ft<sup>2</sup>)



DAY 172, NOON  
PEAK & DESIGN POINT

\* All unmarked surfaces have no direct incident flux

FIGURE 3.1-4d INCIDENT FLUXES - INTERNAL NONABSORBING SURFACES  
SOUTH CAVITY

**TABLE 3.1-1 THERMOPHYSICAL PROPERTIES OF COMMERCIAL GRADE MOLTEN SALT MIXTURE  
(60% NaNO<sub>3</sub> + 40% KNO<sub>3</sub> BY WEIGHT)**

**Specific Heat, BTU/LB-F :**

$$C_p = .4464 - 8.644 \times 10^{-5} T$$

**Density, LB/FT<sup>3</sup> :**

$$= 129.4 - 2.119 \times 10^{-2} T$$

**Viscosity, LB/FT-HR :**

$$= 50.07 - 0.1339 T + 1.292 \times 10^{-4} T^2 - 4.268 \times 10^{-8} T^3$$

**Thermal Conductivity, BTU/FT-HR-F :**

$$= 0.2532 + 6.27 \times 10^{-5} T$$

**Melting Temperature Range (Onset to Complete Melt), F:**

$$T_m = 429 - 473$$

**Heat of Fusion, BTU/LB :**

$$H_f = 46.8$$

**NOTES :** T = Temperature in F; Equations and Data Valid from Melt Temp. to 1100 F

**MAXIMUM ALLOWABLE TRACE ELEMENTS BY PERCENT WEIGHT :**

Cl	: 0.30	Al <sub>2</sub> O <sub>3</sub>	: 0.03
SO <sub>4</sub>	: 0.23	Ca	: 0.03
CO <sub>3</sub>	: 0.11	SiO <sub>2</sub>	: 0.02
Alkali	: 0.10	Fe	: 0.01
OH	: 0.21	Insolubles	: 0.10
H <sub>2</sub> O	: 0.50		

### 3.1.5 Turndown Ratio

3.1.5.1 Steady State and Operating Cloud Cover Transients - The RS shall be capable of meeting the temperature requirements specified under 3.1.4.1 and 3.1.4.2 at part load conditions ranging from 25% to 115% of the rating specified under 3.1.1.

3.1.5.2 Minimum Absorbed Thermal Power - The RS shall be capable of sustained operation (with salt flow) at a minimum absorbed power of 10% of the rating specified under 3.1.1.1, with inlet salt temperatures as specified under 3.1.4.1.a, and outlet temperatures not exceeding those under 3.1.4.1.b.

3.1.6 Operating Modes-Normal - The RS shall be capable of functioning in the following operating modes, within the constraints specified herein.

3.1.6.1 Operating Definitions - The normal operating modes involve combinations of 20 major operational sequences labeled a through u on Figure 3.1-5. The sequences pertaining to any given operational mode and their order of execution, are indicated by the numbers in the matrix blocks. Some of the sequences are only used on an as required basis as shown on the figure.

a. Cold Startup

This operation brings the receiver from a dry and empty state at ambient temperature to quasi-steady state operation, through the eight sequences (a through h) shown on Figure 3.1-5.

b. Diurnal Startup

This operation entails the five sequences indicated on Figure 3.1-5, and brings the RS from hot standby to steady state operation.

c. Sustained Operation

This mode includes all steady state operation specified under 3.1.5 and 3.1.5.

d. Operating Cloud Cover Transient

This transient entails operation during intermittent cloud passages between periods of steady state operation. Generally it involves repetitions of sequences j-l-m-n-h-i of Figure 3.1-5.

e. Hot Standby During Prolonged Cloud Passage.

The flexibility shall be provided to use alternate combinations of sequences o,p,q,r,s and u (Figure 3.1-5), depending on the duration of the cloud passage. The combinations shall include (in order of decreasing durations of the cloud passage):

OPERATIONAL MODES

**NOTES** : Numbers in the Matrix Blocks Correspond to the Approximate Order in which the Operational Sequences are Executed

OPERATIONAL SEQUENCES

	Cold Startup	Diurnal Startup	Sustained Operation (25-115% Load)	Operating Cloud Cover Transient	Hot Standby During Prolonged Clouds	Hot startup Following Cloud Passage	Diurnal Shutdown & Overnight Hold	Prolonged Shutdown
a. Trace heat RS to above salt freezing point	1							
b. Heliostats to standby point	2	1			1			
c. Open cavity doors	3	2			2			
d. Preheat absorbing panels with "warmup" heliostats - as required	4							
e. Fill RS with salt from cold storage tank	5							
f. Establish minimum flow (25%)	6	3			3			
g. Ramp-up power (bring heliostats on target )	7	4			4			
h. Establish "design conditions" (set point temps.)	8	5		5	5			
i. Steady sustained operation (clear sky or haze)			1	6	6			
j. Transient operation - Intermittent clouds, acceptable energy levels				1				
k. Sequence deleted								
l. Establish minimum flow required for maintaining outlet temperature				2				
m. Reduce number of heliostats on target for recovery from cloud transient (if required)				3				
n. Return to full heliostat power w. temp. control				4				
o. Remove heliostats from target to standby					1	1	1	
p. Close cavity doors					2	2	2	
q. RS to "hot standby" configuration (valves & heaters)					3	3	3	
r. Establish circulation through receiver					4	4	4	
s. Intermittent charging of RS buffer tank from TES					5	5		
t. Drain RS into TES							5	
u. Heliostats to stow position					6	6	6	

FIGURE 3.1-5 MAJOR SEQUENCES COMPRISING NORMAL OPERATIONAL MODES

- Sequence o-p-q-r-s-u (as shown on Figure 3.1-5)
- Sequence o-p-q-r-s
- Sequence o-p-s

- f. Hot Startup Following Cloud Passage  
This sequence is same as diurnal startup.
- g. Diurnal Shutdown and Overnight Hold  
The sequences are identical with those of prolonged cloud passage of very long duration where the system is put on hot standby. (Figure 3.1-5).
- h. Prolonged Shutdown  
The object of this operation is to drain the RS and allow it to cool down to ambient temperatures. (Sequences o-p-q-r-t-u on Figure 3.1-5).

### 3.1.6.2 Constraints on Operating Modes

- Freezing of salt, including the formation of dispersed solid particles shall be prevented by insuring that the fluid transport equipment in contact with the salt is preheated to at least 11C (20°F) above the incipient freezing point of the salt (246C or 475°F).
- The amount of salt discharged into the hot storage tank at RS outlet temperatures below those specified under 3.1.4.1 shall be controlled by the operator.
- Entrapment of air pockets in the heat absorbing panels of the receiver shall be prevented.
- Metal temperature in contact with salt shall not exceed 600 C (1112°F) during steady-state operations.
- Peak tube metal temperatures shall not exceed 649 C (1200°F) during steady state operating conditions.

### 3.1.6.3 Cycles for Cyclic Operation

<u>Cyclic Operation</u>	<u>Cyclic Life</u>
Cold Startup and Prolonged Shutdown	1,000
Diurnal Startup and Shutdown	10,000
Operating Cloud Cover Transient, and Hot Standby and Recovery	40,000

3.1.7 Operating Modes - Emergency - The RS shall be capable of safe, automatically controlled shutdown (without operator attention) resulting from the following emergency conditions. In combination, the total cycles for these events shall not exceed 200.

	<u>No. of Events</u>
a. Molten salt pump trip	100
b. Heliostat field scram	100
c. Loss of electrical power to the heliostat field	10
d. Failure of any molten salt pipe	10
e. Failure of a panel tube	10
f. Loss of receiver, collector, or salt flow control	5
g. Loss of site electrical power	5
h. Failure or improper operation of isolation, relief, or control valves	20
i. Loss of pneumatics	10

3.1.8 Availability and Reliability - The RS shall be designed for 95% availability, based on reliability and maintainability assessments exclusive of insolation conditions. Consideration shall be given in the design to achieving high reliability by providing design and operating margins and utilizing sound engineering design practices.

3.1.9 Maintainability

- a. The Receiver Subsystem shall be designed so that potential maintenance locations can be easily reached and components such as electronic units, motors, drives, etc. can be readily replaced.
- b. Elements subject to wear and damage, such as supporting wheels, gears, etc., should be easily serviced and replaced.
- c. The subsystem should be capable of being serviced by personnel of skills typical of those utilities currently employ for maintenance, and should require a minimum of specialized equipment or tools.
- d. Individual tubes and panels shall be replaceable.

3.1.10 Thermal Coating Requirements

- a. Heat absorbing surfaces shall be coated with high temperature black paint (Pyromark 2400 or equivalent) having the following properties on installation: solar absorptivity =  $.95 \pm .02$ , thermal emissivity =  $.90 \pm .02$ .
- b. Reflective coating on external surfaces exposed to induced environments per 3.2.9 shall consist of high temperature white paint (Pyromark 2400 series or equivalent) having the following properties on installation: solar absorptivity =  $.32 \pm .02$ , thermal emissivity =  $.84 \pm .02$ .



3.2 Environmental Conditions for Design, Operation, and Survival

3.2.1 Reference Site - The reference site shall be Barstow, California (As specified in "Pilot Plant Environmental conditions - OPDD Appendix C", Aerospace Report No. ATR-78 (7695-05), Revision 1, 15 August 1978.

3.2.2 Insolation - Refer to 3.1.1.2.

3.2.3 Dynamic Performance

- a. The maximum rate of change of incident flux shall be assumed as that which would result from passage of an opaque cloud across an otherwise clear sky where the sharp leading or trailing edges of the shadow move across the collector field at a velocity of 13 meters per second (29 MPH).
- b. The definition (per 3.1.1.6-b) and modeling of cloud transients for purposes of control subsystem and thermo-structural design shall be based on the insolation variation data reported in Aerospace Report No. ATR-80 (7747)-1, 1 March 1980.

3.2.4 Sun Angle

The sun azimuth and elevation angles assumed for the design point shall be those associated with the time of the day and year at which the solar power to the receiver is at a maximum (for the given field layout), at the insolation levels given by 3.2.2.

3.2.5 Wind

- a. Design Point - Performance requirements shall be met for wind speeds up to 3.5 m/sec (8MPH) at a reference height of 10 m (33 feet)
- b. Wind Speed/Frequency Specification - at reference height of 10 meters:

<u>Speed, m/s</u>	<u>Frequency/Percent</u>
0 - 2	29
2 - 4	21
4 - 6	19
6 - 8	14
8 - 10	8
10 - 12	5
12 - 14	3
14 -	Less than 1

- c. Wind Velocity Profile - Shall be assumed to vary exponentially with height to the 0.15 power, where the reference height is taken as 10 m (33 feet), according to the following model:

$$V_h = V_1 (h/h_1)^c$$

where:  $V_h$  = mean wind speed at height  $h$   
 $V_1$  = wind speed at reference height  $h_1$   
 $h_1$  = reference height (assume 10 meters)  
 $c = 0.15$

- d. Receiver hot salt temperature requirements shall be met for wind speeds up to 14 m/sec (31 MPH) over ambient temperature ranges of 0 to 50C (32 to 122°F).
- e. Maximum Operating Wind Speed - 16 m/sec (36 MPH) at the reference height. At wind speeds higher than maximum operating, the plant shall be shut down, with the cavity doors closed.
- f. Survival - The receiver subsystem shall be capable of surviving winds with a maximum reference speed, including gusts of 40 m/s (90 mph).
- g. The reinforced concrete tower shall be designed for a basic wind pressure of 30 psf (per UBC map area), in accordance with ACI 307-79, "Specification for the Design and Construction of Reinforced Concrete Chimneys."

### 3.2.6 Ambient Temperatures

- a. Design Point - Wet bulb: 23C (74°F); Dry Bulb: 28C (82.6°F).
- b. Range of Performance - the receiver subsystem shall be capable of meeting performance requirements over the ambient temperature range from 0 to 50C (32 to 122°F).
- c. Operation - There is no minimum temperature for operation of the RS.

### 3.2.7 Snow, Hail, Rain and Ice

The receiver subsystem shall survive a static snow load of 248 Pa (5 lb/ft<sup>2</sup>) and a snow deposition rate of 0.3 m (1 ft) in 24 hours.

The receiver subsystem shall survive hail impact up to the following limits:

Diameter	25 mm (1 in)
Specific Gravity	0.9
Terminal Velocity	23 m/s (75 fps)

The receiver subsystem shall survive the following rainfall conditions:

Average annual - 750 mm (30 in)  
Maximum 24-hr rate - 75 mm (3 in)

The receiver subsystem shall survive freezing rain and ice deposits in a layer 50 mm (2 in) thick.

3.2.8 Earthquake - The reinforced concrete tower shall be seismically designed in accordance with ACI 307-79. "Specification for the Design and Construction of Reinforced Concrete Chimneys," for UBC (1973) Seismic Zone 3 with a Use Factor of 2.0. For the resulting tower design, seismic response spectrum analyses of a tower and receiver model shall be made to determine the horizontal and vertical design accelerations at the receiver level. For these analyses, the horizontal and vertical response spectra provided in U.S. Nuclear Regulatory Commission Regulatory Guide 1.60 shall be normalized to peak ground accelerations of 0.10 g and 0.25 g for the operational and survival earthquakes, respectively. Damping for the tower shall be taken as 0.01 and 0.02 of critical damping for the operational and survival earthquakes, respectively. The seismic forces on piping and equipment shall be statically computed by multiplying the mass of the component by the horizontal and vertical accelerations derived from the tower response spectrum analyses. The distributions of the seismic forces shall be in accordance with the distribution of weight throughout the component.

3.2.9 Induced Environments - The receiver subsystem shall be capable of surviving the following solar flux levels on its external surfaces:

- a. Spillage, with intensities up to levels not exceeding 23,000 BTU/HR-FT<sup>2</sup> on aperture frame (must be 304 ss painted with white pyromark), and distributions as shown on Figure 3.1.4a, b, and c.
- b. Flux patterns generated along the path of heliostat images between the standby point and aim points during power ramp-up, shutdown, scram, and other focusing and de-focusing operations, for the combinations of intensity and exposure times represented by the curve on Figure 3.1-6.
- c. Fluxes due to stray heliostats (as a result of possible pointing errors or heliostat pointing system malfunctions), up to levels not exceeding 1.46 w/m<sup>2</sup> (5000 BTU/FT<sup>2</sup>-HR).
- d. Fluxes resulting from loss of electrical power to the heliostat field and subsequent drifting of the aim points due to the motion of the sun, as depicted on Figures 3.1-7a, 3.1-7b, and 3.1-7c, for the North, East (as shown, west opposite), and South apertures, respectively.

The receiver subsystem shall be capable of surviving conditions a, b and c above without damage. Sacrificial materials may be used, as required, to provide thermal protection during d to minimize damage.

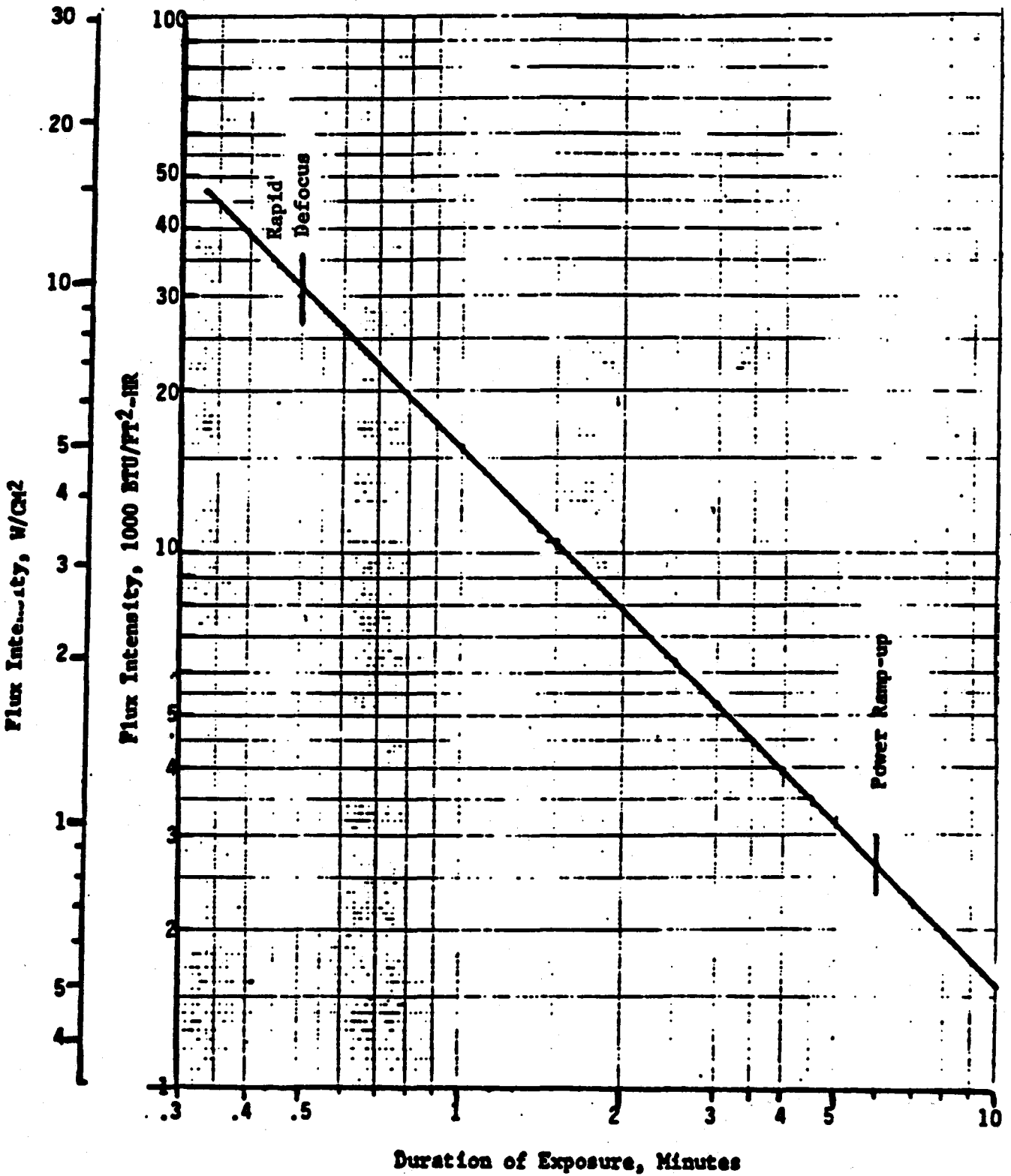
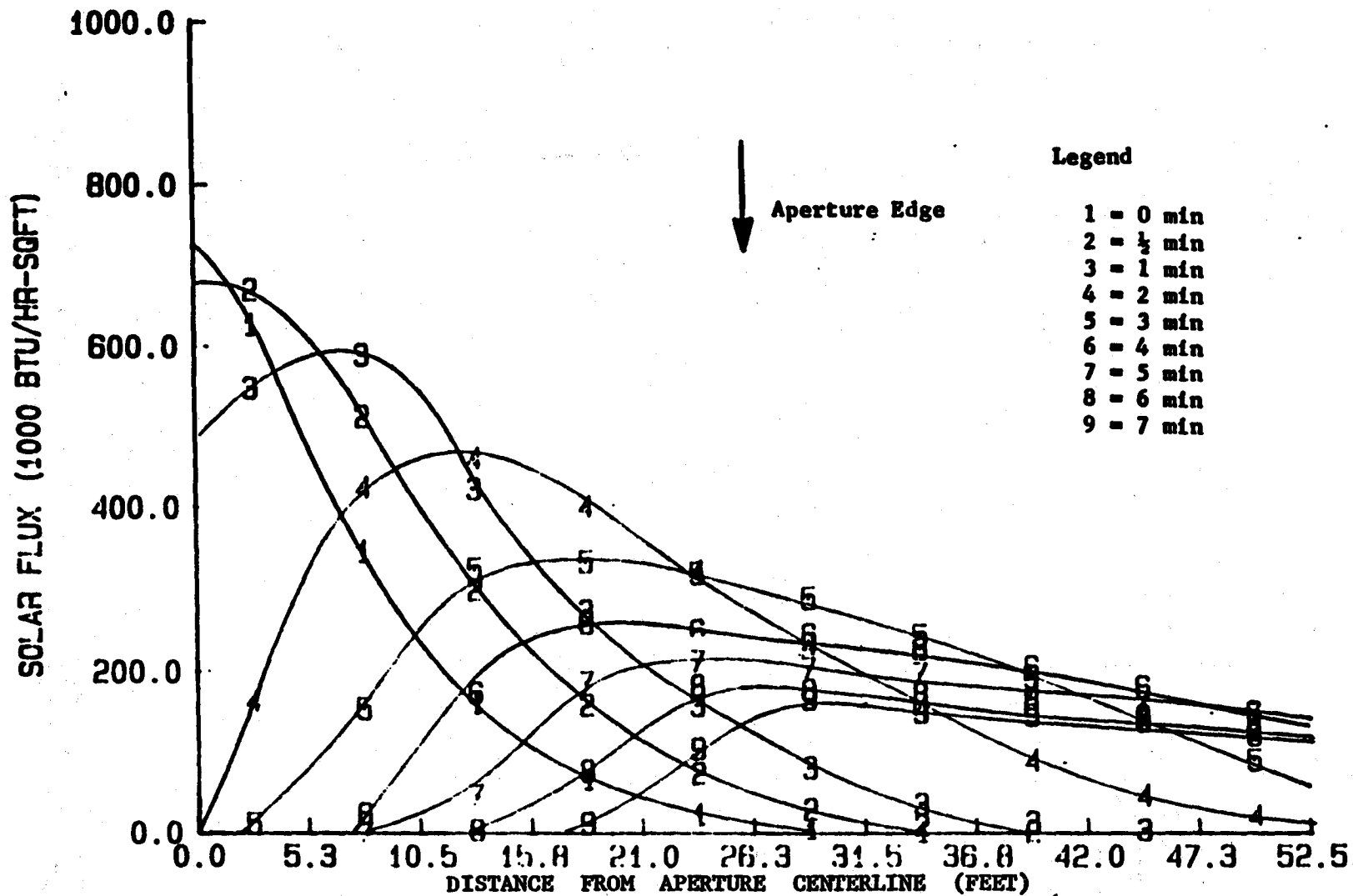


FIGURE 3.1-6 INTENSITY / DURATION CURVE FOR INDUCED FLUXES DURING HELIOSTAT TRANSITIONS BETWEEN STANDBY POINT AND TARGET



**FIGURE 3.1-7a FLUX TRANSIENTS FOLLOWING LOSS OF POWER TO COLLECTOR FIELD - NORTH APERTURE**

A-41

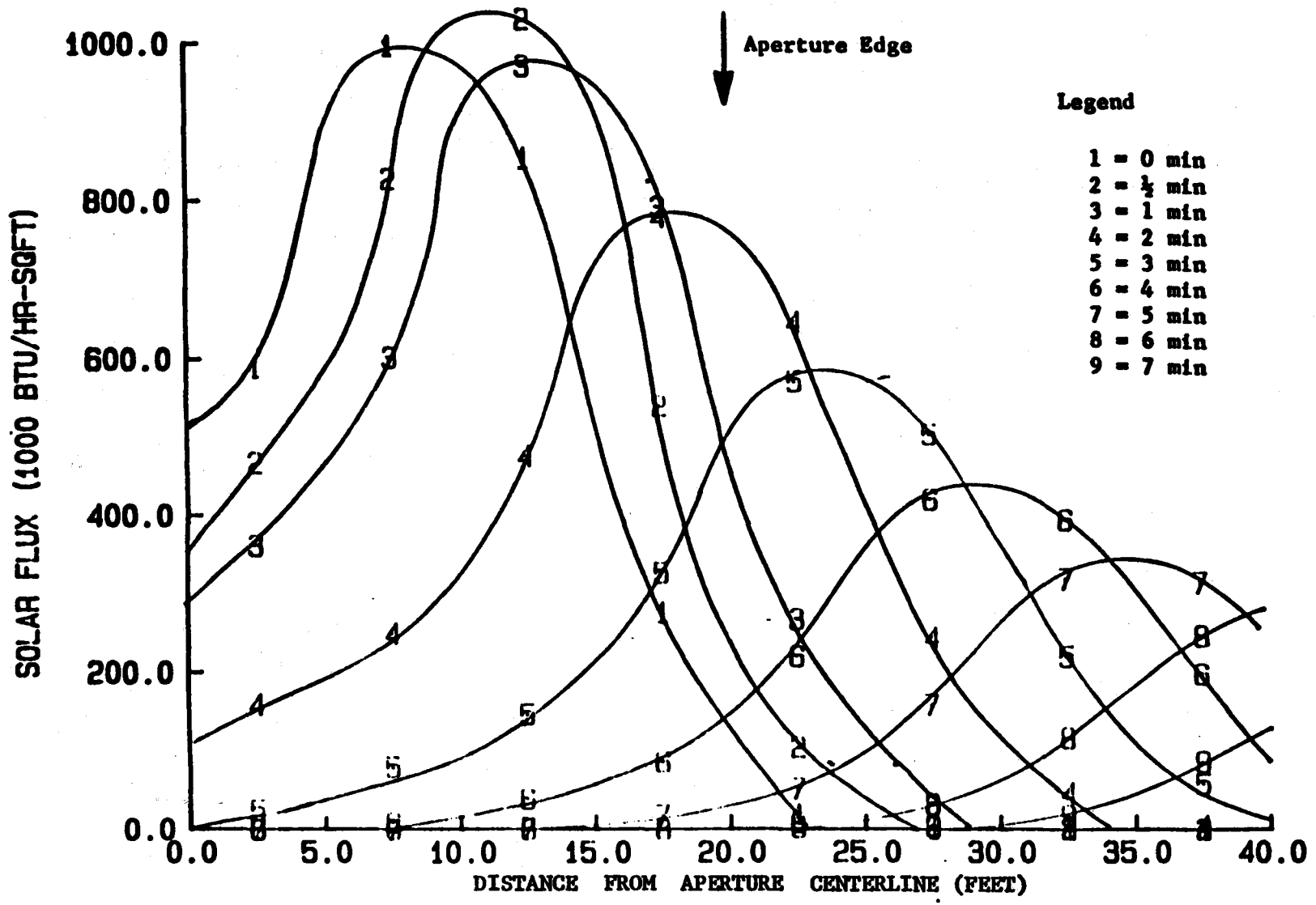


FIGURE 3.1-7b FLUX TRANSIENTS FOLLOWING LOSS OF POWER TO COLLECTOR FIELD - EAST APERTURE

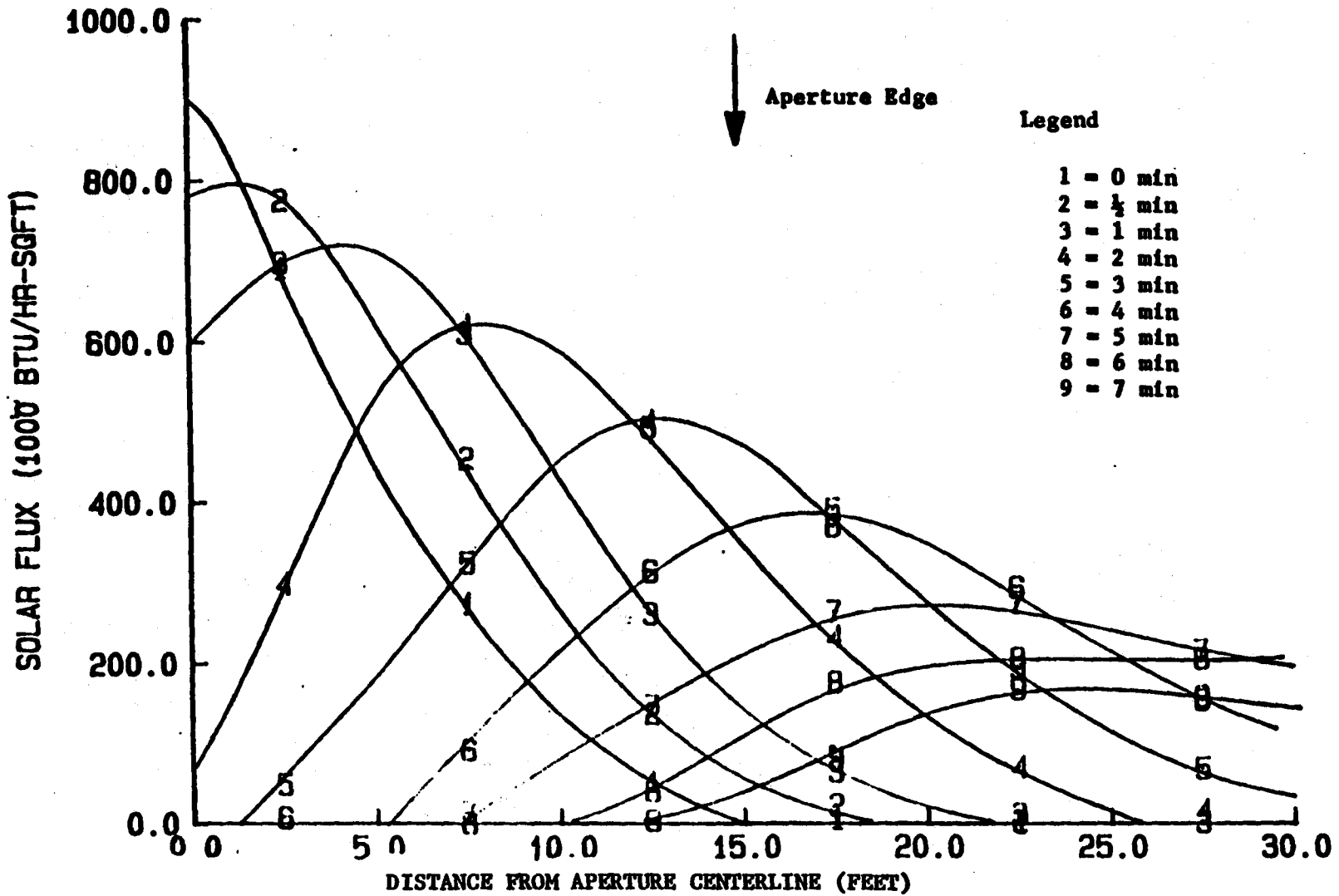


FIGURE 3.1-7c FLUX TRANSIENTS FOLLOWING LOSS OF POWER TO COLLECTOR FIELD - SOUTH APERTURE

### 3.3 Molten Salt Compatibility Requirements

3.3.1 Drainability - The receiver subsystem, including heat absorbing panels, headers, interconnecting piping, surge- and collection tanks, the riser and the downcomer shall be completely drainable to the cold or hot storage tanks.

- a. The drain paths shall be carefully laid out with due consideration to the time required for the boundary layer flow phase of the draining process. Drain lines shall have a minimum slope of 1 cm/m.
- b. All valves shall be drainable valves.
- c. The drain paths shall be insulated, and provided with trace heating that is not adversely affected by a subsystem or station electrical power failure.
- d. All valves shall be equipped with manual override capability, so that they can be opened in case of electrical power or control system failure.
- e. Provisions shall be made for the detection and/or elimination of accumulation of frozen salt due to valve leakage downstream of the drain valves, so that the drain path may be kept free throughout the operation of the RS.

### 3.3.2 Freeze and Thaw Considerations

- a. The RS shall be designed to handle salt in the liquid phase only.
- b. The design of the RS shall be such as to prevent incipient or bulk freezing of the salt in any and all parts of the subsystem.
- c. Local thawing shall not be relied on as an expedient means of correcting a freeze-up situation. If thawing becomes necessary, careful consideration shall be given to the fact that the melting of the salt mixture results in a significant increase in salt specific volume, thus creating a potential for failure of closed containers.

3.3.3 Heat Tracing - Heat tracing shall be provided as required to prevent freezing of salt within fluid transport equipment during fill, drain, and standby operations, consistent with the requirements of Paragraphs 3.1 and 3.3.

### 3.3.4 Salt Chemistry - Control of Degradation

- a. The blanketing atmosphere above high-temperature molten salt shall be air, free of carbon dioxide and water vapor.
- b. Continuous purging of molten salt containers with gases other than air is not acceptable.



- c. Provisions shall be made in the design of the RS for periodic sampling of molten salt for chemical analysis.

### 3.4 Subcomponent Requirements

#### 3.4.1 Fluid Transport Equipment

The fluid transport equipment may consist of the following components:

Heat Absorption Panels, Screen Tubes, Headers, and Connecting Piping  
Surge/Buffer Tank,  
Collection Tank and Recirculation Pipe  
Riser, and  
Downcomer

The design temperatures, pressures, and materials of fabrication for each of these components are listed in Table 3.4-1. The detailed requirements for the design of these components are identified below.

##### 3.4.1.1 Heat Absorption Panels, Headers, and Connecting Piping

- a. Configuration - The heat absorption panels shall be arranged in 4 parallel circuits or control zones, each consisting of multiple vertical passes. Each pass will consist of multiple tubes assembled into a membrane wall panel as shown on Figure 3.4-1.

At each end of the membrane wall the tubes will be welded into a header. Panels shall be arranged in a four cavity configuration consisting of four double "wing" walls and a central "box" core of panels heated from one side only. The panels are hung independently from each other by supporting the top headers from the upper structure leaving them free to expand longitudinally downward. Each panel butts against the adjacent panel to provide a relatively light tight enclosure.

Provisions shall be made to drain and vent all panels and interconnecting piping. Drain lines will conduct the flow into the collection tank.

- b. Thermal Hydraulic Design

Parallel panel flow paths shall be designed to maintain metal temperature gradients within structurally acceptable limits and salt outlet temperature within the specified range.

- c. Structural Design

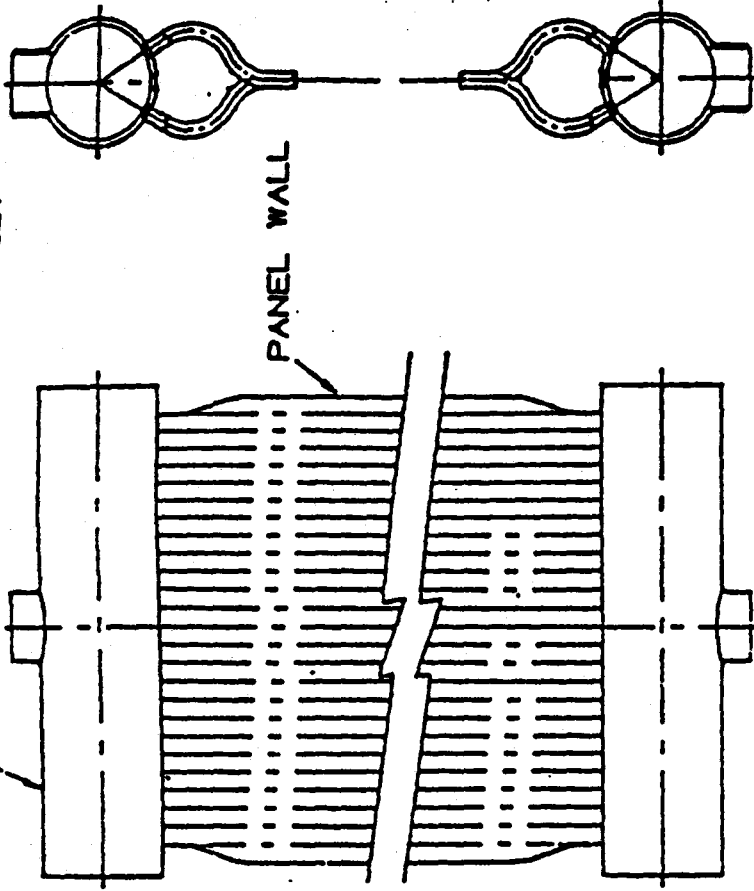
Pressure Boundary - The panels (including interconnecting piping) shall be designed and fabricated to Section VIII Division 1 of the ASME Pressure Vessel code. Supplemental requirements for cyclic-elevated temperature modes will be applied as necessary.

**TABLE 3.4-1 DESIGN TEMPERATURES, PRESSURES, AND MATERIALS**

	<u>TEMPERATURE</u> °C (F)	<u>PRESSURE</u> PSI	<u>MATERIAL</u>
Heat Absorbtion Panels	649 (1200)	400	Alloy 800 H
Screen Tubes	649 (1200)	400	Alloy 800 H
Panel Headers & Connecting Piping	593 (1100)	400	304 SS
Surge/Buffer Tank	438 ( 800)	500	Carbon Steel
Collection Tank	593 (1100)	80	304 SS
Riser (From Surge/Buffer Tank)	316 (600)	500	Carbon Steel
Downcomer (To Collection Tank)	593 (1100)	80	304 SS

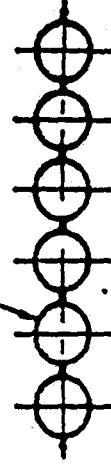
HEADER 12 3/4" O.D.  
PIPE (2 RECD PER PANEL)

PANEL WALL

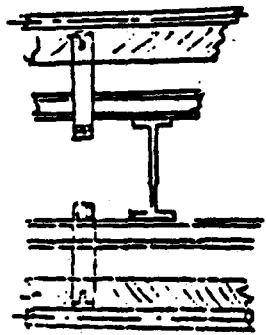


HEAT ABSORPTION PANEL

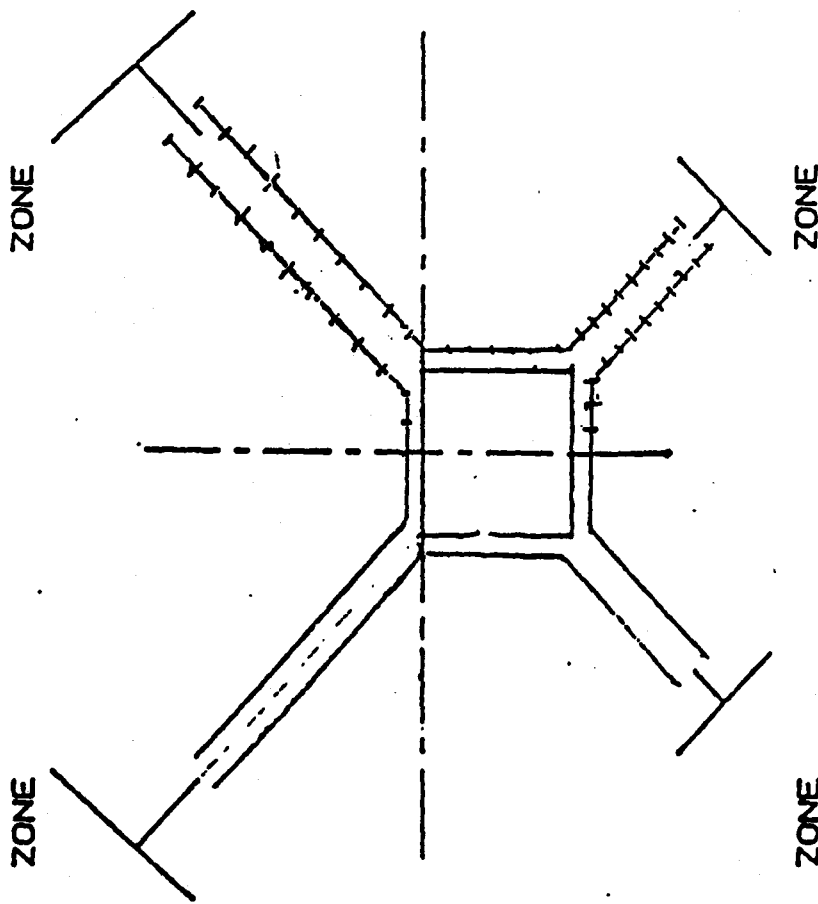
2" DIA TUBES



MEMBRANE WALL



PANEL SUPPORT BEAM



PANEL LAYOUT

FIGURE 3.4-1 PANEL WALL AND CAVITY ARRANGEMENT

Panel/Structural - The heat absorption panels and supports shall be designed to sustain internal pressure, deadweight, wind loading, and applicable seismic loading conditions. Lateral supports will be applied as necessary to restrict lateral deflection of the panels.

Interconnecting Piping - The design of the interconnecting piping shall allow for differential expansion loads (mechanical and thermal). The stress limits will be in accordance with the ASME, BPV Code, Section VIII, Division 1.

Corrosion Allowance - 10 mils on all pressure boundary parts.

#### 3.4.1.2 Surge/Buffer and Collection Tanks

Code Requirements - The collection and surge/buffer tanks shall be designed to meet Section VIII Division 1 of the ASME Pressure Vessel Code.

Capacity - Surge/Buffer Tank - The capacity of the surge/buffer tank shall be consistent with the requirement to provide emergency cooling to the absorption panels in the event of loss of site electrical power, with heliostat defocusing provided by the movement of the sun only.

Capacity - Collection Tank - The collection tank capacity shall provide (in conjunction with the surge/buffer tank) sufficient thermal storage to sustain salt circulation in the panels during hot standby, for periods not exceeding 8.0 hours. The maximum storage temperature shall be 427°C (800°F).

Supplemental Source of Heat - A supplemental source of heat of capacity TBD shall be provided to extend hot standby capability to TBD hours.

Thermal Insulation - Both tanks shall be insulated with 8 inches of calcium silicate block insulation with aluminum lagging.

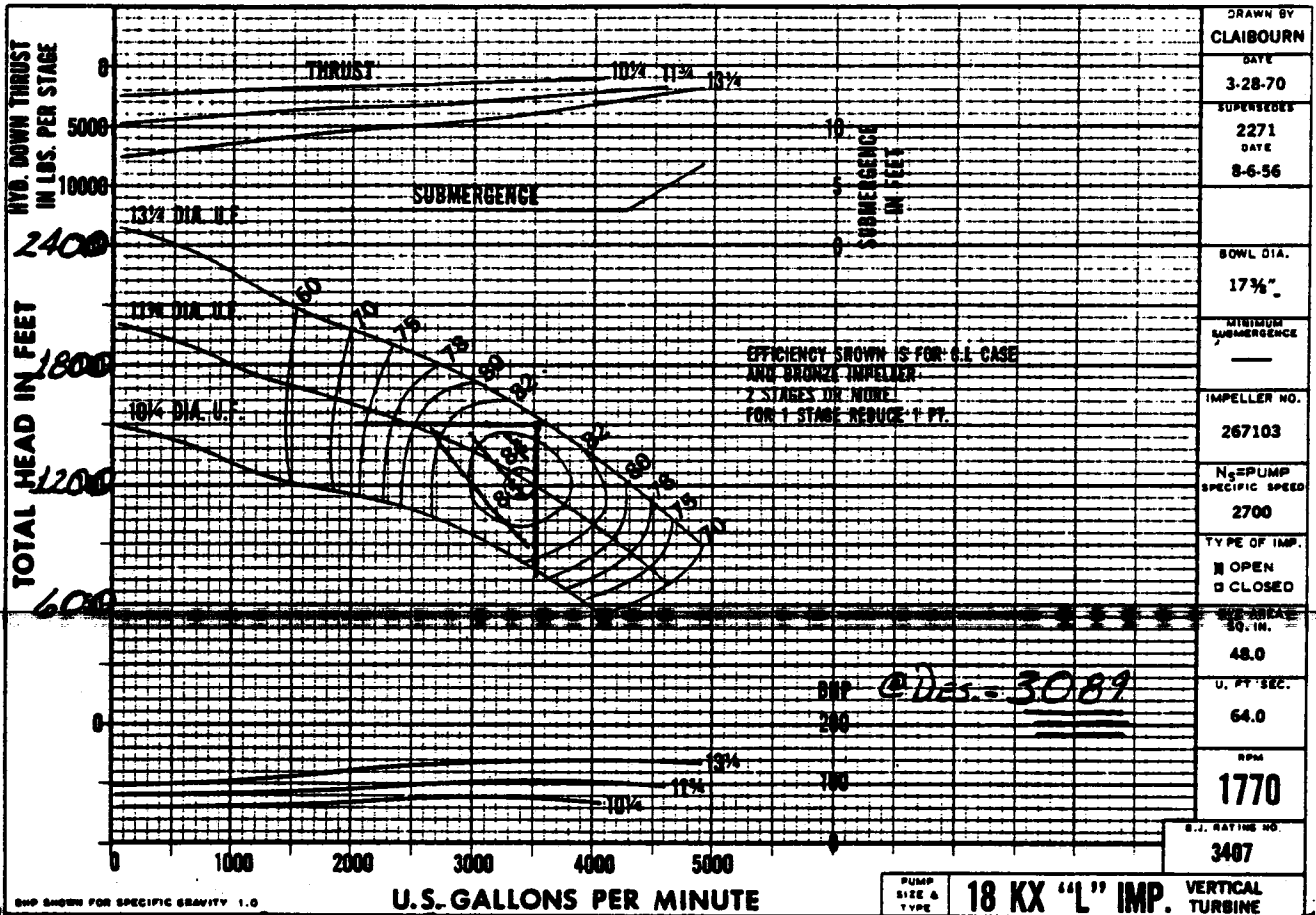
#### 3.4.1.3 Riser and Downcomer Piping

The riser and downcomer piping will be designed to provide a maximum of 125% of design flow to and from the receiver in the top of the tower. Both riser and downcomer shall be routed with multiple expansion loops as required to compensate for thermal expansion. Supports for the piping will be designed to sustain deadweight and seismic loading conditions. The piping will be designed to conform to the rules of ANSI B31.1, Power Piping.

An energy dissipation device in the form of a collection tank level control valve will be provided. The location of this device shall be at the base of the tower.

#### 3.4.2 Auxiliaries - Molten salt receiver subsystem auxiliaries include cold salt booster pumps, off line piping, valves, heat tracing, insulation, and auxiliary electric power equipment. Requirements for these auxiliaries are described in the following subsections.

- 3.4.2.1 Cold Salt Booster Pumps - The cold salt booster pumps shall be located inside the tower on a platform at an elevation of 10.7 meters (35 feet) above the tower base. Two half capacity pumps shall be provided. The pumps shall take suction from the discharge piping of the salt circulating pumps and deliver cold salt to the receiver. Each pump shall be provided with a total developed head sized to overcome the piping and static losses plus a 15% design margin. Pump performance shall be in accordance with Figure 3.4-2. The pumps shall be capable of draining by gravity a drainage sump.
- 3.4.2.2 Off Line Piping - Receiver subsystem piping shall be designed to meet the code requirements of ANSI B31.1. Hot salt piping shall be Type 304 stainless steel. Cold salt piping shall be ASTM A106 Gr B carbon steel. Pipe wall thickness shall be selected based on design pressure and temperature conditions. Pipe size shall be selected based on providing reasonable fluid velocity and pressure loss.
- 3.4.2.3 Valves - Valves shall meet the code requirements of ANSI B16.34. Hot salt valves shall be 316SS. Cold salt valves shall be carbon steel. Valves 50mm (2 inches) and smaller shall be socket welded; those larger than 50mm (2 inches) shall be butt welded.
- 3.4.2.4 Heat Tracing - Heat tracing, consisting of trace heaters and controls shall be provided for piping and equipment to meet the following requirements.
- a. Trace heaters shall be electrically powered with 480 volt supply.
  - b. Trace heaters shall be mineral insulated (M.I.), Inconel sheathed type for surfaces of high (572C, 1061°F) operating temperatures.
  - c. Trace heaters shall be flexible, self-limiting, parallel circuit type with a monitor conductor for surfaces of low (65C, 149°F maximum) operating temperature.
  - d. Controls shall be provided to disconnect electrical power to trace heaters when maximum operating temperatures are exceeded.
  - e. Monitoring shall be provided for heat trace temperatures during startup, shutdown and transient operation.
  - f. Controls shall be provided to maintain a minimum molten salt temperature of 277C (530°F) during process non-operating condition.
  - g. Controls shall be provided to de-energize heating cables at approximately 288C (550°F) during process operating condition.



MOLTEN SALT PUMPS - DUTY: 3520 GPM @ 1500', 1.9 S.G.  
12 STG.

FIGURE 3.4-2 PUMP PERFORMANCE

3.4.2.5 Pipe Insulation - Pipe insulation shall be calcium silicate with aluminum jacketing. The thickness of hot salt piping insulation shall be 150mm (6 in.) and cold salt piping insulation shall be 140mm (5.5 in.).

3.4.2.6 Auxiliary Electric Power Equipment - The auxiliary electric power system shall provide for the distribution of electric power to RS components. The system shall be designed to meet the power requirements of all RS loads during start-up, shutdown, and the other operating modes of the solar plant. The electrical equipment in this system shall be selected to meet the following requirements.

- a. Motor starting
- b. Short circuit duty
- c. Load current duty
- d. Voltage regulation
- e. Future load additions
- f. Alternate power supply sources

The voltage levels selected shall be 4160 volt switchgear for motors and loads of 261 kW (350 hp) and up; 480 volt secondary unit substations for motors and loads above 75 kW (100 hp) and below 261 kW (350 hp); 480 volt motor control centers for motor-operated valves, motors and loads of 75 kW (100 hp) and less.

3.4.3 Receiver Support Tower - The receiver support tower shall be designed to support the solar receiver, withstanding gravitational, wind, and seismic loads as designated in 3.2.8. Also, the tower shall be designed to provide support for the molten salt piping and electrical cables in the receiver subsystem.

The tower shall be constructed of reinforced concrete. It shall be 155 meters (508'6") tall and have a tapered, circular shell with a larger base than top. The tower foundation shall be a reinforced concrete mat, supported if necessary by piles. The foundation shall be designed to meet the following requirements.

- a. No uplift will be permitted on any portion of the foundation under lateral loadings.
- b. The maximum settlement over the life of the solar plant shall not exceed 0.025m (1 inch) total or 0.019m (0.75 inches) differential between points across the diameter of the foundation.
- c. The bearing stress on the soil shall not be permitted to exceed the allowable bearing stress; otherwise, piles shall be used.

Tower accessories shall include an elevator, caged ladder, equipment room, pump platform, lighting, communication equipment, and lightning protection. The elevator and ladder shall provide access to both the equipment room and the receiver.

#### **3.4.4 Controls and Instrumentation**

##### **3.4.4.1 Functional Requirements**

- a. Control salt outlet temperatures within limits specified under 3.1.4.1 and 3.1.4.2 by controlling the salt flow rate to the heat absorption panels to match variations in solar input.
- b. Monitor peak metal temperatures -determined by a combination of direct (radiometer) and indirect (calculation from other available temperature data) measurements- and provide warning and alarm signals to the Operational Control System.
- c. Protect the receiver from overtemperature by the incorporation of an override feature that automatically increases the salt flow rates to values above those required by heat balance if safe local temperatures are exceeded.
- d. Provide time-integrated absorbed energy and temperature data to the Operational Control System as inputs to salt management decisions.
- e. Provide thermal cycle count information to the Operational Control System as inputs to life management decisions (including shutdowns during intermittent cloud passages).
- f. Monitor static or quasi-static salt temperatures during hot standby, and provide temperature warnings and alarms to the operator and Operational Control System.
- g. Provide remote and local manual override capability for all control functions.
- h. Detect failure modes (e.g. loss of salt flow, loss of pump pressure, salt overtemperature, etc.), provide warning and alarm signals to Operational Control, and initiate safe shutdown in case of failures.

##### **3.4.4.2 System Description - The control subsystem shall be of the digital type comprising the following major components:**

- a. Flow sensors
- b. Temperature sensors



- c. Flux sensors (sun sensors in the heliostat field and/or radiometers with view of the absorbing panels)
- d. Pressure sensors and differential pressure sensors
- e. Analog-to-digital converters (including thermocouple reference junctions)
- f. Multiplexers
- g. De-multiplexers
- h. Control equipment necessary for the implementation of the control algorithm
- i. CRT's and other data display equipment (located in the central control room)
- j. Data bus.
- k. Terminal boards, linking the sensors to the A/D converters, and the De-multiplexers to I/P converters for control of the valves, and to contactors or relays for control of electrical equipment.

#### 3.4.4.3 Physical Requirements

- a. Flow sensors shall be wedge type or equivalent to facilitate draining.
- b. Acceptable types of thermocouples:
  1. Mineral-insulated metallic-sheathed thermocouple probe assemblies to measure molten salt temperatures at receiver inlet and outlet and within headers. The probes shall meet the following requirements:
    - Sensor: Type K (Chromel Alumel), ungrounded;
    - Sheath Material & Size: Inconel 702 (or equivalent), 0.125" OD x 0.017 to 0.023" wall (approximately).
    - Termination Style: Screw Cover Head
    - Immersion Length: As required to penetrate through 1/2 pipe diameter
    - Total Length: As required to assure that the screw cover head is exposed to ambient in order to maintain its temperature below 371C (700°F).
    - Mounting Method: replaceable weld joint
    - Response: Time constant not exceeding 1 second.
  2. Ungrounded, sheathed thermocouples, with tabs welded to tubes, pipes, headers, or structures, for long-life operational duty.

3. Grounded thermocouples, directly welded to tubes, pipes, headers or structures, for temporary duty (e.g. engineering data), used in conjunction with:
    - Data-loggers, or other data acquisition equipment that is not susceptible to grounding-noise.
    - In conjunction with MV-to-I converters, when the signal is used by a control computer.
  4. Connecting wire shall be sheathed 16 AWG "thermocouple-grade" (premium) chromel-alumel wire.
- c. Redundancy shall be included as appropriate to protect from catastrophic failures
  - e. Thermocouple locations shall be consistent with structural and functional requirements.
  - f. The attachment of thermocouple junctions to tubes, pipes, and headers shall be by welding, except when thermowells are used.
  - g. Dual data buses with automatic fail over shall be used.
  - h. Control equipment shall incorporate dual microprocessors and memories with automatic fail-over.
  - i. Control equipment shall be provided with uninterruptable power.
  - j. All control valves shall be pneumatically connected for fail safe operation.
  - k. Electronic circuitry shall be protected from adverse environmental conditions (overheating, dust, etc).

#### 3.4.4.4 Interface Requirements

- a. Data processing, conversion to engineering units and recording shall be the function of the Operational Control System
- b. Emergency shutdown (scram) signals generated by the RS control subsystem shall be processed and executed by the Heliostat Array Controller (HAC)
- c. The Operational Control System shall have the capability to override (by pre-programmed or manual control) the RS control subsystem
- d. The controller-to-process interfaces within the RS are represented by the terminal boards described under 3.4.4.2 k.

#### 3.4.5 Structural Steel

### 3.4.5.1 Codes, Material, Loads

- a. Codes - All structural steel and connections shall be designed, detailed, fabricated, and erected according to the following codes and standards:

AISC	- (American Institute of Steel Construction)
ANSI A58.1	- (American National Standards Institute)
AWS	- (American Welding Society)
ASTM	- (American Society for Testing and Materials)
OSHA	- (Occupational Safety and Health Act)
UBC	- (Uniform Building Code)

#### Local Building Codes

- b. Materials

1. Structural steel shall be fabricated from ASTM A36 or A572 GR-50 steel. Structural steel includes columns, beams, base plates, diagonal bracing, gusset plates, door frames, kickplate, ladders, safety cages, etc.
2. Anchor bolts shall be made from A307 steel.
3. Connection bolts shall be A325, type 1, high-strength steel.
4. Grating for platforms, walkways, and stairs shall be made of rectangular, welded steel with 1 1/4" x 3/16" bearing bars spaced on 1 3/16" centers and cross bars on 4" centers. Abrasive nosing shall be provided on the head of all stair treads.
  - a. Grating shall be made from ASTM A569 steel and painted according to Section 3.4.5.5.
  - b. Clips for fastening grating sections to the support steel shall be attached using 1/4" self-tapping lag screws.
5. Checkered plate shall be 5/16" thick A283D steel and painted according to Section 3.4.5.5.
  - a. Checkered plates shall be attached to the support steel using 3/8" x 2" long slotted, flathead counter-sunk machine screws with heavy nut. Screws shall be made from A307 steel.
6. Handrails shall be made from 1 1/2" diameter A501 schedule 40 pipe and painted according to Section 3.4.5.5.

- c. Loads - The steel shall be designed to support and transmit to the tower all loads which it is subjected to, including:
1. Dead loads, which include the weights of all components permanently attached to the structure such as siding, roofing, absorption panels, pumps, piping, steel, platforms, etc.
  2. Wind Loads - Per Section 3.2.5.
  3. Earthquake Loads - Per Section 3.2.8, except that all members in the braced frame shall be designed for 1.25 times the earthquake load. Connections shall be designed for the earthquake load without increasing the allowable stresses by one-third.
  4. Snow and Ice - Per Section 3.2.7.
  5. Operating Loads - Includes pressure, transient pressure, friction, and live loads. The live loads for floors (access platforms and receiver floor) shall be 100 lbs./sq. ft. and for the roof, 25 lbs./sq. ft. (or snow and ice load, whichever is worse). Stairs shall be designed for 125 lbs./sq. ft. or a concentrated load of 100 lbs. at the center of the stairs, whichever is greater. Maximum deflection due to live load shall be 1/360 of the member span.
  6. The steel shall also be designed for the heat flux requirements of Section 3.2.9.

#### 3.4.5.2 Platforms and Walkways

- a. Access platforms shall be provided for all equipment requiring regular maintenance and inspection. Access platforms shall be accessible from walkways, temporary or permanent ladders, stairs, or scaffolding.
  1. Access platforms shall have a minimum of 3'-0" clear space around those parts of equipment requiring access.
  2. Walkways shall be a minimum 3'-0 in width.
  3. A minimum headroom of 7'-0 in required above all platforms and walkways.
- b. The receiver floor shall be equipped with access hatches for removal and installation of receiver components.

**3.4.5.3 Cavity Enclosure** - The cavity enclosure consists of a roof, floor and sides located around the absorption panels and aperture door frame. The cavity enclosure shall conform to the following requirements:

- a. The cavity enclosures shall withstand dead, live, wind, ice, snow, and seismic loads as defined elsewhere in this specification.
- b. Heat Flux Spillage (See Section 3.2.9).
- c. Cyclic loadings defined in Par. 3.1.6 and 3.1.7.
- d. Cavity design temperature to be used shall be 700°F.
- e. Cavity enclosure shall be insulated to minimize heat loss and protect the support steel from excessive heat.
- f. The roof shall have sufficient drainage.
- g. Access openings shall be installed in the roof and floor.
- h. Consideration shall be given in the design of the floor and roof for absorption panel replacement.
- i. The thermal coating requirements are identified in Para. 3.1.10.

**3.4.5.4 Connections**

- a. Structural steel shall be connected using 7/8" diameter ASTM A325 high-strength bearing type bolts with threads excluded from the shear plane.
- b. All connections shall be designed to resist all shears, moments, and axial forces resulting from the loads in Section 3.4.2.1-C. The ratio of actual stress to allowable stress for connections shall be limited to 1.00 for all load combinations.
- c. Anchor bolts shall be designed for a minimum uplift of 81 kips with no increase in the allowable stresses permitted.

**3.4.5.5 Painting**

- a. Structural steel shall be cleaned to Structural Steel Painting Council SP6 specifications before it is painted.
- b. All structural steel grating, checkered plate, and handrails should have one shop coat of heat-resistant primer (TBD) applied before shipment to the field.
- c. All steel not covered with insulation shall be painted with (TBD) after erection.
- d. All paints and primers shall be applied according to manufacturer's specifications.

**3.4.6 Cavity Aperture and Door**

3.4.6.1 Aperture - The receiver apertures shall be designed to meet the thermal requirements of 3.1.1.5d, 3.1.1.6c, and 3.2.9. During normal operation, the aperture frame shall be designed to protect hardware on the cavity from spillage effects. An arrangement providing adequate protection with minimal maintenance requirements shall be designed for this purpose.

A system of sacrificial shielding shall be included with the capability of protecting the molten salt system pressure boundary and the major structural steel components from damage resulting from the conditions of 3.2.9d.

3.4.6.2 Door - The cavity doors will be designed to meet the following requirements:

- a. Withstand maximum seismic and wind loads.
- b. Protect heat absorption panels from high wind loads.
- c. Restrict heat loss from the cavity during nightly shutdowns.
- d. The main door structure and the thermal insulation shall be totally separate in order to prevent warping.
- e. The door shall be as light as possible.
- f. In order to restrict heat loss from the cavity due to infiltration, the design of the doors will incorporate a seal arrangement that meets the following:
  1. The sealing surfaces should be protected from the solar radiation and thermally outside the cavities.
  2. A high temperature elastomer seal such as silicone is acceptable.
  3. Redundant seals shall be used.
  4. The seal surfaces should be adjustable relative to the door and receiver structure to assure good mating surface and allow adjustments to account for tolerances.
  5. There should be no rubbing on the seal during door opening or closing.
  6. After closing, a distributed force is required on the seal to be effective.
- g. Locate tracks to avoid direct impingement of solar flux.

4.0 INTERFACE DEFINITIONS AND REQUIREMENTS

4.1 Collector Subsystem - The Collector Subsystem shall reflect solar radiation into the receiver in a manner which satisfies receiver heat flux requirements. The final definition of the Collector Subsystem interface shall be based on an iterative process between the Receiver Subsystem and the Collector Subsystem contractors, involving the following elements:

4.1.1 Total Reflected Power - 355 Mwt at the design point, with 950 w/m<sup>2</sup> insolation.

4.1.2 Geometrical Interface - The heliostat field shall be of the surrounding type, with approximate dimensions as shown on Figure 4.1-1. The distribution of incident power on the four cavities, expressed in percent of thermal rating, shall be approximately as follows:

	<u>Design Point</u>	<u>Peak Points</u>
North Cavity:	38.5	44.3 (Day 355 Solar Noon)
South Cavity	13.3	13.3 (Day 172 Solar Noon)
East Cavity	24.1	25.9 (Day 172 14:00 Hours)
West Cavity	24.1	25.9 (Day 172 10:00 Hours)
	<u>100.0</u>	

4.1.3 Functional Interface

a. Aim Point Strategy - See Addendum A for exact tables of Aim Point Strategies

North - Table A.1  
East - Table A.2  
South - Table A.3

b. Standby Point Coordinates - Standby point locations shall be specified at safe distances from the receiver to permit access of personnel to the tower top with the heliostats at standby. Possible drifting of the standby points as a result of loss of power to the heliostat field (refer to 3.2.9 d) shall not result in overheating of the external structure of the RS.

c. De-focusing (normal field power) - The collector subsystem shall have the capability to de-focus all heliostats from the receiver within 30 seconds following a scram command initiated by the RS, Operational Control System, or by manual override.

d. De-focusing following loss of field power - The collector subsystem controls shall be designed to allow for flexibility with respect to receiver safety. This design shall allow execution of any one of several predefined safety strategies--these strategies should be selectable as options at collector start-up, and the capability should exist for the operator to select a new option anytime while the system is running, except while a particular option is being exercised.

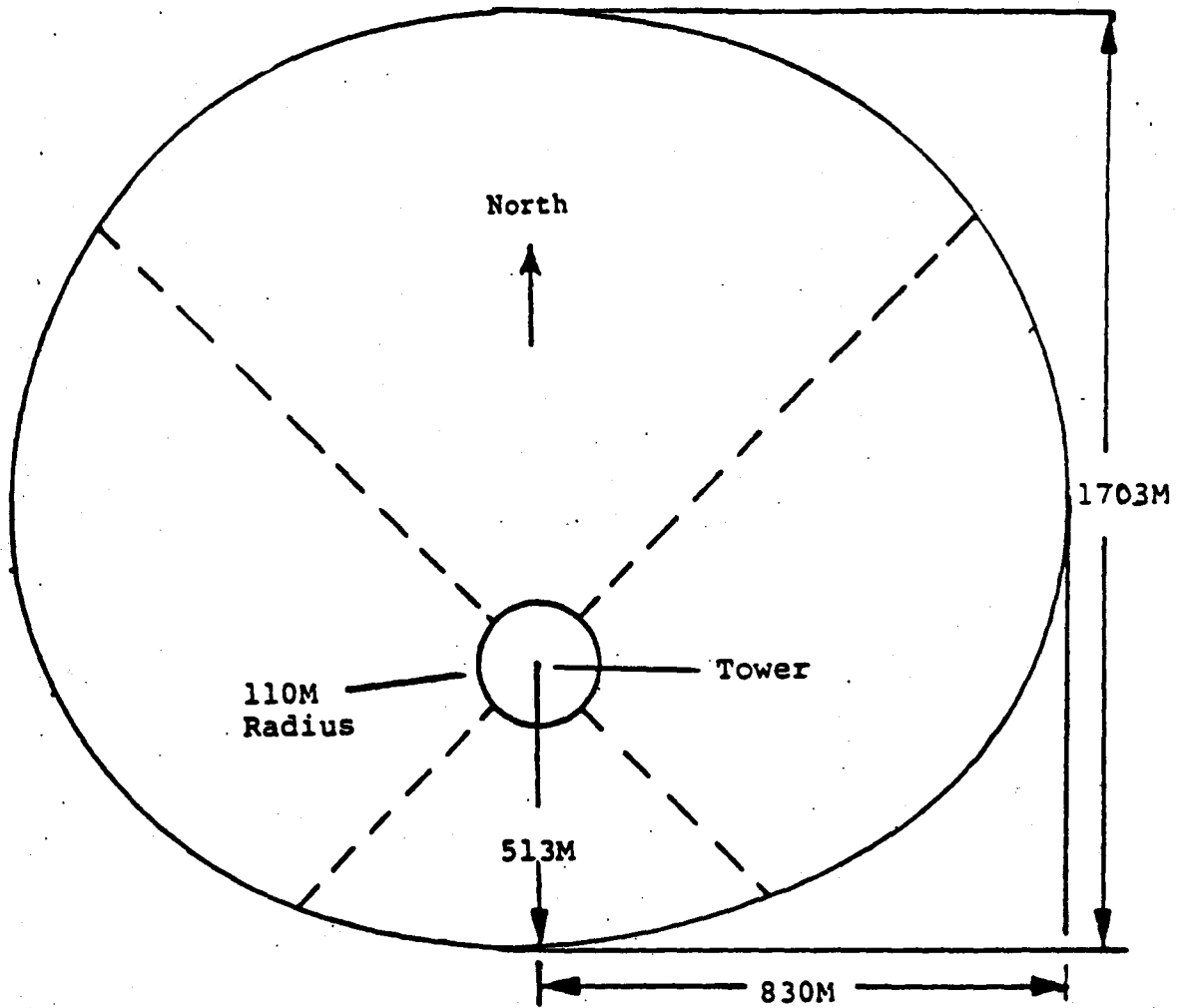


FIGURE 4.1-1 HELIOSTAT FIELD LAYOUT



In the situation where the full field loses power all field controllers (HFC) and heliostat controllers (HC) lose memory and the collector subsystem controller shall automatically reinitialize both the HFCs and HCs when power is restored and implement the preselected scram strategy.

The collector subsystem shall have as a minimum the capability to execute any of the following scram strategies:

OPTION 1: Within 60 seconds of power restoration, all heliostat must be automatically removed from the receiver.

OPTION 2: Within 120 seconds of power restoration, all heliostat must be automatically removed from the receiver in a preset incremental approach. This option combines HC initialization in groups of 256 HCs followed by a de-focus command. This combination would be repeated 32 times for up to 8192 heliostats. The time allotted includes 7 seconds for HFC initialization and command retries in addition to central processing and disk overhead.

OPTION 3: This option would allow for the optimum combination of initialization and de-focus commands as defined in Option 2. By stacking the initialization commands together (back-to-back in groups of 256) and then issuing the de-focus command, the scram time will approach the 60 seconds given in Option 1. This optimum strategy should be defined by a joint effort between the collector and receiver contractors.

- e. Power Ramp-up - The collector subsystem shall be capable of re-focusing the heliostats from standby to aim in a pre-programmed and continuous fashion in 6 minutes. This is not recommended following a power failure.
- f. Warmup Heliostats - The capability shall be provided to preheat the receiver absorber panels with reflected solar energy without overheating, by the use of pre-selected groups of heliostats. Warmup must be possible for any insolation condition.

4.2 Energy Storage Subsystem - The interfaces between the receiver subsystem and the energy storage subsystem consist of hot and cold salt flows through piping at the common subsystem boundary. Warmup must be possible for any insolation condition.

#### 4.3 Master Control Subsystem

- The receiver control is resident within the MCS and interfaces with the receiver through high and low level signal lines. These consist of

- a. Thermocouple measurements,
- b. Flow transmitters,
- c. Level transmitters and switches,
- d. Pressure transmitters and switches,
- e. Analogue control signal driving valve actuation.

All digital to analogue, analogue to digital conversion and signal conditioning will be performed within the MCS. Similarly, the valve actuations, transmitters and switches are part of the receiver subsystem and not the MCS.

#### 4.4 Electric Power Supply Subsystem - The interfaces between the receiver subsystem and the electric power generation subsystem consist of electrical wiring at the subsystem boundary, including:

- a. Auxiliary Electric Power System
  - Normal AC power and alternate or backup supply
  - Uninterruptible power supply
- b. Grounding
- c. Communications

The power supply will be 4,160 Volts and 6,500 KVA (maximum subsystem demand). The interface point for the incoming line will be 0.305m (1 ft) outside the tower at grade elevation.

5.0 FABRICATION REQUIREMENTS

5.1 Fabrication Quality Assurance - Quality Assurance for fabrication of the receiver pressure boundary components shall be based on the requirements of the ASME Code. Quality Assurance for fabrication of the receiver structural steel shall be based on the requirements of AISC. Quality Assurance for concrete work and erection shall be based on the requirements of ACI, UBC and local building codes.

5.2 Fabrication Process - The pressure boundary components of the receiver subsystem shall be shop welded, assembled, pressure tested and ASME Code stamped. Final subsystem pressure testing shall be performed as a field procedure. Pressure testing must precede Code Stamping.

Heat Treatment - The need for heat treating after forming operations shall be evaluated and if necessary, temperature, hold times, and heat up and cool down rates in heat treatment procedures shall be specified.

Surface Finish - The finish of surfaces subject to non-destructive examination shall be in accordance with Code requirements. Unless otherwise determined by the Supplier, all other surfaces shall be acceptable in the "as-formed" condition. Pressure boundaries shall not violate minimum wall thickness requirements.

Welding - Welding materials used for fabricating shall comply with the requirements of the ASME Code Section VIII, Section I, Section IX, and applicable welding procedures.

5.3 Cleanliness - Care shall be taken to prevent unnecessary contamination of surfaces by dirt producing operations such as machining and grinding. Surfaces to be welded shall be clean and free of scale, rust, oil, grease, and other foreign material. Equipment shall be suitable for installation at the user's site without additional cleaning.

5.4 Painting - Where appropriate, components shall be painted before shipping.

5.5 Spare Parts/Tooling - A list of spare parts for operation shall be developed. The list of spare parts to be stocked at the site shall include those parts and tools likely to be damaged or expended during delivery and/or operation.

5.6 Shipping and Handling - Shipping rigs and/or containers shall be provided to secure and protect components during shipment to the user's site. Open nozzles shall be sealed with temporary plugs or caps. Procedures for off-loading and lifting components shall be defined in the Operation and Maintenance Manual.

6.0 MAINTENANCE

Provisions shall be made for dry layup, inspection, and panel repair for the components of the receiver subsystem. Chemical cleaning of the system is not considered necessary.

6.1 Dry Layup - During system shutdown when the receiver subsystem or any part of it is to be drained of salt, provisions shall be made to provide a pressurized air atmosphere free of carbon dioxide and moisture within the system.

6.2 Inspection - Provisions shall be made to make the cavity absorption surface accessible during plant shutdown for visual inspection of the external surface. These examinations will allow detection of any evidence of:

- Salt leakage.
- Deterioration of tube base metal or welds.
- Gross deformation of panels caused by thermal stress, wind, or seismic loadings.
- Deterioration of the special purpose paint.

Ready access to pumps, valves, and the drive mechanisms associated with the cavity doors shall be provided in order to facilitate routine inspection and maintenance of these components.

6.3 Absorption Panel Repair - In the event of a tube failure, two methods of repair shall be available:

- Local repair in place
- Panel replacement

The technique for local repair shall consist of either spot weld repair or replacement of the defective section of tube. Specialized weld preparation, welding, inspection, and repainting methods will be part of this procedure.

The technique for replacement of a single absorption panel will include methods for removing the defective panel from the cavity, lowering it to the ground, and erecting and re-installing a replacement panel. Equipment and access required to perform this repair technique (including a crane of sufficient capacity and access hatches into each cavity) shall be incorporated into the receiver subsystem design.

6.4 Spare Parts/Tooling - The spare parts to be stocked at the site shall include those parts and tools likely to be damaged or expended during delivery and/or operation.

7.0 SPECIAL REQUIREMENTS

7.1 Certification - Marking and certification of pressure vessels shall conform with code requirements.

7.2 Operation and Maintenance Manual - An operation and maintenance manual shall be provided. This manual shall include instructions for:

- a) Unloading and receipt inspection;
- b) Installation and post-installation inspection and checkout;
- c) Testing, startup, and operation;
- d) In-service inspection;
- e) Preventive maintenance and trouble shooting;
- f) Corrective maintenance and post-correction check-out;
- g) Limits and precautions to be taken during filling, testing, startup, shutdown, and layup operations.

7.3 Safety - The receiver subsystem shall be designed to minimize safety hazards to operating and service personnel, the public, and equipment. Electrical components shall be insulated and grounded. All components with elevated temperatures shall be insulated against contact with or exposure to personnel. Any moving elements shall be shielded to avoid entanglements, and safety override controls/interlocks shall be provided for servicing.

ADDENDUM A TO THE  
RECEIVER SUBSYSTEM AND REQUIREMENTS  
SPECIFICATION

HELIOSTAT AIMING STRATEGY

ADDENDUM A - Table A1: NORTH APERTURE

		HELIOSTAT COORDINATES	
ROW NO	AIM NO	X(I)	Y(I)
02	00	83.37,	3882.86
02	00	249.96,	3875.71
02	00	416.10,	3861.40
02	00	581.49,	3839.98
02	00	745.79,	3811.47
02	00	908.72,	3775.94
05	13	103.02,	3598.28
05	13	257.41,	3590.54
05	00	411.28,	3576.17
05	00	564.43,	3555.24
05	00	716.53,	3527.71
05	00	867.28,	3493.72
05	00	1016.46,	3453.27
05	00	1163.73,	3406.45
05	00	1308.91,	3353.34
05	00	1451.66,	3294.05
05	00	1591.71,	3228.73
05	00	1728.85,	3157.41
08	13	71.59,	3333.46
08	13	214.60,	3327.32
08	13	357.25,	3315.05
08	13	499.21,	3296.65
08	13	640.25,	3272.20
08	13	780.14,	3241.69
08	13	918.56,	3205.21
08	13	1055.30,	3162.82
08	00	1190.11,	3114.63
08	00	1322.72,	3060.66
08	00	1452.87,	3001.05
08	00	1580.36,	2935.92
08	00	1704.93,	2865.39
08	00	1826.36,	2789.57
08	00	1944.40,	2708.60
08	00	2058.90,	2622.61
08	00	2169.56,	2531.83
08	00	2276.25,	2436.35
11	08	88.45,	3088.64
11	08	220.93,	3082.02
11	08	353.05,	3069.68
11	08	484.48,	3051.70
11	08	615.02,	3028.08
11	08	744.45,	2998.88
11	08	872.50,	2964.17
11	08	998.94,	2923.98
11	00	1123.51,	2878.41
11	00	1246.05,	2827.52
11	00	1366.29,	2771.42
11	00	1483.97,	2710.24
11	00	1598.96,	2644.03
11	00	1710.97,	2572.97
11	00	1819.83,	2497.15
11	00	1925.37,	2416.74
11	00	2027.34,	2331.83
11	00	2125.56,	2242.66
14	09	61.42,	2860.79
14	09	184.18,	2855.51
14	09	306.59,	2844.98
14	09	428.44,	2829.20

14	09	549.47,	2808.20
14	09	669.51,	2782.02
14	09	788.31,	2750.72
14	09	905.66,	2714.34
14	09	1021.35,	2672.97
14	08	1135.16,	2626.67
14	08	1246.84,	2575.49
14	08	1356.25,	2519.62
14	08	1463.17,	2459.06
14	00	1567.37,	2394.00
14	00	1668.68,	2324.51
14	00	1766.94,	2250.73
14	00	1861.92,	2172.81
14	00	1953.49,	2090.89
17	09	75.88,	2650.07
17	09	227.39,	2641.37
17	09	378.18,	2624.05
17	09	527.68,	2598.10
17	09	675.52,	2563.65
17	09	821.09,	2520.80
17	09	964.00,	2469.69
17	09	1103.73,	2410.47
17	08	1239.85,	2343.38
17	08	1371.90,	2268.57
17	08	1499.46,	2186.36
17	08	1622.13,	2096.99
17	00	1739.45,	2000.73
17	00	1851.09,	1897.91
20	10	93.67,	2452.66
20	10	233.86,	2443.31
20	10	373.29,	2425.92
20	10	511.48,	2400.59
20	10	647.99,	2367.39
20	10	782.41,	2326.42
20	10	914.23,	2277.83
20	10	1043.10,	2221.79
20	09	1168.49,	2158.47
20	09	1290.11,	2088.07
20	09	1407.46,	2010.84
20	08	1520.22,	1926.98
20	08	1628.00,	1836.85
20	08	1730.43,	1740.69
23	11	65.03,	2271.04
23	11	194.88,	2263.59
23	11	324.08,	2248.76
23	11	452.23,	2226.51
23	10	578.90,	2196.99
23	10	703.67,	2160.28
23	10	826.11,	2116.48
23	10	945.85,	2065.72
23	03	1062.52,	2008.21
23	03	1175.67,	1944.14
23	09	1284.99,	1873.66
23	09	1390.11,	1797.06
23	09	1490.66,	1714.58
23	00	1586.33,	1626.46
26	11	80.28,	2102.37
26	11	240.38,	2090.13
26	11	399.08,	2065.72
26	11	555.44,	2029.27
26	04	708.59,	1980.98
26	03	857.60,	1921.17



26	03	1001.63,	1850.17
26	03	1139.78,	1768.42
26	10	1271.34,	1676.32
26	10	1395.49,	1574.49
29	12	99.01,	1944.10
29	12	247.01,	1930.88
29	12	393.53,	1906.44
29	11	537.79,	1870.88
29	04	678.90,	1824.42
29	04	816.03,	1767.33
29	04	948.45,	1699.95
29	02	1075.32,	1622.68
29	02	1195.95,	1535.94
29	09	1309.60,	1440.24
32	12	68.70,	1799.29
32	12	205.74,	1788.82
32	12	341.53,	1767.92
32	12	475.39,	1736.72
32	12	606.46,	1695.42
32	04	733.98,	1644.24
32	04	857.24,	1583.48
32	04	975.48,	1513.47
32	04	1088.08,	1434.69
32	04	1194.31,	1347.52
35	06	84.74,	1663.86
35	06	211.38,	1652.54
35	06	336.81,	1631.61
35	06	460.26,	1601.19
35	06	581.03,	1561.40
35	05	698.42,	1512.55
35	05	811.74,	1454.90
35	05	920.30,	1388.76
35	04	1023.54,	1314.52
35	04	1120.82,	1232.63
38	06	97.90,	1536.83
38	06	253.54,	1518.94
38	06	406.56,	1485.32
38	06	555.37,	1436.33
38	05	698.45,	1372.46
38	05	834.27,	1294.41
38	05	961.47,	1202.94
38	05	1078.73,	1099.00
41	06	72.37,	1420.95
41	06	216.37,	1406.25
41	06	358.13,	1376.98
41	06	496.19,	1333.48
41	06	629.13,	1276.17
41	06	755.54,	1205.63
41	05	874.10,	1122.62
41	05	983.65,	1028.01
44	07	89.14,	1311.63
44	07	221.95,	1295.78
44	07	352.46,	1266.52
44	06	479.32,	1224.16
44	06	601.21,	1169.15
44	06	716.89,	1101.99
44	06	825.15,	1023.45
44	06	924.89,	934.31
47	07	61.71,	1211.70
47	07	184.51,	1199.17
47	07	305.41,	1174.20
47	07	423.12,	1137.09

47	06	536.48,	1088.21
47	06	644.25,	1028.07
47	06	745.40,	957.30
47	06	838.80,	876.60
50	07	75.92,	1116.98
50	07	226.34,	1096.44
50	07	372.60,	1055.76
50	07	512.00,	995.62
50	06	641.99,	917.21
50	06	760.19,	821.91
53	07	93.21,	1027.38
53	07	231.36,	1005.34
53	07	365.25,	964.78
53	07	492.42,	906.49
53	06	610.52,	831.5
53	06	717.41,	741.30
56	07	64.30,	946.08
56	07	191.70,	928.70
56	07	315.58,	894.21
56	07	433.66,	843.30
56	07	543.76,	776.89
56	07	643.89,	696.19
59	07	77.89,	858.42
59	07	231.10,	830.40
59	07	376.77,	775.25
59	07	510.10,	694.81
62	07	93.40,	770.43
62	07	230.51,	741.03
62	07	360.10,	687.46
62	07	477.95,	611.44
65	07	62.66,	690.77
65	07	185.96,	668.20
65	07	303.18,	623.84
65	07	410.49,	559.11
68	07	72.87,	601.08
68	07	214.37,	566.27
68	07	343.43,	498.65
71	07	83.99,	517.68
71	07	205.25,	482.61
71	07	314.60,	419.58
74	07	87.04,	427.03
74	07	217.58,	377.59
02	00	-83.37,	3882.86
02	00	-249.96,	3875.71
02	00	-416.10,	3861.40
02	00	-581.49,	3839.98
02	00	-745.79,	3811.47
02	00	-908.72,	3775.94
05	13	-103.02,	3598.28
05	13	-257.41,	3590.54
05	00	-411.28,	3576.17
05	00	-564.43,	3555.24
05	00	-716.53,	3527.71
05	00	-867.28,	3493.72
05	00	-1016.46,	3453.27
05	00	-1163.73,	3406.45
05	00	-1308.91,	3353.34
05	00	-1451.66,	3294.05
05	00	-1591.71,	3228.73
05	00	-1728.85,	3157.41
08	13	-71.59,	3333.46
08	13	-214.60,	3327.32

08	13	-357.25,	3315.05
08	13	-499.21,	3296.65
08	13	-640.25,	3272.20
08	13	-780.14,	3241.69
08	13	-918.56,	3205.21
08	13	-1055.30,	3162.82
08	00	-1190.11,	3114.63
08	00	-1322.72,	3060.66
08	00	-1452.87,	3001.05
08	00	-1580.36,	2935.92
08	00	-1704.93,	2865.39
08	00	-1826.36,	2789.57
08	00	-1944.40,	2708.60
08	00	-2058.90,	2622.61
08	00	-2169.56,	2531.83
08	00	-2276.25,	2436.35
11	08	-88.45,	3088.64
11	08	-220.93,	3082.02
11	08	-353.05,	3069.68
11	08	-484.48,	3051.70
11	08	-615.02,	3028.08
11	08	-744.45,	2998.88
11	08	-872.50,	2964.17
11	06	-998.94,	2923.98
11	00	-1123.51,	2878.41
11	00	-1246.05,	2827.52
11	00	-1366.29,	2771.42
11	00	-1483.97,	2710.24
11	00	-1598.96,	2644.03
11	00	-1710.97,	2572.97
11	00	-1819.83,	2497.15
11	00	-1925.37,	2416.74
11	00	-2027.34,	2331.83
11	00	-2125.56,	2242.66
14	09	-61.42,	2860.79
14	09	-184.18,	2855.51
14	09	-306.59,	2844.98
14	09	-428.44,	2829.20
14	09	-549.47,	2808.20
14	09	-669.51,	2782.02
14	09	-788.31,	2750.72
14	09	-905.66,	2714.34
14	09	-1021.35,	2672.97
14	08	-1135.16,	2626.67
14	08	-1246.84,	2575.49
14	08	-1356.25,	2519.62
14	08	-1463.17,	2459.06
14	00	-1567.37,	2394.00
14	00	-1668.68,	2324.51
14	00	-1766.94,	2250.73
14	00	-1861.92,	2172.81
14	00	-1953.49,	2090.89
17	09	-75.88,	2650.07
17	09	-227.39,	2641.37
17	09	-378.18,	2624.05
17	09	-527.68,	2598.10
17	09	-675.52,	2563.65
17	09	-821.09,	2520.80
17	09	-964.00,	2469.69
17	09	-1103.73,	2410.47
17	08	-1239.85,	2343.38
17	08	-1371.90,	2268.57

17	08	-1499.46,	2186.36
17	08	-1622.13,	2096.99
17	00	-1739.45,	2000.73
17	00	-1851.09,	1897.91
20	10	-93.67,	2452.66
20	10	-233.86,	2443.31
20	10	-373.29,	2425.92
20	10	-511.48,	2400.59
20	10	-647.99,	2367.39
20	10	-782.41,	2326.42
20	10	-914.23,	2277.83
20	10	-1043.10,	2221.79
20	09	-1168.49,	2158.47
20	09	-1290.11,	2088.07
20	09	-1407.46,	2010.84
20	08	-1520.22,	1926.98
20	08	-1628.00,	1836.85
20	08	-1730.43,	1740.69
23	11	-65.03,	2271.04
23	11	-194.88,	2263.59
23	11	-324.08,	2248.76
23	11	-452.23,	2226.51
23	10	-578.90,	2196.99
23	10	-703.67,	2160.28
23	10	-826.11,	2116.48
23	10	-945.85,	2065.72
23	10	-1062.52,	2008.21
23	10	-1175.67,	1944.14
23	03	-1284.99,	1873.66
23	03	-1390.11,	1797.06
23	09	-1490.66,	1714.58
23	00	-1586.33,	1626.46
26	11	-80.28,	2102.37
26	11	-240.38,	2090.13
26	11	-399.08,	2065.72
26	11	-555.44,	2029.27
26	04	-708.59,	1980.98
26	03	-857.60,	1921.17
26	03	-1001.63,	1850.17
26	03	-1139.78,	1768.42
26	10	-1271.34,	1676.32
26	10	-1395.49,	1574.49
29	12	-99.01,	1944.10
29	12	-247.01,	1930.88
29	12	-393.53,	1906.44
29	11	-537.79,	1870.88
29	04	-678.90,	1824.42
29	04	-816.03,	1767.33
29	04	-948.45,	1699.95
29	02	-1075.32,	1622.68
29	02	-1195.95,	1535.94
29	09	-1309.60,	1440.24
32	12	-68.70,	1799.29
32	12	-205.74,	1788.82
32	12	-341.53,	1767.92
32	12	-475.39,	1736.72
32	12	-606.46,	1695.42
32	04	-733.98,	1644.24
32	04	-857.24,	1583.48
32	04	-975.48,	1513.47
32	04	-1088.08,	1434.69
32	04	-1194.31,	1347.52

35	06	-84.74,	1663.86
35	06	-211.38,	1652.54
35	06	-336.81,	1631.61
35	06	-460.26,	1601.19
35	06	-581.03,	1561.40
35	05	-698.42,	1512.55
35	05	-811.74,	1454.90
35	05	-920.30,	1388.76
35	04	-1023.54,	1314.52
35	04	-1120.82,	1232.63
38	06	-97.90,	1536.83
38	06	-253.54,	1518.94
38	06	-406.56,	1485.32
38	06	-555.37,	1436.33
38	05	-698.45,	1372.46
38	05	-834.27,	1294.41
38	05	-961.47,	1202.94
38	05	-1078.73,	1099.00
41	06	-72.37,	1420.95
41	06	-216.37,	1406.25
41	06	-358.13,	1376.98
41	06	-496.19,	1333.48
41	06	-629.13,	1276.17
41	06	-755.54,	1205.63
41	05	-874.10,	1122.62
41	05	-983.65,	1028.01
44	07	-89.14,	1311.63
44	07	-221.95,	1295.78
44	07	-352.46,	1266.52
44	06	-479.32,	1224.16
44	06	-601.21,	1169.15
44	06	-716.89,	1101.99
44	06	-825.15,	1023.45
44	06	-924.89,	934.31
47	07	-61.71,	1211.70
47	07	-184.51,	1199.17
47	07	-305.41,	1174.20
47	07	-423.12,	1137.09
47	06	-536.48,	1088.21
47	06	-644.25,	1028.07
47	06	-745.40,	957.30
47	06	-838.80,	876.60
50	07	-75.92,	1116.98
50	07	-226.34,	1096.44
50	07	-372.60,	1055.76
50	07	-512.00,	995.62
50	06	-641.99,	917.21
50	06	-760.19,	821.91
53	07	-93.21,	1027.38
53	07	-231.36,	1005.34
53	07	-365.25,	964.78
53	07	-492.42,	906.49
53	06	-610.52,	831.5
53	06	-717.41,	741.30
56	07	-64.30,	946.08
56	07	-191.70,	928.70
56	07	-315.58,	894.21
56	07	-433.66,	843.30
56	07	-543.76,	776.89
56	07	-643.89,	696.19
59	07	-77.89,	858.42
59	07	-231.10,	830.40

59	07	-376.77.	775.25
59	07	-510.10.	694.81
62	07	-93.40.	770.43
62	07	-230.51.	741.03
62	07	-360.10.	687.46
62	07	-477.95.	611.44
65	07	-62.66.	690.77
65	07	-185.96.	668.20
65	07	-303.18.	623.84
65	07	-410.49.	559.11
68	07	-72.87.	601.08
68	07	-214.37.	566.27
68	07	-343.43.	498.65
71	07	-83.99.	517.68
71	07	-205.25.	482.61
71	07	-314.60.	419.58
74	07	-87.04.	427.03
74	07	-217.58.	377.59

AIM

=	1.0
01	0.0,0.0,2.
02	0.0,0.0,4.
03	0.0,0.0,6.
04	0.0,0.0,8.
05	0.0,0.0,10.
06	0.0,0.0,12.
07	0.0,0.0,14.
08	0.0,0.0,-2.
09	0.0,0.0,-4.
10	0.0,0.0,-6.
11	0.0,0.0,-8.
12	0.0,0.0,-10.
13	0.0,0.0,-1.
00	0. , 0. , 0.
	x , y , z

AIM POINT COORDINATES

ADDENDUM A - Table A2: EAST APERTURE

ROW NO	AIM NO	HELIOSTAT COORDINATES	
		X(I)	Y(I)
10	01	2292.16,	2187.80
10	01	2383.96,	2087.41
10	01	2471.39,	1983.15
10	01	2554.23,	1875.24
13	01	2109.49,	2042.49
13	01	2195.22,	1950.07
13	01	2276.91,	1854.05
13	01	2354.40,	1754.60
13	01	2427.56,	1651.92
13	01	2496.23,	1546.18
13	01	2560.30,	1437.61
13	01	2619.65,	1326.36
13	01	2674.18,	1212.71
16	01	1993.51,	1848.96
16	01	2096.07,	1731.87
16	01	2191.71,	1609.07
16	01	2280.19,	1481.02
16	01	2361.22,	1348.15
16	01	2434.48,	1210.81
16	20	2499.77,	1069.54
16	20	2556.89,	924.73
16	20	2605.61,	776.93
16	20	2645.80,	626.53
19	01	1825.17,	1733.77
19	01	1921.40,	1626.49
19	01	2011.29,	1513.89
19	01	2094.63,	1396.31
19	01	2171.10,	1274.16
19	21	2240.46,	1147.85
19	21	2302.47,	1017.77
19	09	2356.93,	884.34
19	09	2403.68,	748.02
19	09	2442.52,	609.28
19	09	2473.40,	468.50
19	09	2496.16,	326.21
19	09	2510.73,	182.84
19	09	2517.10,	38.88
22	01	1705.85,	1589.74
22	01	1794.01,	1489.52
22	20	1876.29,	1384.43
22	20	1952.44,	1274.79
22	21	2022.19,	1160.98
22	21	2085.31,	1043.36
22	06	2141.61,	922.33
22	18	2190.85,	798.28
22	09	2232.95,	671.61
22	09	2267.72,	542.74
22	09	2295.05,	412.10
22	09	2314.87,	280.08
22	09	2327.10,	147.14
22	09	2331.73,	13.75
22	09	2328.68,	-119.68
22	09	2318.02,	-252.75
22	09	2299.78,	-384.97
22	09	2273.99,	-515.94
25	01	1564.68,	1486.33
25	20	1647.19,	1394.37
25	20	1724.26,	1297.82

25	09	1795.71,	1197.03
25	09	1861.26,	1092.34
25	06	1920.71,	984.04
25	18	1973.86,	872.53
25	10	2020.58,	758.13
25	10	2060.64,	641.30
25	10	2093.97,	522.34
25	10	2120.41,	401.64
25	10	2139.93,	279.66
25	10	2152.40,	156.76
25	10	2157.85,	33.33
25	10	2156.24,	-90.19
25	10	2147.55,	-213.45
25	10	2131.80,	-335.95
25	10	2109.10,	-457.41
25	10	2079.47,	-577.36
25	22	2043.02,	-695.37
25	22	1999.88,	-811.14
25	22	1950.17,	-924.23
28	01	1470.42,	1352.97
28	09	1569.31,	1236.89
28	09	1659.07,	1113.60
28	22	1739.18,	983.85
28	17	1809.13,	848.35
28	10	1868.58,	707.90
28	10	1917.10,	563.35
28	11	1954.47,	415.48
28	11	1980.49,	265.22
28	11	1994.96,	113.42
28	11	1997.78,	-39.04
28	11	1988.99,	-191.30
28	11	1968.61,	-342.42
28	11	1936.75,	-491.56
28	11	1893.64,	-637.82
28	22	1839.48,	-780.37
28	22	1774.62,	-918.39
28	21	1699.39,	-1051.04
28	21	1614.28,	-1177.58
31	21	1344.21,	1268.82
31	21	1437.09,	1162.58
31	22	1521.54,	1049.63
31	22	1597.16,	930.53
31	17	1663.46,	805.99
31	11	1720.09,	676.80
31	11	1766.71,	543.66
31	11	1803.03,	407.34
31	11	1828.85,	268.63
31	11	1844.01,	128.38
31	11	1848.40,	-12.60
31	11	1842.07,	-153.54
31	11	1825.01,	-293.57
31	11	1797.29,	-431.88
31	11	1759.13,	-567.71
31	22	1710.71,	-700.19
31	22	1652.34,	-828.63
31	22	1584.33,	-952.22
31	22	1507.10,	-1070.26
31	21	1421.08,	-1182.11
31	21	1326.79,	-1287.03
34	21	1257.96,	1157.47
34	17	1342.57,	1058.16
34	17	1419.34,	952.71



34	10	1487.88,	841.69
34	16	1547.72,	725.75
34	11	1598.57,	605.60
34	11	1640.10,	481.95
34	11	1672.09,	355.44
34	11	1694.30,	226.90
34	12	1706.70,	97.01
34	12	1709.13,	-33.40
34	12	1701.59,	-163.65
34	11	1684.17,	-292.94
34	11	1656.90,	-420.53
34	11	1620.03,	-545.66
34	23	1573.70,	-667.61
34	23	1518.19,	-785.69
34	23	1453.85,	-899.17
34	22	1381.05,	-1007.44
34	21	1300.18,	-1109.83
34	21	1211.76,	-1205.76
37	17	1177.15,	1055.79
37	16	1278.33,	930.73
37	16	1366.29,	796.02
37	04	1440.11,	653.08
37	12	1499.00,	503.37
37	12	1542.40,	348.45
37	12	1569.83,	189.93
37	12	1580.98,	29.46
37	12	1575.80,	-131.33
37	12	1554.31,	-290.78
37	12	1516.71,	-447.21
37	12	1463.43,	-599.01
37	23	1395.00,	-744.58
37	23	1312.12,	-882.47
37	22	1215.67,	-1011.24
40	04	1096.02,	966.36
40	04	1188.54,	849.99
40	04	1268.75,	724.83
40	12	1335.81,	592.18
40	12	1389.09,	453.37
40	12	1427.97,	309.90
40	12	1452.05,	163.19
40	12	1461.14,	14.83
40	12	1455.07,	-133.73
40	12	1433.94,	-280.87
40	12	1397.98,	-425.13
40	12	1347.56,	-564.95
40	24	1283.19,	-698.94
40	23	1205.53,	-825.71
40	23	1115.37,	-943.92
43	04	997.00,	909.57
43	03	1084.27,	803.57
43	03	1160.29,	689.26
43	02	1224.33,	567.78
43	02	1275.67,	440.45
43	02	1313.83,	308.56
43	02	1338.37,	173.46
43	02	1349.10,	36.58
43	02	1345.82,	-100.69
43	02	1328.63,	-236.91
43	02	1297.69,	-370.66
43	02	1253.30,	-500.62
43	02	1195.95,	-625.35
43	02	1126.20,	-743.63

43	04	1044.84,	-854.22
46	04	934.96,	824.37
46	03	1013.90,	725.12
46	03	1082.34,	618.33
46	02	1139.55,	505.18
46	02	1184.99,	386.77
46	02	1218.16,	264.37
46	02	1238.70,	139.24
46	02	1246.44,	12.63
46	02	1241.29,	-114.07
46	02	1223.28,	-239.60
46	02	1192.60,	-362.66
46	02	1149.56,	-481.95
46	02	1094.67,	-596.25
46	03	1028.40,	-704.39
46	03	951.50,	-805.24
49	03	875.25,	745.69
49	03	968.10,	620.43
49	02	1043.13,	483.75
49	02	1098.97,	338.18
49	02	1134.63,	186.38
49	02	1149.43,	31.17
49	02	1143.06,	-124.64
49	02	1115.70,	-278.15
49	02	1067.80,	-426.54
49	02	1000.28,	-567.05
49	03	914.36,	-697.17
52	03	786.97,	709.87
52	02	875.74,	596.84
52	02	948.45,	472.86
52	02	1003.73,	340.22
52	02	1040.51,	201.28
52	02	1058.19,	58.66
52	02	1056.38,	-85.04
52	02	1035.16,	-227.20
52	02	994.90,	-365.15
52	02	936.37,	-496.39
52	03	860.59,	-618.50
52	03	769.02,	-729.26
55	03	739.43,	637.23
55	02	818.82,	531.33
55	02	883.19,	415.68
55	02	931.29,	292.35
55	02	962.29,	163.68
55	02	975.58,	31.95
55	02	970.95,	-100.29
55	02	948.45,	-230.74
55	02	908.49,	-356.95
55	02	851.86,	-476.57
55	03	779.55,	-587.43
55	03	692.90,	-687.52
58	02	661.74,	596.91
58	02	736.44,	501.90
58	02	797.56,	397.63
58	02	844.02,	286.09
58	02	874.96,	169.26
58	02	889.82,	49.34
58	02	888.31,	-71.52
58	02	870.46,	-191.04
58	02	836.60,	-307.05
58	02	787.39,	-417.42
58	02	723.68,	-520.11

58	02	646.65,	-613.25
61	02	615.48,	514.46
61	02	698.02,	395.30
61	02	757.77,	263.22
61	02	792.74,	122.57
61	02	801.86,	-22.11
61	02	784.80,	-166.04
61	02	742.12,	-304.56
61	02	675.19,	-433.13
61	14	586.21,	-547.57
64	02	567.48,	445.96
64	02	638.48,	336.58
64	02	688.61,	216.17
64	02	716.30,	88.71
64	02	720.56,	-41.63
64	02	701.30,	-170.60
64	02	659.15,	-294.06
64	14	595.47,	-407.87
64	14	512.36,	-508.36
67	02	487.56,	407.54
67	02	570.79,	279.23
67	02	620.99,	134.78
67	02	635.20,	-17.52
67	02	612.62,	-168.76
67	14	554.55,	-310.23
67	14	464.36,	-433.75
70	02	441.07,	332.51
70	02	507.74,	217.48
70	02	545.01,	89.89
70	02	550.68,	-42.95
70	02	524.47,	-173.26
70	14	467.91,	-293.57
73	02	360.63,	295.30
73	02	435.49,	166.17
73	02	465.68,	19.95
73	02	448.09,	-128.31
73	14	384.54,	-263.38
76	02	330.51,	179.92
76	02	375.39,	26.18
76	02	352.26,	-132.31

AIM	=	1.0
01	=	0.0,0.0,0.0
02		0.0,-2.25,10.0
03		0.0,-2.25,8.0
04		0.0,-2.25,6.00
05		0.0,-2.25,4.00
06		0.0,-2.25,2.00
07		0.0,-2.25,1.00
08		0.0,-2.25,-1.0
09		0.0,-2.25,-2.0
10		0.0,-2.25,-4.
11		0.0,-2.25,-6.
12		0.0,-2.25,-8.
13		0.0,-2.25,-10.
14		0.0,2.25,10.
15		0.0,2.25,8.
16		0.0,2.25,6.
17		0.0,2.25,4.
18		0.0,2.25,2.
19		0.0,2.25,1.
20		0.0,2.25,-1.
21		0.0,2.25,-2.

22 U.0,2.25,-4.  
23 0.0,2.25,-6.  
24 0.0,2.25,-8.  
25- 0.0,2.25,-10.

00 0. , 0. , 0.  
x y z

AIM POINT COORDINATES

ADDENDUM A - Table A3 : SOUTH APERTURE

ROW NO	AIM NO	HELIOSTAT COORDINATES	
		X(I)	Y(I)
31	00	1259.60,	-1352.84
31	00	1152.77,	-1444.96
34	00	1148.87,	-1265.83
34	00	1049.00,	-1349.75
34	00	943.00,	-1425.84
34	00	831.52,	-1493.58
34	00	715.18,	-1552.64
34	07	594.68,	-1602.67
37	00	1077.51,	-1157.30
37	00	954.38,	-1260.78
37	07	821.32,	-1351.23
37	07	679.78,	-1427.71
37	08	531.19,	-1489.38
37	08	377.13,	-1535.64
37	08	219.12,	-1566.02
37	08	58.89,	-1580.16
40	00	977.42,	-1086.14
40	00	862.00,	-1179.84
40	07	737.66,	-1261.34
40	08	605.70,	-1329.74
40	08	467.45,	-1384.40
40	08	324.37,	-1424.75
40	08	177.92,	-1450.31
43	00	919.64,	-987.72
43	07	814.52,	-1076.07
43	08	700.98,	-1153.23
43	08	580.18,	-1218.49
43	08	453.37,	-1271.15
43	08	321.88,	-1310.65
43	08	187.04,	-1336.57
43	08	50.26,	-1348.64
46	07	833.82,	-926.56
46	08	735.36,	-1006.48
46	08	629.29,	-1076.00
46	08	516.69,	-1134.37
46	09	398.78,	-1180.99
46	09	276.70,	-1215.41
46	10	151.77,	-1237.22
49	01	783.55,	-841.53
49	01	662.49,	-939.82
49	02	529.23,	-1020.79
49	09	386.28,	-1083.02
49	10	236.18,	-1125.31
49	10	81.76,	-1146.93
52	02	699.96,	-795.76
52	03	585.89,	-883.13
52	03	461.02,	-954.29
52	04	327.65,	-1007.89
52	04	188.29,	-1042.93
52	04	45.47,	-1058.85
55	02	627.95,	-747.30
55	03	521.09,	-825.38
55	04	404.62,	-888.31
55	04	280.71,	-934.86
55	05	151.64,	-964.26
58	02	588.61,	-669.15
58	03	492.68,	-742.64
58	04	387.66,	-802.45

55	13	213.32,	-541.33
58	05	158.33,	-877.02
58	05	38.22,	-890.38
61	03	516.07,	-614.13
61	15	397.11,	-696.97
61	15	265.19,	-757.08
61	05	124.64,	-792.44
64	04	447.47,	-566.33
64	15	338.22,	-637.59
64	15	217.98,	-688.05
64	06	90.58,	-716.07
67	13	378.74,	-510.23
67	13	245.86,	-585.95
67	11	98.72,	-627.72
70	15	351.08,	-426.44
70	15	239.04,	-497.96
70	06	113.12,	-540.64
73	05	281.56,	-371.45
73	06	149.67,	-441.43
76	05	235.27,	-293.70
76	06	91.80,	-364.92
31	00	-1259.60,	-1352.84
31	00	-1152.77,	-1444.96
34	00	-1148.87,	-1265.83
34	00	-1049.00,	-1349.75
34	00	-943.00,	-1425.84
34	00	-831.52,	-1493.58
34	00	-715.18,	-1552.64
34	07	-594.68,	-1602.67
37	00	-1077.51,	-1157.30
37	00	-954.38,	-1260.78
37	07	-821.32,	-1351.23
37	07	-679.78,	-1427.71
37	08	-531.19,	-1489.38
37	08	-377.13,	-1535.64
37	08	-219.12,	-1566.02
37	08	-58.89,	-1580.16
40	00	-977.42,	-1086.14
40	00	-862.00,	-1179.84
40	07	-737.66,	-1261.34
40	08	-605.70,	-1329.74
40	08	-467.45,	-1384.40
40	08	-324.37,	-1424.75
40	08	-177.92,	-1450.31
43	00	-919.64,	-987.72
43	07	-814.52,	-1076.07
43	08	-700.98,	-1153.23
43	08	-580.18,	-1218.49
43	08	-453.37,	-1271.15
43	08	-321.88,	-1310.65
43	08	-187.04,	-1336.57
43	08	-50.26,	-1348.64
46	07	-833.82,	-926.56
46	08	-735.36,	-1006.48
46	08	-629.29,	-1076.00
46	08	-516.69,	-1134.37
46	09	-398.78,	-1180.99
46	09	-276.70,	-1215.41
46	10	-151.77,	-1237.22
49	01	-783.55,	-841.53
49	01	-662.49,	-939.82
49	02	-529.23,	-1020.79

44	09	- 386.28,	-1083.02
49	10	- 236.18,	-1125.31
49	10	- 81.76,	-1146.93
52	02	- 699.96,	-795.76
52	03	- 585.89,	-883.13
52	03	- 461.02,	-954.29
52	04	- 327.65,	-1007.89
52	04	- 188.29,	-1042.93
52	04	- 45.47,	-1058.85
55	02	- 627.95,	-747.30
55	03	- 521.09,	-825.38
55	04	- 404.62,	-888.31
55	04	- 280.71,	-934.86
55	05	- 151.64,	-964.26
58	02	- 588.61,	-669.15
58	03	- 492.68,	-742.64
58	04	- 387.66,	-802.45
58	14	- 275.52,	-847.53
58	05	- 158.33,	-877.02
58	05	- 38.22,	-890.38
61	03	- 516.07,	-614.13
61	14	- 397.11,	-696.97
61	14	- 265.19,	-757.08
61	05	- 124.64,	-792.44
64	04	- 447.47,	-566.33
64	14	- 338.22,	-637.59
64	14	- 217.98,	-688.05
64	06	- 90.58,	-716.07
67	12	- 378.74,	-510.23
67	12	- 245.86,	-585.95
67	11	- 98.72,	-627.72
70	04	- 351.08,	-426.44
70	05	- 239.04,	-497.96
70	06	- 113.12,	-540.64
73	05	- 281.56,	-371.45
73	06	- 149.67,	-441.43
76	05	- 235.27,	-293.70
76	06	- 91.80,	-364.92

AIM

	=1.0
01	0.0,0.0,1.0
02	0.0,0.0,2.0
03	0.0,0.0,3.0
04	0.0,0.0,4.0
05	0.0,0.0,5.0
06	0.0,0.0,6.0
07	0.0,0.0,-1.0
08	0.0,0.0,-2.0
09	0.0,0.0,-3.0
10	0.0,0.0,-4.0
11	0.0,0.0,0.0
12	-5.0,0.0,0.0
13	5.0,0.0,0.0
14	-5.0,0.0,5.0
15	5.0,0.0,5.0
00	0.0,0.0,0.0

x y z  
AIM POINT COORDINATES

**Appendix B**  
**Elevated Temperature Analysis**



## TABLE OF CONTENTS

	PAGE
ELEVATED TEMPERATURE ANALYSIS	
Summary .....	B-1
1. Creep/Fatigue Evaluation - Solar 100 Analysis .....	B-1
2. Simplified Inelastic Creep/Fatigue Procedure	
for Sandia Receiver Panels .....	B-2
3. Assessment of Membrane Wall Program .....	B-3
4. Effect of Membrane Wall Construction .....	B-5
5. Thermal Hydraulic Analysis .....	B-8
6. Stresses at Critical Section .....	B-11
7. Leading Cycle .....	B-18
8. Elastic Analysis by CREEPF Program .....	B-20
9. Inelastic Analysis by Simplified Method .....	B-23
References .....	B-29
CREEP-FATIGURE ANALYSIS USING SUPPLEMENTAL ELEVATED TEMPERATURE RULES .....	B-30
CREEP RATCHETING EVALUATION .....	B-31
SUPPLEMENTAL ELEVATED TEMPERATURE RULES FOR SECTION VIII DIVISION 1 .....	B-73

## Summary

The design of the receiver panels for cyclic elevated temperature service, which includes creep-fatigue effects, is a vital part of the mechanical design analysis. Thermal stresses and strains are produced in the panels by high, nonuniform incident heat fluxes which are cyclic in nature. The effects of creep and fatigue become significant because of the elevated temperatures involved, the duration, cyclic characteristic, and peak levels of the thermal loading. A detailed creep/fatigue analysis of the Sandia solar receiver panels was conducted based on the ASME Code Case N-47 and the elastic and inelastic creep/fatigue evaluations of the Solar 100 receiver panels. The evaluation involved a temperature and stress analysis of the tube-web finite element model using the Membrane Wall computer program. The results are used in conjunction with the computer program CREEPF and the inelastic fatigue curves of Code Case N-47 to calculate the total damage. The worst panel examined under direct heating was found to have a combined creep-fatigue damage that fell within the damage envelope. The geometrical configuration of the absorption panels was therefore acceptable for the given heat flux distribution and the design life of the receiver.

### (1) Creep/Fatigue Evaluation - Solar 100 Analysis

The Creep/Fatigue Report on the receiver panel tubes of Solar 100 by K. H. Hsu (Ref. 1), provides a detailed study using elastic, single element uniaxial inelastic and three dimensional inelastic methods. The basic analytical procedure consists of five steps:

- 1) A thermal-hydraulic analysis to predict salt temperatures inside the tubes and net absorbed heat fluxes.
- 2) A two-dimensional thermal finite element analysis to predict the tube metal temperature distribution.

- 3) An elastic analysis and elastic creep/fatigue evaluation to locate the critical section of the tube.
- 4) An inelastic analysis to predict stresses and strains for the given temperature distribution.
- 5) A stress/strain evaluation to predict the creep and fatigue damages.

These analyses required extensive work using computer programs GRID(91349), ABTA (91349), FETAP (91447), FESAP (91424), CLASS (91417), CREEPF (09017), and ADINA (09019). The GRID program generates the finite element tube model to be used for the analysis. ABTA and FETAP create the temperature distributions around the tube for input to FESAP, which obtains the thermal stresses. The CLASS program resolves the stresses into membrane, bending, and peak components for use in CREEPF, which calculates the strains and the creep and fatigue damage factors. The ADINA program calculates the inelastic stresses and strains for creep and fatigue evaluations based on the Code Case N-47 inelastic rules.

(2) Simplified Inelastic Creep/Fatigue Procedure for Sandia Receiver Panels

Based on a conclusion from the Solar 100 Creep/Fatigue Report, a simplified inelastic creep/fatigue evaluation procedure was proposed. This study shows that the procedure can be used in conjunction with the Membrane Wall Program (157) for performing creep/fatigue analysis of the Sandia solar receiver panels with the following provisions:

- 1) The Membrane Wall Program (MWP) contains its own model and also generates temperature distributions and stress results in the same output run. The use of program 157 eliminates tedious computer work using GRID, ABTA, FETAP, and FESAP finite element programs.
- 2) Stresses from the MWP have been checked with those results from FESAP in order to verify and warrant its use.

- 3) The receiver panels of Solar 100 consist of tangent tubes as opposed to the membrane wall construction of the Sandia receiver panels. A correlation between the two has to be made in order to demonstrate the insignificance of the web with regard to the critical section of the panel wall.
- 4) The stress results from the MWP can be linearized and resolved into components by hand. Therefore, the CLASS program will not be needed.
- 5) In the proposed simplified inelastic creep/fatigue evaluation, the fatigue damage usage fraction is determined from the total strain range using the elastically calculated fatigue curves of Code Case N-47. This procedure is used in analyzing the Sandia panels with references to the Solar 100 Report as needed.

(3) Assessment of Membrane Wall Program

Comparisons of the MWP and FESAP results are shown in Tables 1 and 2. The proximity of these stress results implies that the MWP gives an adequate assessment of the thermal stress distribution in the absorption panels.

# Babcock & Wilcox ENGINEERING CALCULATIONS

**SUBJECT:** CREEP/FATIGUE ANALYSIS

PANEL DESIGN CONDITIONS:

HEAT FLUX =  $45,400 \frac{\text{BTU}}{\text{HR} \cdot \text{FT}^2}$   
 FILM COEFFICIENT =  $1166 \frac{\text{BTU}}{\text{HR} \cdot \text{FT}^2 \cdot \text{°F}}$   
 SALT TEMPERATURE = 885 °F

TABLE 1

SOURCE	STRESS COMPONENTS @ TUBE CROWN			MAX. STRESS INTENSITY
	$\sigma_r$	$\sigma_t$	$\sigma_z$	
MEMBRANE WALL PROGRAM (REF. 2)	0	-9061	-36592	36592
FESAP (REF. 1)	297	-9439	-38098	38395

ALL STRESSES IN PSI.

$\frac{38395 - 36592}{38395} = 0.047 \rightarrow 4.7\% \text{ DIFFERENCE}$

PANEL DESIGN CONDITIONS:

HEAT FLUX =  $83300 \frac{\text{BTU}}{\text{HR} \cdot \text{FT}^2 \cdot \text{°F}}$   
 FILM COEFFICIENT =  $1254 \frac{\text{BTU}}{\text{HR} \cdot \text{FT}^2 \cdot \text{°F}}$   
 SALT TEMPERATURE = 1012 °F

TABLE 2

SOURCE	STRESS COMPONENTS @ TUBE CROWN			MAX. STRESS INTENSITY
	$\sigma_r$	$\sigma_t$	$\sigma_z$	
MEMBRANE WALL PROGRAM (REF. 2)	0	-1931	-19492	19492
FESAP (REF. 1)	171	-5434	-20844	21015

$\frac{21015 - 19492}{21015} = 0.072 \rightarrow 7.2\% \text{ DIFFERENCE}$

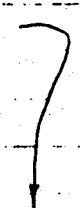

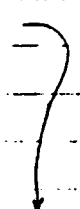
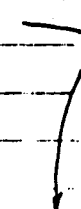
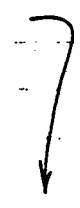
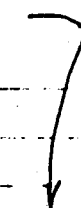
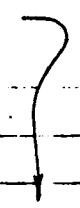
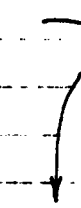
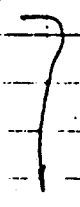
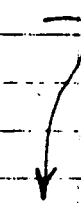
(4) Effect of Membrane Wall Construction

Table 3 shows stress results for tangent tubes vs. a membrane wall under the same conditions. Stresses are given for the various panel locations in Figure 1. The critical section for either panel configuration occurs at the tube crown. The presence of a web affects the circumferential gradient of the tube and hence the stress pattern, particularly at the tube-to-web juncture. However, it does not alter the location of the worst stress, nor does it alter greatly the magnitude of the maximum stress in the panel.

# Babcock & Wilcox ENGINEERING CALCULATIONS

**SUBJECT:** CREEP / FATIGUE ANALYSIS

TABLE 3

SALT TEMP.	HEAT FLUX (BTU/HR.-FT <sup>2</sup> )	MEMBRANE WALL			TANGENT TUBES		
		Loc.	T(°F)	σ (PSI)	Loc.	T(°F)	σ (PSI)
600°F 	155,000 	1	879	-47067	1	879	-50437
		2	793	-20785	2	793	-22577
		3	600	+19890	3	600	+18026
		4	718	-5601	4	615	+12449
		5	826	-33163	5	—	—
		6	750	-12284	6	—	—
700°F 	120,000 	1	892	-32783	1	891	-37847
		2	827	-12798	2	827	-13977
		3	700	+13723	3	700	+12122
		4	783	-4512	4	710	+8263
		5	865	-25007	5	—	—
		6	807	-9494	6	—	—
800°F 	117,000 	1	968	-28496	1	968	-30589
		2	908	-9928	2	908	-11244
		3	800	+11581	3	800	+10134
		4	874	-4352	4	809	+7030
		5	951	-23127	5	—	—
		6	897	-8918	6	—	—
900°F 	108,000 	1	1043	-27243	1	1043	-26035
		2	990	-7848	2	990	-8974
		3	900	+9737	3	900	+8763
		4	964	-3912	4	907	+5845
		5	1032	-20310	5	—	—
		6	984	-7892	6	—	—
1000°F 	80,000 	1	1100	-16762	1	1100	-18009
		2	1062	-5182	2	1062	-5961
		3	1000	+6684	3	1000	+6015
		4	1045	-2771	4	1005	+3978
		5	1094	-14381	5	—	—
		6	1060	-5587	6	—	—

REFERENCES: 3 and 4.

# Babcock & Wilcox ENGINEERING CALCULATIONS

SUBJECT: CREEP / FATIGUE ANALYSIS

MEMBRANE WALL PANEL TUBE MODEL:

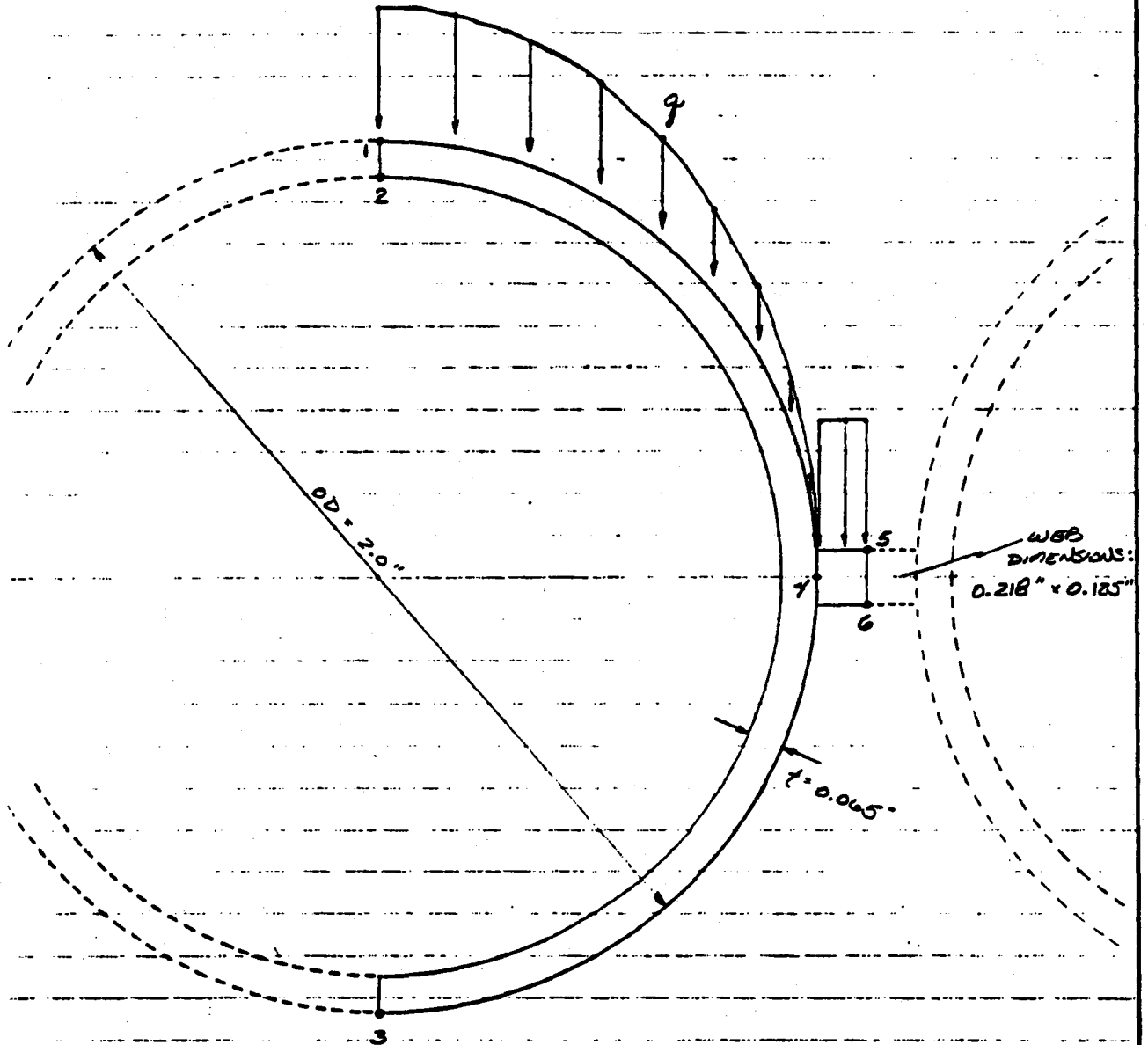


FIGURE 1



(5) Thermal-Hydraulic Analysis

A functional analysis of the receiver subsystem provides thermal-hydraulic data for input into the MWP. Molten salt temperatures, inside tube film coefficients, and heat flux distributions are provided in Table 4 and Figure 2. The two panel areas that are most likely subjected to the most severe creep and/or fatigue damage are those exposed to the highest heat flux and those that see the highest metal temperatures. Both of these cases were tested for creep/fatigue damage in the Solar 100 report, with the worst case being the panel receiving the highest heat flux. It is perceived that the most critical conditions (as far as creep and fatigue are concerned) for the Sandia receiver exist in Panel 2, North Cavity ( $T_{\text{salt}} = 600^{\circ}\text{F}$ , Flux = 155.000 Btu/Hr-Ft<sup>2</sup>).

# Babcock & Wilcox ENGINEERING CALCULATIONS

SUBJECT:

(°F) SALT TEMPERATURE	(BTU/HR·FT <sup>2</sup> ·°F) h - SOLAR 100	(BTU/HR·FT <sup>2</sup> ·°F) h - SNLL
550	798	766
600	866	836
650	935	911
700	1002	988
750	1064	1064
800	1119	1135
850	1166	1200
900	1205	1256
950	1239	1305
1000	1275	1351
1050	1318	1399

TABLE 4 - FILM COEFFICIENTS

flow rates : SOLAR 100 ≈ 1.2067 × 10<sup>6</sup> lb/hr (15 TUBES)  
 SNLL ≈ 1.171 × 10<sup>6</sup> lb/hr (15 TUBES)

# Babcock & Wilcox ENGINEERING CALCULATIONS

SUBJECT:

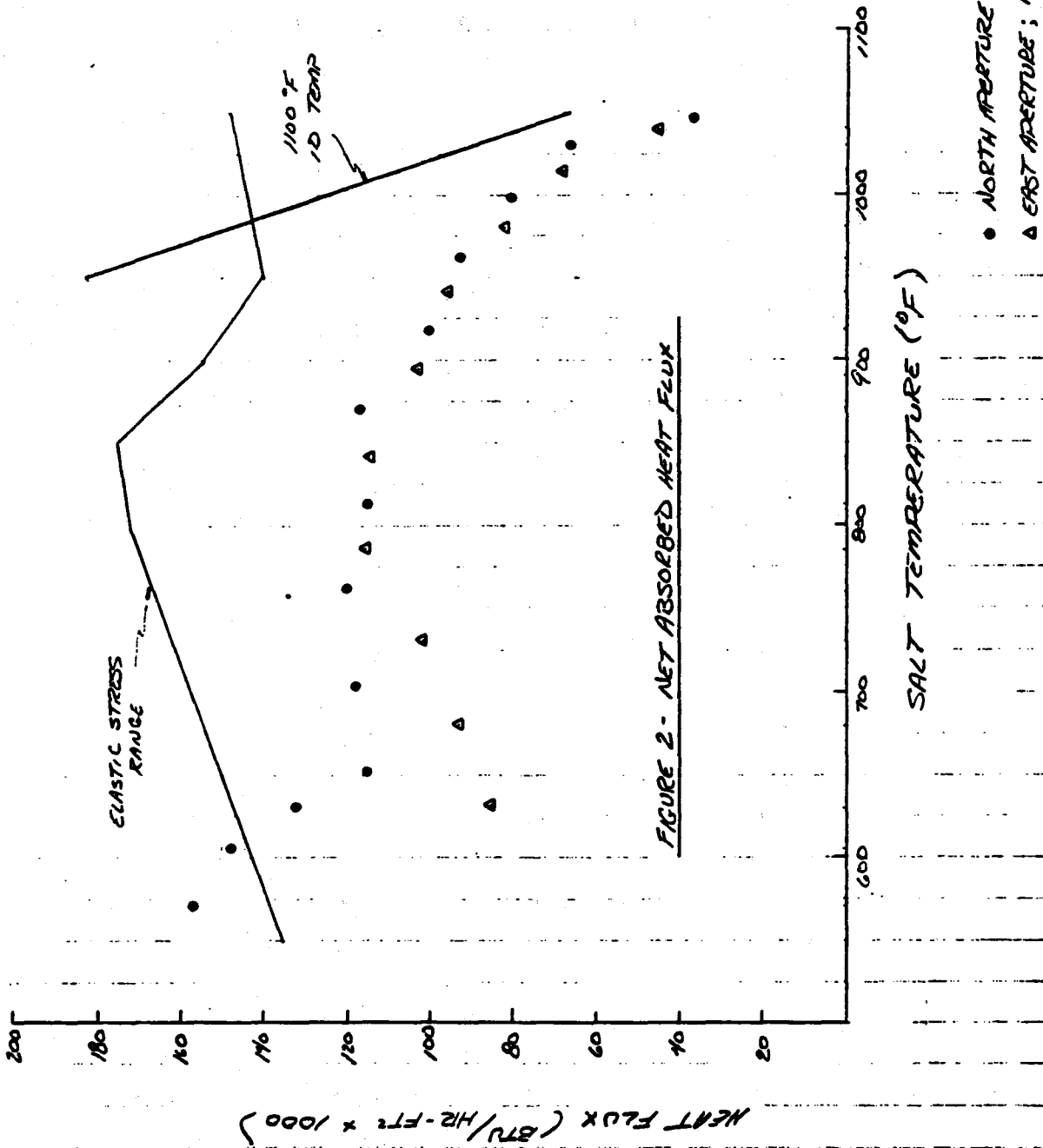


FIGURE 2 - NET ABSORBED HEAT FLUX

(6) Stresses at Critical Section

For the previously mentioned conditions, the steady state thermal stresses at a section through the tube crown are given in Table 5. These values are generated by the MWP for the tube model shown in Figure 3. The stresses through the section are resolved into membrane, bending, and peak components by linearization (see Figures 4, 5, and 6). This is required for input to the CREEPF program.

# Babcock & Wilcox ENGINEERING CALCULATIONS

SUBJECT: PROGRAM 157 DATA (TUBE @ CROWN)

POINT	RADIUS	STRESS COMPONENTS (PSI)			
		$\sigma_r$	$\sigma_\theta$	$\sigma_z$	$\tau_{rz}$
A	1.000"	0	-9263	-77064	0
B	0.975"	148	-2272	-36949	0
C	0.960"	152	1986	-30941	0
D	0.950"	115	-5087	-26631	0
E	0.942"	61	-7541	-23259	0
F	0.935"	0	9578	-20485	0

TABLE 5

# Babcock & Wilcox ENGINEERING CALCULATIONS

SUBJECT: PROGRAM 157 TUBE MODEL

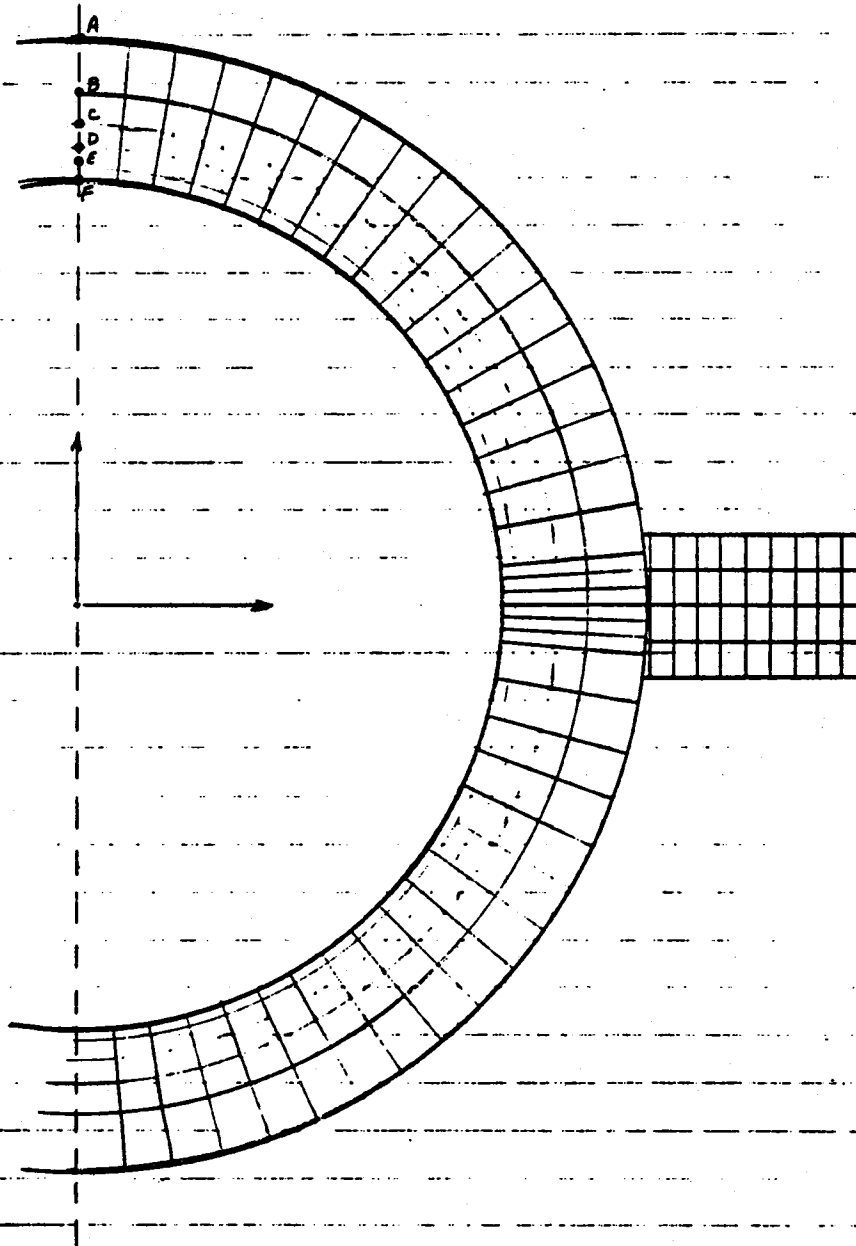


FIGURE 3

# Babcock & Wilcox ENGINEERING CALCULATIONS

SUBJECT: LOAD CONTROLLED STRESS COMPONENTS

LOAD CONTROLLED STRESSES ARE MEMBRANE STRESSES  
DUE TO PRESSURE LOADS. DUE TO SIMILARITY OF  
DESIGN CONDITIONS BETWEEN SOLAR-100 AND  
SANDIA CONTRACTS, THE LOAD CONTROLLED STRESSES,  
BASED ON A CONSTANT PRESSURE OF 500<sup>PSI</sup>, ARE  
OBTAINED FROM THE CREEP / FATIGUE EVALUATIONS  
MADE ON SOLAR 100.

$$\sigma_r = -268 \text{ PSI}$$

$$\sigma_\theta = 7223 \text{ PSI}$$

$$\sigma_z = 58 \text{ PSI}$$

$$\tau_{rz} = 1 \text{ PSI}$$

# Babcock & Wilcox ENGINEERING CALCULATIONS

SUBJECT: LINEARIZATION OF STRESS  
COMPONENTS (RADIAL)

## LINEARIZED RADIAL STRESSES (THERMAL)

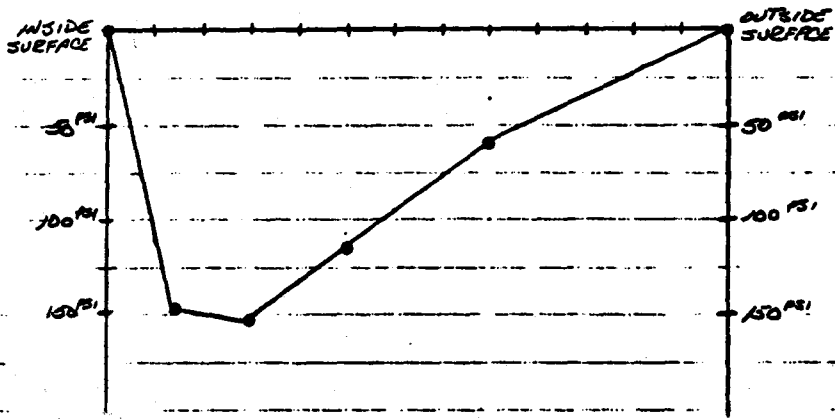


FIGURE 4 (REF. 3)

FOR CONSERVATISM  $\sigma_{r, \text{OUTSIDE}} = \sigma_{r, \text{INSIDE}} = 150 \text{ PSI}$

PEAK THERMAL STRESSES ARE TOTAL STRESSES MINUS  
MEMBRANE + BENDING STRESSES DUE TO THERMAL  
LOAD ONLY.



# Babcock & Wilcox ENGINEERING CALCULATIONS

SUBJECT: LINEARIZATION OF STRESS ...  
COMPONENTS (CIRCUMFERENTIAL)

## LINEARIZED CIRCUMFERENTIAL STRESSES (THERMAL)

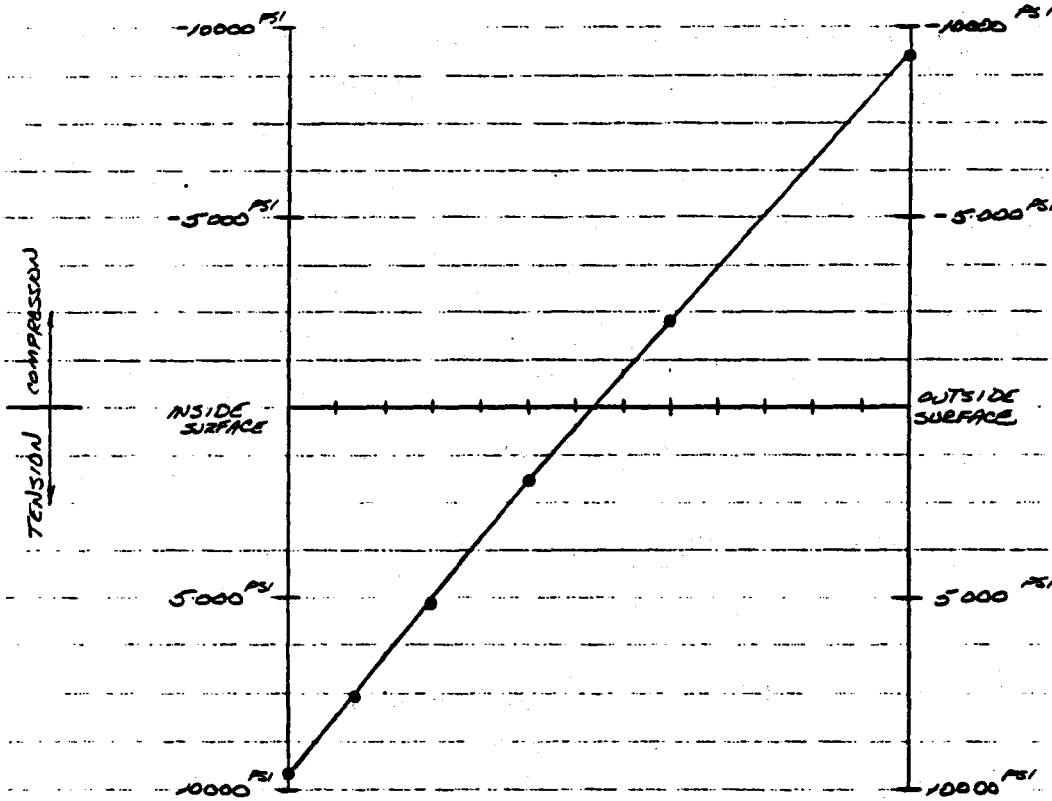


FIGURE 5 (REF. 3)

SINCE DISTRIBUTION IS VERY NEARLY LINEAR, THE PEAK THERMAL CIRCUMFERENTIAL STRESS COMPONENTS WILL BE TAKEN AS ZERO.

# Babcock & Wilcox ENGINEERING CALCULATIONS

SUBJECT: LINEARIZATION OF STRESS  
COMPONENTS (LONGITUDINAL)

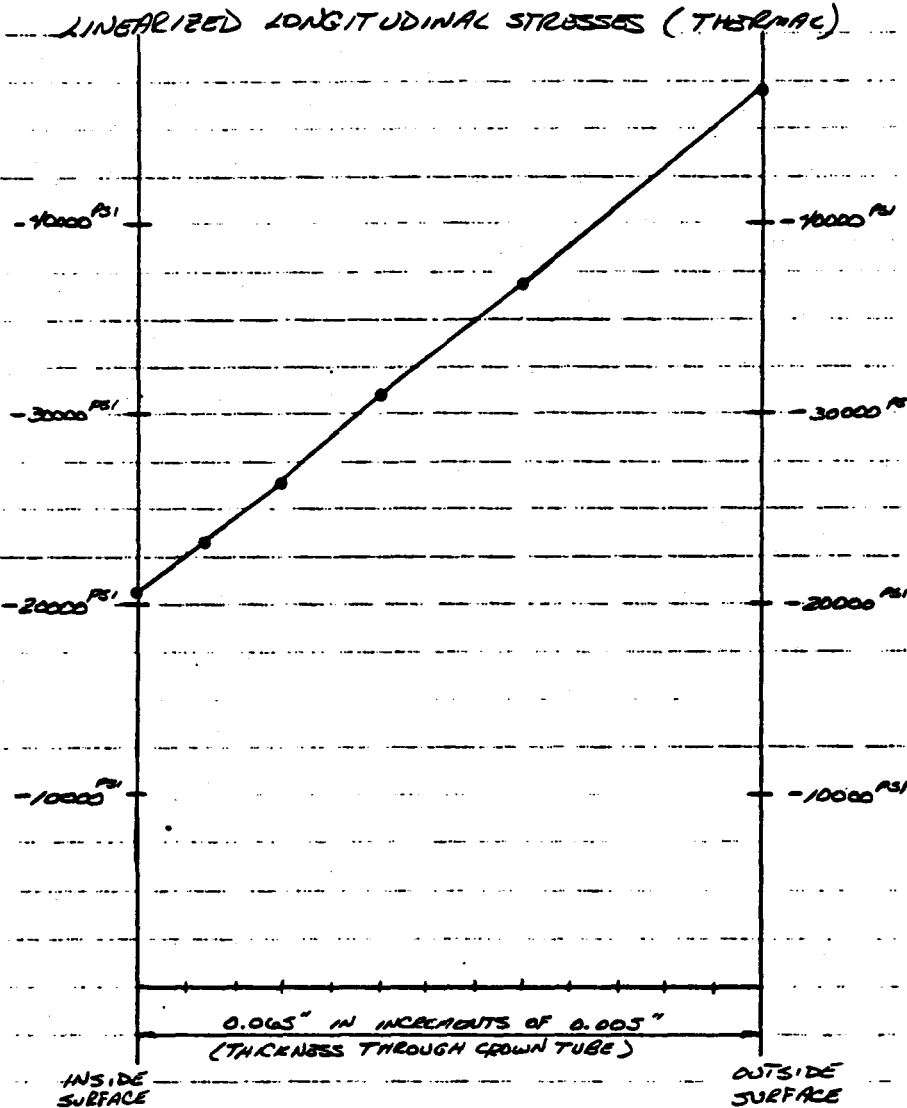


FIGURE 6 (REF. 3)

SINCE THE DISTRIBUTION IS VERY NEARLY LINEAR, THE  
PEAK THERMAL LONGITUDINAL STRESS COMPONENTS WILL  
BE TAKEN AS ZERO.

(7) Loading Cycle

In order to simplify the complex operating history to which the receiver panels will be subjected, a repetitive cycle similar to the one used in the Solar 100 analysis is proposed. The cycle is assumed to ramp up to full power for a duration of 2 hours, then ramp down to hot standby at the end of the cycle. The panels are assumed to be subjected to 50,000 of these cycles throughout its design life of 30 years or 100,000 hours. The thermal cycle used in CREEPF is shown in Figure 7.

# Babcock & Wilcox ENGINEERING CALCULATIONS

SUBJECT: SIMPLIFIED CYCLE FOR  
CREEP / FATIGUE ANALYSIS

ASSUMED THERMAL TRANSIENT AND STEADY  
STATE EVENTS FOR SIMPLIFIED CYCLE :

$$q = 155000 \frac{\text{BTU}}{\text{HR} \cdot \text{FT}^2}$$

$$T_{\text{SALT}} = 600^\circ\text{F}$$

$$h = 836 \frac{\text{BTU}}{\text{HR} \cdot \text{FT}^2 \cdot \text{F}}$$

$$q = 0 \frac{\text{BTU}}{\text{HR} \cdot \text{FT}^2}$$

$$T_{\text{SALT}} = 550^\circ\text{F}$$

$$h = 836 \frac{\text{BTU}}{\text{HR} \cdot \text{FT}^2 \cdot \text{F}}$$

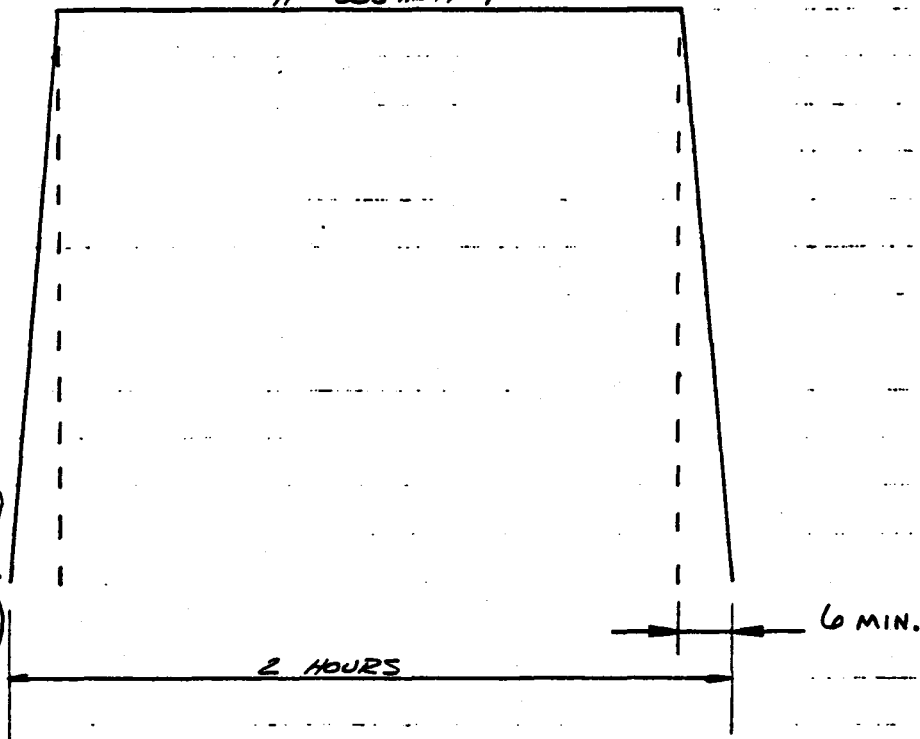


FIGURE 7

(8) Elastic Analysis by CREEPF Program

Table 6 contains a list of stress components for input to CREEPF. The purpose of CREEPF is to perform a creep-fatigue analysis for components operated in an elevated temperature environment. Using the elastic analysis option of the program, the maximum equivalent strain range is calculated along with the fatigue and creep damage fractions. The total damage factor exceeds the Code Case N-47 allowable of 1.0 by a large margin. The elastic method of analysis for creep/fatigue evaluation is very conservative as compared to the inelastic procedure.

# Babcock & Wilcox ENGINEERING CALCULATIONS

**SUBJECT: LOAD & DISPLACEMENT CONTROLLED  
STRESS COMPONENTS**

LOAD & DISPLACEMENT CONTROLLED STRESSES ARE  
MEMBRANE + BENDING STRESSES DUE TO  
PRESSURE AND THERMAL LOADS.

RADIUS	COMPONENT	(PSI) PRESSURE	(PSI) THERMAL	(PSI) PRESSURE + THERMAL
1.000"	r	-268	0	-268
	θ	7223	-9263	-2040
	z	58	-47064	-47006
0.975"	r	-268	148	-120
	θ	7223	-2272	4951
	z	58	-36949	-36891
0.960"	r	-268	152	-116
	θ	7223	1986	9209
	z	58	-30941	-30883
0.950"	r	-268	115	-153
	θ	7223	5087	12310
	z	58	-26631	-26573
0.942"	r	-268	61	-207
	θ	7223	7541	14764
	z	58	-23259	-23201
0.935"	r	-268	0	-268
	θ	7223	9578	16801
	z	58	-20485	-20427

TABLE 6 (REF. 3)

SHEAR STRESSES ARE SMALL AND TAKEN AS ZERO.

# Babcock & Wilcox ENGINEERING CALCULATIONS

SUBJECT: ELASTIC STRESS COMPONENTS AT  
TUBE CROWN POINT

STRESS CLASSIFICATION	STRESS COMPONENTS (PSI)			PRINCIPAL STRESSES (PSI)			STRESS INTENSITIES (PSI)			MAX STRESS INTENSITY
	$\sigma_r$	$\sigma_\theta$	$\tau_{r\theta}$	$\sigma_1$	$\sigma_2$	$\sigma_3$	$S_e$	$S_s$	$S_i$	
LOAD CONTROLLED	-268	7224	4	7224	96	-268	7128	364	-7492	7492
LOAD + DISPLACEMENT CONTROLLED	-268	16801	0	16801	-268	-20127	17069	20159	-37228	46738
PEAK THERMAL	150	0	0	150	0	0	150	0	-150	150

TABLE 7

(9) Inelastic Analysis by Simplified Method

Using the simplified solution suggested in the Solar 100 report, the maximum equivalent strain range calculated in the program is used in the inelastic fatigue curve of Figure T-1420-1C (for Alloy 800H). Using log interpolation and the tabular values of Table T-1420-1C,  $N_d$  (the number of allowable cycles), for a temperature of 879°F and a strain range of 0.001833 in/in, is calculated to be 61,000 cycles. Using 50,000 as the number of applied cycles results in a fatigue damage fraction of 0.818. The creep damage is regarded as being insignificant due to the "low" metal temperature (879°F). Therefore, the total damage is due almost exclusively to fatigue and falls within the allowable damage envelope in Figure 8. The receiver panel geometry and flux pattern identified on this contract are acceptable.



CASE (continued)

N-47-17

CASES OF ASME BOILER AND PRESSURE VESSEL CODE

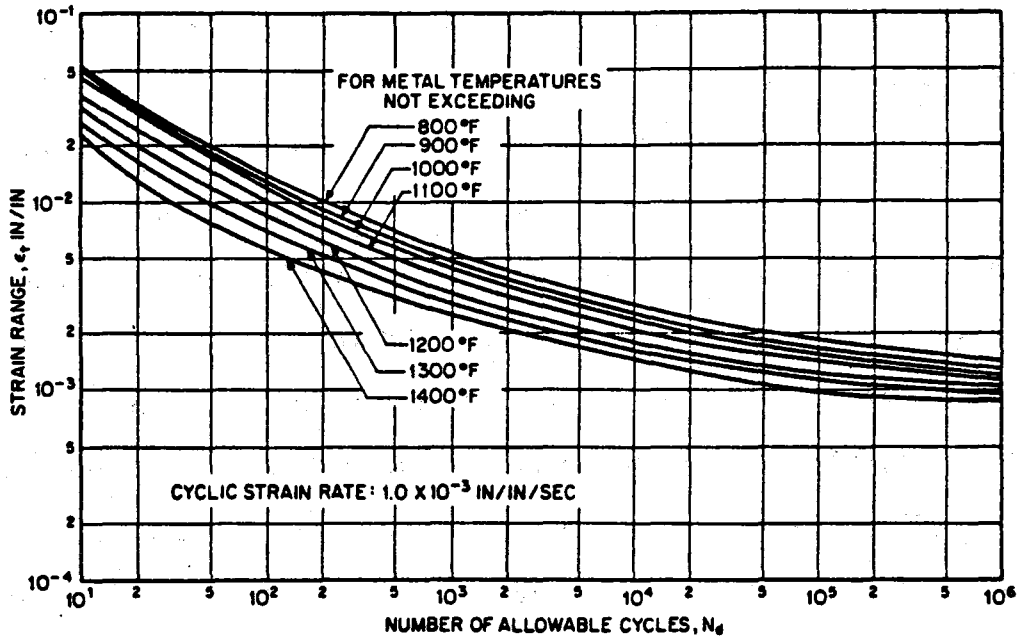


Fig. T-1420-1C Design fatigue strain range,  $\epsilon_f$ , for Ni-Fe-Cr Alloy 800H

Table T-1420-1C

Design Fatigue Strain Range,  $\epsilon_f$ , for Ni-Fe-Cr Alloy 800H

$N_d$ Number of Cycles <sup>a</sup>	$\epsilon_f$ , Strain Range (in./in.) at Temperature							
	800 F	879	900 F	1000 F	1100 F	1200F	1300 F	1400 F
10 <sup>1</sup>	.0513		.0498	.0468	.0378	.0308	.0263	.0231
2x10 <sup>1</sup>	.0328		.0313	.0298	.0243	.0198	.0168	.0129
4x10 <sup>1</sup>	.0218		.0208	.0190	.0163	.0130	.0113	.00866
10 <sup>2</sup>	.0139		.0129	.0119	.01	.00823	.00725	.00566
2x10 <sup>2</sup>	.0103		.00939	.00861	.00722	.00603	.00535	.00426
4x10 <sup>2</sup>	.00777		.00699	.00641	.00542	.00463	.00405	.00331
10 <sup>3</sup>	.00537		.00489	.00441	.00392	.00328	.00285	.00254
2x10 <sup>3</sup>	.00427		.00379	.00351	.00312	.00261	.0023	.00209
4x10 <sup>3</sup>	.00347		.00314	.00291	.00259	.00213	.00195	.00176
10 <sup>4</sup>	.00277		.00249	.00233	.0021	.00174	.00159	.00143
2x10 <sup>4</sup>	.00242		.00219	.00201	.00182	.00155	.00142	.00125
4x10 <sup>4</sup>	.00215		.00193	.0018	.00162	.0014	.00127	.00109
10 <sup>5</sup>	.00187	.0017	.00164	.00151	.00139	.00122	.00115	.000959
2x10 <sup>5</sup>	.00169	.00158	.00149	.00141	.00128	.00113	.00105	.000919
4x10 <sup>5</sup>	.00157	.00148	.00139	.00129	.00121	.00108	.000987	.000889
10 <sup>6</sup>	.00139	.0013	.00129	.00119	.00112	.00103	.000937	.000869

<sup>a</sup>Cyclic strain rate: 1x10<sup>-3</sup> in./in./sec.

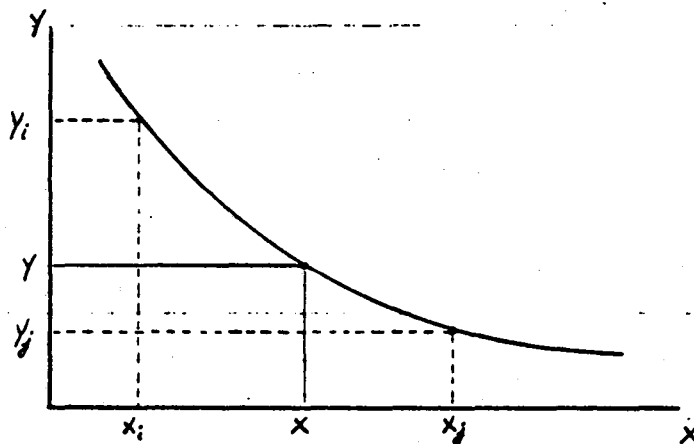
# Babcock & Wilcox ENGINEERING CALCULATIONS

SUBJECT: CREEP/FATIGUE ANALYSIS  
894-0012-45

MAXIMUM EQUIVALENT STRAIN RANGE =  $1.835 \times 10^{-3}$   $\mu\text{/IN}$

← RESULTS OF  
CREEP PROGRAM  
(COMPUTER RUN ETSGTWS)

THIS VALUE IS USED TO ENTER THE DESIGN FATIGUE CURVES OF CODE CASE N-17.  
FROM SECTION VIII, DIVISION 2, APPENDIX 5,  
A FORMULA FOR INTERPOLATION BETWEEN TABULAR VALUES BASED ON DATA REPRESENTATION ON A LOG-LOG PLOT CAN BE USED TO DETERMINE  $N_d$ , THE NUMBER OF ALLOWABLE DESIGN CYCLES.

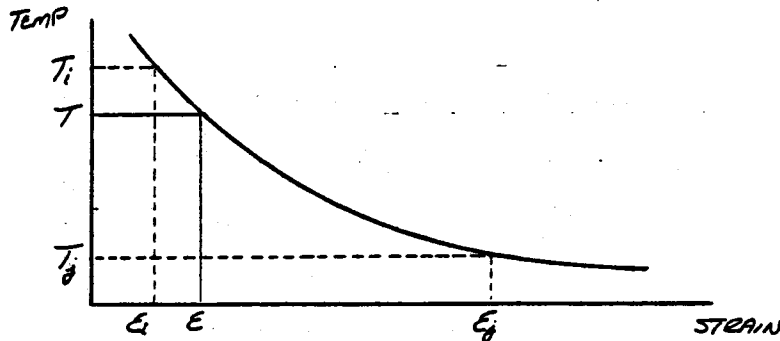


for  $y_i > y_j$  :

$$X = \left[ \frac{X_j}{X_i} \right]^{\frac{\log(Y_i/Y)}{\log(Y_i/Y_j)}} \cdot X_i$$

# Babcock & Wilcox ENGINEERING CALCULATIONS

SUBJECT: CREEP/FATIGUE ANALYSIS  
894-0012-45



FROM TABLE T-1420-1C (CODE CASE N-47) :

$$\begin{array}{ll}
 T_i = 900^\circ\text{F} & E_i = 0.00193 \text{ in./in.} \\
 T_j = 800^\circ\text{F} & E_j = 0.00215 \text{ in./in.} \\
 T = 879^\circ\text{F} & E = ?
 \end{array}$$

$$E = \left[ \frac{0.00215}{0.00193} \right]^{\left[ \frac{\log(900/879)}{\log(900/800)} \right]} \times 0.00193 = \underline{0.0019722 \text{ in./in.}}$$

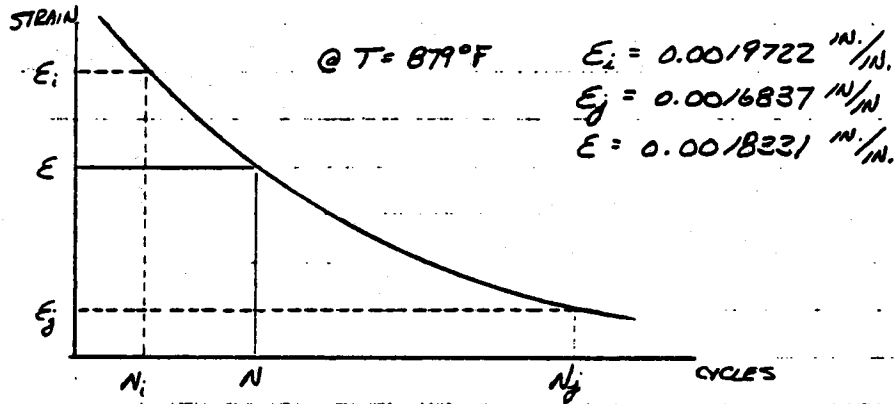
FROM TABLE T-1420-1C :

$$\begin{array}{ll}
 T_i = 900^\circ\text{F} & E_i = 0.00187 \text{ in./in.} \\
 T_j = 800^\circ\text{F} & E_j = 0.00164 \text{ in./in.} \\
 T = 879^\circ\text{F} & E = ?
 \end{array}$$

$$E = \left[ \frac{0.00187}{0.00164} \right]^{\left[ \frac{\log(900/879)}{\log(900/800)} \right]} \times 0.00164 = \underline{0.0016837 \text{ in./in.}}$$

# Babcock & Wilcox ENGINEERING CALCULATIONS

**SUBJECT:** CREEP / FATIGUE ANALYSIS  
894-0012-75



$N_i = 40000 \text{ CYCLES}$

$N_j = 10^5 \text{ CYCLES}$

$N = ?$

$$N = \left[ \frac{10^5}{4 \times 10^4} \right]^{\frac{\log(.0019722/.0018331)}{\log(.0019722/.0016837)}} \times 40000 = 61,100 \text{ CYCLES}$$

FATIGUE DAMAGE FRACTION ( USING 50000 AS  
# OF APPLIED CYCLES ) :

$$\frac{n}{N_d} = \frac{50000}{61100} = \underline{\underline{0.818}}$$

# Babcock & Wilcox ENGINEERING CALCULATIONS

SUBJECT: CREEP/FATIGUE ANALYSIS  
894-0012-45

(COMBINED) CREEP/FATIGUE DAMAGES @ TUBE CROWN :

<u>ELASTIC ANALYSIS</u>	<u>SIMPLIFIED INELASTIC ANALYSIS</u>
$U^c = 0.0055$	$U^c = 0.0055$
$U^f = 125.9446$	$U^f = 0.8183$
TOTAL = 125.95	TOTAL = 0.8238

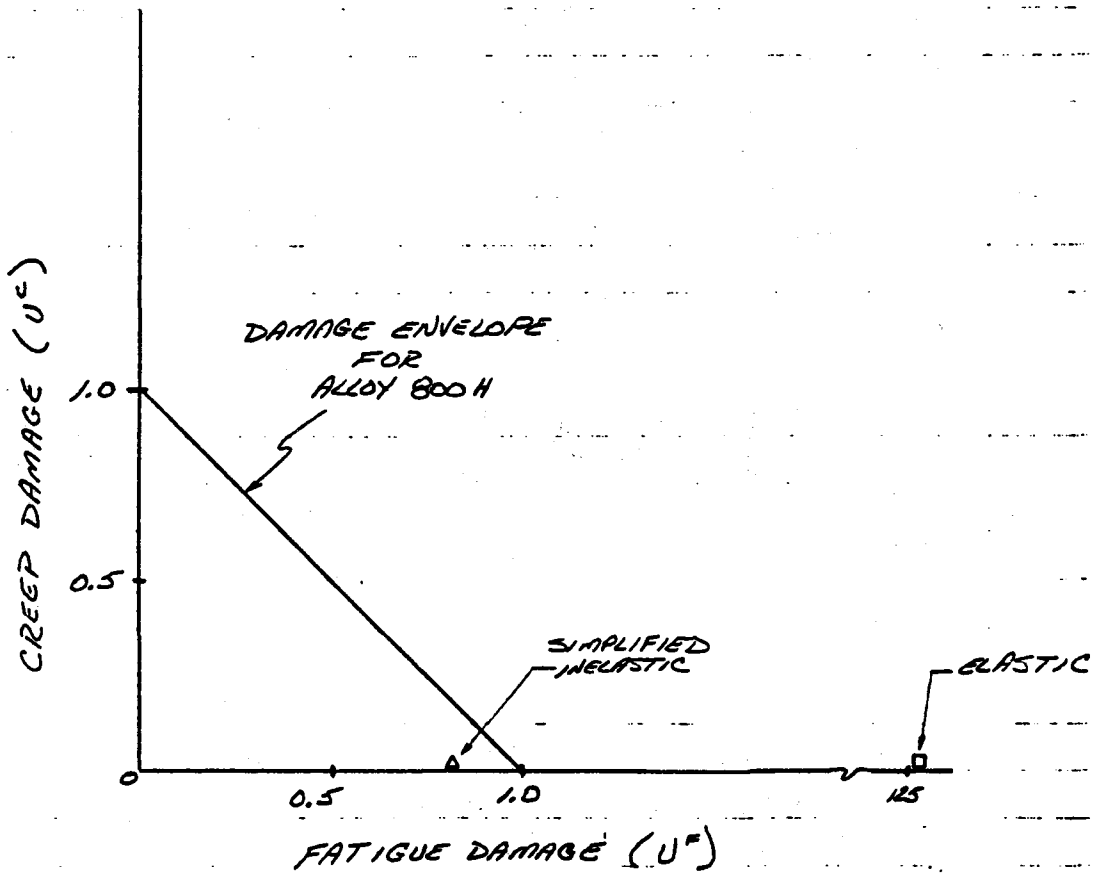


FIGURE 8 (REF. 6)

## References

1. Hsu, K. H., "Elastic and Inelastic Creep/Fatigue Evaluations of Solar Receiver Panel Tube Based on ASME Code Case N-47," Babcock & Wilcox Company.
2. B&W Computer Program 157 - Membrane Wall Program, Computer Run ITSDV7V.
3. B&W Computer Program 157 - Membrane Wall Program, Computer Run ITSDVBA.
4. B&W Computer Program 157 - Membrane Wall Program, Computer Run ITSDVCO.
5. ASME Boiler and Pressure Vessel Code Case N-47, Revision 17.
6. B&W Computer Program 09017 - CREEPF, Rev. 9-0, "Creep-Fatigue Analysis per Code Case 1592 and N-47," Computer Run EJSGJW5.

## CREEP-FATIGUE ANALYSIS USING SUPPLEMENTAL ELEVATED TEMPERATURE RULES

The criteria for creep-fatigue analysis as outlined in Code Case N-47 contains a detailed procedure which emphasizes the particular needs of the nuclear applications for which they were developed. However, special construction, diverse loading conditions, and difficult modes and consequences of failure of solar power systems are among some of the reasons for the necessity of the development of alternate design rules. Consequently, the Supplemental Elevated Temperature Rules for ASME Section VIII, Division 1, has been developed to eliminate some of the conservatisms built into Code Case N-47, and also to account for some failure modes which may not be considered as important for nuclear systems. The major design features of the creep-fatigue criteria include:

1. Using an equivalent strain range in the less conservative inelastic design fatigue curves as also proposed in the simplified inelastic creep-fatigue evaluations of K. H. Hsu.
2. An upper bound of the primary plus secondary stress is set as the yield strength rather than the 25% increase of the yield strength suggested by Code Case N-47.

Complete rules and commentary are found in this Appendix.

The Sandia absorption panels were further analyzed for creep-fatigue damage using the supplemental design rules. Two cases were analyzed, and the total damage fraction in either case did not exceed the allowable established by the damage envelope for Alloy 800H. Further investigation of the available flux and stress data indicated that the panel design and heat flux distribution are acceptable using the creep-fatigue criteria of the Supplemental Elevated Temperature Rules.

## CREEP RATCHETING EVALUATION

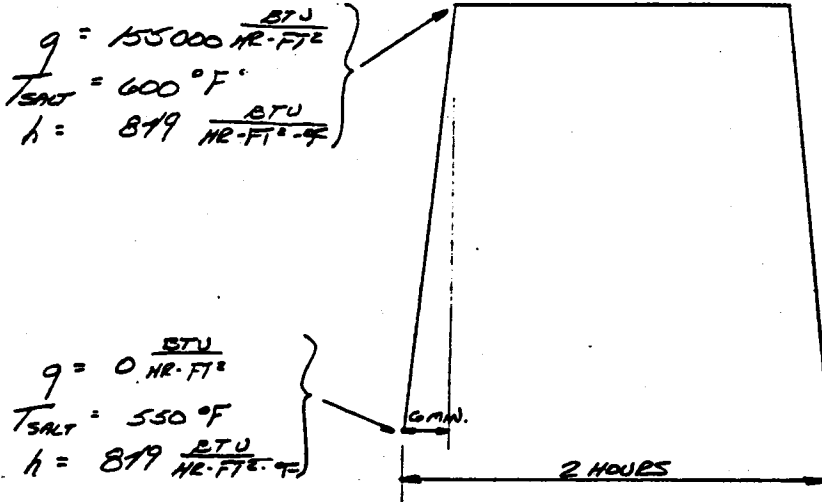
Significant creep ratcheting strain, by 3251.2(a), occurs above the temperature where  $S_m$  equals  $S_t$  at  $10^5$  hours. For Alloy 800H, this is at  $1070^\circ\text{F}$  from Figure 3251.2.2. The combination of X and Y parameters for primary and secondary stress range at and above this temperature will result in an "effective creep stress" considerably less than yield stress. At an "effective creep stress" equal to yield, the accumulative strain for  $10^5$  hours at  $1100^\circ\text{F}$  will be less than 1/2% as compared to an allowable limit of 1-1/2%.



# Babcock & Wilcox ENGINEERING CALCULATIONS

**SUBJECT:** CREEP FATIGUE ANALYSIS ACC. TO Suppl. Elev. Temp. Rules

ASSUMED THERMAL TRANSIENT EVENT :



ELASTIC STRESS COMPONENTS @ TUBE CROWN

STRESS CATEGORY	STRESS COMPONENTS (Psi)			PRINCIPAL STRESSES (Psi)			STRESS INTENSITIES (Psi)			MAX. STRESS INTENSITY
	$\sigma_r$	$\sigma_\theta$	$\sigma_z$	$\sigma_1$	$\sigma_2$	$\sigma_3$	$S_1$	$S_2$	$S_3$	
PRESSURE	-268	7224	96	7224	96	-268	7128	364	-7192	7192
PRESSURE + THERMAL	-268	-2039	-16968	-268	-2039	-16968	7771	11929	16700	16700

RESOLVE STRESSES INTO PLASTIC AND ELASTIC STRAIN COMPONENTS :

$$STRESS INTENSITY (P + TH) = 16700 \text{ PSI}$$

$$S_y (@ 879^\circ F) = 16443 \text{ PSI}$$

$$S_{P+TH} > S_y \rightarrow \epsilon_{pm}^p = \frac{\sigma_{eff} - S_y}{E}$$

$$\text{where } \sigma_{eff} = \frac{1}{\sqrt{2}} \sqrt{(\sigma_r - \sigma_\theta)^2 + (\sigma_\theta - \sigma_z)^2 + (\sigma_z - \sigma_r)^2}$$

# Babcock & Wilcox ENGINEERING CALCULATIONS

**SUBJECT:** CREEP-FATIGUE ANALYSIS ACC.  
TO Suppl. Elev. Temp. Rules

$$\sigma_{\text{eff}} = \frac{1}{\sqrt{2}} \sqrt{(-268 + 2039)^2 + (-2039 + 16968)^2 + (-16968 + 268)^2}$$

$$= 15870 \text{ PSI}$$

$$E_{P+TA}^P = \frac{15870 - 16443}{21.25 \times 10^6} = 1.212 \times 10^{-3} \text{ in/in}$$

INELASTIC STRAIN COMPONENT:

$$E_r^P = \frac{E_{P+TA}^P}{\sigma_{\text{eff}}} \left[ \sigma_r - \frac{1}{2}(\sigma_o + \sigma_e) \right]$$

$$= \frac{1.212 \times 10^{-3}}{15870} \left[ -268 - \frac{1}{2}(-2039 - 16968) \right] = 6.467 \times 10^{-4} \text{ in/in}$$

$$E_o^P = \frac{E_{P+TA}^P}{\sigma_{\text{eff}}} \left[ \sigma_o + \frac{1}{2}(\sigma_r + \sigma_e) \right]$$

$$= \frac{1.212 \times 10^{-3}}{15870} \left[ -2039 - \frac{1}{2}(-268 - 16968) \right] = 5.705 \times 10^{-4} \text{ in/in}$$

$$E_e^P = \frac{E_{P+TA}^P}{\sigma_{\text{eff}}} \left[ \sigma_e - \frac{1}{2}(\sigma_r - \sigma_o) \right]$$

$$= \frac{1.212 \times 10^{-3}}{15870} \left[ -16968 - \frac{1}{2}(-268 - 2039) \right] = -1.211 \times 10^{-3} \text{ in/in}$$

# Babcock & Wilcox ENGINEERING CALCULATIONS

**SUBJECT:** CREEP-FATIGUE ANALYSIS ACC.  
TO Suppl. Elev. Temp. Rules

ELASTIC STRAIN COMPONENTS :

$$E_r^e = \frac{S_r}{\sigma_{eff} E} [\sigma_r - \nu (\sigma_o + \sigma_e)]$$

where  $\frac{S_r}{\sigma_{eff} E} = \frac{16443}{(45846)(21.25 \times 10^3)}$

$$= 1.479 \times 10^{-8}$$

$$E_r^e = 1.479 \times 10^{-8} [-268 - 0.3636 (-2039 - 16968)]$$

$$= 2.595 \times 10^{-7} \text{ in/in}$$

$$E_o^e = 1.479 \times 10^{-8} [-2039 - 0.3636 (-268 - 16968)]$$

$$= 2.238 \times 10^{-7} \text{ in/in}$$

$$E_e^e = 1.479 \times 10^{-8} [-16968 - 0.3636 (-268 - 2039)]$$

$$= -6.822 \times 10^{-7} \text{ in/in}$$

# Babcock & Wilcox ENGINEERING CALCULATIONS

**SUBJECT:** CREEP-FATIGUE ANALYSIS ACC.  
TO Suppl. Elev. Temp. Rules

CALCULATE TOTAL STRAIN COMPONENTS:

$$\begin{aligned} \epsilon_r^T &= \epsilon_r^f + \epsilon_r^c \\ &= 6.407 \times 10^{-4} + 2.595 \times 10^{-4} = 9.002 \times 10^{-4} \text{ in/in} \end{aligned}$$

$$\begin{aligned} \epsilon_o^T &= \epsilon_o^f + \epsilon_o^c \\ &= 5.705 \times 10^{-4} + 2.238 \times 10^{-4} = 7.943 \times 10^{-4} \text{ in/in} \end{aligned}$$

$$\begin{aligned} \epsilon_e^T &= \epsilon_e^f + \epsilon_e^c \\ &= -1.211 \times 10^{-3} + (-6.822 \times 10^{-4}) = -1.893 \times 10^{-3} \text{ in/in} \end{aligned}$$

EQUIVALENT STRAIN RANGE:

$$\begin{aligned} \Delta \epsilon_{equiv.} &= \frac{\sqrt{2}}{3} \sqrt{(\Delta \epsilon_r - \Delta \epsilon_o)^2 + (\Delta \epsilon_o - \Delta \epsilon_e)^2 + (\Delta \epsilon_e - \Delta \epsilon_r)^2} \\ &= \frac{\sqrt{2}}{3} \sqrt{(9.002 \times 10^{-4} - 7.943 \times 10^{-4})^2 + (7.943 \times 10^{-4} + 1.893 \times 10^{-3})^2 + (-1.893 \times 10^{-3} - 9.002 \times 10^{-4})^2} \\ &= \underline{\underline{1.828 \times 10^{-3} \text{ in/in}}} \end{aligned}$$

# Babcock & Wilcox ENGINEERING CALCULATIONS

**SUBJECT:** CREEP-FATIGUE ANALYSIS ACC.  
TO Suppl. Elev. Temp. Rules

for  $E_{equiv.} = 1.828 \times 10^{-3} \frac{IN}{IN} @ 879^{\circ}F,$

$N_d = 61,100 \text{ CYCLES}$

**CREEP DAMAGE CALCULATION:**

$P_m \text{ (PRIMARY STRESS INTENSITY)} = 7492 \text{ PSI}$

$S_1 \text{ (PRIMARY + SECONDARY STRESS INTENSITY)} = 46700 \text{ PSI}$

$\sigma_{eff} \text{ (EFFECTIVE STRESS)} = 45840$

STEP 1 - Calculate and determine the following stress quantities:

1)  $(P_m + 0.5 S_1) = 7492 + 0.5(46700)$   
 $= 30842 \text{ PSI}$

2) MINIMUM YIELD STRENGTH @ THE AVERAGE WALL TEMPERATURE ( $S_{yk}$ )

$T_{avg. wall} = 700^{\circ}F$

$S_{yk} = 17470 \text{ PSI}$

SELECT LESSER OF 1) AND 2) AS  $S_{k1}$ .

$S_{k1} = 17470 \text{ PSI}$

# Babcock & Wilcox ENGINEERING CALCULATIONS

**SUBJECT:** CREEP - FATIGUE ANALYSIS ACC.  
TO Suppl. Elev. Temp. Rules

STEP 2 - Calculate the following stress quantities:

1)  $T_{eff} = 45840 \text{ PSI}$

2) LARGEST PRINCIPAL TENSILE COMPONENT OF THE  
PRIMARY + SECONDARY STRESS COMPONENTS  
= 0

SELECT LARGER OF 1) AND 2) AS  $S_{K_2}$ ...

$S_{K_2} = 45840 \text{ PSI}$

$S_{K_1} < S_{K_2} \Rightarrow S_K = 17470 \text{ PSI}$

ACCORDING TO TABLE 3252.3.4 (EXPECTED MINIMUM STRESS-  
TO-RUPTURE VALUES FOR ALLOY 800H), FOR  $S_K = 16675 \text{ PSI}$   
@ 879 °F, CREEP DAMAGE IS INSIGNIFICANT.

TOTAL DAMAGE:

$$\frac{m}{N_d} = \frac{t}{T_d} = \frac{50000}{61100} = 0.818 < 1.0$$

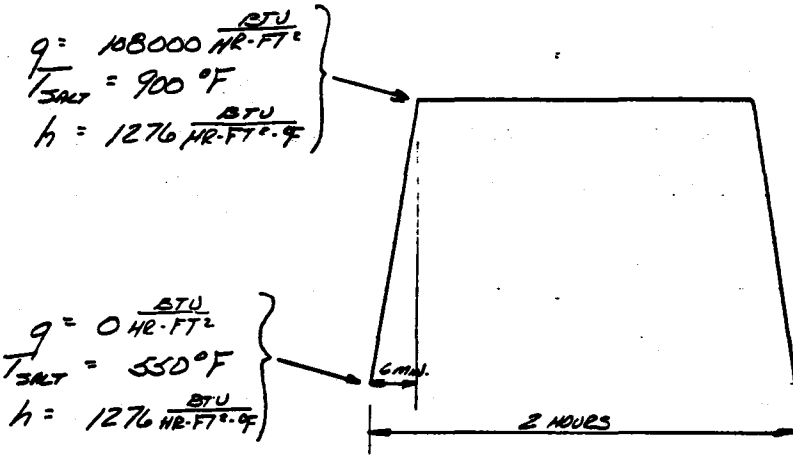
OK.

DESIGN IS ACCEPTABLE!

# Babcock & Wilcox ENGINEERING CALCULATIONS

**SUBJECT:** CREEP - FATIGUE ANALYSIS ACC.  
TO Suppl. Elev. Temp. Rules

ASSUMED THERMAL TRANSIENT EVENT :



STRESS CATEGORY	(PSI) STRESS COMPONENTS			(PSI) PRINCIPAL STRESSES			(PSI) STRESS INTENSITIES			MAX. STRESS INTENSITY
	$\sigma_x$	$\sigma_y$	$\sigma_z$	$\sigma_1$	$\sigma_2$	$\sigma_3$	$S_1$	$S_2$	$S_3$	
PRESSURE	-268	7221	96	7221	96	-268	7128	364	-7492	7492
PRESSURE + THERMAL	-268	1252	-21147	1252	-268	-21147	1520	23879	-25100	25100

## FATIGUE DAMAGE CALCULATION

STEP 1 - RESOLVE STRESSES INTO PLASTIC STRAIN COMPONENTS :

$$\text{STRESS INTENSITY (P+TH)} = 25100 \text{ PSI}$$

$$S_y (@ 1043 \text{ } ^\circ\text{F}) = 15581 \text{ PSI}$$

# Babcock & Wilcox ENGINEERING CALCULATIONS

**SUBJECT:** CREEP-FATIGUE ANALYSIS ACC.  
TO Suppl. Elev. Temp. Rules

$$S_{P+T} > S_y \rightarrow \epsilon_{P+T}^p = \frac{\sigma_{eff} - S_y}{E}$$

where  $\sigma_{eff} = \frac{1}{\sqrt{2}} \sqrt{(\sigma_1 - \sigma_0)^2 + (\sigma_0 - \sigma_2)^2 + (\sigma_2 - \sigma_1)^2}$

$$\begin{aligned} \sigma_{eff} &= \frac{1}{\sqrt{2}} \sqrt{(-268 - 1252)^2 + (1252 - 24147)^2 + (-24147 - 268)^2} \\ &= 24675 \text{ psi} \end{aligned}$$

$$\epsilon_{P+T}^p = \frac{24675 - 15584}{23.33 \times 10^6} = 3.896 \times 10^{-4} \text{ in/in}$$

INELASTIC STRAIN COMPONENTS:

$$\begin{aligned} \epsilon_1^p &= \frac{\epsilon_{P+T}^p}{\sigma_{eff}} \left[ \sigma_1 - \frac{1}{2}(\sigma_0 + \sigma_2) \right] \\ &= \frac{3.896 \times 10^{-4}}{24675} \left[ -268 - \frac{1}{2}(1252 - 24147) \right] = 1.765 \times 10^{-4} \text{ in/in} \end{aligned}$$

$$\begin{aligned} \epsilon_0^p &= \frac{\epsilon_{P+T}^p}{\sigma_{eff}} \left[ \sigma_0 - \frac{1}{2}(\sigma_1 + \sigma_2) \right] \\ &= \frac{3.896 \times 10^{-4}}{24675} \left[ 1252 - \frac{1}{2}(-268 - 24147) \right] = 2.125 \times 10^{-4} \text{ in/in} \end{aligned}$$

$$\begin{aligned} \epsilon_2^p &= \frac{\epsilon_{P+T}^p}{\sigma_{eff}} \left[ \sigma_2 - \frac{1}{2}(\sigma_1 + \sigma_0) \right] \\ &= \frac{3.896 \times 10^{-4}}{24675} \left[ -24147 - \frac{1}{2}(-268 + 1252) \right] = -3.89 \times 10^{-4} \text{ in/in} \end{aligned}$$



**Babcock & Wilcox**  
**ENGINEERING CALCULATIONS**

**SUBJECT:** CREEP-FATIGUE ANALYSIS ACC.  
TO Suppl. Elev. Temp. Rules

STEP 2 - RESOLVE STRESSES INTO ELASTIC STRAIN COMPONENTS :

$$E_r^e = \frac{S_r}{\sigma_{eff} E} [\sigma_r - \nu(\sigma_o + \sigma_i)]$$

$$\text{where } \frac{S_r}{\sigma_{eff} E} = \frac{15584}{(24675)(23.33 \times 10^6)}$$
$$= 2.707 \times 10^{-8}$$

$$E_r^e = 2.707 \times 10^{-8} [-268 - 0.3697(1252 - 21147)]$$
$$= 2.218 \times 10^{-4} \frac{in}{in}$$

$$E_o^e = 2.707 \times 10^{-8} [1252 - 0.3697(-268 - 21147)]$$
$$= 2.782 \times 10^{-4} \frac{in}{in}$$

$$E_i^e = 2.707 \times 10^{-8} [-21147 - 0.3697(-268 + 1252)]$$
$$= -6.635 \times 10^{-4} \frac{in}{in}$$

# Babcock & Wilcox

## ENGINEERING CALCULATIONS

**SUBJECT:** CREEP-FATIGUE ANALYSIS ACC.  
TO Suppl. Elev. Temp. Rules

STEP 3 - CALCULATE TOTAL STRAIN COMPONENTS :

$$\begin{aligned} \epsilon_r^T &= \epsilon_r^p + \epsilon_r^c \\ &= 1.765 \times 10^{-4} + 2.218 \times 10^{-4} = 3.983 \times 10^{-4} \text{ in./in.} \end{aligned}$$

$$\begin{aligned} \epsilon_\theta^T &= \epsilon_\theta^p + \epsilon_\theta^c \\ &= 2.125 \times 10^{-4} + 2.782 \times 10^{-4} = 4.907 \times 10^{-4} \text{ in./in.} \end{aligned}$$

$$\begin{aligned} \epsilon_z^T &= \epsilon_z^p + \epsilon_z^c \\ &= -3.89 \times 10^{-4} - 6.635 \times 10^{-4} = -1.0525 \times 10^{-3} \text{ in./in.} \end{aligned}$$

STEP 4 - CALCULATE EQUIVALENT STRAIN RANGE :

$$\begin{aligned} \Delta \epsilon_{\text{equiv.}} &= \frac{\sqrt{2}}{3} \sqrt{(\Delta \epsilon_r - \Delta \epsilon_\theta)^2 + (\Delta \epsilon_\theta - \Delta \epsilon_z)^2 + (\Delta \epsilon_z - \Delta \epsilon_r)^2} \\ &= \frac{\sqrt{2}}{3} \left[ (3.983 \times 10^{-4} - 4.907 \times 10^{-4})^2 + (4.907 \times 10^{-4} + 1.0525 \times 10^{-3})^2 \right. \\ &\quad \left. + (-1.0525 \times 10^{-3} - 3.983 \times 10^{-4})^2 \right]^{1/2} \\ &= \underline{9.994 \times 10^{-4} \text{ in./in.}} \end{aligned}$$

ACCORDING TO TABLE 3252.3.2 (DESIGN FATIGUE STRAIN RANGE), FOR  $\Delta \epsilon_{\text{equiv.}} = 9.994 \times 10^{-4} \text{ in./in. @ } 1043 \text{ }^\circ\text{F}$ , FATIGUE DAMAGE IS INSIGNIFICANT.

**Babcock & Wilcox**  
**ENGINEERING CALCULATIONS**

**SUBJECT:** CREEP-FATIGUE ANALYSIS ACC.  
TO Suppl. Elev. Temp. Rules

CREEP DAMAGE CALCULATION

$$P_m \text{ (PRIMARY STRESS INTENSITY)} = 7492 \text{ PSI}$$

$$S_i \text{ (PRIMARY + SECONDARY STRESS INTENSITY)} = 25400 \text{ PSI}$$

$$S_{\text{eff}} \text{ (EFFECTIVE STRESS)} = 24675 \text{ PSI}$$

STEP 1 - Calculate and determine the following stress quantities:

$$\begin{aligned} 1) (P_m + 0.5 S_i) &= 7492 + 0.5(25400) \\ &= 20192 \text{ PSI} \end{aligned}$$

2) MINIMUM YIELD STRENGTH @ THE AVERAGE WALL TEMPERATURE ( $S_{yk}$ )

$$T_{\text{avg. wall}} = 950 \text{ }^\circ\text{F}$$

$$S_{yk} = 16075 \text{ PSI}$$

SELECT LESSER OF 1) AND 2) AS  $S_k$ .

$$S_k = 16075 \text{ PSI}$$

**Babcock & Wilcox  
ENGINEERING CALCULATIONS**

**SUBJECT:** CREEP-FATIGUE ANALYSIS ACC.  
TO Suppl. Elev. Temp. Rules

STEP 2 - Calculate the following stress quantities :

1)  $T_{eff} = 24675 \text{ PSI}$

2) LARGEST PRINCIPAL TENSILE COMPONENT OF THE  
PRIMARY + SECONDARY STRESS COMPONENTS  
= 0

SELECT LARGER OF 1.) AND 2.) AS  $S_{K2}$ .

$S_{K2} = 24675 \text{ PSI}$

$S_{K1} < S_{K2} \Rightarrow S_K = 16075 \text{ PSI}$

ACCORDING TO TABLE 3252.3.4 (EXPECTED MINIMUM  
STRESS-TO-RUPTURE VALUES FOR ALLOY 800H), FOR  $S_K = 15730 \text{ PSI}$   
@  $1043^\circ\text{F}$ , CREEP DAMAGE IS INSIGNIFICANT.

$\therefore$  TOTAL DAMAGE IS NEGLIGIBLE.

DESIGN IS ACCEPTABLE!

SUPPLEMENTAL ELEVATED TEMPERATURE RULES  
FOR SECTION VIII DIVISION 1

Introduction and Purpose

The basic design code for the SGS components is Section VIII Division 1 of the ASME Code. For elevated temperature service this code does address a primary creep failure mode due to pressure and dead loading conditions. There are however other creep related effects which should be addressed, therefore supplemental rules have been developed for guidance.

References 20, 22 and 14 are the principal references used in the development of the rules. Some of the material in paragraphs 3252 and 3260 are contained in reference 14, "An Interim Structural Design Standard, Jan. 1979." In the following paragraphs, the supplementary rules are presented, followed by a brief commentary on the development of the rules.

REVISION NO.	REVISION DATE	DESCRIPTION	PREPARED BY
0	Oct. 30,1981	Original Issue	EML
1	March 19,1982	Redefined stress parameter under 3251.1 Revised criteria for total creep damage in 3252.3 Revised the procedure for creep damage calculation in 3252.3 (d) Added section 3262.3 for time dependent buckling Added values for yield strength in Table 3251.1 Added Figure 3252.3.5 for creep- fatigue damage	EML

Supplementary Elevated Temperature Design Rules

For Section VIII-Division 1

-3000 DESIGN

-3100 GENERAL REQUIREMENTS FOR DESIGN

-3111 ACCEPTABILITY - An acceptable design is one which meets the requirements given below.

(a) the design satisfies the general design requirements of -3100 and the appropriate component rules in -3200.

-3200 DESIGN RULES (VESSEL)

-3210 GENERAL - The design of the pressure vessels and the vessel parts shall conform to the design requirements of -3200.

-3220 BASE DESIGN RULES

The design shall conform to the requirements of Section VIII-Division 1 of the ASME Boiler and Pressure Vessel Code. Additional requirements stated in -3250 shall also be met.

-3250 ADDITIONAL REQUIREMENTS - The additional requirements of -3251 and -3252 shall be satisfied if -3220 is used.

The buckling limits of -3260 may be used for those configurations and loading conditions for which buckling rules or charts are not provided in Section VIII-Division 1.

3251 CREEP RATCHETING EVALUATION - Ratcheting requirements for shells can be considered met for normal operating cycles if the limits of 3251.2 is satisfied. Each cycle may be evaluated independently in determining the final accumulated strain.

#### 3251.1 Parameters

(a) The following definitions apply to 3251.2 for stresses across a shell thickness.

$$x = \frac{\sigma_p}{S_y}$$

where  $\sigma_p$  is the primary pressure membrane stress and  $S_y$  is the average of the  $S_y$  values at the maximum and minimum wall-averaged temperatures during the operating cycle being evaluated. Table 3251.1 lists values for  $S_y$ .

$$y = \frac{Q_r}{S_y}$$



where  $Q_R$  is the maximum range of secondary stress occurring with X during the operating cycle being evaluated.

- (b) The following definitions apply to 3251.2 for stresses across the shell cross section.

$$x = \left( \sigma_p + \frac{\sigma_b}{1.27} \right) / S_y$$

where  $\sigma_p + \frac{\sigma_b}{1.27}$  is the primary membrane and primary

bending adjusted for bending distribution

$$y = \frac{Q_r}{S_y}$$

where  $Q_R$  is maximum range of secondary stress occurring with X during the operating cycle being evaluated.

- (c) The secondary thermal stress from radial gradients shall be based on the linearized radial gradient.

## 3251.2 Ratcheting Limits

- (a) The procedure in this paragraph may be used for shells remote from geometric and material discontinuities to show that the limits for creep ratcheting are satisfied for the stress parameter of X and Y (3251.1) occurring at temperatures in the creep regime. These temperatures are defined as those for which  $S_m$  equals  $S_t$  for  $10^5$  hours and where  $S_m$  and  $S_t$  are as defined in the ASME Code Case N-47. Figures 3251.2.1 and 3251.2.2 give these temperatures for Type 304 and Alloy 800H. Non-axisymmetric loads such as the bending of a pipe or vessel may be included as axisymmetric loads and the rules applied.

The elastically calculated primary and secondary stresses are used to determine an "effective creep stress"  $\sigma_c$ , which in turn is used to determine a total ratcheting strain. The effective creep stress  $\sigma_c$ , for any combination of loading is given in Figure 3252.2.2 in dimensionless form.

(b) The isochronous stress strain curves of T-1800 in Appendix T of Code Case N-47 may be used to obtain the creep ratcheting strain. The total service life may be subdivided into temperature-time blocks and the strain increment for each block may be evaluated separately. The strain increments for each time temperature block shall be added to obtain the total ratcheting strain. The resulting value shall be limited to 1.5%.

-3252 CREEP-FATIGUE EVALUATION - The following requirements on creep-fatigue evaluation apply to elevated temperature service.

-3252.2 RULES TO DETERMINE NEED FOR CREEP-FATIGUE ANALYSIS - A creep-fatigue evaluation need not be made provided the total number of significant load cycles is less than 25. If this condition is not met, a detailed creep-fatigue analysis shall be made in accordance with -3252.3. The load cycle is significant if any of the following is true:

(a) The range of the elastically calculated primary stress intensity is greater than 1.25 times the maximum allowable stress in Section VIII-Division 1.

- (b) The range of the elastically calculated, secondary stress intensity range is greater than 1.5 times the maximum allowable stress in Section VIII-Division 1.
- (c) The range of elastically calculated peak stress intensity range using a stress concentration factor of 2.5 at local structural discontinuities, unless otherwise specified, is greater than twice the allowable stress amplitude at  $10^6$  cycles from the design fatigue curves in Figures -3252.2.2.3.

-3252.3 CREEP-FATIGUE ANALYSIS

- (a) All significant load conditions shall be evaluated for accumulated creep and fatigue damage including hold time and strain rate effects. For a design to be acceptable, the creep and fatigue damage shall satisfy the following relation:

$$\sum_{j=1}^p \left[ \frac{n}{N_d} \right]_j + \sum_{k=1}^q \left[ \frac{t}{T_d} \right]_k \leq D \quad (1)$$

where

D = total creep-fatigue damage from Figure 3252.3.4

n = number of applied cycles of loading condition, j.

$N_d$  = number of design allowable cycles of loading condition, j.  $N_d$  is determined from one of the design fatigue curves in Figures -3252.3.1 or 3252.3.2 corresponding to the maximum metal temperature during the cycle. The design fatigue curves were determined from completely reversed loading conditions at strain rates greater than, or equal to those noted on the curves.

t = time duration of the load condition, k.

$T_d$  = allowable creep rupture time at a given stress or an effective stress from load,  $k$ .  $T_d$  values are obtained by the procedure outlined in -3252.3 (d).

- (b) Equivalent Strain Range Calculation - An equivalent strain range is used to determine  $N_d$ . When the Design Specification contains a histogram delineating a specific loading sequence, the strain range shall be calculated for the cycles described by the histogram. If the sequence of loading is not defined by the Design Specification, then an appropriate method of combining cycles shall be applied. The equivalent strain range is computed according to one of the following procedures:

Procedure 1 -General Case

Step 1 - Calculate all strain components for the strain history ( $\epsilon_x, \epsilon_y, \epsilon_z, \nu_{xy}, \nu_{yz}, \nu_{zx}$  versus time) for the complete cycle.

Step 2 - Select a time when conditions are at an extreme for the cycle, either maximum or minimum. Refer to this time point by a subscript  $i$ . In some cases it may be necessary to try different points in time to find the one which results in the largest value of equivalent strain range.

Step 3 - Calculate the history of the change in strain components by subtracting the values at the time, t, from the corresponding components at each point in time during the cycle. For example:

$$\Delta \varepsilon_x = \varepsilon_x - \varepsilon_{xi}$$

$$\Delta \varepsilon_y = \varepsilon_y - \varepsilon_{yi}$$

Step 4 - Calculate the equivalent strain range for each point in time.

$$\Delta \varepsilon_{equiv} = \frac{\sqrt{2}}{3} \left[ (\Delta \varepsilon_x - \Delta \varepsilon_y)^2 + (\Delta \varepsilon_y - \Delta \varepsilon_z)^2 + (\Delta \varepsilon_z - \Delta \varepsilon_x)^2 + \frac{3}{2} (\Delta \nu_{xy}^2 + \Delta \nu_{yz}^2 + \Delta \nu_{zx}^2) \right]^{1/2} \quad (2)$$

Procedure 2- Applicable Only When the Principal Strains do not Rotate

Step 1. No change from Step 1 of Procedure 1.

Step 2. Determine the principal strains versus time for the cycle.

Step 3. At each time interval of Step 2, determine the strain differences  $\epsilon_1 - \epsilon_2$ ,  $\epsilon_2 - \epsilon_3$ ,  $\epsilon_3 - \epsilon_1$ .

Step 4. Determine the history of the change in strain differences by subtracting the values at the time,  $t$ , from the corresponding values at each point in time during the cycle.

Designate these strain difference changes as:

$$\Delta(\epsilon_1 - \epsilon_2) = \epsilon_{12} - \epsilon_{12i}$$

$$\Delta(\epsilon_2 - \epsilon_3) = \epsilon_{23} - \epsilon_{23i}$$

$$\Delta(\epsilon_3 - \epsilon_1) = \epsilon_{31} - \epsilon_{31i}$$

Step 5. Compute the equivalent strain range as:

$$\Delta\epsilon_{equiv} = \frac{\sqrt{2}}{3} \left[ \Delta(\epsilon_1 - \epsilon_2)^2 + \Delta(\epsilon_2 - \epsilon_3)^2 + \Delta(\epsilon_3 - \epsilon_1)^2 \right]^{1/2} \quad (3)$$

(c) Fatigue Damage Evaluation

- 1) For the fatigue damage term the strain range  $\epsilon_T$  is used with the design fatigue curve Figures 3252.3.1 and 3252.3.2 to determine  $N_d$ .



- 2) The maximum total equivalent strain is obtained from the following:

$$\epsilon_T = K_\epsilon \epsilon_\epsilon + K_\epsilon^2 \epsilon_p + \epsilon_F \quad (4)$$

where

$\epsilon_T$  = the derived maximum strain for the loading condition

$\epsilon_\epsilon$  = the elastic strain in the region under consideration, exclusive of strain concentration

$K_\epsilon$  = the theoretical elastic strain-concentration factor

$\epsilon_p$  = the inelastic strain in the region under consideration, exclusive of strain concentration and peak thermal strains

$\epsilon_F$  = peak thermal strain associated with the peak thermal stress intensity

The value,  $\epsilon_p$ , is determined by subtracting the elastic strain component;  $\epsilon_e$  from the calculated total nominal strain,  $\epsilon_{equiv}$ .  $\epsilon_{equiv}$  can also be expressed as the total nominal strain,  $\epsilon_n$ , and is the sum of the load-controlled strain and deformation-controlled strain, exclusive of strain concentration and peak thermal strain. The load-controlled strain is determined by entering the appropriate isochronous stress-strain curve at a stress intensity equivalent to the load-controlled stress intensity in the region under consideration. The deformation-controlled strain is determined from the elastically calculated stress intensity due to the applied deformation.

$$\epsilon_n = \epsilon_{load-controlled} + (S_{strain-controlled}/E)$$

- 3) Equation (4) results in a conservative value of the maximum strain  $\epsilon_t$ , relative to the nominal strain level  $\epsilon_{equiv}$  or  $\epsilon_n$  when compared to the values obtained by the use of the Neuber equation. A more accurate and less conservative value may be obtained by following the procedure in Paragraph T-1432 (d) of Appendix T of ASME code case N-47.

(d) Creep-Damage Calculation -Creep damage calculations may be done by the following procedure for elastic analysis. The quantities are defined as:

- $P_m$  = Primary stress intensity
- $S_1$  = Primary + secondary stress intensity for sustained operating conditions in the load cycle k
- $S_y$  = Minimum yield strength
- $S_k$  = Stress quantity used to determine the allowable creep rupture time  $T_d$
- $\sigma_{eff}$  = Effective stress for the sustained operating conditions in the load cycle k
- $\sigma_i$  = Principal stresses
- k = Subscript of load condition

Step 1 - Calculate and determine the following stress quantities:

- 1)  $(P_m + 0.5 S_1)_k$
- 2)  $S_{yk}$  is the minimum yield strength at the average wall temperature for the sustained operating condition being analyzed in the load cycle condition k.

Select the lesser of 1) and 2) as  $S_{k1}$

Step 2 - Calculate the following stress quantities:

- 1) Effective stress:

$$\sigma_{eff} = \frac{1}{\sqrt{2}} \left[ (\sigma_1 - \sigma_2)^2 + (\sigma_2 - \sigma_3)^2 + (\sigma_3 - \sigma_1)^2 \right]^{1/2}$$

- 2) The largest principal tensile stress component of the primary-plus-secondary stresses during the sustained portion of the load cycle  $k$  being analyzed.

Select the larger of 1) and 2) above and designate as  $S_{k2}$ . If this value is less than  $S_{k1}$  from step 1, use this quantity as  $S_k$  in Step 3. If this value is greater than  $S_{k1}$ , use  $S_{k1} = S_k$  in Step 3.

Step 3 - Enter the stress-to-rupture curves in Figure 3252.3.3 and Table 3252.3.3 or Figure 3252.3.4 and Table 3252.3.4, with  $S_k$  from Step 2 to determine the value of allowable time  $T_d$ .

-3260 BUCKLING INSTABILITY LOADS

-3261 GENERAL REQUIREMENTS

- (a) Scope of Rules - The stability limits in Section VIII-Division 1 and 2 pertain only to specific geometrical configurations under specific loading conditions. These limits include the effects of initial geometrical imperfections permitted by fabrication tolerances. The rules in Paragraphs -3131, and -3132 of Code Case N-253 provide additional limits which are applicable to general configurations and loading conditions that may cause buckling or instability.

(b) Load-Controlled and Strain-Controlled Buckling - For the limits specified in -3262.2, distinction is made between load-controlled buckling and strain-controlled buckling. Load-controlled buckling is characterized by continued application of an applied load in the post-buckling regime leading to failure, as exemplified by collapse of tube under external pressure. Strain-controlled buckling is characterized by the immediate reduction of load due to strain-induced deformations. Even though it is self-limiting, strain-controlled buckling should be avoided to guard against failure by fatigue, excessive strain, loss of function due to excessive deformation, and interaction with load-controlled buckling.

(c) Interaction of Load-Controlled and Strain-Controlled Buckling - For conditions under which strain-controlled and load-controlled buckling may interact, as exemplified by elastic follow-up, the higher load factors applicable to load-controlled buckling shall be used for the combination of load-controlled and strain-controlled loadings.

- (d) Effect of Initial Geometry Imperfections - For load-controlled buckling, the effects of initial geometrical imperfections and tolerances shall be considered in the time-independent calculations according to the requirements of Paragraph -3262.2. In calculating the instability strain under pure strain-controlled buckling, the effects of geometrical imperfections and tolerances, whether initially present or induced by service, need not be considered.
- (e) Strain-Controlled Buckling - The evaluation of strain-controlled buckling is not mandatory. However, the strain-controlled buckling limits provided in -3262.2 may be used if such evaluation is deemed necessary.
- (f) Creep Buckling - The evaluation of time-dependent buckling is not mandatory.

-3262 BUCKLING LIMITS (Time-Independent)

-3262.1 Buckling limits of Section VIII-Division 1 or Division 2 shall apply. These rules provide buckling charts which are applicable to limited geometrical configurations under specific loading conditions. For general configurations and loading conditions, and for materials and temperatures for which limits of Section VIII-Divisions 1 or 2 do not apply, the limits of -3132 of Code Case N-253 may be used.

-3262.2 For load-controlled buckling, the load factor, and for strain-controlled buckling, the strain factor, shall equal or exceed the values given in Table -3262-2.

Table -3262-2 Buckling Limits

Loads	Load Factor <sup>1</sup>	Strain Factor <sup>1,3</sup>
Design	3.0 <sup>2</sup>	1.67
Testing <sup>4</sup>	2.25	1.67
Normal Operating		
Steady State	3.0	1.67

<sup>1</sup>Load (Strain) = Load (strain) which would cause instant instability at the design or actual service temperature Design or expected load (strain).

<sup>2</sup> Changes in configuration induced by service need not be considered in calculating the buckling load.

<sup>3</sup> For thermally-induced strain-controlled buckling, the strain factor is applied to loads induced by thermal strain. To determine the buckling strain, it may be necessary to artificially induce high strains concurrent with the use of realistic stiffness properties. The use of an "adjusted" thermal expansion coefficient is one technique for enhancing the applied strains without affecting the associated stiffness characteristics.

<sup>4</sup> These factors apply to hydrostatic, pneumatic, and leak tests.

-3262.3 Time-Dependent Buckling - To protect against load-controlled time-dependent creep buckling, it shall be demonstrated that instability will not occur during the specified lifetime for a load history obtained by multiplying the specified Service Loading by the factor given in Table 3262.3. A design factor is not required for purely strain-controlled buckling because strain-controlled loads are reduced concurrently with resistance of the structure to buckling when creep is significant.

Table 3262.3

Time-Dependent Load-Controlled Buckling  
Factors

Service Loadings

Normal Operating

Steady State

1.5



Table 3251.1

Yield Strength Values,  $S_y$ , vs. Temperature

Temp., F	304 SS	316 SS	Ni-Fe-Cr Alloy 800H
	(Stresses in ksi Units)		
RT	30.0	30.0	25.0
100	28.8	29.2	24.3
200	25.0	25.8	22.5
300	22.5	23.3	21.1
400	20.7	21.4	20.0
500	19.4	19.9	19.0
600	18.2	18.8	18.3
700	17.7	18.1	17.5
750	17.3	17.8	17.2
800	16.8	17.6	17.0
850	16.5	17.4	16.6
900	16.2	17.3	16.5
950	15.9	17.1	16.2
1000	15.6	17.0	16.0
1050	15.2	16.7	15.8
1100	14.7	16.5	15.6
1150	14.4	16.4	15.5
1200	14.1	16.2	15.3
1250	13.7	15.8	15.1
1300	13.2	15.3	14.7
1350	12.5	14.9	14.5
1400	11.6	14.4	14.0
1450	10.6	13.8	13.5
1500	9.5	13.1	13.0
1550			12.0
1600			11.2

Table 3251.2.1  
 Smt - Allowable Stress Intensity Values, Ksi  
 Type 304 SS - 30-YS, 75-UTS (30-YS, 70-UTS)

Temp. °F	1 hr	10 hr	30 hr	10 <sup>2</sup> hr	3 x 10 <sup>2</sup> hr	10 <sup>3</sup> hr	3 x 10 <sup>3</sup> hr	10 <sup>4</sup> hr	3 x 10 <sup>4</sup> hr	10 <sup>5</sup> hr	3 x 10 <sup>5</sup> hr
800	15.1	15.1	15.1	15.1	15.1	15.1	15.1	15.1	15.1	15.1	15.1
850	14.8	14.8	14.8	14.8	14.8	14.8	14.8	14.8	14.8	14.8	14.8
900	14.6	14.6	14.6	14.6	14.6	14.6	14.6	14.6	14.6	14.6	14.6
950	14.3	14.3	14.3	14.3	14.3	14.3	14.3	14.3	14.3	14.3	14.2
1000	14.0	14.0	14.0	14.0	14.0	14.0	14.0	14.0	13.1	11.1	9.3
1050	13.6	13.6	13.6	13.6	13.6	13.6	13.6	12.2	10.3	8.7	7.3
1100	13.2	13.2	13.2	13.2	13.2	13.2	11.5	9.7	8.2	6.8	5.7
1150	12.9	12.9	12.9	12.9	12.9	11.0	9.3	7.7	6.4	5.3	4.4
1200	12.7	12.7	12.7	12.2	10.6	8.9	7.4	6.1	5.1	4.1	3.4
1250	12.3	12.3	11.9	10.3	8.7	7.2	5.9	4.9	4.0	3.2	2.7
1300	11.9 (11.8)	11.4	10.0	8.5	7.0	5.9	4.8	3.9	3.2	2.5	2.1
1350	10.9 (10.5)	9.7	8.4	7.1	5.9	4.8	3.9	3.1	2.5	2.0	1.6
1400	9.5 (9.0)	8.1	6.9	5.9	4.8	3.9	3.1	2.5	2.0	1.6	1.2
1450	8.2 (7.5)	6.8	5.8	4.6	3.8	3.0	2.4	1.9	1.5	1.2	0.9
1500	7.0 (6.4)	5.3	4.4	3.5	2.8	2.2	1.7	1.3	1.0	0.8	0.6

Figure 3251.2.1 Smt - Type 304 SS

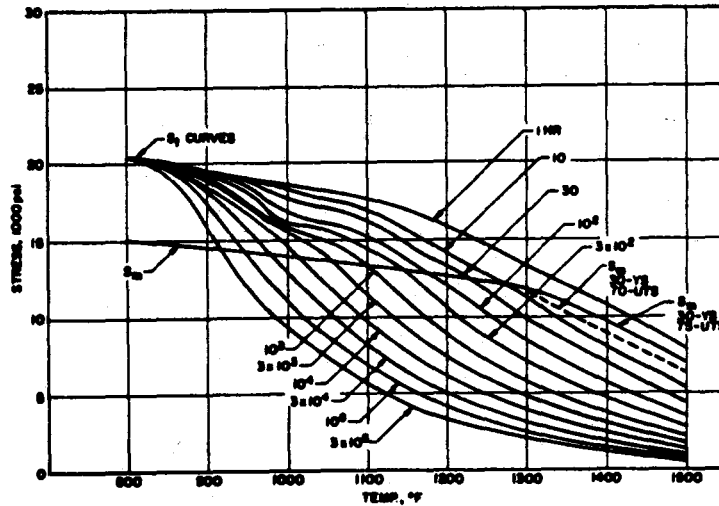


Table 3251.2.2  
 Ni-Fe-Cr (Alloy 800H), Smt Allowable Stress Intensity Values, Ksi

Temp. °F	1 hr	10 hr	30 hr	100 hr	300 hr	1000 hr	3000 hr	10,000 hr	30,000 hr	100,000 hr	300,000 hr
800	15.3	15.3	15.3	15.3	15.3	15.3	15.3	15.3	15.3	15.3	15.3
850	15.1	15.1	15.1	15.1	15.1	15.1	15.1	15.1	15.1	15.1	15.1
900	14.8	14.8	14.8	14.8	14.8	14.8	14.8	14.8	14.8	14.8	14.8
950	14.6	14.6	14.6	14.6	14.6	14.6	14.6	14.6	14.6	14.6	14.6
1000	14.4	14.4	14.4	14.4	14.4	14.4	14.4	14.4	14.4	14.4	14.4
1050	14.3	14.3	14.3	14.3	14.3	14.3	14.3	14.3	14.3	14.3	14.3
1100	14.1	14.1	14.1	14.1	14.1	14.1	14.1	14.1	13.6	11.7	10.3
1150	13.9	13.9	13.9	13.9	13.9	13.9	13.9	12.0	10.5	9.1	8.0
1200	13.8	13.8	13.8	13.8	13.8	12.5	10.9	9.4	8.2	7.2	6.4
1250	13.5	13.5	13.5	13.3	11.5	9.8	8.6	7.5	6.6	5.8	5.1
1300	13.2	13.2	12.4	10.5	9.1	7.9	6.9	6.0	5.3	4.6	4.1
1350	12.0	11.4	9.9	8.4	7.4	6.4	5.6	4.9	4.3	3.7	3.3
1400	11.0	9.2	8.0	6.8	6.0	5.2	4.6	4.0	3.5	3.0	2.6

Figure 3251.2.2  $S_{mt}$  - Ni-Fe-Cr (Alloy 800H)

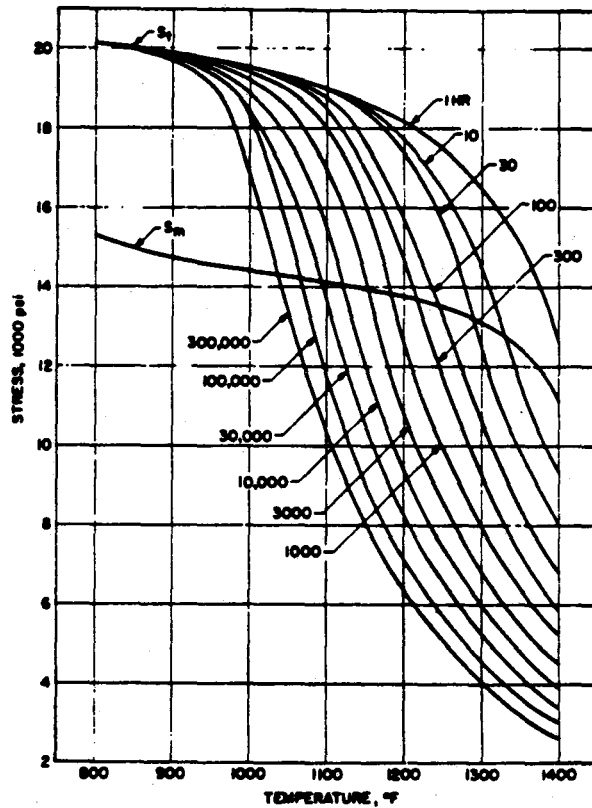


Figure 3252.2.2 Strain Limits Using Elastic Analysis

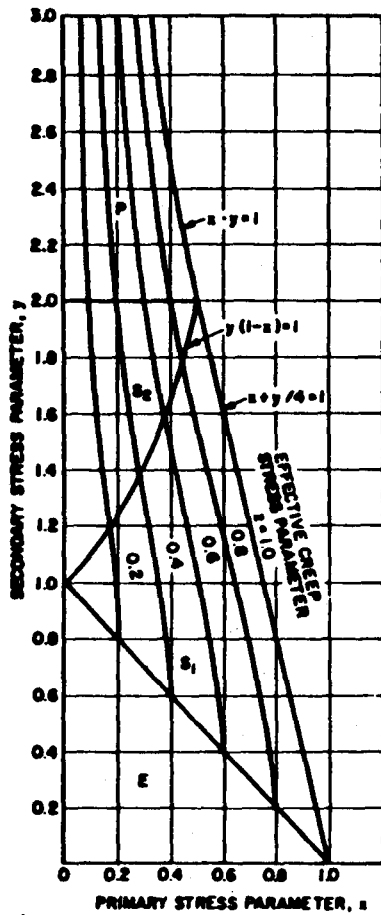


Figure 3252.2.3 Design Fatigue Strength,  $S_a$ , For High-Alloy Steels and Ni-Cr-Fe Alloys up to 1200°F

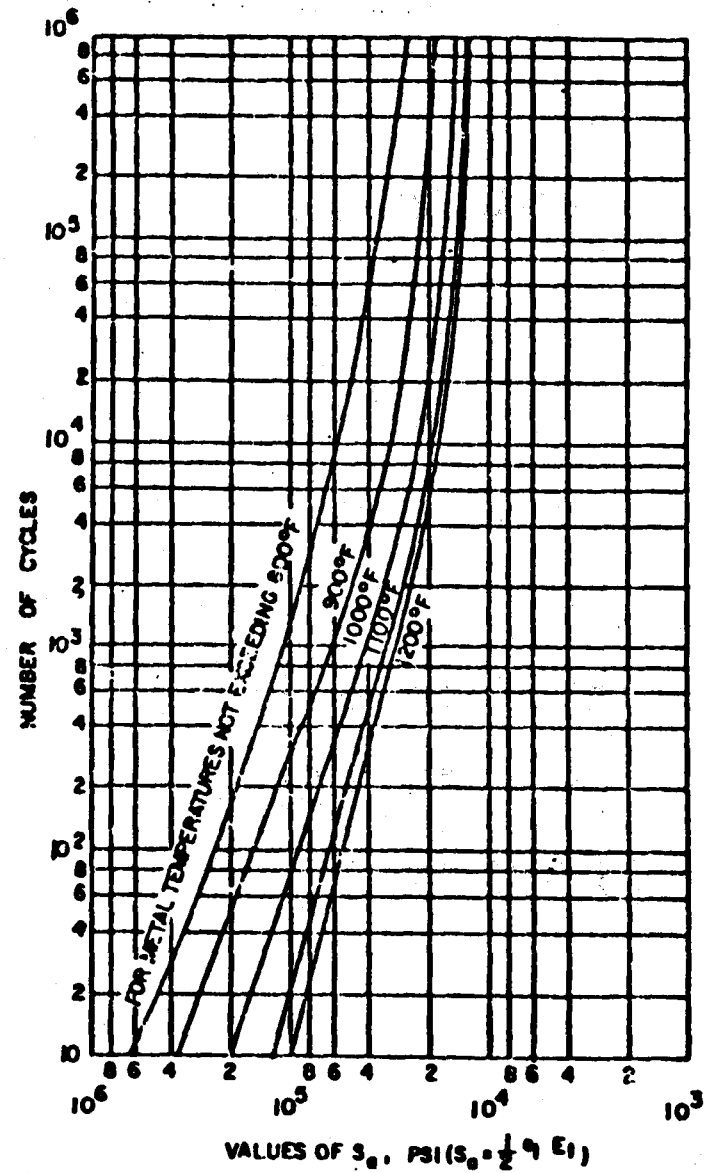


Table 3252.3.1  
Design Fatigue Strain Range,  $\epsilon_t$ , for 304 SS

$N_f$ Number of Cycles*	$\epsilon_t$ Strain Range (in./in.) at Temperature						
	100 F	800 F	900 F	1000 F	1100 F	1200 F	1300 F
10	0.051	0.050	0.0465	0.0425	0.0382	0.0335	0.0297
20	0.036	0.0345	0.0315	0.0284	0.025	0.0217	0.0186
40	0.0263	0.0246	0.0222	0.0197	0.017	0.0146	0.0123
$10^2$	0.018	0.0164	0.0146	0.0128	0.011	0.0093	0.0077
$2 \times 10^2$	0.0142	0.0125	0.011	0.0096	0.0082	0.0069	0.0057
$4 \times 10^2$	0.0113	0.00965	0.00845	0.00735	0.0063	0.00525	0.00443
$10^3$	0.00845	0.00725	0.0063	0.0055	0.0047	0.00385	0.00333
$2 \times 10^3$	0.0067	0.0059	0.0051	0.0045	0.0038	0.00315	0.00276
$4 \times 10^3$	0.00545	0.00485	0.0042	0.00373	0.0032	0.00263	0.0023
$10^4$	0.0043	0.00385	0.00335	0.00298	0.0026	0.00215	0.00185
$2 \times 10^4$	0.0037	0.0033	0.0029	0.00256	0.00226	0.00187	0.00158
$4 \times 10^4$	0.0032	0.00287	0.00254	0.00224	0.00197	0.00162	0.00138
$10^5$	0.00272	0.00242	0.00213	0.00188	0.00164	0.00140	0.00117
$2 \times 10^5$	0.0024	0.00215	0.0019	0.00167	0.00145	0.00123	0.00105
$4 \times 10^5$	0.00215	0.00192	0.0017	0.0015	0.0013	0.0011	0.00094
$10^6$	0.0019	0.00169	0.00149	0.0013	0.00112	0.00096	0.00084

\*Cyclic strain rate:  $1 \times 10^{-3}$  in./in./sec.

Figure 3252.3.1 Design Fatigue Strain Range,  $\epsilon_t$ , For 304 SS

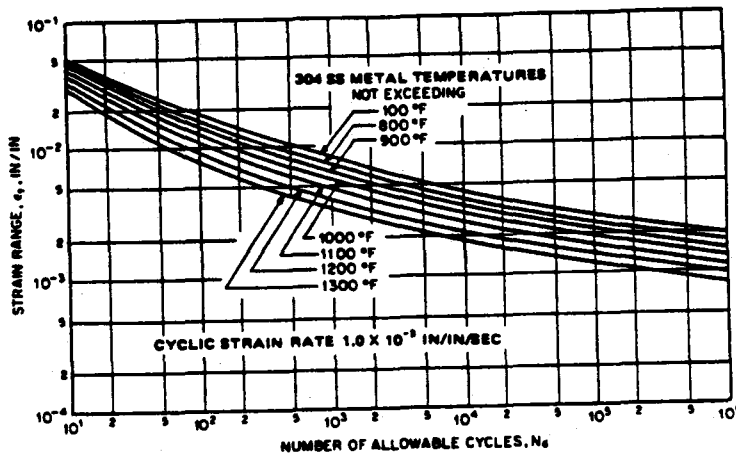


Table 3252.3.2  
Design Fatigue Strain Range,  $\epsilon_t$ , For Ni-Fe-Cr, Alloy 800H

$N_d$ Number of Cycles*	$\epsilon_t$ , Strain Range (in./in.) at Temperature						
	800 F	900 F	1000 F	1100 F	1200 F	1300 F	1400 F
10 <sup>1</sup>	.0513	.0498	.0468	.0378	.0308	.0263	.0231
2x10 <sup>1</sup>	.0328	.0313	.0298	.0243	.0198	.0168	.0129
4x10 <sup>1</sup>	.0218	.0208	.0190	.0163	.0130	.0113	.00866
10 <sup>2</sup>	.0139	.0129	.0119	.01	.00823	.00725	.00566
2x10 <sup>2</sup>	.0103	.00939	.00861	.00722	.00603	.00535	.00426
4x10 <sup>2</sup>	.00777	.00699	.00641	.00542	.00463	.00405	.00331
10 <sup>3</sup>	.00537	.00489	.00441	.00392	.00328	.00285	.00254
2x10 <sup>3</sup>	.00427	.00379	.00351	.00312	.00261	.0023	.00209
4x10 <sup>3</sup>	.00347	.00314	.00291	.00259	.00213	.00195	.00176
10 <sup>4</sup>	.00277	.00249	.00233	.0021	.00174	.00159	.00143
2x10 <sup>4</sup>	.00242	.00219	.00201	.00182	.00155	.00142	.00125
4x10 <sup>4</sup>	.00215	.00193	.0018	.00162	.0014	.00127	.00109
10 <sup>5</sup>	.00187	.00164	.00151	.00139	.00122	.00115	.000959
2x10 <sup>5</sup>	.00169	.00149	.00141	.00128	.00113	.00105	.000919
4x10 <sup>5</sup>	.00157	.00139	.00129	.00121	.00108	.000987	.000889
10 <sup>6</sup>	.00139	.00129	.00119	.00112	.00103	.000937	.000869

\*Cyclic strain rate:  $1 \times 10^{-3}$  in./in./sec.

Figure 3252.3.2 Design Fatigue Strain Range,  $\epsilon_t$ , For Ni-Fe-Cr Alloy 800H

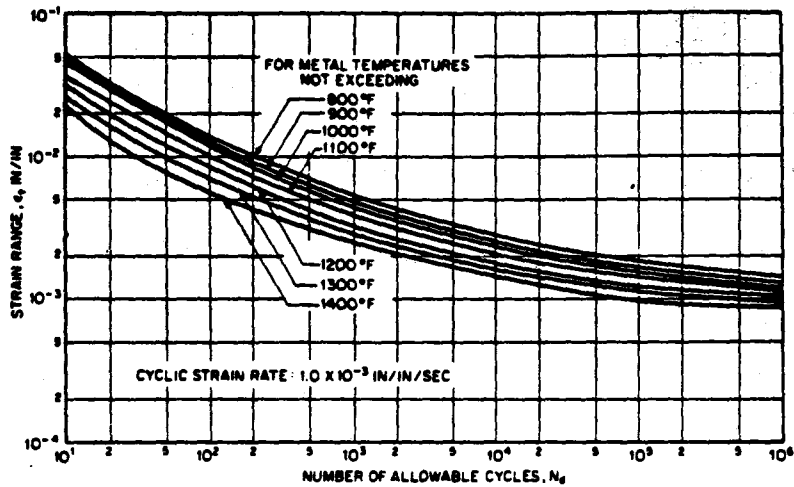


Table 3252.3.3  
 Expected Minimum Stress-To-Rupture Values For Type 304 SS, Ksi

Temp., °F	1 hr	10 hr	30 hr	10 <sup>2</sup> hr	3 x 10 <sup>2</sup> hr	10 <sup>3</sup> hr	3 x 10 <sup>3</sup> hr	10 <sup>4</sup> hr	3 x 10 <sup>4</sup> hr	10 <sup>5</sup> hr	3 x 10 <sup>5</sup> hr
800	57	57	57	57	57	57	57	57	51	44.3	39
850	54.5	54.5	54.5	54.5	54.5	54.5	50.2	45.4	40	34.7	30.5
900	55.5	55.5	55.5	55.5	51.5	46.9	41.2	36.1	31.5	27.2	24
950	54.2	54.2	51	48.1	43	38.0	33.5	28.8	24.9	21.2	18.3
1000	52.5	50	44.5	39.8	35	30.9	26.5	22.9	19.7	16.6	14.0
1050	50	41.9	37	32.9	28.9	25.0	21.6	18.2	15.5	13.0	11.0
1100	45	35.2	31	27.2	23.9	20.3	17.3	14.5	12.3	10.2	8.6
1150	38	29.5	26	22.5	19.3	16.5	13.9	11.6	9.6	8.0	6.6
1200	32	24.7	21.5	18.6	15.9	13.4	11.1	9.2	7.6	6.2	5.0
1250	27	20.7	17.9	15.4	13	10.8	8.9	7.3	6.0	4.9	4.0
1300	23	17.4	15	12.7	10.5	8.8	7.2	5.8	4.8	3.8	3.1
1350	19.5	14.6	12.6	10.6	8.8	7.2	5.8	4.6	3.8	3.0	2.4
1400	16.5	12.1	10.3	8.8	7.2	5.8	4.7	3.7	3.0	2.3	1.9
1450	14.0	10.2	8.8	7.3	5.8	4.6	3.8	2.9	2.3	1.8	1.4
1500	12.0	8.6	7.2	6.0	4.9	3.8	3.0	2.4	1.8	1.4	1.1

Figure 3252.3.4 Minimum Stress-To-Rupture Values For Type 304 SS, Ksi

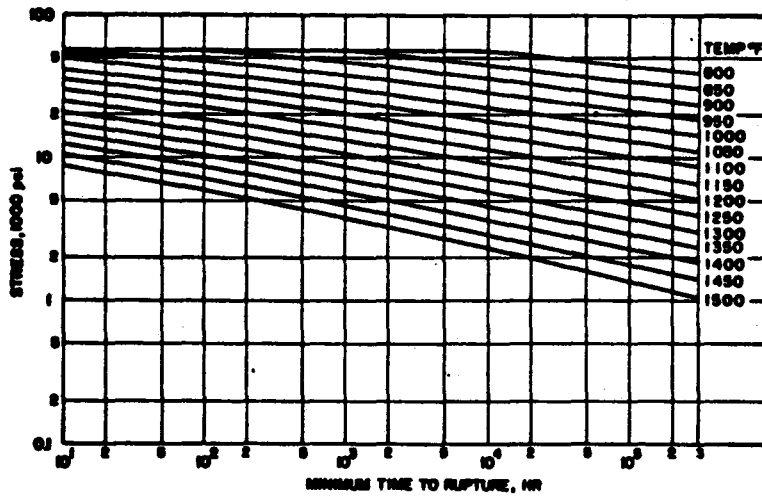


Table 3252.3.4  
 Expected Minimum Stress-To-Rupture Values For Ni-Fe-Cr Alloy 800H, Ksi

Temp., °F	1 hr	3 hr	10 hr	30 hr	100 hr	300 hr	1000 hr	3000 hr	10000 hr	30000 hr	100000 hr	300000 hr
800	60.7	60.7	60.7	60.7	60.7	60.7	60.7	60.7	60.7	60.7	60.7	60.7
850	60.7	60.7	60.7	60.7	60.7	60.7	60.7	60.7	60.7	57.5	53.5	49.3
900	60.7	60.7	60.7	60.7	60.7	60.7	57.9	53.8	49.4	45.5	41.5	38.0
950	60.7	60.7	60.7	60.7	59.0	54.7	50.1	46.1	41.9	38.2	34.4	31.2
1000	60.7	60.7	60.7	56.3	51.5	47.2	42.8	39.0	35.0	31.6	28.2	25.4
1050	60.7	58.5	53.5	49.0	44.3	40.3	36.1	32.6	29.0	25.9	22.9	20.4
1100	56.1	51.4	46.5	42.2	37.8	34.0	30.1	26.9	23.7	21.1	18.4	16.3
1150	49.3	44.7	40.0	36.0	31.8	28.4	24.9	22.1	19.3	17.0	14.7	12.9
1200	42.9	38.5	34.1	30.3	26.6	23.5	20.5	18.0	15.5	13.6	11.7	10.2
1250	37.0	32.9	28.8	25.4	22.1	19.3	16.7	14.5	12.5	10.9	9.3	8.1
1300	31.6	27.8	24.1	21.0	18.2	15.8	13.5	11.7	10.0	8.6	7.4	6.4
1350	26.0	23.4	20.1	17.5	14.9	12.9	10.9	9.4	8.0	6.9	5.8	5.0
1400	22.6	19.6	16.7	14.4	12.2	10.4	8.8	7.5	6.4	5.5	4.6	4.0

Figure 3252.3.4 Minimum Stress-To-Rupture Values For Ni-Fe-Cr Alloy 800H, Ksi

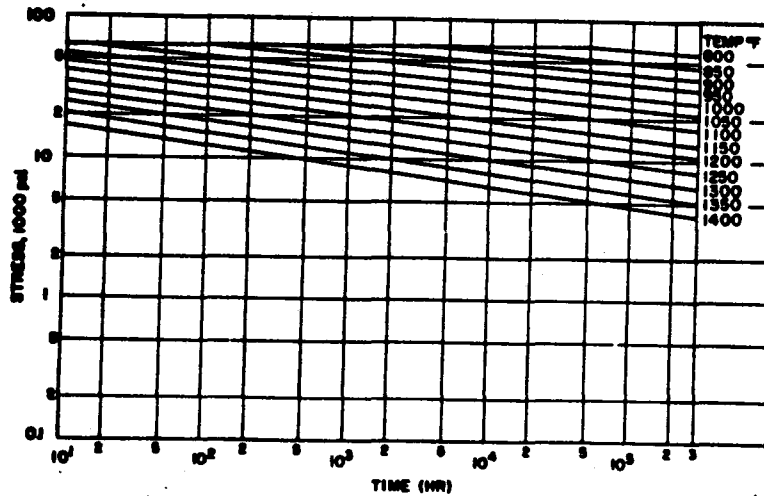
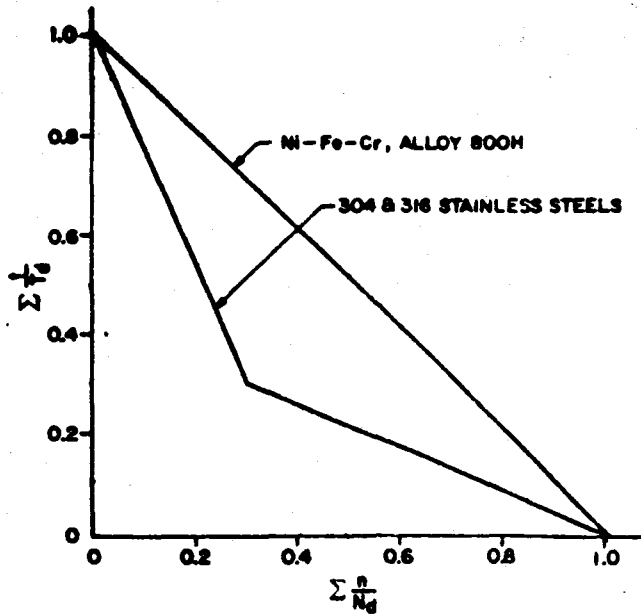




Table 3252.3.5  
Creep-fatigue damage envelope



Commentary to the Supplemental Elevated Temperature  
Rules for Section VIII Division 1

Introduction and Purpose

The basic design code for the SGS and receiver components is Section VIII Division 1 of the ASME Code. For elevated temperature service this code does address a primary creep failure mode due to pressure and dead loading conditions. There are however other creep related effects which should be addressed, therefore supplemental rules have been developed for guidance.

References 20, 22, and 14 are the principal references used in the development of the rules. Some of the material in paragraphs 3252 and 3260 are contained in reference 14, "An Interim Structural Design Standard, Jan. 1979".

-3251 Evaluation for the potential ratcheting of the main shell pressure boundaries is necessary for several reasons:

- 1) There is very little creep-fatigue data existing for conditions where the mean strain may be continually rising. When ratcheting occurs the mean strain continually rises leading to unknown effects on creep-fatigue damage.
- 2) In low temperature design by Section III, the limit of  $3 S_m$  assures shakedown and therefore the determination of peak fatigue stress ranges by elastic analysis will be valid. Although for elevated temperature the  $3 S_m$  limit need not apply, there should be some assurance that shakedown limits are not excessively exceeded in order again that elastically calculated peak stresses can validly be used for fatigue evaluations.
- 3) The ratcheting evaluation results of accumulated strain are needed for comparison to safe limits for progressive distortion.

O'Donnell in Reference 21 points out that the procedure in his report (and incorporated in N-47) does not account for strain hardening and could be approximated by using a higher effective yield strength. In these supplementary rules strain hardening could be accounted for by using a value of yield exhibiting strain hardening. However, until strain hardening values are available, the yield strength values given in reference 20 will be used.

-3251.2 The requirements of paragraph T-1324 of Appendix T (Reference 20) limits the ratcheting rules to locations away from structural discontinuities. This is consistent with the development work done in Reference 21. O'Donnell in Reference 21 has developed the upper bound accumulated strain due to creep-ratcheting using the concept of interacting circumferential principal stresses for the thermal stresses and membrane pressure stress. Since there will not in general be primary bending across the vessel walls, the procedure will apply to cylindrical or spherical shells having primary membrane stress and secondary thermal bending stresses through the vessel wall. Therefore, the creep-ratcheting procedure in the supplementary rules will apply only to cylindrical and spherical shells at locations removed at least an attenuation length of  $2.5\sqrt{RT}$  away from geometric or material structural discontinuities.

O'Donnell in Reference 21 uses the maximum surface stress as the linearized stress and states that this is conservative. In the supplementary procedure the actual linearized value will be used.

Reference 20 limits the elastic stress ratcheting procedure to loading cases where at least one stress extreme is below the creep regime. In the supplementary rules this requirement is deleted, and the procedure will be used without this restriction. The reason being that an elastic analysis alternative is not available, therefore it can be used without restriction and consider the effect in setting the limits.

The procedure can also be used for circular cross-sectional bending and longitudinal pressure membrane, e.g., piping or shells. In this case, there could be primary bending in addition to primary membrane. The expression for the stress parameter  $X$  in this case is based on using a bending distribution factor of  $K_t = 1.27$  for thin tubes as discussed in Section 5.4 of Reference 22.

- 3251.2 (b) (1) CC N-47 requires that the effective creep stress  $\sigma_c$  be increased by 1.25. This is a result of basing the evaluation on minimum isochronous curves and making the assumption that they will be 25% lower than the "average" curves given in T-1800 of N-47. This is discussed in Reference 22 Section 6.4.2. In this procedure the evaluation will be based on the average curves, therefore the 1.25 will be replaced by 1.
- (2) O'Donnell in Reference 21 concludes the residual stresses relax, therefore do not influence long term effects. However, because of the uncertainties of weld material properties and degree of residuals, strain limits for weld was recommended to be reduced by an arbitrary amount of one-half. The resulting limits were set to e 1% for base metal and 1/2% for weld metal. However, Section 6.2 of Reference 20 sets a limit 1% for membrane strain and 2% for bending. The stress parameters for the ratcheting rules are both membrane and bending.

Therefore, this procedure will allow for this by setting the limit at an average value of 1.5%. The concern for welds has not been conclusively proven and since there is conservatism in the rules, the limit of 1.5% will also apply to welds.

- (3) CC N-47 in paragraph T-132(d) requires consideration of stress "elastic follow-up". As discussed in Section 9.3 of Reference 22, this concern is addressed mainly to piping where the system can have significant unbalanced stiffness. This section cites that a "built-in" cylinder is another example, however, admits that requiring it to be included as a primary bending source is conservative and not fully justified. Therefore in this procedure, this conservative follow-up requirement will not be applied.

- 3252.3 (c) (1) The effect of fatigue life due to slow strain rates or cycling with hold times has not been well defined or quantified. One of the factors known to be involved is the relaxation of peak residual thermal stresses. In this supplementary procedure fatigue will be evaluated using the continuous cycling fatigue design curves in lieu of the conservative hold time fatigue curves, and the effect of the peak residual thermal stresses will be included in determining the creep life-fraction ratio. This will avoid double counting creep that may be done by using hold time curves.

(2) The equation for determining the maximum strain is from Reference 21 Section 7.72. This equation is considered to be the most appropriate for these simplified rules and is judged to provide adequate conservatism in accounting for plastic strain concentration.

3252.3(d)

In section 7.7.3 of reference 22 the philosophy and assumptions are given for the rules developed for determining the time fraction of creep damage. Because of residual stress relaxation it was assumed that an upper bound of primary plus secondary stress during a sustained condition would be the yield strength. The rules as written in N-47 Appendix T-1433 required a factor of 1.25 to be applied. A surmise is that this factor is to adjust the minimum values of yield strength to an average value. In the Supplementary rules the factor is reduced to 1. The reason for this is that the stress to rupture curves used in finding the allowable time are based on minimum times to rupture, therefore the additional conservatism of applying the 1.25 factor is not required in order to have a safe analysis. In other words, it is consistent to use minimum yield strength for correlation with minimum stress rupture data.

There are test data results cited in Section 4 of reference 14 that show for types 304 and 316 stainless steels, only the tensile stress contributes to creep damage. However, insufficient data are available to verify this for Incoloy 800 material, therefore the "effective stress" should be used. The Supplementary rules provide steps for analyzing either case to assure that the most valid quantity is considered.

Appendix T-1431 of reference 20 limits the total creep-fatigue damage to unity for an elastic analysis. In the Supplementary rules the total creep-fatigue damage is limited to the more conservative creep-damage envelope based on Figure T-1420-2 of reference 20. The reason for this change is that the Supplementary rules allow the use of the less conservative inelastic fatigue curves, therefore any unaccounted for cyclic hold time creep will be covered by the additional conservatism in the damage envelope.





# **Appendix C**

## **Control System Design**

Handwritten text, possibly a signature or name, located in the center of the page.

# TABLE OF CONTENTS

	Page
Glossary	C-1
Summary	C-3
1. Introduction	C-4
1.1 Previous Control System Analysis	
1.2 The Cloud Transient Problem	
1.3 The Receiver Configuration	
1.4 Control Requirements	
1.5 Control Techniques	
1.6 Method of Analysis	
2. Two Point Temperature Feedback	C-11
2.1 Description	
2.2 Simulation Runs	
2.3 Conclusions	
3. Quasi-FeedForward Control (QFFC)	C-19
3.1 Basic QFFC	
3.2 QFFC with Salt Temperature Limitation	
3.3 QFFC with Salt and Wall Temperature Limitation	
3.4 Optimal Filters	
3.5 Optimal Control	
3.6 Maximum Thermal Load	
3.7 Group Cloud Transient	
4. Control for Start-up and Operation	C-51
4.1 Salt Flow Control Functions	
4.2 Salt Flow Control During Receiver Operation	
4.3 Receiver Warm and Fill Procedure	
4.4 Receiver Trip Conditions	
5. Control Hardware	C-59
5.1 Salt Flow Control Valves	
5.2 Hardware for Control Algorithms	
5.3 Instrumentation for Control and Data Acquisition	
6. Conclusions	C-70

## Glossary

$T_{O_{sp}}$	= required temperature of salt leaving receiver (set-point)
$\dot{m}_D$	= demanded salt flow rate
$T_m$	= mid-point temperature measurement
$T_{m_r}$	= mid-point temperature reference (set-point)
$T_o$	= end-point temperature measurement
$T_{o_r}$	= end-point temperature reference
$Cl, \epsilon T_o$	= control gains
$\Delta t$	= sample period
$Q_E$	= estimated absorbed power
$\dot{m}$	= measured salt flow rate
$C_p$	= $\partial H / \partial T$ for salt
$m$	= mass of salt in receiver
$T_o$	= temperature of salt leaving receiver
$T_i$	= temperature of salt entering receiver
$\dot{T}$	= differential of temperature w.r.t. time
$N$	= number of panels in the receiver
$m_n$	= mass of salt in panel n
$T_{o_n}$	= temperature of salt leaving panel n
$m$	= valve stem position, $m \in [0,1]$
$R$	= valve rangeability (assumed = 50)
$a_*$	= fractional open of valve, $a \in [0,1]$
$\rho$	= density of salt
$\Delta P_{v_{min}}$	= the pressure drop across the valves fully open
QFFC	= Quasi-Feedforward Control
OQFFC	= Optimal Quasi-Feedforward Control

## Summary

This report documents the results of a study into the control of a thermal receiver. The study was centered on a quad-cavity receiver and analyzed the effect of passing cloud on performance. The result for an advanced control algorithm show the receiver to be controllable within the temperature constraints imposed even in a worst case environment.

# 1. INTRODUCTION

## 1.1 Previous Control System Analysis

The development of the Molten Salt Receiver Subsystem (RS) control system has been based on previous work performed by Martin Marietta. The past analysis made use of a computer simulation to predict performance using two control concepts: two point temperature feedback (ref 1) and quasi-feedforward control (ref 2). In each case, the aim was to control salt outlet temperature from the receiver while random, unmeasured solar fluxes impinged onto the receiver.

The first technique, two point temperature feedback, uses two reference points on the receiver to generate error for control command. The errors in the salt outlet temperature and salt temperature measurement part way along the receiver are both used to determine the required salt flow. As will be shown, this technique suffers two draw backs. First, the mid-point temperature reference is sensitive to changes in the spacial distribution of flux. Secondly, the flux disturbance period tends to be significantly faster than the salt residence time between temperature measurement locations. These two problems present a conflict in setting control gains that will be both stable and effective in minimizing the errors.

One method of eliminating this problem is to measure salt temperature at the header of every panel on the receiver. This ensures a residence time between measurements that is sufficiently smaller than the flux disturbance period. These measurements are used to estimate absorbed thermal power which in turn is used to set the control demand. This quasi-feedforward control (QFFC) has been demonstrated using both simulation techniques and the Salt Receiver Experiment at Sandia Labs, Albuquerque. Figure 1.1 show results from the SRE where a simple form of QFFC was employed.

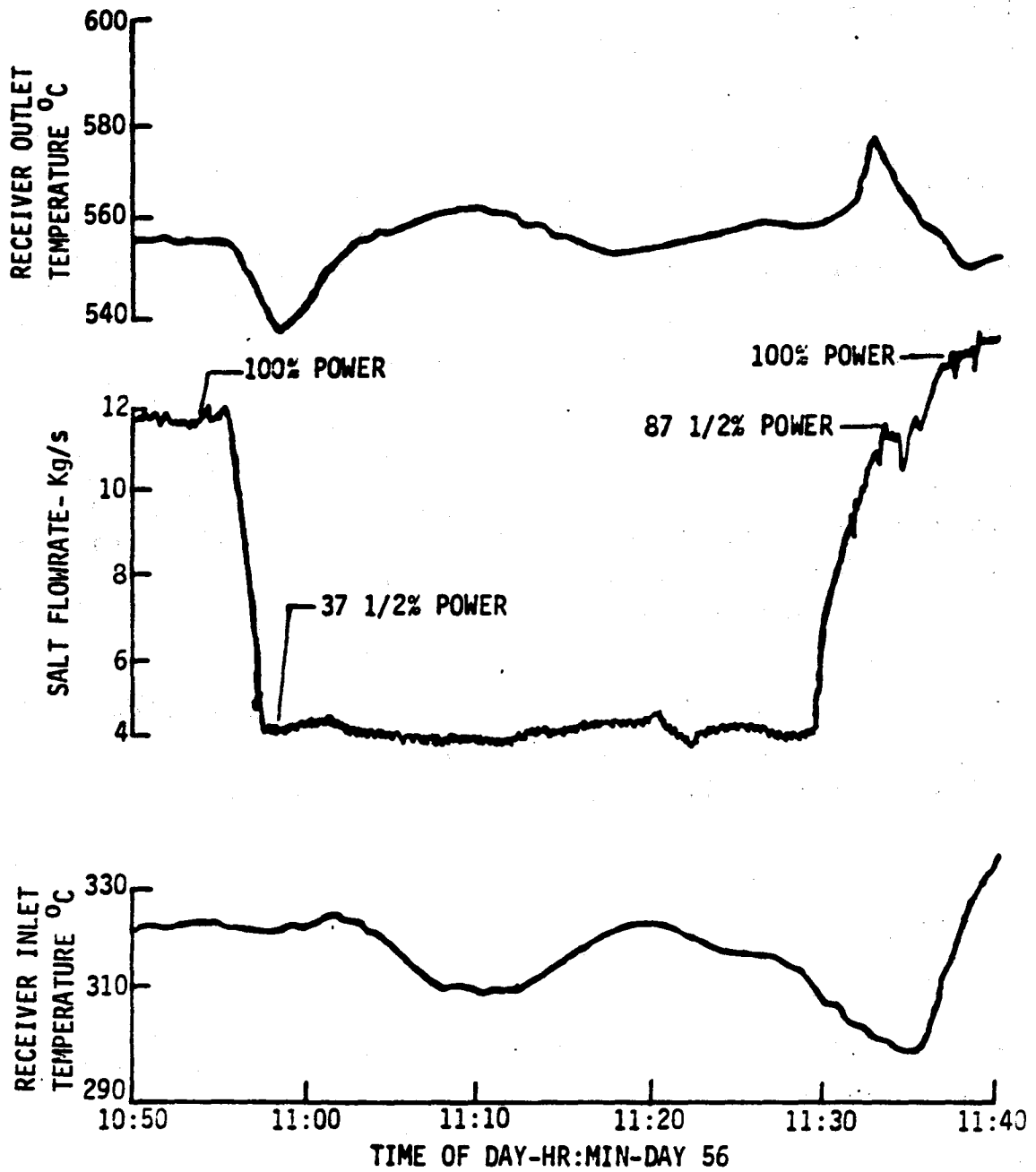


FIGURE 1.1 - SRE RESPONSE TO FLUX DISTURBANCE WITH QUASI-FEEDFORWARD CONTROL (EXPERIMENTAL DATA)



With the QFFC developed during the present program, deviations from set-points are minimized even with the most severe cloud transients. The development also illustrated the ability of QFFC to ensure against overheating the receiver tubes during severe transients.

## 1.2 The Cloud Transient Problem

The analysis of the RS control problem has been centered on what is considered to be the most severe transient. This is represented by a cloud moving off a field of heliostats such that the flux pattern is varied not just in time but in space also.

This presents two severe problems for the control system. First, the salt flow through the receiver (with the cloud over the field) is initially low resulting in very large residence times and a consequent tendency towards instability. Secondly, the variation in flux patterns that increase in magnitude affects an overheating of the receiver. As the thermal design is so close to limits, such deviation could be damaging and are thus undesirable.

Analysis has been generally limited to this worst case condition as defined in paragraph 1.4.4. It will be shown that such a cloud transient is controllable using an advanced form of QFFC.

## 1.3 The Receiver Configuration

The Receiver schematic shown in Figure 1.2 shows the configuration considered in this study. The essential features are:

- a. The salt flow through each of the four sets of panels (control zones) can be controlled independently.

CHKD BY \_\_\_\_\_ DATE \_\_\_\_\_ JOB NO \_\_\_\_\_

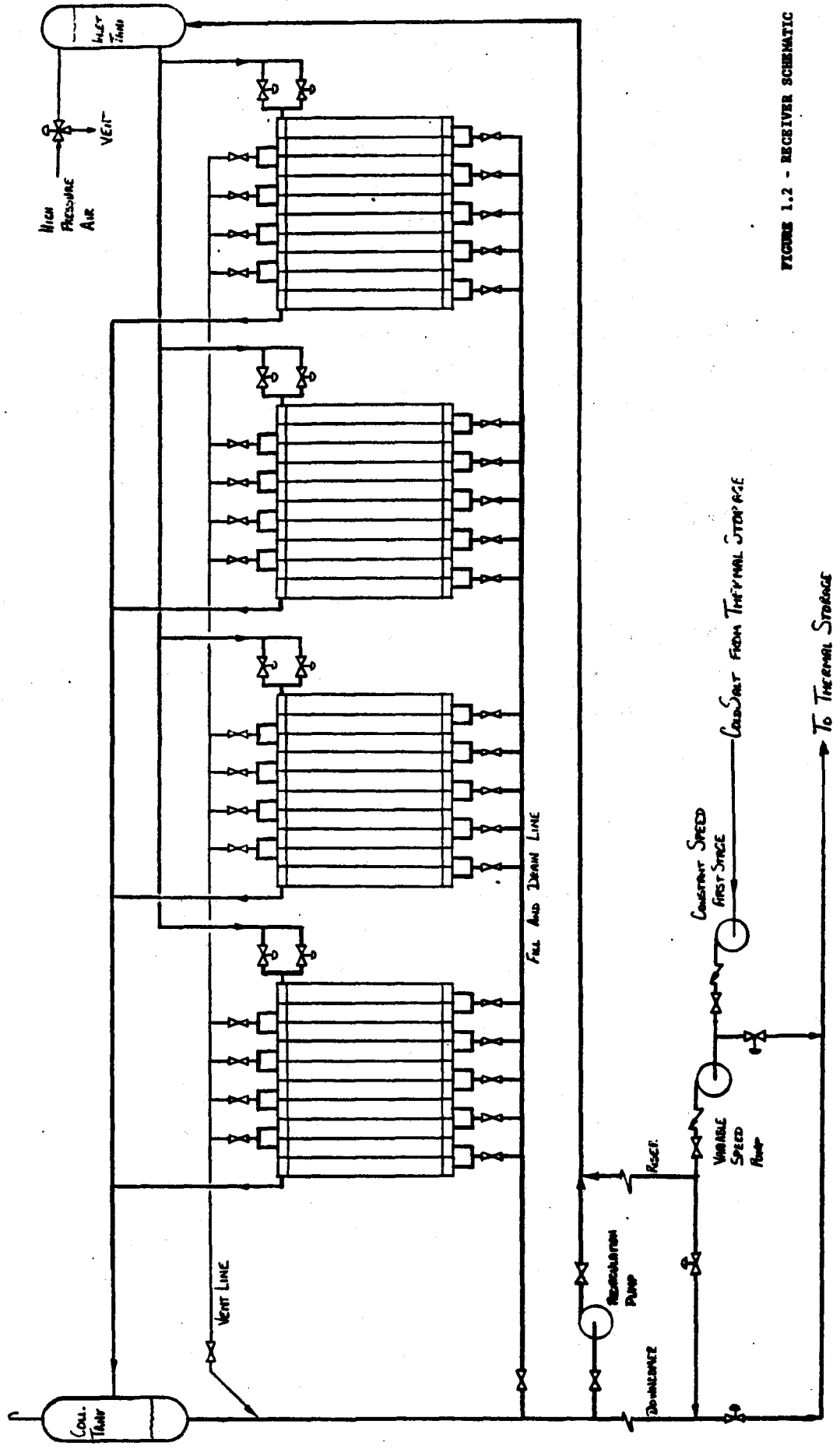


FIGURE 1.2 - RECEIVER SCHEMATIC

b. The salt flow through a panel is controlled by two parallel acting valves which work independently using a common set-point (flow rate). This ensures against one valve sticking, with the risk of damaging a panel through overheating.

c. Each control zone consists of 10 panels.

It has been assumed throughout the study that the pressure head across the surge tank and collection tank is constant. Therefore, the maximum flow rate capability between the two remains constant.

#### 1.4 Control Requirements

Paragraph 1.2 presented the type of cloud transient which the control system must be capable of handling. As such, it forms part of the control requirements. The remaining requirements used in the control system evaluation are outlined below.

##### 1.4.1 Steady State Operation

a. Salt inlet to RS:  $288 \pm 15^{\circ}\text{C}$  ( $550 \pm 27^{\circ}\text{F}$ )

b. Salt leaving RS:  $565 \pm 5^{\circ}\text{C}$  ( $1050 \pm 10^{\circ}\text{F}$ )

##### 1.4.2 Operating Cloud Cover Transients

a. Salt inlet to RS:  $288 \pm 15^{\circ}\text{C}$  ( $550 \pm 27^{\circ}\text{F}$ )

b. Salt leaving RS:  $565 \pm 30^{\circ}\text{C}$  ( $1050 \pm 53^{\circ}\text{F}$ )

1.4.3 Load variation: The RS shall be capable of meeting the temperature requirements stated in paragraphs 1.4.1 and 1.4.2 at part load conditions ranging from 25% to 116% of the design rating.

1.4.4 Cloud Transients: The RS shall be capable of controlling a transient in the flux distribution caused by a cloud or clouds traversing the heliostat field a speed no greater than 13 m/s.

## 1.5 Control Techniques

The initial aim of the analysis was to investigate the application of two-point temperature feedback and QFFC to the cloud transient problem as applied to a quad-cavity receiver. As will be shown, the two-point temperature feedback scheme was soon discarded due to its inability to tightly control a dissimilar cloud transient.

Quasi-feedforward was then developed with the following objectives:

- i) Apply QFFC such that standard PID controllers can be applied to control salt-flow,
- ii) Introduce an override in QFFC such that the salt temperature does not exceed 1080°F,
- iii) Introduce an additional override in QFFC such that the panel wall exterior temperature does not exceed 1200°F,
- iv) Investigate the use of an optimal control strategy.

Objectives ii) and iii) are not part of the control requirements outlined in para. 1.4, but were included as a means to safeguard the operation of the receiver.

Objective iii) also required the development of an optimal filter to minimize numerically induced noise. Objective iv) was proposed to improve control by minimizing salt temperature error leaving the panel, thus steering the control such that it was less prone to hit the temperature limits and induce control override.

Each of the techniques derived by the objectives have been investigated and their relative performances compared.

## 1.6 Method of Analysis

By using salt flow through the panels to control salt outlet temperatures, the process becomes non-linear as the outlet temperature is inversely proportional to salt flow. Although analytical techniques can be used to investigate such a system, it was deemed expedient to use simulation alone for the study. The reasoning behind this decision is centered on the availability of MITAS as an accurate simulation tool to predict temperatures across the receiver. To achieve this, it is necessary to include the control algorithms as subroutines in this code.

To this end, a simple FORTRAN program was written which predicts receiver performance with sufficient accuracy (MITAS) for the purposes of this development. The control algorithm was developed as a subroutine within this simple program and on completion transferred to the MITAS program for evaluation. This technique led to an efficient method of control design minimizing the effort required using the more expensive MITAS program.

### References

1. Solar Central Receiver Dynamic Control Study, July 1981, Martin Marietta Corp. Rep. No. R81-44002-1.
2. Control Simulations of a Molten Salt Solar Thermal Central Receiver, Martin Marietta Corp. De Rocher, Melchior, McMordie

## 2. TWO POINT TEMPERATURE FEEDBACK

### 2.1 Description

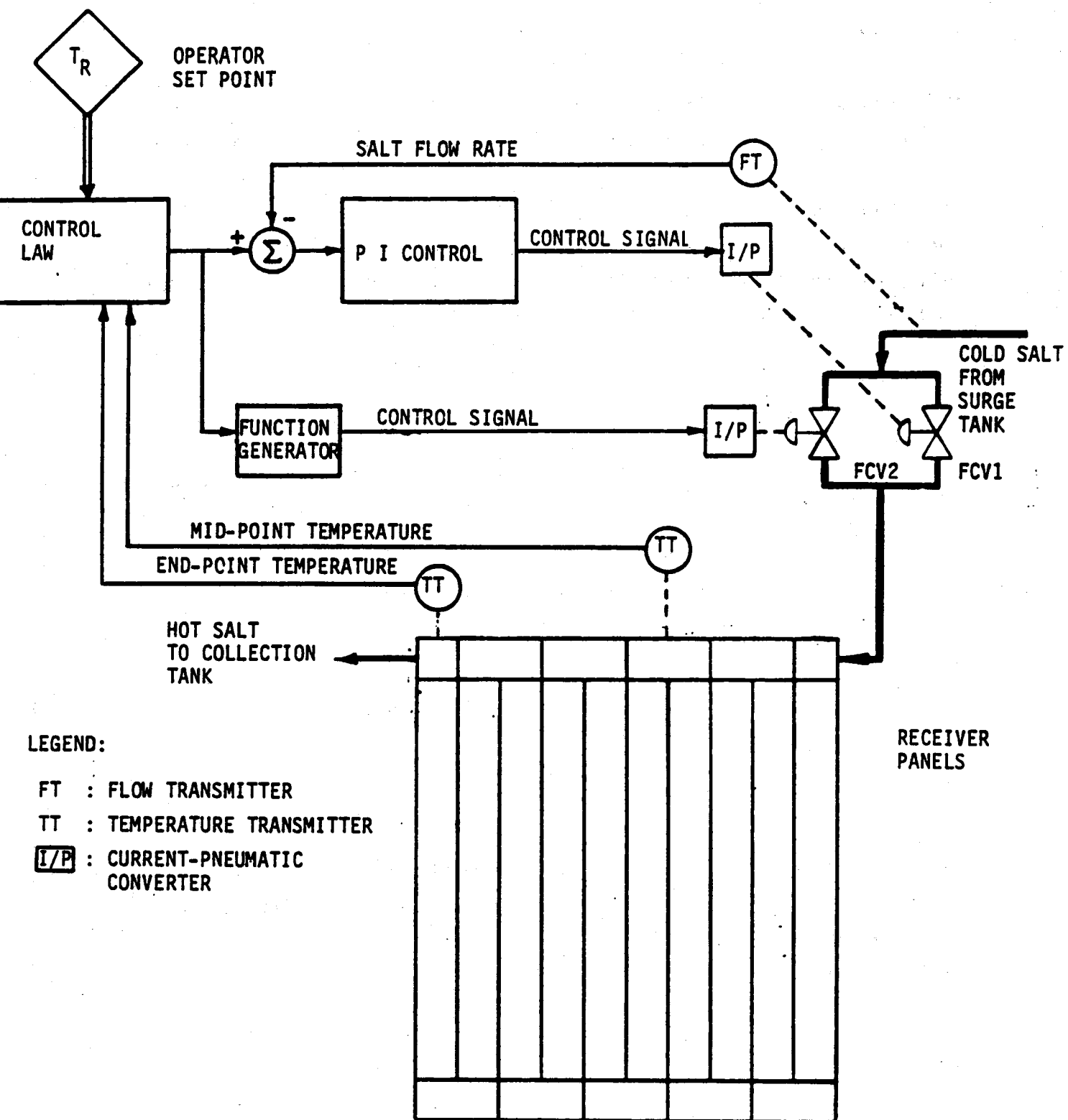
The control configuration is illustrated in Figure 2.1. This diagram shows the control system superimposed onto the receiver panel assembly.

The control algorithm uses two temperature measurements: the end point and a midpoint. These are compared with references, operator set-point, and are used to generate a demanded salt flow rate. This demand is formulated using the control law described below:

$$\dot{m}_d = \Delta t \sum \left\{ Cl(T_m - T_{m_r}) + \Delta t \sum \left[ \frac{T_o - T_{o_r}}{\epsilon T_o} \right] \cdot \left( \frac{T_o - T_{o_r}}{\epsilon T_o} \right) \right\} \quad (2.1)$$

where:  $\dot{m}_d$  = demanded salt flow rate,  
 $T_m$  = mid-point temperature measurement,  
 $T_{m_r}$  = mid-point temperature reference (set-point),  
 $T_o$  = end-point temperature measurement,  
 $T_{o_r}$  = end-point temperature reference,  
 $Cl, \epsilon T_o$  = control gains,  
 $\Delta t$  = sample period.

As described in the introduction, the demanded salt flow rate is used to position Flow Control Valve 2 (FCV2) and the salt-flow rate error is corrected via Flow Control Valve 1 (FCV1). This will be further explained later in the text.



LEGEND:

- FT : FLOW TRANSMITTER
- TT : TEMPERATURE TRANSMITTER
- I/P : CURRENT-PNEUMATIC CONVERTER

TWO POINT TEMPERATURE FEEDBACK SCHEMATIC

Figure 2.1

The control algorithm works in two ways. An error in the temperature profile is first noted by the mid-point term,  $T_m - T_{mr}$ . This error is integrated to correct the salt flow rate for thermal balance. Due to cloud induced changes in the spacial distribution of flux, the reference temperature,  $T_{mr}$ , set by the operator will often be in error. To correct for this, the output temperature error,  $T_o - T_{or}$ , is integrated twice so that in steady-state, it will outweigh any error introduced by using an incorrect mid-point temperature reference.

Three control limits are placed on this law, modifying 2.1 to:

$$\dot{m}_d = \Delta t \sum \left\{ Cl(T_m - T_{mr}) + \Delta t \sum \left[ \frac{T_o - T_{or}}{\epsilon T_o} \right] \cdot \left( \frac{T_o - T_{or}}{\epsilon T_o} \right) \right\} \quad (2.2)$$

The RHS limits the maximum salt flow acceleration demanded; this prevents the control from becoming divergently unstable.

The limit on the LHS is to prevent the control law from demanding either less than 25% or greater than 125% of the full-load salt flow rate. The minimum level limit, 25% has a two fold purpose:

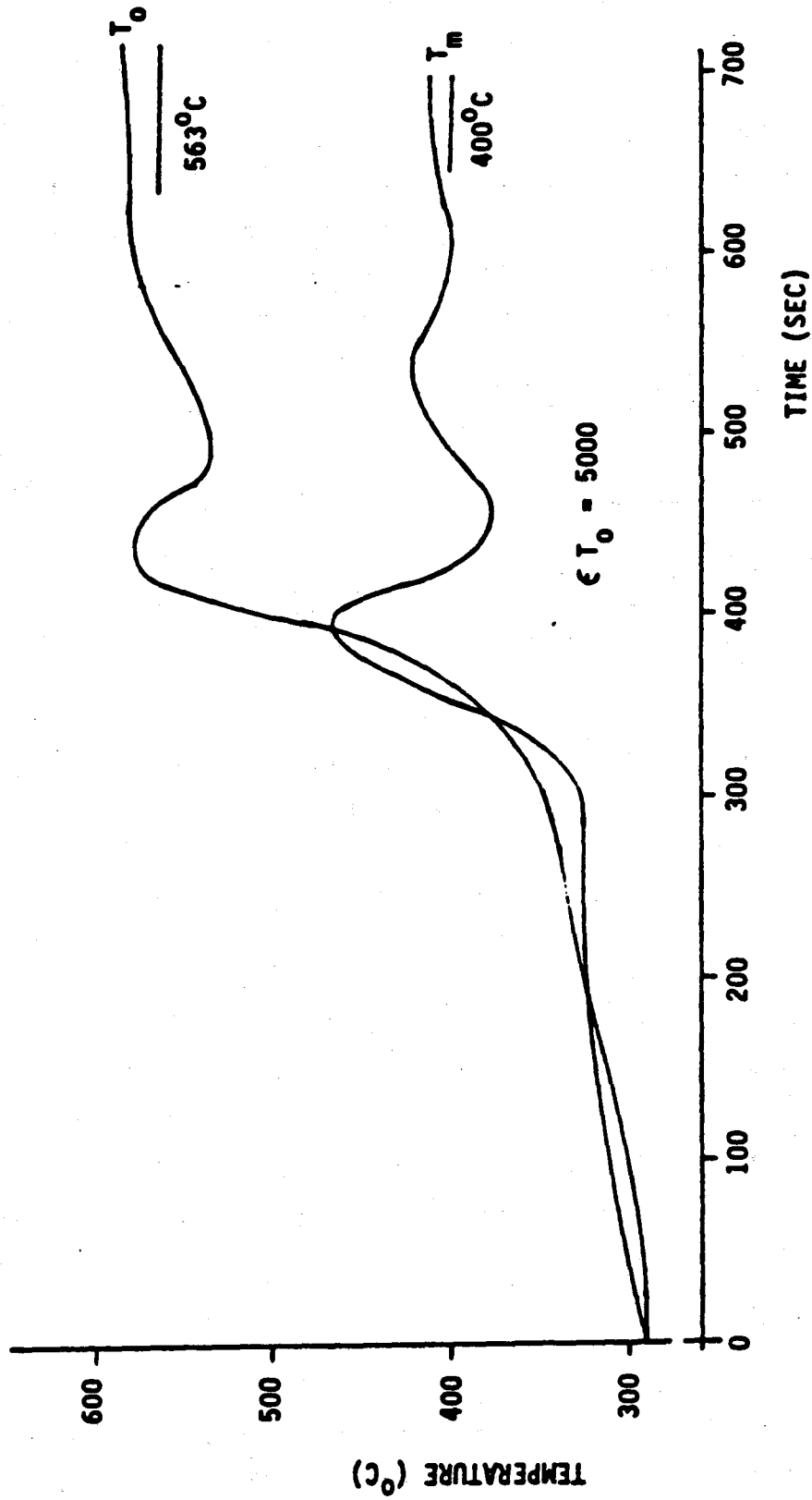
- a. It ensures flow rate when a cloud moves onto the field.
- b. As flow reduces, the residence time increases. Too large a residence time produces instability, which is prevented by this limit.

## 2.2 Simulation Results

Figure 2.2 shows the results from using the control law (2.2) to compute flow using a self-similar transient. This type of transient is



SELF-SIMILAR LOAD SWING: 10% Load  $t \leq 300$  Sec  
100% Load  $t \geq 340$  Sec

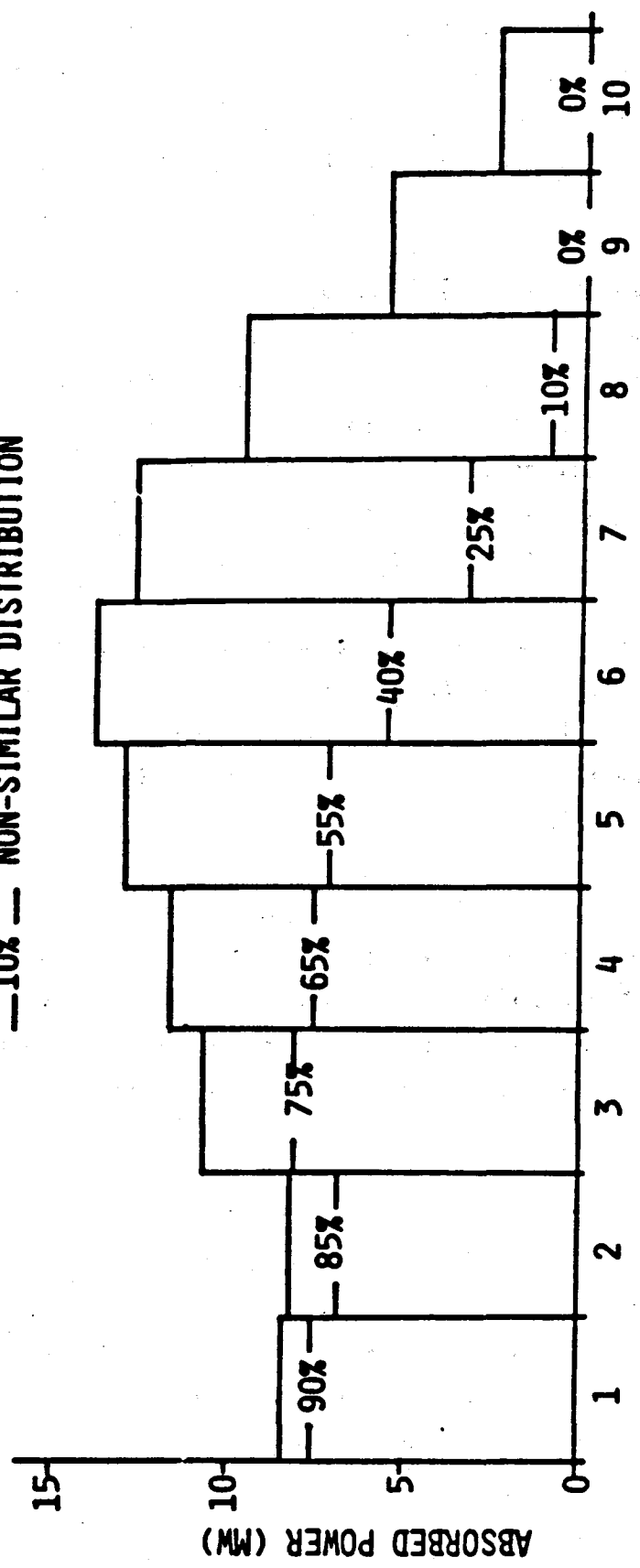


TWO POINT TEMPERATURE FEEDBACK: SELF SIMILAR LOAD SWING

Figure 2.2

—— 100% LOAD DISTRIBUTION

——10%—— NON-SIMILAR DISTRIBUTION



PANEL NUMBER

PANEL WISE FLUX DISTRIBUTIONS

Figure 2.3

hypothetical in that there is no distortion in the flux spatial distribution. In this case, the flux was held at 10% of the design point until 300 secs, and then ramped up to 100% in 40 seconds. The control gains for this run were set heuristically and represent the best achievable performance.

The mid-point temperature reference was set assuming the distribution of absorbed power shown in Figure 2.3. The same mid-point reference was then used for a second simulation run this time with the power level attenuated to a distorted profile. This profile is shown superimposed onto Figure 2.3, and is an arbitrary choice, not representative of any particular cloud but used solely for investigation of performance. The results are shown in Figure 2.4.

As can be seen in Figure 2.4, the temperatures converge onto the set-points relating to the 100% power level, but an attenuation to the distorted levels of Figure 2.3 results in an error in the salt outlet temperature. The error is corrected by reducing  $\epsilon T_c$ , as shown, but this tends to upset stability.

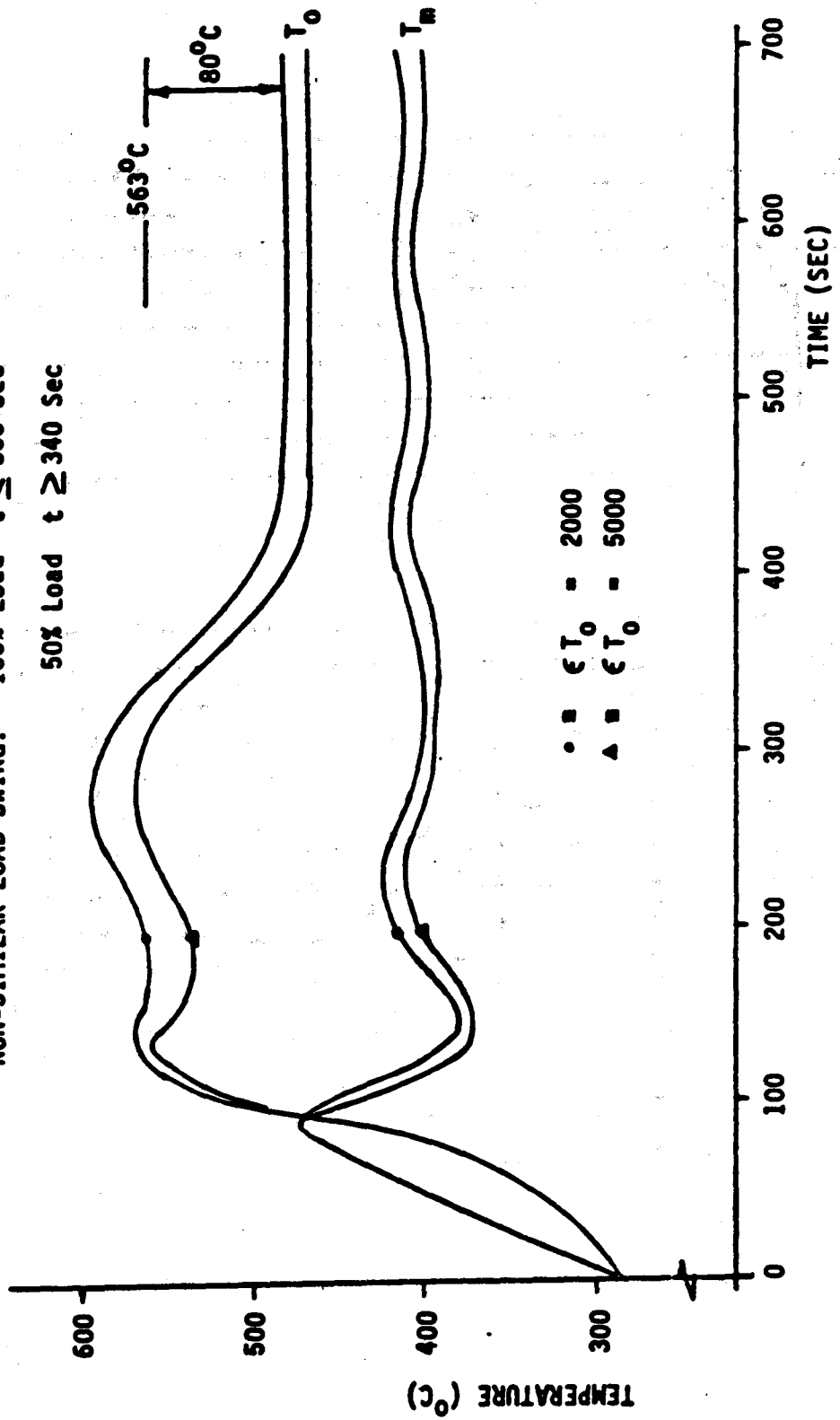
These results are pessimistic in that a hypothetical distortion in the flux distribution is used to simulate cloud cover. Figure 2-5 shows results for the MITAS model using a realistic cloud. The results show the same effect, which although not so severe, show the algorithm to be unable to control when clouds cover part of a field of heliostats.

## 2.3 Conclusions

The justification for the control algorithm defined by 2.1 is based on a brief analysis of a suitable Liapunov function. Further detailed analysis would have been warranted had the results been more promising. Consequently, no further analysis was performed as the quasi-feedforward control, described in the next section, promised better performance.

NON-SIMILAR LOAD SWING: 100% Load  $t \leq 300$  Sec

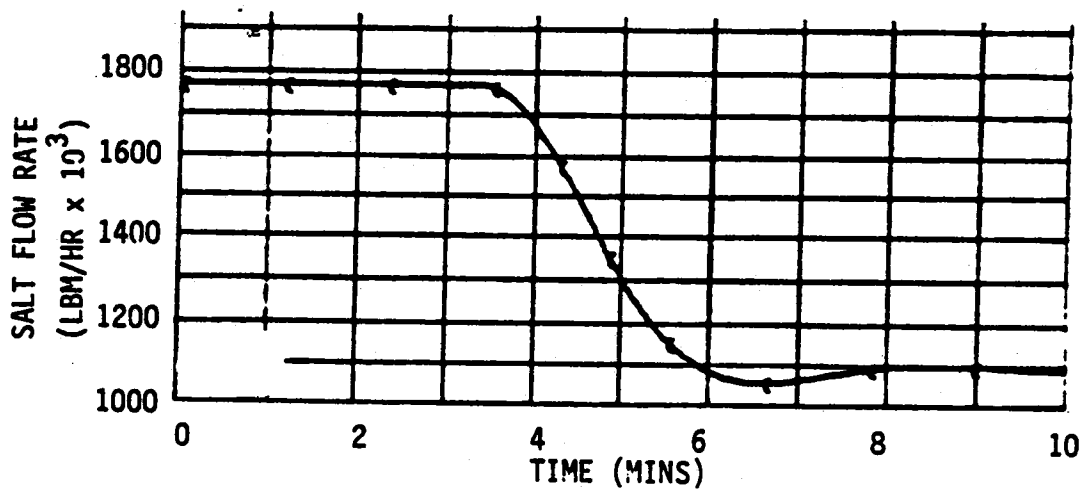
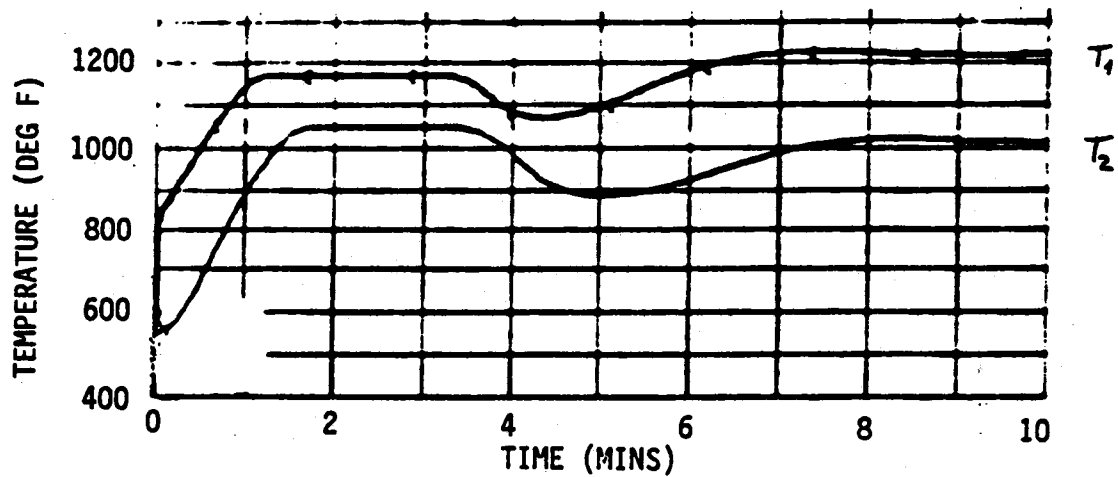
50% Load  $t \geq 340$  Sec



• =  $\epsilon T_0 = 2000$   
▲ =  $\epsilon T_0 = 5000$

RESPONSE TO DISTORTION ON FLUX DISTRIBUTION

Figure 2.4



T<sub>1</sub>: PEAK METAL TEMPERATURE  
 T<sub>2</sub>: SALT OUTLET TEMPERATURE

### 3. QUASI-FEED FORWARD CONTROL

#### 3.1 Basic QFFC

The principle of QFFC is to estimate the thermal power absorbed by the receiver in order to set the required salt flow rate by thermal balance. The algorithm used to estimate the absorbed power is commonly called an observer, and in this application can be expressed as:

$$Q_E = \dot{m} C_p (T_o - T_i) + m C_p \dot{T} \quad (3.1)$$

where:  $Q_E$  = estimated absorbed power  
 $\dot{m}$  = measured salt flow rate  
 $C_p$  = specific heat of salt  
 $m$  = mass of salt within the node  
 $T_o$  = temperature of salt leaving the node  
 $T_i$  = temperature of salt entering the node  
 $\dot{T}$  = differential of salt temperature with respect to time.

Equation 3.1 is an accurate means of calculating absorbed thermal power during steady state when the outlet temperature is constant. During transients it is a first order approximation as long as  $\dot{T}$  is approximately the same throughout the node. Therefore, a panel-wise application of equation 3.1 can be used to calculate absorbed power during both steady-state and transient operation.

To thermally balance the receiver we use:

$$\dot{m}_D = \frac{Q_E}{C_p (T_{o_{sp}} - T_i)} \quad (3.2)$$

where  $T_{o_{sp}}$  = required temperature of salt leaving receiver (set-point)  
 $\dot{m}_D$  = demanded salt flow rate

Figure 3.1 illustrates the application of this method to the receiver. As shown, the temperature of each header is used with the mass of salt in each panel to calculate the absorbed power using:

$$\frac{Q_E}{C_p} = \dot{m}(T_{oN} - T_i) + \sum_{n=1}^N m_n \dot{T}_{o_n} \quad (3.3)$$

where:  $N$  = number of panels in the receiver  
 $m_n$  = mass of salt in panel  $n$   
 $T_{o_n}$  = temperature of salt leaving panel  $n$

Using equations 3.2 and 3.3 the salt flow demand is determined. This demand is used to control two parallel operating valves as before, one operating open loop via a function generator, the second operating using flow feedback to correct flow errors. This arrangement ensures correct salt flow should one of the two valves jam.

To emulate the control system in the computer model, equation 3.3 was expressed in digital form as:

$$Q_E/C_p = \dot{m}(T_o(t) - T_i(t)) + \sum_{i=1}^N m_i \left[ \frac{T_i(t) - T_i(t + \Delta t)}{\Delta t} \right] \quad (3.4)$$

where:  $\Delta t$  = sample period (set at 1 second).

This control algorithm was then evaluated against an E-W cloud moving off the heliostat field - a worst case: Figure 3.2 shows the total absorbed power as a history.

Figures 3.3a and 3.3b show the results, the notation for these diagrams is given in Table 3.1. The figures show a receiver starting from warm standby (550°F) with flux instantaneously focused onto the panels from a field partially covered by cloud. The receiver is allowed to heat-up after which the cloud is removed from East to West after 10 minutes. The history of salt outlet temperature shows a stable response with minimal overshoots. This is to be compared with two-point temperature feedback, Figure 2.4, where the temperature overshoots and suffers steady-state errors.

Figure 3.3a also shows the parallel valve action. The valve operating open loop uses a position function which assumes the second valve is 50% open. It then moves with salt flow demand. The flow feedback valve moves only to correct small errors in salt flow moving about the 50% position.

Figure 3.3b shows the salt-flow and salt flow demand coefficients (normalized by maximum salt flow rate). The demand never reaches the maximum limit (1) and the flow always follows the demand closely.

The main conclusion to be drawn from these results is the need to minimize the overshoot in salt temperature shown in Figure 3.3a. It is desirable to keep the salt temperature below 1100°F.

### 3.2 QFFC with Salt Temperature Limitations

One method of minimizing the temperature overshoot is to move the minimum salt flow rate according to the temperature of the salt in each header. Using the same observer and thermal balance equation we have:

$$\frac{Q_E}{C_P}(t,n) = \dot{m} (T_N(t) - T_n(t)) + \sum_{i=n+1}^N m_i \left[ \frac{T_i(t) - T_i(t+\Delta t)}{\Delta t} \right] \quad (3.5)$$

for the observer, and for the thermal balance

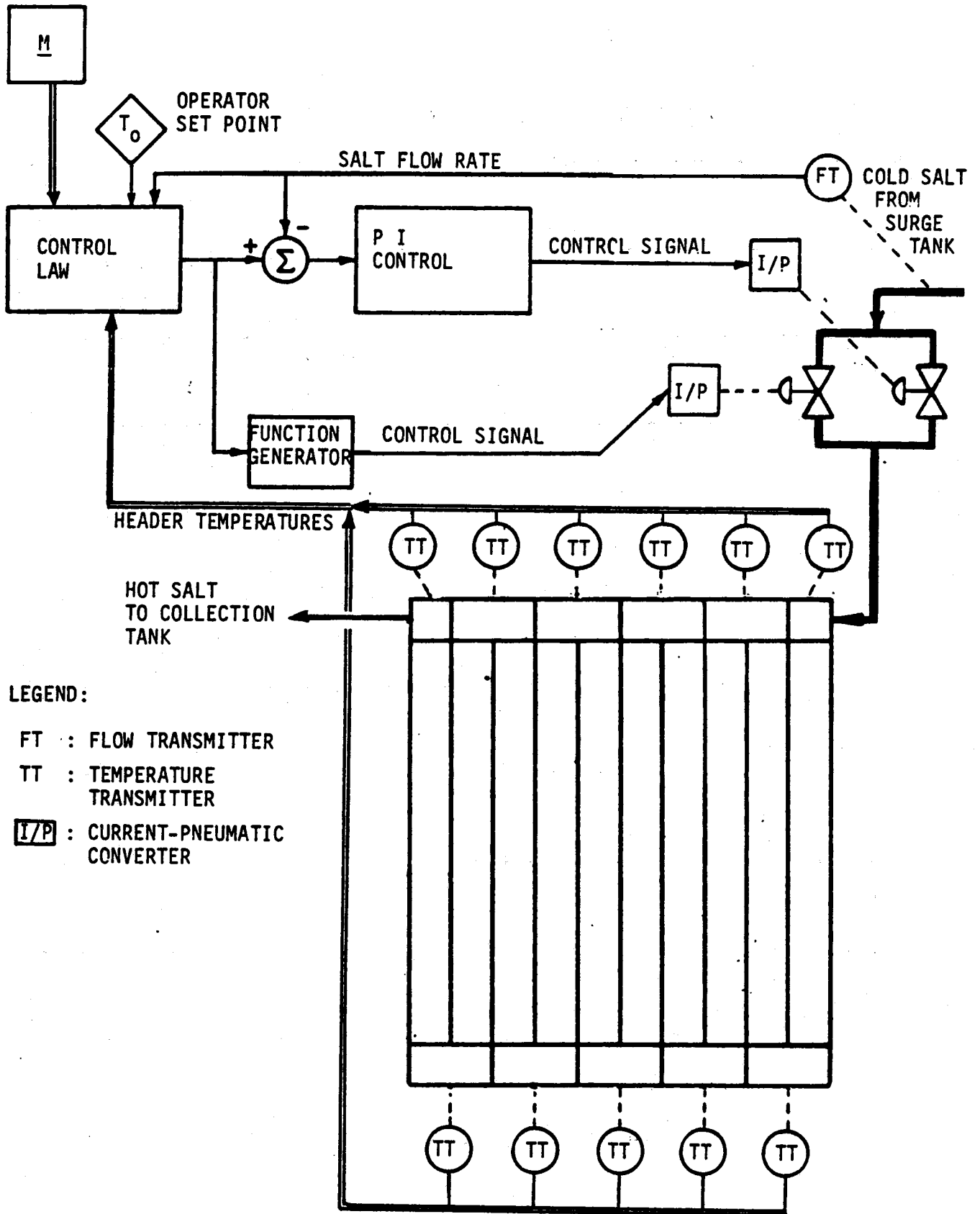
$$\dot{m}_k = \frac{Q_E(t,k)}{C_P(T_{MAX} - T_k)} \quad (3.6)$$

where  $T_{MAX}$  = maximum salt outlet temperature  
 $T_k$  = salt temperature of header to panel k



TABLE 3.1 - FIGURE CONVENTION OF SIMULATION RESULTS

<b>Figure a:</b>	
Receiver Outlet Temperature	⊙
Peak Metal Temperature	△
Valve, open loop	△
feedback loop	⊙
<b>Figure b:</b>	
Peak Metal Temp. to be controlled	⊙
Estimate of controlled Metal Temp.	△
Normalized Flow Demand	⊙
Normalized Flow Measured	△
Normalized Flow Demand	⊙
Normalized Minimum Flow Level	△



LEGEND:

FT : FLOW TRANSMITTER

TT : TEMPERATURE TRANSMITTER

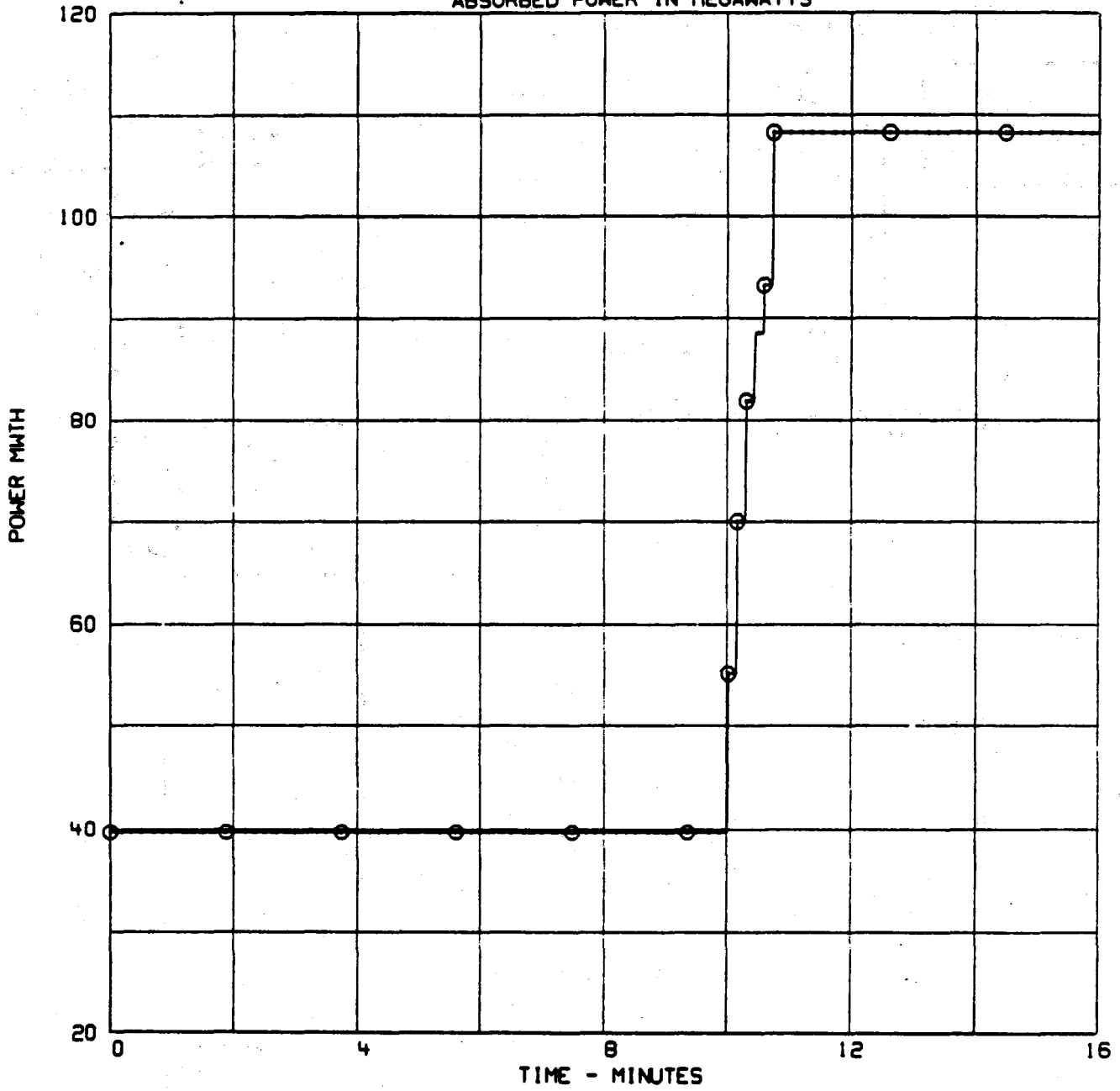
I/P : CURRENT-PNEUMATIC CONVERTER

QUASI-FEEDFORWARD SCHEMATIC

Figure 3.1

# TRANSIENT SYSTEM ANALYSIS MODEL

ABSORBED POWER IN MEGAWATTS



E-W Cloud: Absorbed Power Transient

Figure 3.2

# TRANSIENT SYSTEM ANALYSIS MODEL

## RECEIVER OUTLET AND PEAK METAL TEMPERATURE

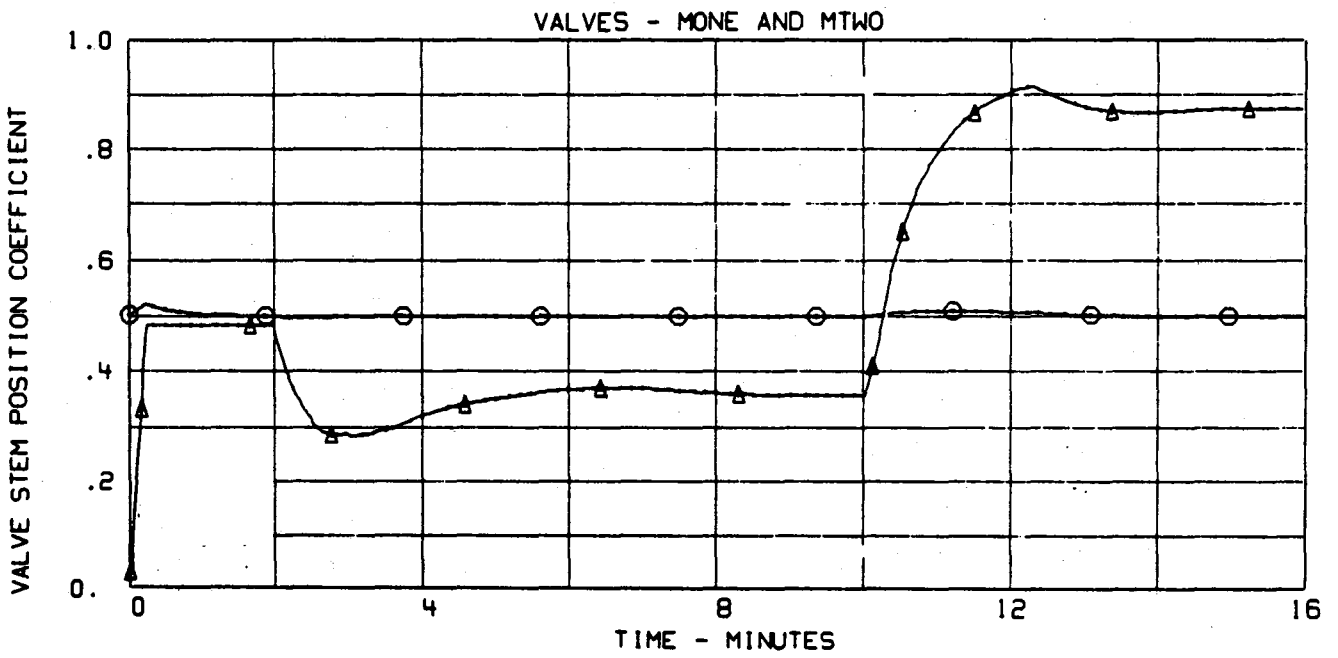
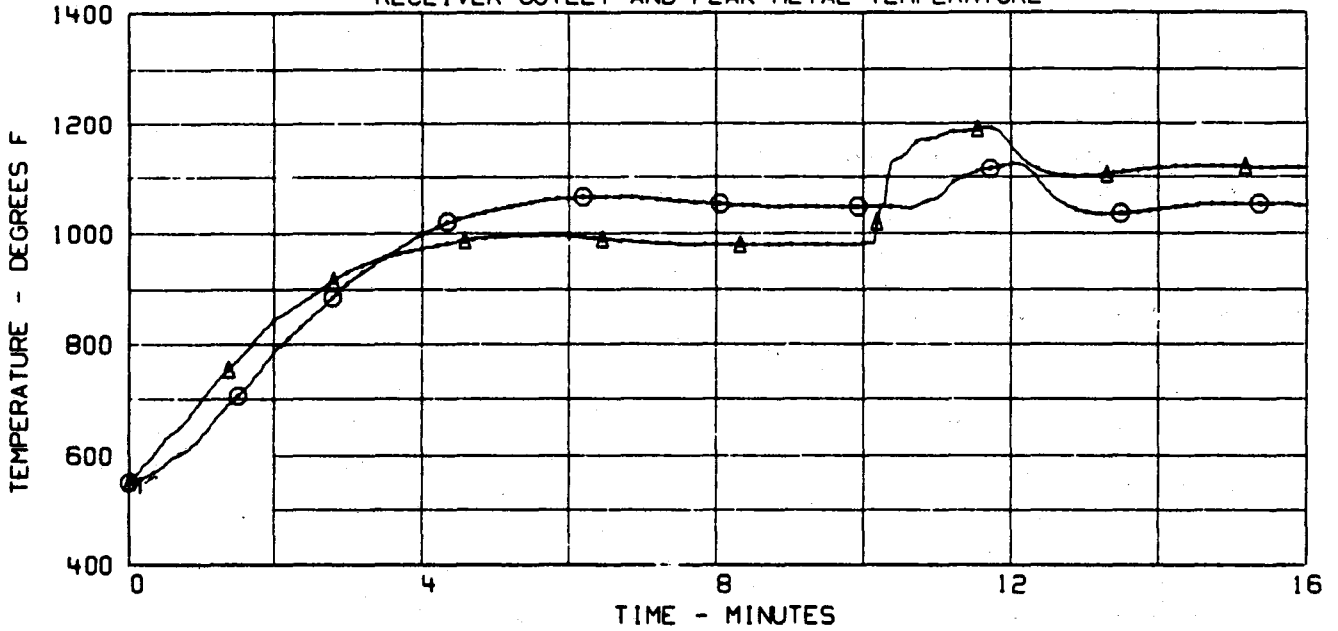
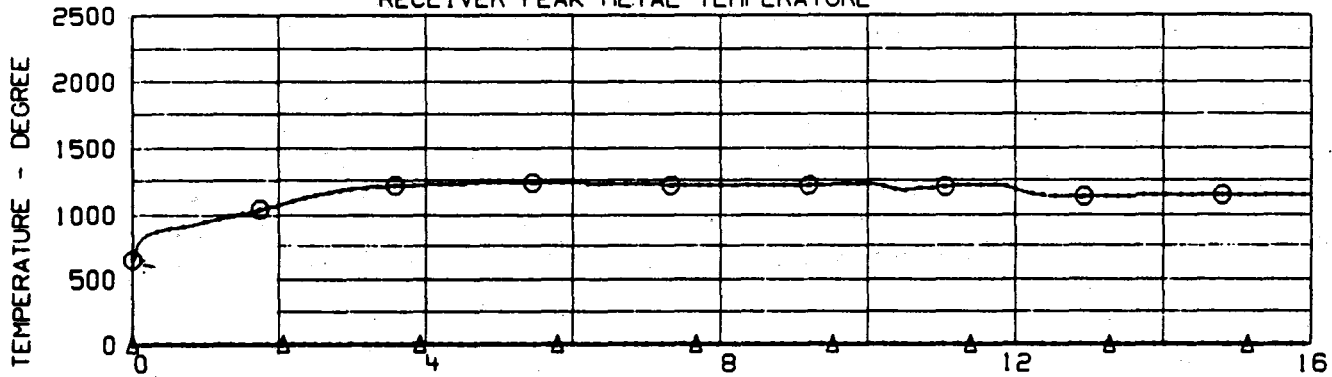


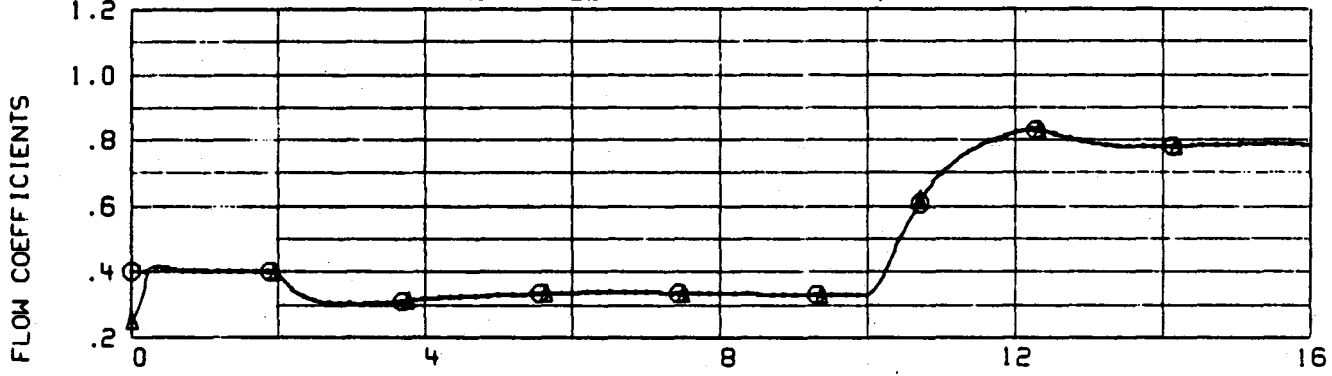
Figure 3.3a

# TRANSIENT SYSTEM ANALYSIS MODEL

## RECEIVER PEAK METAL TEMPERATURE



## NORMALIZED FLOWS - FCOEFFD, FCOEFF



## NORMALIZED FLOWS - FCOEFFD, FCOEFFM

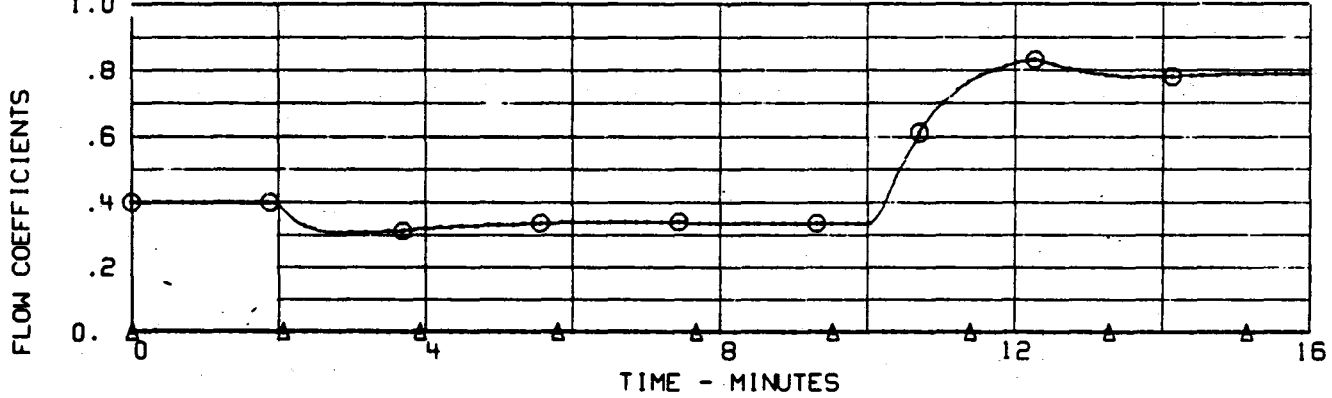


Figure 3.3b

Equation 3.5 is used to calculate the power absorbed from panel n to the end of the zone. Equation 3.6 is used to calculate flow for thermal balance from panel k to the end of the zone. For a receiver with N panels, there are N values for  $\dot{m}_k$ , and the largest must be chosen i.e.,

$$\dot{m}_{\min} = \max_{\dot{m}} \left\{ \dot{m}_{25\%}, \dot{m}_k = f(Q_E(t,k), T_{\text{MAX}}, T_k) \right\}, \forall k \in [1, N] \quad (3.7)$$

Note the absolute minimum flow rate of 25% of the design flow ( $\dot{m}_{25\%}$ ).

In flow diagram form, this new algorithm is shown in Figure 3.4. This algorithm was tested against the E-W cloud transient (Figure 3.2), results are shown in Figure 3.5a and 3.5b. As can be seen, the salt temperature overshoot is effectively limited. However, Figure 3.5b shows the history for the minimum flow rate (FCOEFFM). There is oscillatory motion during transients and a filter on demanded flow is required to dampen the effect on demanded flow. A more stable response would allow the salt to reach the limit (set-point) 1080°F .

### 3.3 QFFC with Salt and Wall Temperature Limits

As pointed out in the Introduction, one of the objectives of the control technique is to provide overrides to prevent excess metal temperatures. Consequently, an adaptive model has been defined to predict wall temperatures. Figure 3.6 illustrates this model where measured wall temperature, via a radiometer, is correlated with absorbed power, salt flow rate and salt inlet temperature.

The heat transfer equations for the control mode are:

$$Q = \dot{m}_p C_p (T_{s_0} - T_{s_1}) \quad (3.8)$$

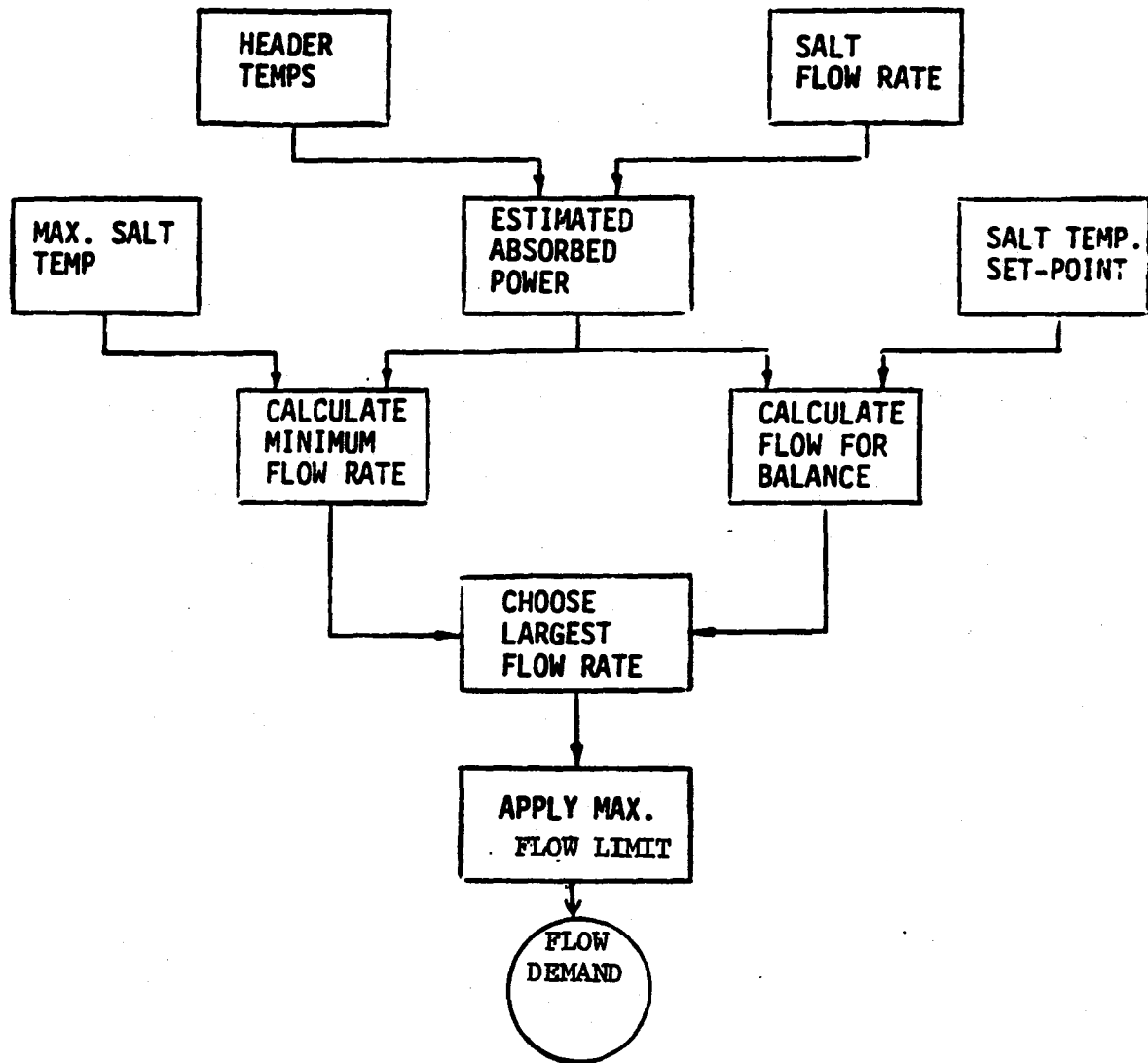


FIGURE 3.4 - QUASI FEEDFORWARD CONTROL

# TRANSIENT SYSTEM ANALYSIS MODEL

## RECEIVER OUTLET AND PEAK METAL TEMPERATURE

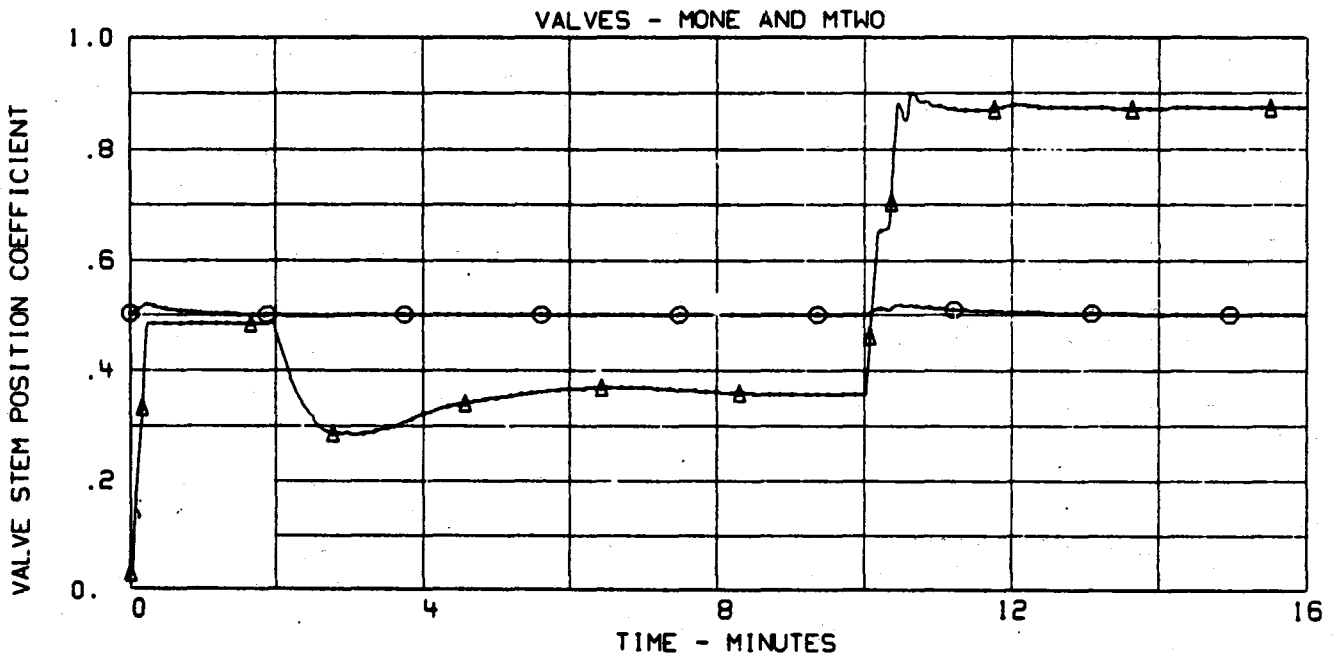
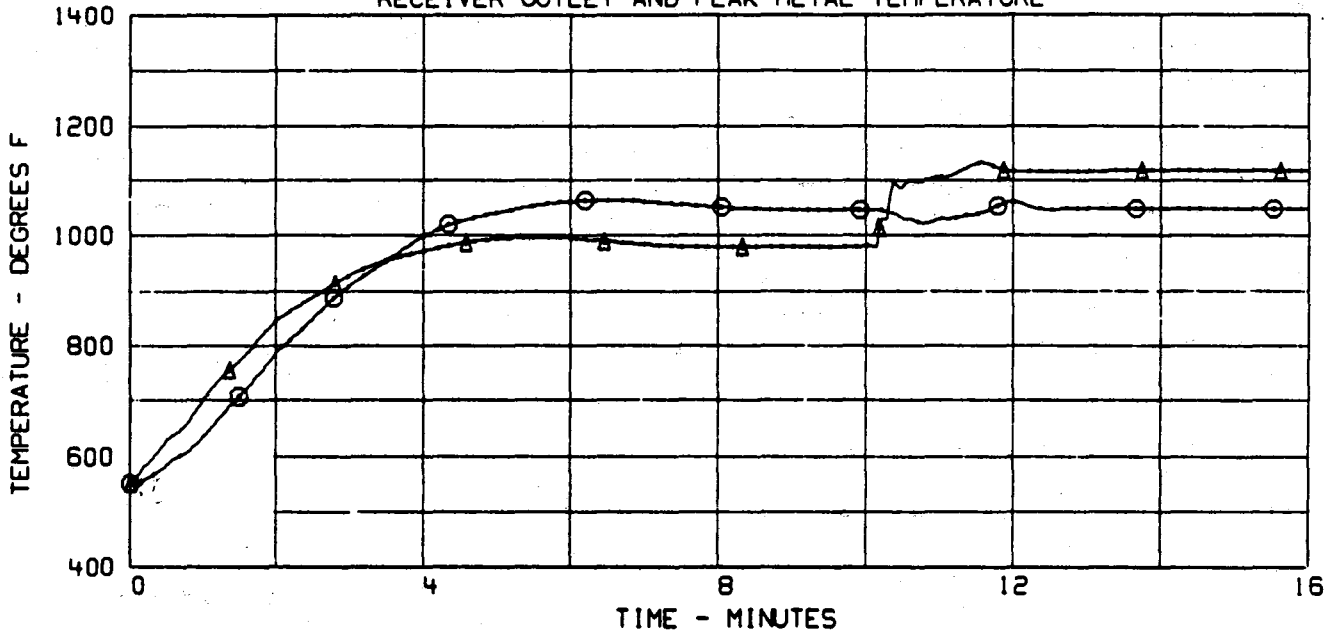


Figure 3.5a



# TRANSIENT SYSTEM ANALYSIS MODEL

## RECEIVER PEAK METAL TEMPERATURE COMPARISON

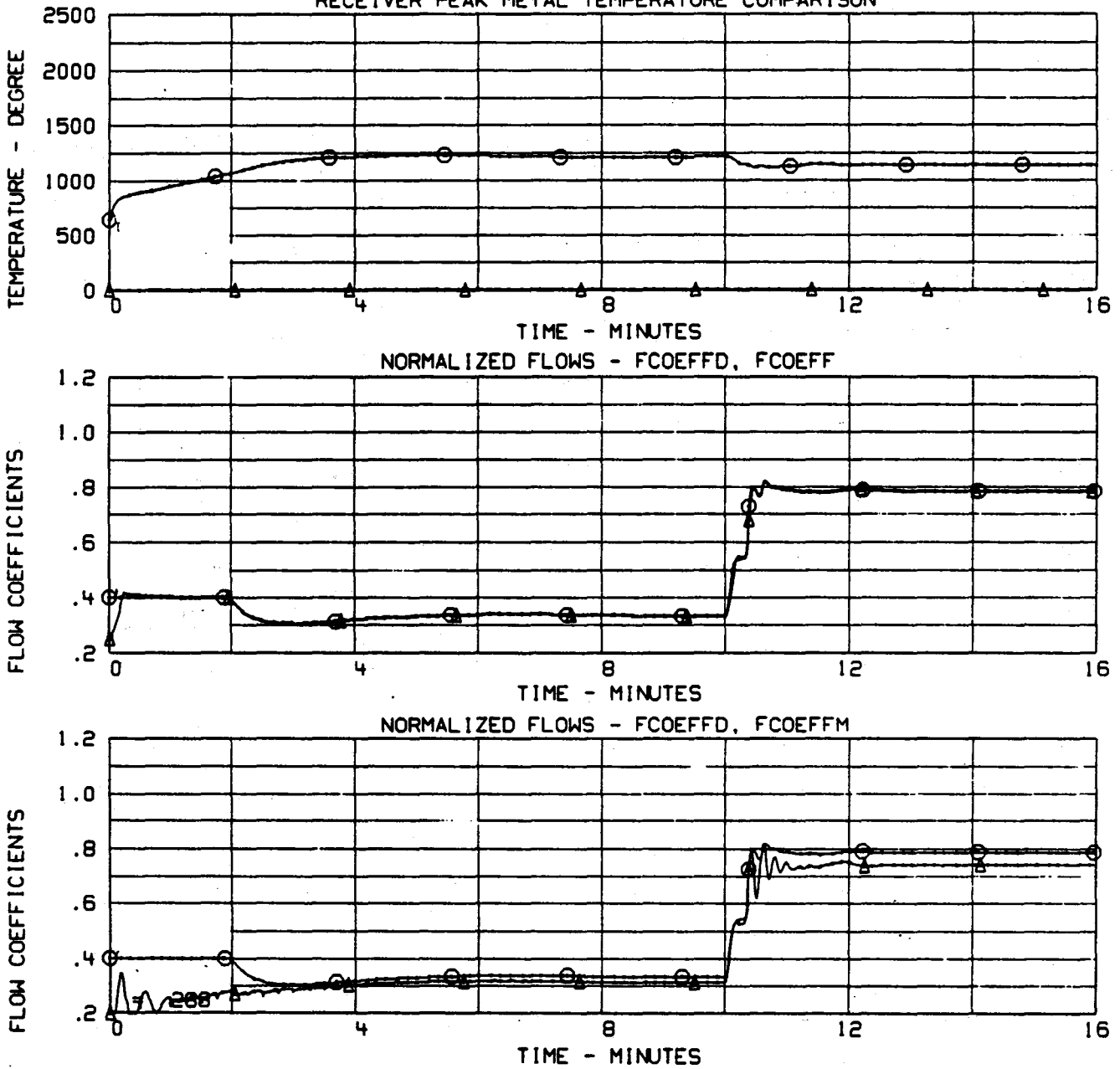
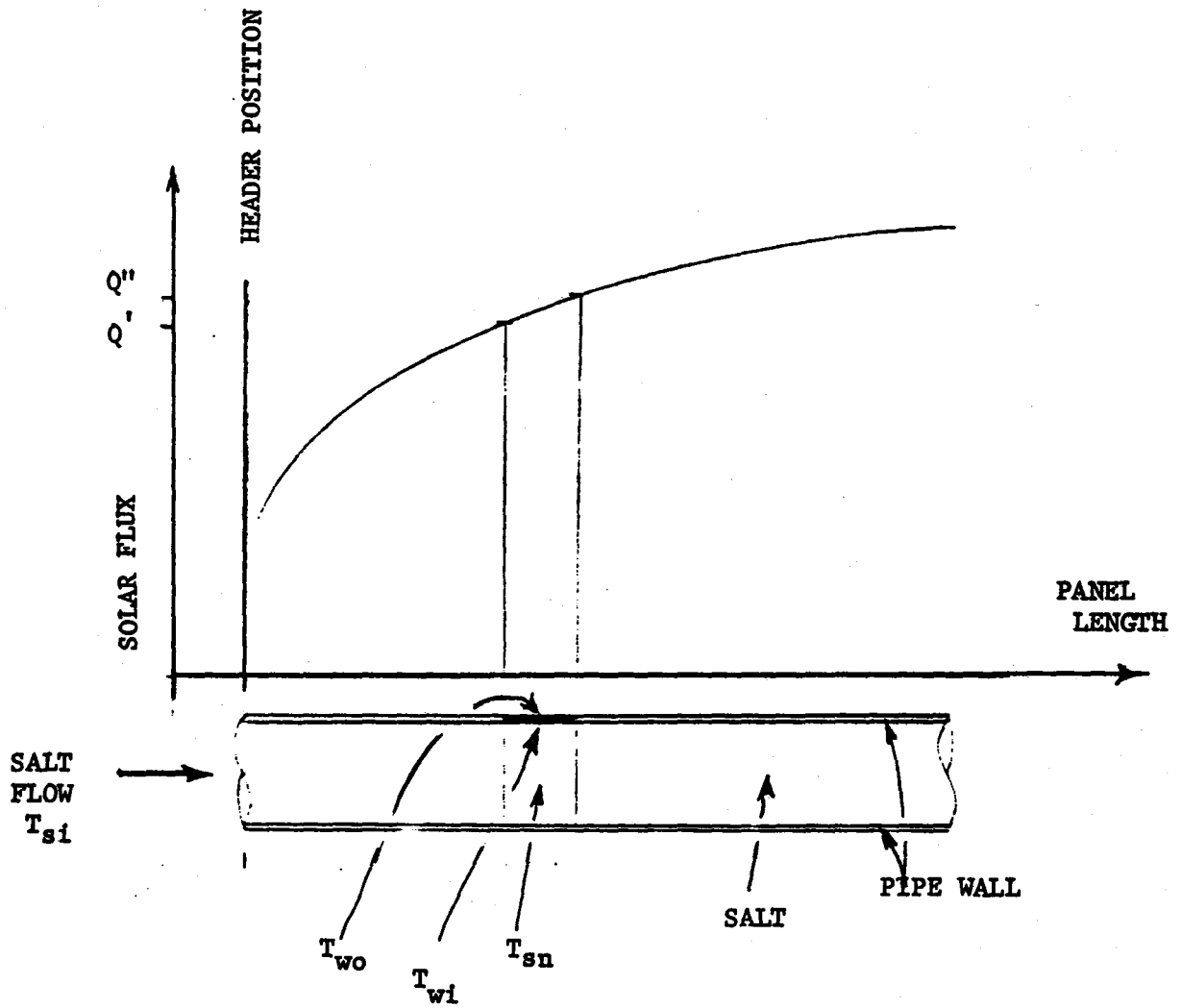


Figure 3.5b



- $T_{si}$  = Salt Temperature Entering Panel
- $T_{wo}$  = Outside Wall Temperature
- $T_{wi}$  = Inside Wall Temperature
- $T_{sn}$  = Salt Temperature Within Controlled Node

FIGURE 3.6 - WALL TEMPERATURE PREDICTIVE MODEL

$$G_s(T_{s_n} - T_{w_i}) + G_w(T_{w_o} - T_{w_i}) = 0 \quad (3.9)$$

$$G_w(T_{w_i} - T_{w_o}) + Q = 0 \quad (3.10)$$

hence:

$$\dot{m}C_p(T_{s_n} - T_{s_i}) = \frac{Q' + Q''}{2} \quad (3.11)$$

Equations 3.8-3.11 yield the model form:

$$T_{w_o} = T_{s_i} + \frac{\frac{1}{2}(Q' + Q'')/C_p}{\dot{m}} + Q' \frac{G_s + G_w}{G_s G_w} \quad (3.12)$$

$$\text{i.e. } T_{w_o} = f(Q, T_{s_i}, \dot{m}) \quad (3.13)$$

From equation 3.12 we define an adaptive model.

$$T_{w_e} = T_{s_i} + [Q/C_p] \cdot \left(\frac{k_1}{\dot{m}} + k_2\right) \quad (3.14)$$

The radiometer measurements of wall temperature is used to generate samples,  $T_{w_m}$ , and the terms  $k_1$  and  $k_2$  are determined as regression coefficients  $\hat{k}_1$ ,  $\hat{k}_2$  using as a cost function:

$$J = \sum_j (T_{w_m} - T_{w_e})_j^2 \quad (3.15)$$

$$\text{and } \frac{\partial J}{\partial k_1} = \frac{\partial J}{\partial k_2} = 0 \rightarrow \hat{k}_1, \hat{k}_2 \quad (3.16)$$

Hence, the optimal predicted wall temperature is

$$T_{w_p} = T_{s_i} + Q_E' \left( \frac{\hat{k}_1}{\dot{m}} + \hat{k}_2 \right) \quad (3.17)$$

Equation 3.17 can be rewritten in the form:

$$\dot{m}_{\min} = \frac{Q_{E_1} + \hat{k}_1 Q_{E_2}}{C_p [T_{w_o} - T_i] - \hat{k}_2 Q_{E_2}} \quad (3.18)$$

where:  $\dot{m}_{\min}$  = minimum salt flow rate  
 $T_{w_o}$  = wall temperature limit (maximum)  
 $Q_{E_1}$  = power absorbed before panel being controlled  
 $Q_{E_2}$  = power absorbed by panel being controlled

and the minimum flow can be computed using the header temperature feeding the controlled panel. Hence, the biggest minimum-limit flow is chosen as for the salt limit control case (equation 3.7). The observer is again used to determine the fluxes.

Figure 3.7a and 3.7b show results with the algorithm predicting wall temperature alone. Figure 3.7b compares peak metal temperature ( $\odot$ ) with that predicted by equation 3.17 ( $\Delta$ ). As can be seen, the algorithm requires some time to settle during transients.

The limit applied for Figure 3.7 was 1400°F. To see the effect of wall temperature limiting, this was reduced to 1200°F, the results are shown in Figures 3.8a and 3.8b. Comparison of Figures 3.7b and 3.8b show the wall temperature to be limited to 1200°F as desired, where before it peaked at 1250°F. Comparison of Figures 3.7a and 3.8a show the salt temperature during startup to asymptotically converge on the set point with no overshoot. This is due to 1200°F being a design point for the panel being controlled. Further comparison between the two runs shows the noisy effect wall temperature limits had on flow and valve demands. These effects were minimized by replacing the suboptimal filters with optimal filters.

### 3.4 Optimal Filters

The wall temperature control introduced too much noise into the control for sub-optimal filters. Consequently, optimal filters were employed for the type:

$$\theta_e(t) = \theta(t_0) + [t-t_0] \dot{\theta} \quad (3.19)$$

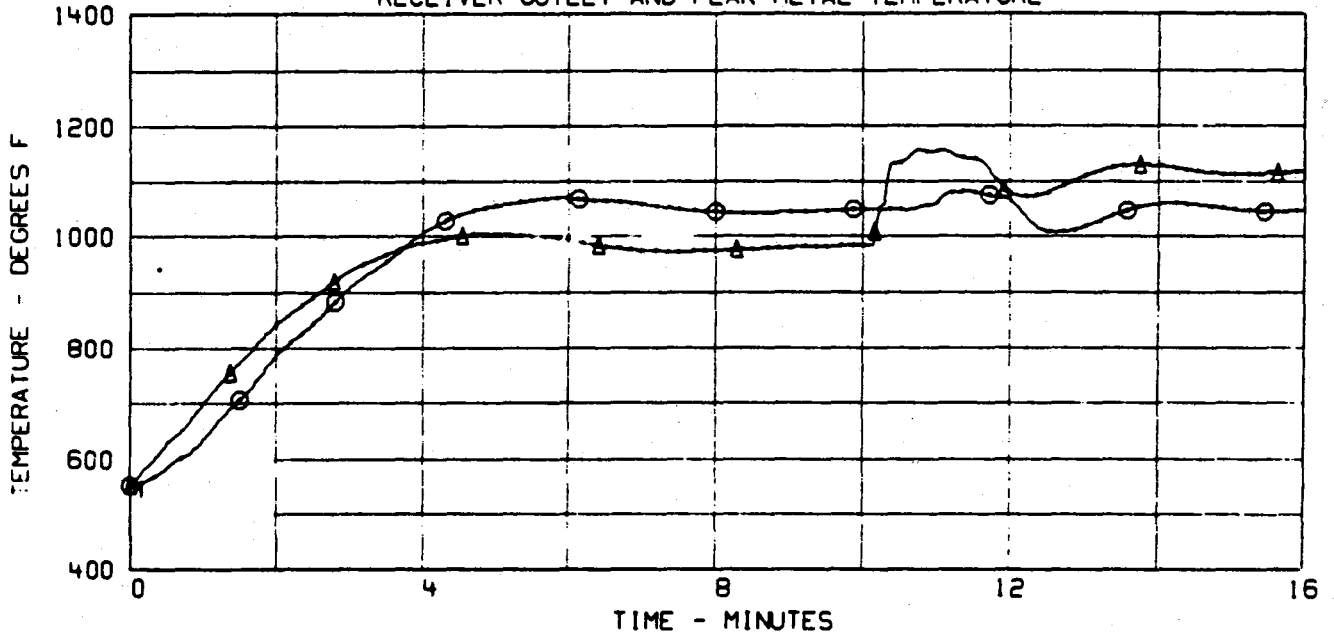
and the variable to be filtered compared with  $\theta_e$  using the cost function

$$J = \sum_i (\theta_m - \theta_e)^2 \quad (3.20)$$

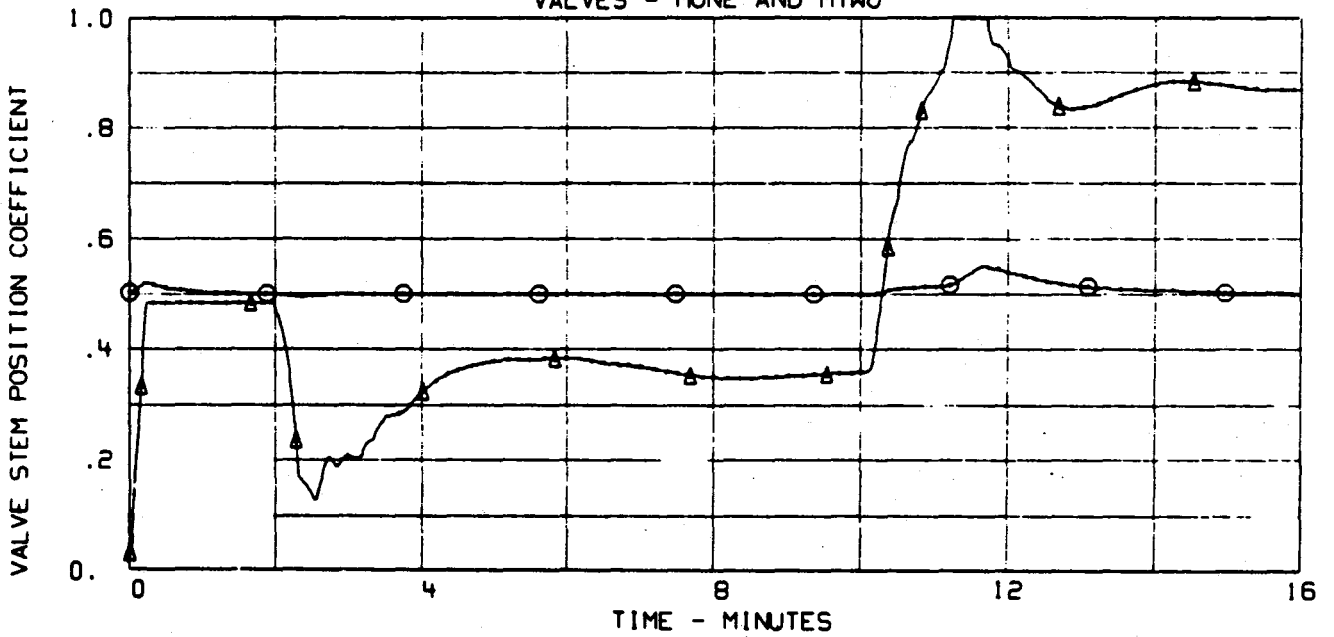
$$\text{hence } \frac{\partial J}{\partial \theta_0} = \frac{\partial J}{\partial \dot{\theta}} = 0 \rightarrow \hat{\theta}_0 \text{ and } \hat{\dot{\theta}} \quad (3.21)$$

# TRANSIENT SYSTEM ANALYSIS MODEL

## RECEIVER OUTLET AND PEAK METAL TEMPERATURE



## VALVES - MONE AND MTWO



# TRANSIENT SYSTEM ANALYSIS MODEL

## RECEIVER PEAK METAL TEMPERATURE COMPARISON

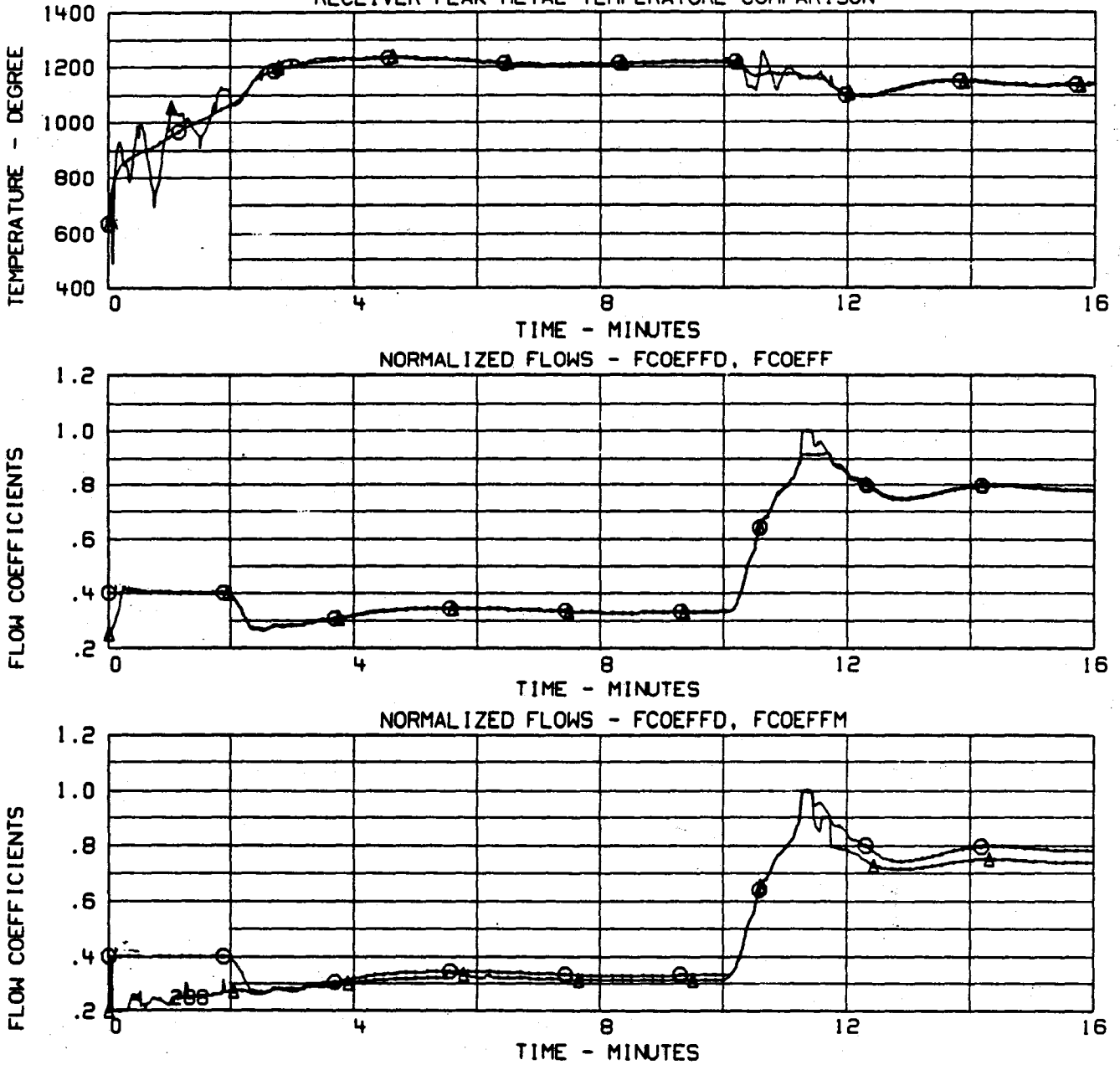
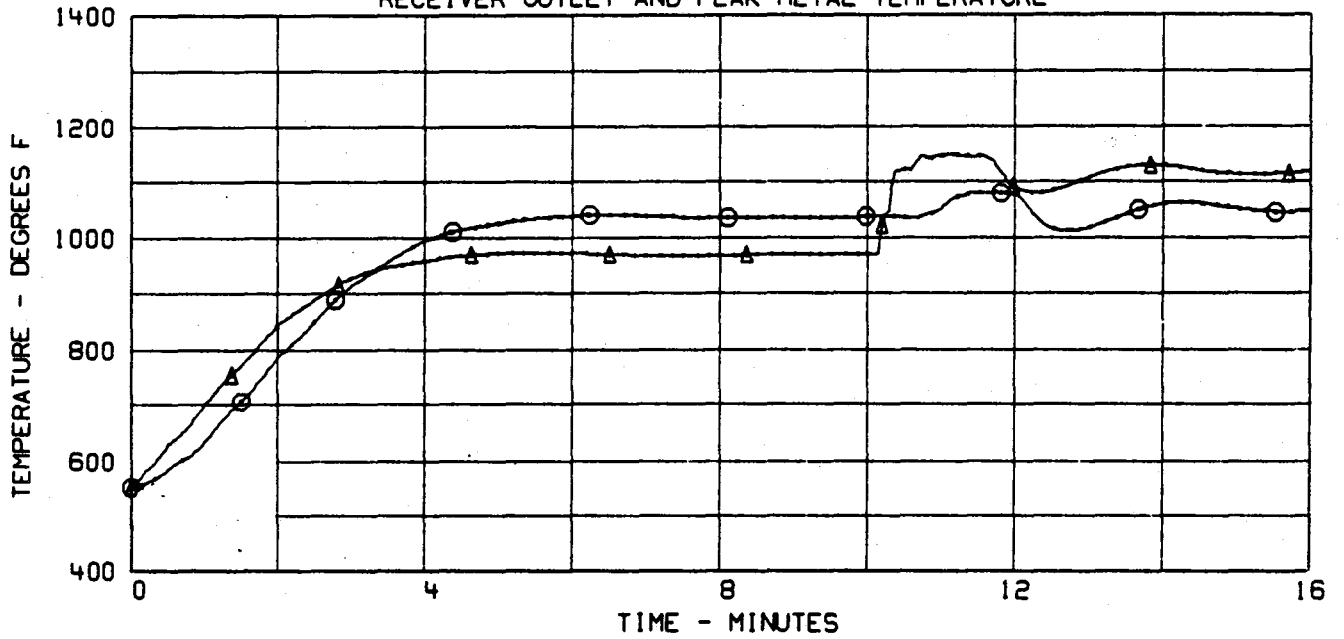


Figure 3.7b

# TRANSIENT SYSTEM ANALYSIS MODEL

## RECEIVER OUTLET AND PEAK METAL TEMPERATURE



## VALVES - MONE AND MTWO

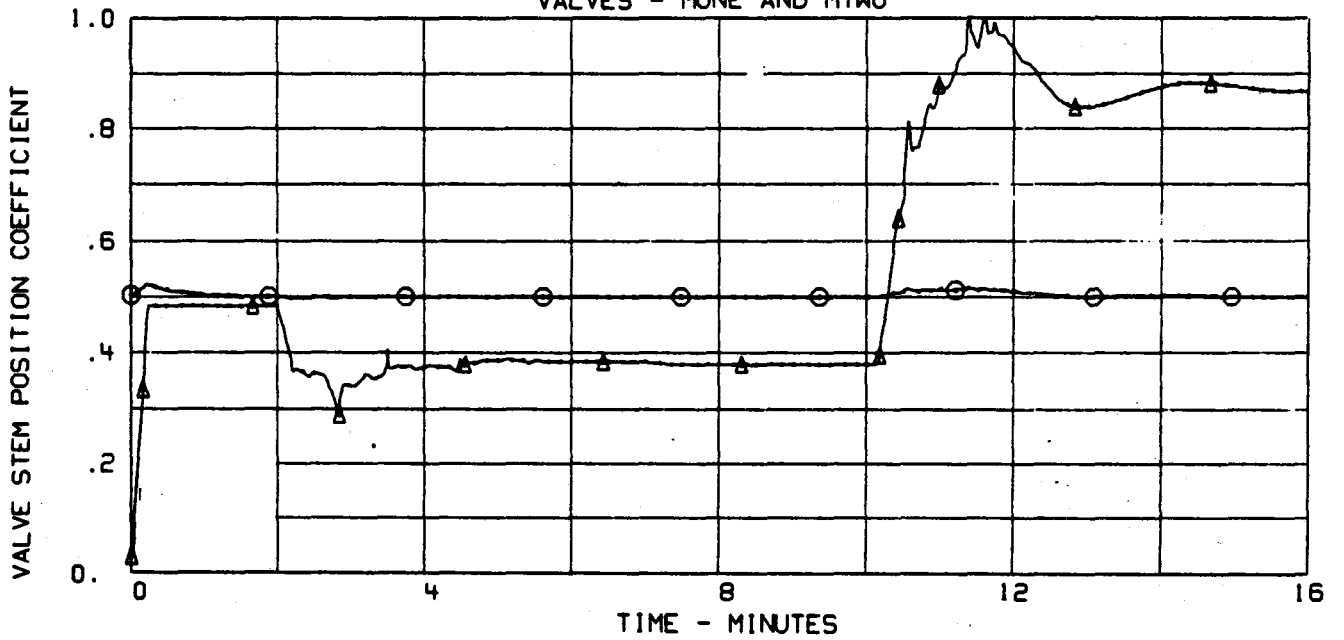


Figure 3.8a



# TRANSIENT SYSTEM ANALYSIS MODEL

## RECEIVER PEAK METAL TEMPERATURE COMPARISON

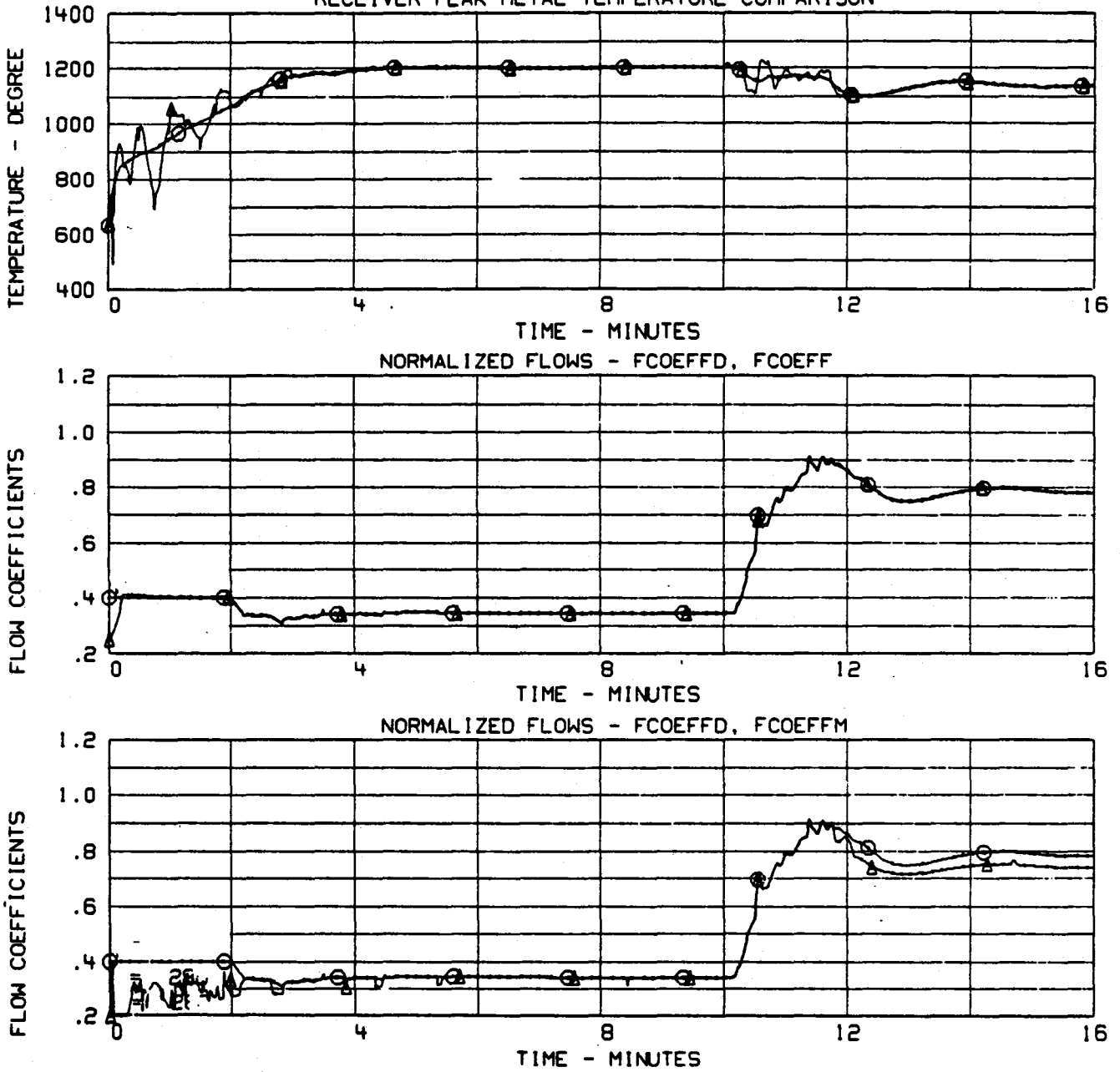


Figure 3.8b

giving the filtered variable:

$$\hat{\theta}_e(t) = \hat{\theta}(t_0) + [t-t_0] \cdot \hat{\dot{\theta}} \quad (3.22)$$

This filter was used on each estimate of absorbed power and the demanded flow to smooth numerically induced noise.

### 3.5 Optimal Control

Suboptimal control used a thermal balance across the receiver to achieve the correct salt temperature at the outlet (ref. equations 3.2 and 3.4). This technique is susceptible to errors during transients when shifts in flux distribution causes distortions in the temperature spacial profile. Such distortions cannot be absolutely controlled. At best, the consequent errors in outlet temperature can only be minimized. This leads to an optimal control strategy where an optimal flow rate is defined as that which minimizes the sum of the square of the predicted outlet temperature errors from each panel header in a control zone. This is described mathematically by the cost function:

$$J = \sum_{n=1}^N (T_{o,sp} - T_{o,n})^2 \quad (3.23)$$

where N = number of panels

n = panel

$T_{o,sp}$  = outlet temperature set-point

$T_{o,n}$  = predicted outlet temperature from panel n

The outlet temperature is predicted by the steady state thermal balance equation.

$$T_{O_n} = T_{i_n} + \frac{Q_{E_n}}{\dot{m}C_p} \quad (3.24)$$

where  $Q_{E_n}$  = observed absorbed power between panel 'n' and exit  
 $T_{i_n}$  = salt temperature at panel 'n'

Substituting 3.24 into 3.23 the cost is minimized w.r.t. the control variable,  $\dot{m}$  (salt flow rate), hence

$$\frac{dJ}{d\dot{m}} = 0 \rightarrow \dot{m}_d = f(Q_E, T_i, T_{O_{sp}}) \quad (3.25)$$

Equation 3.25 constitutes Optimal Quasi-FeedForward Control( OQFFC).

Results from the implementation of the control are shown in Figure 3.9. These can be compared with their sub-optimal equivalent in Figures 3.7. The comparison does not show significant difference other than the period 2 to 4 minutes. In comparison to the sub-optimal, OQFFC is less prone to be driven by the salt-temperature limit control; this can be seen in normalized flow history for demand and minimum flows.

There are definite advantages in using this type of optimal control; as yet, insufficient work has been performed to fully realize them. Areas for future investigation should include:

- a. use of weighting factors in equation 3.23 to better minimize the outlet error,

# TRANSIENT SYSTEM ANALYSIS MODEL

## RECEIVER OUTLET AND PEAK METAL TEMPERATURE

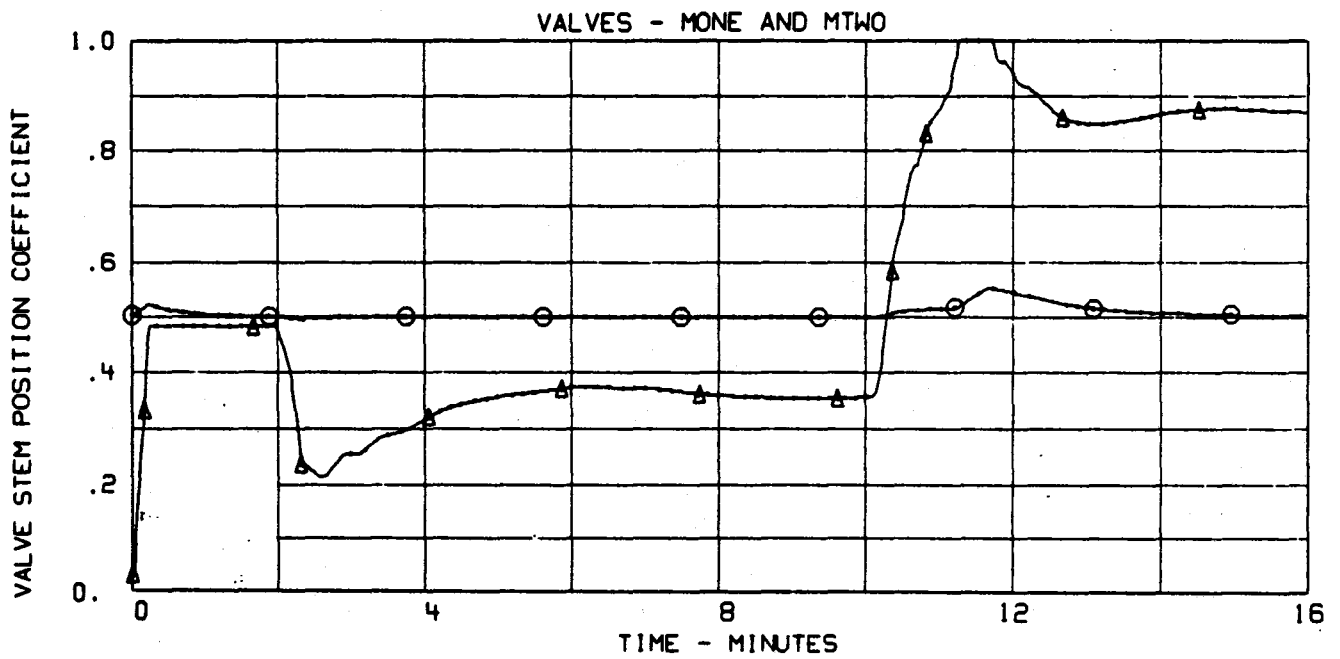
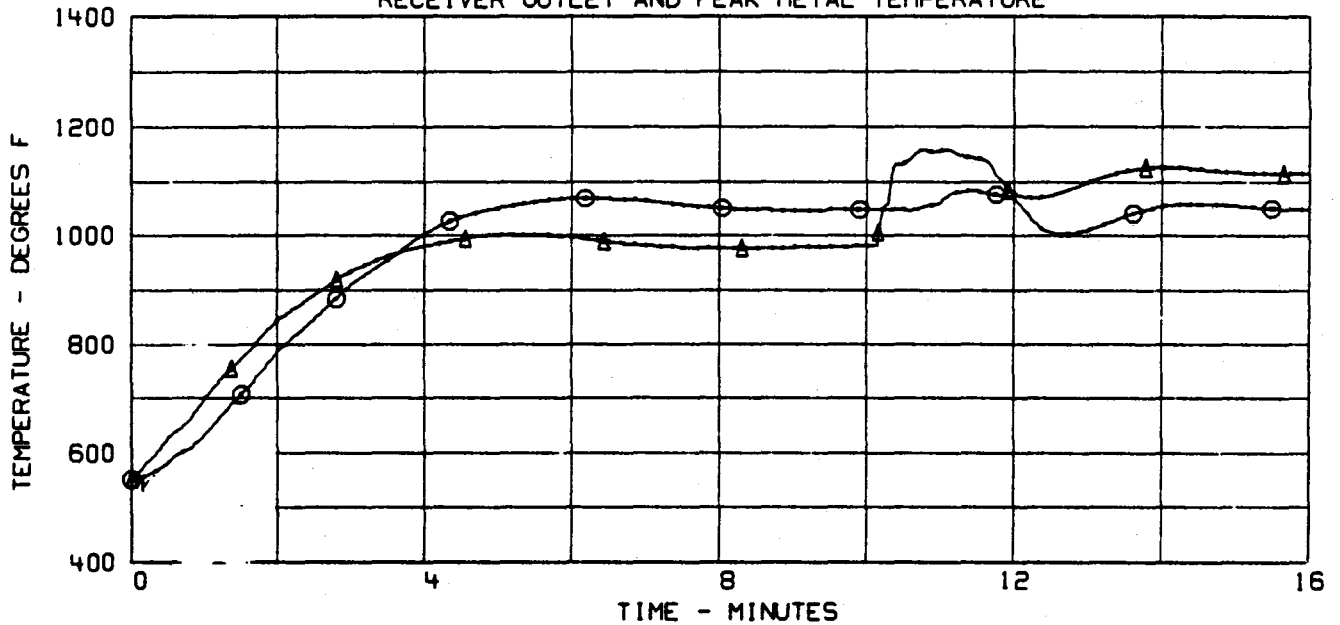


Figure 3.9a

# TRANSIENT SYSTEM ANALYSIS MODEL

## RECEIVER PEAK METAL TEMPERATURE COMPARISON

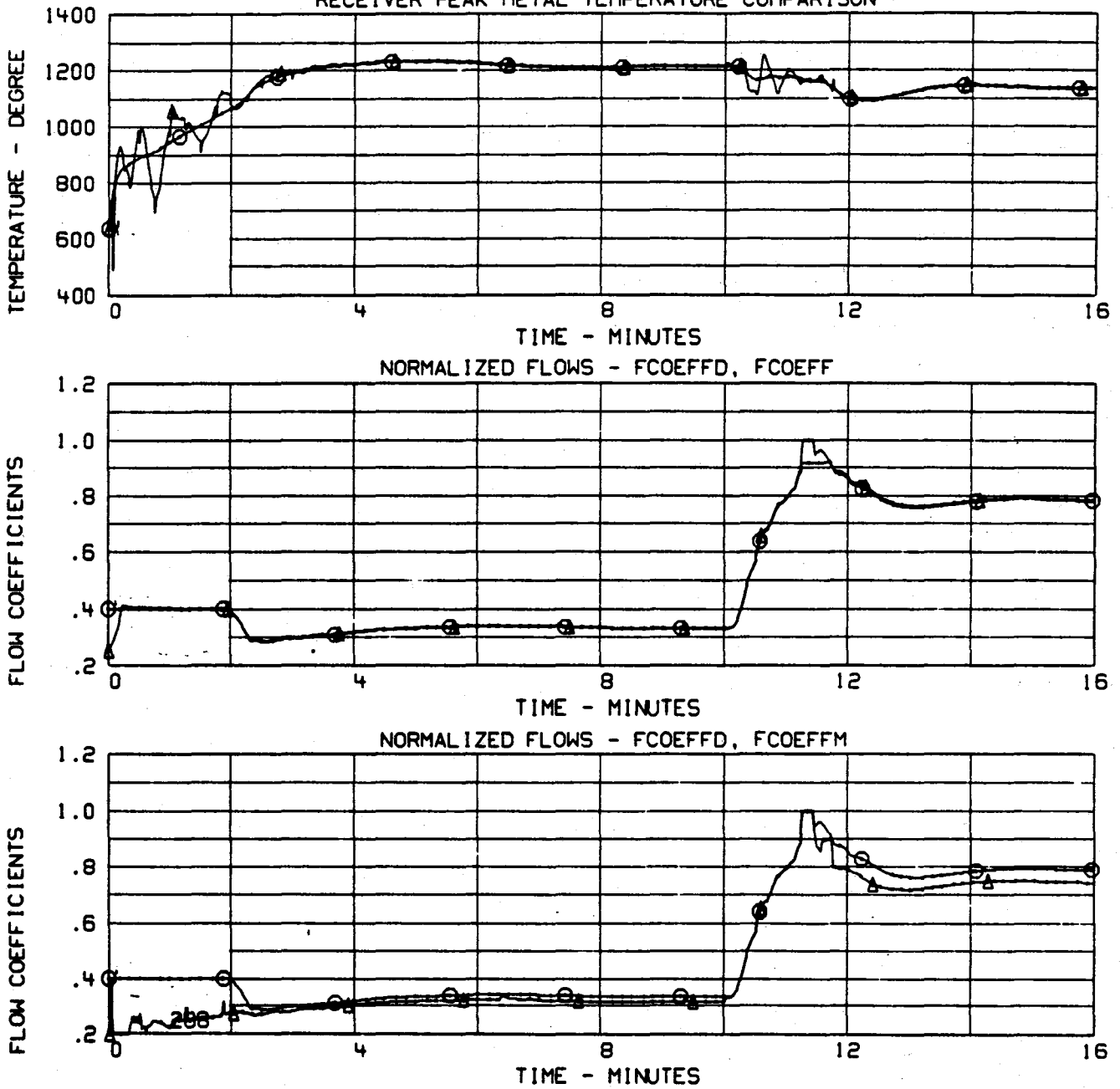


Figure 3.9b

- b. integration of salt temperature limits into equation 3.23 to "steer" the receiver away from limiting temperatures.

The latter feature, b, was attempted using a barrier function, but this led to undesirable effects on stability and was abandoned.

### 3.6 Maximum Thermal Load

The baseline design does not use the maximum feasible thermal power generated by the heliostat field at midday. With all the heliostats operating, a maximum relative power would be 116%. Using this as a new level, the same cloud transient was re-run to determine whether a flow rate maximum of 125% design load would be sufficient.

Figure 3.10 show the results which should be compared with the standard run shown in Figure 3.8. Note that the wall temperature limit of 1200°F was again applied as shown in Figure 3.10b.

Figure 3.10a shows the salt temperature to overshoot and not be controlled to 1080°F as defined by the limits set point. The cause of this is obvious from the valve histories of MONE and MTWO. As can be seen, the higher flux level of 116% requires the feed forward valve to be fully open. This results in a flow error, illustrated by the flow and demand histories shown in Figure 3.10b. This error drives the feedback controlled valve which corrects the error. It can be seen from the response of that valve that there is scope for improvement. A revision to the control of the parallel valves would enable the salt temperature overshoot to be reduced.

However, even without the revision to the control systems, the receiver was safely controlled through this extreme transient.

# TRANSIENT SYSTEM ANALYSIS MODEL

## RECEIVER OUTLET AND PEAK METAL TEMPERATURE

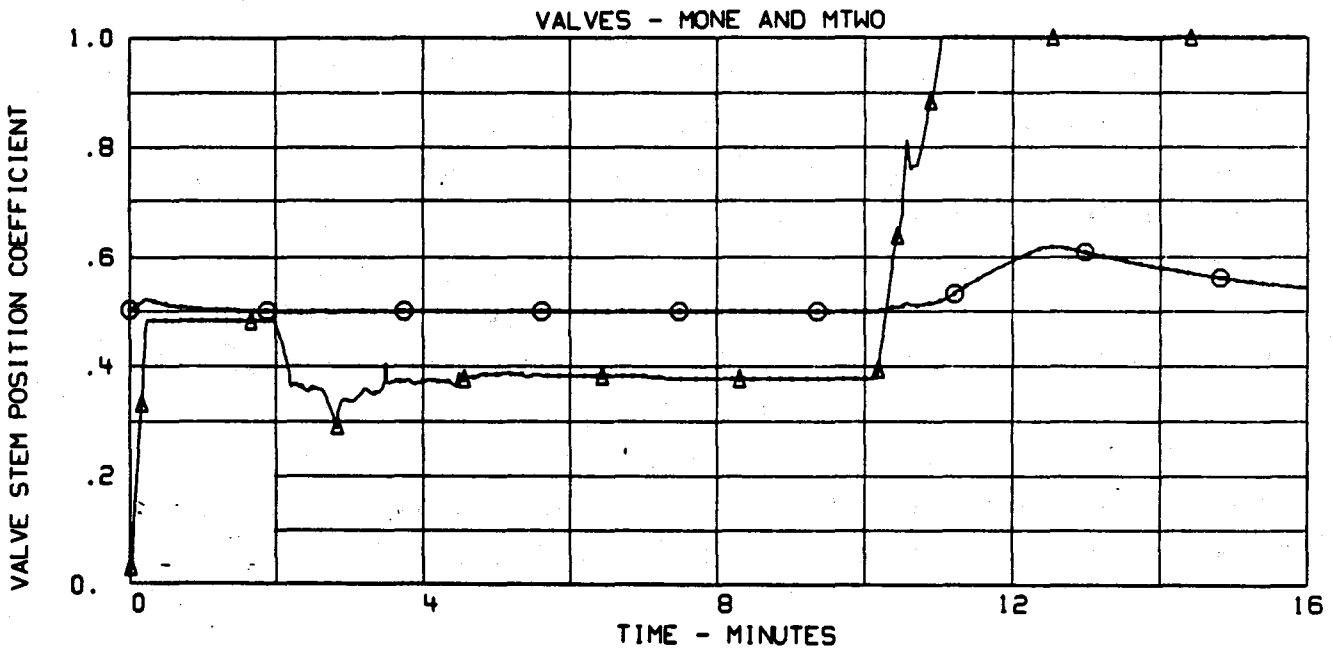
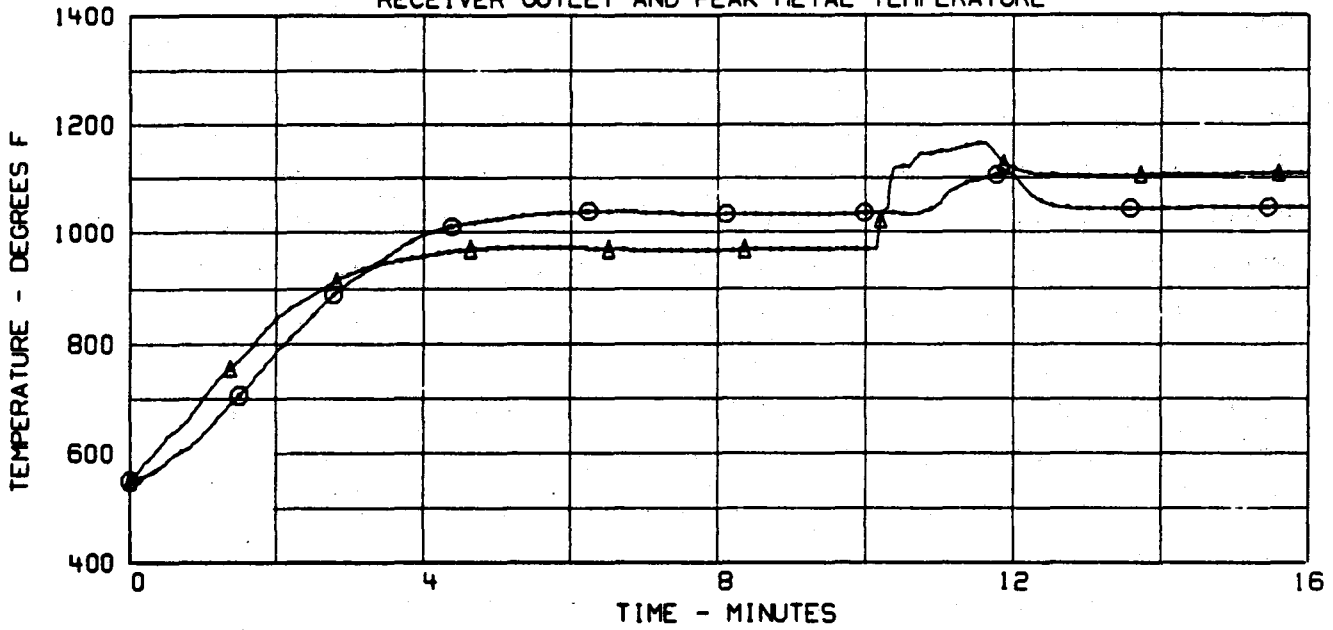


Figure 3.10a

# TRANSIENT SYSTEM ANALYSIS MODEL

## RECEIVER PEAK METAL TEMPERATURE COMPARISON

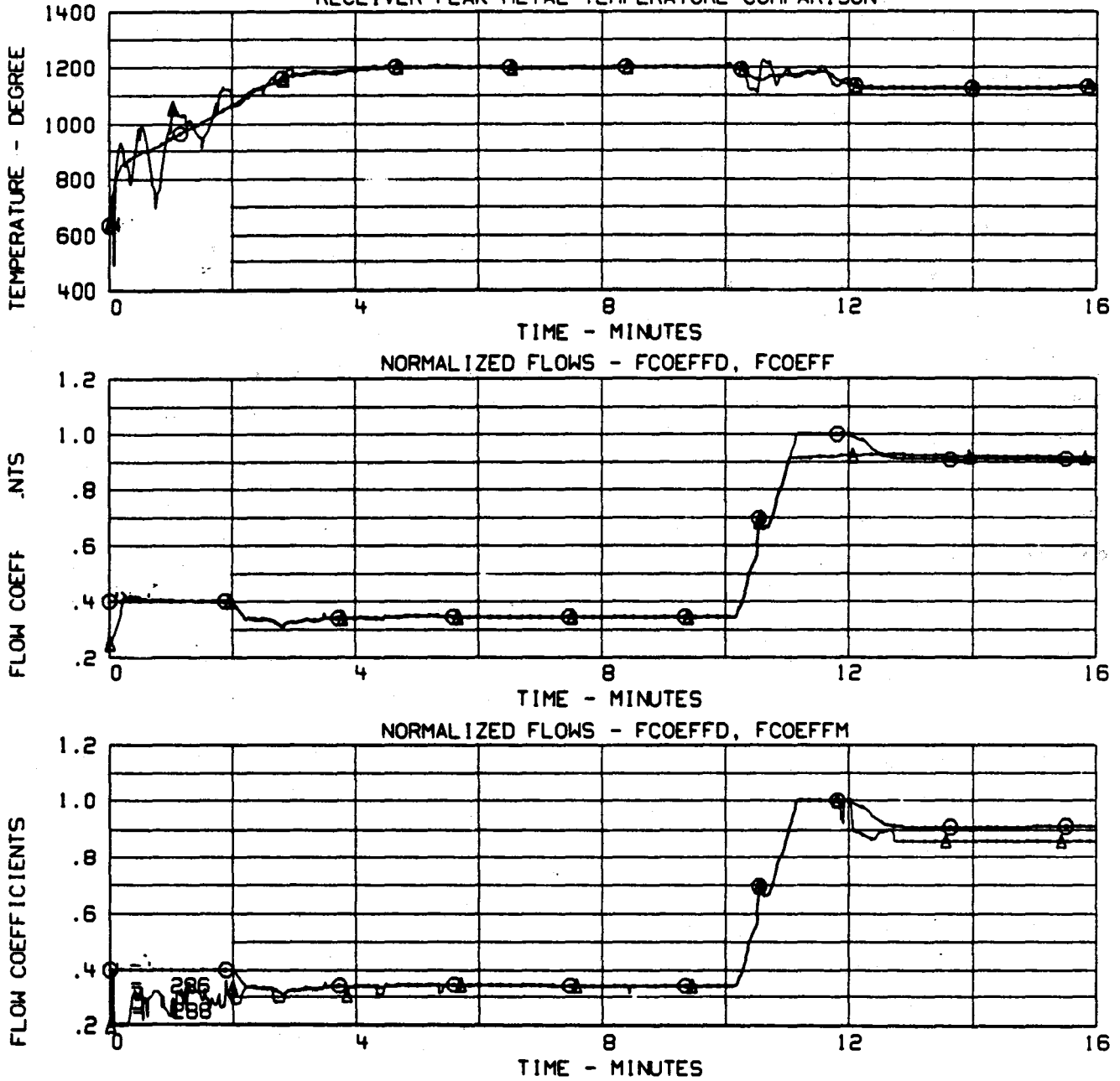


Figure 3.10b



### 3.7 Group Cloud Transient

The partial cover cloud transient was considered a worst case due to the distorted flux profile producing large temperature overshoots. In addition to this a further transient has been investigated; the group cloud transient.

The group cloud transient consists of a number of clouds sequentially crossing the field distorting the flux profile by casting shadows which traverse the receiver. The consequent effect on absorbed power is illustrated by the history shown in Figure 3.11a.

The results are shown in Figures 3.11, b, c, and d. As can be seen, the control algorithm successfully cycles the salt flow to match absorbed power and the salt outlet temperature is kept well within tolerable limits. Comparison of flow demand and the minimum flow level show the effect of salt temperature limit in minimizing the temperature overshoot.

In conclusion, it can be seen that the group cloud transient can be controlled well within limits.

TRANSIENT SYSTEM ANALYSIS MODEL -

ABSORBED POWER IN MEGAWATTS

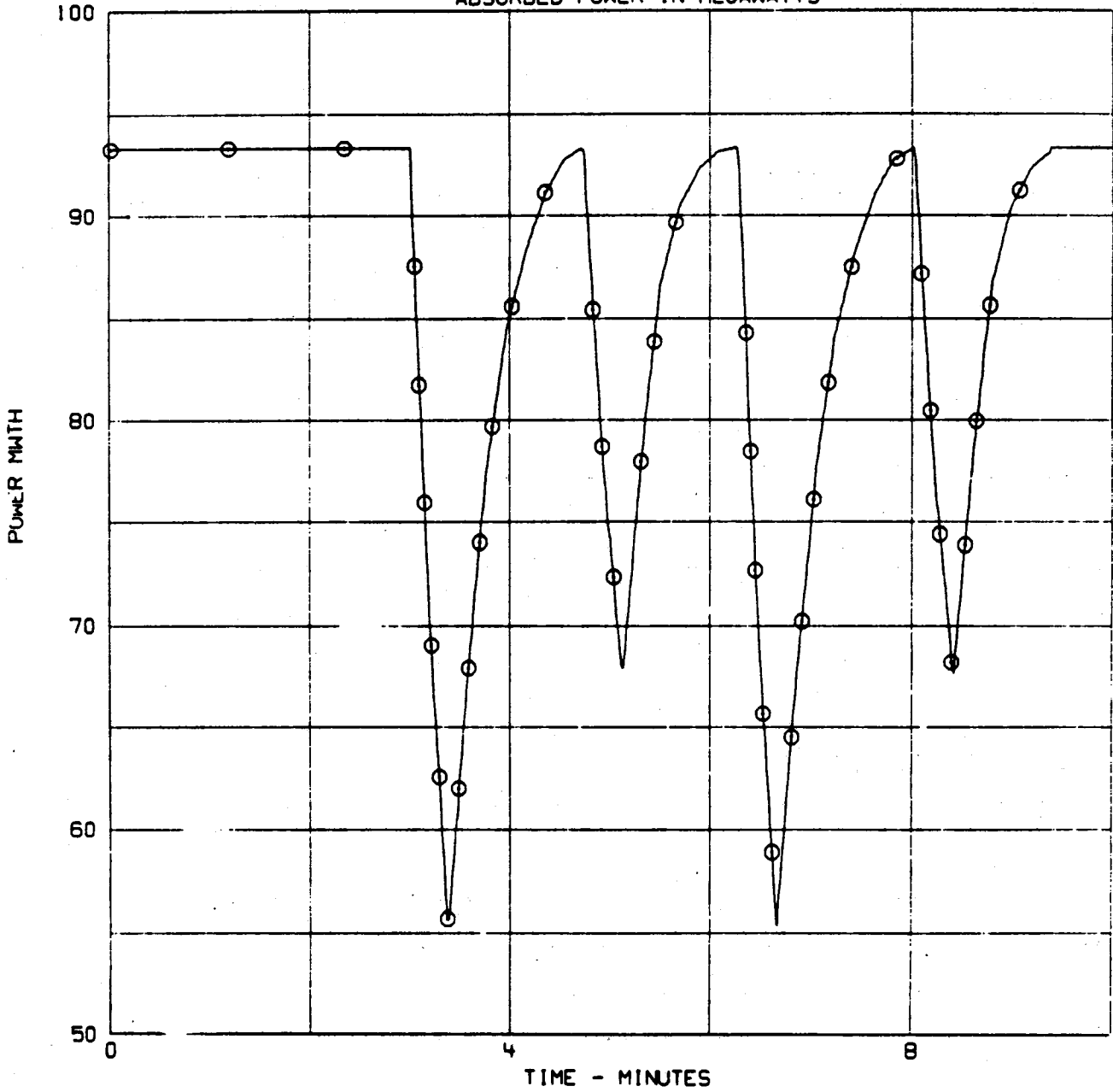


Figure 3.11a

TRANSIENT SYSTEM ANALYSIS MODEL -  
RECEIVER OUTLET AND PEAK METAL TEMPERATURE

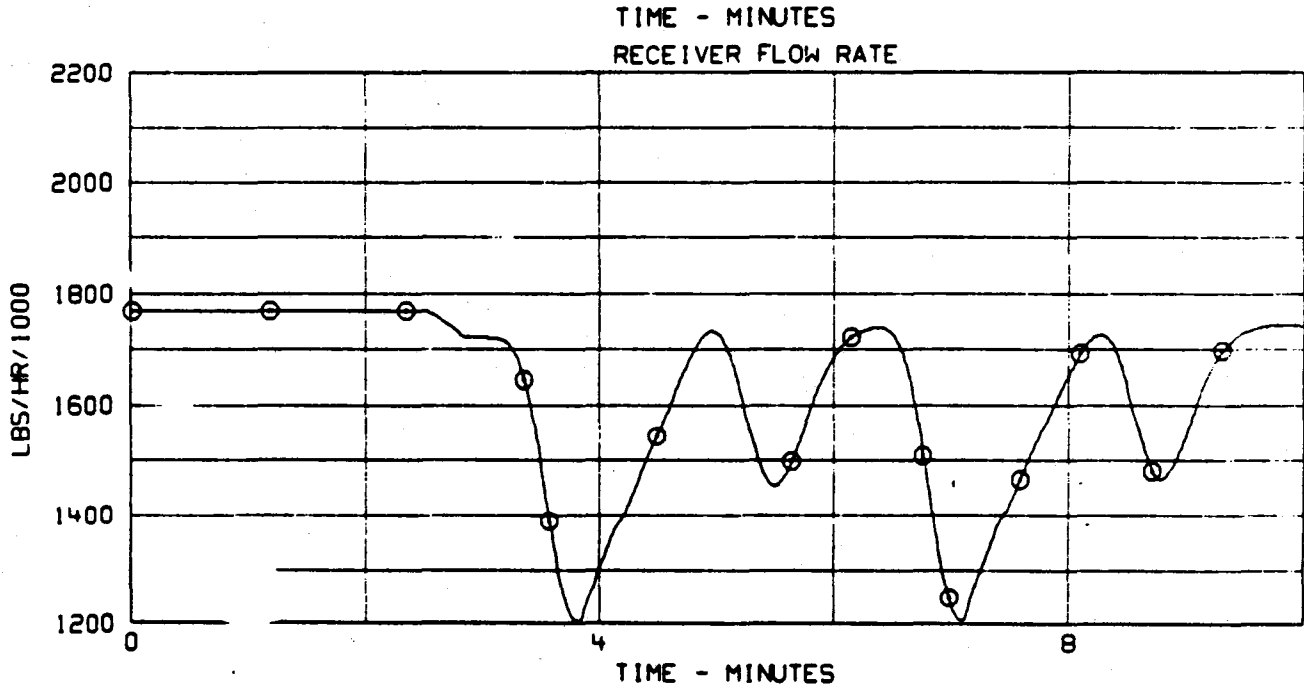
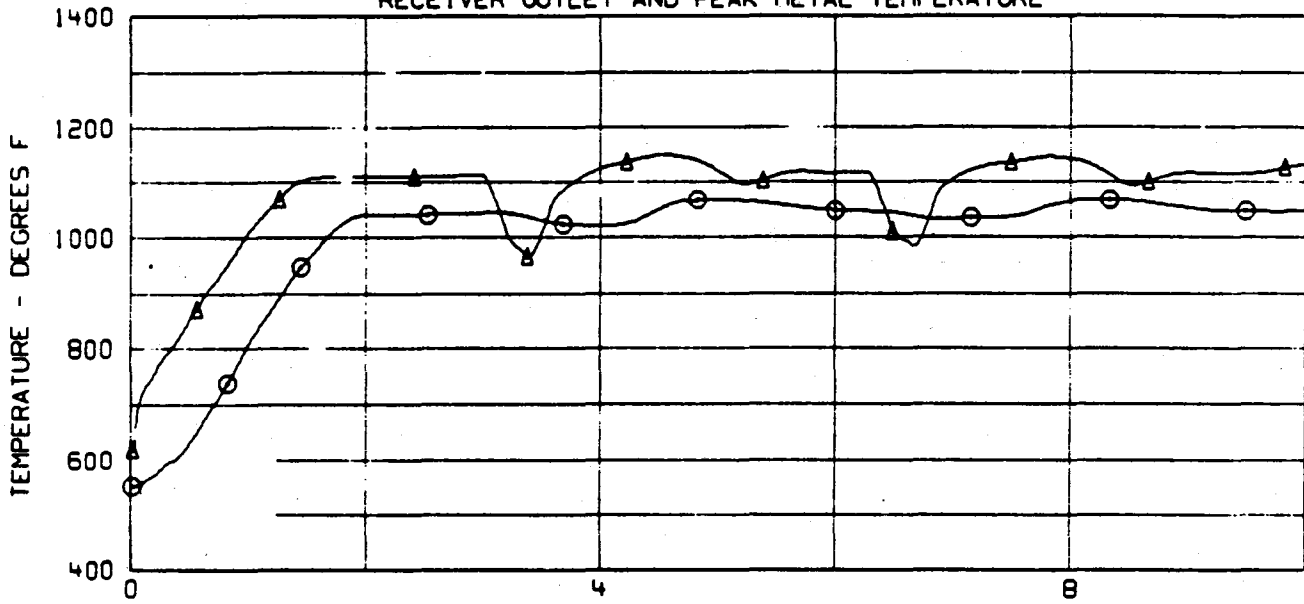
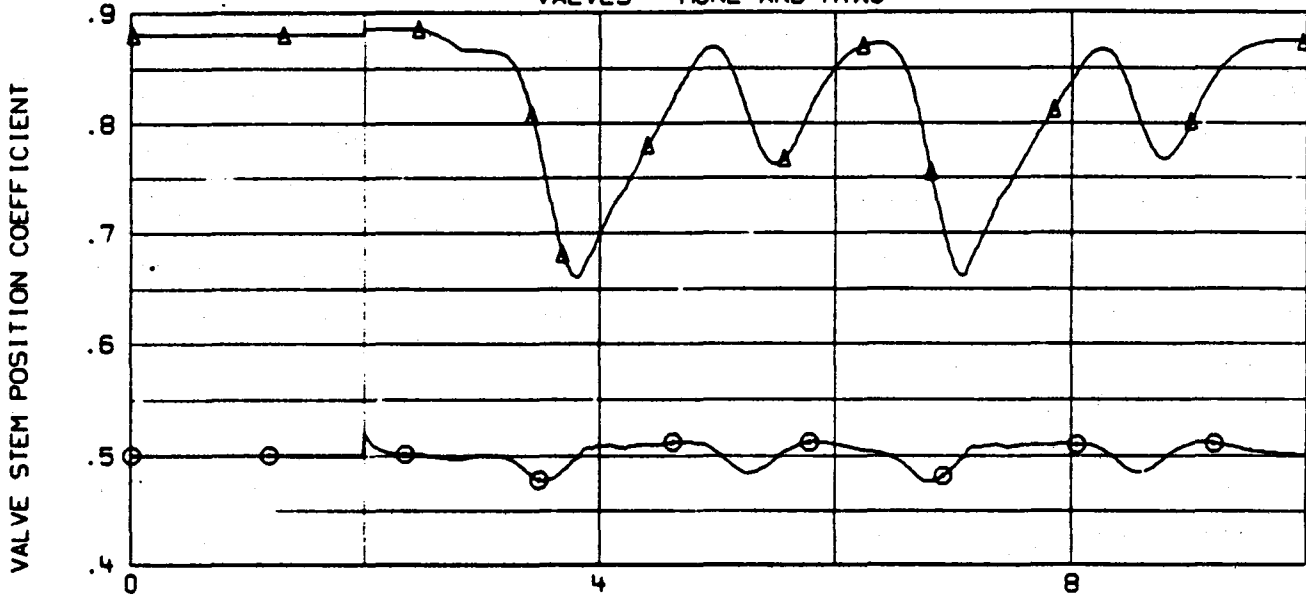


Figure 3.11b

# TRANSIENT SYSTEM ANALYSIS MODEL

## VALVES - MONE AND MTWO



## RECEIVER PEAK METAL TEMPERATURE COMPARISON

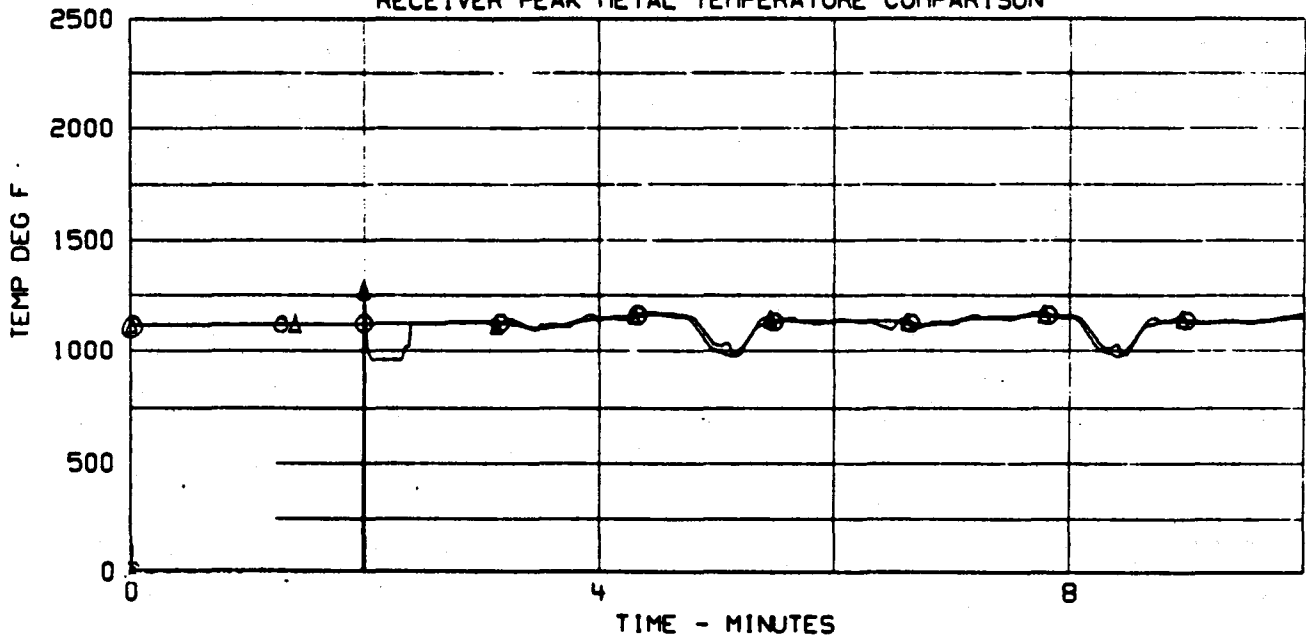
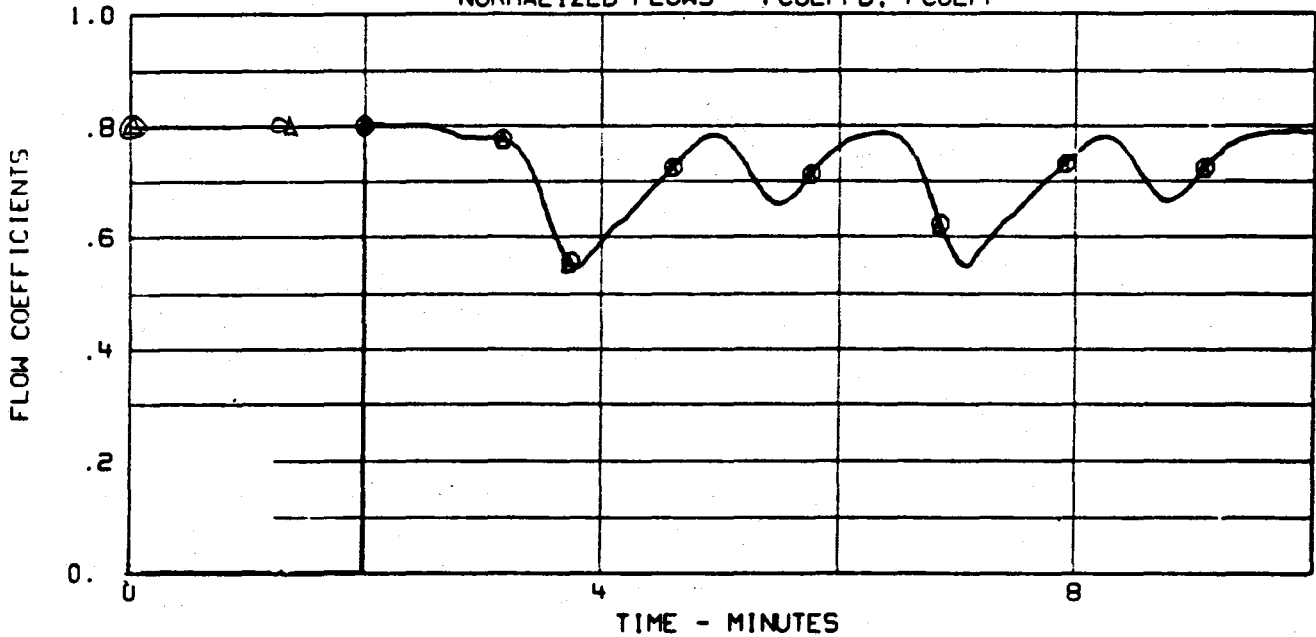


Figure 3.11c

# TRANSIENT SYSTEM ANALYSIS MODEL

NORMALIZED FLOWS - FCOEFFD, FCOEFF



NORMALIZED FLOWS - FCOEFFD, FCOEFFM

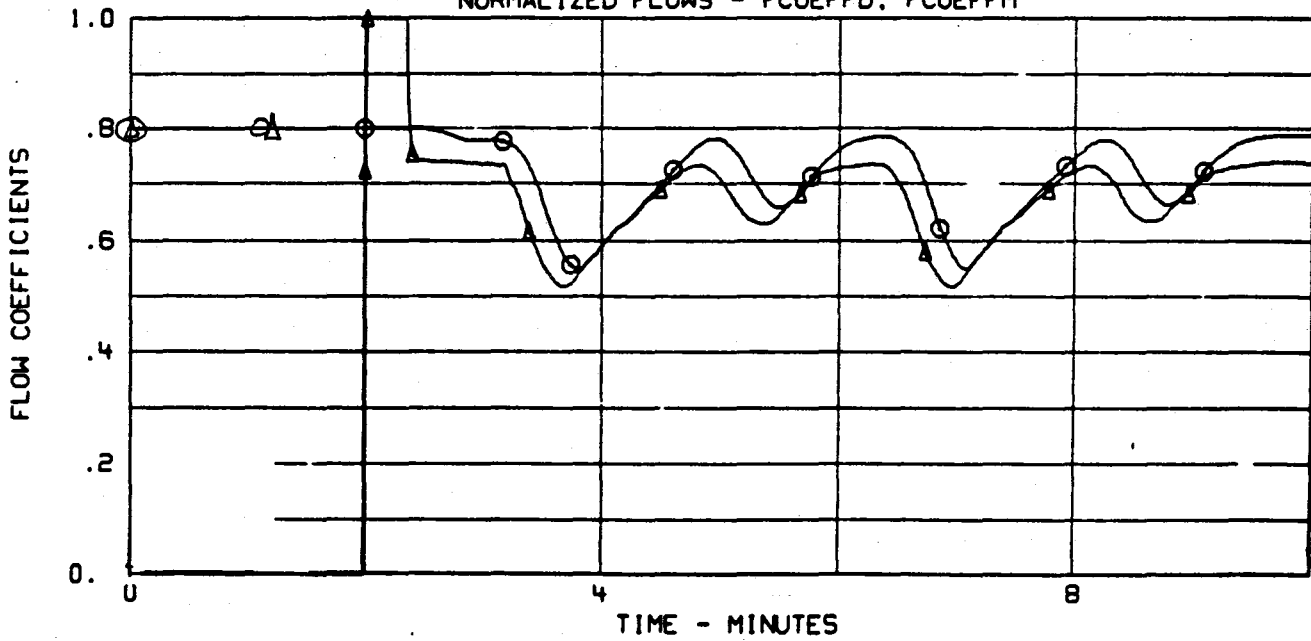


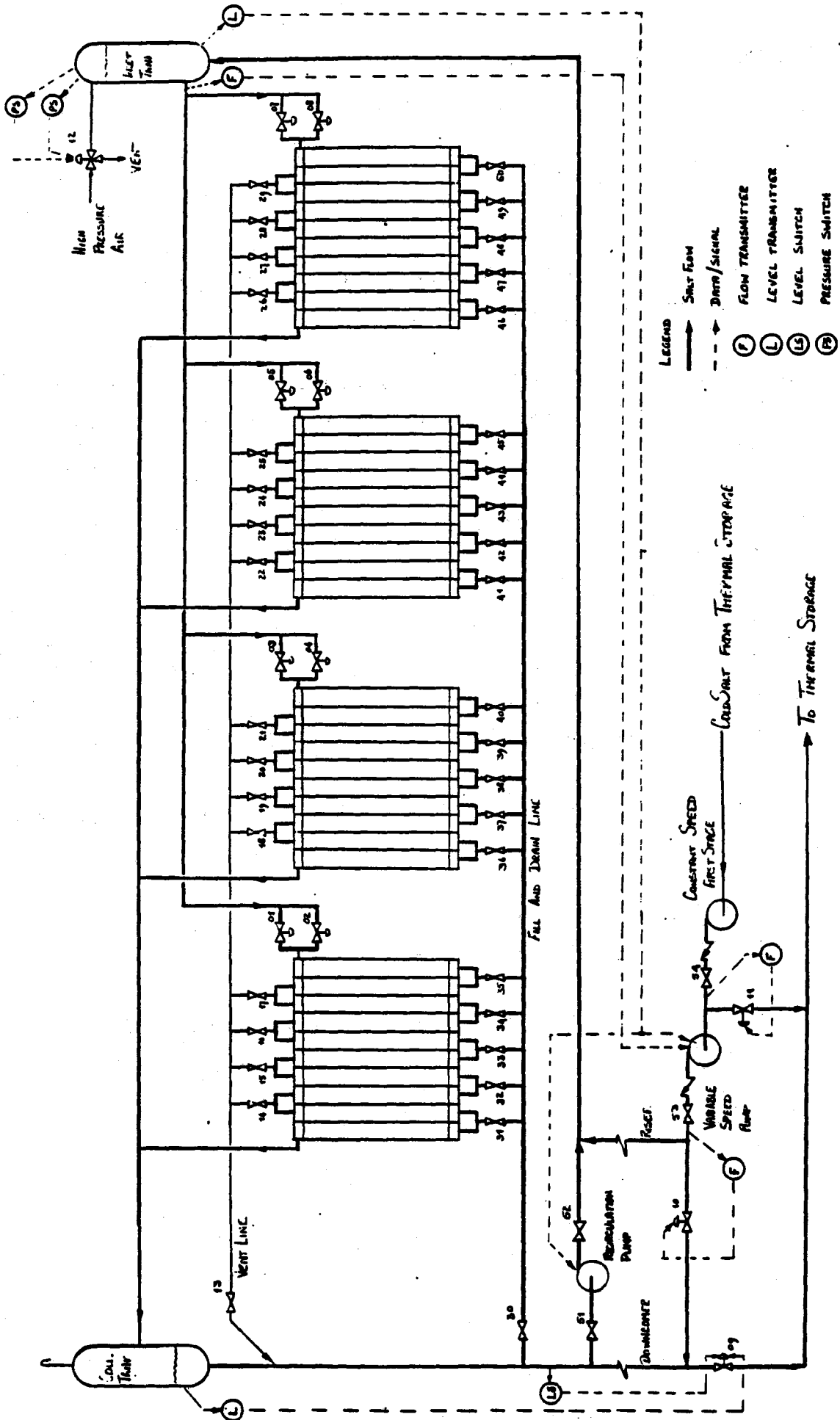
Figure 3.11d

## 4. CONTROL FOR STARTUP AND OPERATION

### 4.1 Salt Flow Control Functions

The general controls for the receiver are shown in figure 4.1. The control functions include:

- a) Collection Tank level control, ensuring single phase flow of salt in the downcomer and dissipating excess fluid energy across the valve (09),
- b) Inlet Tank level control is used to minimize the parasite power of the cold salt feed pumps.
- c) Minimum Flow controls using valves 10 and 11 ensure a minimum flow through the feed pumps (they could also be used to control the temperature of the salt returned to thermal storage such that the salt could be dumped into the cold salt tank if required).
- d) Recirculation Pump control is used during overnight standby to circulate salt.
- e) Inlet Tank pressure control is bang-bang type used for initial pressurization and emergency usage.
- f) During hot salt generation, the salt flow through the receiver is controlled by valves 01-08 as explained in the next section.



- LEGEND
- Salt Flow
  - Drain/Signal
  - (P) Flow Transmitter
  - (L) Level Transmitter
  - (LS) Level Switch
  - (PS) Pressure Switch

RECEIVER CONTROL SCHEMATIC

FIGURE 4: C-52

## 4.2 Salt Flow Control During Receiver Operation

The previous chapter described the use of QFFC and it's application to the thermal receiver. The control function diagram as applied to one zone is shown in Figure 4.2. Included are additional features for system redundancy. These minimize the down-time due to failures as well as maximizing the safety of the receiver. These features are:

- a) Header Temperature Auction selects the median value of three independent measurements of each header temperature. This level of integrity can include the low-level signal sensor and A-D converter by inputting each measurement on independent boards. Hence, any one of the three measurements of header temperature from the thermocouple through to the A-D converter can fail without loss of control of that panel. Process controllers generally include the necessary firmware to implement this strategy.
- b) Flow Sensor Redundancy is achieved by measuring the flow from the inlet tank feeding all four zones. This can be used to back-up any one of the flow sensors related to the eight FCV's. Identification of a failed flow sensor is made via the knowledge of inlet tank pressure and the position of each FCV.
- c) Flow Control Valves are redundant in that even with one FCV out of commission, the control can be reconfigured to control flow using the remaining parallel valve.

## 4.3 Receiver Warm and Fill Procedure

The startup of the receiver requires the following steps.

- 1) Warm the receiver with trace heating and heliostats.



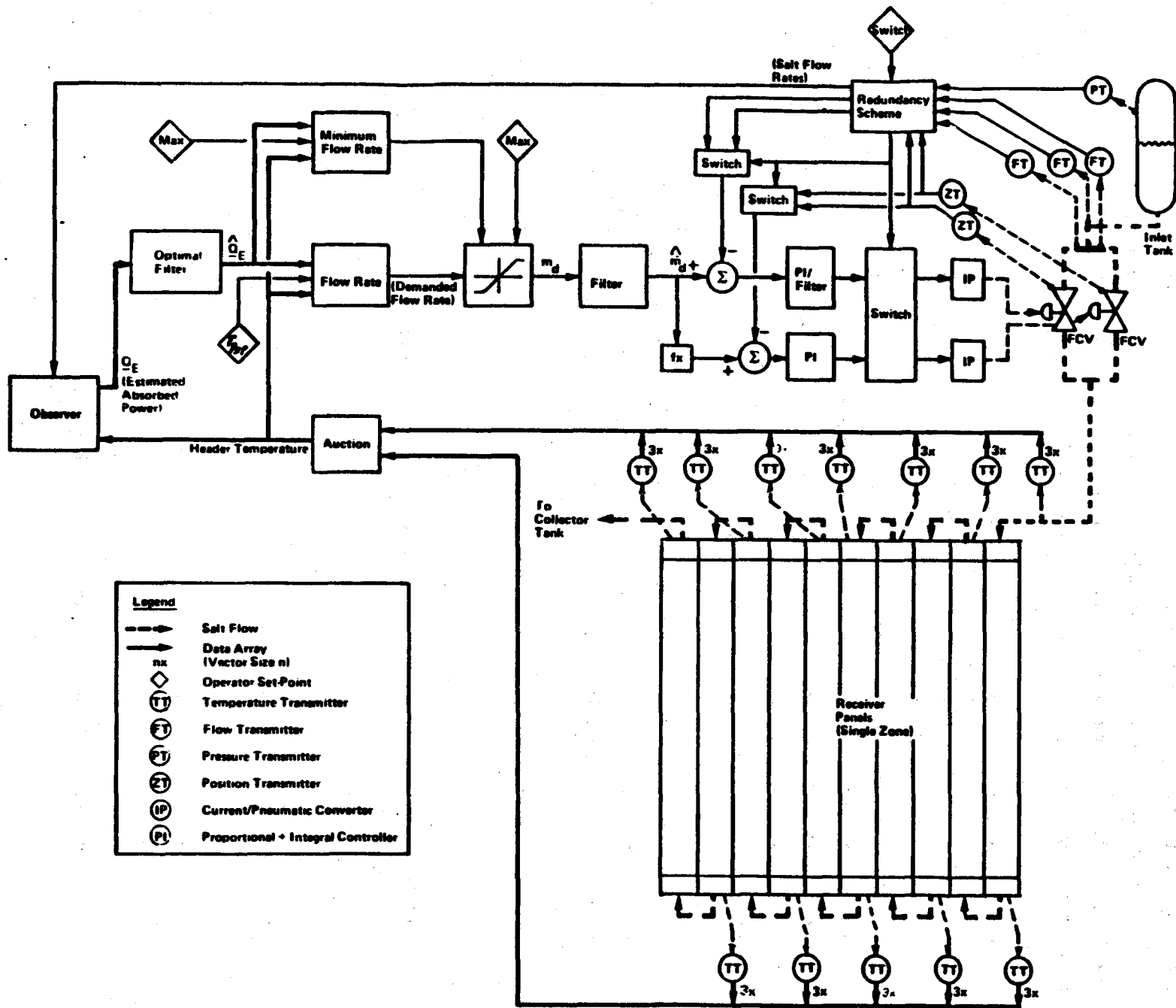


FIGURE 4.2 - CONTROL SYSTEM SCHEMATIC

2) Fill the receiver with cold salt (@ 550°F).

This prewarm of the receiver, step one, requires feedback to the operator indicating panel temperature. For this purpose the thermocouple probes situated in the panel headers can be used. But additional measurements of the tube temperature will be required. To this end radiometers situated in each cavity will be focused on specific panels areas which are indicative of the receiver temperature (three in each cavity should suffice). The trace heaters used for prewarm also require thermocouple measurements: up to ten trace heaters will be used with two thermocouples measuring the control temperature.

In total, instrumentation for prewarm, required in addition to that for control, can be summarized as:

- i) 3 radiometers per cavity,
- ii) up to 20 thermocouples.

Having warmed the receiver, the fill procedure can be commenced. This sequence of events is summarized by Table 4.1 and assumes salt flow to the pumps has been established.

TABLE 4.1 - RECEIVER FILL PROCEDURE

<u>STEP</u>	<u>FUNCTION</u>
1	Start pumps with V09-10 open and V11 controlling minimum flow through constant speed pumps.
2	Open V01-08 and V12-50.
3	Enable collection tank level control via V09.
4	On stabilizing tank levels: Close V01-08, V13-29 and V31-50.
5	Change V09 level setpoint to empty drain/fill line.
6	Close V30, then reset V09 level set point.
7	With stable collection tank level, apply inlet Tank level control to V10 and variable speed pump control.
8	Pressurize Inlet Tank via V12.

#### 4.4 Receiver Trip Conditions

The trip conditions outlined in Table 4.2 will first alarm the operator when they exceed certain bounds. If the condition continues to deteriorate and exceed a second bound, the receiver will trip. The consequences of a receiver trip will be the immediate defocus of the heliostats.

All of the instrumentation requirements for the trip function are covered by those of the startup and normal operation of the receiver.

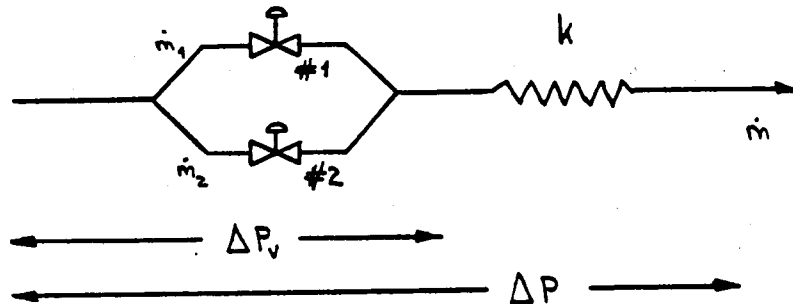
**TABLE 4.2 - RECEIVER TRIP CONDITIONS**

1. Inlet Tank; pressure loss, low level
2. Cold Salt Pumps; pressure loss, low cold salt sump level
3. Outlet Tank; level too high
4. Pneumatic Power; excessive valve positioning error due to loss of pneumatic power
5. Receiver Panels; excessive heating (temperatures)
6. Receiver Door; accidental closure
7. Instrumentation; multiple failures

5. CONTROL HARDWARE

5.1 Salt Flow Control Valves

In choosing the type of flow control valve it is necessary to consider the linearity of the installed flow characteristics. The following analysis pertains to the parallel valves FCV1 and FCV2 configured as shown below:



- where:  $\dot{m}_*$  = salt flow rate  
 $\Delta P_v$  = pressure drop across valves  
 $\Delta P$  = total pressure drop to atmospheric  
 $k$  = receiver pressure drop constraint of proportionality

The flow through both valves is defined by:

$$\dot{m} = a_1 C_v (\rho \Delta P_v)^{1/2} \quad \text{_____} \quad (5.1)$$

$$\dot{m}_2 = a_2 C_v (\rho \Delta P_v)^{1/2} \quad \text{_____} \quad (5.2)$$

where both valves are sized to give the same  $C_v$  at 100% open, and

$a_x$  = fractional open of valve,  $a \in [0,1]$

$\rho$  = density of salt

the pressure drop across the whole is:

$$\Delta P = \Delta P_v + km^2 \quad (5.3)$$

Defining the non-dimensionilized flow as

$$f = \frac{\dot{m}}{\dot{m}_{MAX}} \quad (5.4)$$

and substituting 5.3 into 5.4, we have:

$$f^2 = \frac{\Delta P - \Delta P_v}{\Delta P - \Delta P_{v_{min}}} \quad (5.5)$$

where  $\Delta P_{v_{min}}$  is the pressure drop across the valves fully open.

From equation 5.1 and 5.2 we have:

$$\dot{m}^2 = (\dot{m}_1 + \dot{m}_2)^2 = C_v^2 \rho \Delta P_v (a_1 + a_2)^2 \quad (5.6)$$

$$\dot{m}_{MAX}^2 = \left( \dot{m}_{1_{MAX}} + \dot{m}_{2_{MAX}} \right)^2 = C_v^2 \rho \Delta P_{v_{min}}^4 \quad (5.7)$$

Hence, equations 5.4, 5.6 and 5.7 yield:

$$f^2 = \frac{\Delta P_v}{\Delta P_{v_{min}}} \cdot \left( \frac{a_1 + a_2}{2} \right)^2 \quad (5.8)$$

combining 5.5 with 5.8

$$f = \frac{1}{\left[ 1 + \frac{\Delta P_{v_{\min}}}{\Delta P} \left\{ \left( \frac{2}{a_1 + a_2} \right)^2 - 1 \right\} \right]^{\frac{1}{2}}} \quad (5.9)$$

From equation 5.9 the linearity of a valve set can be investigated. For this two types have been considered:

$$\text{Linear Valve: } a = m \quad (5.10)$$

$$\text{Equal \% Valve: } a = R^{m-1} \quad (5.11)$$

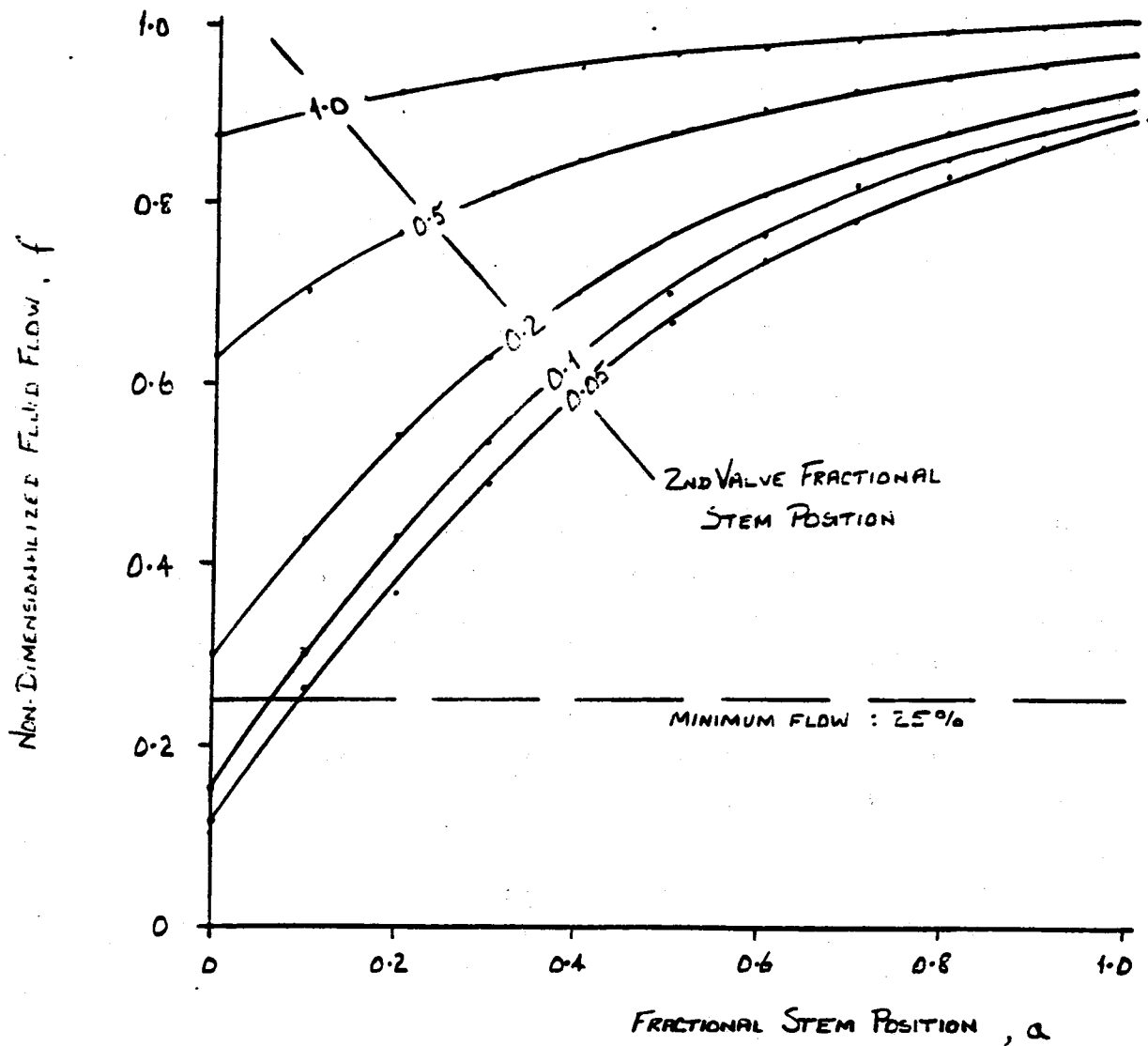
where:  $m$  = valve stem position,  $m \in [0,1]$   
 $R$  = rangeability (assumed = 50)

Figures 5.1 and 5.2 shown the flow characteristics for both types of valves. Comparing the two figures it can be concluded the equal percentage valve give the best flow vs position characteristics for the following reasons:

- a) Linear Valves have a large stem travel to achieve full flow, stem travel should be minimized.
- b) Linear Valves give non-linear flow characteristics over the mid-range of operation and a low gain over the high-flow range.
- c) Equal percentage valves need only be operated between 40% and 100% open due to the 25% minimum flow operation.
- d) Over the majority of working range (50-100%) the equal percentage valves yield good linearity, simplifying feedback control.

For these reasons, equal percentage valves should be used for receiver flow control. Hence, the flow characteristics described by Figure 5.2 were implemented in the control subroutine used for the MITAS results.

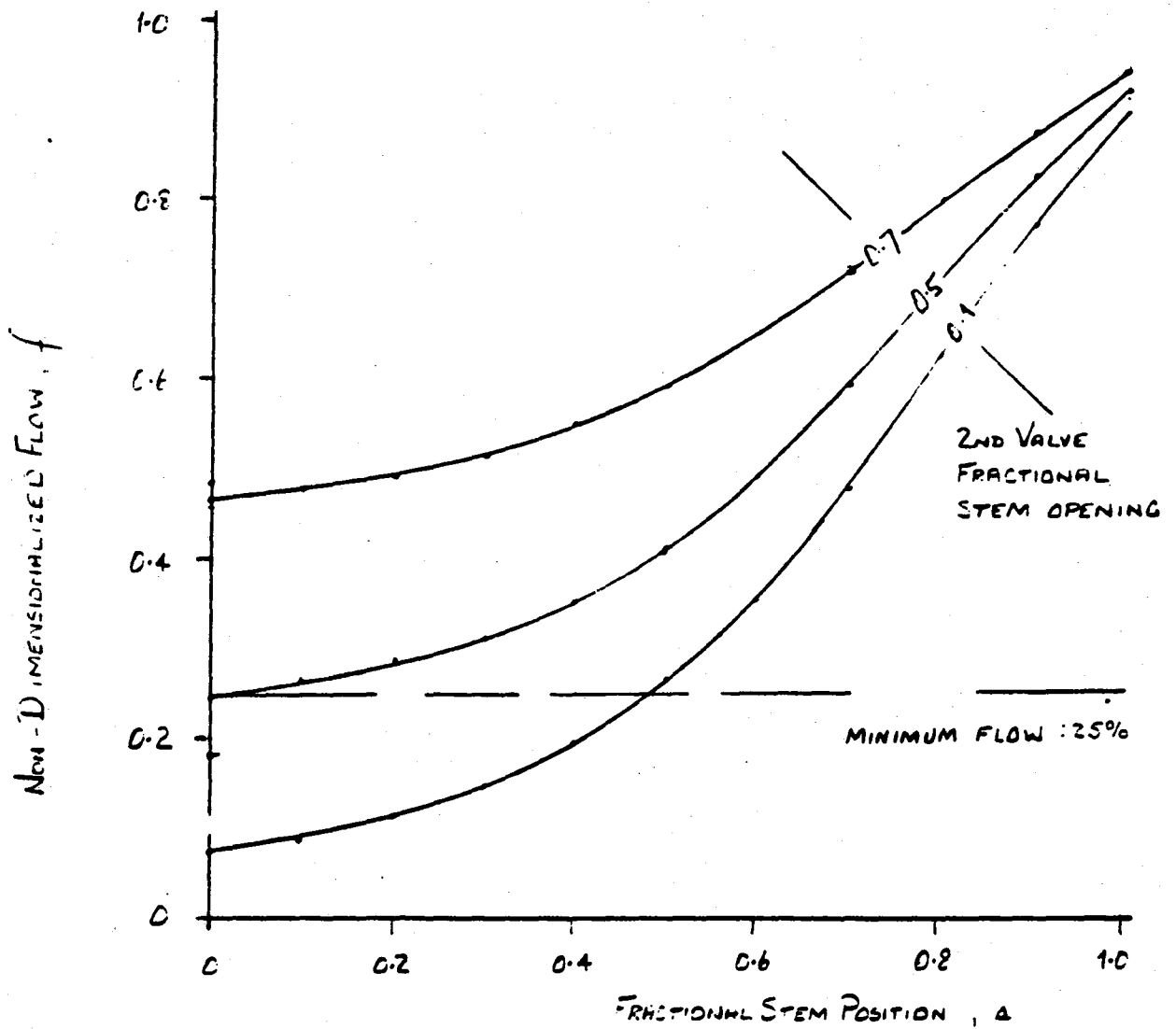




PRESSURE RATIO :

$$\left\{ \frac{\Delta P_{V_{MIN}}}{\Delta P_{MAX}} \right\} = 0.10$$

INSTALLED FLOW CHARACTERISTIC : LINEAR VALVES



PRESSURE RATIO :  $\left( \frac{\Delta P_{V_{MIN}}}{\Delta P_{MAX}} \right)$

INSTALLED FLOW CHARACTERISTIC : EQUAL % VALVES

## 5.2 Hardware for Control Algorithms

The general controls outlined by Figure 4.1 consist of standard PID type controls and can be realized using hardware readily available. The receiver flow control algorithm, however, is non-standard as it consists of a specialized control algorithm.

There is the option to use one of three possible control algorithms: simple OFFC, OQFFC with a limit on salt temperature and OQFFC with optimal filtering and the control of panel wall temperature. The first two cases can be solved using PID controllers as will be shown, but the optimal filtering and wall temperature control require software more advanced than a PID.

The simple QFFC and OQFFC with salt temperature limit both use a PID type algorithm to construct an observer. Recall, the digital form of an observer is:

$$\frac{Q_E}{C_p} = \dot{m}(T_o - T_i) + \sum_{n=1}^N m_n \frac{(T_n(t+\Delta t) - T_n(t))}{\Delta t} \quad (5.12)$$

The digital form of the PID controller is:

$$\Theta = k_p \left[ \epsilon + \frac{\Delta t}{T_I} \sum \epsilon + \frac{T_D}{\Delta t} \cdot (\epsilon(t+\Delta t) - \epsilon(t)) \right] \quad (5.13)$$

As can be seen, the two forms can be equated making the following observations:

$$\frac{Q_E}{C_p} = \sum_{n=0}^N \theta_n \quad (5.14)$$

$$\theta_o = k_p \varepsilon \quad (5.15)$$

where  $k_p = \dot{m}$  (adaptive gain)  
 $\varepsilon = (T_o - T_i)$

$$\theta_k = k_p \left[ \varepsilon_k(t+\Delta t) + \frac{T_D}{\Delta t} (\varepsilon_k(t+\Delta t) - \varepsilon_k(t)) \right] - \varepsilon_k(t+\Delta t) \quad (5.16)$$

where  $k_p = 1$   
 $\varepsilon = T_n$   
 $T_D = m_n$  (constant)  
 $k =$  panel reference (1 through N)

The remainder of the blocks used in the simple QFFC and OQFFC with salt temperature limits are found in the standard software of digital controllers.

The application of panel wall temperature control requires the use of data histories of the optimal filters and adaptive model. These take the form of FILO stack holding a limited number of samples forming the history. This type of software is not generally available in the PID type controllers. However, this control can be applied when either multi-loop controllers or a larger computer are used for direct digital control. Also, some manufacturers such as Westinghouse provide a calculator type card which could be used for this control. Similarly, Bailey (Network 90) will soon be marketing a micro-processor which can be mounted in the distributed control rack and programmed in BASIC (it

is not limited to specialized software as are the control cards). Consequently, although the panel temperature control algorithm cannot as yet be realized in distributed type systems, it is envisaged that this limitation of hardware will be short lived and would not cause a real problem long term.

### 5.3 Instrumentation for Control and Data Acquisition

The controls defined in the text and for the configuration illustrated in Figure 4.1 have been listed in Table 5.1 and summarized in Table 5.2.

TABLE 5.1 - INSTRUMENTATION LIST

ITEM	MEASUREMENT	RANGE	FUNCTION	QTY	COMMENTS
1	Collection Tank Level		Level feedback to V09	1	
2	Downcomer Level Switch	ON-OFF	Emptying Fill/Drain line during start-up operation	1	
3	Flow through variable Speed Pump		i) Minimum flow through V10 ii) Variable speed control	3	Assuming three pumps in parallel, one flow sensor is required for each
4	Flow through Constant Speed Pump		Minimum flow through V11	1	Assuming the constant speed pumps feed a common header, only one sensor is required
5	Inlet Tank Level		Level feedback to variable speed pumps for trim of flow control	1	
6	Flow from Inlet Tank		i) Provides redundancy to flow measurements through V01-08 ii) Control of variable speed pumps	1	
7	Inlet Tank Pressure Switches	ON-OFF	Bang-Bang control of pressure in inlet tank	2	Generally only used during start-up and emergencies.
8	Inlet Tank Pressure		Used in the FCV redundancy scheme	1	
9	Flow to FCV's		Flow feedback on V01-08	8	Each of the four zones requires two flow sensors
10	Salt Temperature		Used by the absorbed power 'Observer'	144	Each header has three sensors which are auctioned to provide redundancy. These are thermocouple probes.

TABLE 5.1 - INSTRUMENTATION LIST (CONTINUED)

ITEM	MEASUREMENT	RANGE	FUNCTION	QTY	COMMENTS
11	Trace Heater Temperature		Monitor prewarm	20	10 independent measurements
12	Wall metal temperatures		i) Monitor for trip conditions and failures during Hot Salt generation ii) Monitor for pre-warmup by heliostats and trace heating	12	Radiometers must be used for this measurement, 3 per zone.
13	Status of Isolation Valves V13-50	ON-OFF	used during start-up and shut down procedures.	37	
14	Status of Isolation Valves V51-52	ON-OFF	using during warm stand-by	2	
15	Status of Isolation Valves V53-54	ON-OFF	Remote isolation during failures	6	
16	Position of FCV's V01-08		Used by redundancy scheme	8	
17	Position of FCV's V09-11		DA only	3	
18	Position of V12		DA only	1	
19	Motor Speed for variable speed pumps		DA only	3	assuming three pumps
20	Variable speed pump pressure		Failure condition	3	assuming three pumps
21	Constant speed pump pressure		Failure condition	3	assuming the first stage consists of two series pumps.

TABLE 5.2 - INSTRUMENTATION SUMMARY

ITEM	QUANTITY
Thermocouples	164
Radiometers	12
Flow measurements	13
Pressure measurements	10
Level measurements	2
Pressure switches	2
Level switches	1
Valve positions	12
Valve status (open/closed)	45
Motor speed	3



## 6. CONCLUSIONS

- 6.1 Quasi-Feedforward control should be used in preference to two-point temperature feedback control. Two-point temperature feedback control is very sensitive to discrepancy between temperature set-points and flux distribution as well as being prone to instability. In comparison, QFFC uses the one set-point and is thus insensitive to the distortions in flux distribution caused by cloud coverage. In addition to this advantage, QFFC is easily adapted and can be used to limit the peak salt temperatures by over-riding the main control.
- 6.2 Peak metal temperatures on the panel surface can be limit controlled using a radiometer for temperature measurement. The control uses the temperature measurement of the point to be controlled to continuously update an adaptive model. The model is then used to predict the panel temperature in order to control it by over-riding the salt flow rate control. As in the case of salt-temperature limiting, this control is an extension of QFFC.
- 6.3 The control hardware required to implement QFFC is readily available. The PID controller can be adapted for QFFC to implement both QFFC and OQFFC with salt-temperature limiting. However, the availability of a high-level language programmable controller would improve the efficiency and reliability of control as fewer hardware components would be required. Furthermore, this type of controller is required to implement the optimal filtering used for metal-temperature control. The requirement for high-level language for control limits the scope of hardware available if fully distributed control is a further requirement. However, there is no such limitation with DDC and the high-level language type controllers are becoming more available with distributed control hardware as time proceeds. Consequently, implementing the more advanced control algorithms is not considered to be problematic.

6.4 The analysis has shown that a quad-cavity receiver can be tightly controlled, comfortably within the requirements. Further analysis in the area of optimal control would be beneficial. Such study would be aimed at further reducing deviation in salt outlet temperature by modifying the cost function used for optimal control. Further attention to the control of parallel valves would also affect better control.

**Appendix D**  
**Skewed Heating Analysis**

**STRESS ANALYSIS OF THE HEAT ABSORPTION TUBES**

**FOR**

**SKEWED HEATING**

**(TWO-SIDED HEATING)**

**MOLTEN SALT RECEIVER**

**SUBSYSTEM RESEARCH EXPERIMENT**

**THE BABCOCK & WILCOX COMPANY  
CONTRACT 894-0012-45**

**Prepared by  
John P. Reed**

**APPROVED BY J. L. HECHMER  
JUNE 1982  
REPORT NO: 0012-10(S)**

**TABLE OF CONTENTS**

	<b>PAGE</b>
<b>STRESS ANALYSIS OF THE HEAT ABSORPTION TUBES FOR SKEWED HEATING (TWO-SIDED HEATING)</b>	
1. Background and Purpose .....	D-3
2. Geometry and Models .....	D-8
3. Boundary Conditions .....	D-11
4. Thermal Analysis .....	D-13
5. Results .....	D-20
6. Discussion of Results .....	D-42
6.1 General .....	D-42
6.2 Stresses .....	D-45
6.3 Summary .....	D-51
7. Conclusions .....	D-52
8. Recommendations .....	D-53
Appendix A .....	D-54
Appendix B .....	D-71
<b>SUPPLEMENTAL STRESS ANALYSIS OF THE HEAT ABSORPTION TUBES FOR SKEWED HEATING (ONE-SIDED HEATING)</b>	
	D-92
1. Purpose .....	D-93
2. Thermal Analysis .....	D-94
3. Results .....	D-101
4. Conclusion .....	D-102

## 1. BACKGROUND AND PURPOSE

The purpose of this analysis is to determine the change in maximum stress and in the stress distribution for skewed heating from the normal-to-the-panel heating assumption. The effect that shading has on the temperature and stress distribution is included in the evaluation.

Initial analyses of the membrane wall tubes assumed the heat flux normal to the panel; thus, the maximum temperatures and stresses occur at the tube crown and at the midpoint of the web surface. In its true environment, however, each membrane wall tube experiences a unique heating condition relative to its location in the cavity. The maximum heat flux is at an angle (skewed) to the panel and the distribution around the tube is not an area function (i.e., cosine distribution). Also, shading of the web and partial shading of the tube can occur. Heating at any given location is not limited to one angle of incidence, but is a function of a range of angles with heat-flux magnitudes varying throughout this range. This multi-angle of incidence effects both the amount of shading and the non-cosine distribution.

Two locations are evaluated in this report (identified as locations 2 and 3) which are representative of maximum skewed heating conditions. Martin Marietta (MMC) re-developed the skewed heating data for locations 2 and 3 (figure 1) based on the final heliostat aiming strategy for design-point, steady-state, two sided heating.

To accurately study the effects of skewed heating, a two tube model is necessary, because neither the tube crown nor the centerline of the web is a symmetry line for temperature distribution. This is caused by the maximum heat flux being at an angle to the tube crown (figures 2 and 3). The shading problem is also defined graphically in figures 2 and 3. Figure 2 (and to a lesser extent Figure 3) shows that the angle of incidence of the heat flux causes the left hand tube to shade the web and the right side of the tube. Therefore there is little or no heat flux directly to the web or to the tube at the left side of the web. Actual heat flux distributions show some heat flux to the web because there are multi-angles of incidence.

ZONE IV

ZONE I

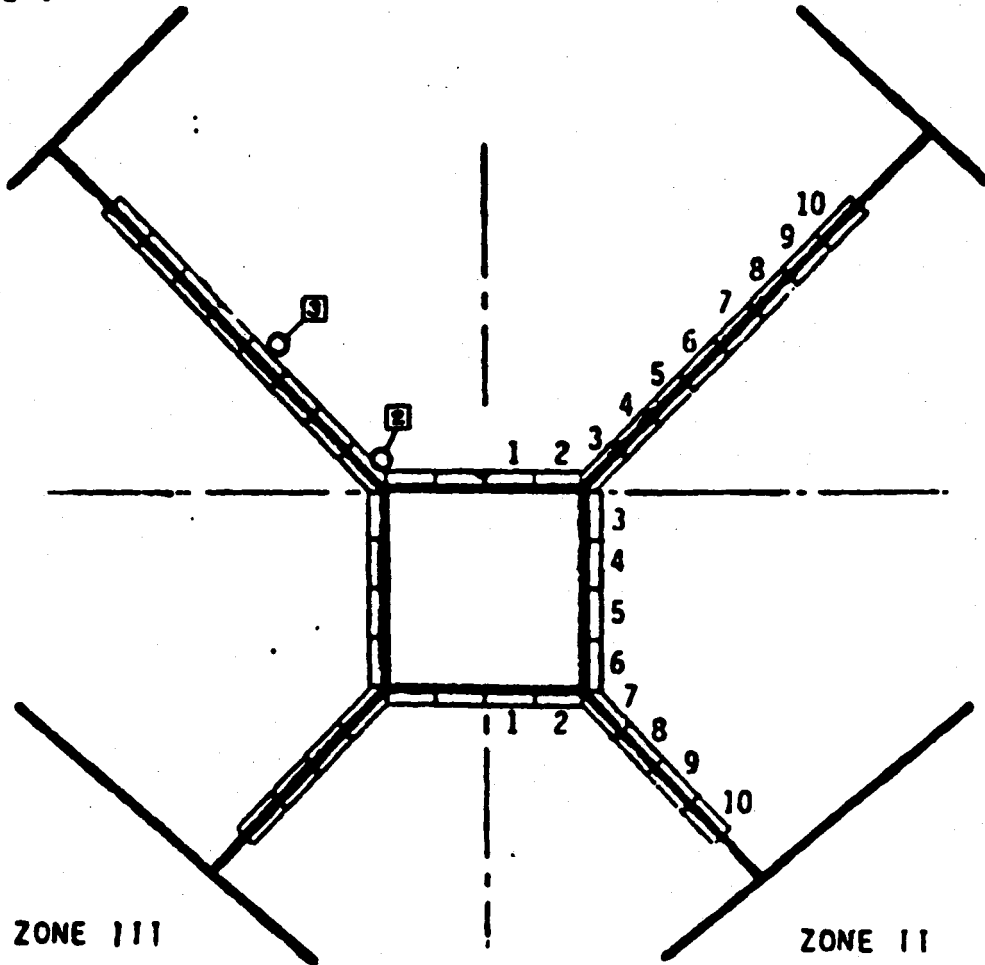
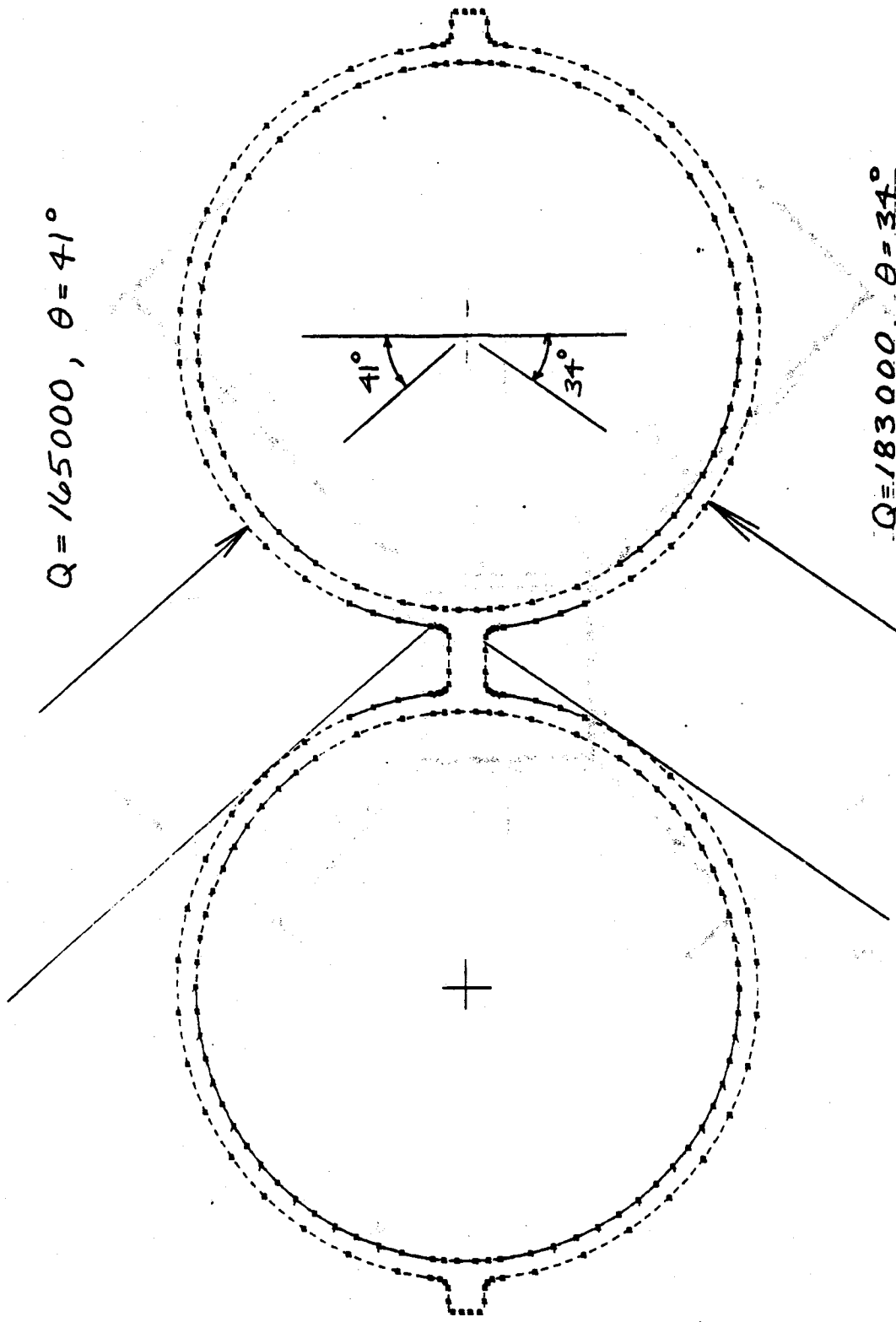


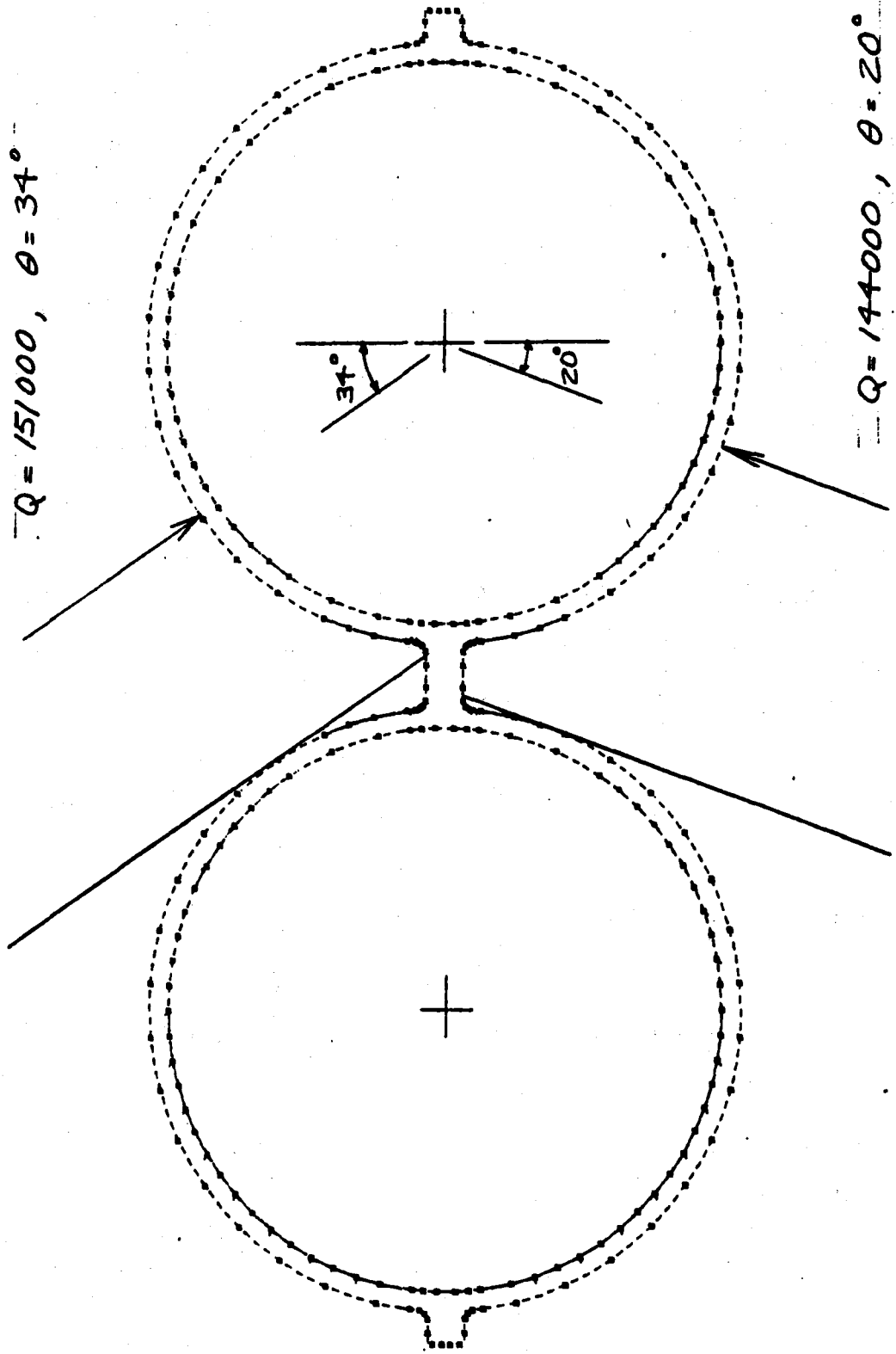
FIGURE 1 - LOCATIONS 2 AND 3





TWO TUBE STRESS MODEL TWENTY NODE 3D ELEMENTS - TYPE 10

FIGURE 2 - LOCATION 2



TWO TUBE STRESS MODEL TWENTY NODE 3D ELEMENTS - TYPE 10

FIGURE 3 - LOCATION 3

## 2. GEOMETRY AND MODELS

The 2" O.D. tube with 0.065 wall thickness is analyzed. The web dimensions are 0.218 inches wide by 0.125 inches thick. The complete geometry consists of two tubes connected by a web and two half webs on either side of the pair of tubes (figure 2 or 3). The use of a two tube model (rather than 3, 4, or more) should give reasonably accurate results, provided that the boundaries are not totally constrained. The blend radius of 40 mils connects the web surface to the tube.

A 2D plane body FETAP model is used for determining the temperature distribution and a 3D one element high FESAP model is used to calculate the resulting thermal stresses. A 3-D model is required to obtain longitudinal stresses. A very refined grid is used for the FETAP analysis to obtain accurate temperatures in regions where shading occurs. 928 8-Node elements with 3207 nodes comprise the 2-D FETAP model.

The 3D FESAP Model is generated from a 2-D (plane body) grid consisting of 216 elements (figure 4a). This 2D Model is layered to create the 3-D FESAP model, one element, 3/16" high (figure 4b). The model has 216 20-node elements and 2009 nodes. The addition of 1064 beam elements to one surface provided uniform axial growth generalized (plane strain) condition.

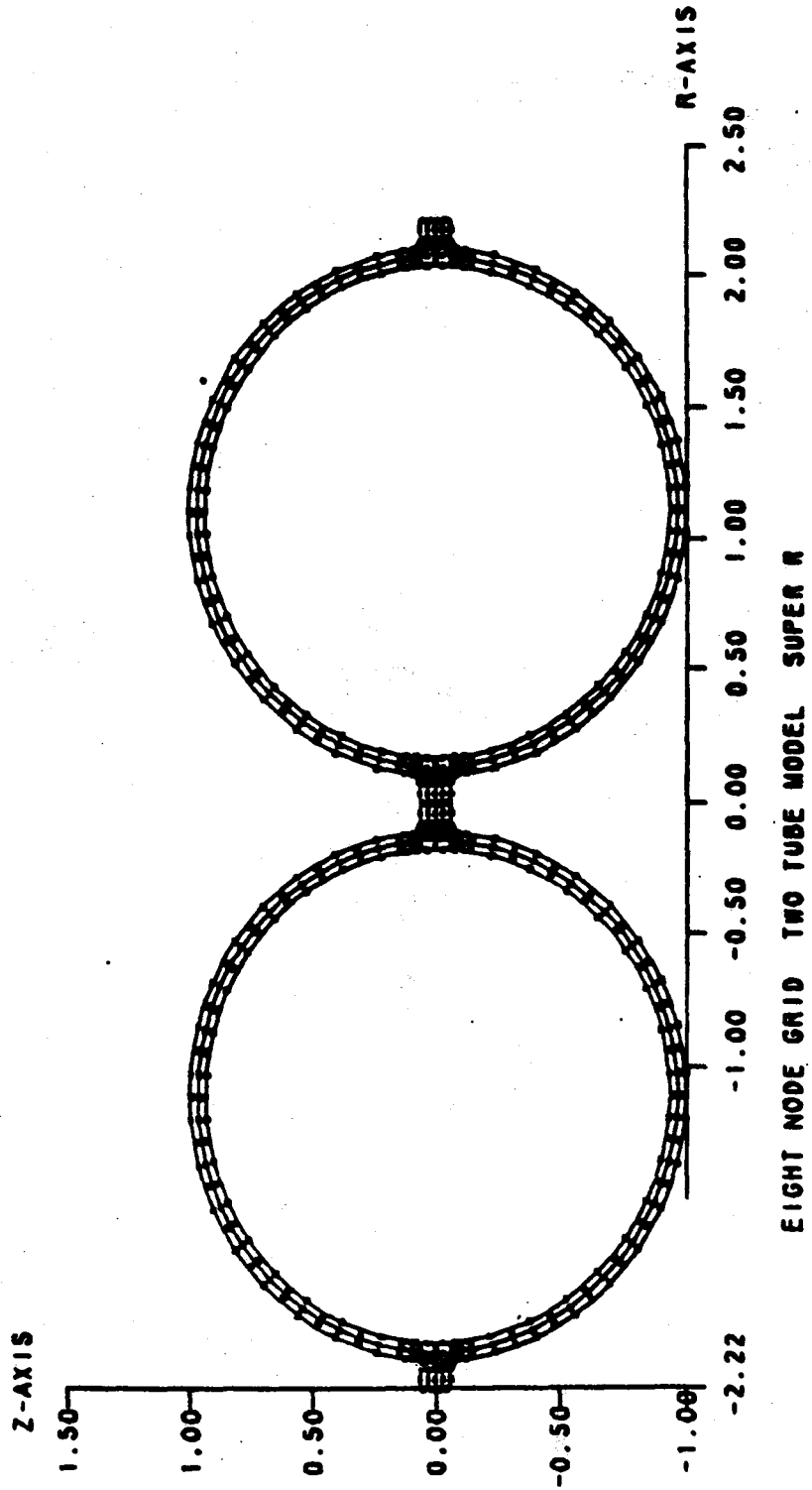


FIGURE 4a - PLANE BODY MODEL TO BE LAYERED

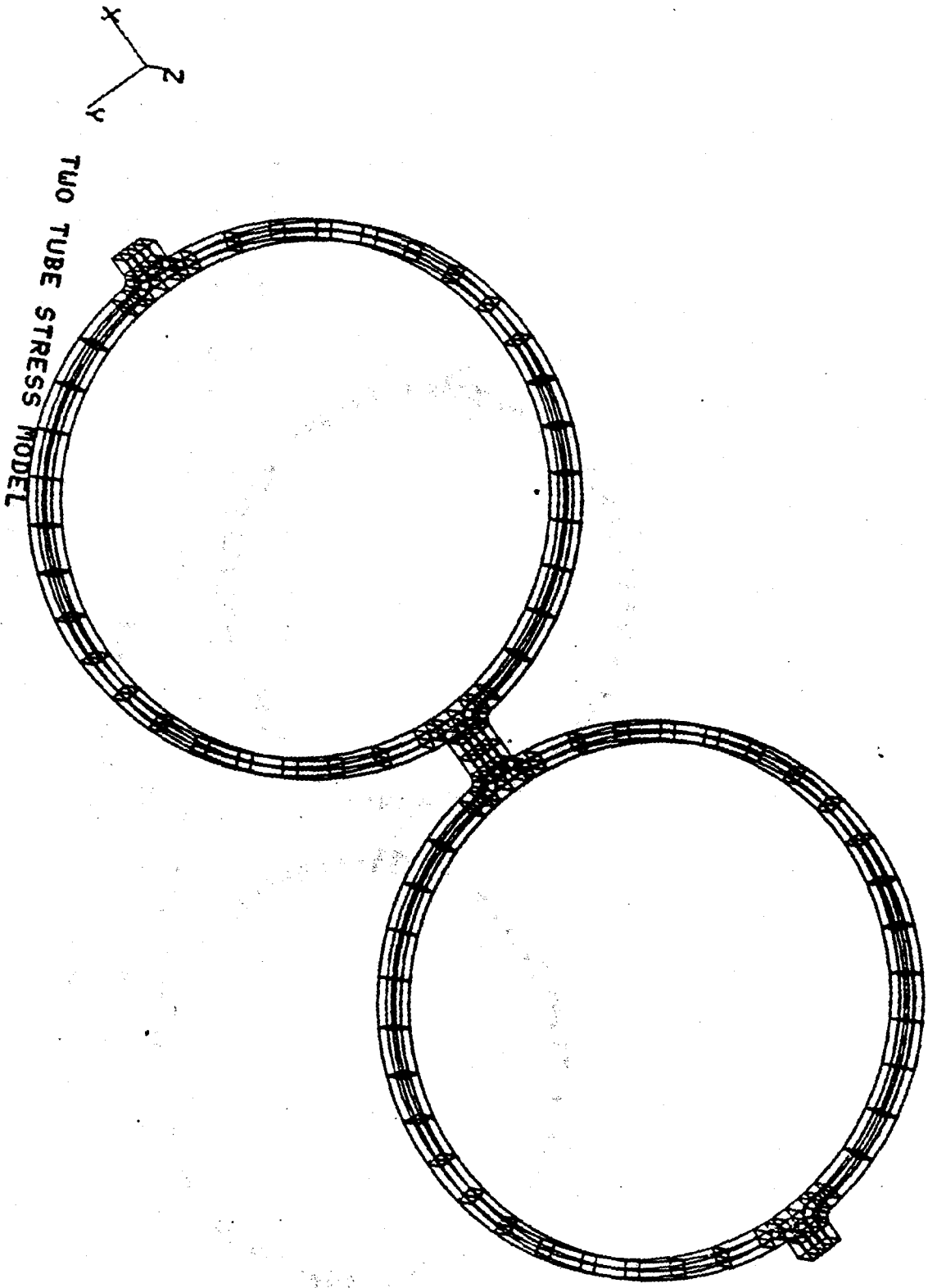


FIGURE 4b -

### 3. BOUNDARY CONDITIONS

The FESAP analysis has generalized plane strain boundary conditions (the top and the bottom surfaces remain plane and parallel). This is obtained by restraining the top nodes against motion in the axial (Z) direction and tying the nodes on the bottom surface so that they all have the same axial displacement. A system of beam elements is used to tie the nodes, instead of the FESAP tie-node option, because this restricts the size of the solution matrix of equations within the FESAP program and saves considerable run time on this type of model.

For the in-plane motions (figure 5), the four midside nodes of the web ends (the upper and lower surface, left and right sides of the model) are restrained in the direction normal to panel (Y). This permits some lateral bowing, but recognizes that these points are common to another tube. The same two nodes on the left side are also restrained in the lateral direction (X) permitting in-plane (or lateral) growth.

UPPER SURFACE CONSTRAINED IN Z-DIRECTION

LOWER SURFACE TIED TOGETHER USING BEAM ELEMENTS

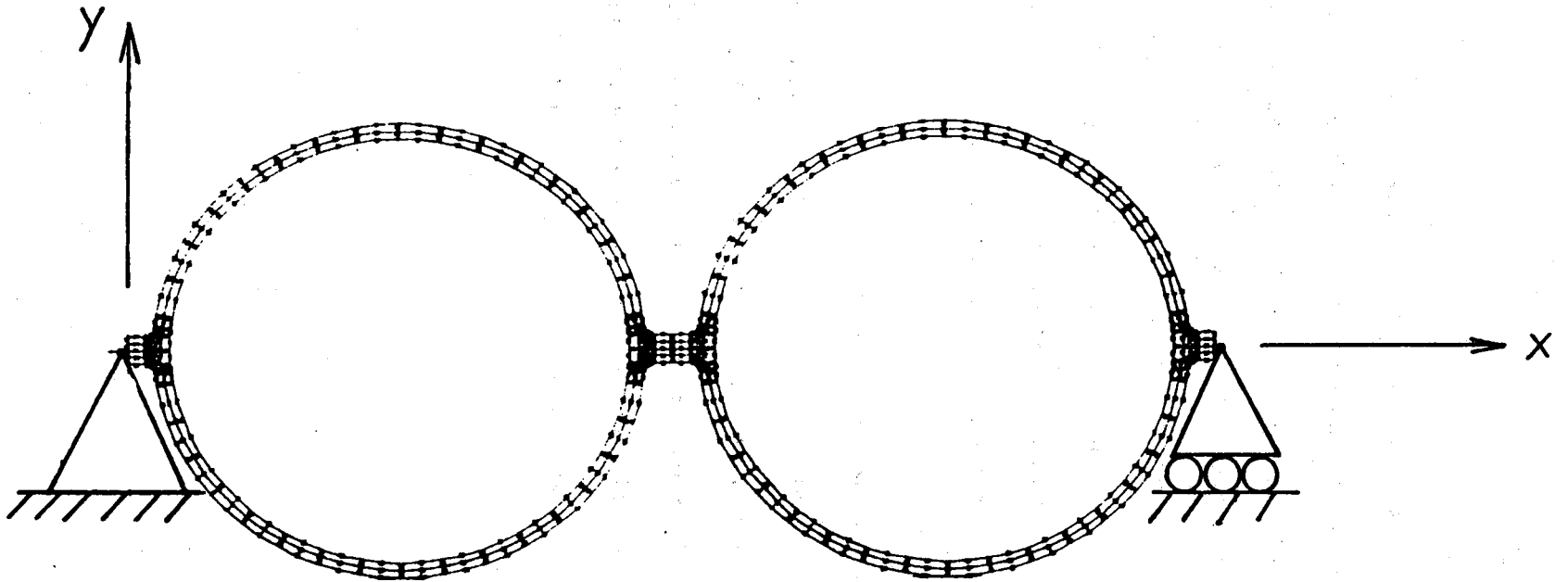


FIGURE 5 - BOUNDARY CONDITIONS FOR 3-D MODEL

#### 4. THERMAL ANALYSES

The design point heat flux at locations 2 and 3 (figure 1) is the thermal load considered in this analysis. Location 2 is on panel 3 and location 3 is on panel 6, both are 2 feet above the aperture centerline. The heat flux distribution was developed by Martin Marietta and is presented in figures A1, A2, A3, and A4 of Appendix A. These figures show a slightly different heat flux to the two tubes plus the left side of the left tube is not shaded. The change in the distribution from one tube to the next tube is slight; therefore, the heat flux data given for the right tube is used in this analysis. Complete shading is evident for the east aperture of location 2 on a portion of the tube and web. The remaining sides display a lesser degree of shading with a variety of distribution occurring on the web. The heat flux is presented at eleven locations ( $16.36^\circ$  increments) around the tube and at 4 locations in the web.

Maximum heat flux values and corresponding angles of incidence were obtained by plotting the Martin Marietta data in polar coordinates (figures A5, A6, A7, and A8 of Appendix A). Unlike direct heating conditions, maximum heat flux does not occur at the tube crown but at some angle from the crown. For location 2, the maximum heat flux is 165,000 at an angle of  $41^\circ$  from the crown (figure A5 of Appendix A); the value at the crown is only 107,700 Btu/HrFt<sup>2</sup>. For location 3, the maximum heat flux and the angle of incidence are not as extreme as location 2. In polar coordinates the distribution is non-circular; therefore, the heat flux distribution around the tube is not a cosine function. The cause of



the non-cosine function may be that the presumed angle of incidence for the heat flux is actually multiple angles of incidence acting in combination with the presence of shading.

An accurate definition of the distribution was obtained by plotting the data on rectangular coordinates (Figure 6). Note that these figures normalize the heat flux to the maximum heat flux.

Figure 6 shows that the heat flux is discontinuous in going from the tube to the web. The heat flux in the tube appears to be converging to zero at the zero angle; whereas, the heat flux in the web is increasing as it approached the zero angle corner. We have no explanation for the discontinuity. This problem is further complicated by the blend radius problem that is discussed in the next paragraph.

The heat flux curves (figure 6) provide input data for the tube surface and web surface, but does not account for the blend radius which actually joins the tube and web. There is no direct means for obtaining the distribution, so some assumptions are needed. The distribution across the blend radius is also a function of the range of angles of incidence; but there is no means of directly determining these angles. Therefore we have used one angle of incidence; we have assumed this to be the angle at which the maximum heat flux occurs. This angle of incidence is used with an extrapolated heat flux value; i.e., the heat flux distribution in the web is extrapolated to the web-to-tube corner; in a similar manner, the heat flux in the tube is extrapolated to the tube-to-web corner. The angle of incidence is projected through each node on the blend radius to a

web or tube location. The heat flux at that tube or web location is assumed to act at the blend radius node. This heat flux is then adjusted for projected area; i.e., the blend radius area associated with the node is projected to the angle of incidence. A typical distribution is shown in Appendix B.

The plot of  $Q/Q_{MAX}$  (figure 6) along the surface of one tube and the web provided the input to FETAP. Carefully reading values from the curves at the angle that defines the location of each surface node maintains the accuracy of the analysis. For the blend radius, values are calculated as described above and are tabulated in appendix B in a manner convenient for FETAP input. Reducing the chance of error during input preparation, a table of weighted nodal areas was assembled using the order of input identical to the table containing the normalized heat flux data. The output is a file of nodal temperatures to be later input to FESAP for calculating stress.

Additional input to FETAP includes fluid temperature and film coefficient; Table 1 contains the data used in the analysis. The standard Material Properties Library is used for conductivity, heat stored capacity and density.

Two grids are used in the analysis. The finer plane body grid for temperature distributions takes into account the presence of shading where sudden changes in heat flow might occur. A courser 3D grid is used for stress analysis. Before inputting the temperature output from FETAP into FESAP, the temperature output had to be sorted by FETERP. The node

locations of the course grid were developed to be identical with nodes of the fine grid; thus no interpolation is needed and no accuracy is lost. Next, a 3-D temperature deck had to be created from the 2-D FETERP output. Since the 3 layers of nodes (3D Model) all have the same heat flux input, the in-plane temperature distributions are identical. Program THERM provided the 3-D temperature deck suitable for FESAP input by layering the plane node temperatures.

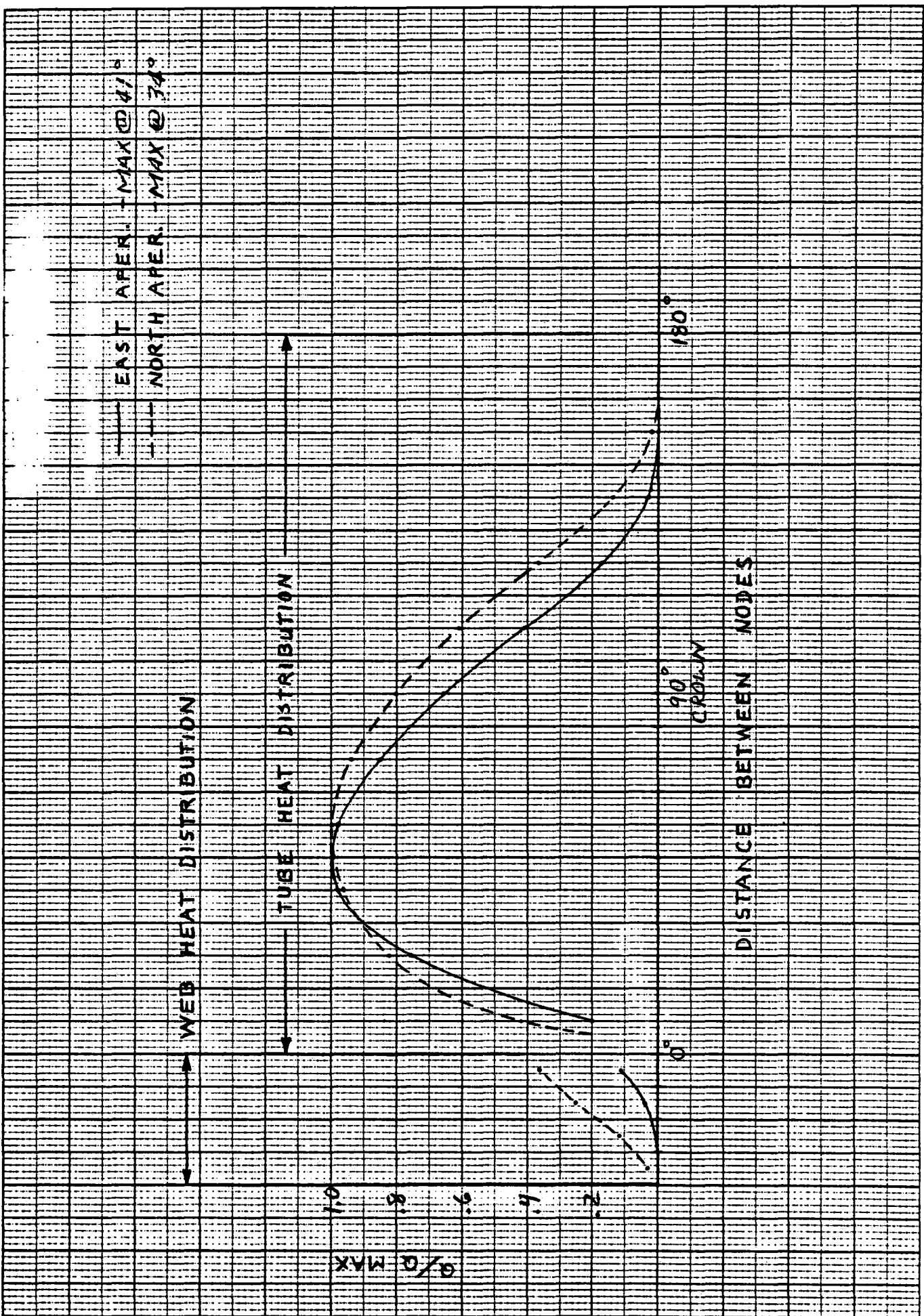


FIGURE 6a - LOCATION 2

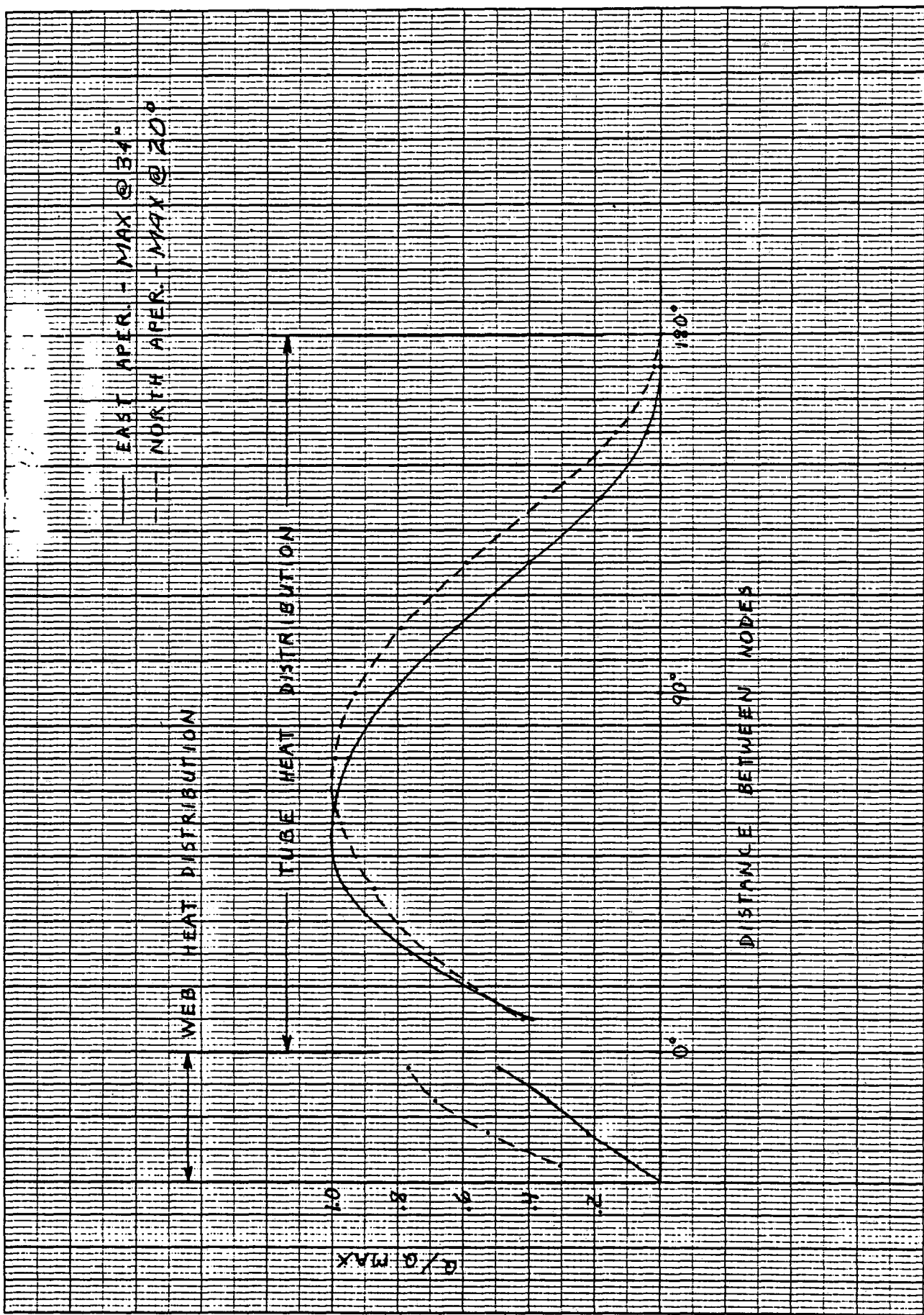


FIGURE 6b CATION 3

TABLE 1

DATA FOR FETAP

	LOC. 2	LOC. 3	UNITS
$Q_1$	1145.8	1048.6	BTU/Hr-IN <sup>2</sup>
$Q_2$	1270.8	1000.0	BTU/Hr-IN <sup>2</sup>
T	652	837	°F
h	930	1200	Btu/HrFt <sup>2</sup>

## 5. RESULTS

Results include a displacement plot of each of the locations (figure 7), temperature contour plots (figures 8 and 9), and maximum, minimum, and effective stress contour plots (figures 10 and 11). The temperature and stress output of the Membrane Wall Program are also discussed and compared to the FESAP results.

The displacement plots (figures 7a and 7b) show that the tubes thermally expand as one would expect and they are compatible with the xy boundary conditions. There does appear to be some lateral bowing; this is further evaluated in figure 7c.

The isotherms (figures 8 and 9) give a clear picture of the temperature distribution. The maximum temperatures occur at the points (i.e., north and east sides of tubes) of maximum heat flux. The web for location 2 is substantially cooler than the tube due to the almost complete shading on one side and the low heat input from the other side. At locations 3, the web may be cooler than the tube, but not by a substantial amount because there is appreciable heat into it. The temperature contours into the web are smooth, indicating that the assumption of heat flux distribution around the blend radius is reasonable.

# TWO TUBE DISPLACEMENT LOC 2

NOTE:  
NODES OF THE MESH WITH  
SOLID BOUNDARY LINES  
ARE DISPLACED AS GIVEN  
FOR LOAD CASE 1 USING  
DISPLACEMENT FACTOR 14.7

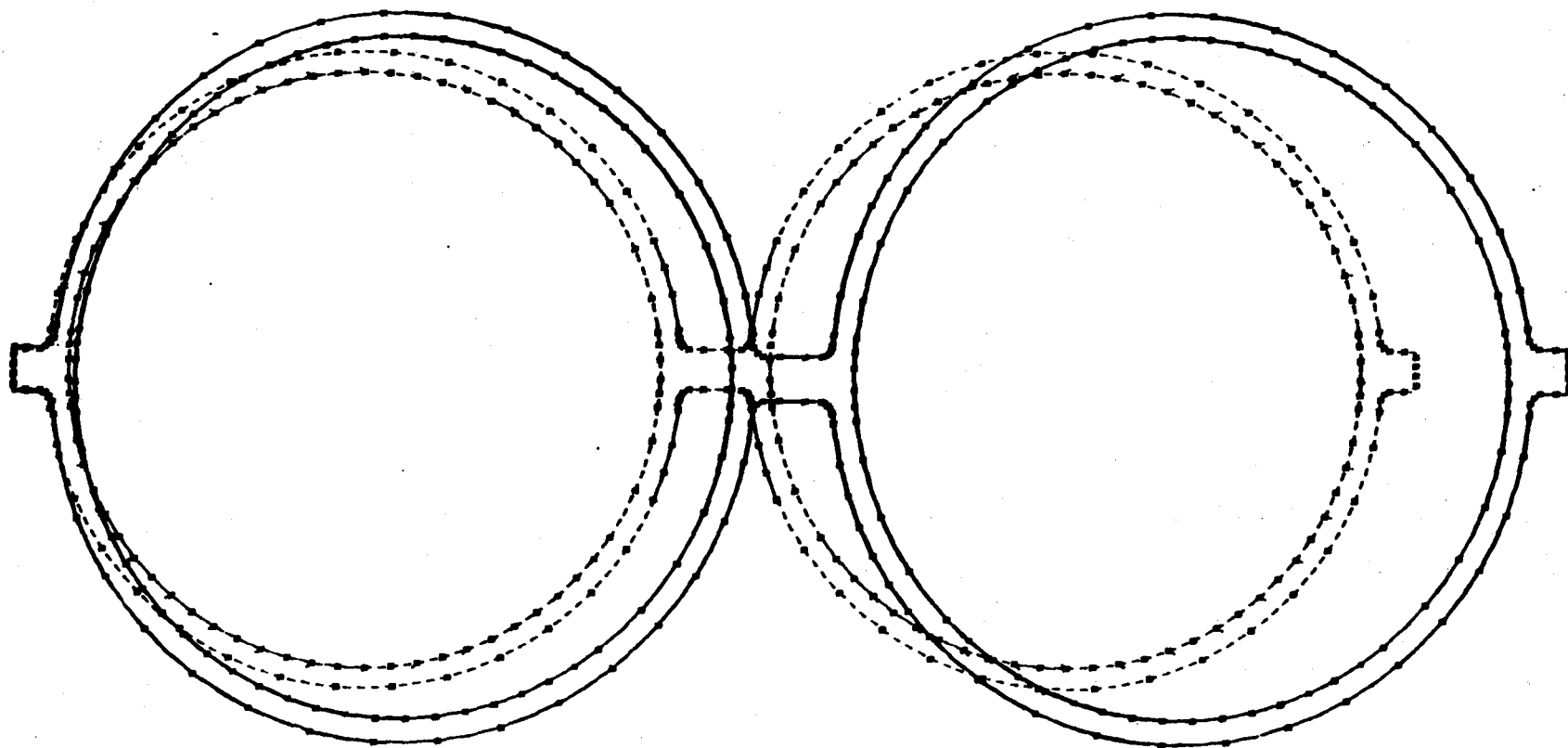


FIGURE 7a - LOCATION 2 DISPLACEMENTS

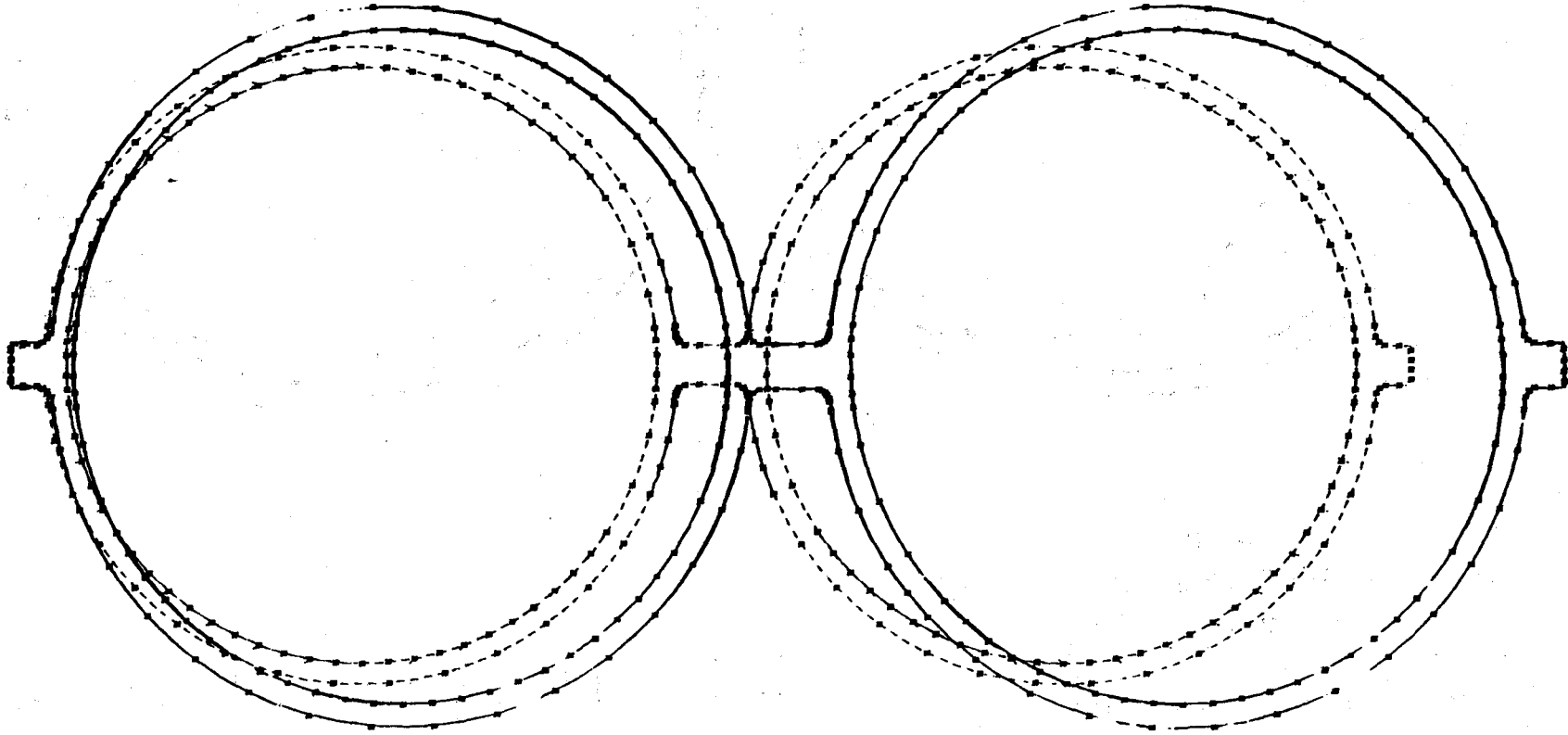
D-21

X



# TWO TUBE DISPLACEMENT LOC 3

NOTE:  
NODES OF THE MESH WITH  
SOLID BOUNDARY LINES  
ARE DISPLACED AS GIVEN  
FOR LOAD CASE 1 USING  
DISPLACEMENT FACTOR 19.6



D-22

X

FIGURE 7b - LOCATION 3 DISPLACEMENTS

$$\theta = \tan^{-1} \left( \frac{DY}{2.218} \right)$$

$$K = \frac{21 \text{ TUBES}}{2} (2\theta)$$

$$S_y = \frac{21}{2} (2.218) \tan \frac{K}{2}$$

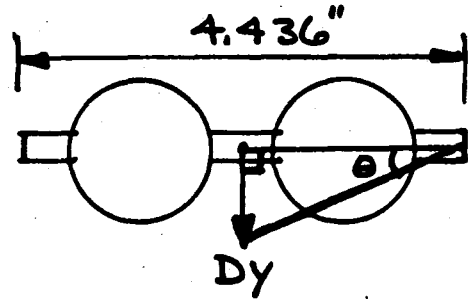
FOR LOCATION #2,

$$DY = -1.271E-3 \text{ "}$$

$$\theta = 0.0328^\circ$$

$$K = 0.6895^\circ$$

$$S_y = \underline{\underline{0.140 \text{ "}}} \quad \underline{\underline{OK}}$$



NODE 845

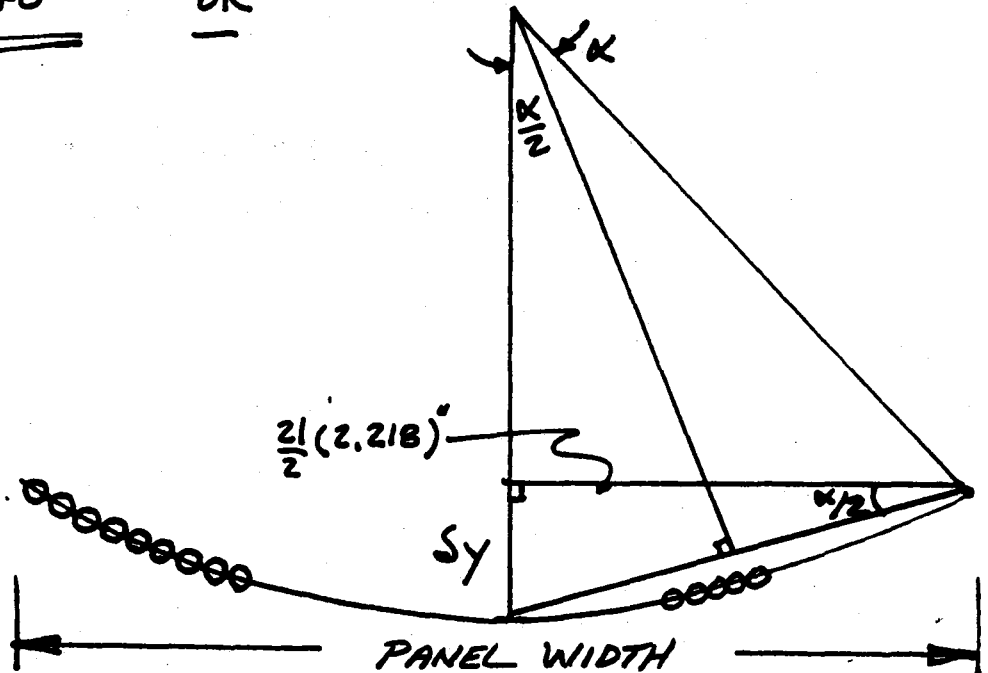
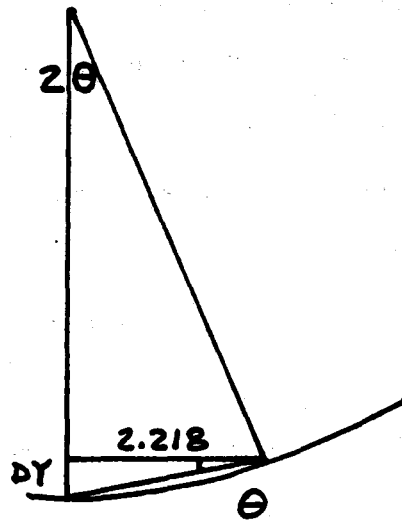


FIGURE 7c - PANEL DISPLACEMENT

It is interesting to note that only a through thickness gradient occurs at the point of maximum heat flux. Moving away from the point of peak heating, the circumferential gradient becomes evident. At 90° from the point of peak heating, the cool region is found. At this point, no temperature gradient is apparent and the tube is at the fluid temperature.

Temperature contour plots of location 3 (figures 9) show similar characteristics. Cool regions again develop where shading occurs, however, heat from the web traveling circumferentially tends to restrict their growth. In the web vicinity, nearly linear gradients are prevalent where the rate of change is gradual. Unlike location 2, location 3 has no heat transfer across the web to the adjacent tube.

Stress contour plots (figures 10 and 11) are presented for locations 2 and 3, for maximum and minimum principal stresses, and for effective stress. The stresses are presented for the two half tubes plus web and for the web-blend radius detail. The direction of the maximum and minimum stress can not be determined from these plots. In the following discussion, the term "Maximum stress" refers to the absolute value of maximum principal stress.

For location 2, the maximum stress occurs at the location of highest heat flux; the output data indicates that this is a compressive stress. The maximum effective stress occurs at the same location, but is lower, reflecting the lower in-plane stresses. The maximum web stresses are substantially lower than the maximum tube stress (28 ksi vs. 44 ksi), which is due to decreased temperature from the shading effect. Also, the web maximum stress is an in-plane stress rather than an axial stress; but even this in-plane stress decreases in going from the tube, to the web, through the web, to the opposite tube.

The stress levels for location 3 are generally lower than at location 2. The maximum stress in the tube is an axial stress and it occurs at the location of maximum heat flux. The maximum effective stress also occurs at the location of maximum heat flux, but the distribution is very complex. There are a number of locations where the effective stress approaches the maximum, which reflects the high in-plane stresses (i.e., the maximum in-plane stresses in the tube approach the maximum axial stresses) and the effect of cold spots due to shading. As with location 2, the effective stresses decrease in going from the tube into the web, again reflecting the decrease in heat flow to the web.

CONTOUR MAP OF TEMPERATURE  
FOR TIME 1.00

CONTOUR IDENT

□	663.46
○	683.29
△	703.11
+	722.93
X	742.76
◇	762.58
↑	782.40
⋈	802.22
Z	822.05
Y	841.87
⋈	861.69
*	881.52
⋈	901.34
	921.16
★	940.99

D-26

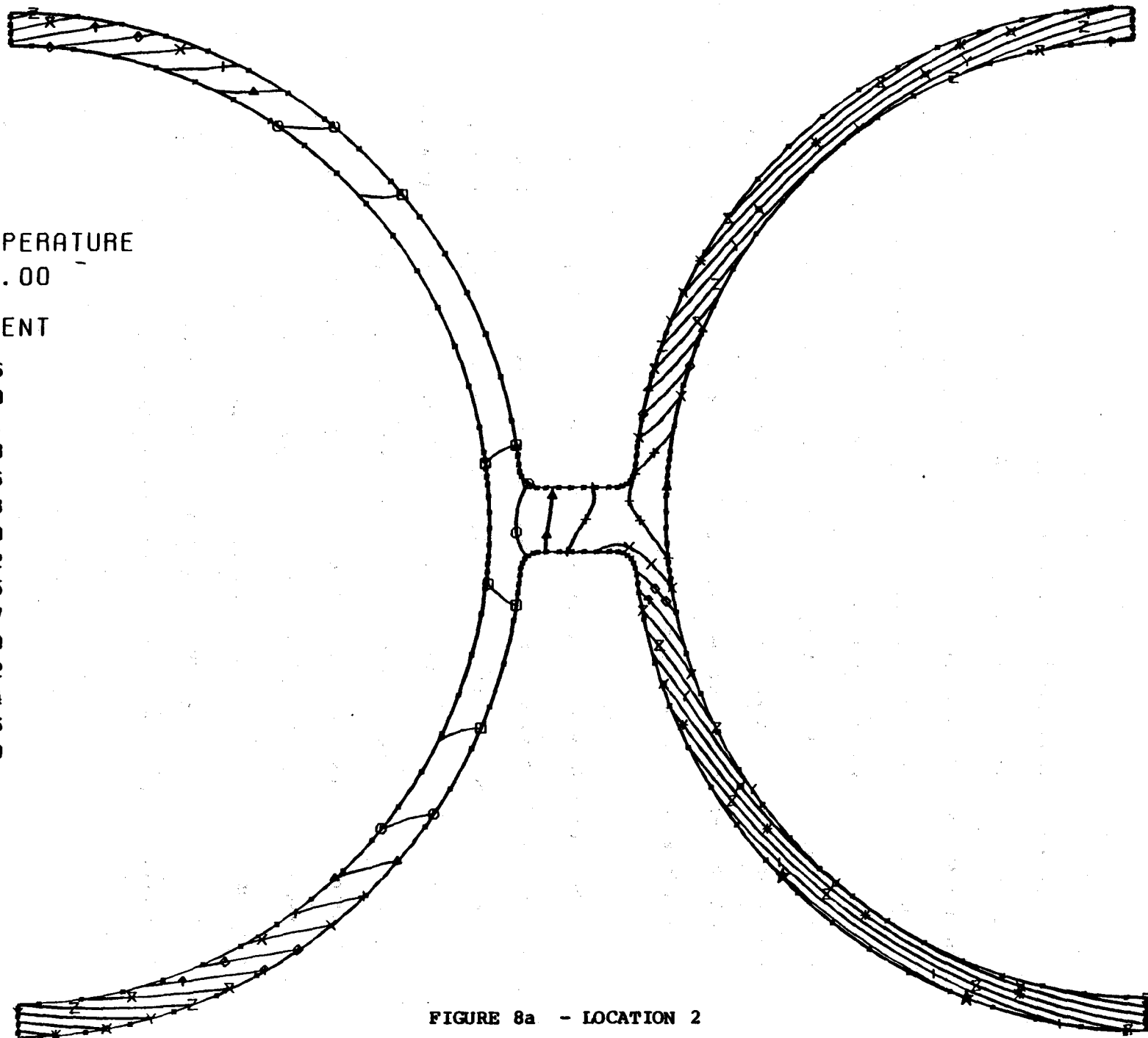
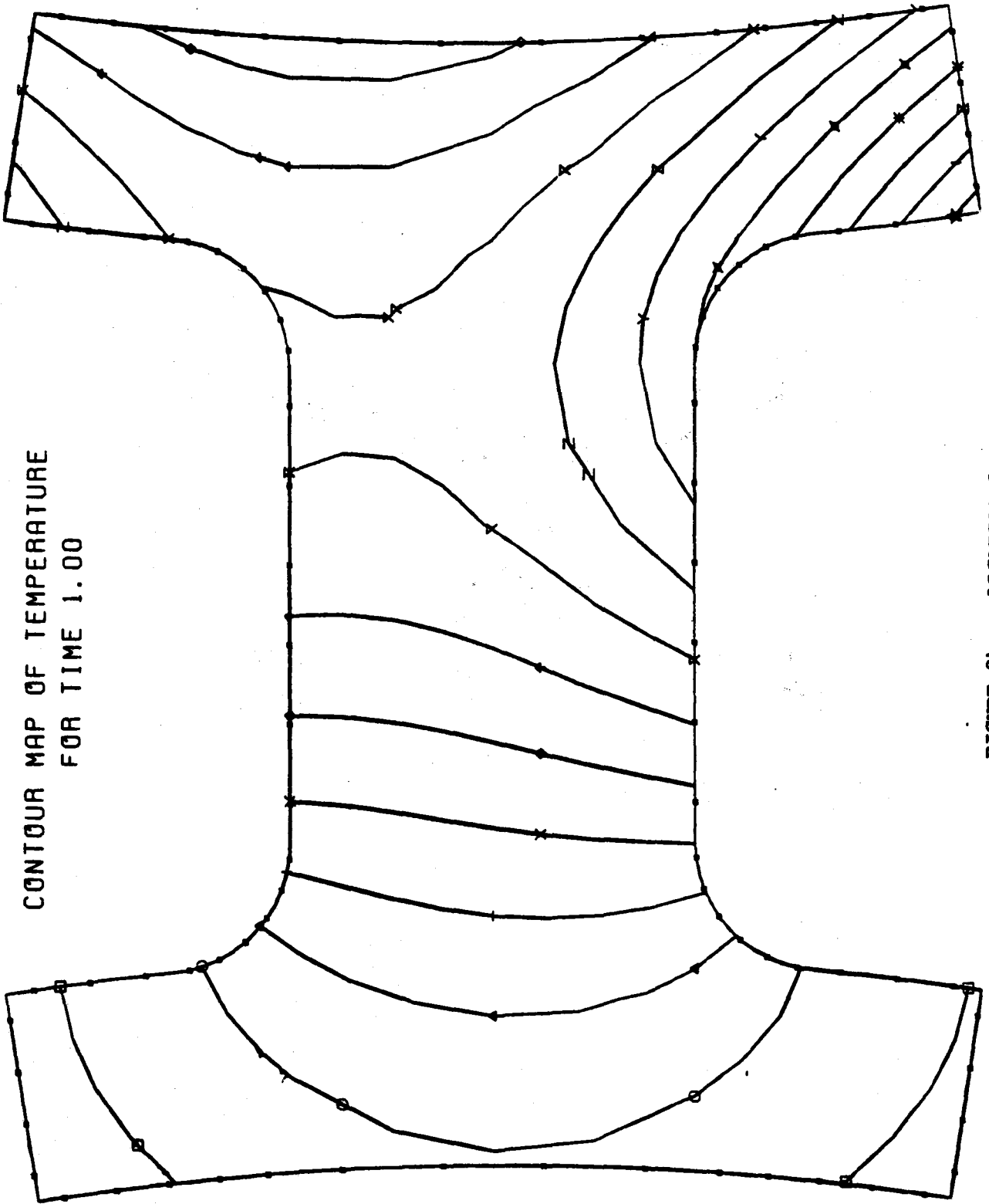


FIGURE 8a - LOCATION 2

CONTOUR MAP OF TEMPERATURE  
FOR TIME 1.00



CONTOUR IDENT

- 664.80
- 673.34
- △ 681.88
- + 690.42
- X 698.96
- ◇ 707.50
- ↑ 716.04
- X 724.58
- Z 733.13
- Y 741.67
- X 750.21
- \* 758.75
- X 767.29
- I 775.83
- ★ 784.37

P. 27

Y

FIGURE 8b - LOCATION 2

CONTOUR MAP OF TEMPERATURE  
FOR TIME 1.00

CONTOUR IDENT

□	846.78
○	860.23
△	873.68
+	887.13
x	900.58
◇	914.03
†	927.48
⋈	940.93
Z	954.38
Y	967.83
⋈	981.28
*	994.73
⋈	1008.18
I	1021.63
☆	1035.08

D-28

Z

X

Y

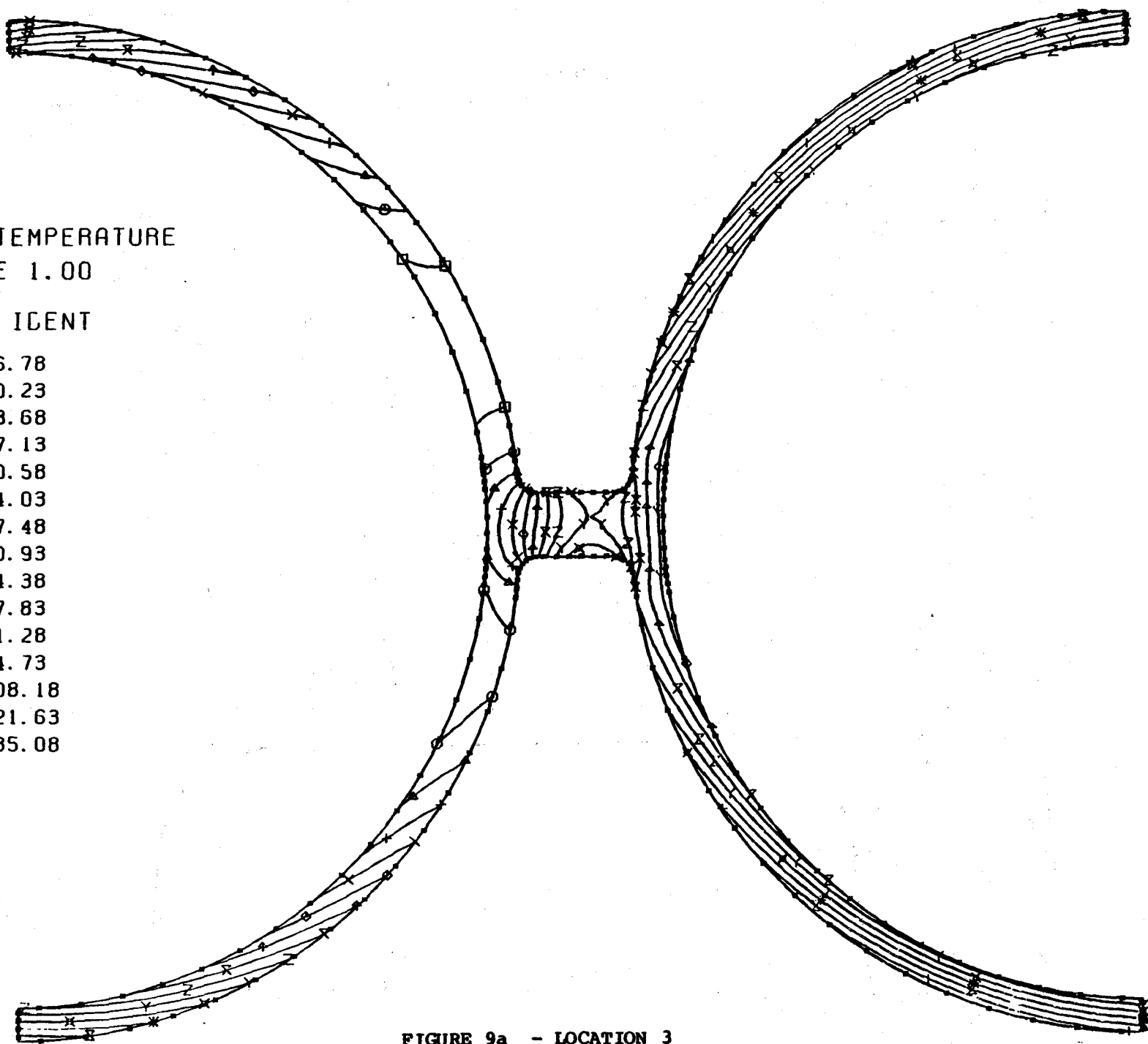
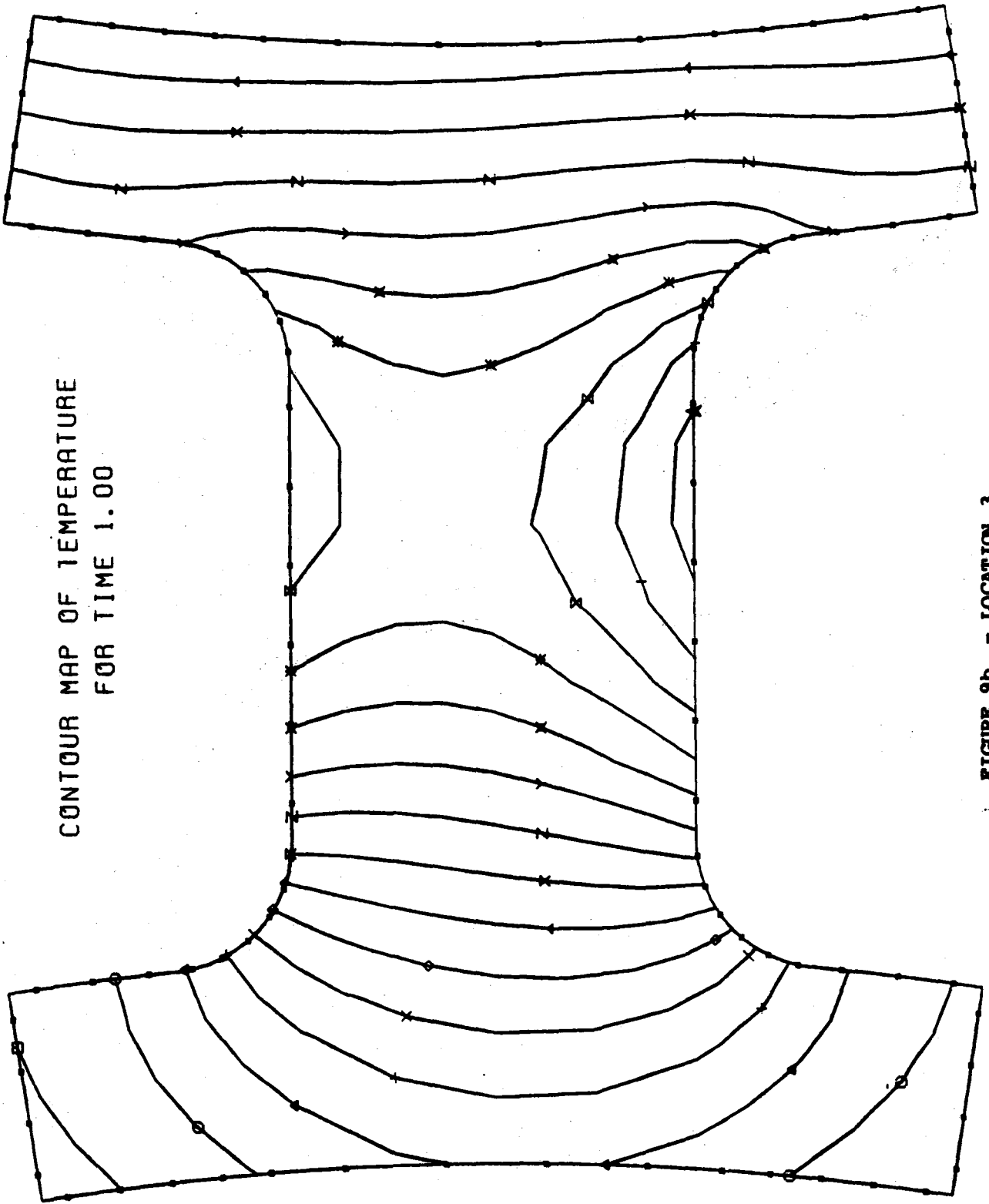


FIGURE 9a - LOCATION 3

CONTOUR MAP OF TEMPERATURE  
FOR TIME 1.00



CONTOUR IDENT

- 857.72
- 867.20
- △ 876.69
- + 886.18
- X 895.66
- ◇ 905.15
- ↑ 914.64
- ⌘ 924.13
- Z 933.61
- Y 943.10
- ⌘ 952.59
- \* 962.07
- ⌘ 971.56
- | 981.05
- ☆ 990.54

FIGURE 9b - LOCATION 3

Y



CONTOUR MAP OF MAXIMUM STRESS  
FOR LOAD CASE 1

CONTOUR IDENT

□	31.91
○	3242.24
△	6452.56
+	9662.89
×	12873.21
◇	16083.54
♣	19293.86
⊗	22504.19
Z	25714.51
Y	28924.84

D-30

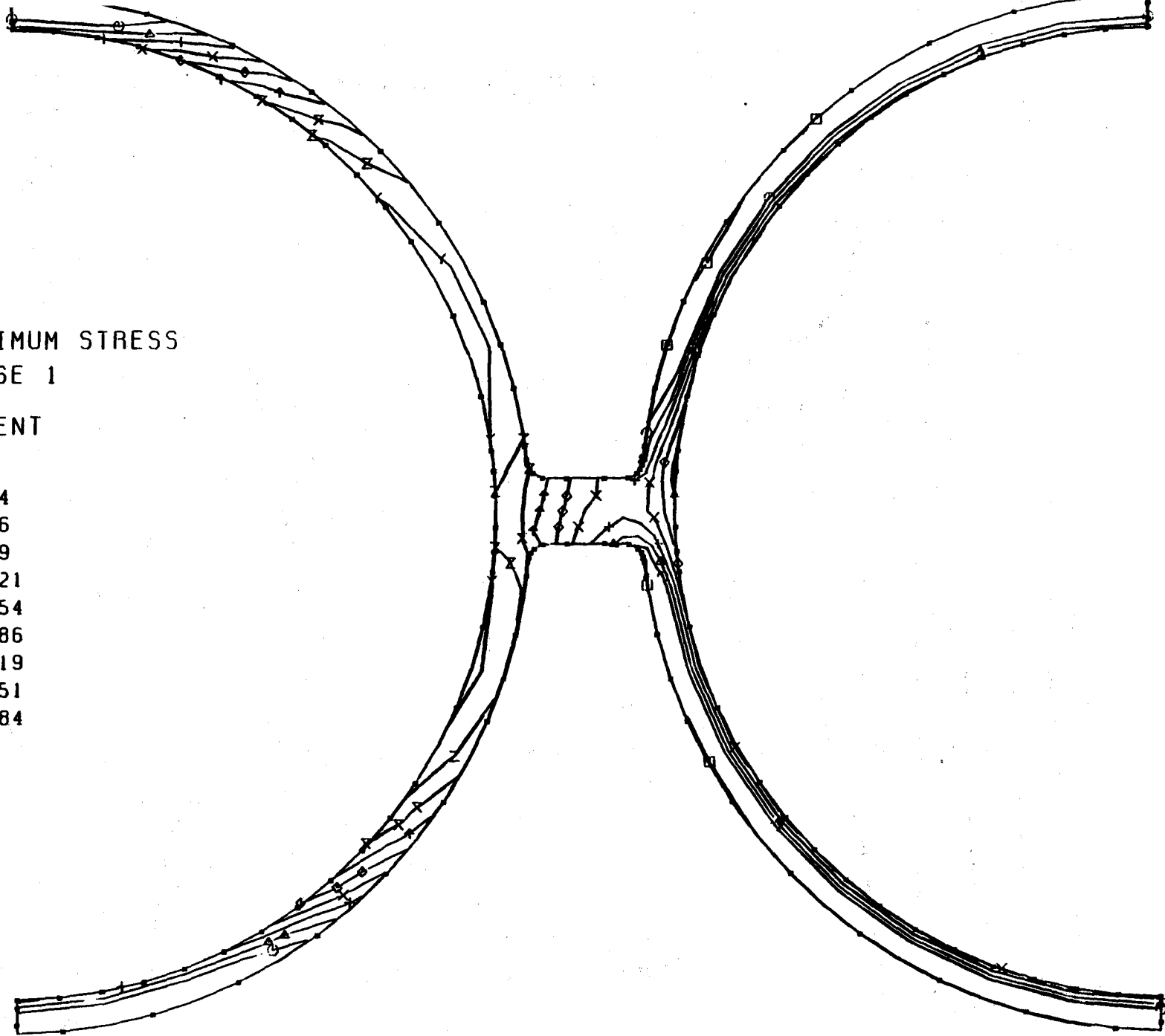
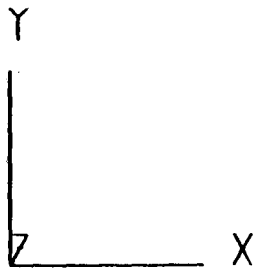
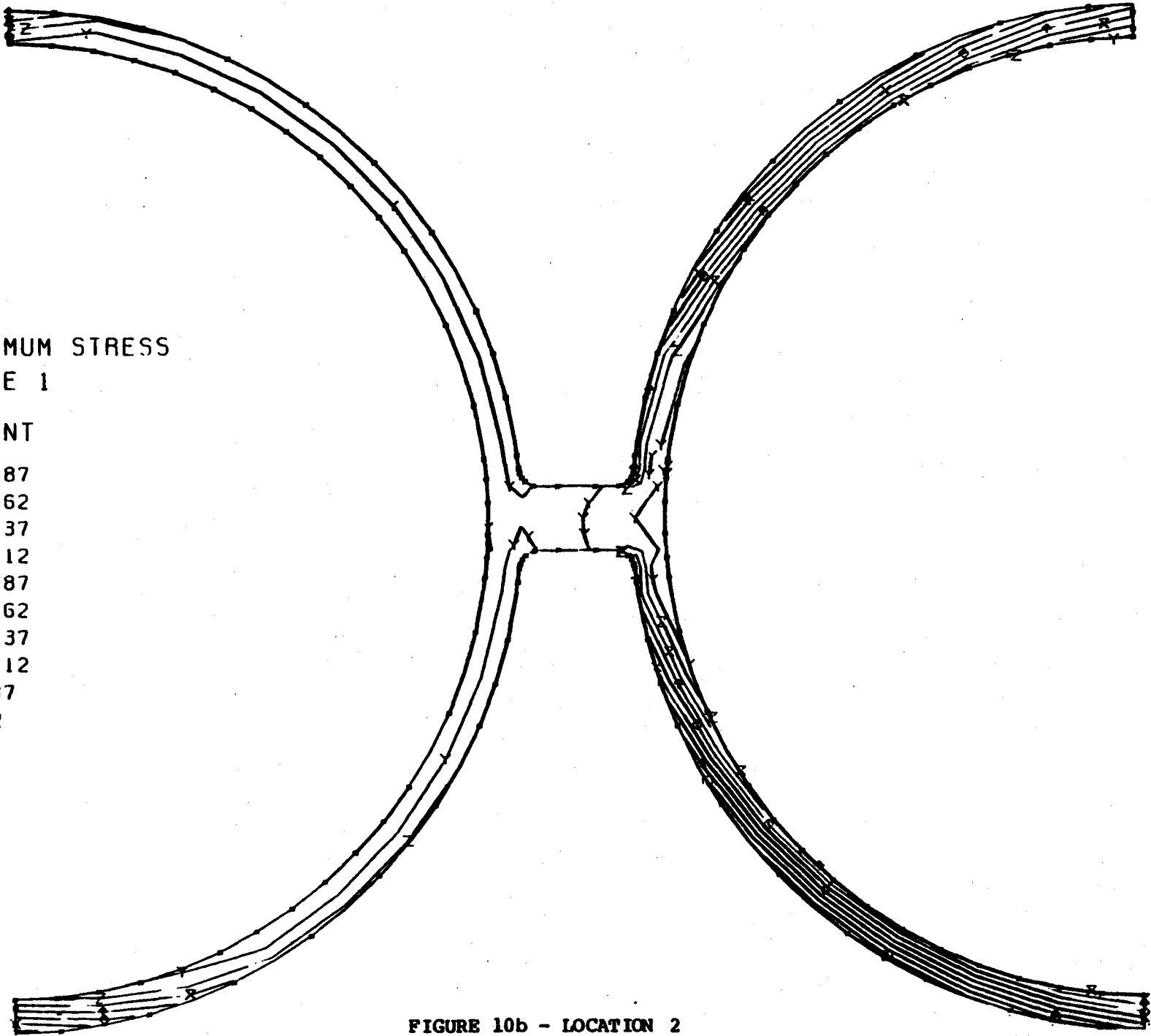


FIGURE 10a - LOCATION 2



CONTOUR MAP OF MINIMUM STRESS  
FOR LOAD CASE 1

CONTOUR IDENT

□	-44015.87
○	-39227.62
△	-34439.37
+	-29651.12
X	-24862.87
◇	-20074.62
↑	-15286.37
*	-10498.12
Z	-5709.87
Y	-921.62

D-31

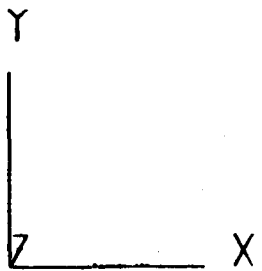


FIGURE 10b - LOCATION 2

CONTOUR MAP OF EFFECTIVE STRESS  
FOR LOAD CASE 1

CONTOUR IDENT

□	3256.29
○	7320.36
△	11384.44
+	15448.51
X	19512.59
◇	23576.66
⋈	27640.74
X	31704.81
Z	35768.89
Y	39832.96

D-32

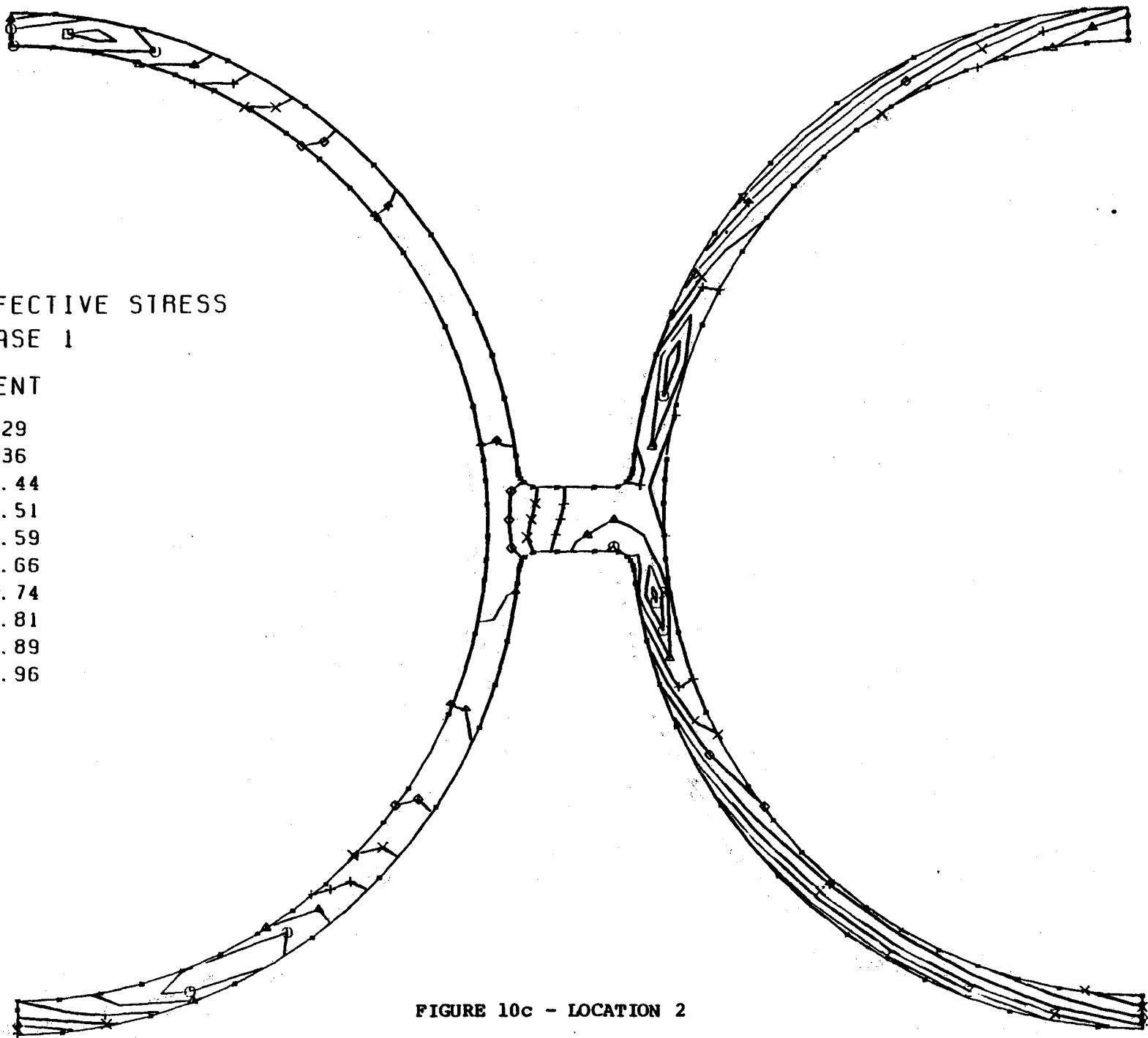
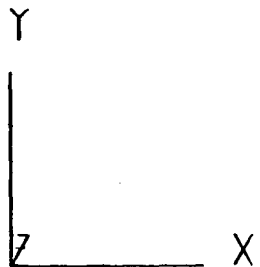
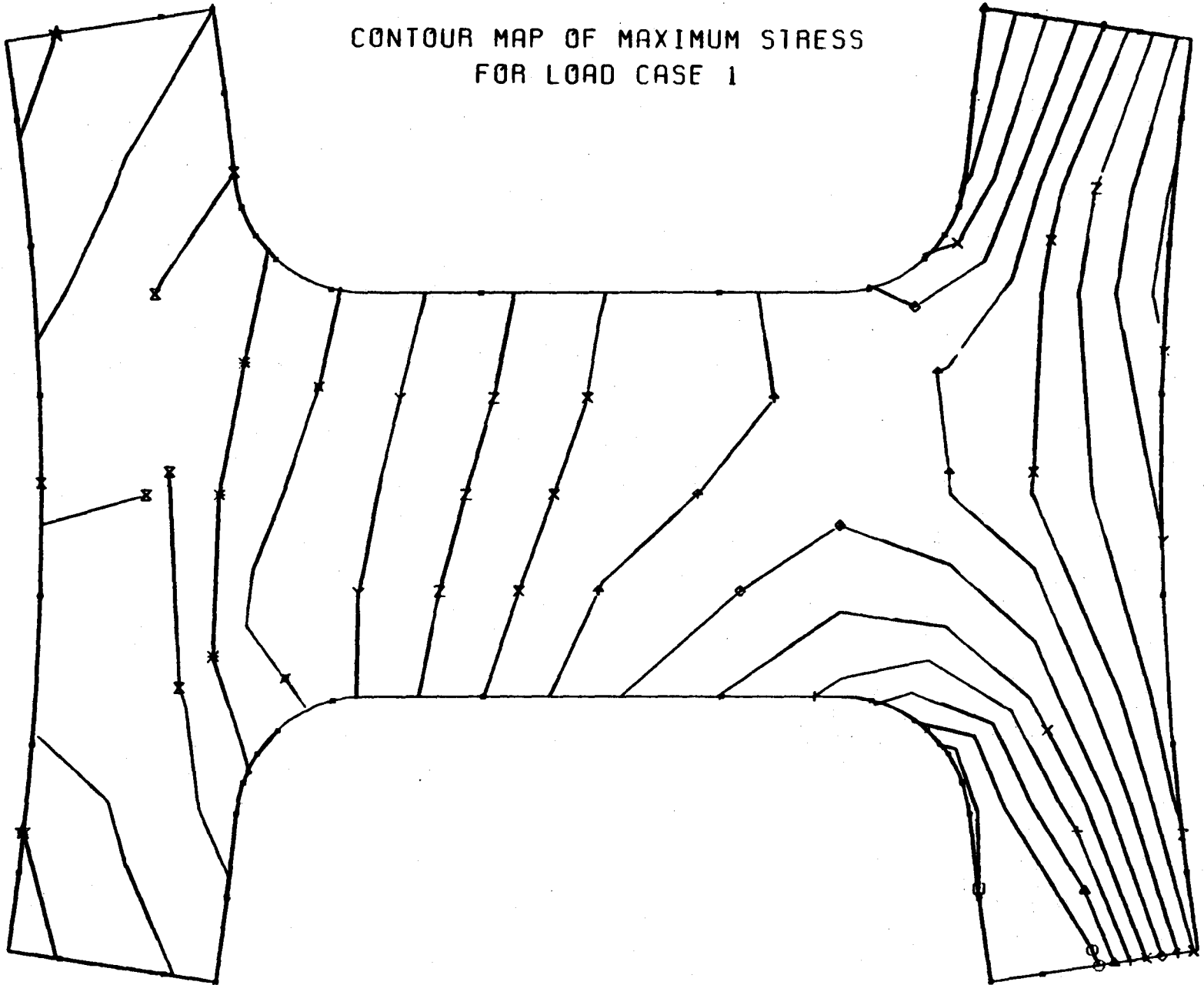


FIGURE 10c - LOCATION 2

CONTOUR MAP OF MAXIMUM STRESS  
FOR LOAD CASE 1

CONTOUR IDENT

□	-456.02
○	1590.95
△	3637.92
+	5684.88
X	7731.85
◇	9778.82
↑	11825.78
X	13872.75
Z	15919.72
Y	17966.68
X	20013.65
*	22060.62
X	24107.58
	26154.55
☆	28201.52



D-33

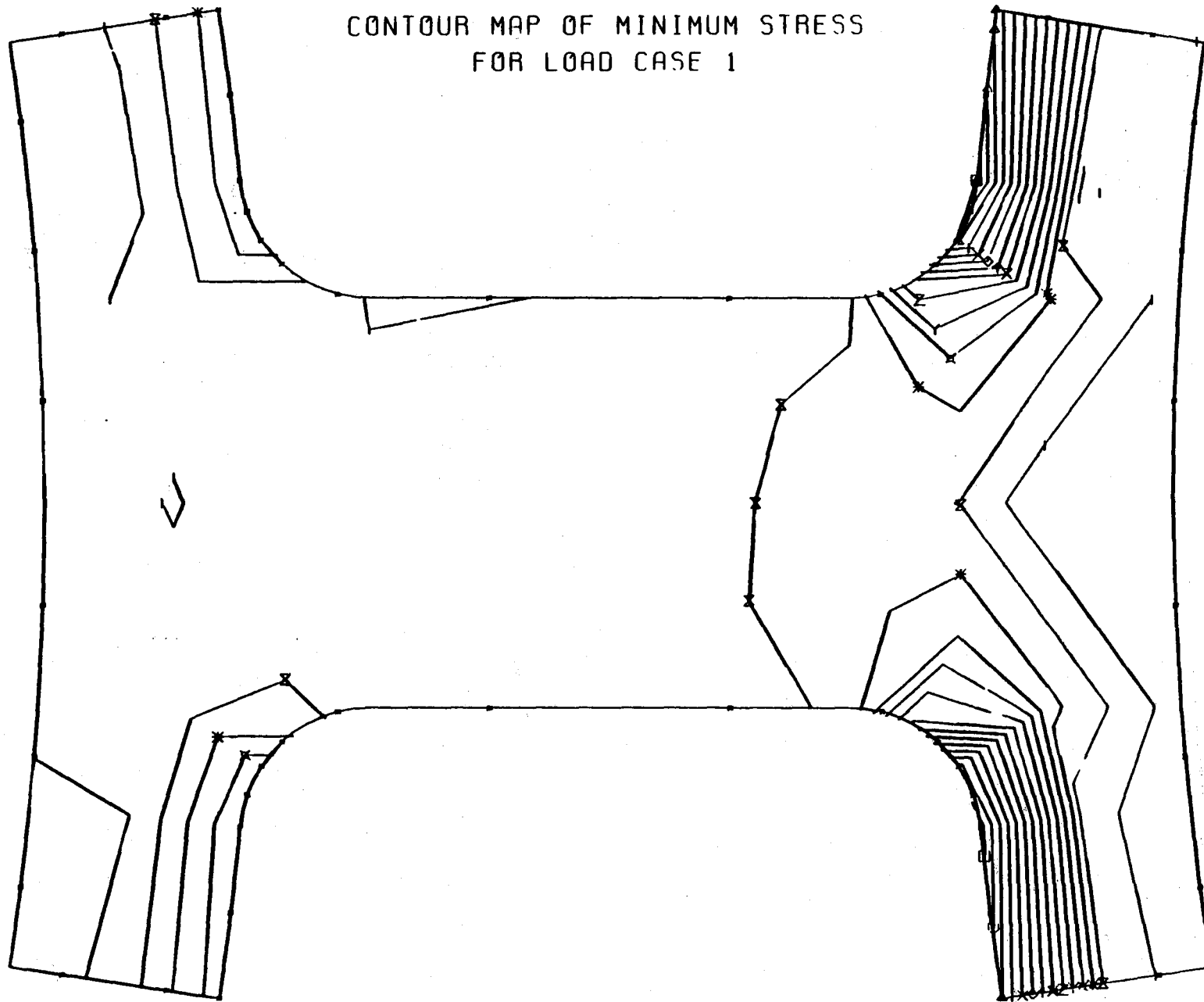
X

FIGURE 10d - LOCATION 2

CONTOUR MAP OF MINIMUM STRESS  
FOR LOAD CASE 1

CONTOUR IDENT

□	-15876.75
○	-14680.25
△	-13483.75
+	-12287.25
x	-11090.75
◇	-9894.25
↑	-8697.75
x	-7501.25
Z	-6304.75
Y	-5108.25
x	-3911.75
*	-2715.25
⊗	-1518.75
	-322.25
★	874.25



D-34

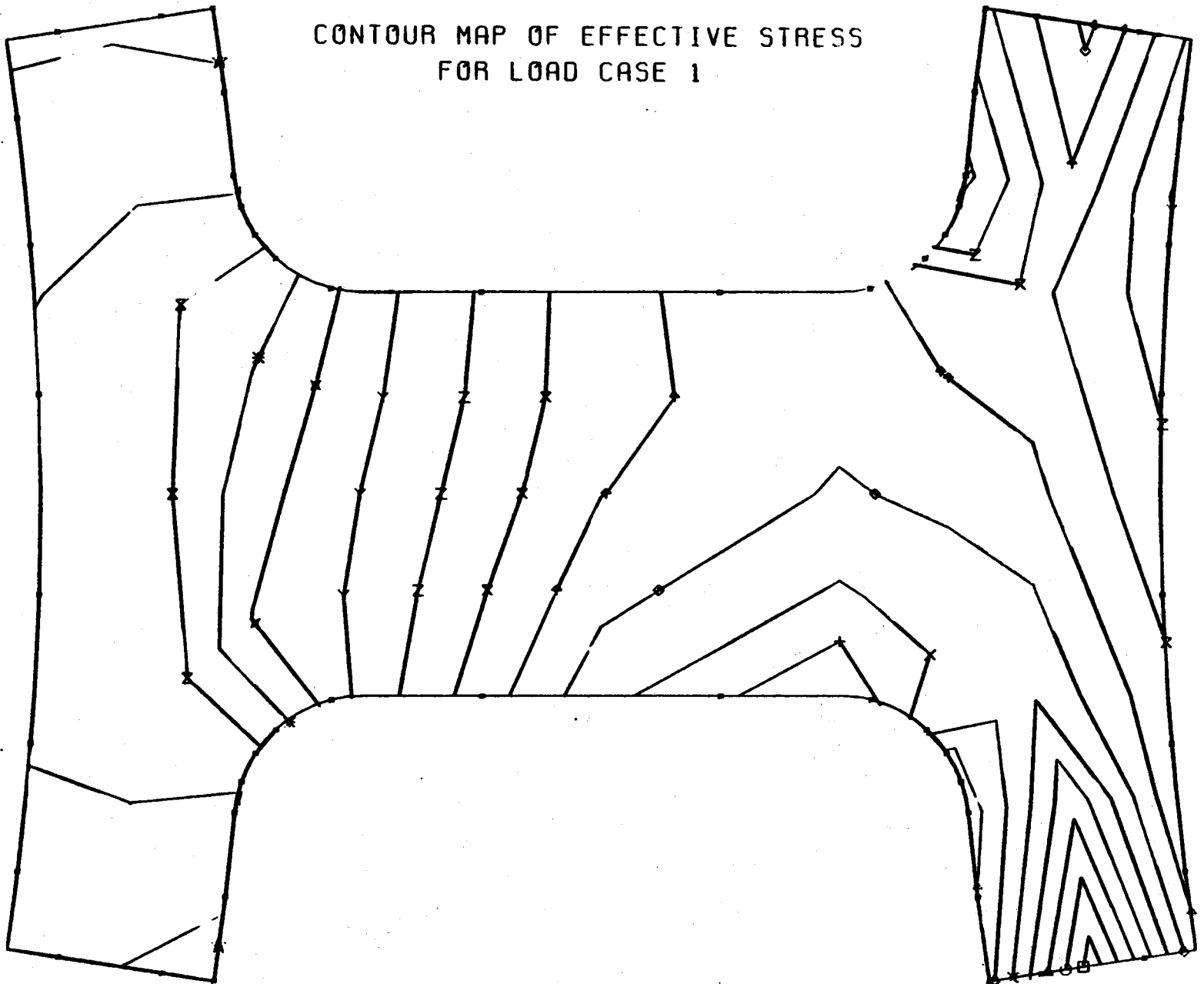
X

FIGURE 10e - LOCATION 2

CONTOUR MAP OF EFFECTIVE STRESS  
FOR LOAD CASE 1

CONTOUR IDENT

□	2789.83
○	4543.98
△	6298.13
+	8052.28
x	9806.43
◇	11560.58
↑	13314.73
×	15068.88
Z	16823.03
Y	18577.18
⊗	20331.33
*	22085.48
⊗	23839.63
	25593.78
★	27347.93



D-35

X

FIGURE 10f - LOCATION 2

CONTOUR MAP OF MAXIMUM STRESS  
FOR LOAD CASE 1

CONTOUR IDENT

□	-446.32
○	2278.03
△	5002.38
+	7726.73
X	10451.08
◇	13175.43
⋈	15899.78
X	18624.13
Z	21348.48
Y	24072.83

D-36

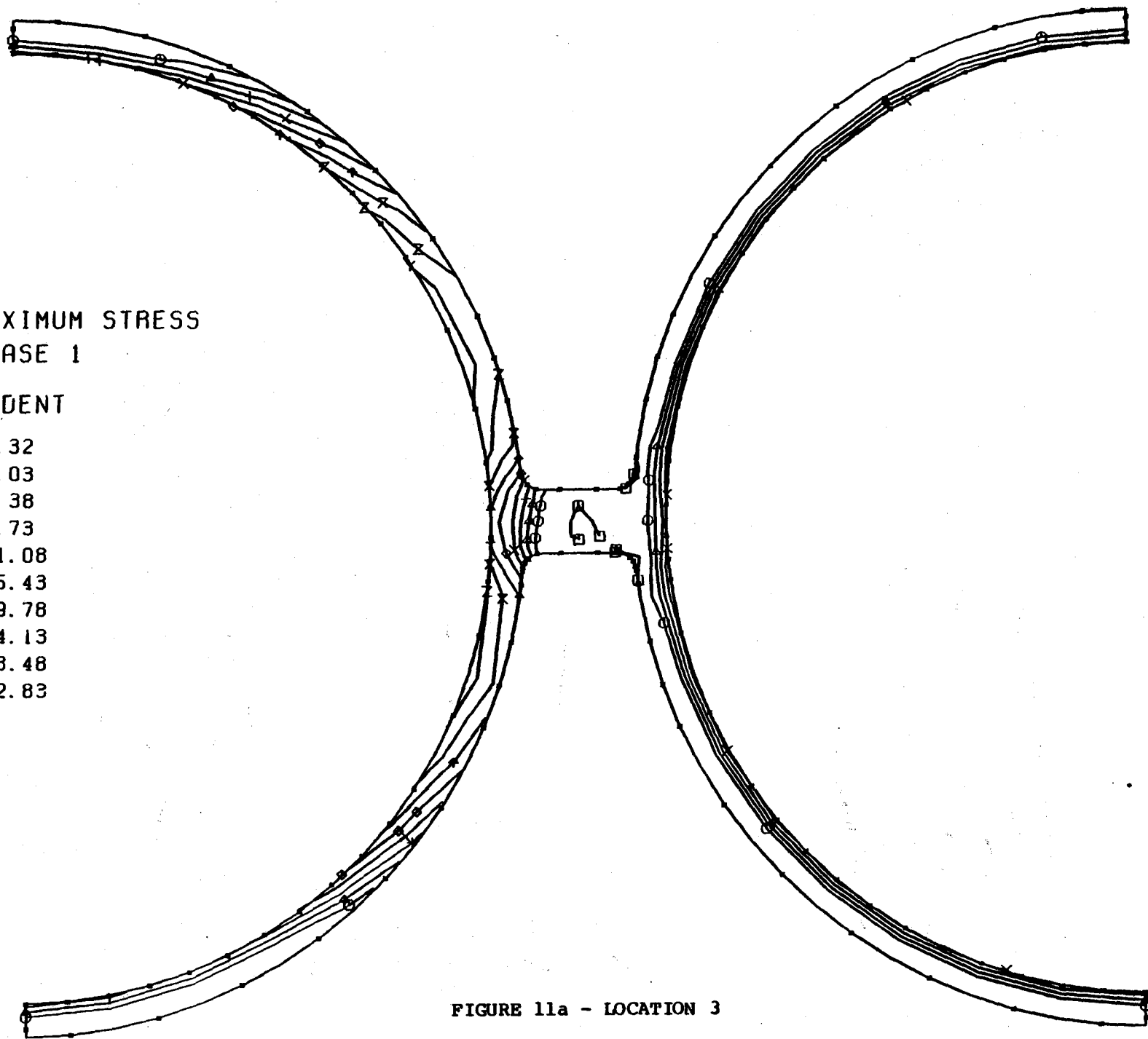


FIGURE 11a - LOCATION 3

CONTOUR MAP OF MINIMUM STRESS  
FOR LOAD CASE 1

CONTOUR IDENT

□	-26254.50
○	-23343.50
△	-20432.50
+	-17521.50
x	-14610.50
◇	-11699.50
↑	-8788.50
x	-5877.50
Z	-2966.50
Y	-55.50

D-37

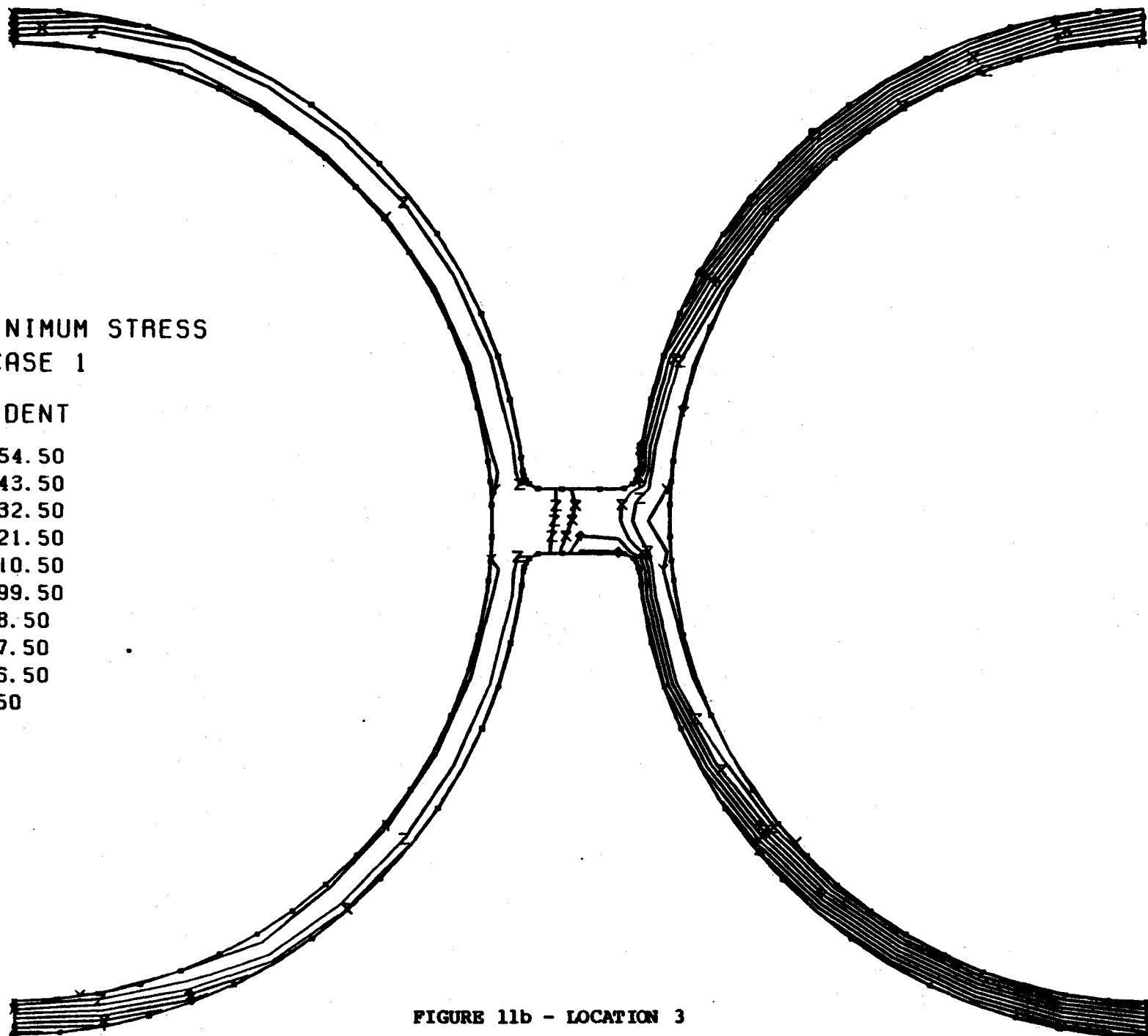
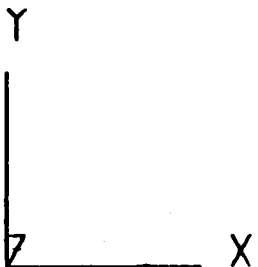


FIGURE 11b - LOCATION 3



CONTOUR MAP OF EFFECTIVE STRESS  
FOR LOAD CASE 1

CONTOUR IDENT

□	1870.96
○	4281.39
△	6691.81
+	9102.24
X	11512.66
◇	13923.09
↑	16333.51
X	18743.94
Z	21154.36
Y	23564.79

D-38

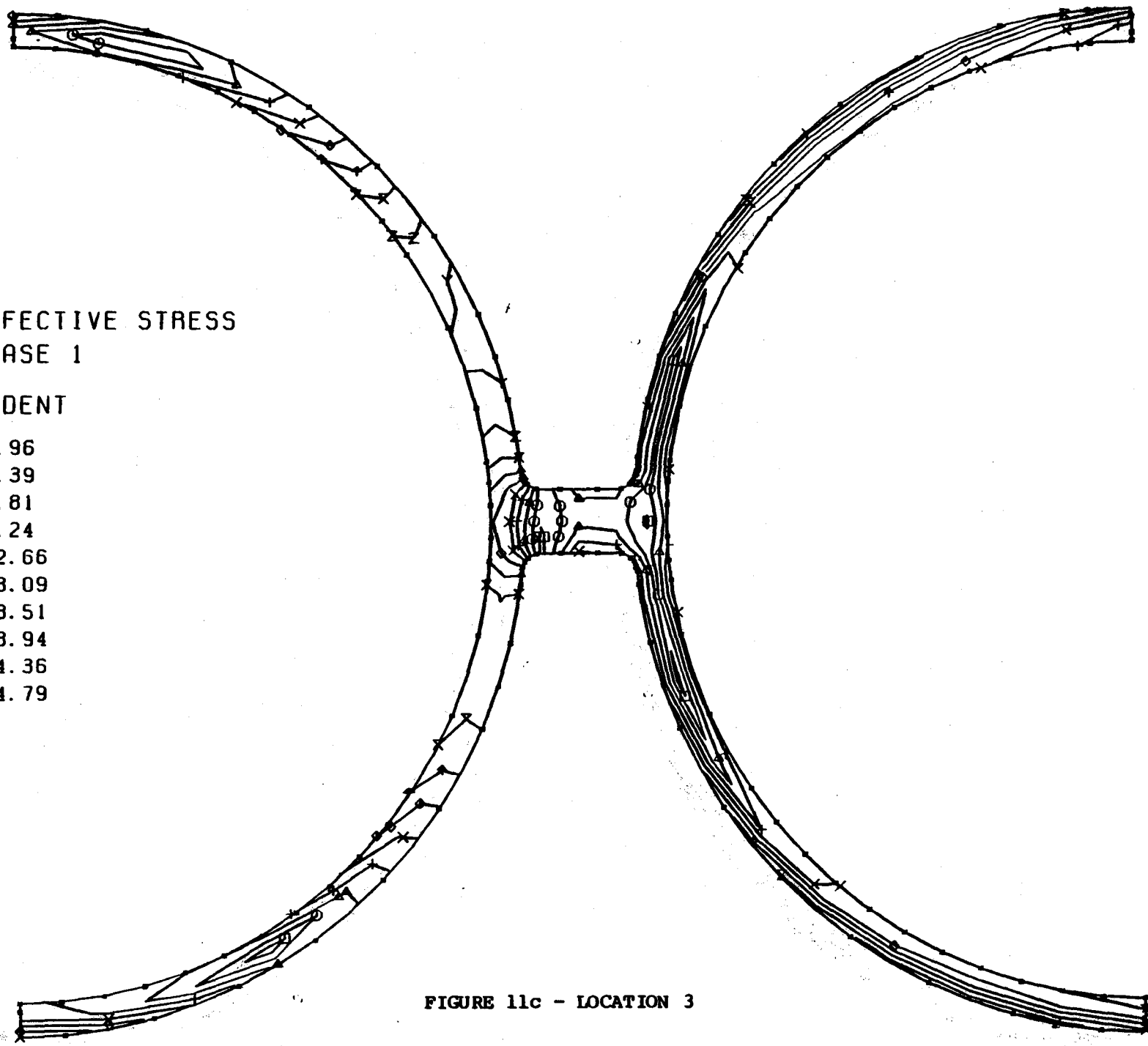
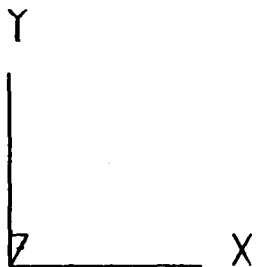
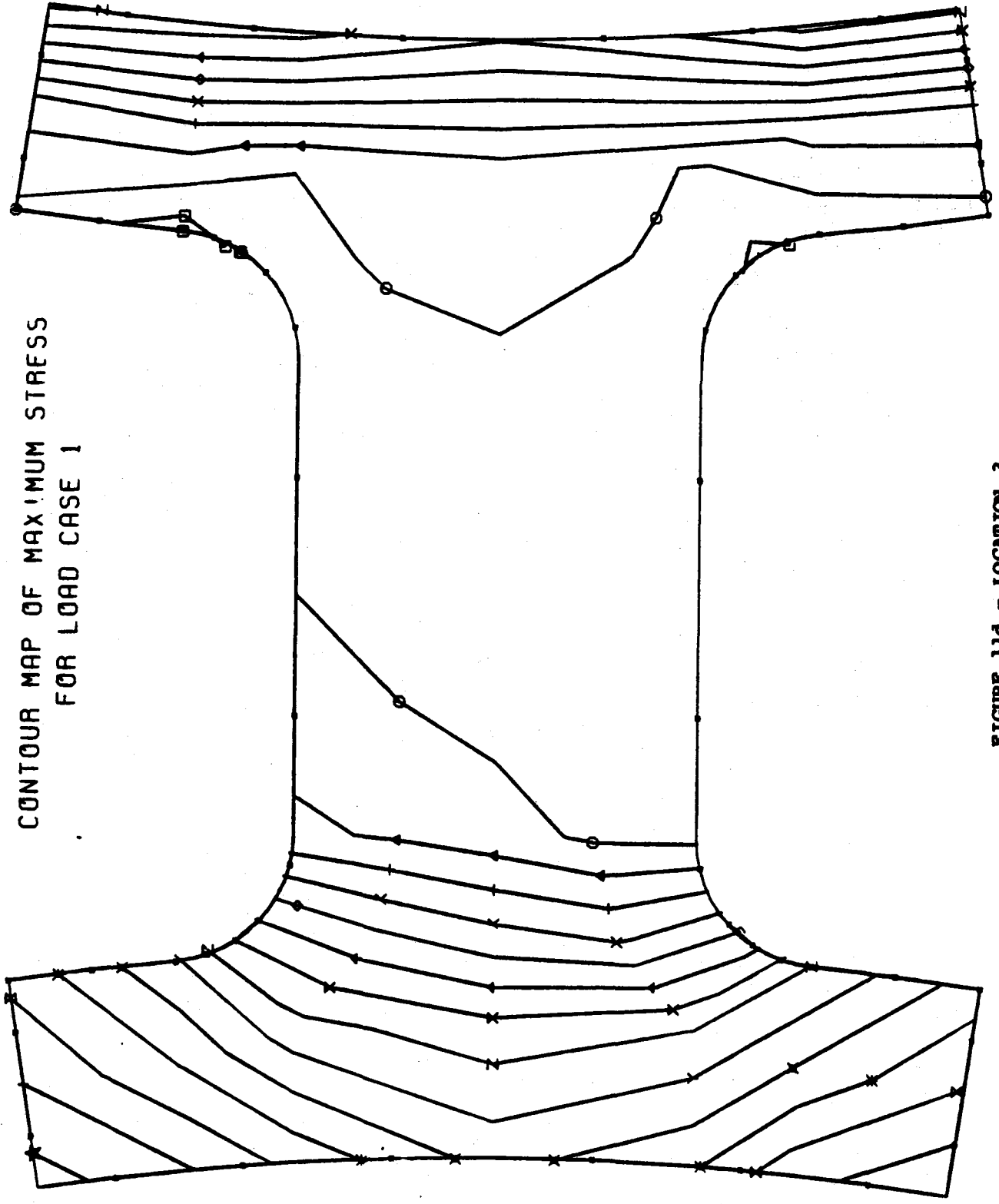


FIGURE 11c - LOCATION 3

CONTOUR MAP OF MAXIMUM STRESS  
FOR LOAD CASE 1



CONTOUR IDENT

- -998.55
- 621.35
- △ 2241.25
- + 3861.15
- X 5481.05
- ◇ 7100.95
- ↑ 8720.85
- X 10340.75
- Z 11960.65
- Y 13580.55
- X 15200.45
- \* 16820.35
- X 18440.25
- | 20060.15
- ★ 21680.05

FIGURE 11d - LOCATION 3

X

CONTOUR MAP OF MINIMUM STRESS  
FOR LOAD CASE 1

CONTOUR IDENT

□	-13336.83
○	-12320.50
△	-11304.17
+	-10287.83
X	-9271.50
◇	-8255.17
⋈	-7238.83
⊗	-6222.50
Z	-5206.17
Y	-4189.83
⊗	-3173.50
*	-2157.17
⊗	-1140.83
	-124.50
☆	891.83

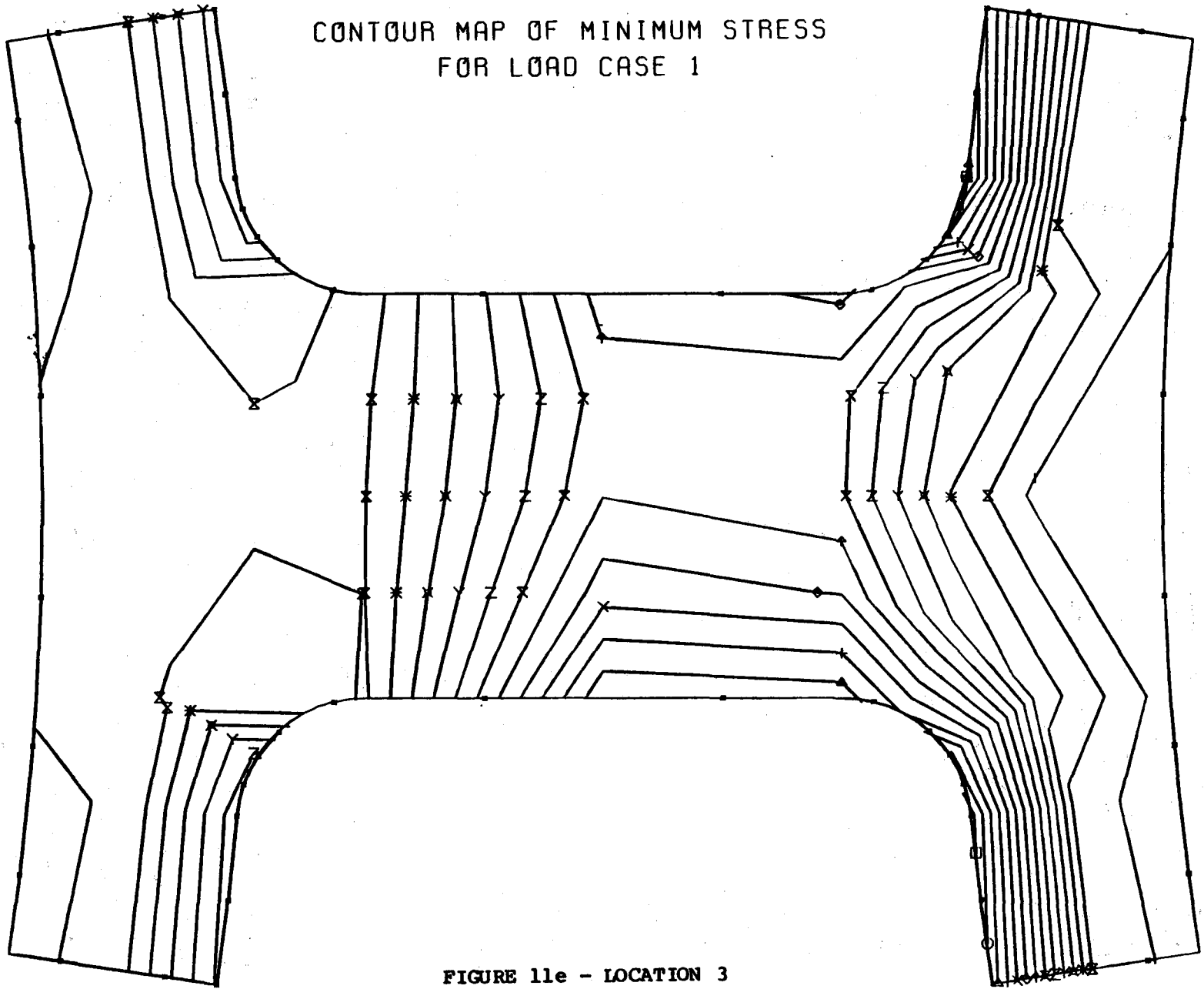
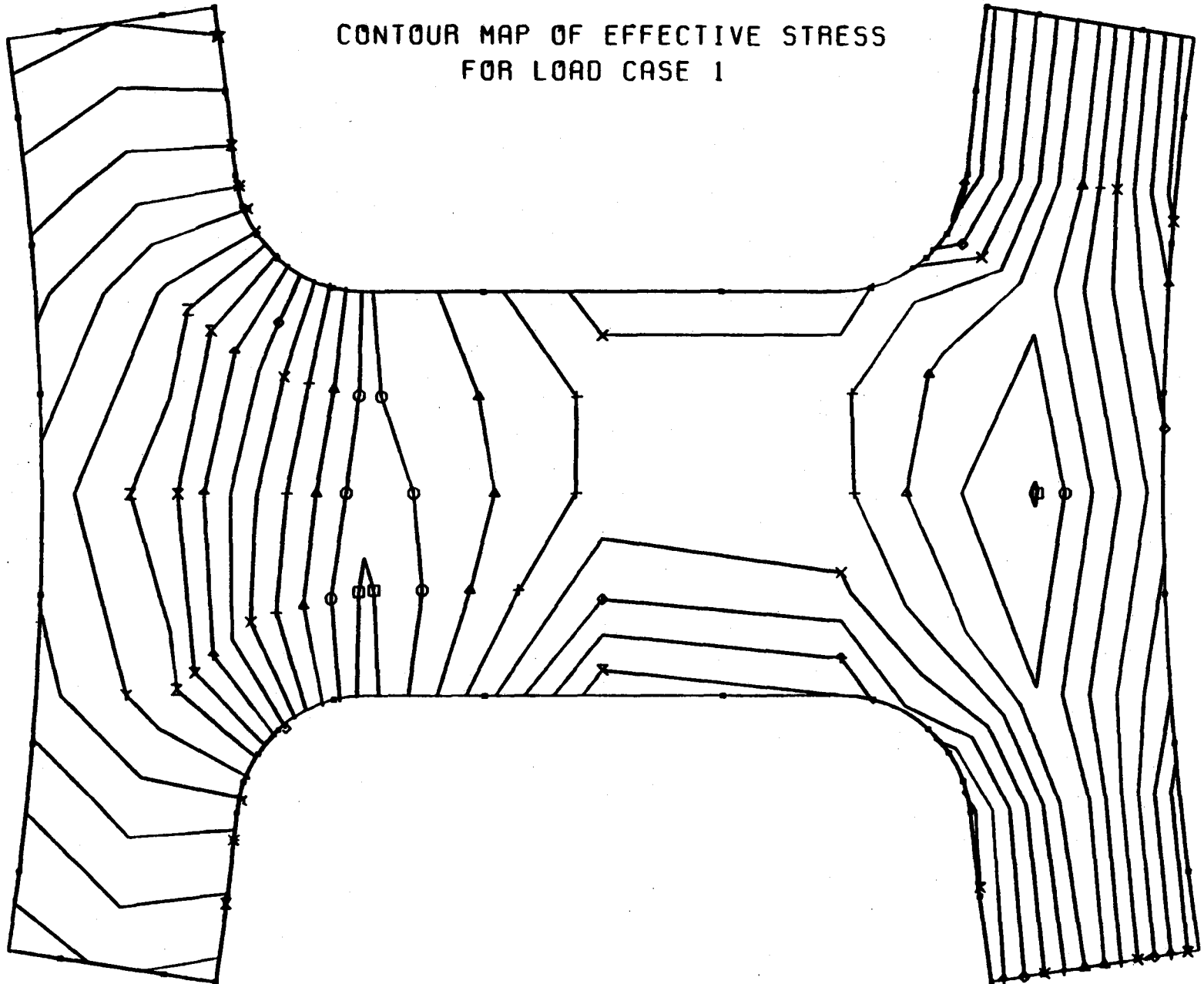


FIGURE 11e - LOCATION 3

CONTOUR MAP OF EFFECTIVE STRESS  
FOR LOAD CASE 1

CONTOUR IDENT

□	1617.48
○	2941.45
△	4265.42
+	5589.38
x	6913.35
◇	8237.32
↑	9561.28
⊗	10885.25
Z	12209.22
Y	13533.18
⊗	14857.15
*	16181.12
⊗	17505.08
	18829.05
★	20153.02



D-41

X

FIGURE 11f - LOCATION 3

## 6. DISCUSSION OF RESULTS

### 6.1 General

The skewed heat flux causes a temperature distribution that is not symmetric about any axis including the tube crown and the web center, which are the geometric axes of symmetry. This causes a bowing in the lateral direction, which has been investigated for location 2. The center of the middle web displaces .0013 inches relative to the outer boundary (figure 7c). For continuous bowing of an entire panel, the accumulated deflection is 0.14 in. This is considered negligible.

The axial displacements revealed less than a 1% spread; therefore, the beam elements are effective in tying the nodes together. The convergence of stresses is within 1% (same node, different elements); the difference in stress between the two tubes is under 3% (symmetry check).

Table 2 contains the maximum temperatures from FETAP and the Membrane Wall Program. The FETAP temperatures result from maximum heating at an angle off the crown; the Membrane Wall Program's maximum temperatures occur at the crown; i.e., in both cases the maximum temperatures occur where the heat flux is maximum. Comparing the maximum temperature of FETAP to those of the Membrane Wall Program, a difference is only one to two degrees is noted; i.e., the temperatures are essentially the same indicating that maximum tube temperature is solely a function of the heat flux and through thickness gradient and is not affected by changing the angle of incidence.

**TABLE 2**

**SUMMARY OF TEMPERATURES**

**FETAP VS. MEMBRANE WALL**

	Location	2		3	
	SIDE	1	2	1	2
Heat Flux		165,000	183,000	151,000	144,000
Tube Temp	FETAP	924.7	957.8	1043.4	1034.6
	Membrane Wall	926.9	956.8	1045.2	1035.6
Mean Temp	FETAP	701		868	
	Membrane Wall	836		964	
Web Temp	FETAP	750		990	
	Membrane Wall	1046		1131	

Table 2 also compares the mean tube wall temperatures of both programs. For location 2, the difference in mean temperatures is 135 F. For location 3, the difference is 96 F. In each case the greater mean temperatures occur for direct insolation; i.e., the Membrane Wall Program gives a higher mean temperature. The stresses are a function of the temperature difference between the temperature at a point and the mean temperature. Since skewed heating decreases the mean temperature, without changing the maximum, one would expect an increase in the maximum compressive stress. The decrease in mean temperature, due to skewed heating, results from shading; i.e., any angle of incidence causes some shading and a resultant cold region.

The angle of incidence accounts for most of the increased temperature difference (decreased mean temperature) but the non-circular plots (polar coordinates) of the heat flux distribution (not a cosine function) are also responsible for a decrease in the mean temperature. The area within the polar coordinate plot is a measure of the total heat input; the cosine function (circle) is a greater area (and thus heat flux) than what was obtained. Therefore a cosine distribution is not conservative in this application since a circular plot offers a lower ratio of maximum heat flux to total heat flux. The higher ratio contributes to a lower mean temperature and therefore higher compressive stress.

Maximum web temperatures (see table 2) are much less for skewed heating (FETAP) than values computed for direct insolation (Membrane Wall Program). Web temperatures appear to decrease as the angle of incidence increases. This undoubtedly is due to increased shading with increased angle of incidence.

## 6.2 STRESSES

A summary of stresses is presented in Table 3 with additional detail in Tables 4, 5, and 6. Stresses in Table 4 are from the lower surface (tube crown) of the model, whereas, Table 5 stresses are maximum for the entire geometry. The maximum, minimum, and effective stresses in the tube for location 2 are 30.5, -46.5, 41.9 KSI; for location 3, these stresses are 25.6, -27.8, 24.9 KSI respectively. The minimum stresses are the maximum compressive stresses; they are axial principal stresses. The maximum stresses are the maximum tensile stresses; they are also axial principal stresses. Table 6 compares maximum tube stress of FESAP and MWP and includes the maximum effective stress obtained from the MWP.

The tube stresses for location 2 are considerably higher than the location 3 stresses. The maximum heat flux is greater for location 2 by 18%; the maximum compressive stress is 67% greater. Maximum effective stress is also greater for location 2 by approximately the same amount, (68%). Location 2 also has higher angles of incidence ( $41^{\circ}$  and  $34^{\circ}$  versus  $34^{\circ}$  and  $20^{\circ}$ ). Thus, we would expect the percent increase in stress to be greater than the percent increase in heat flux which it is.

Table 3 also compares the maximum compressive stresses between skewed and direct insolation (Membrane Wall Program).. The maximum stresses are appreciably higher in the tube for skewed versus direct insolation; e.g., compressive stress increases by 47% for location 2 and 30% for location 3. This stress is primarily due to the difference in temperature between the location being analyzed and the mean temperature of the assembly. The



**TABLE 3****STRESS COMPARISONS****FESAP VS. MEMBRANE WALL**

		LOCATION 2		LOCATION 3	
		FESAP ksi	MEMBRANE WALL ksi	FESAP ksi	MEMBRANE WALL ksi
Tube	Max. Tensile	30.5		25.6	
	Max. Compressive	46.5	31.7	27.8	21.4
	Max. Effective	41.9	27.8	24.9	18.6
Web	Max Tensile	24.0	.5	12.0	.1
	Max Compressive	15.9	47.7	13.9	36.3
	Max. Effective	25.6	47.4	16.6	36.3

temperature difference (maximum temperature minus mean temperature) is 121F for skewed heating versus 41F for direct heating for location 2. The temperature differences are 81F versus 17F for location 3. Therefore it is not surprising that the stresses increase substantially.

The high angle of incidence and shading for location 2 explains the presence of a tensile stress gradients in the web. When the effects of shading reduces web temperatures below the mean temperature, tensile stresses occur and increase with increased shading. On the other hand, the web of location 3 displays compressive stresses because web temperatures are above the mean temperature due to the decreased shading relative to location 2. However, both location 2 and location 3 see substantial shading so the temperatures are reduced. This is reflected in a substantial decrease in web stresses (Table 3).

STRESS (FESAP)

	<u>LEFT TUBE</u>	<u>ELEMENT</u>		<u>RIGHT TUBE</u>	<u>ELEMENT</u>	<u>NODE</u>
<u>LOCATION # 2</u>						
SIG-MAX	29,340	36		28,263	62	178,308
	29,215	35		28,290	61	
	29,208	138		28,285	182	
	29,312	137		28,258	181	
SIG-MIN	- 45,340	5	-	46,492	86	21,426
	- 45,171	4	-	46,264	85	
SIG-EFF	40,737	3		41,883	85	16,426
	40,702	4		41,849	86	
<u>LOCATION #3</u>						
SIG-MAX	23,807	35		23,171	61	178,308
	23,547	36		23,016	62	
	23,788	137		23,165	181	
	23,578	138		23,033	182	
SIG-MIN	- 27,112	25	-	27,805	50	126,251
	- 26,886	26	-	27,610	51	
SIG-EFF	24,877	35		24,345	61	176,306
SIG-EFF	24,630	36		24,213	62	

TABLE 4

MAXIMUM STRESSES

LOCATION #2

		<u>NODE</u>	<u>ELEMENT</u>
SIG-MAX	30,526	632	137
	30,394	632	138
SIG-MIN	- 46,494	426	86
	- 46,264	426	85
SIG-EFF	41,883	426	85
	41,831	426	86

LOCATION #3

		<u>NODE</u>	<u>ELEMENT</u>
SIG-MAX	25,564	632	137
	25,312	632	138
SIG-MIN	- 27,805	251	50
	- 27,610	251	51
SIG-EFF	24,894	176	35
	24,648	176	36

TABLE 5

TUBE STRESS, PSI

LOCATION #2	SIG-MIN.	SIG-EFF
Q = 165,000		
= 41°	-39,365	
= 0°	-24,598*	21,355*
Q = 183,000		
= 34°	-46,494	
= 0°	-31,715*	27,783*
LOCATION #3	SIG-MIN	SIG-EFF.
Q = 151,000		
= 34°	-27,805	
= 0°	-41,420*	18,631*
Q = 144,000		
= 20°	-25,836	
= 0°	-19,145*	16.607*

\* - FROM MEMBRANE WALL PROGRAM

TABLE 6

### 6.3 SUMMARY

Comparison of results between heating at an effective angle of incidence and direct insolation of the Membrane Wall Program reveals identical maximum tube temperatures. Maximum tube temperatures develop at the point of maximum, normal heating and are not affected by an increased angle of incidence or a non-cosine heat distribution around the tube surface. Web temperatures decrease for skewed heating due to the shading (or partial shading) effect (1131F/1046F for Membrane Wall versus 990F for location 3 and 750F for location 2). For location 2, heat flows through the web to adjacent tube from the hot side of the tube.

The tube stresses are considerably higher for skewed heating than for the direct heating (46 ksi vs. 32 ksi for location 2). The increase is attributed to the lower mean temperature with no change in the maximum temperature. Two items are found responsible for causing lower mean temperatures, 1) low temperature regions develop due to shading and 2) lower total heat flow to the tube than the cosine distribution.

The web stresses are considerably lower for skewed heating than for direct heating (25 ksi versus 48 ksi for location 2). This results from lower web temperatures due to shading and the angle of incidence.

## 7. CONCLUSIONS

1. Skewed heating decreases the mean temperature of the tube with no change in the maximum tube temperature but with a substantial decrease in the web temperature.
2. Skewed heating substantially increases the maximum tube stress and decreases the maximum web stress relative to a direct heat input assumption. The amount of increase or decrease is a function of the angle of incidence of the heat flux and the extent that the heat flux distribution is a non-cosine function.
3. The skewed heating will cause some lateral bowing of the panel, but it will be a small amount.
4. The 2 tube Model gives accurate results.

## 8. RECOMMENDATIONS

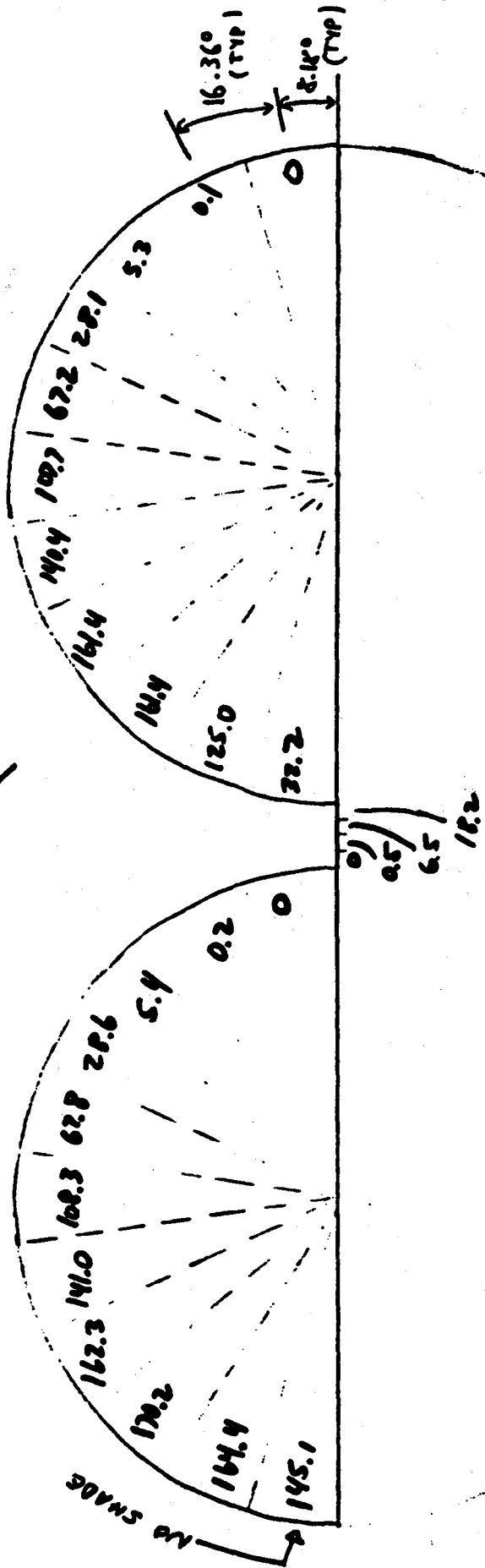
1. All future analyses should use actual heat flux distributions rather than the crown or average with a cosine distribution.
2. The membrane wall program should be rerun for the actual specified heat flux at the locations analyzed rather than the maximum developed in this analyses.



APPENDIX A

DIRECTION TOWARD  
APERTURE CENTER

$Q_{MAX} = 165000, \theta = 41^\circ$



2" 00 Tube  
3/16" hole

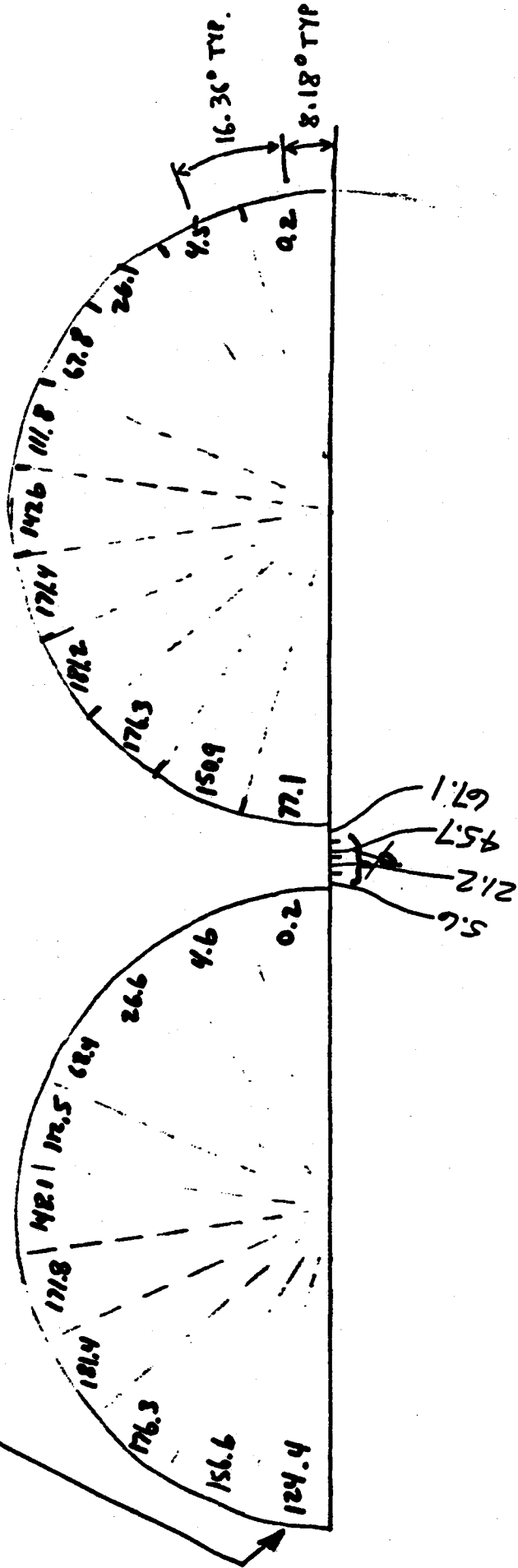
Loc 2

East Aperture (North Wall)  
Bay 172, New.

DIRECTION TOWARD APERTURE CENTER

$Q_{MAX} = 183000, \theta = 34^\circ$

NOTES:  
WITH NO SHADING



North A. (WEST WALL)

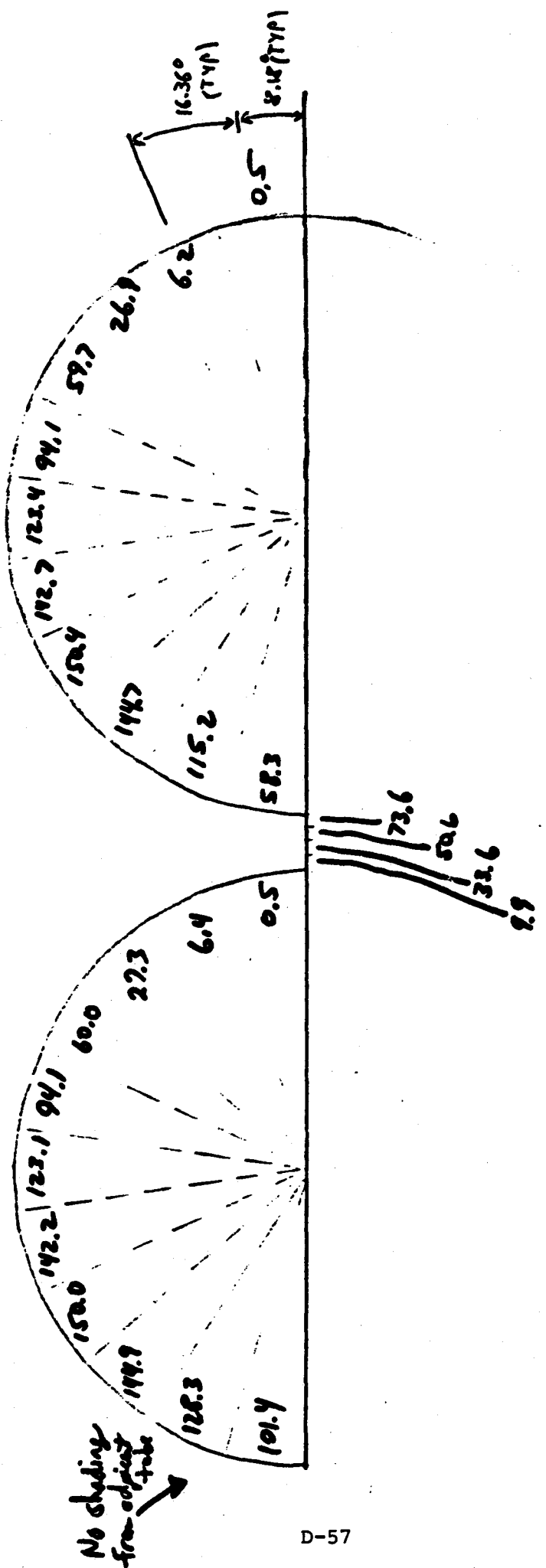
Loc #2

Day 17 2 NOON

2" Tubes  
3/16" Web

DIRECTION TOWARD APERTURE CENTER.

$Q_{MAX} = 151000$ ,  $\theta = 34^\circ$



No shading from adjacent tube

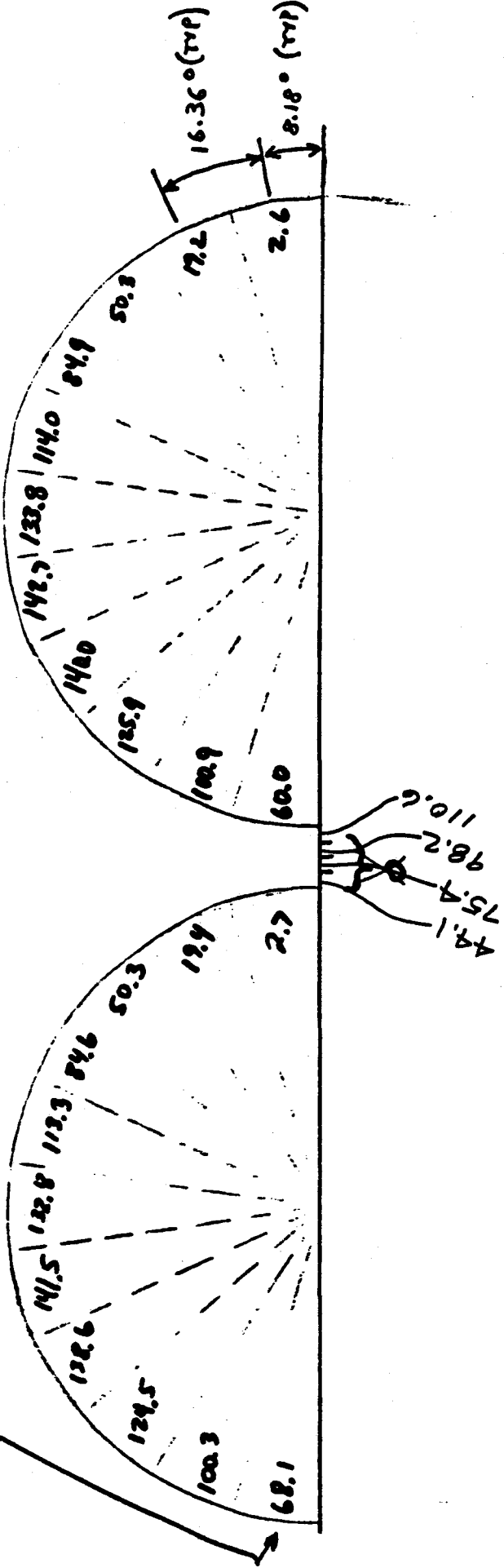
East Aperture (NORTH WALL)  
 Day 172, Noon

Loc 3

2" OD Tube  
 3/16" Web

DIRECTION TOWARD APERTURE CENTER

$Q_{MAX} = 144000, \theta = 20^\circ$

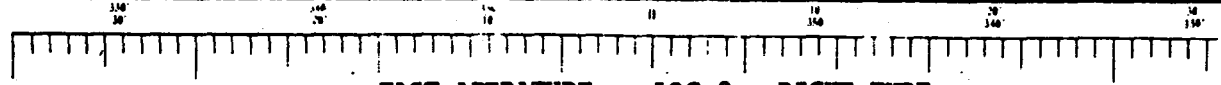
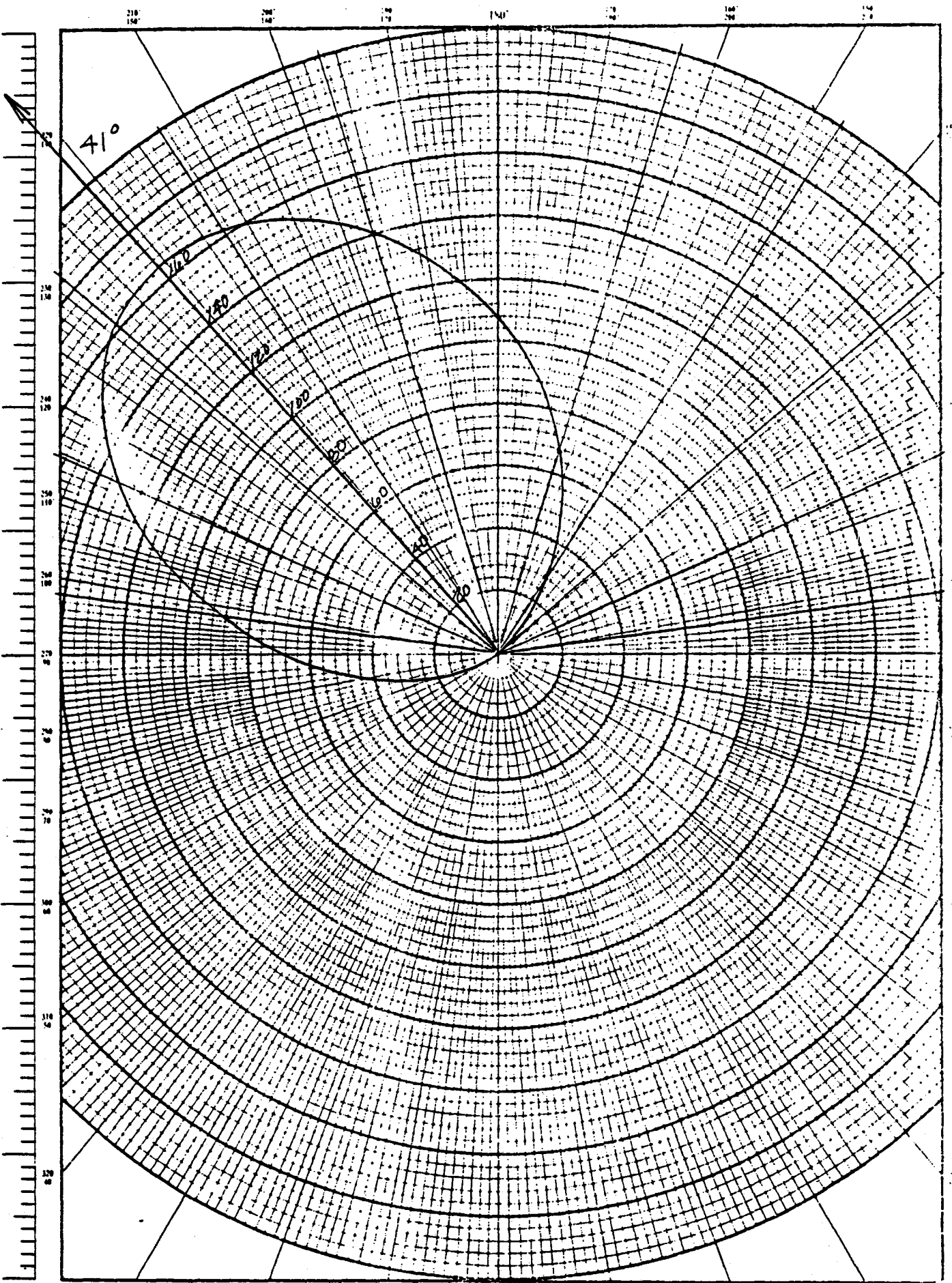


NOTE : WITH NO SHADING

Loc # 3  
(ON WEST WALL) North A.

2" Tube  
3/16" Web

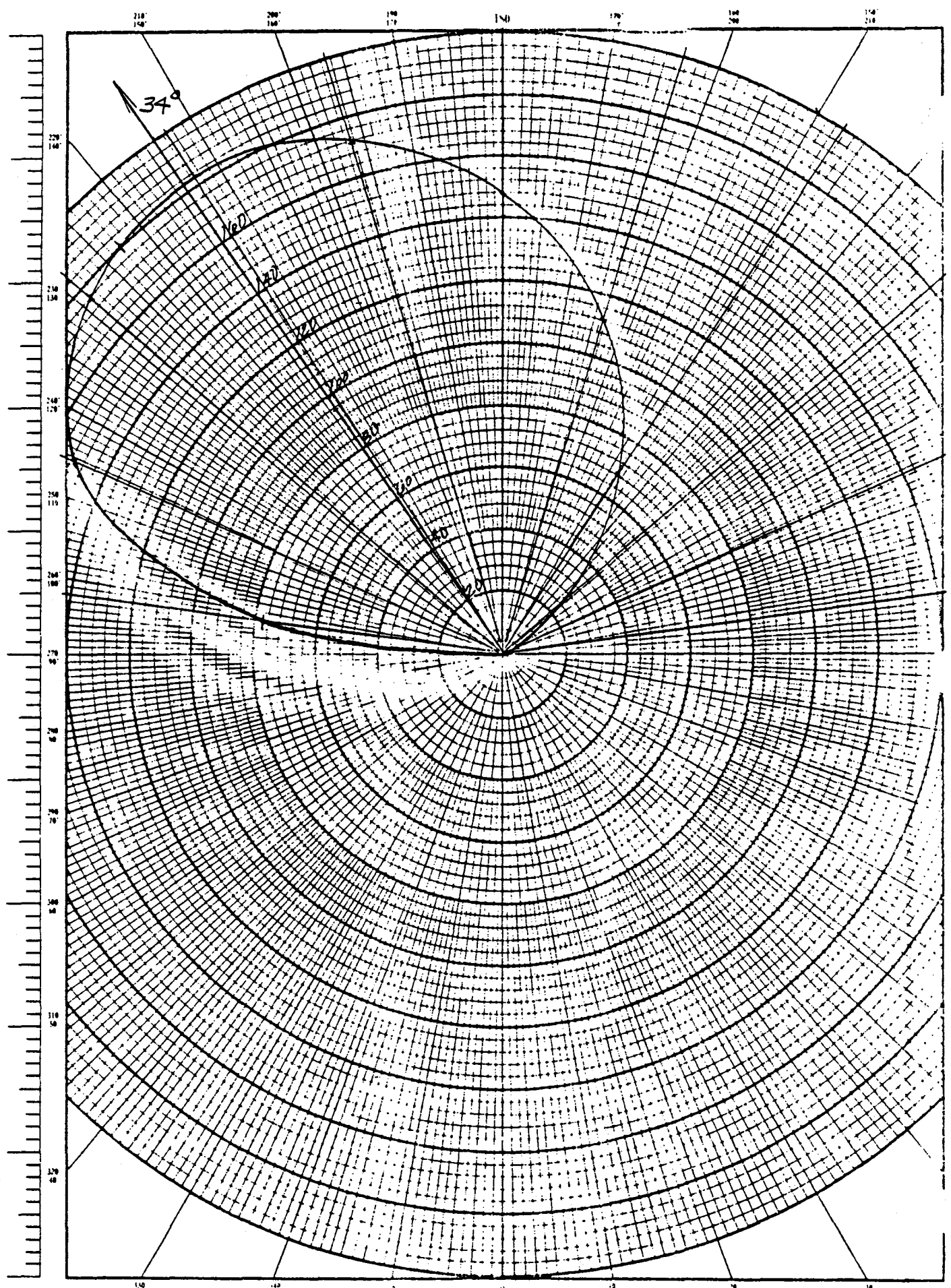
POLAR COORDINATE  
PATENTED BY BRUNNEN



EAST APERTURE - LOC 2 - RIGHT TUBE

D-59

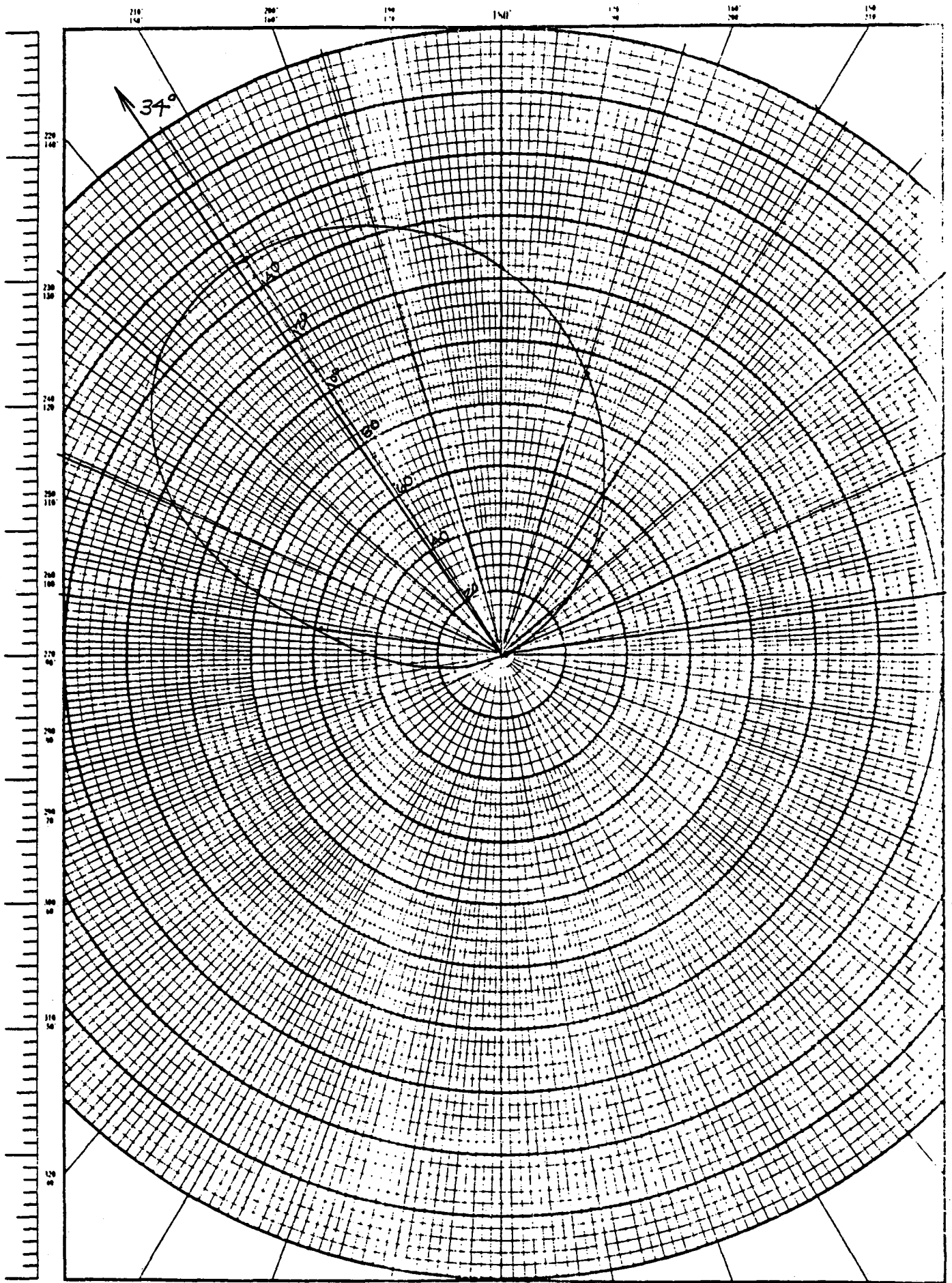
POLAR COORDINATE  
PAPER BY HESTER



NORTH APERTURE - LOC 2 - RIGHT TUBE

D-60

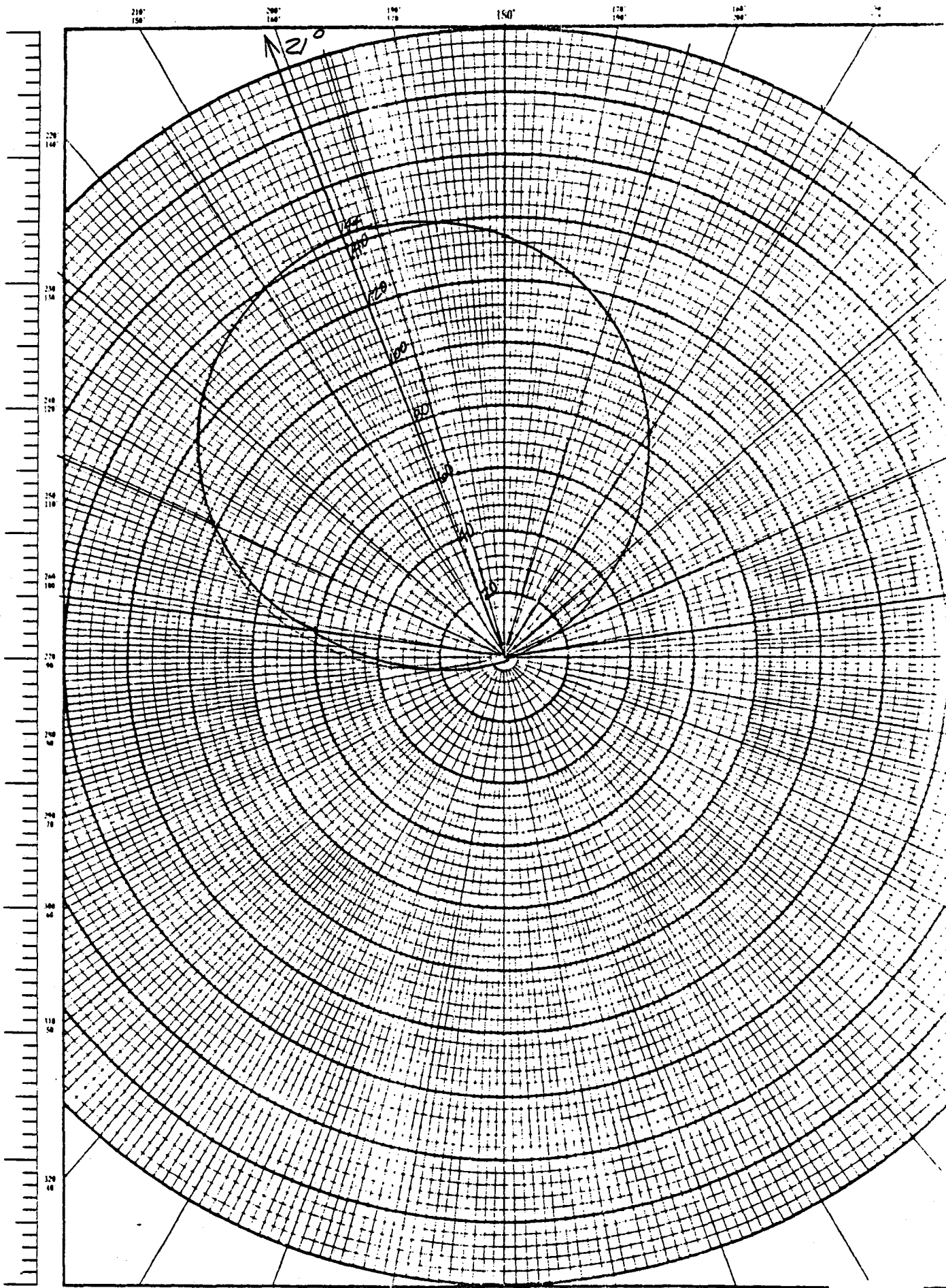
POLAR COORDINATE  
PARTIAL IN INCHES



EAST APERTURE - LOC 3 - RIGHT TUBE

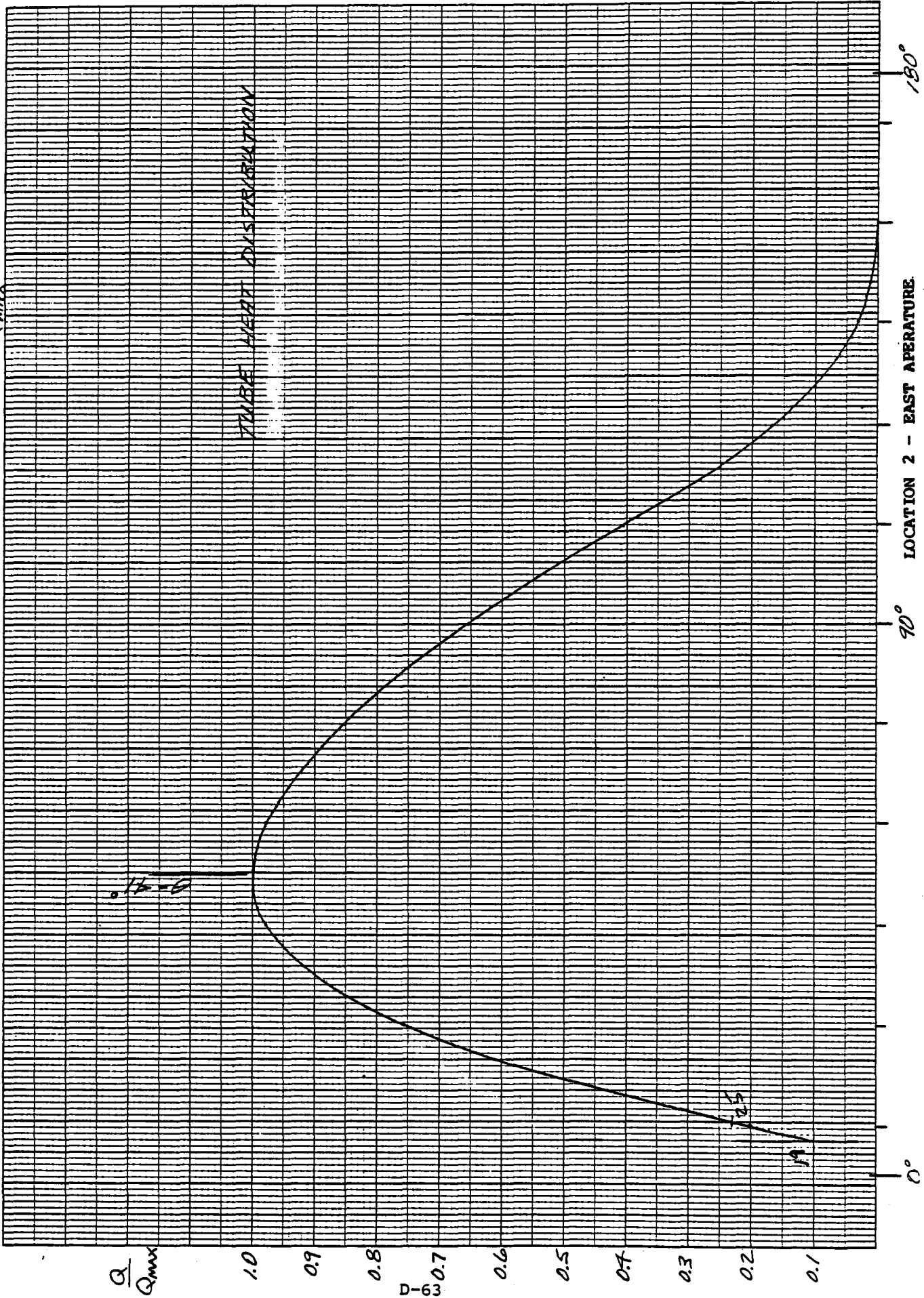
D-61

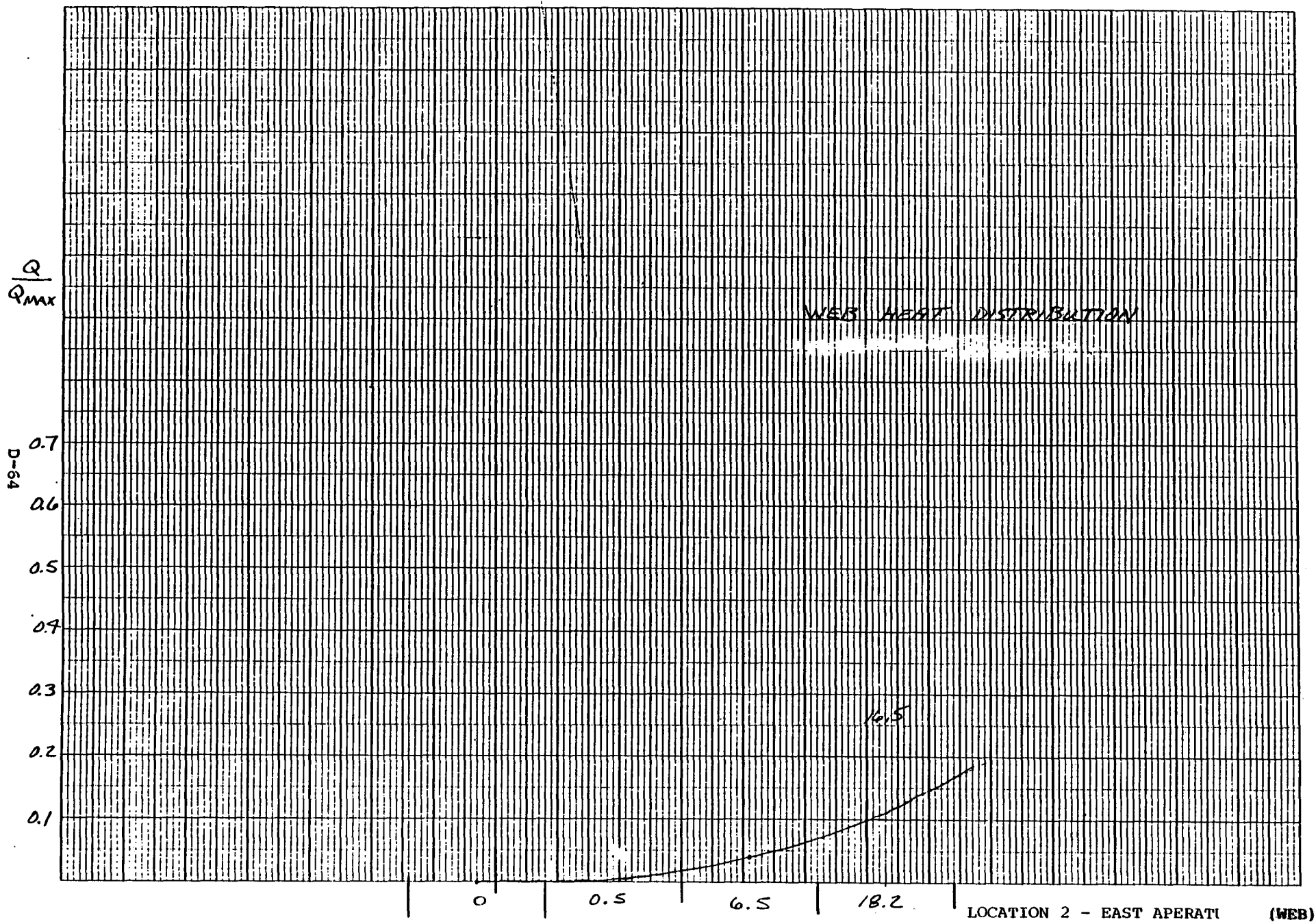




NORTH APERATURE - LOC 3 - RIGHT TUBE

$Q_{MAX} = 165$





$Q_{MAX} = 183$

TUBE HEAT DISTRIBUTION

DISTANCE BETWEEN  
Z AGGDES

0.000

$\frac{Q}{Q_{MAX}}$

1.0

0.9

0.8

0.7

0.6

0.5

0.4

0.3

0.2

0.1

D-65

25

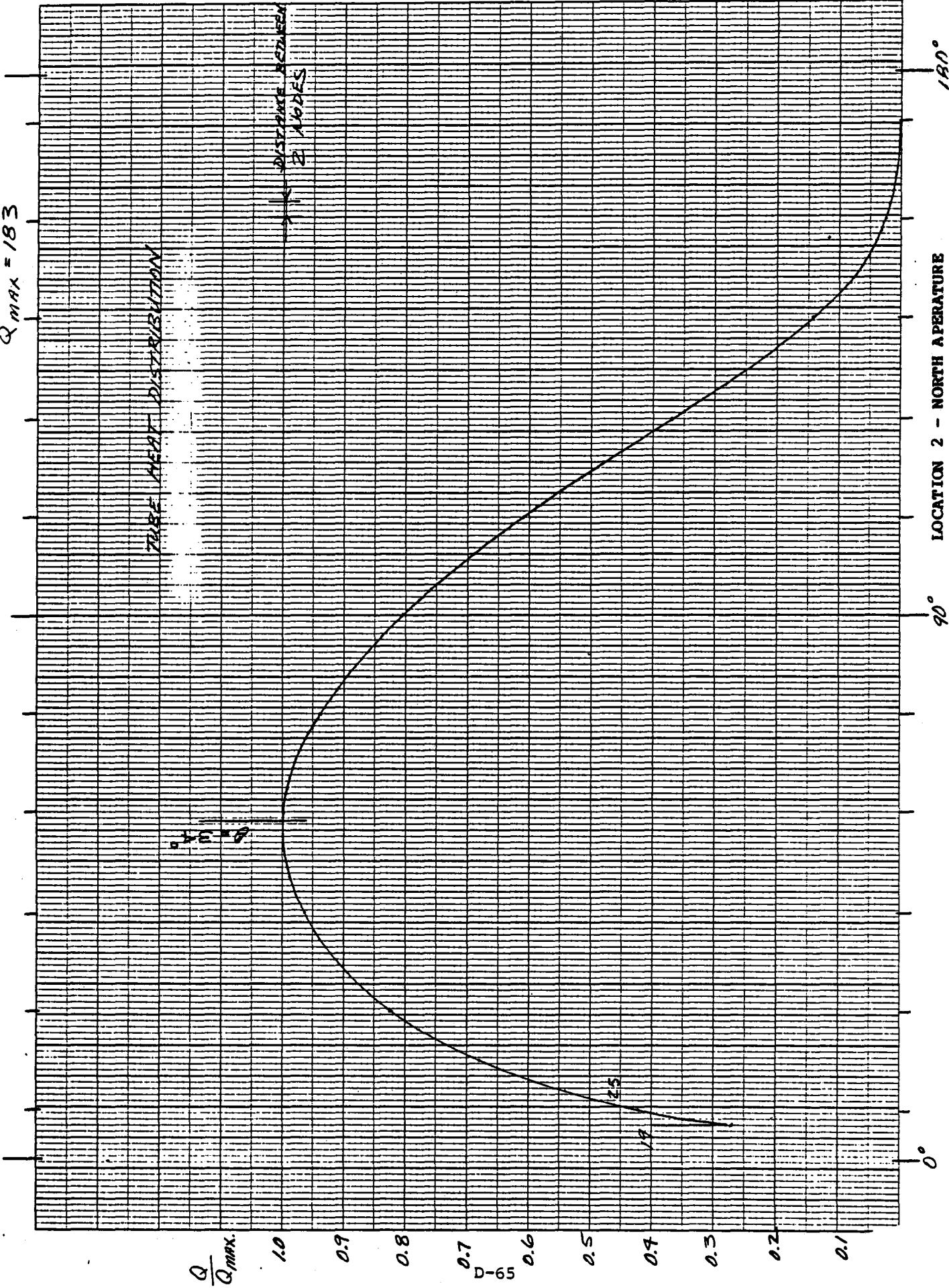
19

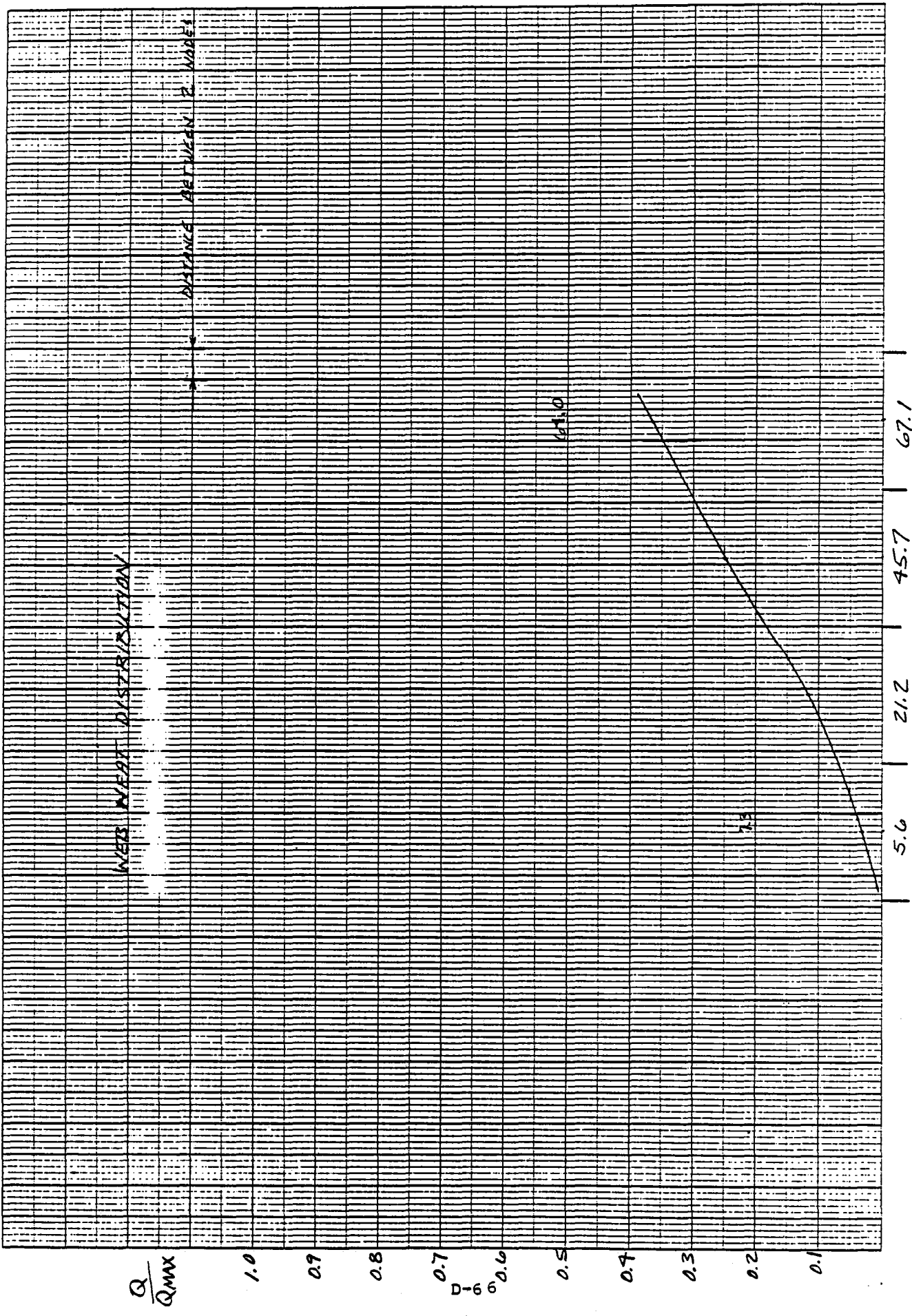
0°

90°

LOCATION 2 - NORTH APERTURE

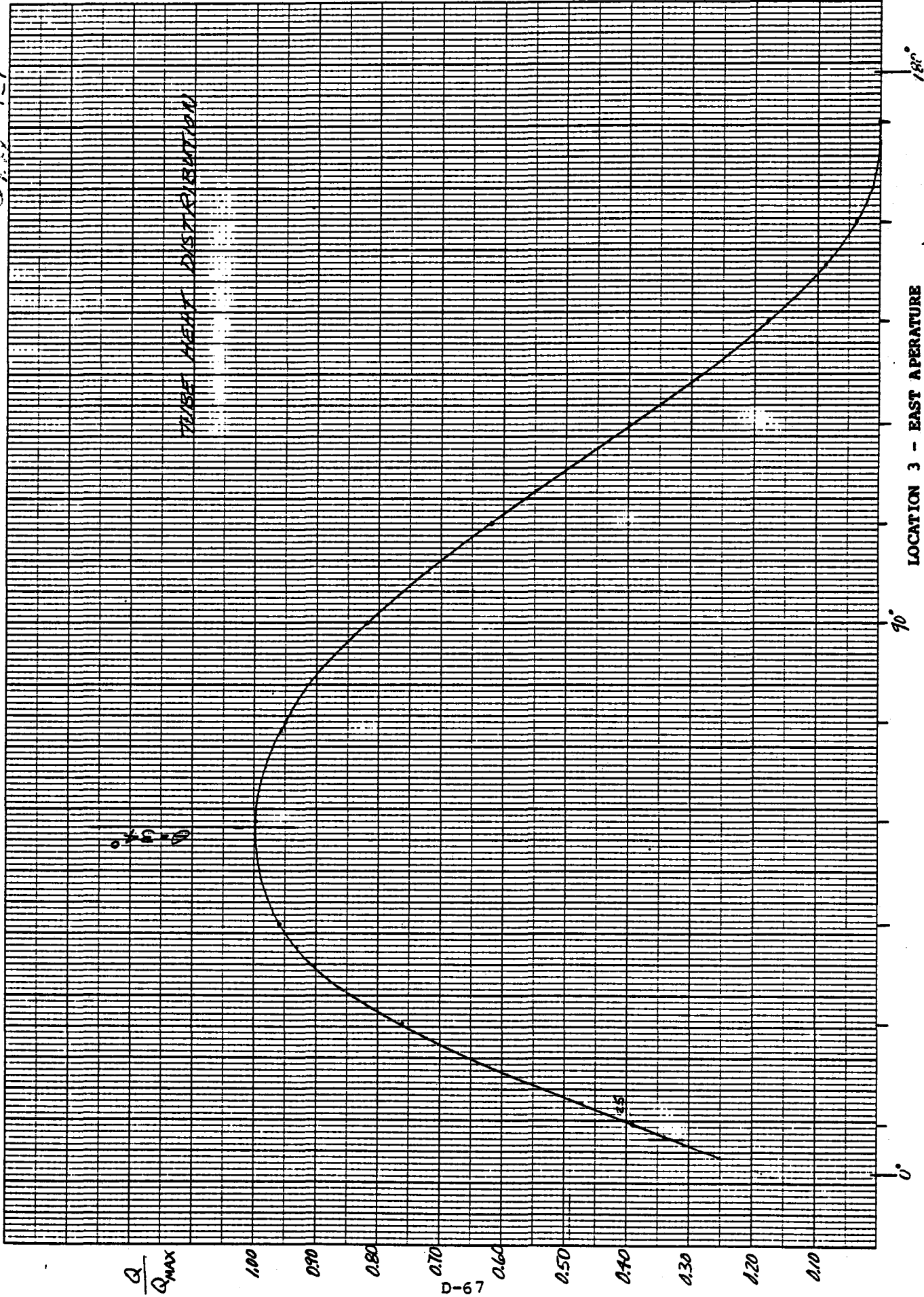
180°





$Q_{MAX} = 1.1$

TUBE HEAT DISTRIBUTION



LOCATION 3 - EAST APERTURE

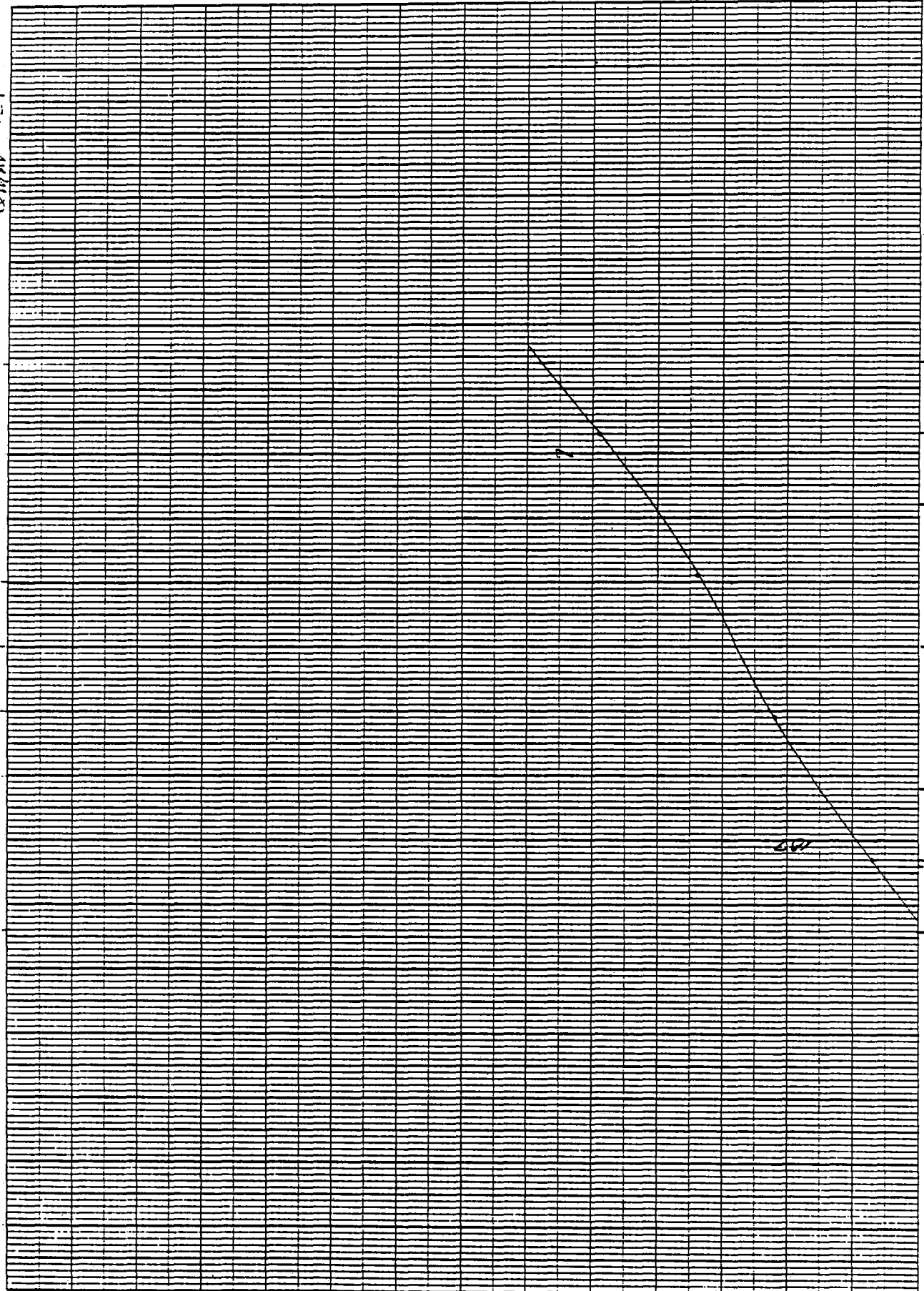
90°

0°

180°

D-67

Q<sub>100</sub> - 151



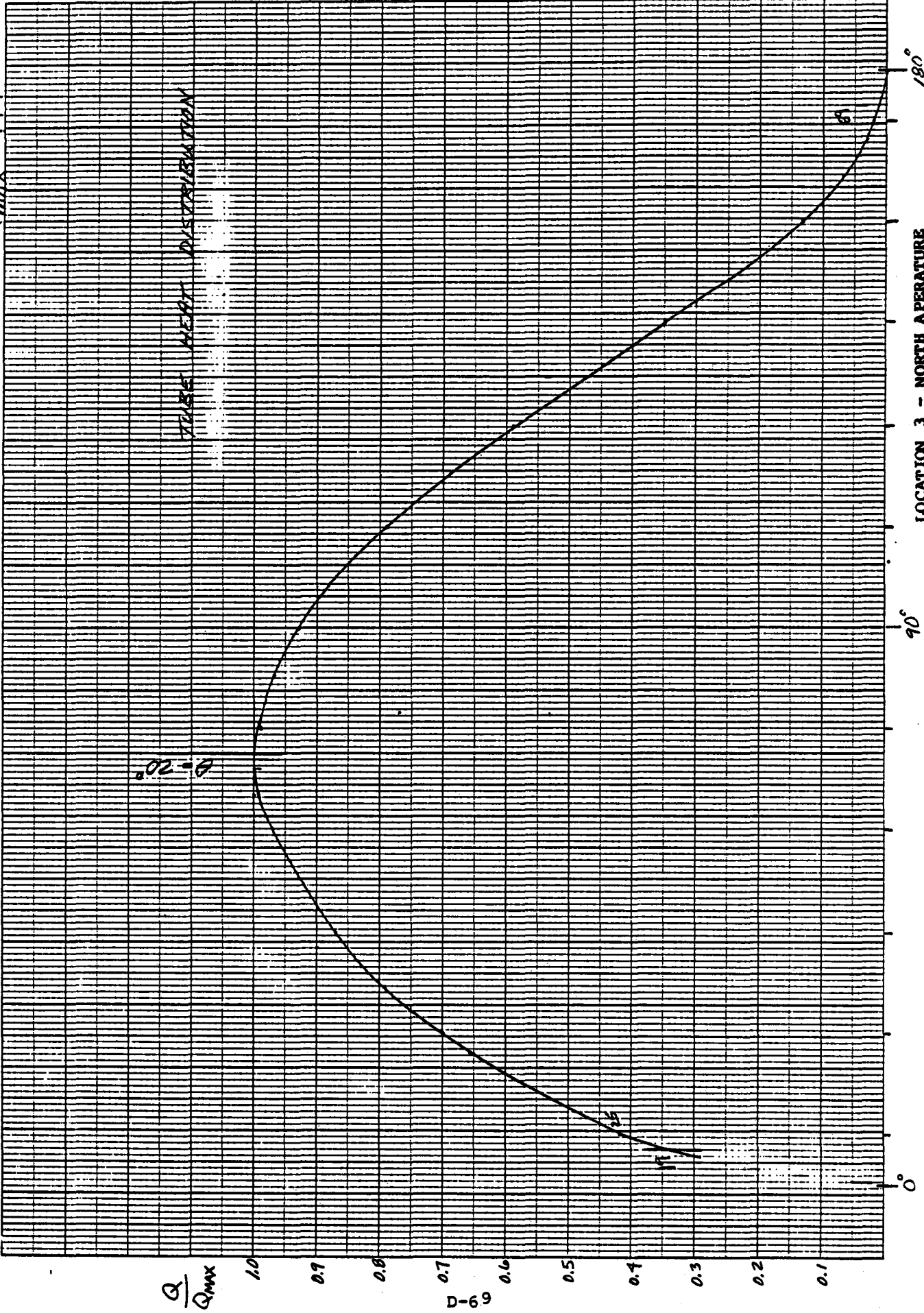
D-68

LOCATION 3 - EAST APER / (WEB)

$Q_{MAX} = 144$

TUBE HEAT DISTRIBUTION

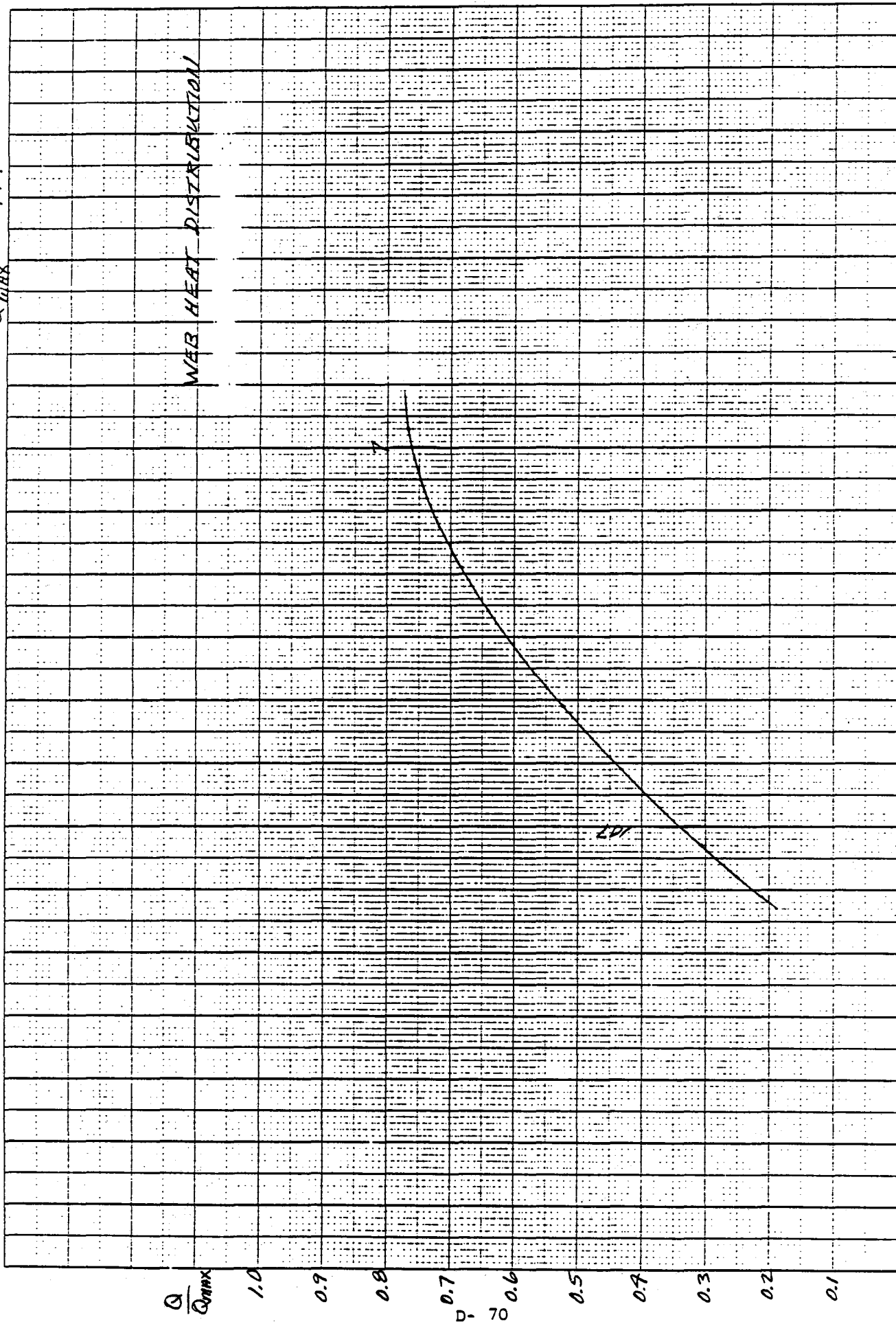
$\theta = 20^\circ$





$Q_{MAX} = 144$

WEB HEAT DISTRIBUTION



LOCATION 3 - NORTH APE (WEB)

APPENDIX B

# Babcock & Wilcox ENGINEERING CALCULATIONS

REFERENCE NO.

SHEET NO.

OF

PREPARED BY:

DATE:

SUBJECT:

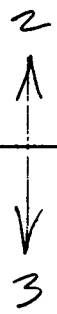
AREAS - 2-TUBE GEOMETRY

CHECKED BY:

REVISION:

## NODAL AREAS (WEIGHTED) - INCHES

1	0.00412	31	0.02957
2	0.01647	32	0.05915
3	0.00823	33	"
4	0.01647	34	"
5	0.00823	35	"
6	0.01647	36	"
7	0.00576	37	"
8	0.00654	38	"
9	0.00327	39	"
10	0.00654	40	"
11	0.00327	41	"
12	0.00654	42	"
13	0.00327	43	"
14	0.00654	44	"
15	0.00327	45	"
16	0.00654	46	"
17	0.00327	47	"
18	0.00654	48	"
19	0.00456	49	"
20	0.01167	50	"
21	0.00584	51	"
22	0.01167	52	"
23	0.00584	53	"
24	0.01167	54	"
25	0.01771	55	"
26	0.05915	56	"
27	0.02957	57	"
28	0.05915	58	"
29	0.02957	59	"
30	0.05915	60	"



<h1>Babcock &amp; Wilcox</h1> <h2>ENGINEERING CALCULATIONS</h2>	REFERENCE NO.	SHEET NO.
	PREPARED BY:	DATE:
SUBJECT:	CHECKED BY:	REVISION:

61	0.02957	3 ↑ — ↓ 2	93	0.00584
62	0.05915		94	0.01167
63	"		95	0.00456
64	"		96	0.00654
65	"		97	0.00327
66	"		98	0.00654
67	"		99	0.00327
68	"		100	0.00654
69	"		101	0.00327
70	"		102	0.00654
71	"	2 ↑ — ↓ 1	103	0.00327
72	"		104	0.00654
73	"		105	0.00327
74	"		106	0.00654
75	"		107	0.00576
76	"		108	0.01647
77	"		109	0.00823
78	"		110	0.01647
79	"		111	0.00823
80	"		112	0.01647
81	"	WEB <del>E</del>	113	0.00823
82	"			
83	"			
84	"			
85	"			
86	"			
87	"			
88	"			
89	0.01771			
90	0.01167			
91	0.00584			
92	0.01167			

4  
↑  
—  
↓  
3

# Babcock & Wilcox ENGINEERING CALCULATIONS

REFERENCE NO.

SHEET NO.

OF

PREPARED BY:

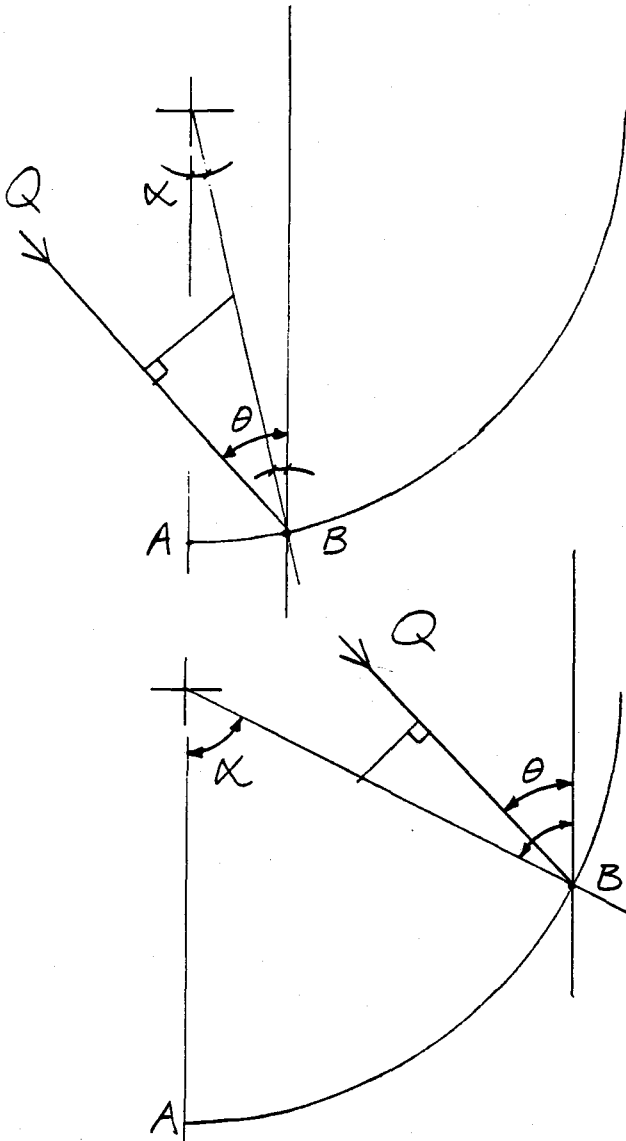
DATE:

SUBJECT:

BLEND RADIUS FLUX DISTRIBUTION

CHECKED BY:

REVISION:



$$\text{FACTOR} = \cos(\theta - \alpha)$$

$$\text{FACTOR} = \cos(\alpha - \theta)$$

AT ANGLE OF INCIDENCE,  $\theta$ ,  $Q$  IS KNOWN AT PT. A TAKEN FROM FLUX PLOT ACROSS WEB. SOLVE FOR  $Q_{\text{NORMAL}}$  WHERE  $Q_N \cos \theta = Q_A$

$$Q_B = \cos|\theta - \alpha| * Q_N$$

$$\text{TEMPFLUX INPUT} = \frac{Q_B}{Q_{\text{MAX.}}}$$

**Babcock & Wilcox**  
**ENGINEERING CALCULATIONS**

REFERENCE NO.	SHEET NO.
	OF
PREPARED BY:	DATE:
CHECKED BY:	REVISION:

SUBJECT:  
 TYPICAL HEAT DISTRIBUTION

FOR BLEND RADIUS

$\frac{Q}{Q_{max}}$

0.80

0.70

0.60

0.50

0.40

0.30

DISTANCE ALONG CURVE



# Babcock & Wilcox ENGINEERING CALCULATIONS

REFERENCE NO.

SHEET NO.

OF

PREPARED BY:

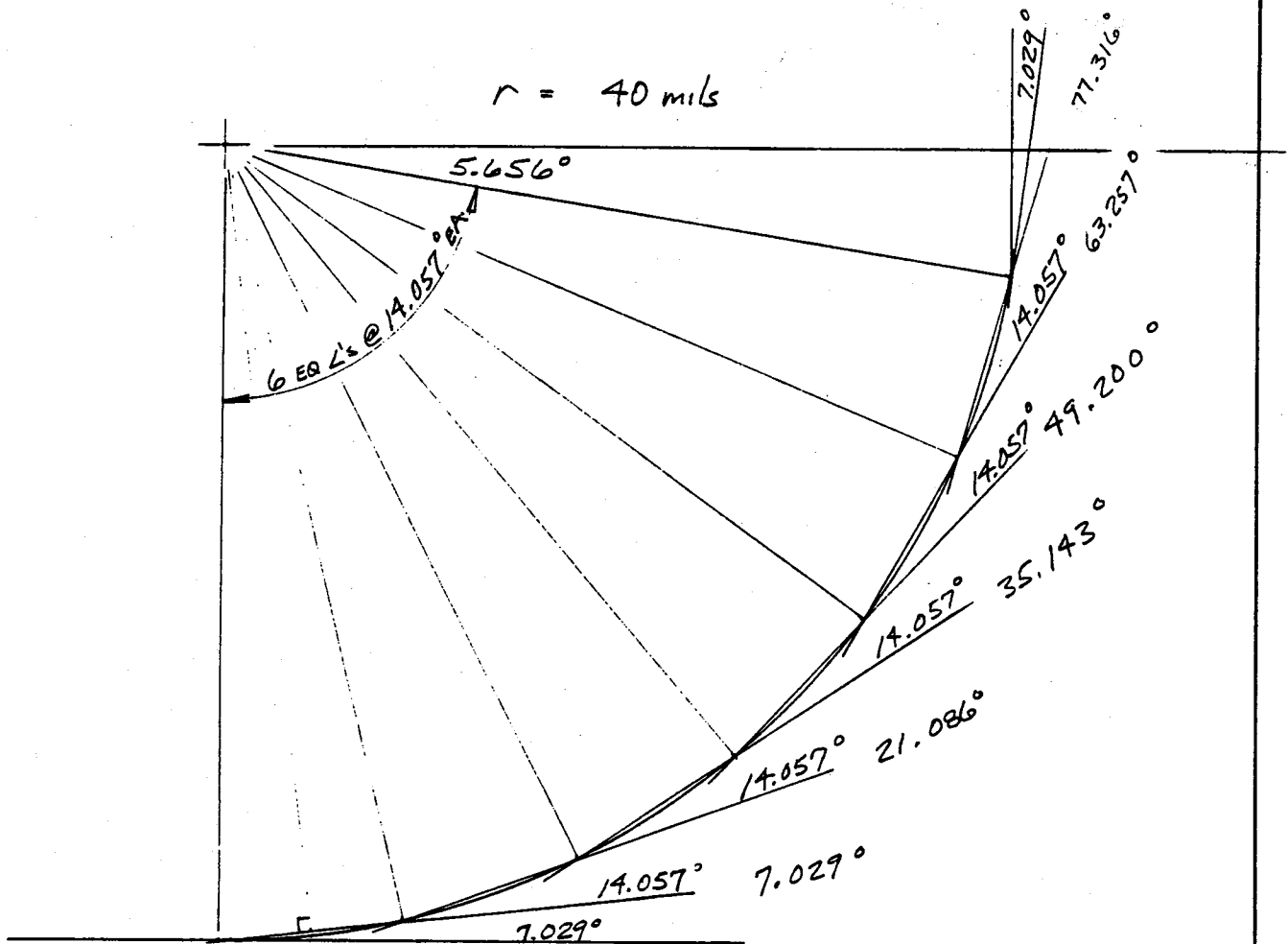
DATE:

SUBJECT:

*BLEND RADIUS*

CHECKED BY:

REVISION:



<b>Babcock &amp; Wilcox</b> <b>ENGINEERING CALCULATIONS</b>	REFERENCE NO.	SHEET NO.
	PREPARED BY:	DATE:
	CHECKED BY:	REVISION:
<b>SUBJECT:</b> BLEND RADIUS, LOC #2 - E. APER.		

$\theta = 41^\circ$

$Q_{MAX} = 165$

$Q_A = 16.5$

$Q_N = \frac{16.5}{\cos 41^\circ} = 21.9$



$NODE \quad \beta = |k - \theta| \quad Q_B = Q_N \cos \beta \quad Q_B / Q_{MAX}$

7	41	16.5	0.100
8	41 - 7.03	18.2	0.110
9	41 - 14.06	19.5	0.118
10	41 - 21.09	20.6	0.125
11	41 - 28.11	21.3	0.129
12	41 - 35.14	21.8	0.132
13	42.17 - 41	21.9	0.133
14	49.20 - 41	21.7	0.131
15	56.23 - 41	21.1	0.128
16	63.26 - 41	20.3	0.123
17	70.29 - 41	19.1	0.116
18	77.32 - 41	17.6	0.107
19	84.34 - 41	15.9	0.097

OPPOSITE BLEND RADIUS IS COMPLETELY SHADED.



# Babcock & Wilcox ENGINEERING CALCULATIONS

REFERENCE NO.

SHEET NO.

OF

PREPARED BY:

DATE:

SUBJECT:

LOCATION #2 - EAST APERATURE

CHECKED BY:

REVISION:

ORDER OF INPUT

↓	$\frac{Q}{Q_{MAX}}$		
1	0.018	31	0.745
2	0.026	32	0.798
3	0.037	33	0.844
4	0.050	34	0.885
5	0.063	35	0.917
6	0.080	36	0.944
7	0.100	37	0.967
8	0.110	38	0.984
9	0.118	39	0.993
10	0.125	40	0.998
11	0.129	41	1.000
12	0.132	42	0.995
13	0.133	43	0.990
14	0.131	44	0.980
15	0.128	45	0.966
16	0.123	46	0.950
17	0.116	47	0.932
18	0.107	48	0.913
19	0.097	49	0.890
20	0.124	50	0.868
21	0.150	51	0.843
22	0.170	52	0.817
23	0.190	53	0.788
24	0.210	54	0.757
25	0.230	55	0.725
26	0.330	56	0.693
27	0.430	57	0.655
28	0.525	58	0.622
29	0.610	59	0.582
30	0.680	60	0.545

# Babcock & Wilcox ENGINEERING CALCULATIONS

REFERENCE NO.

SHEET NO.

OF

PREPARED BY:

DATE:

SUBJECT:

LOC #2 EAST APER.

CHECKED BY:

REVISION:

61	0.505	93	0.0
62	0.465	94	
63	0.424	95	
64	0.380	96	
65	0.340	97	
66	0.297	98	
67	0.258	99	
68	0.224	100	
69	0.190	101	
70	0.161	102	
71	0.135	103	
72	0.110	104	
73	0.088	105	
74	0.068	106	
75	0.051	107	
76	0.036	108	
77	0.027	109	0.001
78	0.019	110	0.002
79	0.012	111	0.004
80	0.007	112	0.010
81	0.003	113	0.018
82	0.001		
83	0.0		
84			
85			
86			
87			
88			
89			
90			
91			
92			

# Babcock & Wilcox ENGINEERING CALCULATIONS

REFERENCE NO.

SHEET NO.

OF

PREPARED BY:

DATE:

SUBJECT:

BLEND RADIUS-LOC #2 - N. AVER

CHECKED BY:

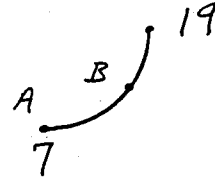
REVISION:

$$\theta = 34^\circ$$

$$Q_{MAX} = 183$$

$$Q_A = 64.0 \text{ (GIVEN)}$$

$$Q_N = \frac{64.0}{\cos 34} = 77.2$$



NODE

$$\beta = |X - \theta|$$

$$Q_B = Q_N \cos \beta$$

$$Q_B / Q_{MAX}$$

7	34°	64.0	0.350
8	34 - 7.03	68.8	0.376
9	34 - 14.06	72.6	0.397
10	34 - 21.09	75.2	0.411
11	34 - 28.11	76.8	0.420
12	35.14 - 34	77.2	0.422
13	42.17 - 34	76.4	0.418
14	49.20 - 34	74.5	0.407
15	56.23 - 34	71.5	0.391
16	63.26 - 34	67.4	0.368
17	70.29 - 34	62.2	0.340
18	77.32 - 34	56.2	0.307
19	84.34 - 34	49.3	0.269

# Babcock & Wilcox ENGINEERING CALCULATIONS

REFERENCE NO.

SHEET NO.

OF

PREPARED BY:

DATE:

SUBJECT:

BLEND RADIUS, LOC #2 - N. APER

CHECKED BY:

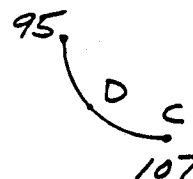
REVISION:

$$\theta = 34^\circ$$

$$Q_{MAX} = 183$$

$$Q_C = 7.3 \text{ (GIVEN FROM PLOT)}$$

$$Q_N = \frac{7.3}{\cos 34^\circ} = 8.8$$



NODE	$\beta = \kappa + \theta$	$Q_D = Q_N \cos \beta$	$Q_D / Q_{MAX}$
------	---------------------------	------------------------	-----------------

95	118.34°	—	0.0
96	111.32	—	0.0
97	104.19	—	0.0
98	97.26	—	0.0
99	90.23	—	0.0
100	83.20	1.04	0.006
101	76.17	2.10	0.011
102	69.11	3.14	0.017
103	62.11	4.12	0.022
104	55.09	5.04	0.028
105	48.06	5.88	0.032
106	41.03	6.64	0.036
107	34°	7.30	0.040

<h2 style="margin: 0;">Babcock &amp; Wilcox</h2> <h3 style="margin: 0;">ENGINEERING CALCULATIONS</h3>	REFERENCE NO.	SHEET NO.
	PREPARED BY:	OF
SUBJECT:	CHECKED BY:	DATE:
LOCATION #2 - NORTH APER.	REVISION:	

1	0.182	31	0.815
2	0.212	32	0.848
3	0.241	33	0.875
4	0.270	34	0.900
5	0.298	35	0.921
6	0.322	36	0.940
7	0.350	37	0.955
8	0.376	38	0.968
9	0.397	39	0.980
10	0.411	40	0.988
11	0.420	41	0.993
12	0.422	42	0.998
13	0.418	43	1.000
14	0.407	44	0.999
15	0.391	45	0.996
16	0.368	46	0.990
17	0.340	47	0.983
18	0.307	48	0.974
19	0.269	49	0.961
20	0.320	50	0.947
21	0.345	51	0.931
22	0.380	52	0.914
23	0.400	53	0.895
24	0.430	54	0.875
25	0.445	55	0.852
26	0.540	56	0.830
27	0.615	57	0.805
28	0.680	58	0.778
29	0.730	59	0.750
30	0.777	60	0.721

<b>Babcock &amp; Wilcox</b> <b>ENGINEERING CALCULATIONS</b>	REFERENCE NO.	SHEET NO.
	PREPARED BY:	DATE:
SUBJECT:	CHECKED BY:	REVISION:

61	0.690	93	0.0
62	0.657	94	↓
63	0.623	95	
64	0.589	96	
65	0.553	97	
66	0.516	98	
67	0.476	99	↓
68	0.437	100	0.006
69	0.400	101	0.011
70	0.360	102	0.017
71	0.323	103	0.022
72	0.283	104	0.028
73	0.248	105	0.032
74	0.213	106	0.036
75	0.182	107	0.040
76	0.152	108	0.058
77	0.125	109	0.077
78	0.100	110	0.098
79	0.076	111	0.121
80	0.060	112	0.150
81	0.044	113	0.182
82	0.033		
83	0.023		
84	0.016		
85	0.010		
86	0.007		
87	0.003		
88	0.001		
89	0.0		
90	↓		
91			
92	↓		

# Babcock & Wilcox ENGINEERING CALCULATIONS

REFERENCE NO.

SHEET NO.

OF

PREPARED BY:

DATE:

SUBJECT:

BLEND RADIUS, LOC. #3 - E. APER.

CHECKED BY:

REVISION:

$$\theta = 34^\circ$$

$$Q_{MAX} = 151$$

$$Q_A = 71 \text{ (GIVEN)}$$

$$Q_N = \frac{71}{\cos 34^\circ} = 85.6$$

NODE	$\beta =$ 1K- $\theta$	$Q_B =$ $Q_N \cos \beta$	$\frac{Q_B}{Q_{MAX}}$
------	---------------------------	-----------------------------	-----------------------

7	34°	71.0	0.470
8	34-7.03	76.3	0.505
9	34-14.06	80.5	0.533
10	34-21.09	83.4	0.553
11	34-28.11	85.1	0.564
12	35.14-34	85.6	0.567
13	42.17-34	84.7	0.561
14	49.20-34	82.6	0.547
15	56.23-34	79.2	0.525
16	63.26-34	74.7	0.495
17	70.29-34	69.0	0.457
18	77.32-34	62.3	0.412
19	84.34-34	54.6	0.362

# Babcock & Wilcox ENGINEERING CALCULATIONS

REFERENCE NO.

SHEET NO.

OF

PREPARED BY:

DATE:

SUBJECT:

BLEND RAD. LOC #3 - E. APER.

CHECKED BY:

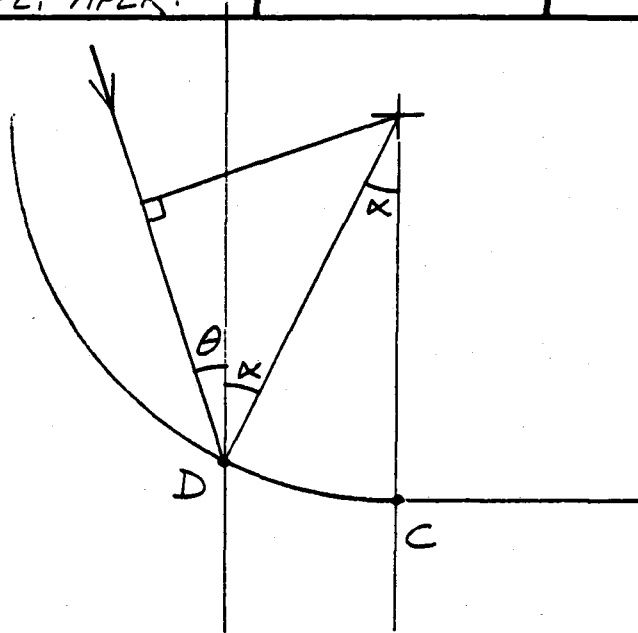
REVISION:

$$\theta = 34^\circ$$

$$Q_C = 14 \text{ (GIVEN)}$$

$$Q_N = \frac{14}{\cos 34^\circ} = 16.9$$

$$Q_{MAX} = 151$$



$$\text{FACTOR} = \cos(\theta + \kappa)$$

$$\text{NODE} \quad \beta = (\kappa + \theta)$$

$$Q_D = Q_N \cos \beta$$

$$\frac{Q_D}{Q_{MAX}}$$

95	118.34	0	0
96	111.32	0	0
97	104.29	0	0
98	97.26	0	0
99	90.23	0	0
100	83.20	2.0	0.013
101	76.17	4.0	0.026
102	69.14	6.0	0.039
103	62.11	7.9	0.052
104	55.09	9.7	0.064
105	48.06	11.3	0.075
106	41.03	12.7	0.084
107	34°	16.9 cos 34° = 14.0	0.093



<b>Babcock &amp; Wilcox</b> <b>ENGINEERING CALCULATIONS</b>	REFERENCE NO.	SHEET NO.
	PREPARED BY:	OF DATE:
SUBJECT: <i>FLUX DATA - FRACTIONS</i>	CHECKED BY:	REVISION:

*LOCATION #3 - EAST APERATURE*

1	0.280			31	0.756
2	0.303			32	0.800
3	0.330			33	0.843
4	0.360			34	0.880
5	0.393			35	0.910
6	0.430			36	0.931
7	<del>0.466</del>	0.470		37	0.950
8	<del>0.550</del>	0.505		38	0.965
9	<del>0.576</del>	0.533		39	0.976
10	<del>0.601</del>	0.553		40	0.985
11	<del>0.611</del>	0.564		41	0.991
12	<del>0.620</del>	0.567		42	0.995
13	<del>0.607</del>	0.561		43	0.998
14	<del>0.594</del>	0.547		44	1.000
15	<del>0.566</del>	0.525		45	0.997
16	<del>0.537</del>	0.495		46	0.987
17	<del>0.493</del>	0.457		47	0.980
18	<del>0.449</del>	0.412		48	0.970
19	0.395			49	0.958
20	0.340			50	0.944
21	0.354			51	0.930
22	0.368			52	0.913
23	0.382			53	0.893
24	0.396			54	0.870
25	0.410			55	0.845
26	0.470			56	0.820
27	0.534			57	0.790
28	0.596			58	0.760
29	0.654			59	0.732
30	0.710			60	0.700

# Babcock & Wilcox ENGINEERING CALCULATIONS

REFERENCE NO.

SHEET NO.

OF

PREPARED BY:

DATE:

SUBJECT:

CHECKED BY:

REVISION:

LOC. #3 - EAST APER.

61	0.668	91	0.0
62	0.634	92	
63	0.600	93	
64	0.565	94	
65	0.530	95	
66	0.495	96	
67	0.460	97	
68	0.421	98	
69	0.387	99	
70	0.350	100	
71	0.316	101	
72	0.281	102	
73	0.249	103	
74	0.218	104	
75	0.190	105	
76	0.160	106	
77	0.088	107	
78	0.068	108	
79	0.050	109	
80	0.035	110	
81	0.012	111	
82	0.008	112	
83	0.003	113	
84	0.002		
85	0.0		
86			
87			
88			
89			
90			

# Babcock & Wilcox ENGINEERING CALCULATIONS

REFERENCE NO.

SHEET NO.

OF

PREPARED BY:

DATE:

SUBJECT:

BLEND RADIUS, LOC. #3 - N. APER.

CHECKED BY:

REVISION:

$$\theta = 20^\circ$$

$$Q_{MAX} = 144$$

$$Q_A = 110 \text{ (GIVEN)}$$

$$Q_N = \frac{110}{\cos 20^\circ} = 117$$



NODE	$\beta =$	$Q_B =$	$\frac{Q_B}{Q_{MAX}}$
	$ x - \theta $	$Q_N \cos \beta$	

7	20°	109.9	0.763
8	20-7.03	114.0	0.792
9	20-14.06	116.4	0.808
10	21.09-20	117.0	0.813
11	28.11-20	115.8	0.804
12	35.14-20	112.9	0.784
13	42.17-20	108.3	0.752
14	49.20-20	102.1	0.709
15	56.23-20	94.4	0.656
16	63.26-20	85.2	0.592
17	70.29-20	74.8	0.519
18	77.32-20	63.2	0.439
19	84.34-20	50.7	0.352

# Babcock & Wilcox ENGINEERING CALCULATIONS

REFERENCE NO.

SHEET NO.

OF

PREPARED BY:

DATE:

SUBJECT:

BLEND RAD - LOC#3 N. RPER

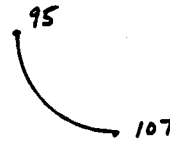
CHECKED BY:

REVISION:

$$\theta = 20^\circ$$

$$Q_C = 49 \text{ (GIVEN)}$$

$$Q_N = \frac{49}{\cos 20^\circ} = 52.1$$



$$Q_{MAX} = 144$$

NODE	$\beta = \alpha + \theta$	$Q_D = Q_N \cos \beta$	$\frac{Q_D}{Q_{MAX}}$
------	---------------------------	------------------------	-----------------------

95	107.34	—	—
96	97.32	—	—
97	90.29	—	—
98	83.26	6.1	0.042
99	76.23	12.4	0.086
100	69.20	18.5	0.128
101	62.17	24.32	0.169
102	55.14	29.78	0.207
103	48.11	34.79	0.242
104	41.09	39.27	0.273
105	34.06	43.2	0.300
106	27.03	46.4	0.322
107	20°	49.0	0.340

# Babcock & Wilcox

## ENGINEERING CALCULATIONS

REFERENCE NO.

SHEET NO.

OF

PREPARED BY:

DATE:

SUBJECT:

HEAT FLUX FRACTIONS - INPUT

CHECKED BY:

REVISION:

LOCATION #3 - NORTH APERTURE

1	<del>0.0</del>	0.611	31	0.694
2	<del>0.0</del>	0.647	32	0.730
3	<del>0.0</del>	0.680	33	0.760
4	<del>0.010</del>	0.705	34	0.790
5	<del>0.040</del>	0.730	35	0.817
6	<del>0.060</del>	0.750	36	0.840
7	<del>0.100</del>	0.763	37	0.860
8	<del>0.120</del>	0.792	38	0.877
9	<del>0.140</del>	0.808	39	0.894
10	<del>0.160</del>	0.813	40	0.911
11	<del>0.180</del>	0.804	41	0.926
12	<del>0.200</del>	0.784	42	0.941
13	<del>0.220</del>	0.752	43	0.955
14	<del>0.240</del>	0.709	44	0.968
15	<del>0.260</del>	0.656	45	0.980
16	<del>0.280</del>	0.592	46	0.990
17	<del>0.300</del>	0.519	47	0.995
18	<del>0.320</del>	0.439	48	1.000
19	<del>0.340</del>	0.352	49	0.998
20	0.360		50	0.996
21	0.374		51	0.990
22	0.390		52	0.985
23	0.400		53	0.977
24	0.420		54	0.968
25	0.425		55	0.956
26	0.477		56	0.945
27	0.524		57	0.930
28	0.574		58	0.914
29	0.615		59	0.895
30	0.656		60	0.875

# Babcock & Wilcox ENGINEERING CALCULATIONS

REFERENCE NO.

SHEET NO.

OF

PREPARED BY:

DATE:

SUBJECT:

CHECKED BY:

REVISION:

Loc. #3 NORTH APER.

61	0.852	93	0.014
62	0.827	94	0.012
63	0.800	- 95	0.010
64	0.774	96	0.008
65	0.744	97	0.006
66	0.714	98	<del>0.004</del> 0.042
67	0.681	99	<del>0.002</del> 0.086
68	0.648	100	<del>0.0</del> 0.128
69	0.614	101	0.169
70	0.580	102	0.207
71	0.543	103	0.242
72	0.506	104	0.273
73	0.470	105	0.300
74	0.433	106	0.322
75	0.398	- 107	0.340
76	0.362	108	0.393
77	0.327	109	0.442
78	0.291	110	0.487
79	0.253	111	0.530
80	0.216	112	0.572
81	0.185	WEB <del>E</del> 113	0.611
82	0.155		
83	0.126		
84	0.102		
85	0.080		
86	0.062		
87	0.046		
88	0.032		
89	0.022		
90	0.020		
91	0.018		
92	0.016		

VOID



**SUPPLEMENTAL STRESS ANALYSIS OF THE HEAT  
ABSORPTION TUBES FOR SKEWED HEATING  
(ONE-SIDED HEATING)**

**MOLTEN SALT RECEIVER  
SUBSYSTEM RESEARCH EXPERIMENT**

**The Babcock & Wilcox Company**

**Contract 894-0012-45**

**Prepared by:  
John P. Reed**

**Approved by:  
E. M. Livingston**

**October 1982**

## Purpose

The purpose of this analysis is to determine the maximum stress levels for one-sided skewed heating and compare results to the normal-to-the-panel heating analysis. The maximum thermal tube stress is also determined for the double wing wall design. The following report supplements the earlier report, Stress Analysis of the Heat Absorption Tubes for Skewed Heating (two-sided heating analysis), written June, 1982.

From the earlier report, the effect of skewed heating increases the tube thermal stress. Since maximum heating exists in the north cavity and maximum skewed heating occurs in both the north and east (west) cavities, it is only necessary to look at Location 2 since it satisfies both conditions. The same heat flux distribution is used as was used previous and is the one supplied by Martin Marietta. The geometry, models, and boundary conditions remain the same and are described in the previous report.

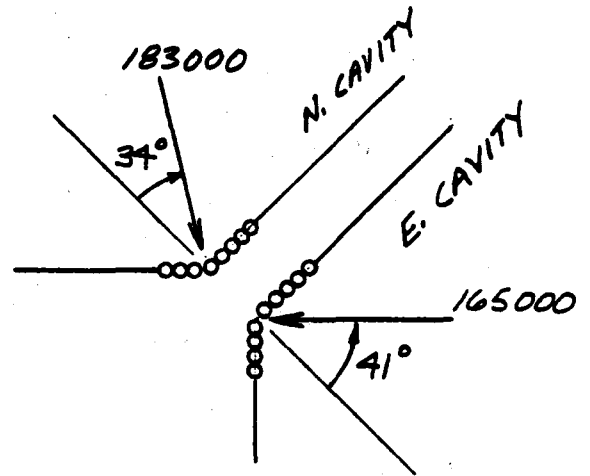


## Thermal Analysis

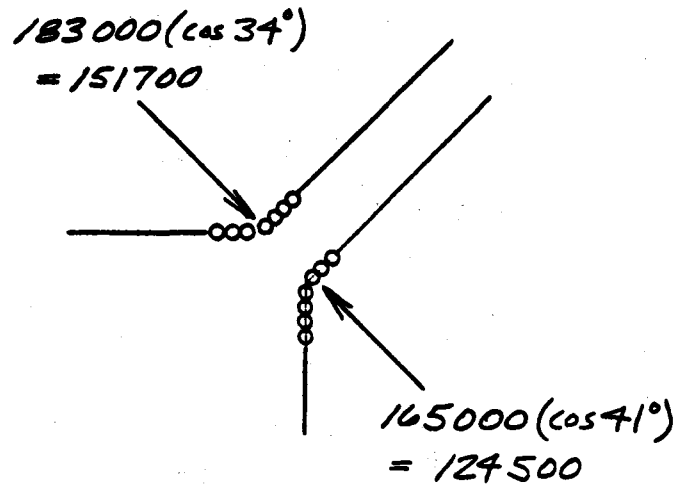
The method of analysis is identical to the two-sided skewed heating analysis for Location #2 except that one-sided heating is applied for the north and east (west) cavities. The existing input files were modified for single sided heating application by changing the heat flow multipliers to zero for the unheated side.

The Membrane Wall Program is used in the analysis to establish a correlation between skewed heating and normal heating. Figure 1 shows the values used for the single-sided skewed heating analysis applied to the double wall configuration. Figure 2 describes the input to the analysis and determination of results. For normal heating, the component of the maximum incident flux is calculated knowing the angle of incidence. The design case, also shown, identifies the flux values corresponding to either type analysis. Two finite element analysis were performed for the skewing heating case. The Membrane Wall Program supplied comparative results for the normal heating case. Assuming that tube stress is linearly proportional to heat flux, maximum tube stress for the design case is easily obtainable by using the Membrane Wall Program for the normal heat flux values and then applying the above relationship to calculate maximum stresses that actually exist for the skewed heating condition. The stresses here are assumed to be elastic. The subject of inelastic stress determination and creep-fatigue is covered in another report. Table 1 contains the data used in the analysis. The material used in the analysis is SB-163 Incoloy 800H.

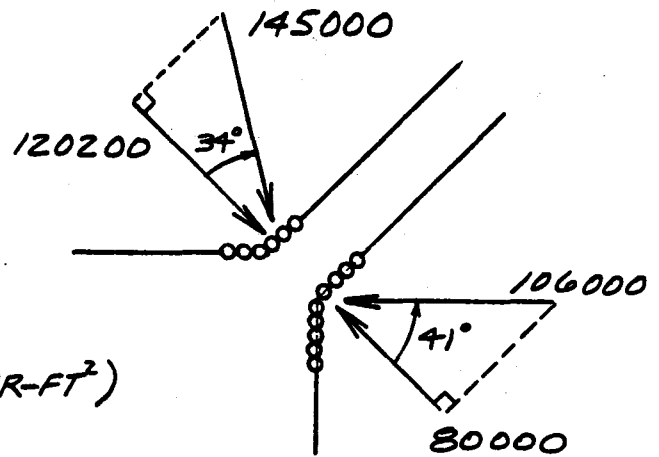
SKEWED HEATING:



NORMAL HEATING:

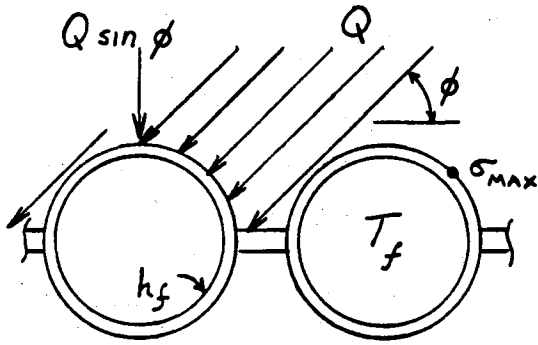


DESIGN CASE:



(Q = HEAT FLUX, BTU/HR-FT<sup>2</sup>)

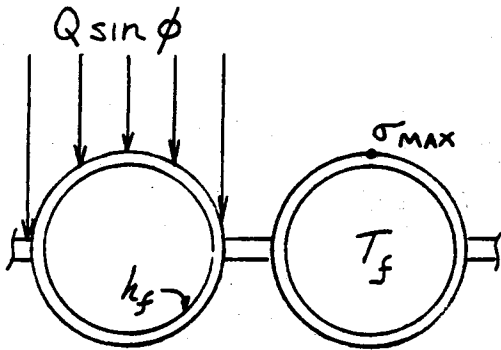
FIGURE 1 - HEAT FLUX DATA FOR LOCATION 2



FINITE ELEMENT ANALYSIS

INPUT  $\{ Q, \phi, T_f, h_f \}_{FEM}$

OUTPUT  $\sigma_{FEM}$

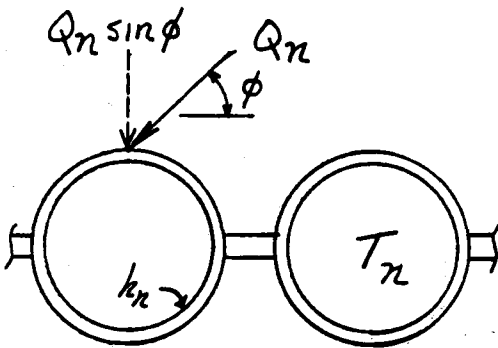


MEMBRANE WALL PROGRAM

INPUT  $\{ Q \sin \phi, T_f, h_f \}_{MWP}$

OUTPUT  $\sigma_{MWP}$

" STRESS INDEX " =  $\frac{\sigma_{FEM}}{\sigma_{MWP}}$



MEMBRANE WALL PROGRAM

INPUT  $\{ Q_n \sin \phi, T_n, h_n \}_n$

OUTPUT  $\sigma_n$

$\sigma_{SKEWED} = \sigma_n \left( \frac{\sigma_{FEM}}{\sigma_{MWP}} \right)$

FIGURE 2 - METHOD OF ANALYSIS

TABLE 1

LOCATION #2

	EAST CAVITY	NORTH CAVITY	UNITS
Panel	3	4	
<u>Finite Element - Skewed</u>			
Heat Flux	165,000	183,000	Btu/Hr-Ft <sup>2</sup> -°F
Fluid Temp.	652	652	°F
Film Coefficient	930	930	Btu/Hr-Ft <sup>2</sup> -°F
<u>Membrane Wall Program - Normal</u>			
Heat Flux	124,500	151,700	
Fluid Temp.	652	652	
Film Coefficient	930	930	
<u>Membrane Wall Program - Normal Design</u>			
Heat Flux	80,000	120,200	
Fluid Temp.	607	652	
Film Coefficient	900	930	

TABLE 2

LOCATION #2

$\sigma_z$  = axial tube stress, ksi

Q = heat flux (max. for analysis) Btu/Hr-Ft<sup>2</sup>-Of

$\theta$  = angle of incidence, degrees

<u>Comparison</u>	<u>Q, <math>\theta</math></u>	<u><math>\sigma_z</math> - normal</u>	<u><math>\sigma_z</math> - skewed</u>	<u><math>\frac{\sigma_z - \text{skewed}}{\sigma_z - \text{normal}}</math></u>
Loc. 2 N. Cavity	183,000 = 34°	-42.8 (Q = 151,700)	-57.4 (Q = 183,000)	1.34
Loc. 2 E. Cavity	165,000 = 41°	-35.1 (Q = 124,500)	-54.0 (Q = 165,000)	1.54

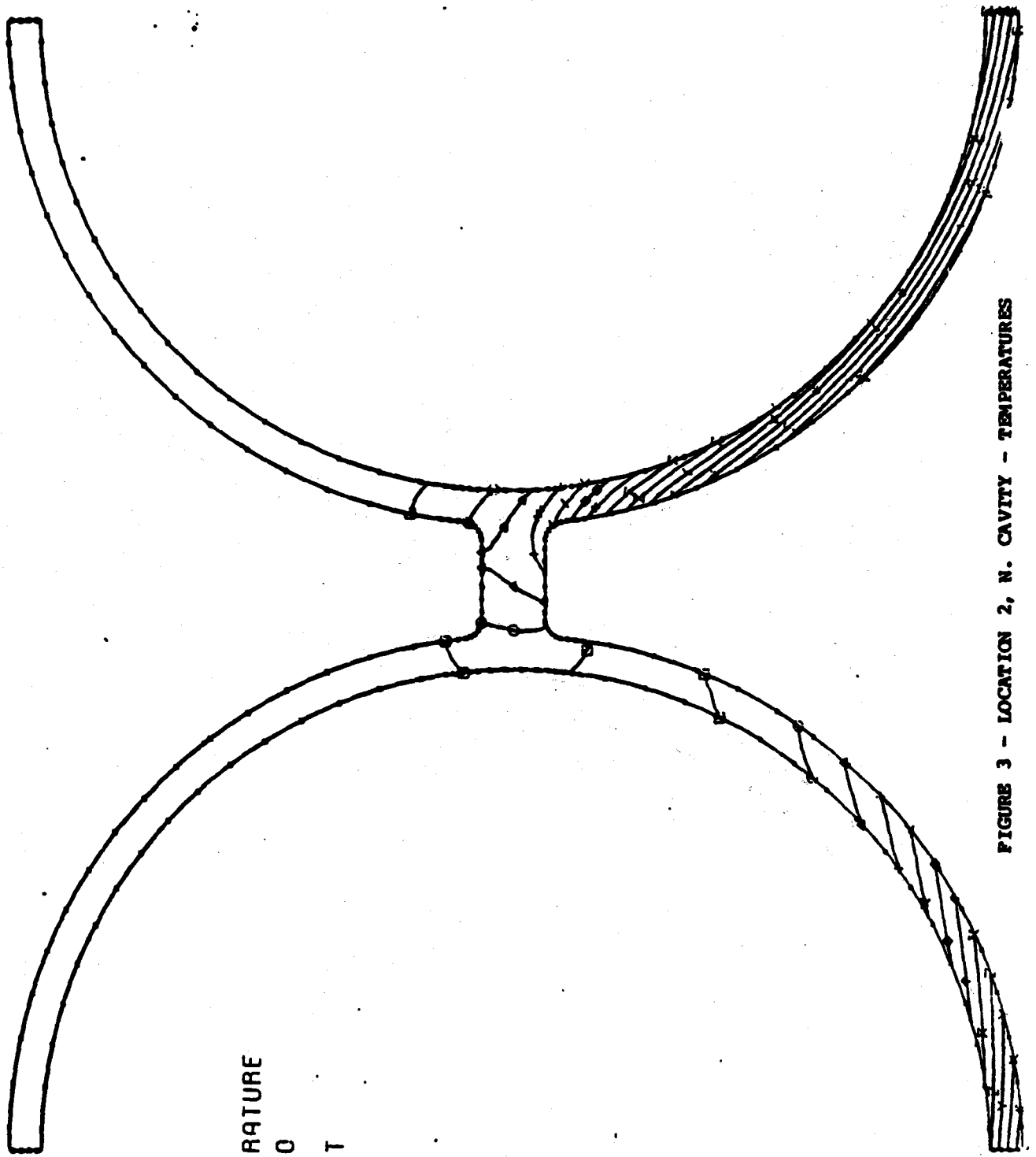
Design

Loc. 2 N. Cavity	145,000 = 34°	-35.5 (Q = 120,200)	-1.34 (35.5) = -47.6
Loc. 2 E. Cavity	106,000 = 41°	-26.0 (Q = 80,000)	-1.54 (26.0) = -40.0

**Max. Metal Temperatures:**

N. Cavity -  $T_{\max} = T_f + T_{O.D. \max.} = 607 + 252 = 859^{\circ}\text{F}$

E. Cavity -  $T_{\max} = 652 + 184 = 836^{\circ}\text{F}$



CONTOUR MAP OF TEMPERATURE  
FOR TIME 1.00

CONTOUR IDENT

- 661.96
- 681.89
- △ 701.82
- + 721.74
- λ 741.67
- ◇ 761.60
- ↑ 781.52
- × 801.45
- z 821.37
- y 841.30
- κ 861.23
- \* 881.15
- Σ 901.08
- | 921.01
- ☆ 940.92

P 99

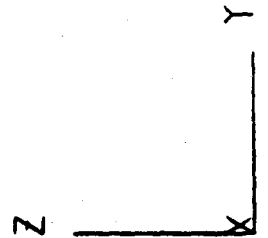


FIGURE 3 - LOCATION 2, N. CAVITY - TEMPERATURES

CONTOUR MAP OF EFFECTIVE STRESS  
FOR LOAD CASE 1

CONTOUR IDENT

□	3980.50
○	9151.50
..	14322.50
+	19493.50
x	24664.50
◇	29835.50
+	35006.50
x	40177.50
Z	45348.50
Y	50519.50

D-100

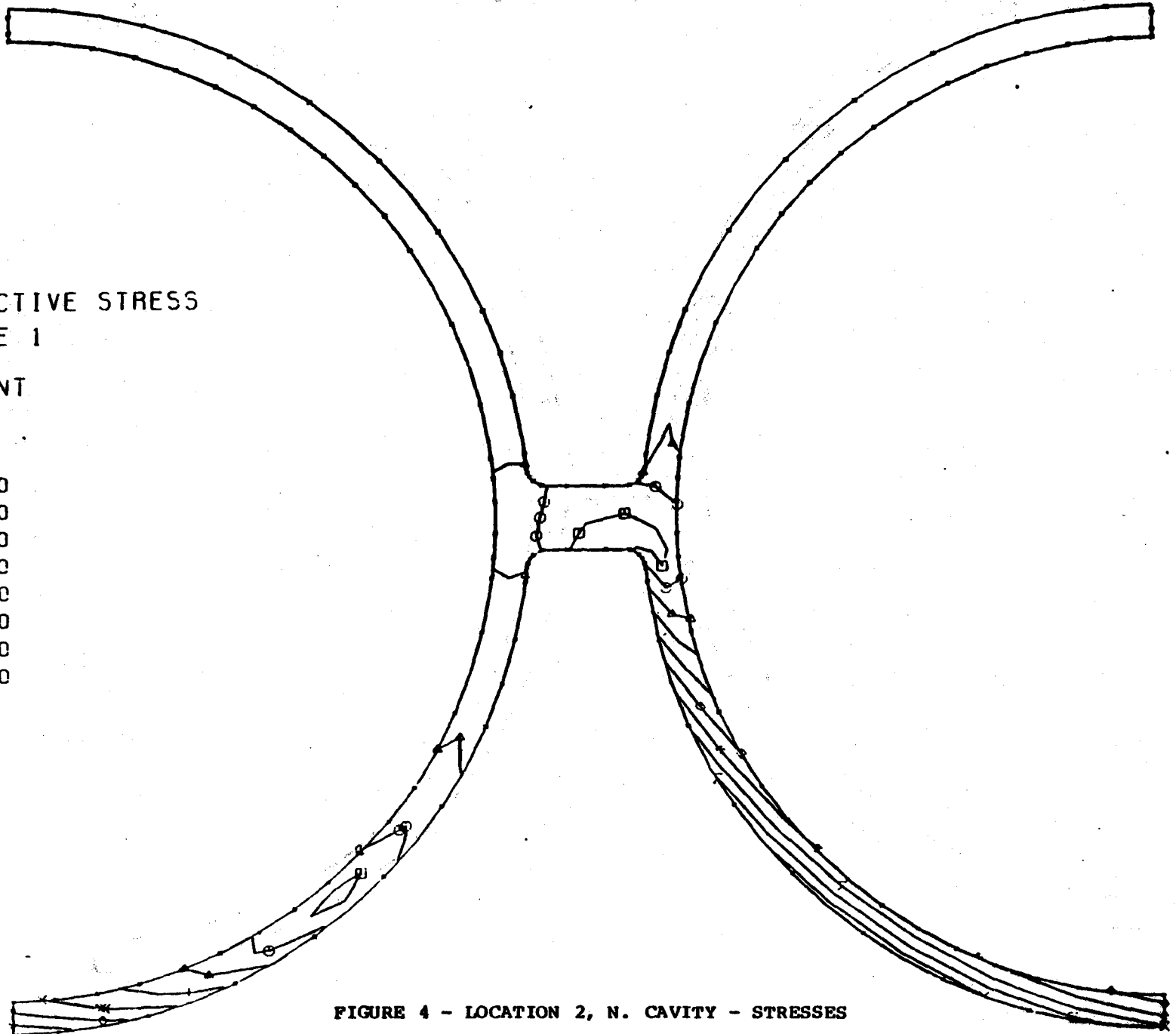
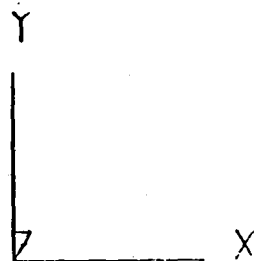


FIGURE 4 - LOCATION 2, N. CAVITY - STRESSES

## Results

The axial stress of skewed heating is 34% higher than the stress level of normal heating for one-sided heating of the north cavity location 2 and the corresponding increase for the east cavity is 54%. Axial tube stress, therefore, increases for increased skewed heating as expected. The controlling axial tube stress is 47.6 ksi (compressive) and exists in panel 4 of the north cavity. The maximum tube stress in panel 3, east cavity, is 40.0 ksi (compressive). The results are summarized in Table 2 and include contour plots of temperature and effective stress distributions.

Figures 3 and 4 are contour plots of temperature and effective stress, respectively, for the north cavity, Location 2. Because of the similarity between these plots and the plots of the 2-sided analysis, only two plots are included in the report and are representative of the remainder.



## Conclusion

The maximum tube stress occurs at Location 2 for one-sided heating of the north cavity. The effects of skewed heating increase axial stress. Axial stress is notably higher for greater angles of incidence. Web temperatures decrease for skewed heating and the gradient is of a lesser severity. Web stresses are also noted to decrease. Maximum tube temperatures remain the same and are directly proportionate to maximum incident heat flux.

**Appendix E**

**Stress Analysis of Full Length**

**Heat Absorption Tubes**

**Stress Analysis  
of  
Full Length Heat Absorption Tubes**

**Molten Salt Receiver  
Subsystem Research Experiment**

**The Babcock & Wilcox Co.**

**Contract No. 894-0012-45**

**Prepared by J.P. Reed**

**Approved by J.L. Hechmer**

**March 1982**

**Report No. 0012-11(S)**

## TABLE OF CONTENTS

	Page
1.0 Purpose and Scope .....	E-3
2.0 Geometry .....	E-4
3.0 FE Model .....	E-4
4.0 Thermal Load .....	E-8
5.0 Mechanical Load and Material Properties .....	E-10
6.0 Boundary Conditions .....	E-10
7.0 Thermal Analysis .....	E-18
8.0 Stress Analysis Results .....	E-24
9.0 Discussion of Results .....	E-65
9.1 Lateral Deflections .....	E-65
9.2 Axial Stresses .....	E-75
9.3 Stress Flux Correlation .....	E-77
10.0 Conclusions .....	E-87
11.0 Recommendations .....	E-88
12.0 Reference .....	E-89

## 1.0 Purpose and Scope

The creep fatigue analysis [1] of the membrane wall tubes is based on generalized plane strain restraint of the tube and a single heat flux input (one location). However the heat absorption panels have no lateral supports to produce the plane strain condition; also the flux distribution varies along the tube length. Since there are no lateral supports to hold the tube straight; it will try to bow to relieve the axial stress caused by the circumferential gradient. The amount of bowing can not be estimated because the temperature gradient varies along the tube length. The effect of axial flux distribution on tube bowing, (lateral deflection) and axial stress is studied in this report.

Flux curves for two-sided, direct heating show that a unique heating condition exists for each panel in the receiver (i.e. the heat flux variation along the length and the front-to-back heat flux imbalance is unique for each panel). Six of the most widely variant conditions are analyzed. Accurate distributions of fluid temperature/film coefficients are incorporated into the analysis. The elements have a high length-to-width aspect ratio; this makes it possible to model such long tubes with a reasonable number of elements. To check the aspect-ratio effect, one case was rerun with the tube length decreased by a factor of four. This analysis is based on the original design and heat flux distributions; i.e., those contained in the proposal.

The condition of one-sided heating is considered for panel 7 of zones 1 and 4.

## 2.0 Geometry

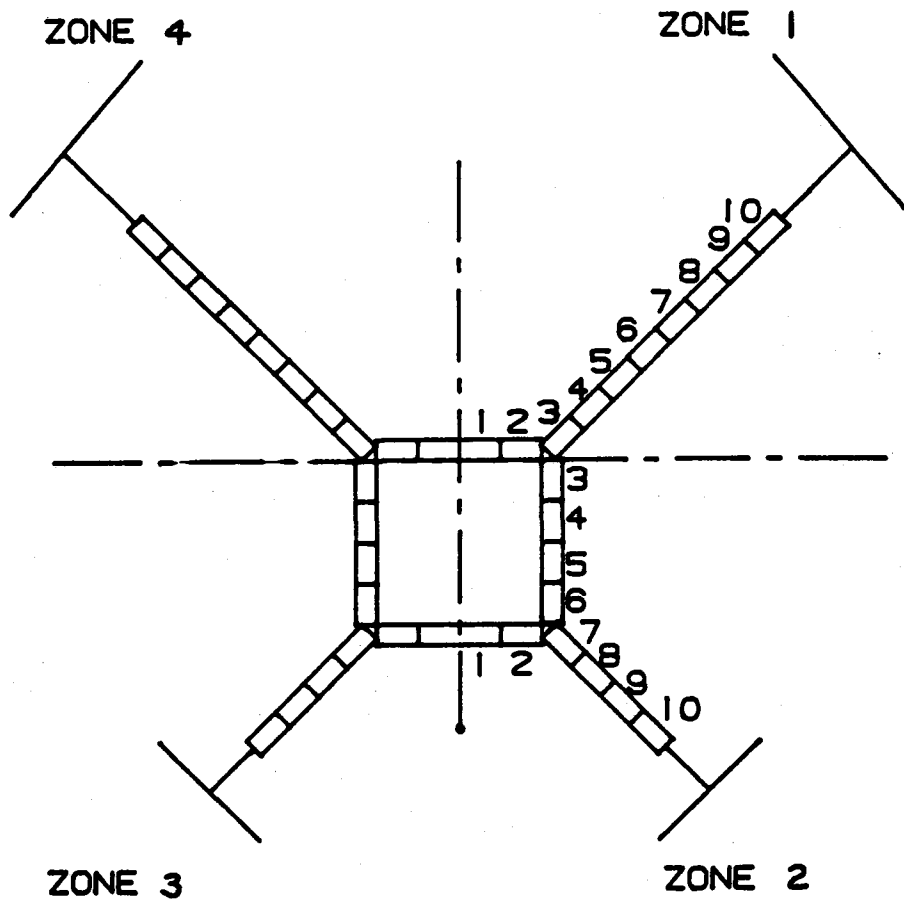
The 2" O.D. tube with a 0.065" wall thickness is analyzed. The web dimensions are 1/4" wide by 1/8" thick; from symmetry, this gives a 1/8" x 1/8" web. The tube length varies from about 63 ft to 72 ft (Figure 1). It is recognized that the 1/4" web width has been decreased to .218" maximum; thus the stress results are not directly applicable.

## 3.0 F.E. Model

To obtain temperatures, a two-dimensional (plane body) grid is used with 8-node elements (Figures 2 and 3). The model is limited to a half tube and a half web because of symmetry. The model has eighteen elements with the web being element 18. This model is used to generate (steady state) temperature distributions in FETAP from flux input corresponding to multiple points along the tube length. The 2-D FETAP temperature output was processed into 3-D FESAP input data by matching it to the FESAP model per the appropriate location.

The interactive program LAYRIT was used to generate the 3D stress grid from the plane body thermal grid. The plane body grid was layered to twenty elements for a total of 360 20-node curved solid elements. Since the tubes are 63 to 72 ft, each layer is about 3.15 to 3.60 ft. high.

Identifying output (element and nodal) information is possible by simply adding 18N to the element number of the 2-D grid and adding 131N to the nodal number of the 2-D grid where N = the number of element layers to the point of investigation along the tube.

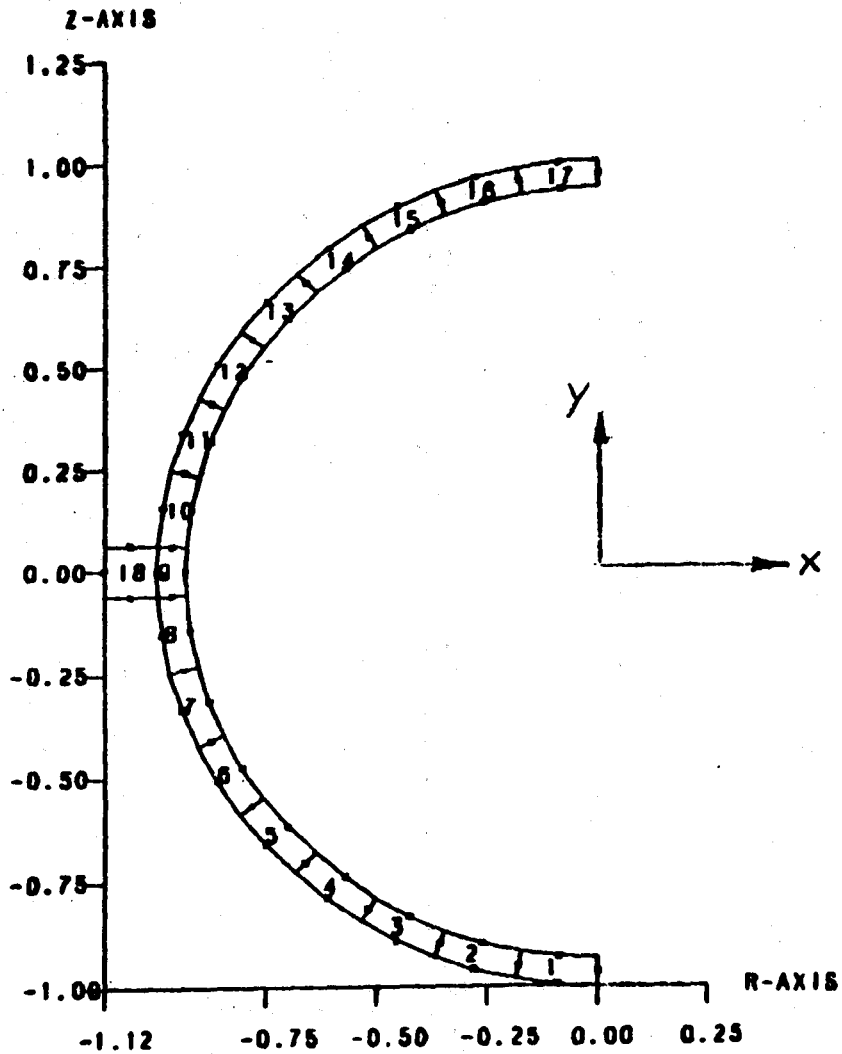


PANEL LAYOUT

PANEL	ZONES	PANEL LENGTH, FT.	
3	1, 4	71.87	71.87 <sup>(1)</sup>
5	↓	68.87	↓
6		68.87	
7		65.65	
8		65.65	
7	2, 3	63.16	↓
7	1, 4	65.65	

- (1) MODEL LENGTH
- (2) QUARTER LENGTH MODEL

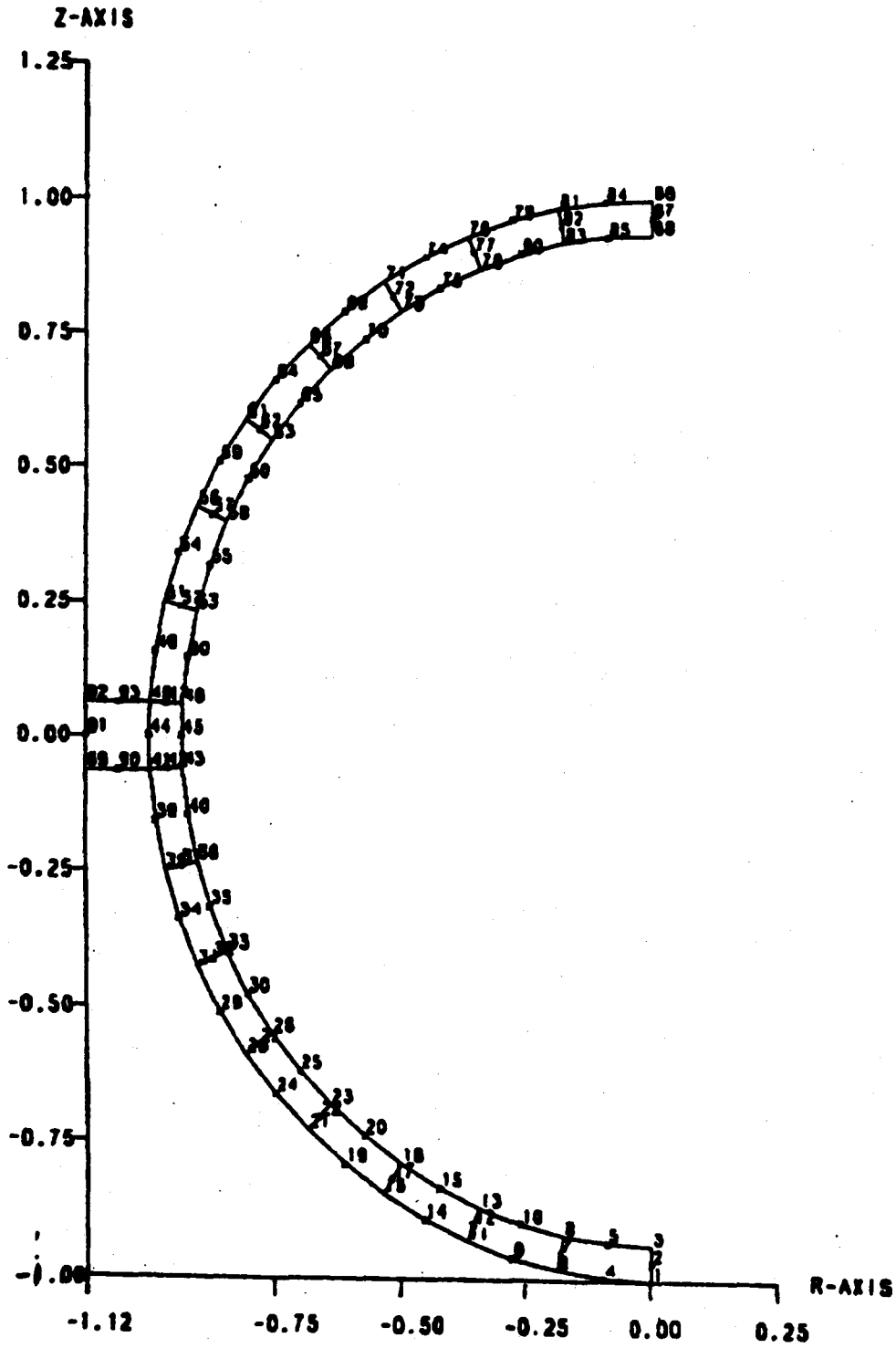
FIGURE 1 - PANEL LENGTHS



EIGHT NODE 2D - 180 DEGREE + ONE WEB

FIGURE 2 - GRID ELEMENT NUMBERS





EIGHT NODE 20 - 180 DEGREE + ONE WEB

FIGURE 3 - GRID NODAL NUMBERS

#### 4.0 Thermal Load

The problem combines the effect of thermal loading with axial dead weight for steady state condition. To decide which panels to analyze, all of the heat flux distributions were evaluated. The Saguaro heat flux distributions are presented for Panels 3, 5, 6, 7, and 8 of Zone 1 and Panel 7 of Zone 2 in Figure 4; these are the ones chosen for analysis. In addition to the two-sided heating shown in Figure 4, Panel 7 is analyzed for one-sided heating.

Great difficulty was encountered in trying to decide which panels to analyze. Based on previous plane body analyses, the maximum axial stress is a function of the magnitude of the heat flux and the imbalance in heat flux between one side of the tube and the other. However, both the magnitude and the imbalance in heat flux vary along the tube so the previous criteria is not valid for judging stress levels. It is believed that the area between the two curves may represent the imbalance; the average heat flux on either side may represent the magnitude. The following evaluation of the chosen panels gives the basic reason for our choices.

Panel 3 has the feature of the north side heat flux always being higher than the east side heat flux; Panel 3 may represent the maximum total imbalance.

Panel 5 is similar to Panel 3 in that the east side heat flux reaches the north side magnitude at one point, but it never becomes larger. Thus the total heat flux imbalance is lower but the maximum heat flux is higher and the imbalance at the maximum heat flux location is higher.

Panel 6 has a reversal in heat flux imbalance; i.e., first the north side is higher, then the east side is higher, and finally the north side is higher. The east side heat flux never becomes much greater than the north side and overall this panel could have less imbalance than Panel 5. It also contains the maximum north side heat flux and the maximum imbalance at the location of maximum heat flux.

Panel 7 extends the heat flux condition of Panel 6; i.e., the east side heat flux increases while the north side decreases. Overall, the north side may have a higher average heat flux but the total imbalance is very low. The maximum heat flux is the same as Panel 6 but the comparable imbalance is lower.

Panel 8 further extends the condition to the point where the east side may have a higher average heat flux. However the total magnitude for Panel 8 is considerably lower than Panel 7.

Panel 7, Zone 2 is most similar to Panel 5 where the south-side, Panel 7 replaces the east side, Panel 5 and the east side, Panel 7 replaces the north side, Panel 5. However for Panel 7, the south side heat flux (max value) exceeds that of the east side, but the east side average heat flux is still greater than that of the south side.

The deflection and stress results are evaluated in terms of the above discussion.

## 5.0 Mechanical Load and Material Properties

The weight of the lower header, interconnecting piping, and salt (header and tube) are applied to the end of the tube as a pressure on the lower face of each element. Tube weight is calculated within the program and is also considered as an axial load in the analyses. It may be important to account for the axial dead-weight load because thermal bowing is reduced as this load increases. However, FESAP is a "small deformation" program, so this reverse bending effect is not seen.

For calculating stresses in FESAP, the standard material properties library is used (material code for Alloy 800H is 11).

## 6.0 Boundary Conditions

The FESAP model is permitted to grow in every direction and bow laterally along the y-axis. Figure 5 shows the type of constraint used in the analysis. By constraining all the nodes at the top in the z-direction, the model is free to grow downward but the top surface is not permitted to rotate. Next, constraining all the nodes in the x-direction (lateral) in a plane normal to the panel and intersecting the centerline (symmetry plane) of the tube enables the modeling of half a tube. The tube grows in the x-direction from this symmetry plane; these nodes can grow in the y-direction (radial). The x-constraint also maintains the assumption that an absorption panel does not bow laterally and assures that twisting due to thermal expansion does not occur. The remaining constraint is that the midside node of the web at the top and bottom of the tube are constrained in the y-direction. The net effect of this system of constraints is a fixed connection developed at the top of the tube and pinned connection at the bottom.

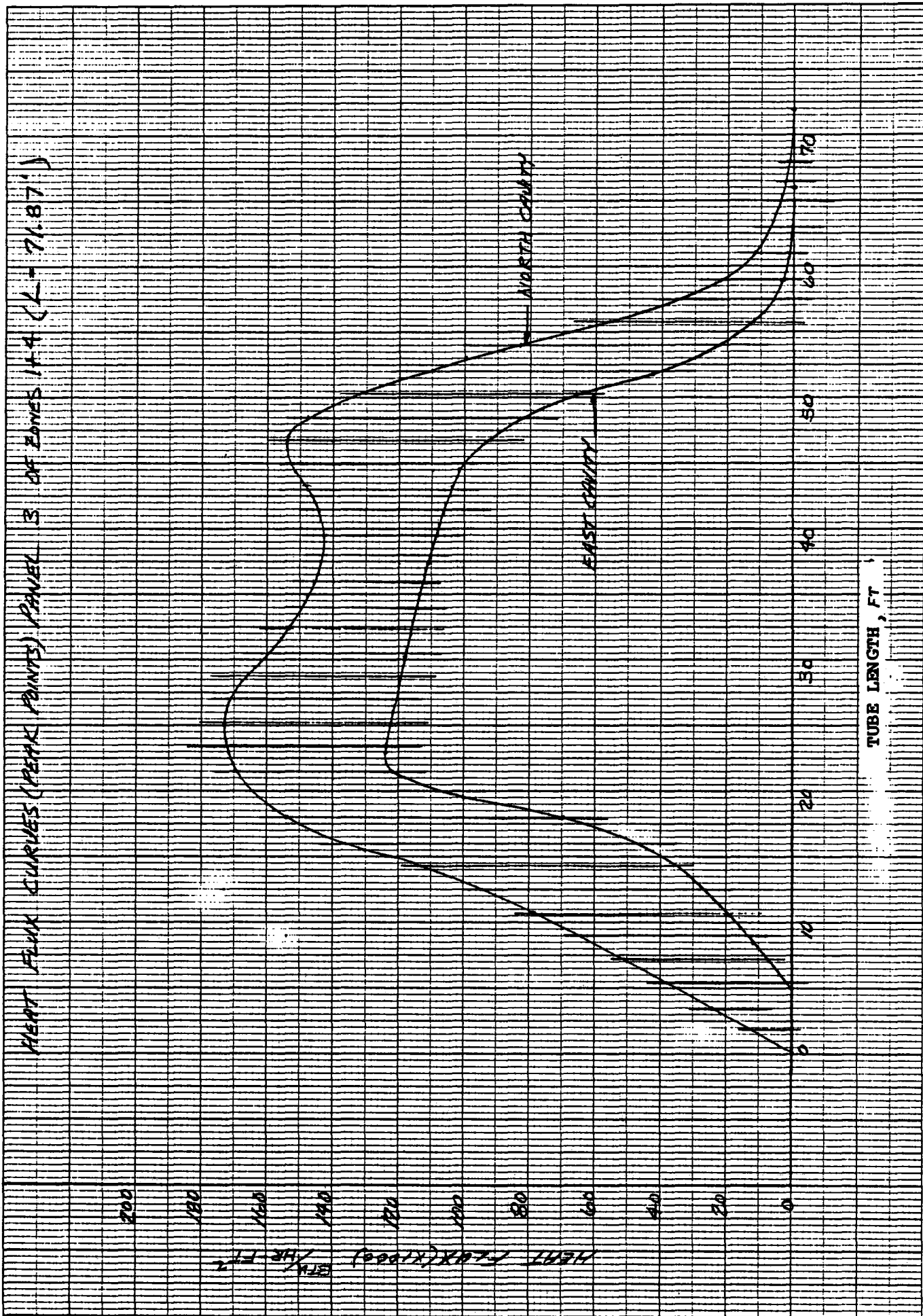


FIGURE 4a - HEAT FLUX CURVES

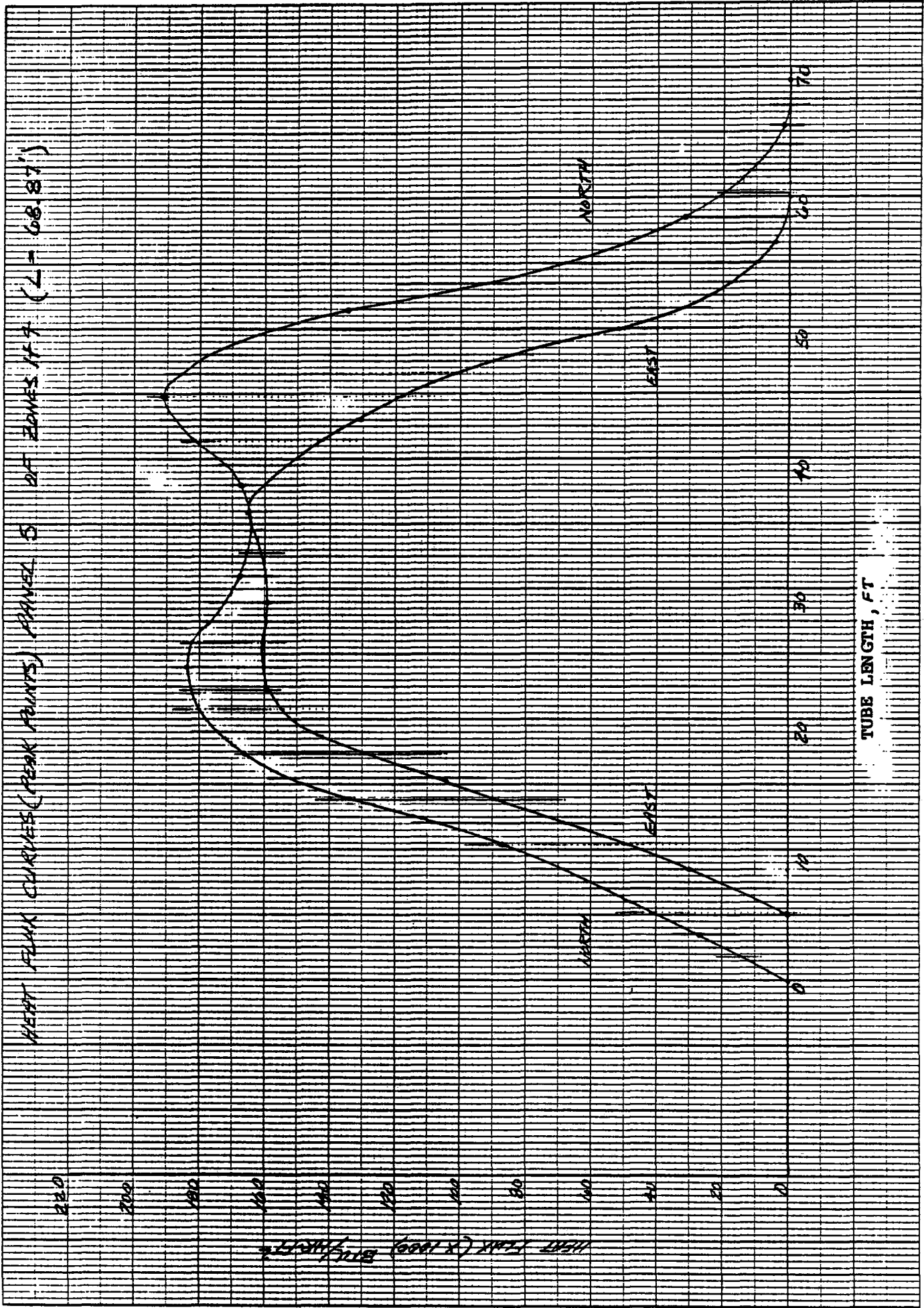


FIGURE 4b - HEAT FLUX CURVES

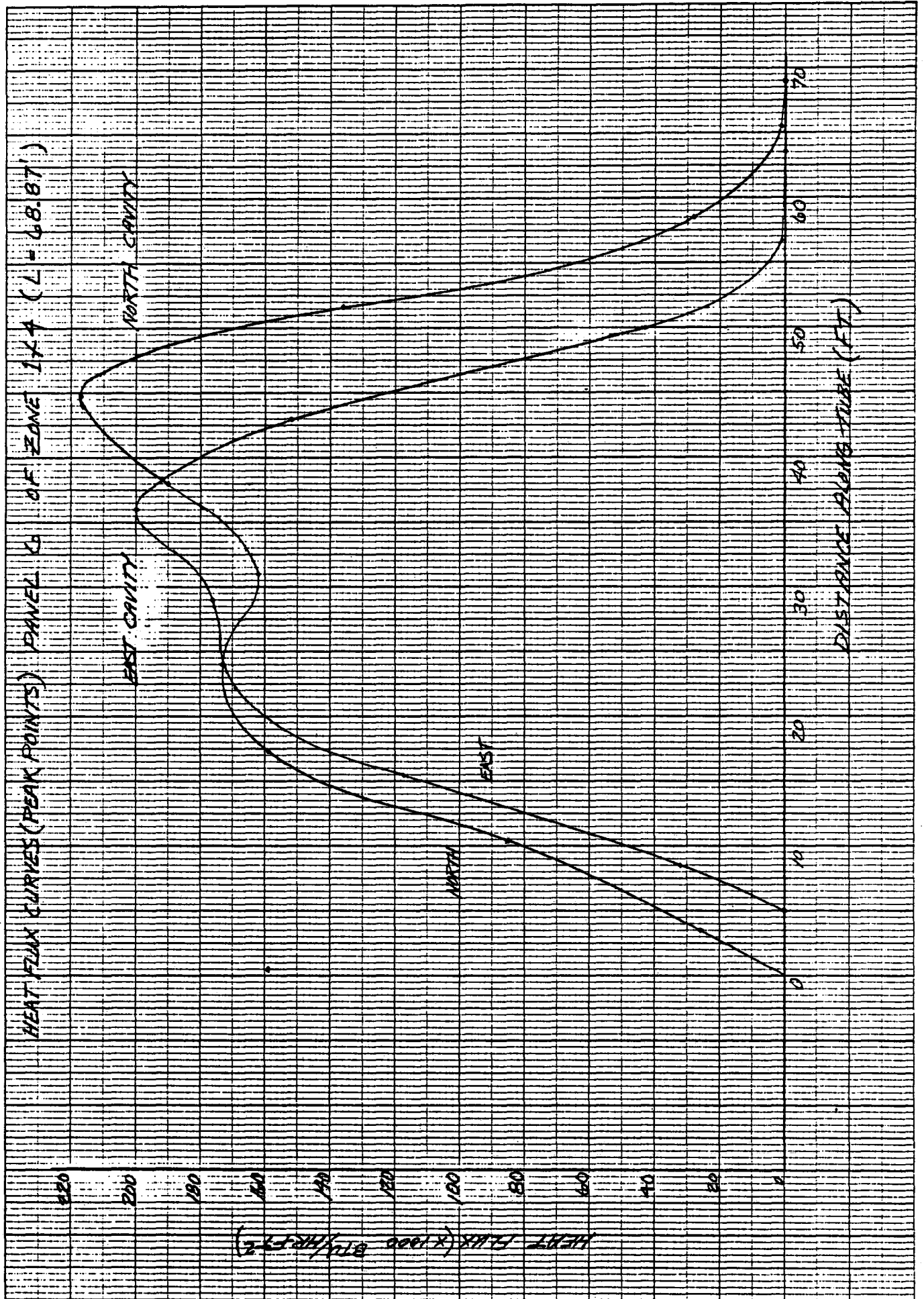


FIGURE 4c - HEAT FLUX CURVES

E-14

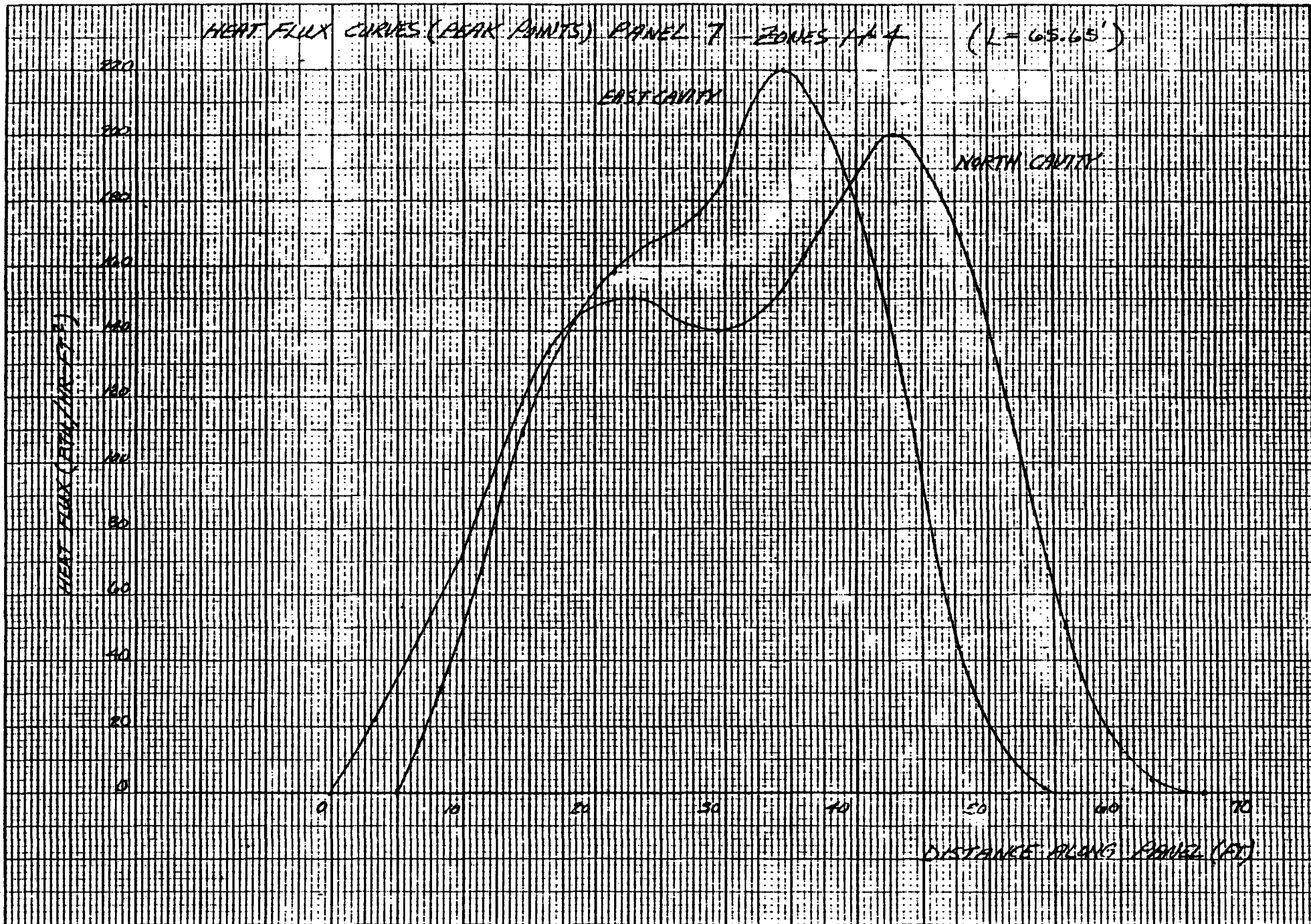


FIGURE 4d - T FLUX CURVES



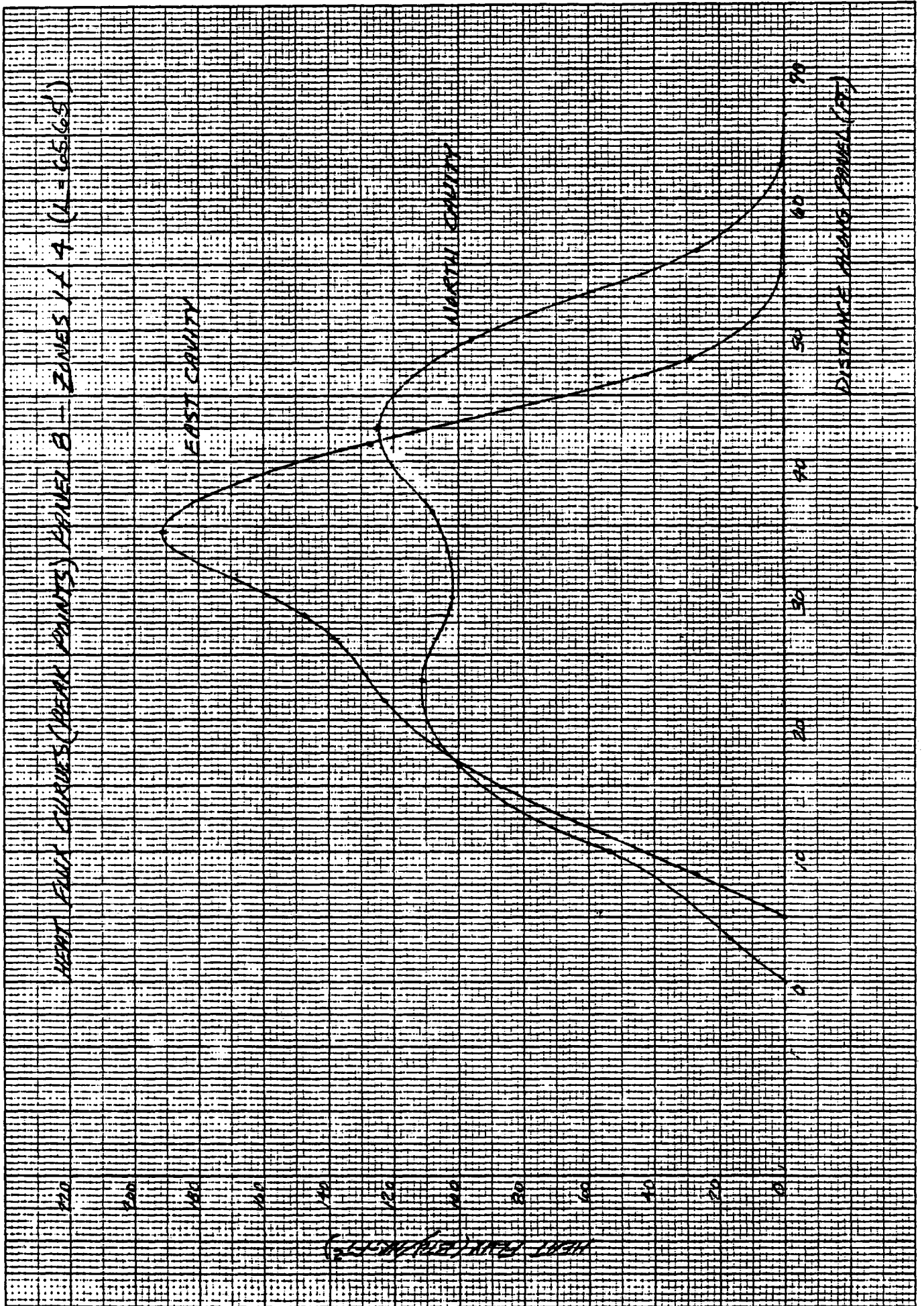


FIGURE 4e - HEAT FLUX CURVES

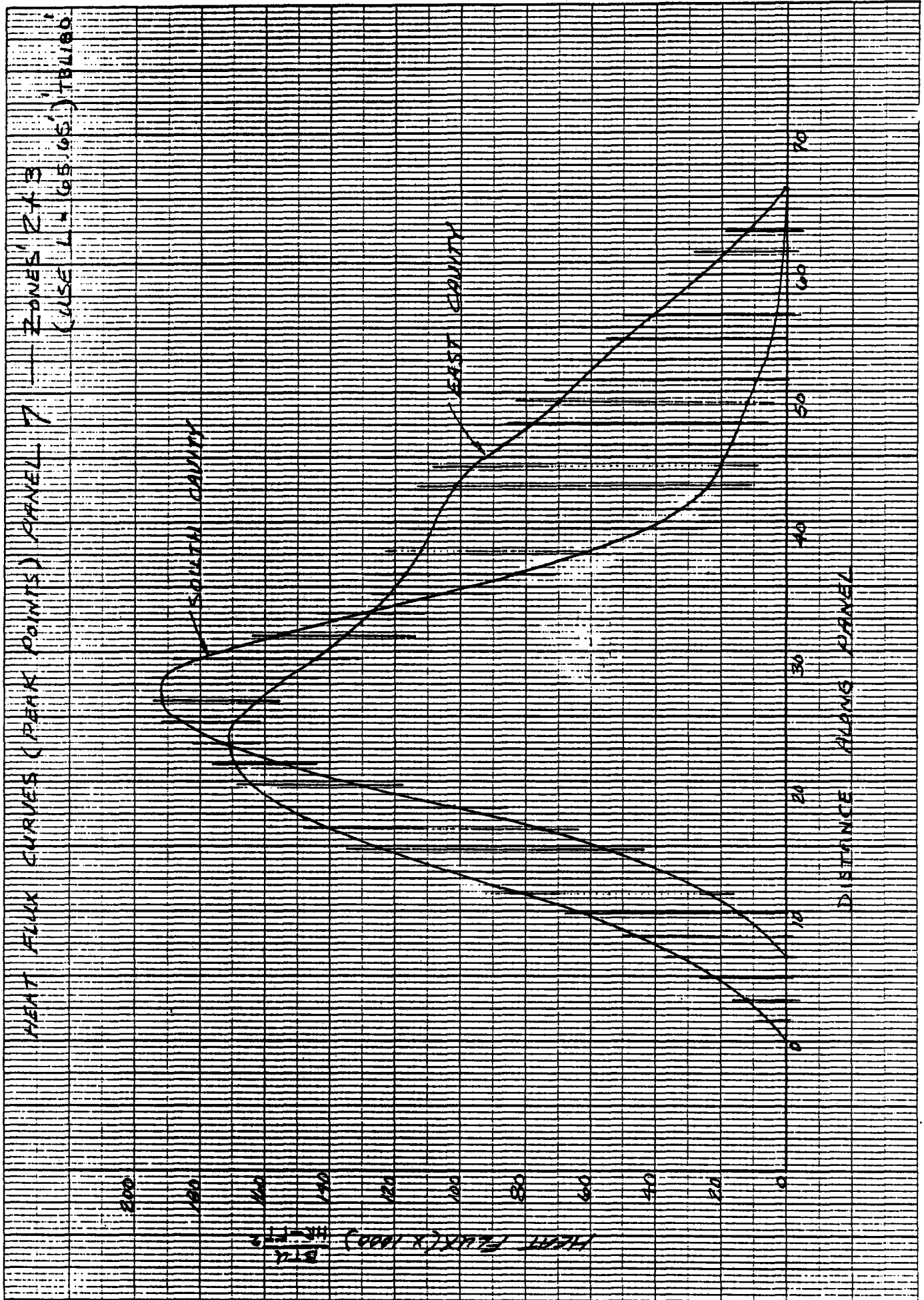


FIGURE 4f - FLUX CURVES

# Babcock & Wilcox ENGINEERING CALCULATIONS

REFERENCE NO.

SHEET NO.

PREPARED BY:

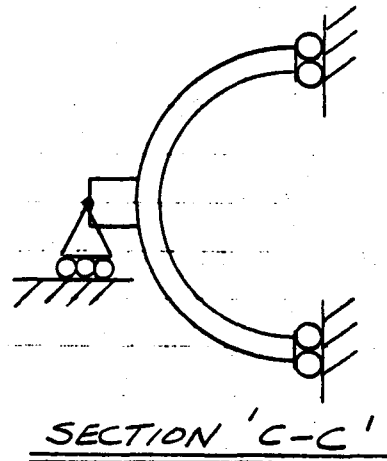
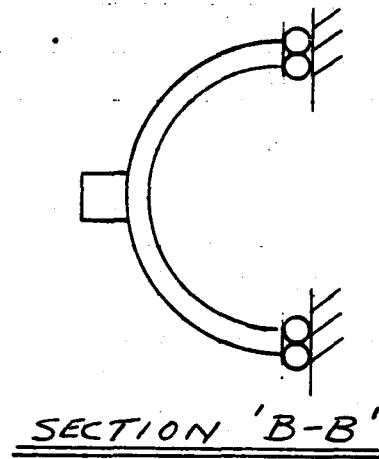
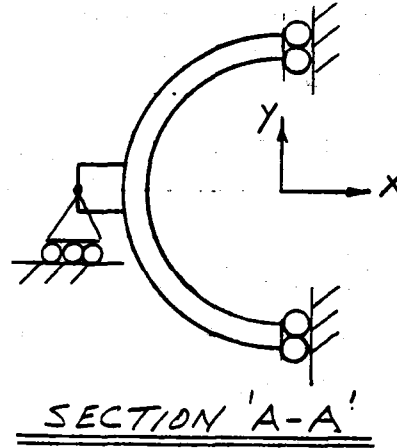
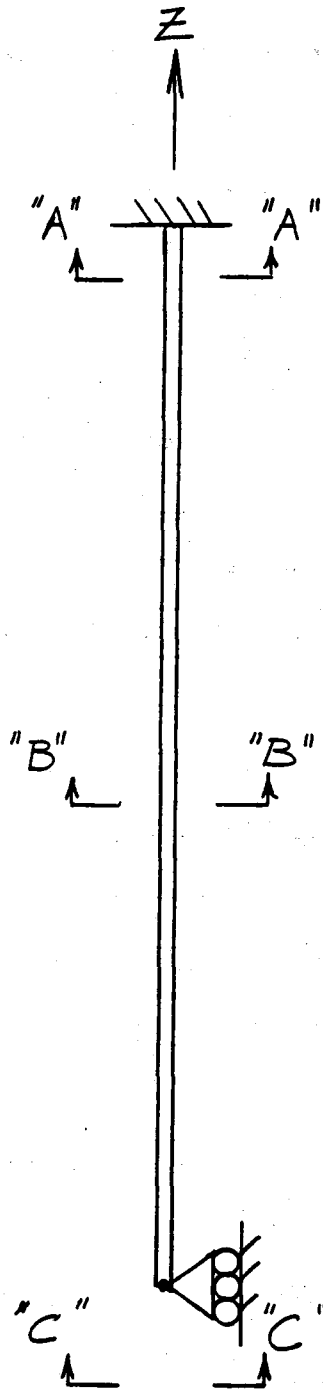
OF  
DATE:

SUBJECT:

*BOUNDARY CONDITIONS*

CHECKED BY:

REVISION:



*FULL LENGTH TUBE*

**FIGURE 5 - BOUNDARY CONDITIONS**

To simulate the pinned connection at the bottom of the tube, tie nodes were considered but not used. Their elimination greatly reduces the number of equations in the stiffness matrix within the program but may affect the accuracy of stresses locally near the bottom of the tube. In reality the design of the header support substantially reduces its rotation, so the pinned connection is probably not justified.

#### 7.0 Thermal Analysis

In order to analyze the tube for the heat-flux distributions, the fluid temperature and film coefficients are needed as a function of distance along the tube. The fluid temperature was calculated using THASOR; the data for Panel 6 is presented in Table 1 and Figure 6. The film coefficient is a function (primarily) of fluid flow; the data in Table 1 is for full flow; i.e., 100% load.

The temperature distribution in the tube was obtained by a series of plane body FETAP analyses, each one representing a nodal plane on the full tube model. Thus, the plane body FETAP output data consists of a series of 21 steady state temperature distributions based on the heat flux at the appropriate elevation. This approach has the built-in assumption that axial heat flow is negligible. THERM, a data processing program, was created for the purpose of reading the FETAP output for each nodal plane and generating a single temperature distribution input tape suitable for input into FESAP. The heat flux was input to FETAP as

weighted values of heat flow (btu/hr) on every node of the plane body grid. Each value was calculated by multiplying maximum heat flux (at the tube crown) by the correct nodal function per element and by projected area of an element which is a cosine distribution. The nodal function for the 8-node element is  $1/6$  to the corner nodes and  $2/3$  to the mid-side nodes. When a corner node is common to two elements,  $1/6$  of the heat flow to each element is input to the node. The cosine function gives the heat flux to each element around the tube circumference. The net result is a single factor for each node which will give the heat flow to that node when multiplied by the maximum heat flux to the plane body model.

Table 2 contains the heat flows used in the analysis. The values listed were determined in a FETAP TEST CASE REPORT and were checked by another method described in Table 3. Functions 1 and 2 of the FETAP input data contained multipliers of the heat flow which yielded correct values at any node along a tube and either side.

<b>Babcock &amp; Wilcox ENGINEERING CALCULATIONS</b>	REFERENCE NO.	SHEET NO. OF
	PREPARED BY:	DATE:
SUBJECT: <i>PANEL 6, ZONE 1</i>	CHECKED BY:	REVISION:

TABLE 1 - TYPICAL FILM COEFFICIENTS

	FLUID TEMP.	FILM COEF.		FLUID TEMP.	FILM COEF.
0	813.0	1238.9	26	859.5	1312.7
1	813.0	1238.9	27	862.5	1316.4
2	813.1	1240.1	28	865.3	1320.0
3	813.3	1241.2	29	868.1	1321.9
4	813.4	1242.4	30	870.8	1323.8
5	813.6	1243.5	31	873.6	1325.7
6	813.7	1244.7	32	876.4	1327.6
7	814.7	1248.0	33	877.8	1327.9
8	815.8	1251.3	34	879.2	1328.2
9	816.8	1254.5	35	880.7	1328.6
10	817.8	1257.8	36	882.1	1328.9
11	820.1	1261.8	37	883.5	1329.2
12	822.4	1265.7	38	883.7	1329.2
13	824.7	1270.0	39	883.9	1329.2
14	827.0	1273.6	40	884.1	1329.3
15	829.6	1276.7	41	884.3	1329.3
16	832.2	1279.8			
17	834.8	1282.8			
18	837.4	1285.9			
19	840.0	1289.0			
20	842.6	1292.3			
21	845.2	1295.6			
22	847.7	1298.8			
23	850.3	1302.1			
24	853.4	1305.4			
25	856.4	1309.1			

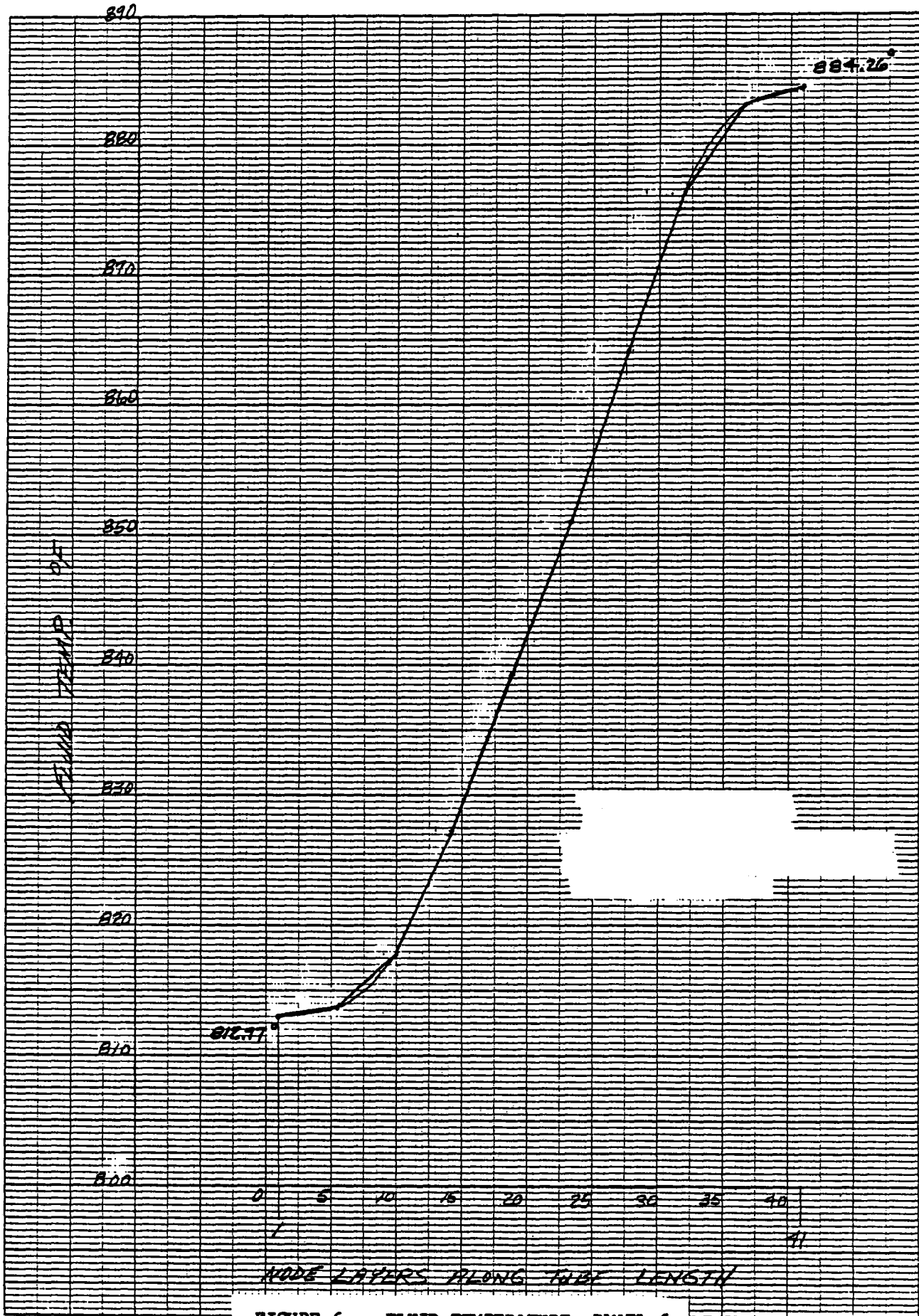


FIGURE 6 - FLUID TEMPERATURE, PANEL 6

THIS IS A CARD IMAGE LISTING OF THE INPUT DATA

11111111112222222222333333333344444444445555555555666666666677777777778  
 12345678901234567890123456789012345678901234567890123456789012345678901234567890

C O L U M N N U M B E R

1 1 1.0 1.0 1 0 1  
 2 1 1.0 1.0 1 0 1  
 3 1 1.0 1.0 1 0 1  
 4 1 1.0 1.0 1 0 1  
 5 1 1.0 1.0 1 0 1  
 6 1 1.0 1.0 1 0 1  
 7 1 1.0 1.0 1 0 1  
 8 1 1.0 1.0 1 0 1  
 9 1 1.0 1.0 1 0 1  
 10 1 1.0 1.0 1 0 1  
 11 1 1.0 1.0 1 0 1  
 12 1 1.0 1.0 1 0 1  
 13 1 1.0 1.0 1 0 1  
 14 1 1.0 1.0 1 0 1  
 15 1 1.0 1.0 1 0 1  
 16 1 1.0 1.0 1 0 1  
 17 1 1.0 1.0 1 0 1  
 18 1 1.0 1.0 1 0 1  
 19 1 1.0 1.0 1 0 1  
 20 1 1.0 1.0 1 0 1  
 21 1 1.0 1.0 1 0 1  
 22 1 1.0 1.0 1 0 1  
 23 1 1.0 1.0 1 0 1  
 24 1 1.0 1.0 1 0 1  
 25 1 1.0 1.0 1 0 1  
 26 1 1.0 1.0 1 0 1  
 27 1 1.0 1.0 1 0 1  
 28 1 1.0 1.0 1 0 1  
 29 1 1.0 1.0 1 0 1  
 30 1 1.0 1.0 1 0 1  
 31 1 1.0 1.0 1 0 1  
 32 1 1.0 1.0 1 0 1  
 33 1 1.0 1.0 1 0 1  
 34 1 1.0 1.0 1 0 1  
 35 1 1.0 1.0 1 0 1  
 36 1 1.0 1.0 1 0 1  
 37 1 1.0 1.0 1 0 1  
 38 1 1.0 1.0 1 0 1  
 39 1 1.0 1.0 1 0 1  
 40 1 1.0 1.0 1 0 1  
 41 1 1.0 1.0 1 0 1  
 42 1 1.0 1.0 1 0 1  
 43 1 1.0 1.0 1 0 1  
 44 1 1.0 1.0 1 0 1  
 45 1 1.0 1.0 1 0 1  
 46 1 1.0 1.0 1 0 1  
 47 1 1.0 1.0 1 0 1  
 48 1 1.0 1.0 1 0 1  
 49 1 1.0 1.0 1 0 1  
 50 1 1.0 1.0 1 0 1  
 51 1 1.0 1.0 1 0 1  
 52 1 1.0 1.0 1 0 1  
 53 1 1.0 1.0 1 0 1  
 54 1 1.0 1.0 1 0 1  
 55 1 1.0 1.0 1 0 1  
 56 1 1.0 1.0 1 0 1  
 57 1 1.0 1.0 1 0 1  
 58 1 1.0 1.0 1 0 1  
 59 1 1.0 1.0 1 0 1  
 60 1 1.0 1.0 1 0 1  
 61 1 1.0 1.0 1 0 1  
 62 1 1.0 1.0 1 0 1  
 63 1 1.0 1.0 1 0 1  
 64 1 1.0 1.0 1 0 1  
 65 1 1.0 1.0 1 0 1  
 66 1 1.0 1.0 1 0 1  
 67 1 1.0 1.0 1 0 1  
 68 1 1.0 1.0 1 0 1  
 69 1 1.0 1.0 1 0 1  
 70 1 1.0 1.0 1 0 1  
 71 1 1.0 1.0 1 0 1  
 72 1 1.0 1.0 1 0 1  
 73 1 1.0 1.0 1 0 1  
 74 1 1.0 1.0 1 0 1  
 75 1 1.0 1.0 1 0 1  
 76 1 1.0 1.0 1 0 1  
 77 1 1.0 1.0 1 0 1  
 78 1 1.0 1.0 1 0 1  
 79 1 1.0 1.0 1 0 1  
 80 1 1.0 1.0 1 0 1  
 81 1 1.0 1.0 1 0 1  
 82 1 1.0 1.0 1 0 1  
 83 1 1.0 1.0 1 0 1  
 84 1 1.0 1.0 1 0 1  
 85 1 1.0 1.0 1 0 1  
 86 1 1.0 1.0 1 0 1  
 87 1 1.0 1.0 1 0 1  
 88 1 1.0 1.0 1 0 1  
 89 1 1.0 1.0 1 0 1  
 90 1 1.0 1.0 1 0 1  
 91 1 1.0 1.0 1 0 1  
 92 1 1.0 1.0 1 0 1  
 93 1 1.0 1.0 1 0 1

TEMP FLUX

NODE NUMBERS

FUNCTION 1  
 220,000 BTU  
 HR-FT<sup>2</sup>  
 (EAST SIDE)

FUNCTION 2  
 154,000 BTU  
 HR-FT<sup>2</sup>  
 (NORTH SIDE)

FUNCTION 1 →  
 FUNCTION 2 →

47.725  
 190.9  
 93.75  
 184.12  
 88.66  
 170.51  
 80.5  
 151.8  
 69.57  
 126.81  
 56.10  
 97.57  
 40.62  
 64.90  
 23.71  
 29.94  
 39.83  
 27.88  
 20.98  
 16.6  
 45.44  
 28.43  
 68.30  
 39.36  
 88.75  
 48.70  
 106.03  
 56.35  
 119.57  
 62.12  
 128.9  
 65.63  
 133.58  
 33.41  
 32.34  
 129.35  
 22.63  
 90.54

WEIGHTED HEAT FLOWS

E-22

11111111112222222222333333333344444444445555555555666666666677777777778  
 1234567890123456789012345678901234567890123456789012345678901234567890

C O L U M N N U M B E R

TABLE 2 - TYPICAL HEAT FLOW INPUT DATA



NODE	FACTOR (AREA)	$\frac{1}{144} \times 220,000 \text{ FLUX} = \frac{\text{BTU}}{\text{HR}}$	NODE	FACTOR	VALUE
1	$\frac{1}{6}$ (0.1886)	= 48.02	66	$\frac{1}{3}$	= 49.00
4	$\frac{2}{3}$	= 191.19	69	$\frac{2}{3}$	= 106.23
6	$\frac{1}{3}$	= 94.34	71	$\frac{1}{3}$	= 56.76
9	$\frac{2}{3}$	= 184.46	74	$\frac{2}{3}$	= 119.80
11	$\frac{1}{3}$	= 89.30	76	$\frac{1}{3}$	= 62.51
14	$\frac{2}{3}$	= 171.14	79	$\frac{2}{3}$	= 129.12
16	$\frac{1}{3}$	= 81.09	81	$\frac{1}{3}$	= 66.04
19	$\frac{2}{3}$	= 151.76	84	$\frac{2}{3}$	= 133.83
21	$\frac{1}{3}$	= 70.00	86	$\frac{1}{6}$	= 33.61
24	$\frac{2}{3}$	= 127.00	89	$\frac{1}{6}$ (0.12696)	= 32.33
26	$\frac{1}{3}$	= 56.43	90	$\frac{2}{3}$ (0.12696)	= 129.31
29	$\frac{2}{3}$	= 97.73	92	$\frac{1}{6}$	= 22.63
31	$\frac{1}{3}$	= 40.87	93	$\frac{2}{3}$	= 90.52
34	$\frac{2}{3}$	= 65.01			
36	$\frac{1}{3}$	= 23.85			
39	$\frac{2}{3}$	= 29.97			
41	$\frac{1}{6}$ (0.12696) + $\frac{1}{6}$ (0.1887)	= 35.32			
46	"	= 24.72			
49	$\frac{2}{3}$	= 20.98			
51	$\frac{1}{3}$	= 16.70			
54	$\frac{2}{3}$	= 45.51			
56	$\frac{1}{3}$	= 28.61			
59	$\frac{2}{3}$	= 68.41			
61	$\frac{1}{3}$	= 39.50			
64	$\frac{2}{3}$	= 88.90			

THE VALUES ON THIS PAGE  
SERVE AS A CHECK ON  
FETAP INPUT DATA —  
FLUX FLOW

SUBJECT: <b>HEAT FLOW (CHECK)</b>	<b>Babcock &amp; Wilcox</b>	
	<b>ENGINEERING CALCULATIONS</b>	
CHECKED BY:	PREPARED BY:	REFERENCE NO.
REVISION:	DATE:	SHEET NO. OF

E-23

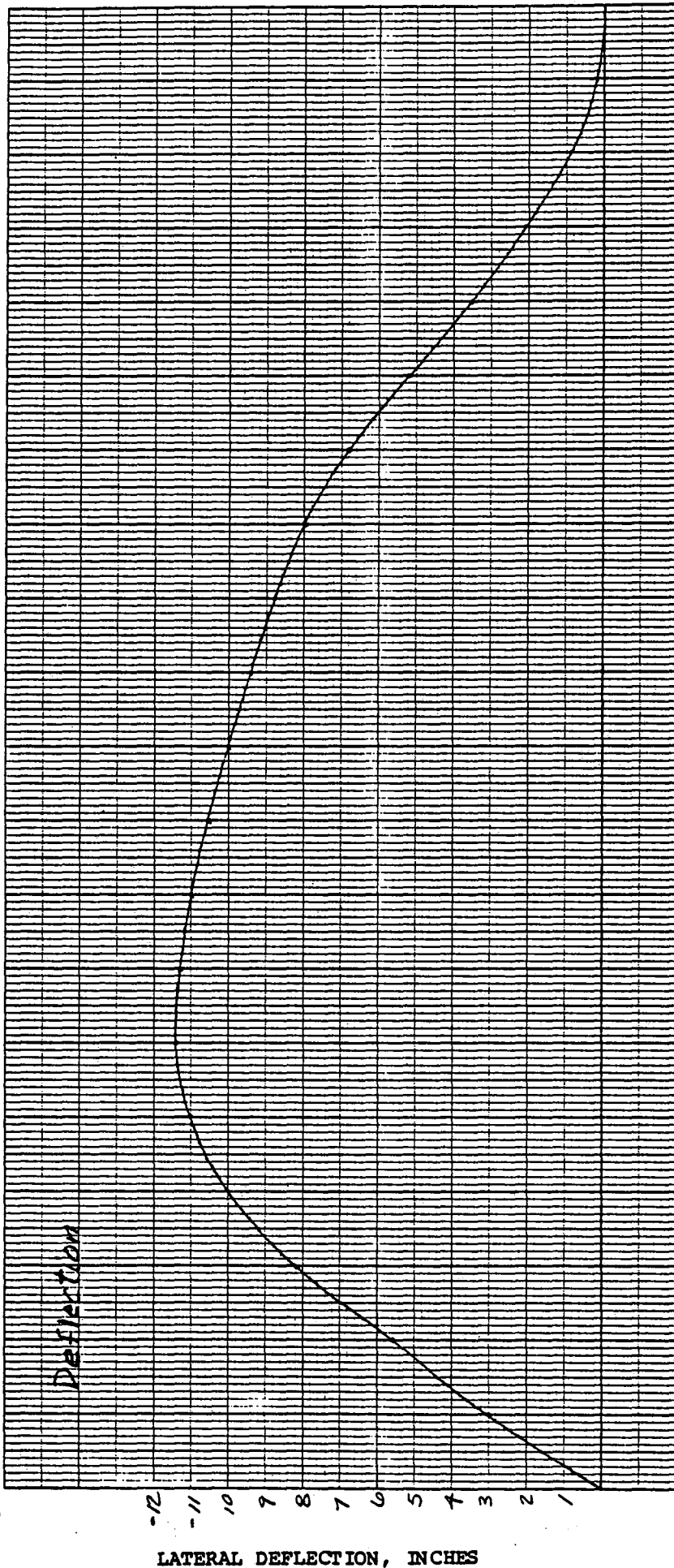
TABLE 3 - HEAT FLOW CALCULATIONS

## 8.0 Stress Analysis Results

The axial stresses are the stresses of interest for this analysis because bowing will affect them; whereas the circumferential stresses are a function of the through-thickness gradient and are not affected by bowing. Lateral deflections are presented in Figures 7a through 7g for the six major conditions evaluated and the check on the effect of tube length (Figure 7g) of Panel 7 reduced by a factor of four. Figures 8a through 8p present the axial stress as a function of length for four locations, i.e.; the two crown locations and the two web extremity locations. Two stress values (same node on different elements) are given for each crown tube location as a check on convergence (i.e., for a converged solution the values would be equal). In addition to the 6 panels, the quarter length tube analysis (Panel 7) and a pin-pin boundary condition analysis is also presented.

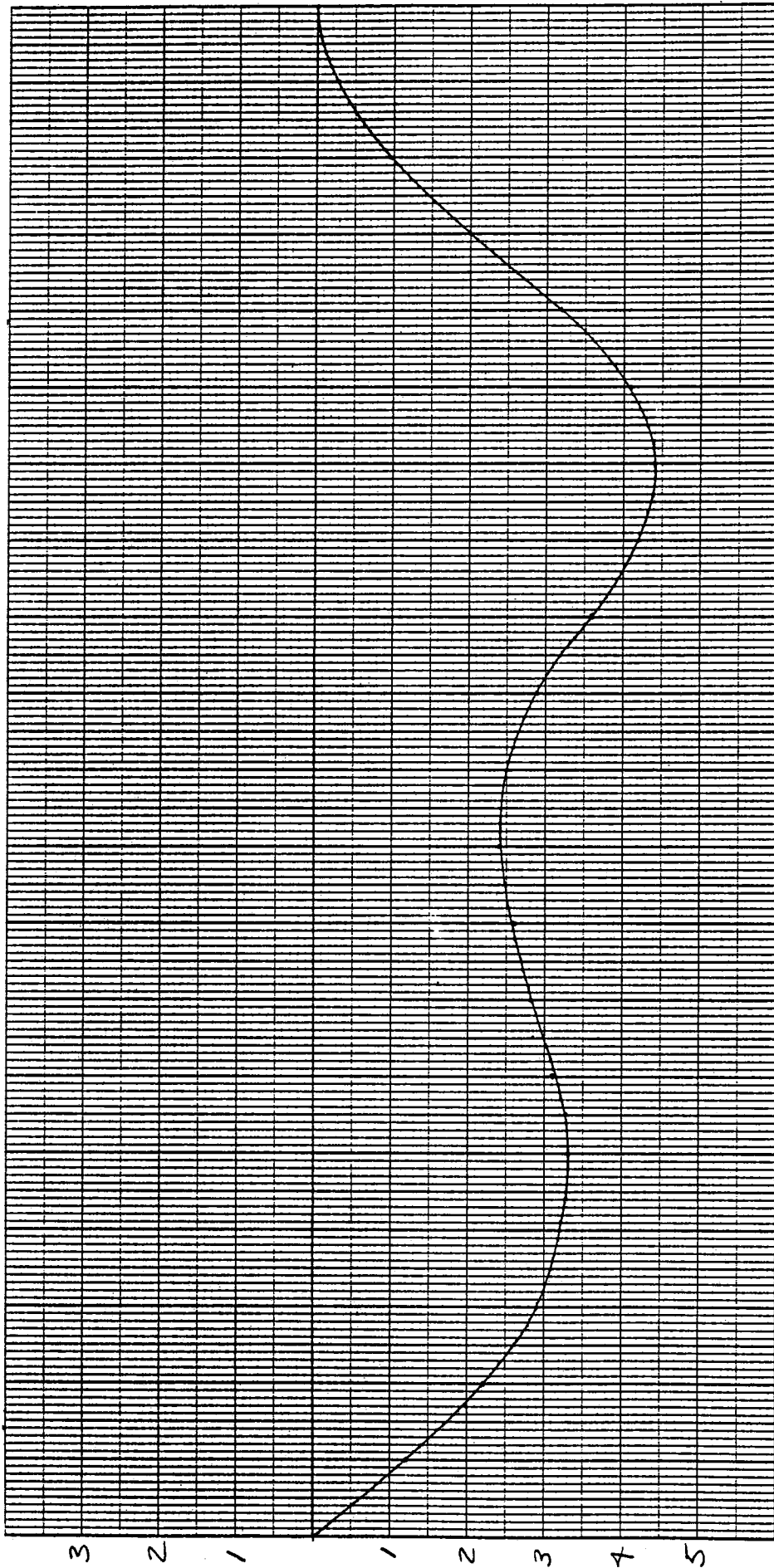
The two axial crown stresses were averaged and replotted for each panel (Figure 9a through 9f); each figure includes both the front and back sides (e.g., north and east sides). Table 7 summarizes Figure 9 by presenting the maximum axial compressive stress for the six locations. From Table 7 the maximum tube stress and the maximum web stress both occur on Panel 6. The stress data is again summarized along with heat flux data in Table 8.

All of the stress plots appear to be free of unreliable numbers except near the ends of the tube; e.g., axial stress at the pinned end should go to zero.



TUBE LENGTH (PANEL 3, ZONE 1 - PEAK HEATING)

FIGURE 7a - TUBE DEFECTION

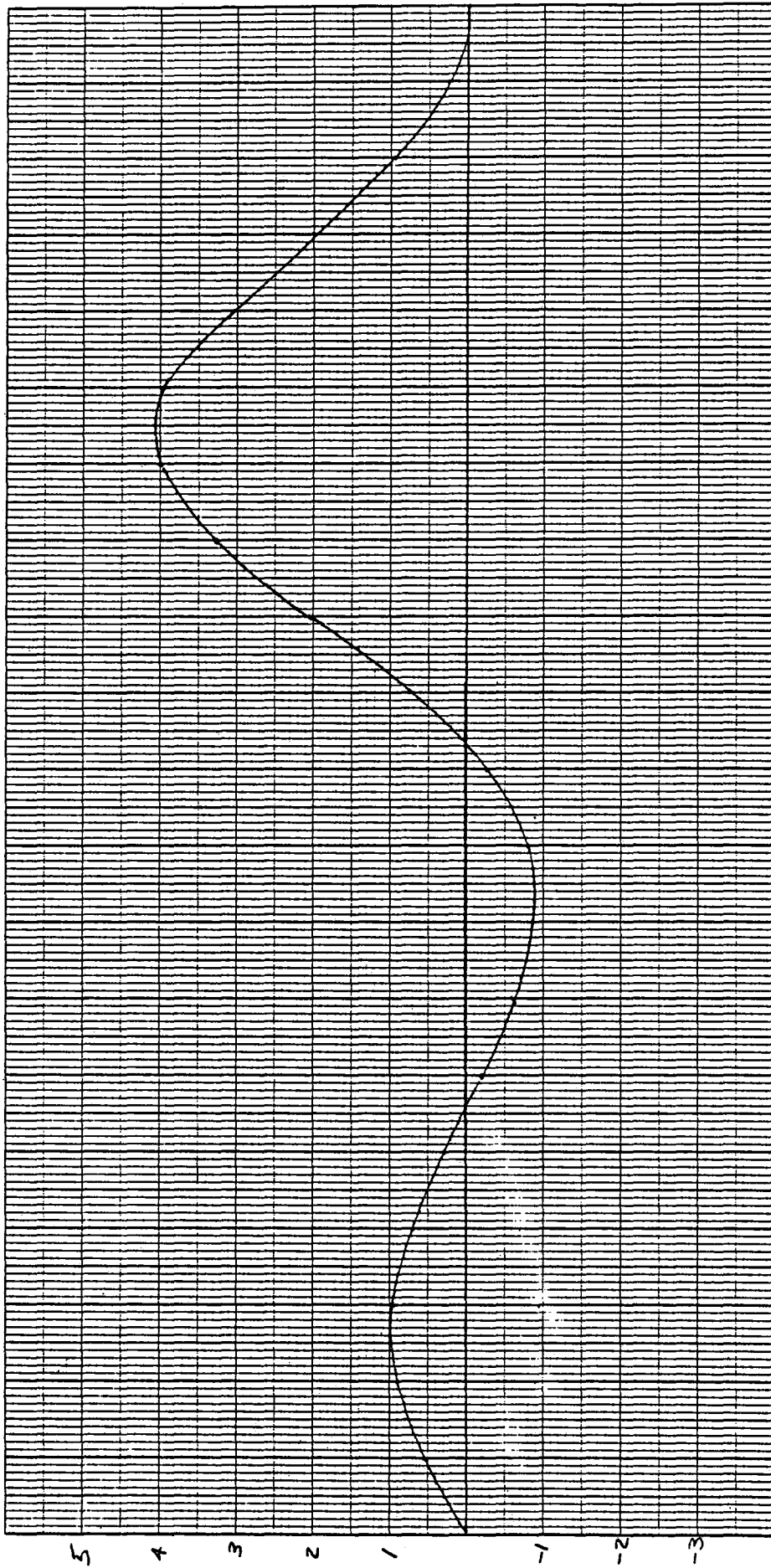


3 2 1 1 2 3 4 5

LATERAL DEFLECTION, INCHES

TUBE LENGTH (PANEL 5, ZONE 1 - PEAK HEATING)

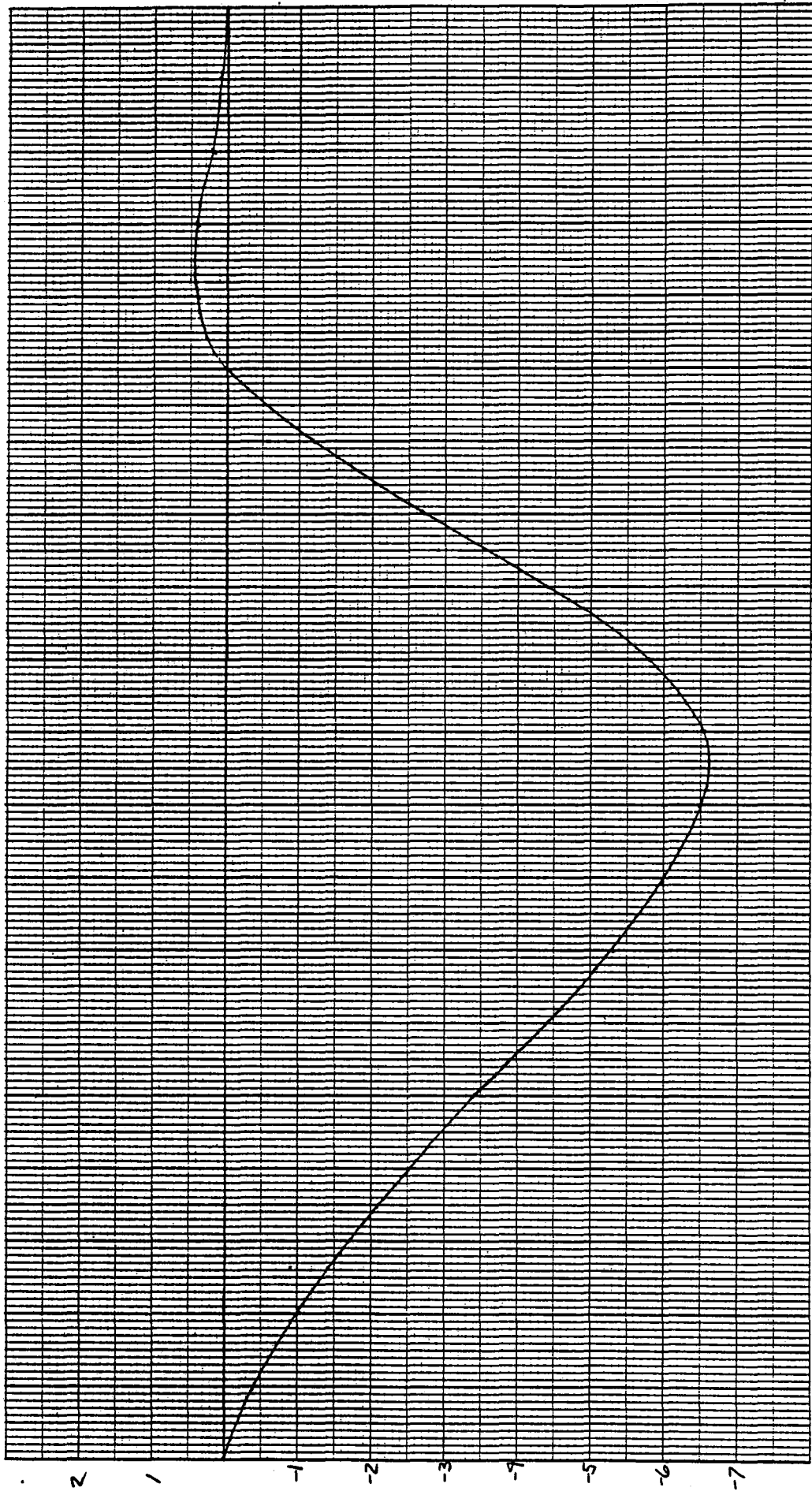
FIGURE 7b - TUBE DELECTION



TUBE LENGTH (PANEL 6, ZONE 1 - PEAK HEATING)

FIGURE 7c - TUBE DEFECTION

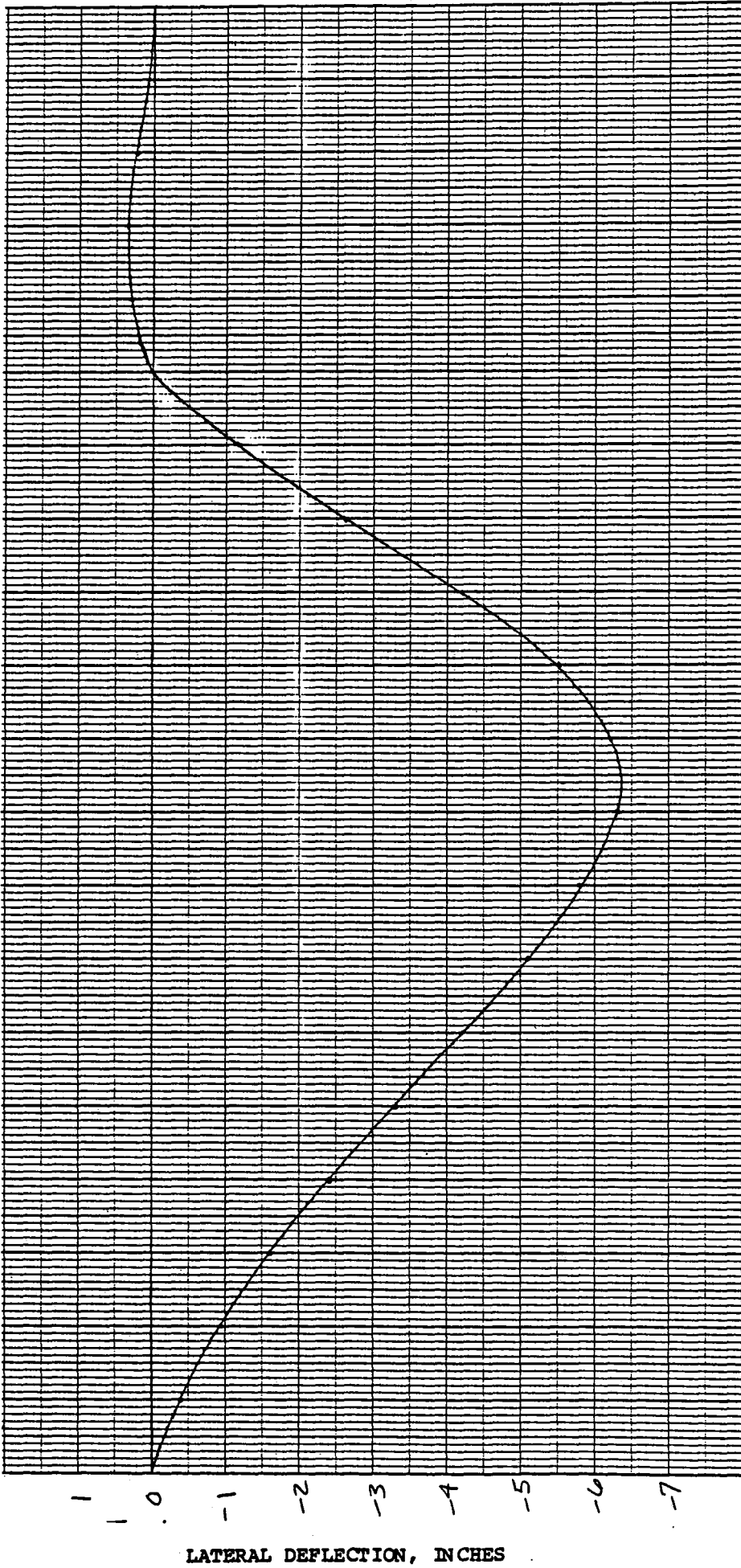
LATERAL DEFLECTION, INCHES



TUBE LENGTH (PANEL 7, ZONE 1 - PEAK HEATING)

FIGURE 7d - TUBE DEFECTION

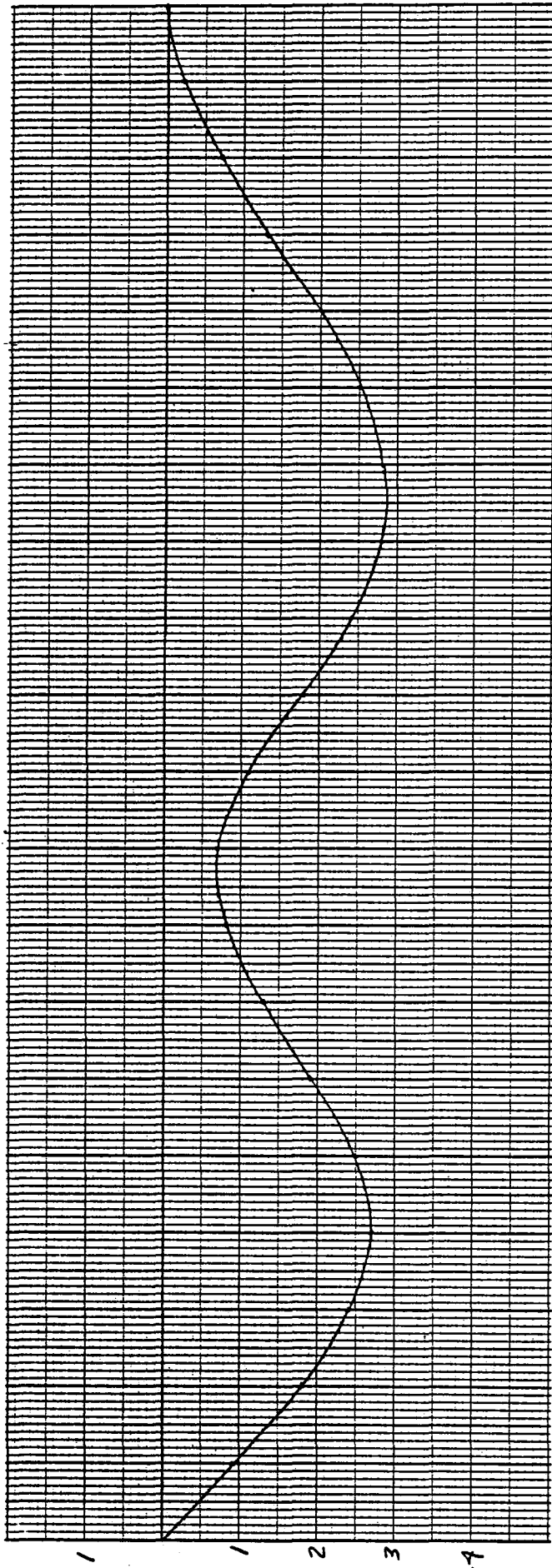
LATERAL DEFLECTION, INCHES



TUBE LENGTH (PANEL 8, ZONE 1 - PEAK HEATING)

FIGURE 7e - TUBE DEFLECTION

LATERAL DEFLECTION, INCHES

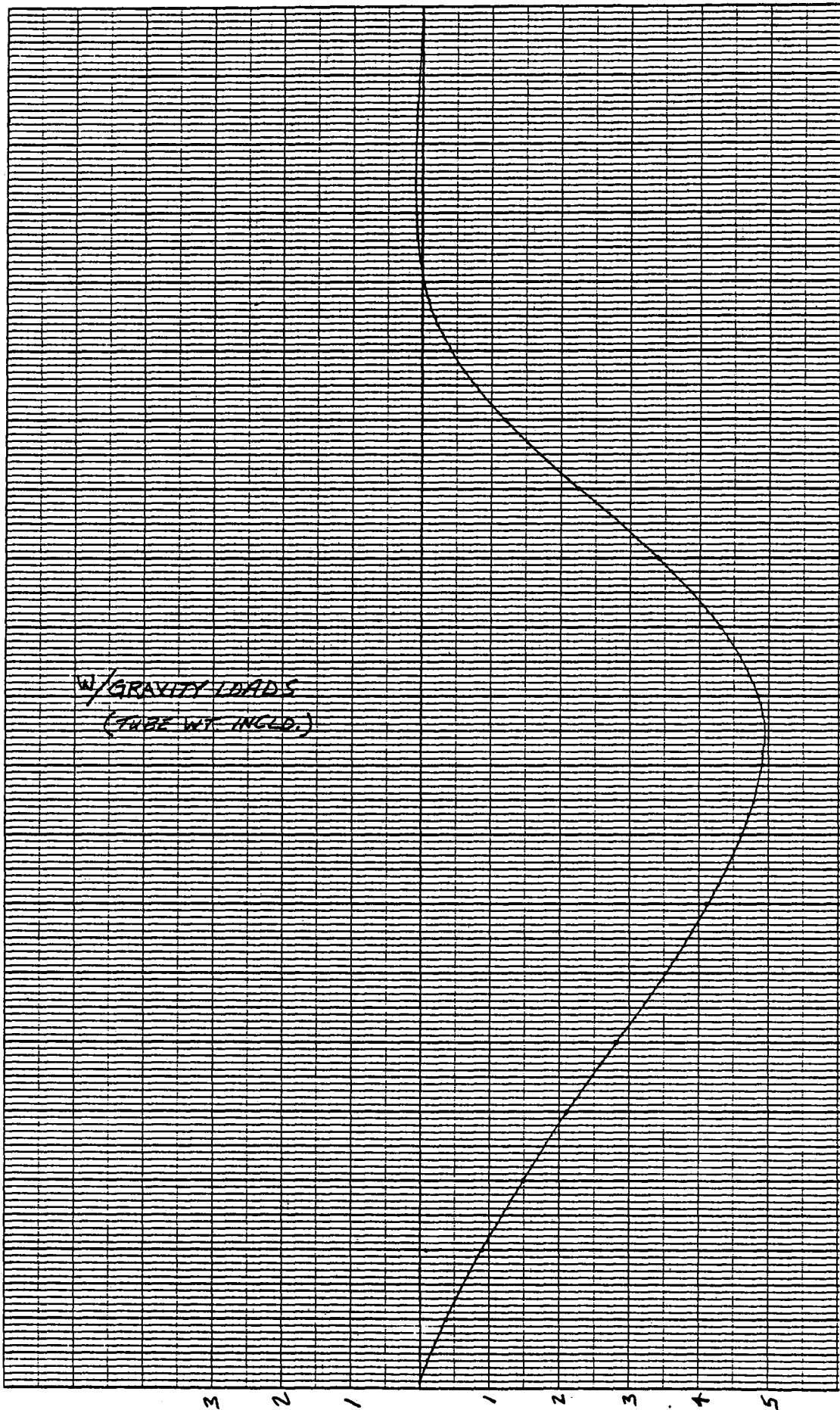


LATERAL DEFLECTION, INCHES

TUBE LENGTH (PANEL 7, ZONE 2 - PEAK HEATING)

FIGURE 7f - TUBE DEFECTION





TUBE LENGTH, L/4 (PANEL 7, ZONE 1 - PEAK HEATING)

FIGURE 7g - TUBE DEFLECTION

LATERAL DEFLECTION, x 10<sup>1</sup> INCHES

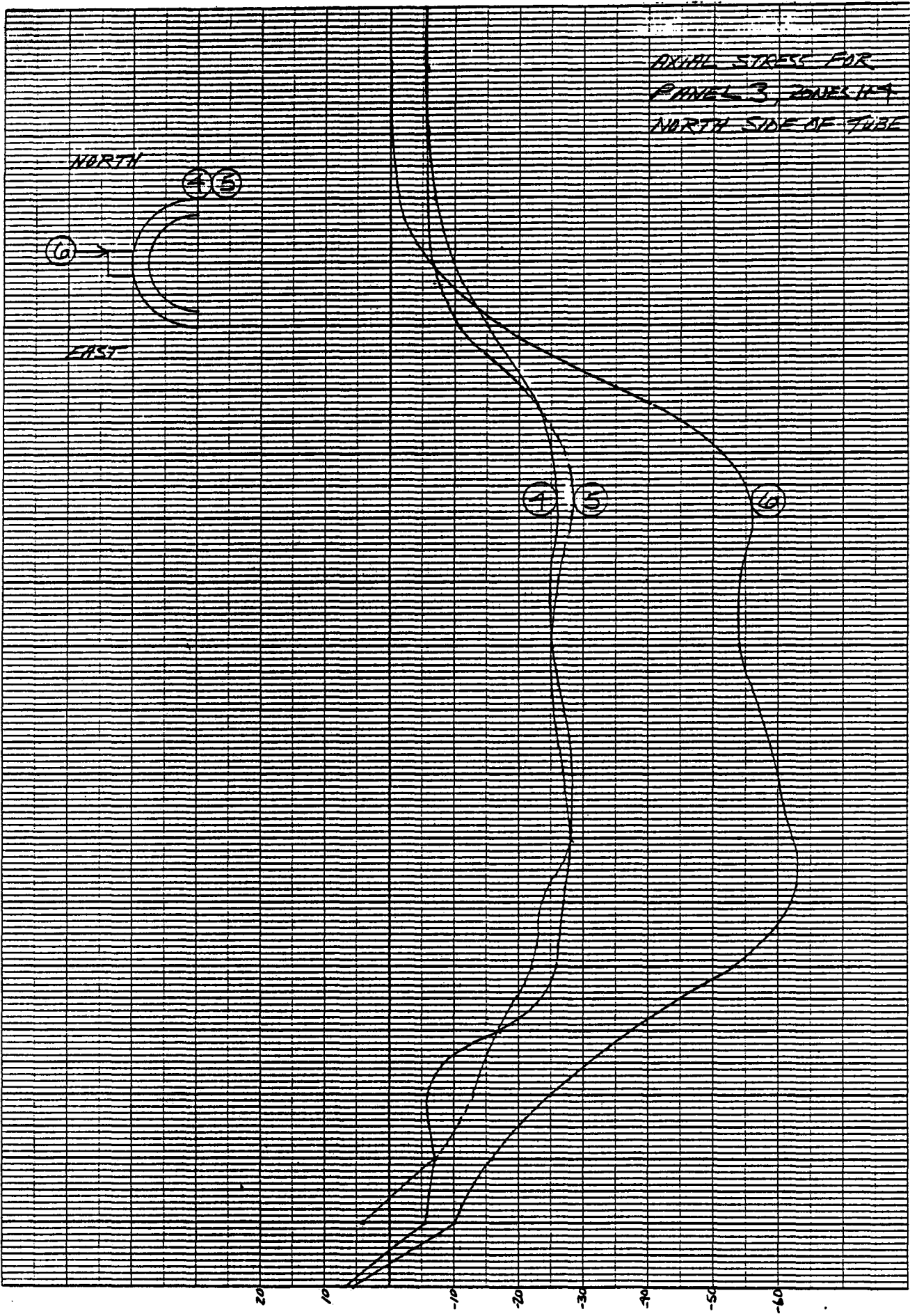


FIGURE 8a - AXIAL STRESS

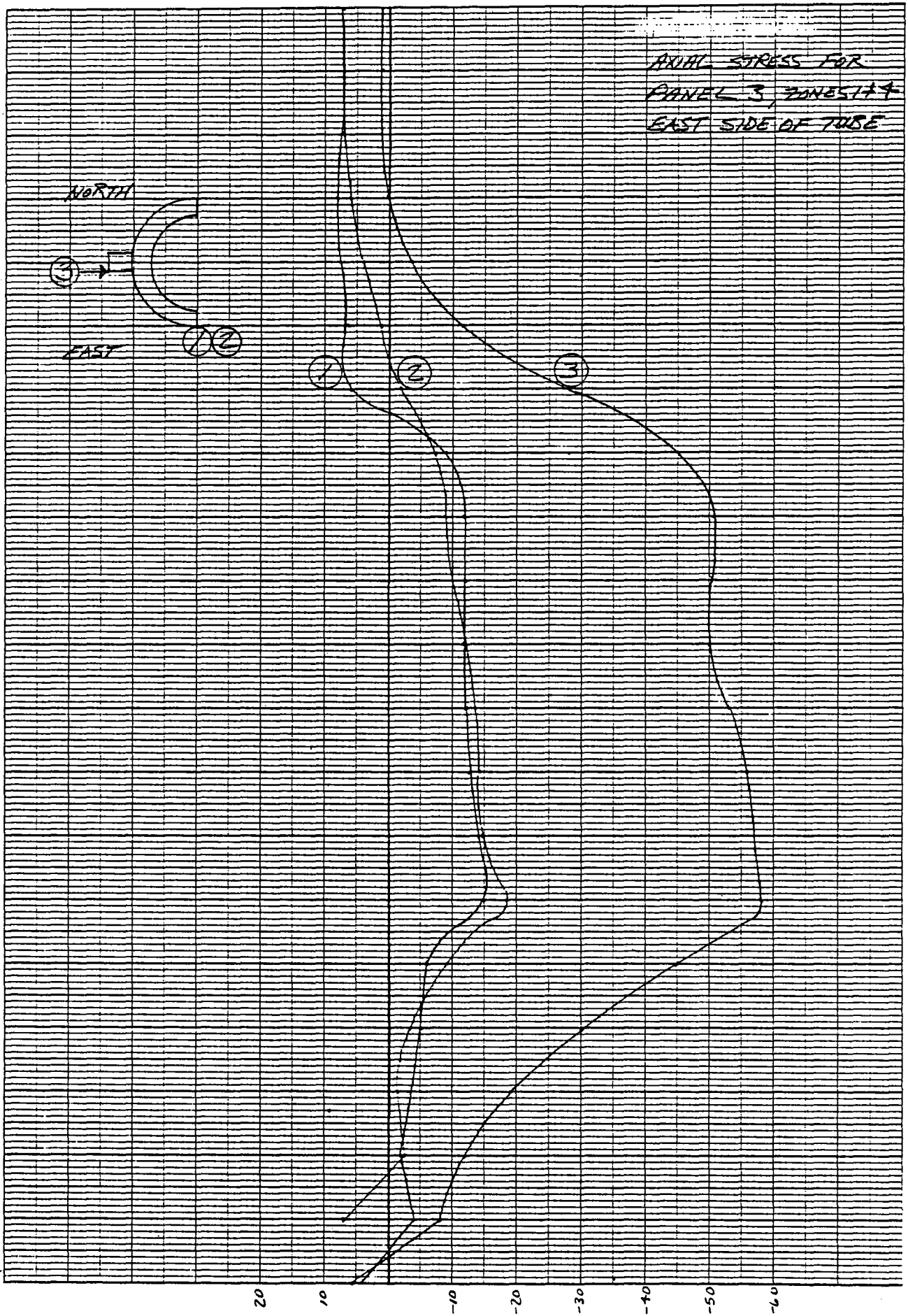


FIGURE 8b - AXIAL STRESS

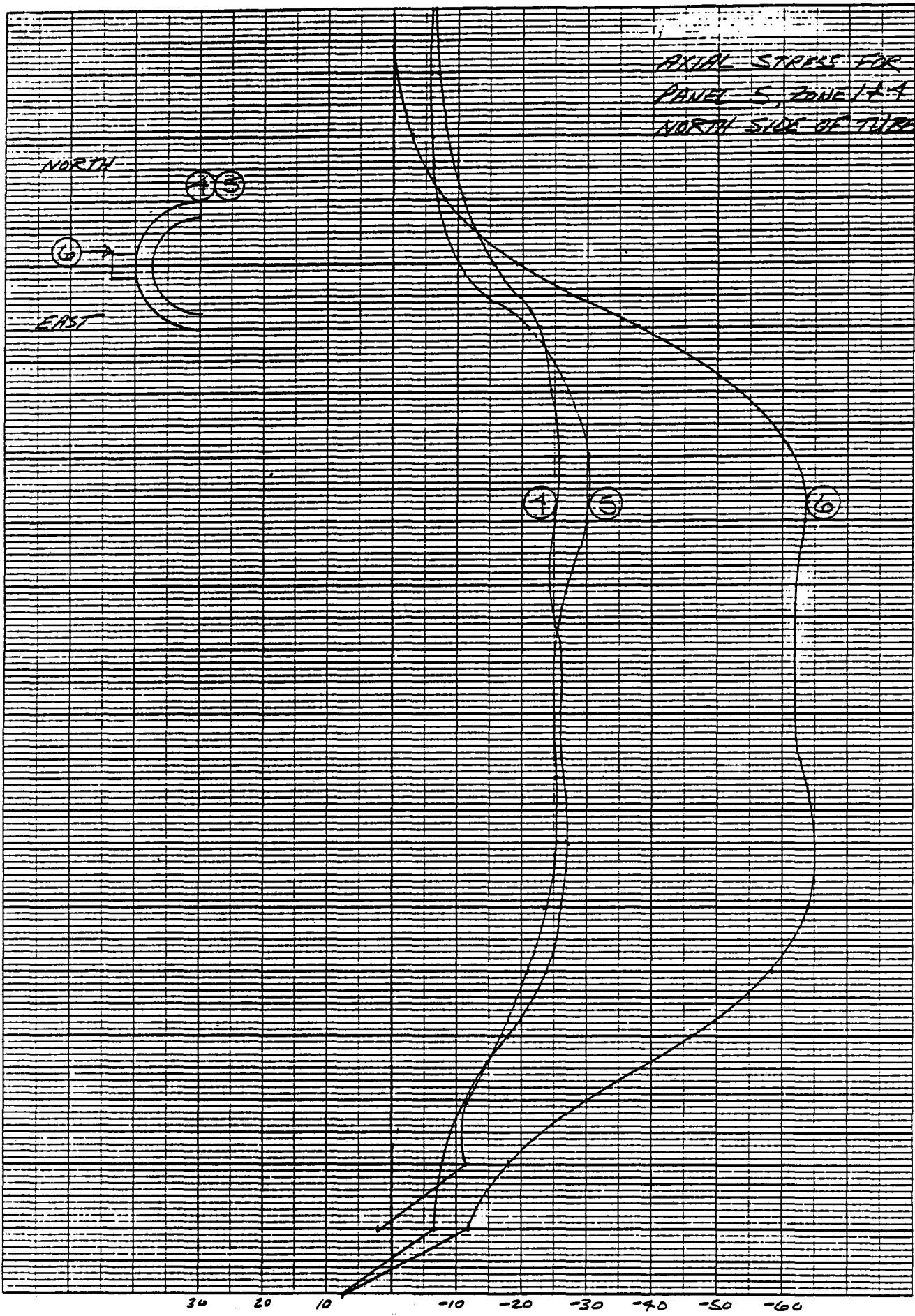
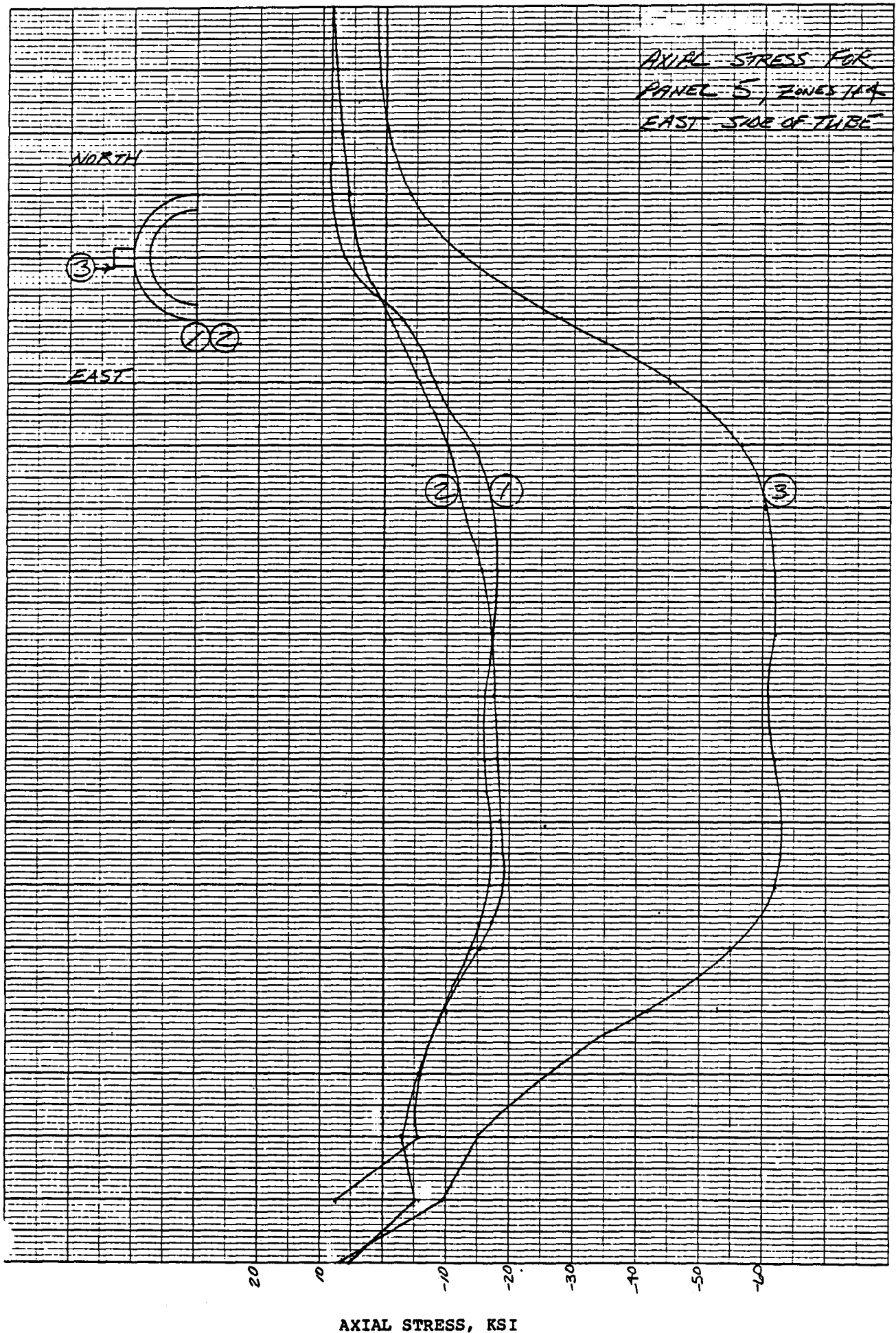


FIGURE 9C - AXIAL STRESS



TUBE LENGTH  
FIGURE 8d - AXIAL STRESS

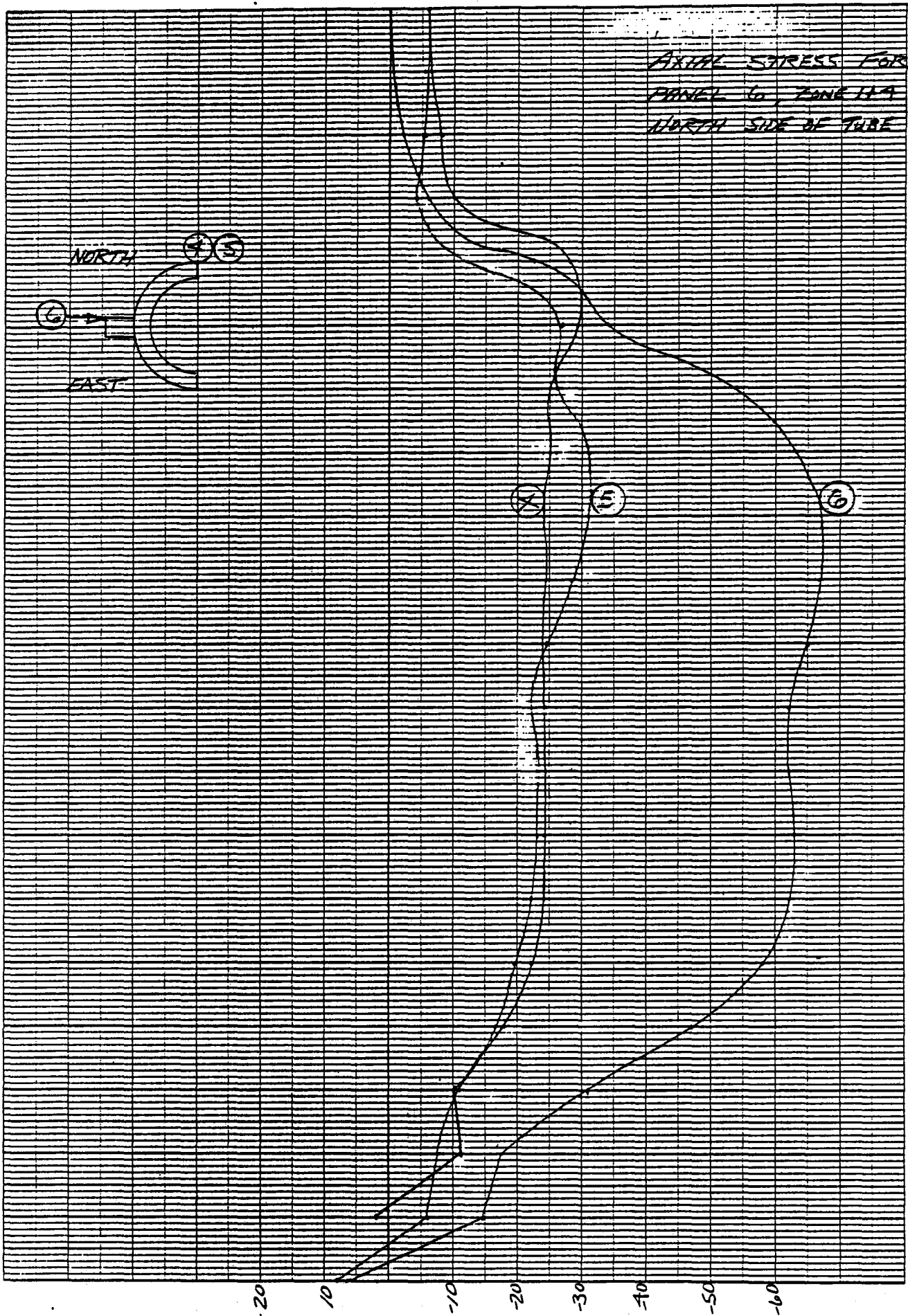
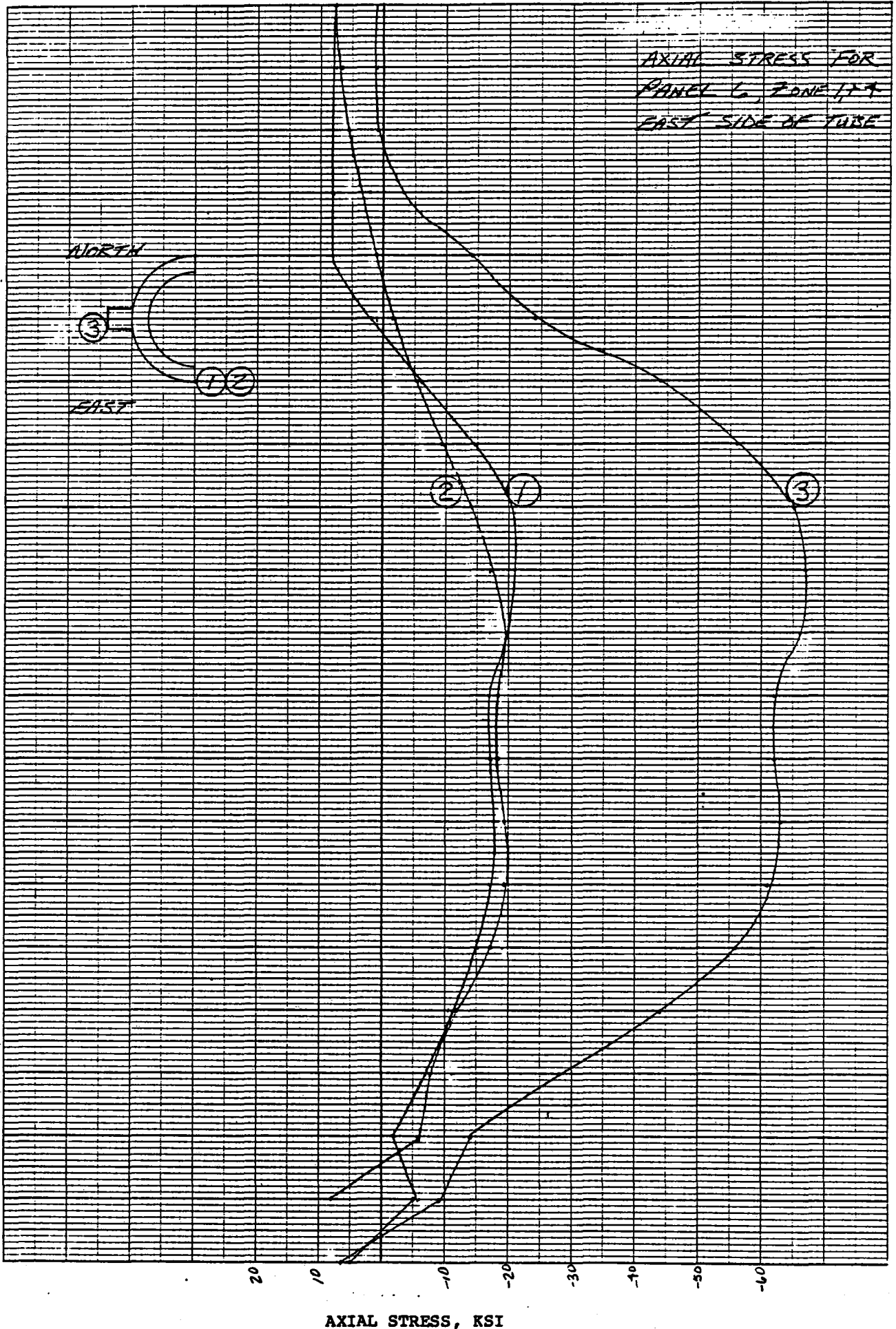
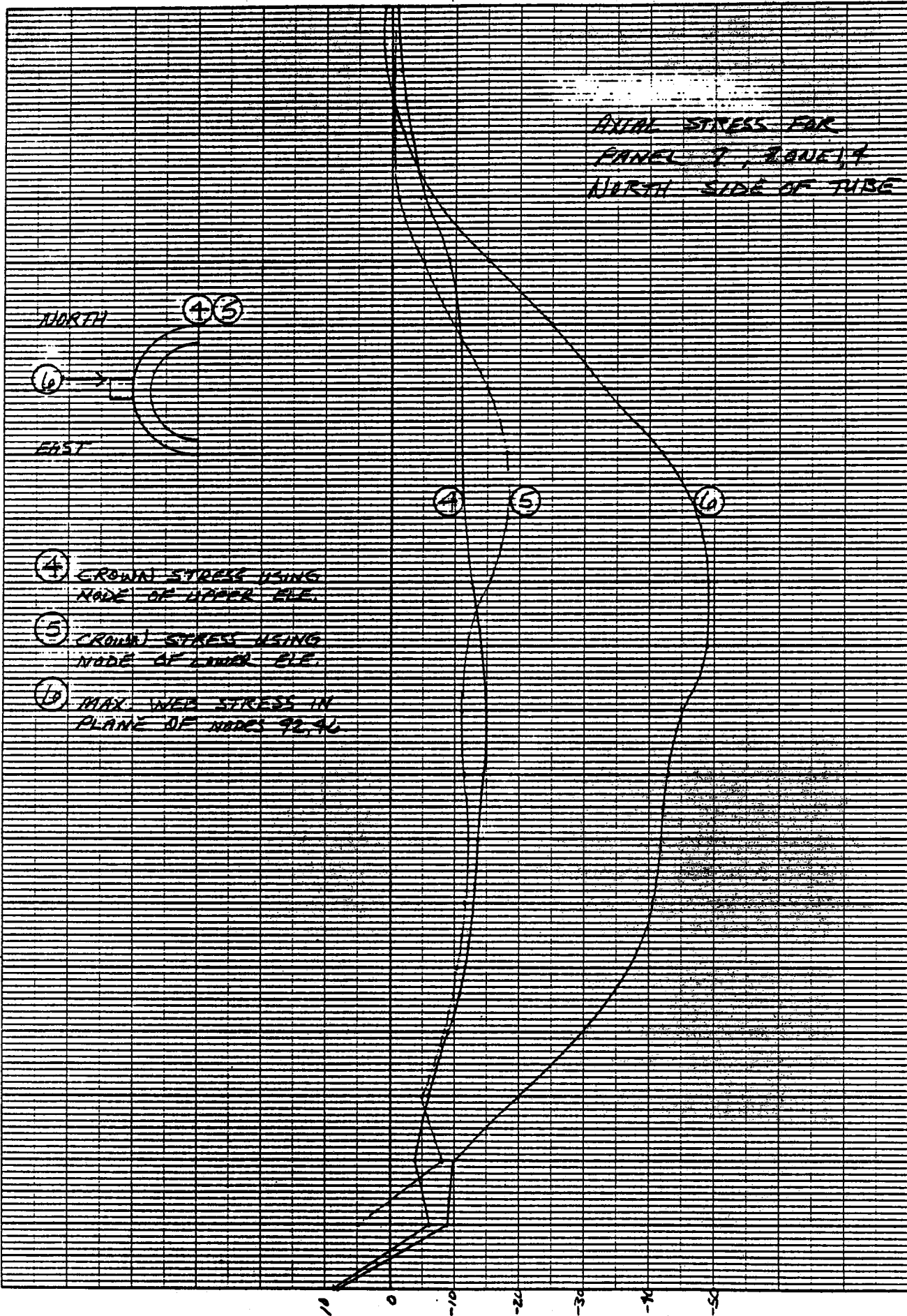


FIGURE 8e - AXIAL STRESS



TUBE LENGTH  
 FIGURE 8f - AXIAL STRESS

AXIAL STRESS FOR  
 PANEL 7, ROW 17  
 NORTH SIDE OF TUBE



④ ⑤

⑥

NORTH  
 EAST

④

⑤

⑥

④ CROWN STRESS USING  
 NODE OF UPPER ELE.

⑤ CROWN STRESS USING  
 NODE OF LOWER ELE.

⑥ MAX. WELD STRESS IN  
 PLANE OF NODES 92, 96

TUBE LENGTH

FIGURE 8g - AXIAL STRESS

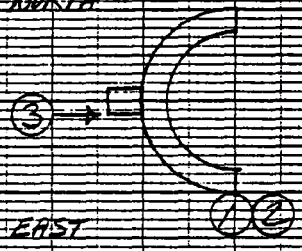
AXIAL STRESS, KSI



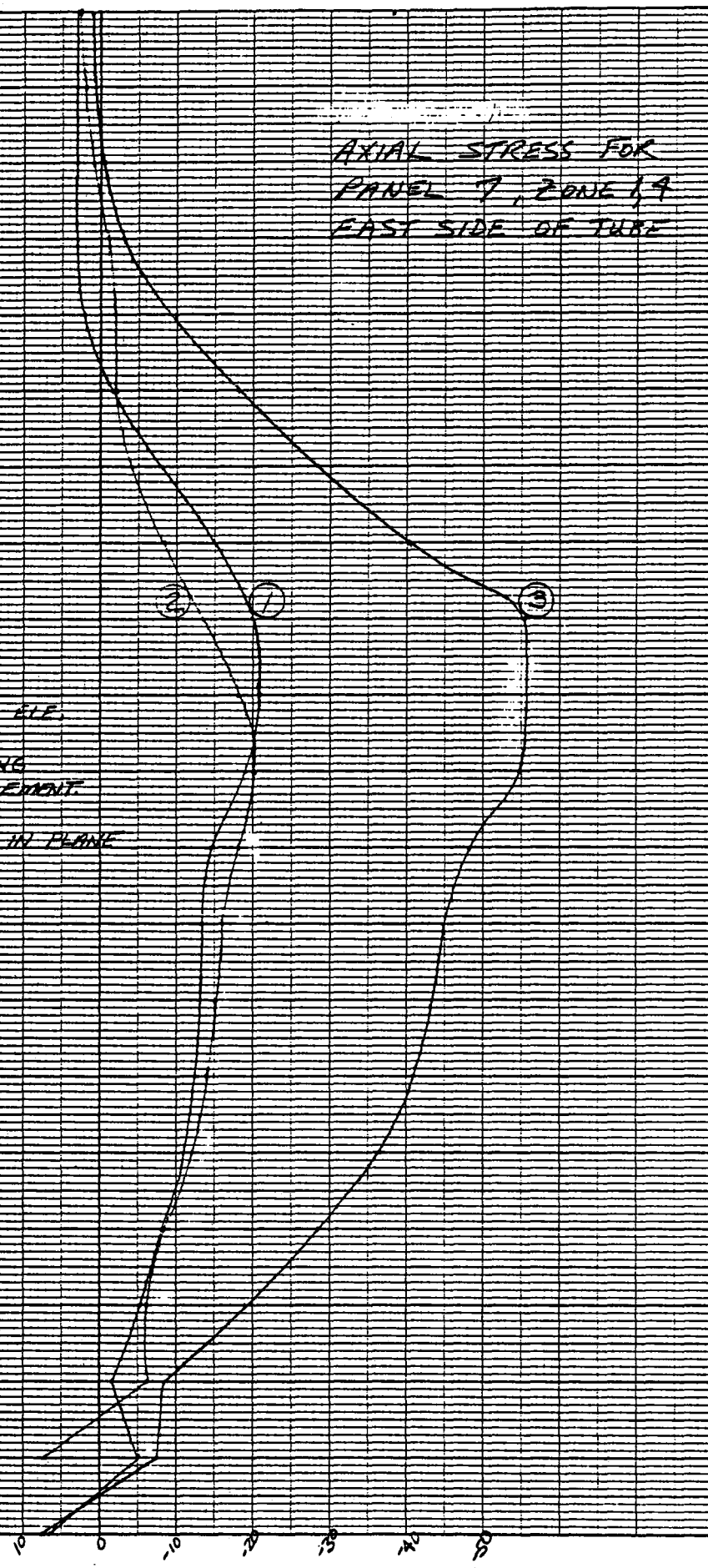
AXIAL STRESS FOR  
 PANEL 7, ZONE 1, 9  
 EAST SIDE OF TUBE

NORTH

EAST



- ① STRESS AT CROWN USING NODE OF UPPER ELE.
- ② CROWN STRESS USING NODE OF LOWER ELEMENT.
- ③ MAX. WEB STRESS IN PLANE OF NODES 89, 91.



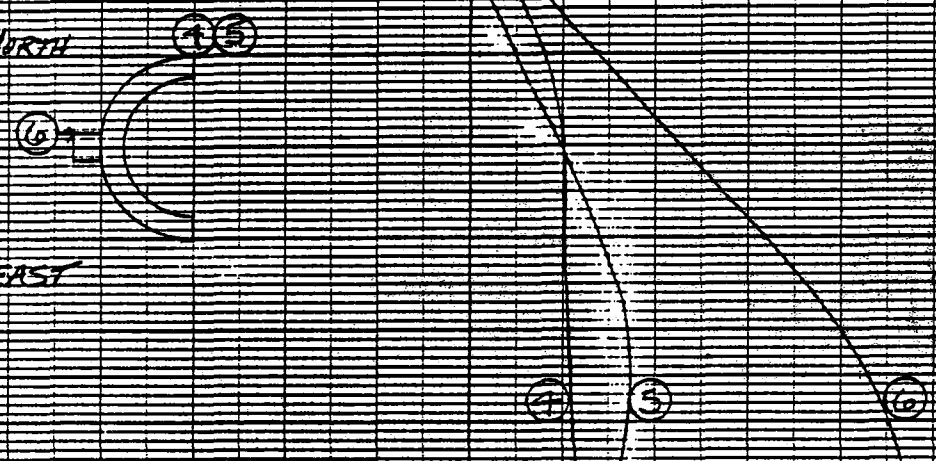
AXIAL STRESS, KSI

TUBE LENGTH

FIGURE 8h - AXIAL STRESS

AXIAL STRESS FOR  
 PANEL 8, ZONE 14  
 NORTH SIDE OF TUBE

NORTH  
 EAST



- (1) CROWN STRESS USING  
 NODE OF UPPER ELEMENT
- (5) CROWN STRESS USING  
 NODE OF LOWER ELEMENT
- (6) MAX. WEB STRESS IN  
 PLANE OF NODES 92, 96

TUBE LENGTH

AXIAL STRESS, KSI

FIGURE 81 - AXIAL STRESS

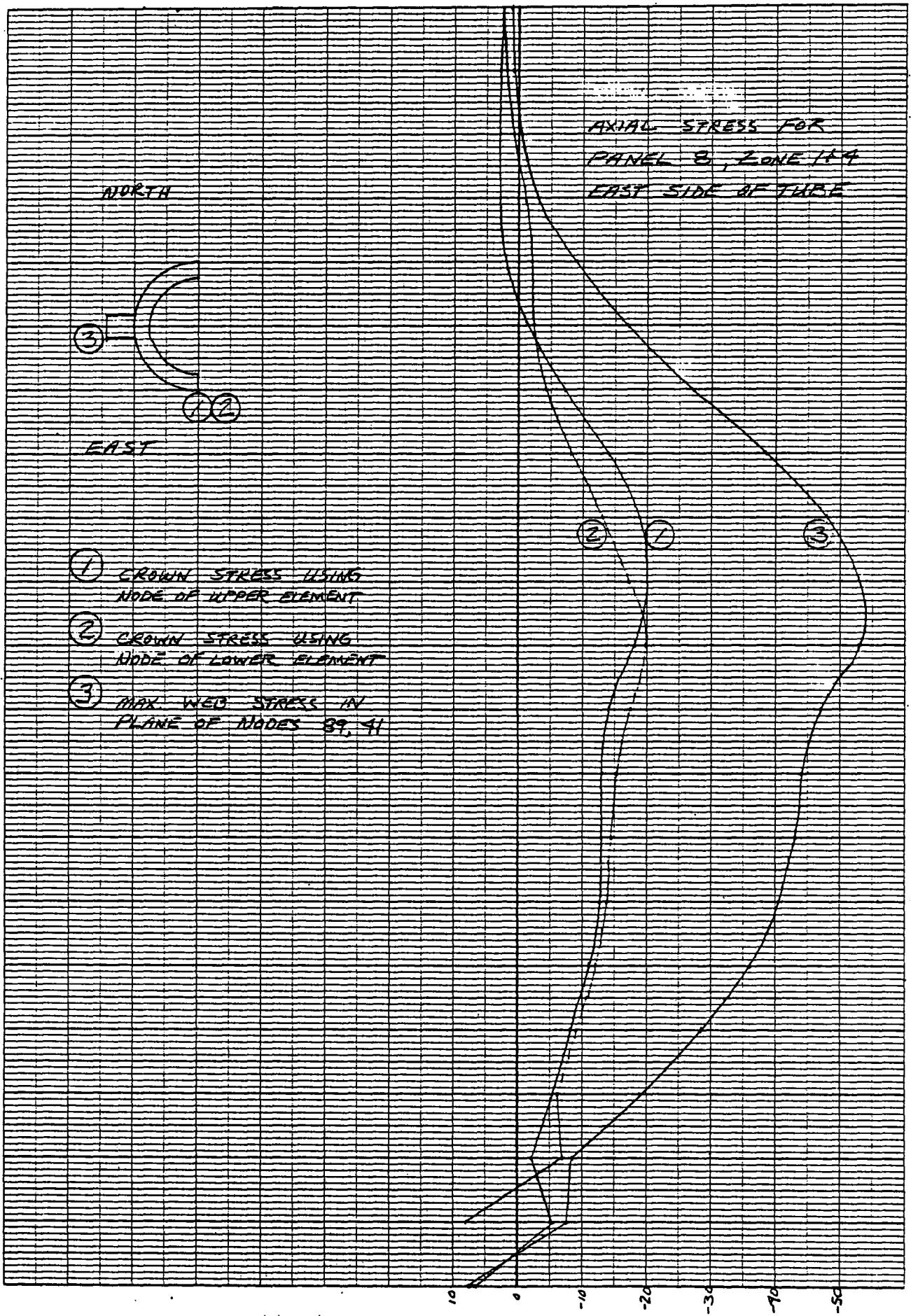


FIGURE 8j - AXIAL STRESS

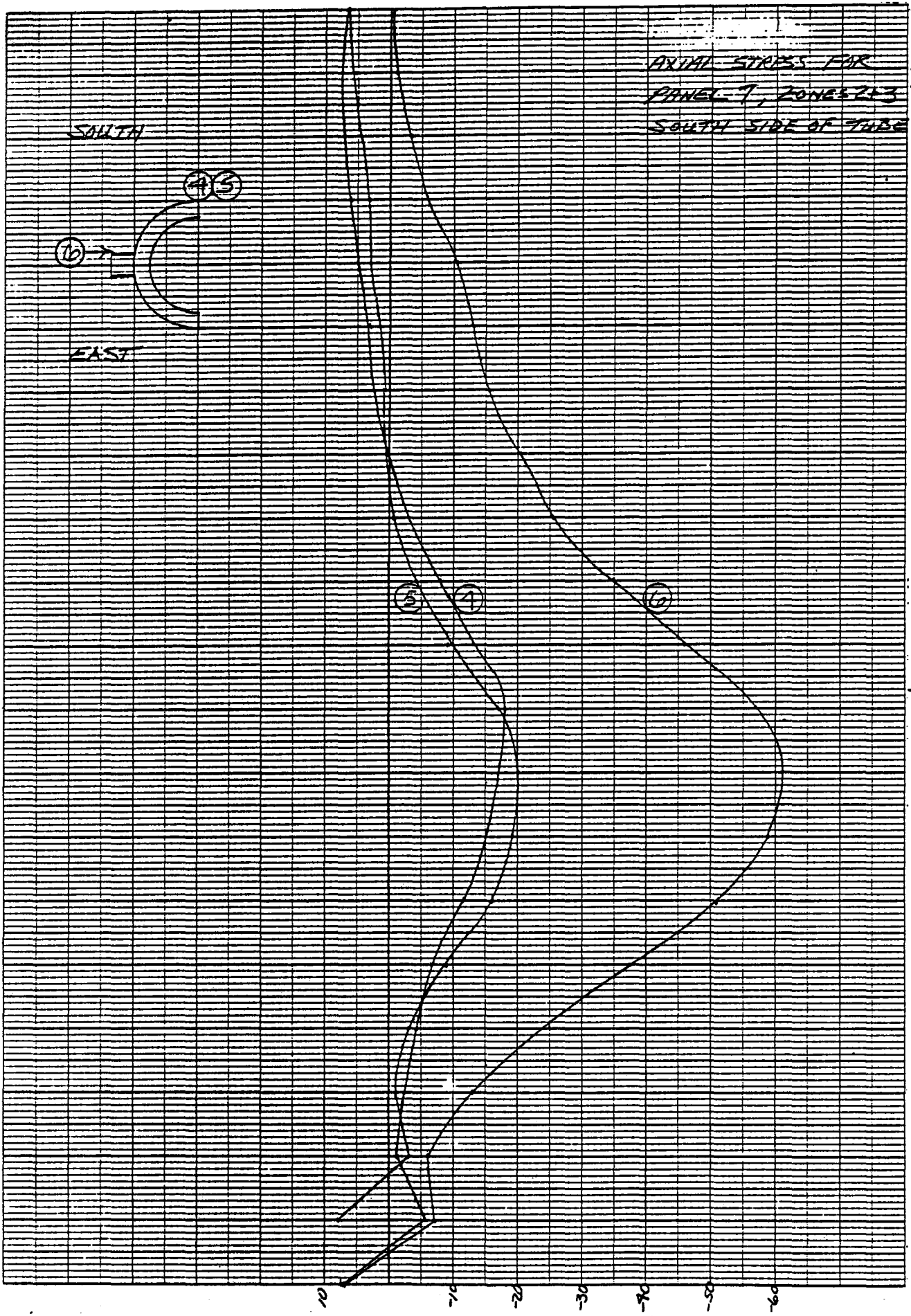


FIGURE 8k - AXIAL STRESS

AXIAL STRESS FOR  
PANEL 7 ZONES 1+3  
EAST SIDE OF TUBE

SOUTH

EAST

③

① ②

⑦

⑧

⑬

10 -10 -20 -30 -40 -50 -60

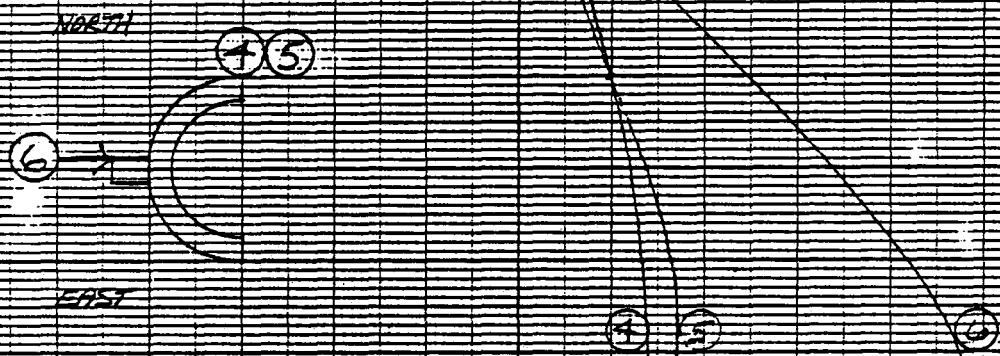
AXIAL STRESS, KSI

TUBE LENGTH

FIGURE 81 - AXIAL STRESS

AXIAL STRESS FOR  
 PANEL 7, ZONE 114  
 NORTH SIDE OF TUBE

(QUARTER LENGTH)



- ① PLOT OF STRESS AT CROWN USING NODE OF UPPER FL.
- ② PLOT OF CROWN STRESS USING NODE OF LOWER FL.
- ③ MAX. WEB STRESS IN PLANE OF NODES 92, 96

10      -10    -20    -30    -40    -50    -60

AXIAL STRESS, KSI

TUBE LENGTH

FIGURE 8m - AXIAL STRESS

AXIAL STRESS FOR  
 PANEL 7, ZONE 1 & 4  
 EAST SIDE OF TUBE

(QUARTER LENGTH)

NORTH

EAST

③

① ②

② ①

③

- ① PLOT OF STRESS AT CROWN USING NODE OF UPPER ELEMENT
- ② PLOT OF CROWN STRESS USING NODE OF LOWER ELEMENT
- ③ MAXIMUM WEB STRESS IN PLANE OF NODES 897 & 1.

ELEMENT #1

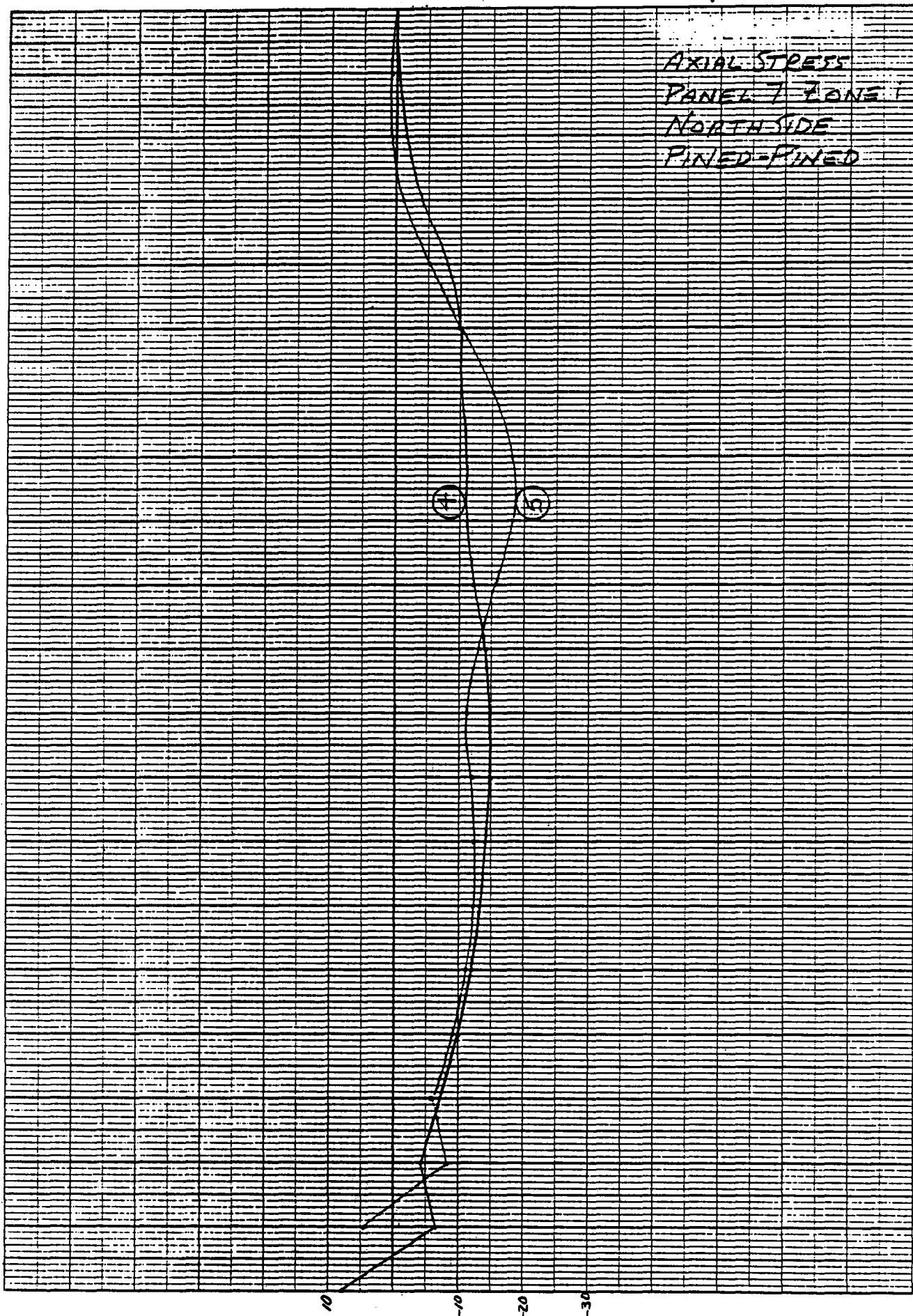


10 0 -10 -20 -30 -40 -50 -60

AXIAL STRESS, KSI

TUBE LENGTH

FIGURE 8n - AXIAL STRESS

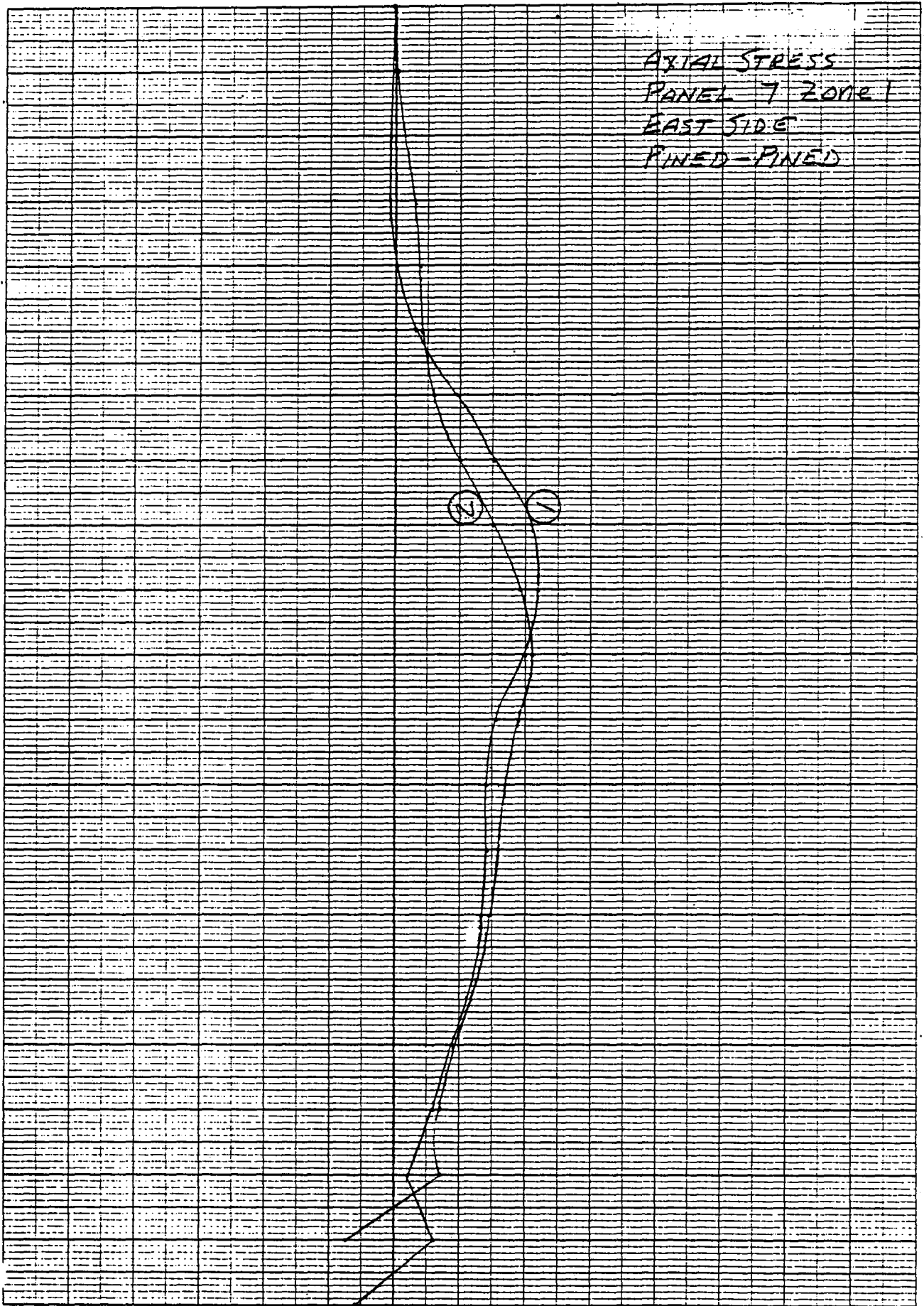


TUBE LENGTH (PIN-PIN CONNECTIONS)

FIGURE 80 - AXIAL STRESS

AXIAL STRESS, KSI

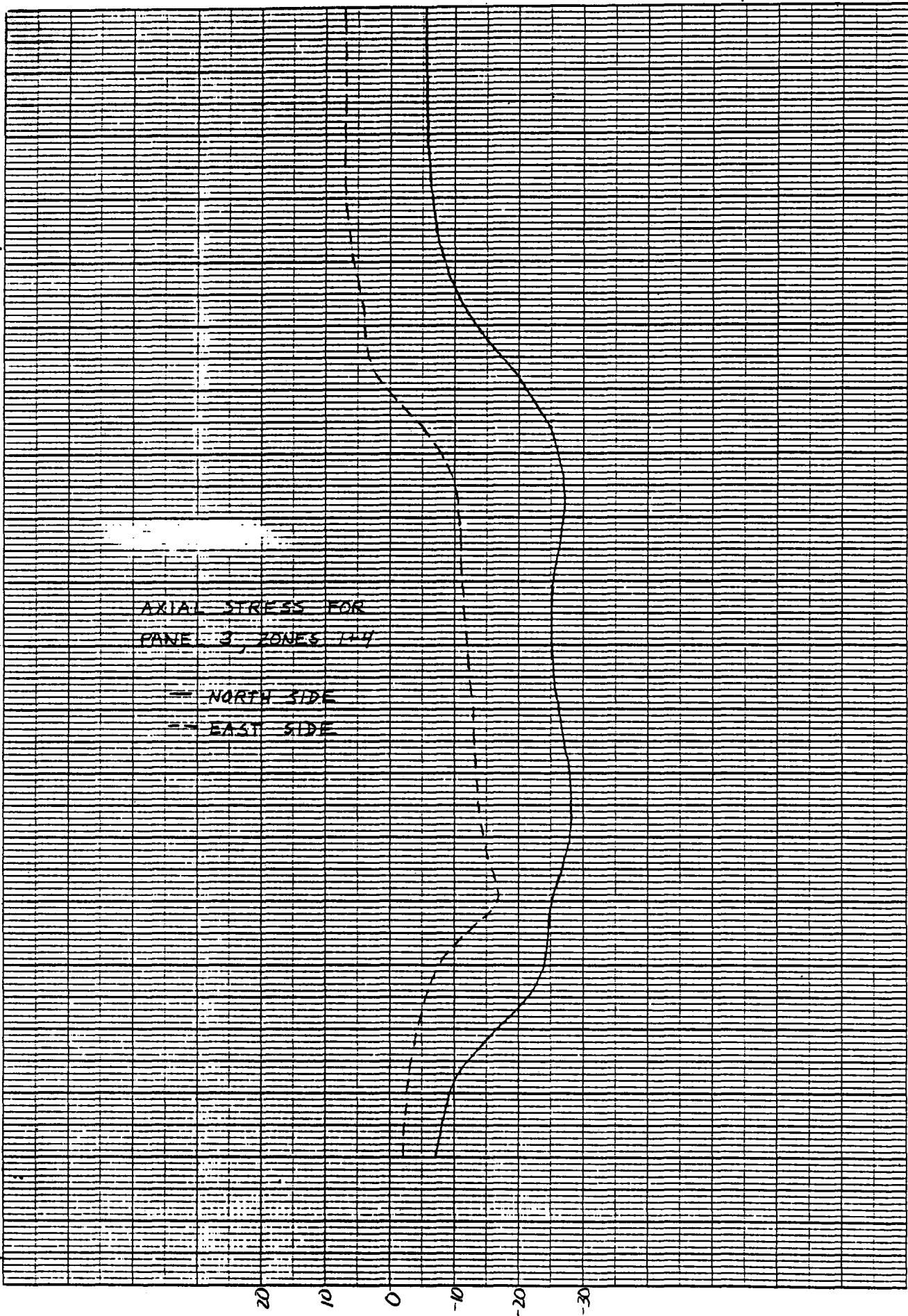




TUBE LENGTH (PIN-PIN CONNECTIONS)

FIGURE 8p - AXIAL STRESS

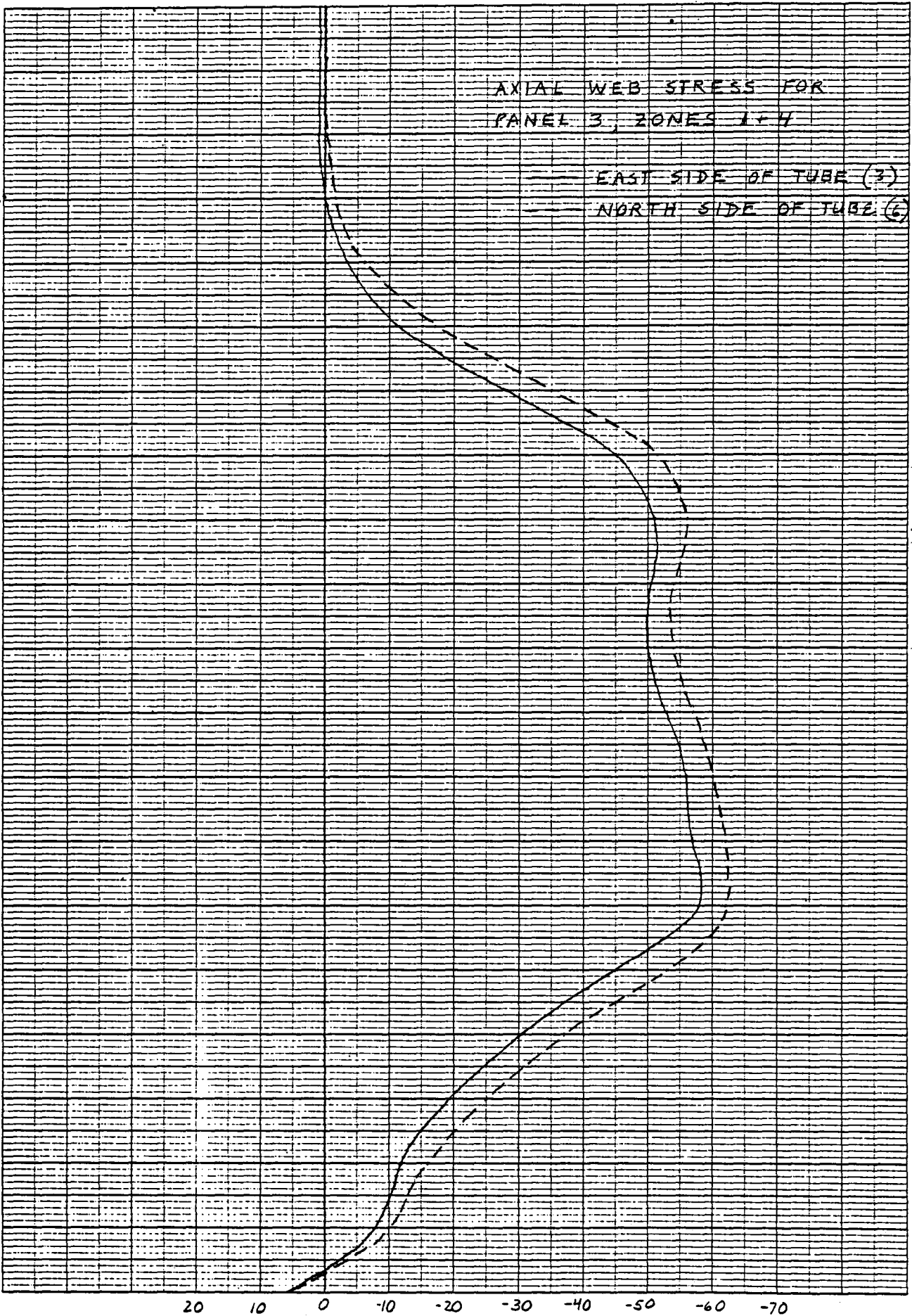
AXIAL STRESS, KSI



TUBE LENGTH

FIGURE 9a - AXIAL STRESS

AXIAL STRESS, KSI



AXIAL STRESS, KSI

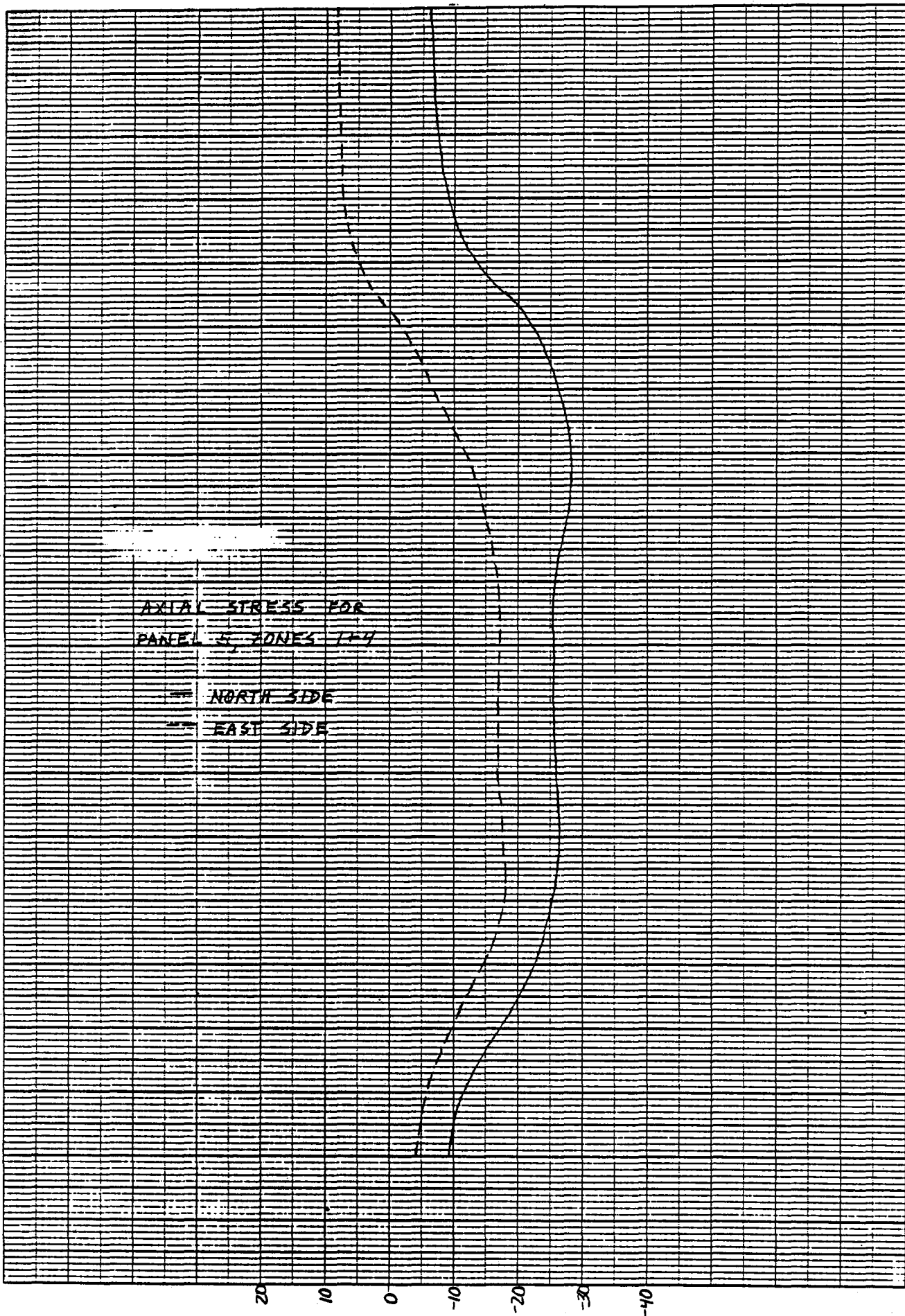
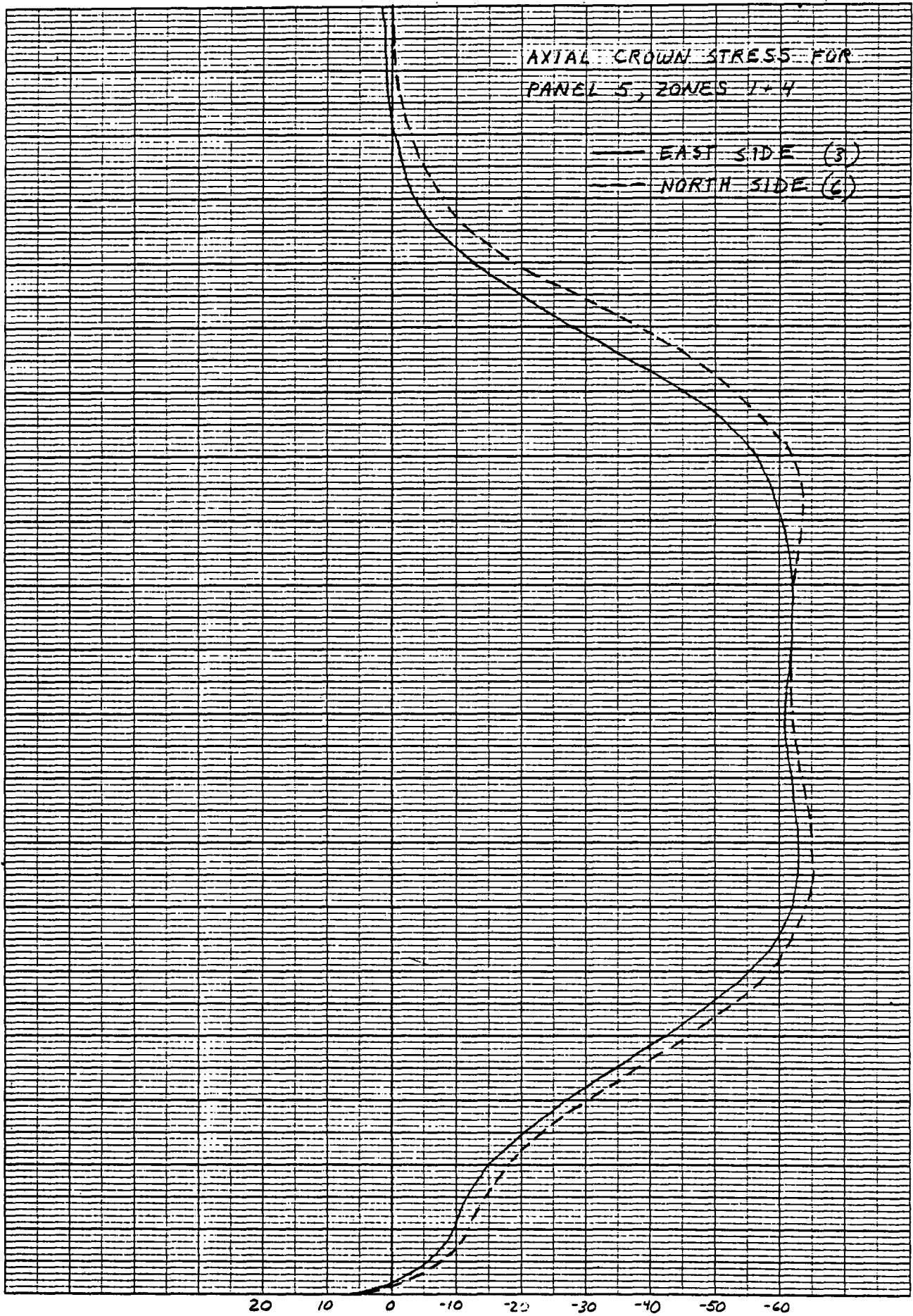
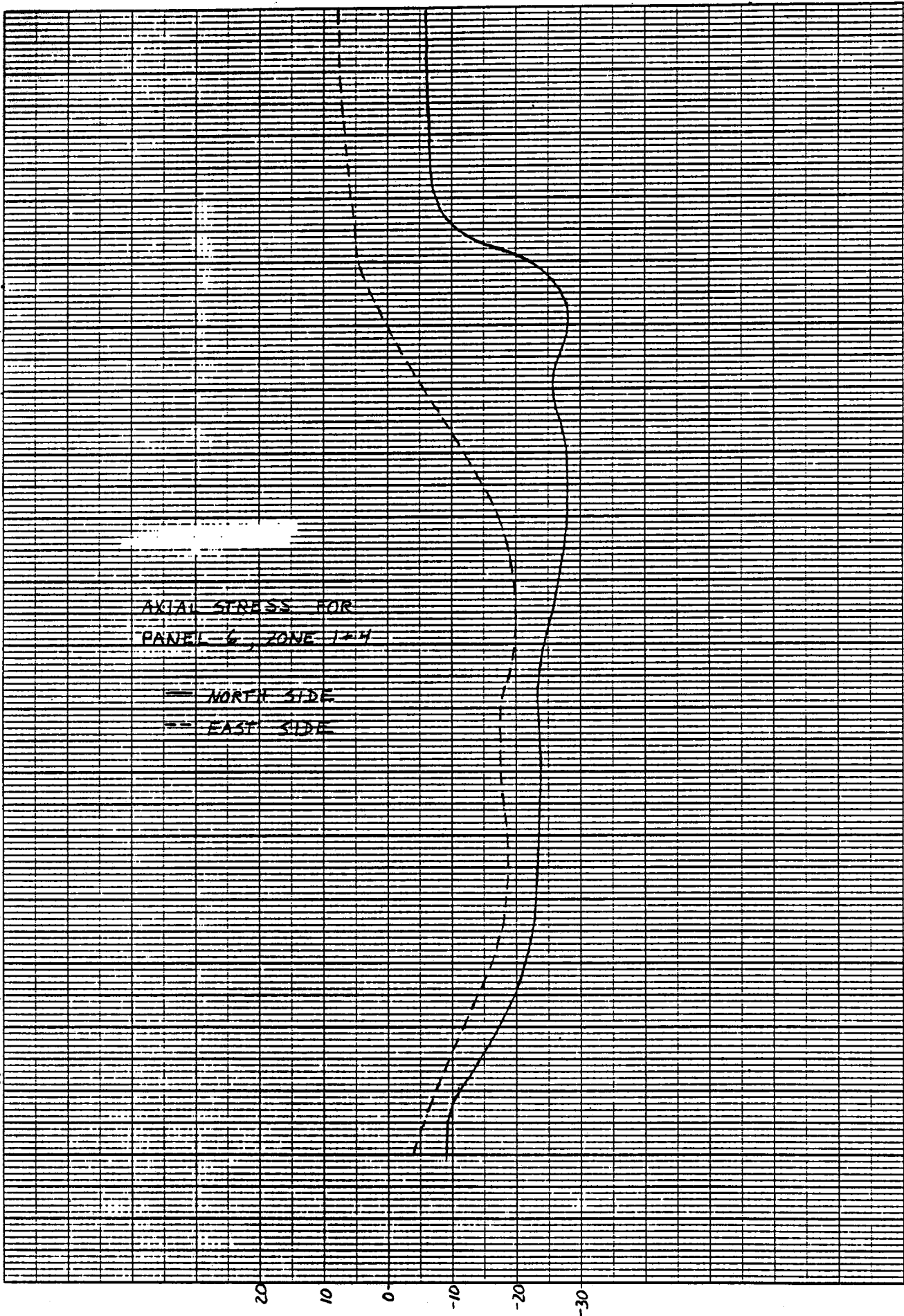


FIGURE 9b - AXIAL STRESS



AXIAL STRESS, KSI



TUBE LENGTH

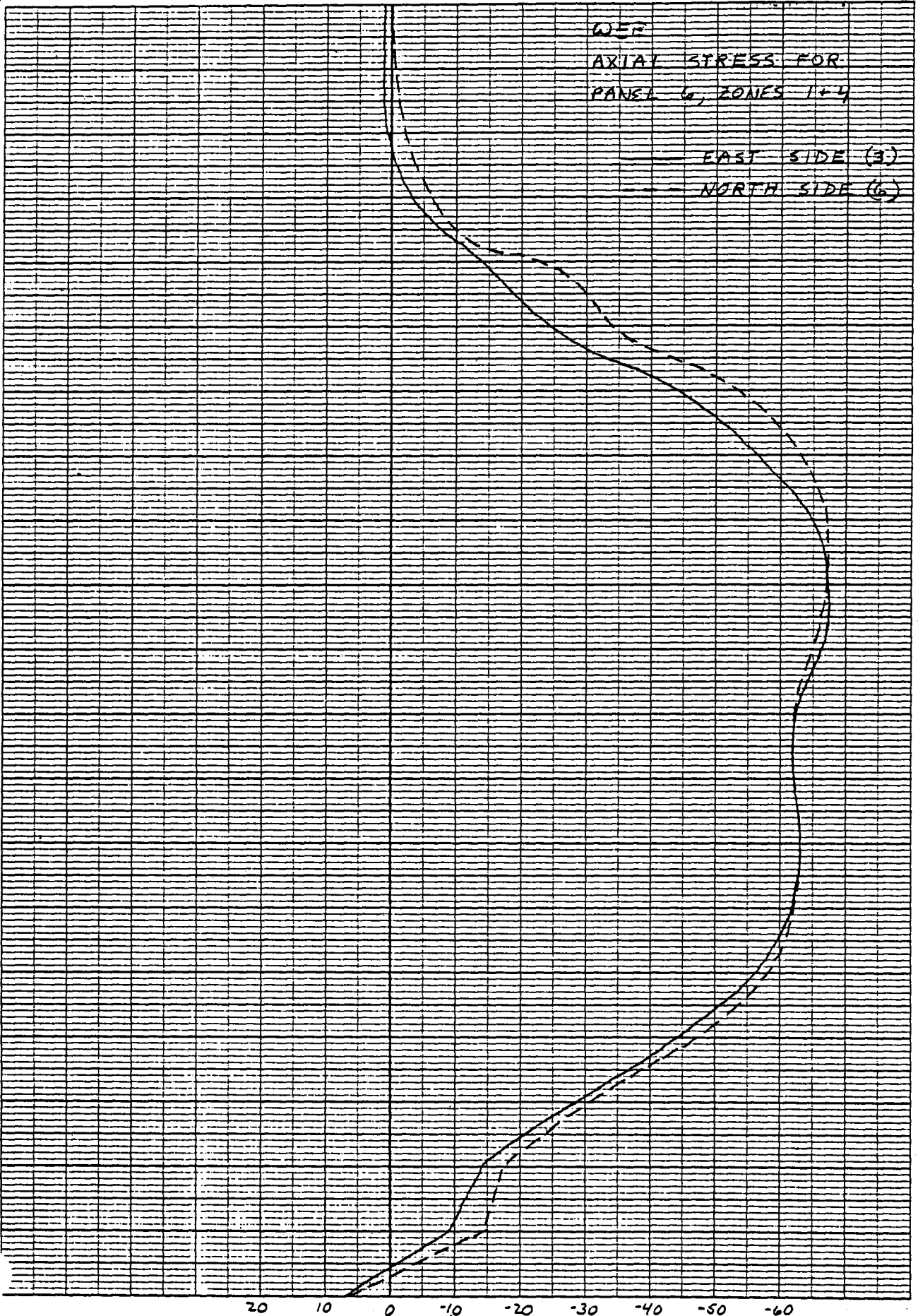
FIGURE 9C - AXIAL STRESS

AXIAL STRESS, KSI

WER  
AXIAL STRESS FOR  
PANEL 6, ZONES 1+4

— EAST SIDE (3)

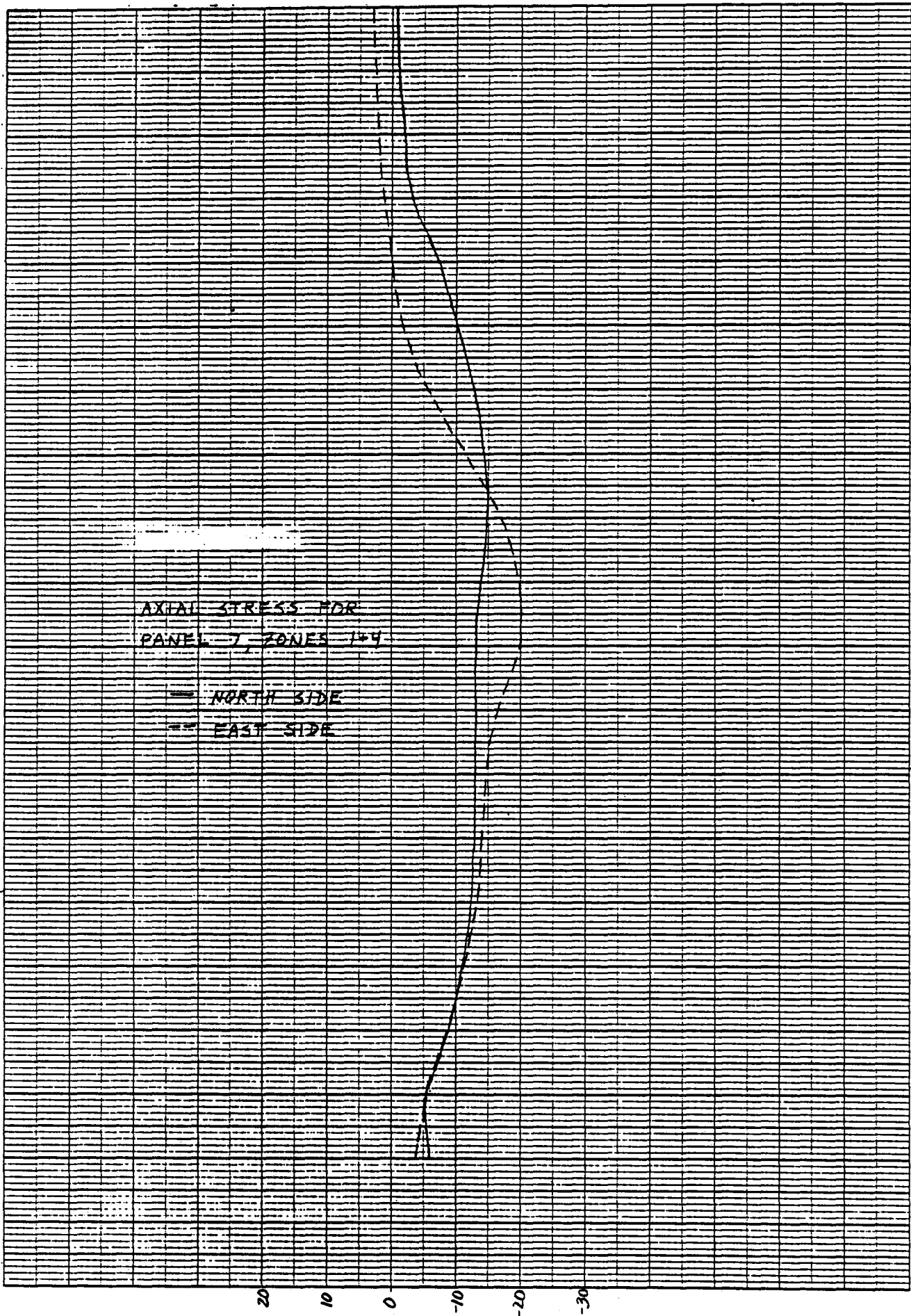
— NORTH SIDE (6)



TUBE LENGTH

20 10 0 -10 -20 -30 -40 -50 -60

AXIAL STRESS, KSI



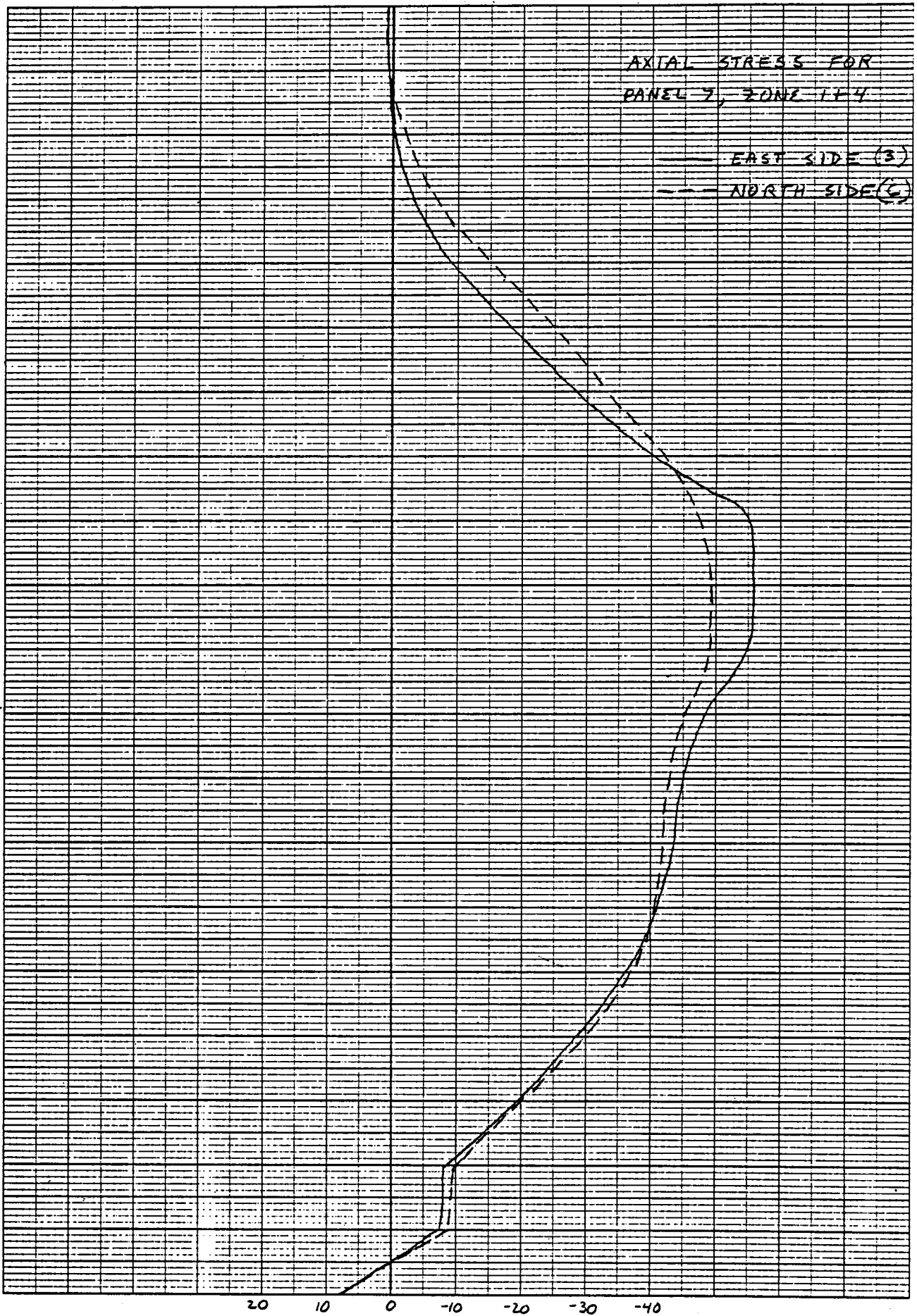
TUBE LENGTH

FIGURE 9d - AXIAL STRESS

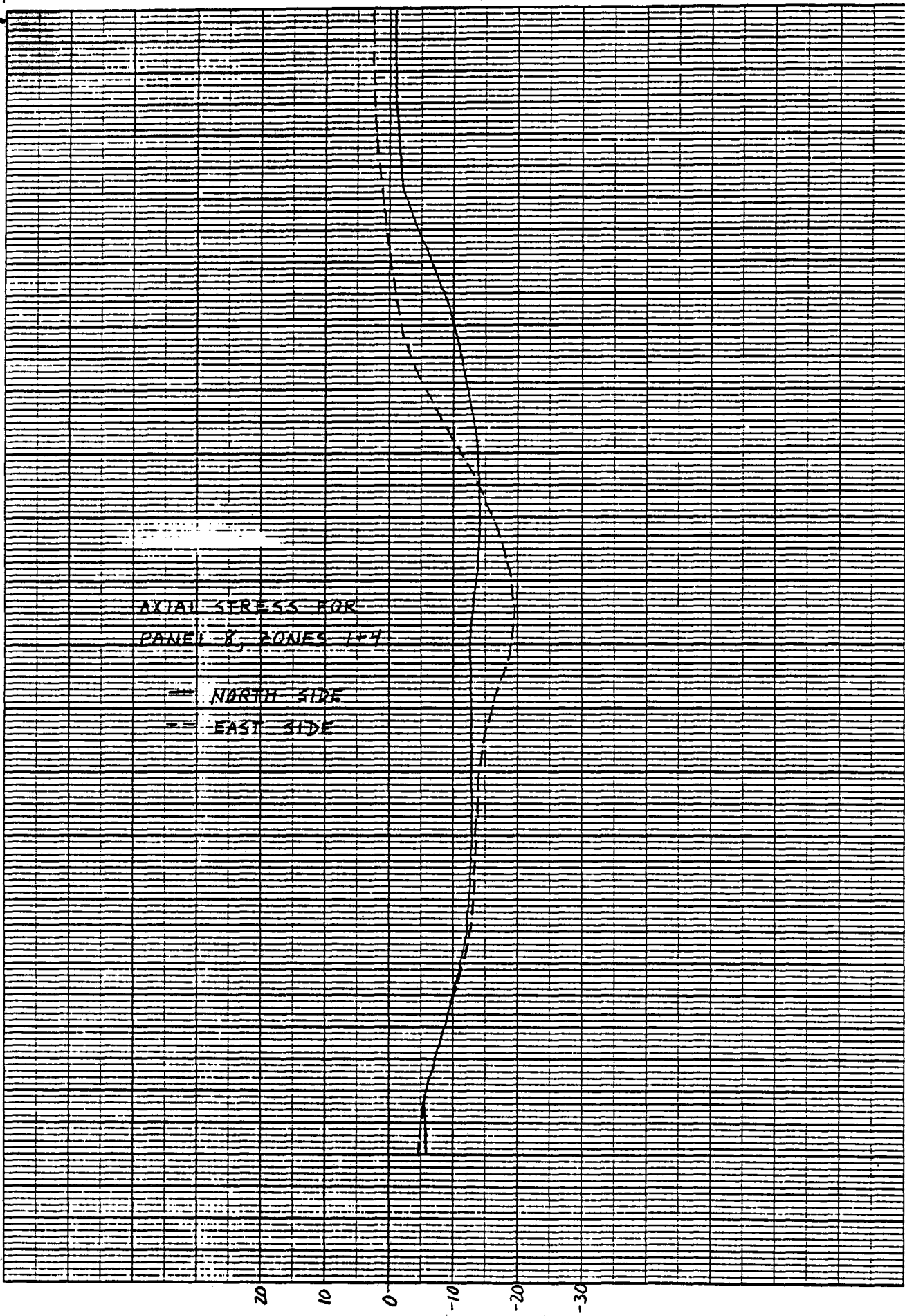
20  
 10  
 0  
 -10  
 -20  
 -30

AXIAL STRESS, KSI





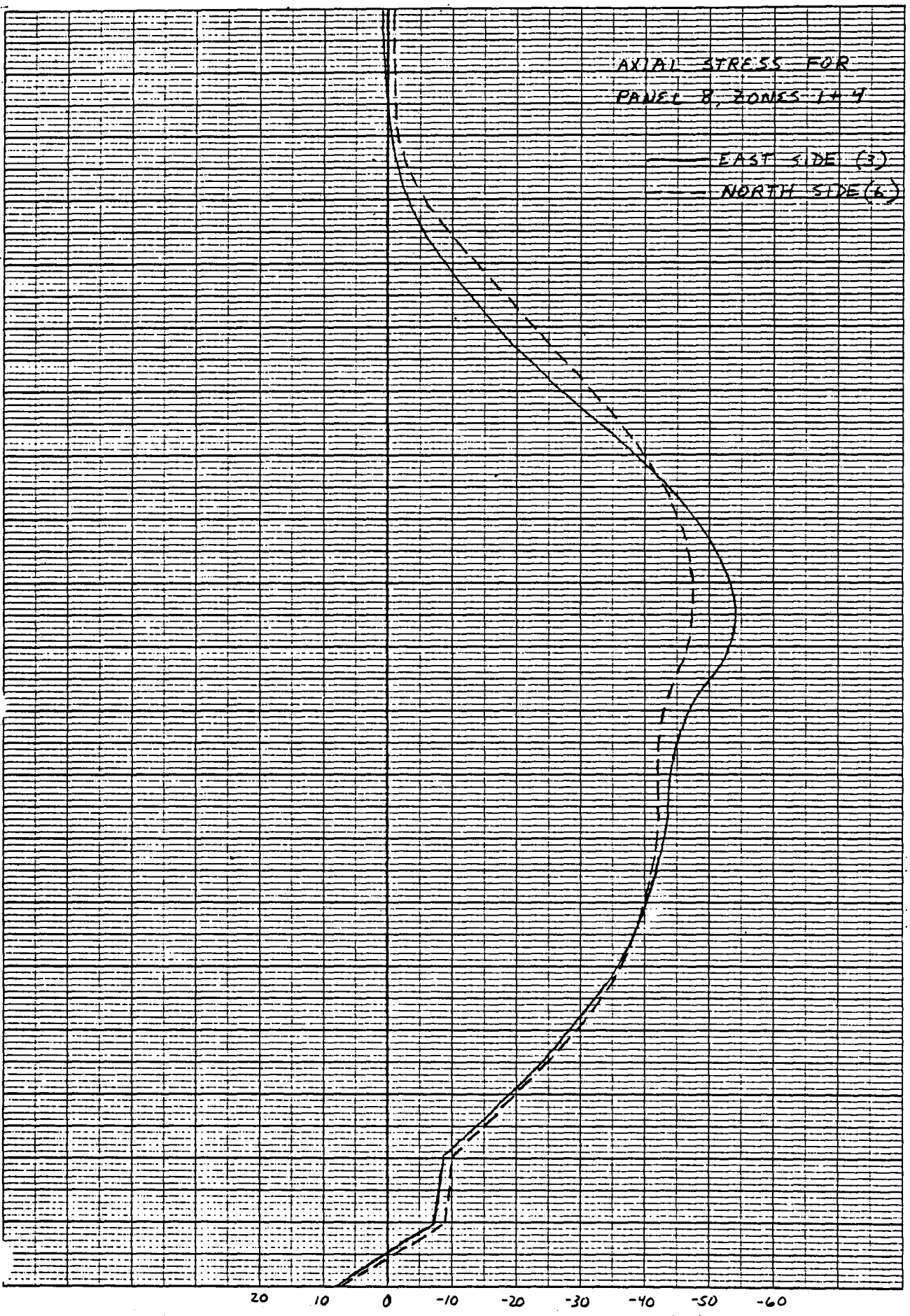
AXIAL STRESS, KSI



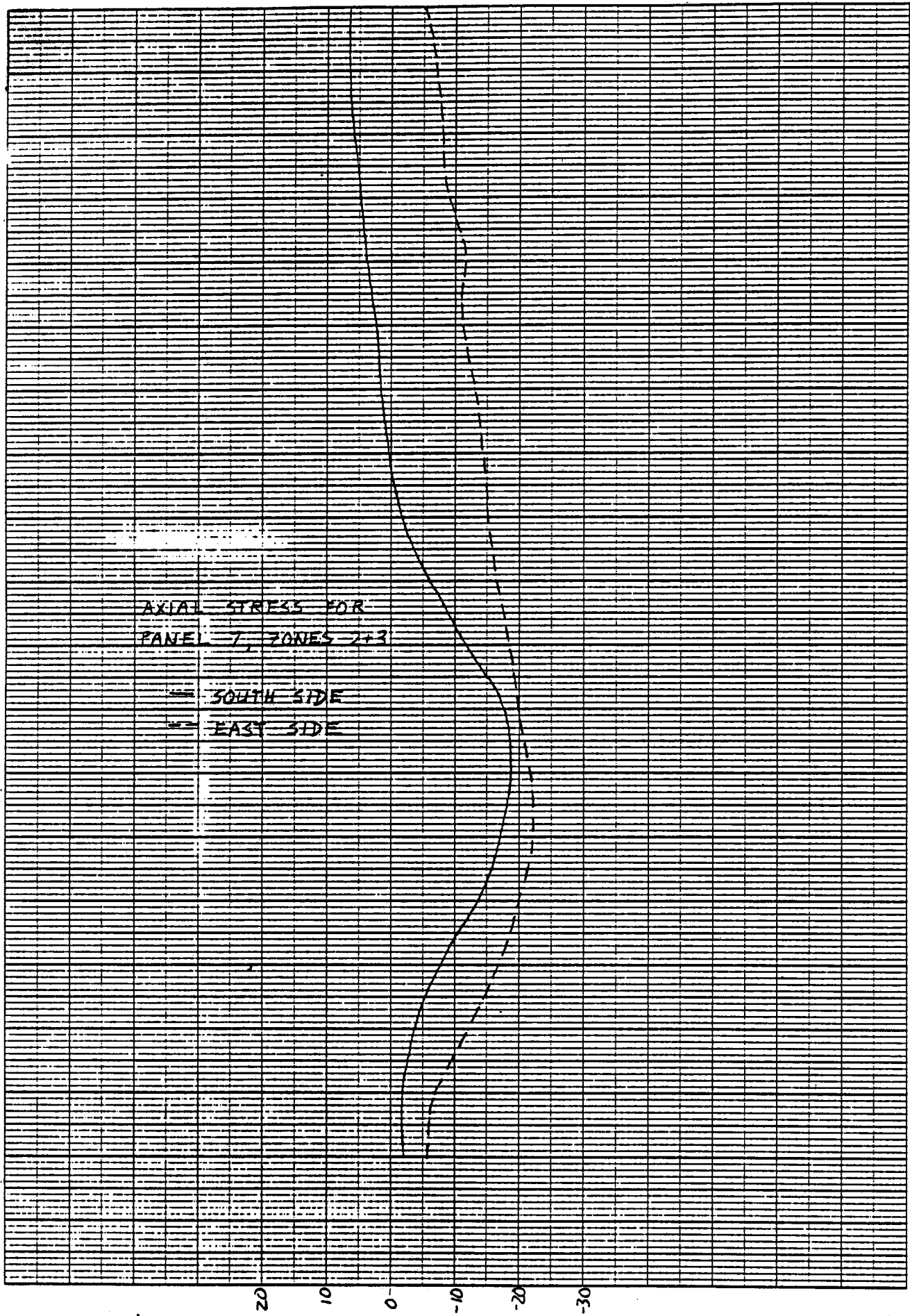
TUBE LENGTH

FIGURE 9e - AXIAL STRESS

AXIAL STRESS, KSI



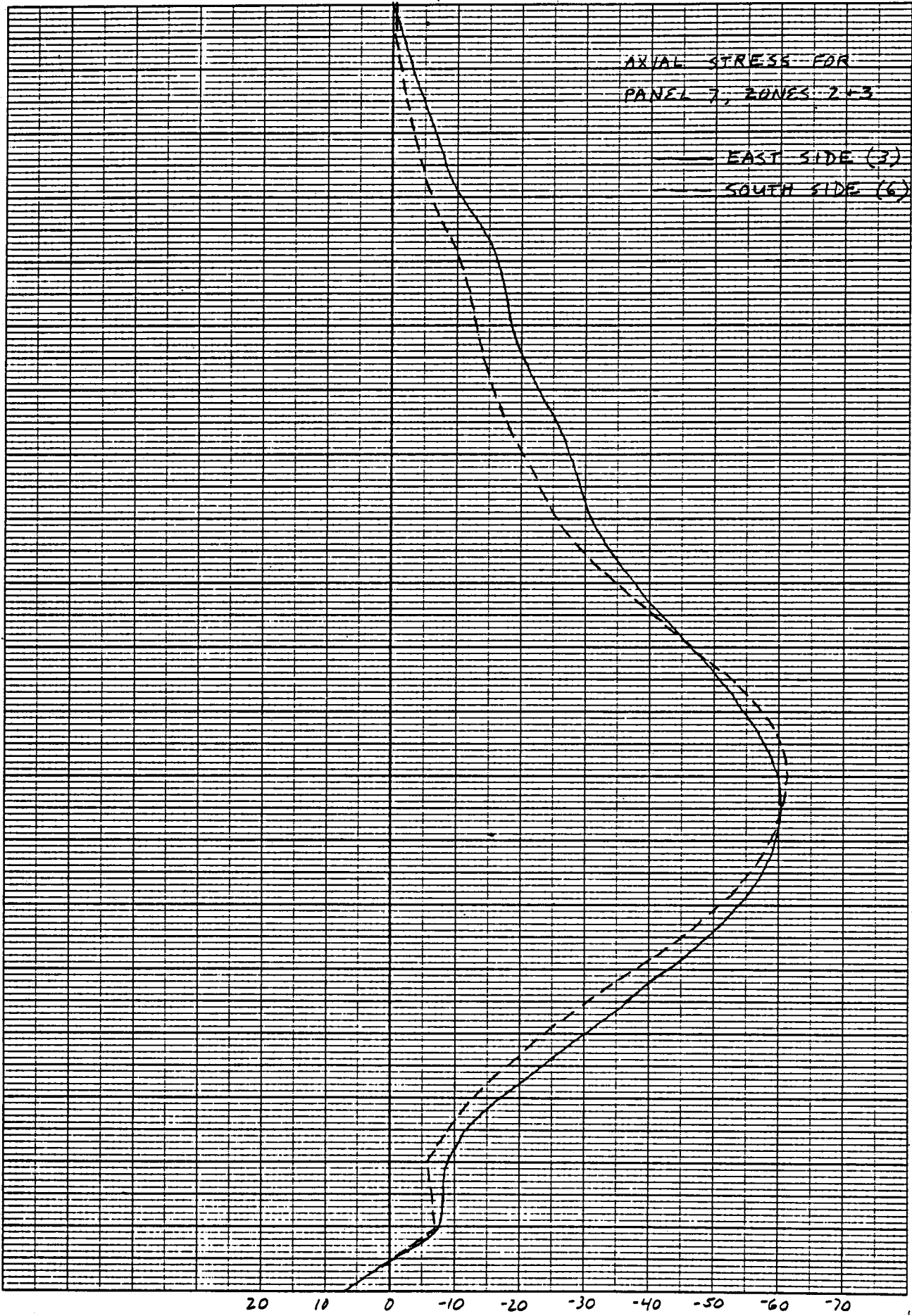
AXIAL STRESS, KSI



AXIAL STRESS, KSI

TUBE LENGTH

FIGURE 9f - AXIAL STRESS



TUBE LENGTH

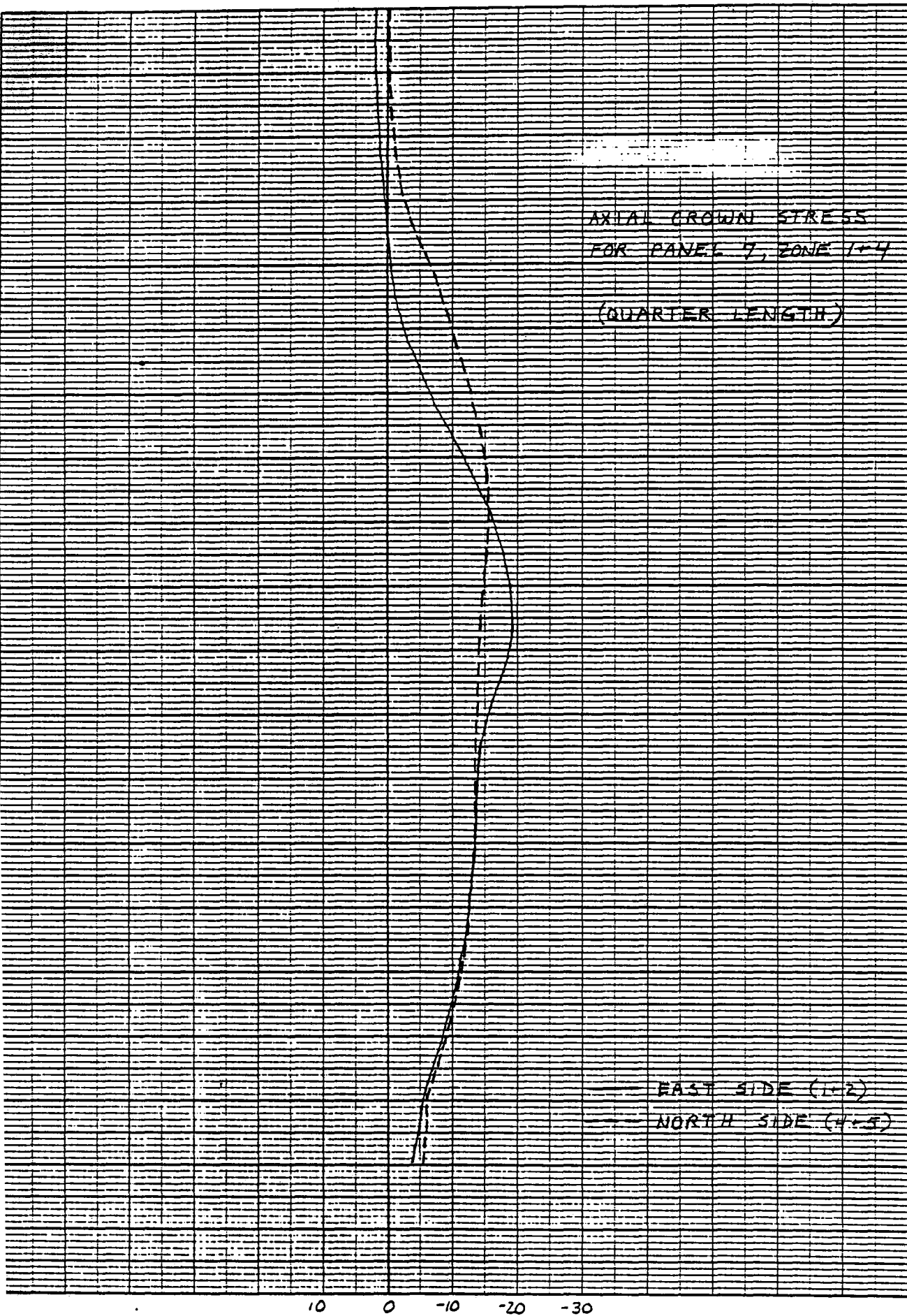
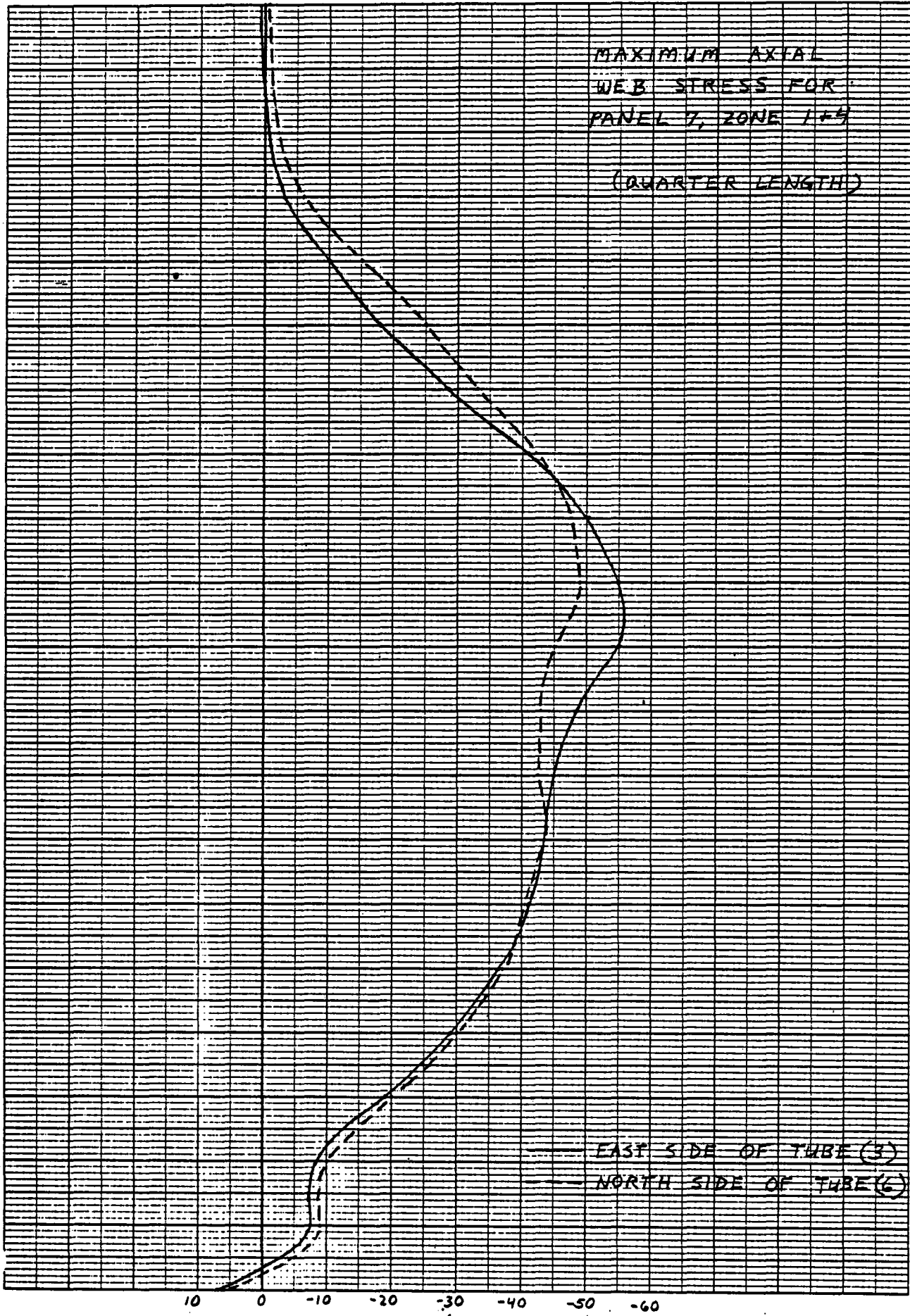


FIGURE 9g - AXIAL STRESS

MAXIMUM AXIAL  
WEB STRESS FOR  
PANEL 7, ZONE 1+4  
(QUARTER LENGTH)

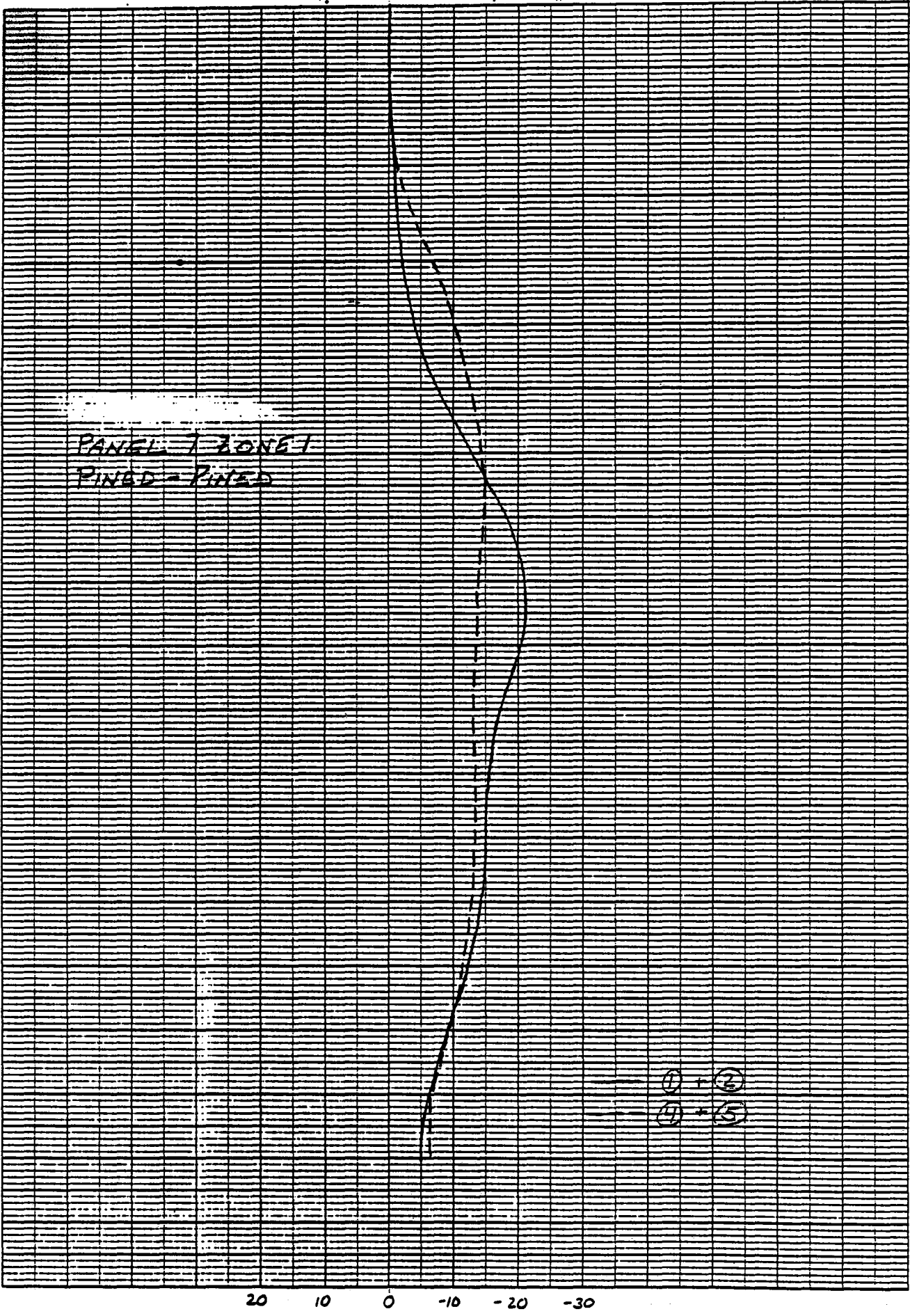


TUBE LENGTH

— EAST SIDE OF TUBE (3)  
- - - NORTH SIDE OF TUBE (6)

10 0 -10 -20 -30 -40 -50 -60

AXIAL STRESS, KSI



20 10 0 -10 -20 -30

AXIAL STRESS, KSI

TUBE LENGTH (PIN-PIN CONNECTIONS)

FIGURE 9h - AXIAL STRESS



TABLE 7

Axial Stresses, ksi (Compressive)

Panel	1	2	3	4	5	6
3	15.0	18.5	58.0	26.0	28.5	63.0
5	17.0	19.2	63.0	25.8	30.2	65.0
6	21.0	16.5	67.0	31.2	24.2	67.2
7	21.0	17.5	55.8	11.2	18.2	49.0
7*	19.5	18.2	55.2	14.0	17.0	49.0
7**	24.0	20.0	60.2	17.0	20.0	61.0
8	18.0	20.0	54.0	17.2	11.0	47.5

- (1) (2) Tube Crown, East Side (2 elements, same node) at max location.
- (3) Web, East Side at max location.
- (4) (5) Tube Crown, North (South) Side (2 elements, same node) at max location.
- (6) Web, North (South) Side at max location

\*quarter length, zone 1 and 4  
 \*\*zone 2 and 3

TABLE 8

Panel	$Q_{max}$ (per side)	$Q_{max}$ (2 sides)	$Q_t$ $Q_t$ $\times 10^3$	$\Delta Q$ max	$Q_t$ $Q_T$ $\times 10^3$	$\sigma_{max}$ Tube	$\sigma_{max}$ Web	Lateral $\delta$ (in)	$\frac{\delta}{\Delta Q_T}$
3	173	300	5.9	50	1.6	28.5	63	11.4	7.1
5	191	310	7.8	70	1.4	30.2	65	4.4	3.1
6	217	335	8.2	100	1.1	31.2	67.2	4.1	3.7
7	220	370	7.8	70	.6	21.0	55.8	6.6	11.0
8	191	295	5.9	85	.1	20.0	54.0	6.4	64.0
7	192	345	5.7	40	1.2	24.0	61.0	2.9	2.4

NOTE: This table was assembled for the purpose of determining correlation only; therefore, units are not shown.

## 9.0 Discussion of Results

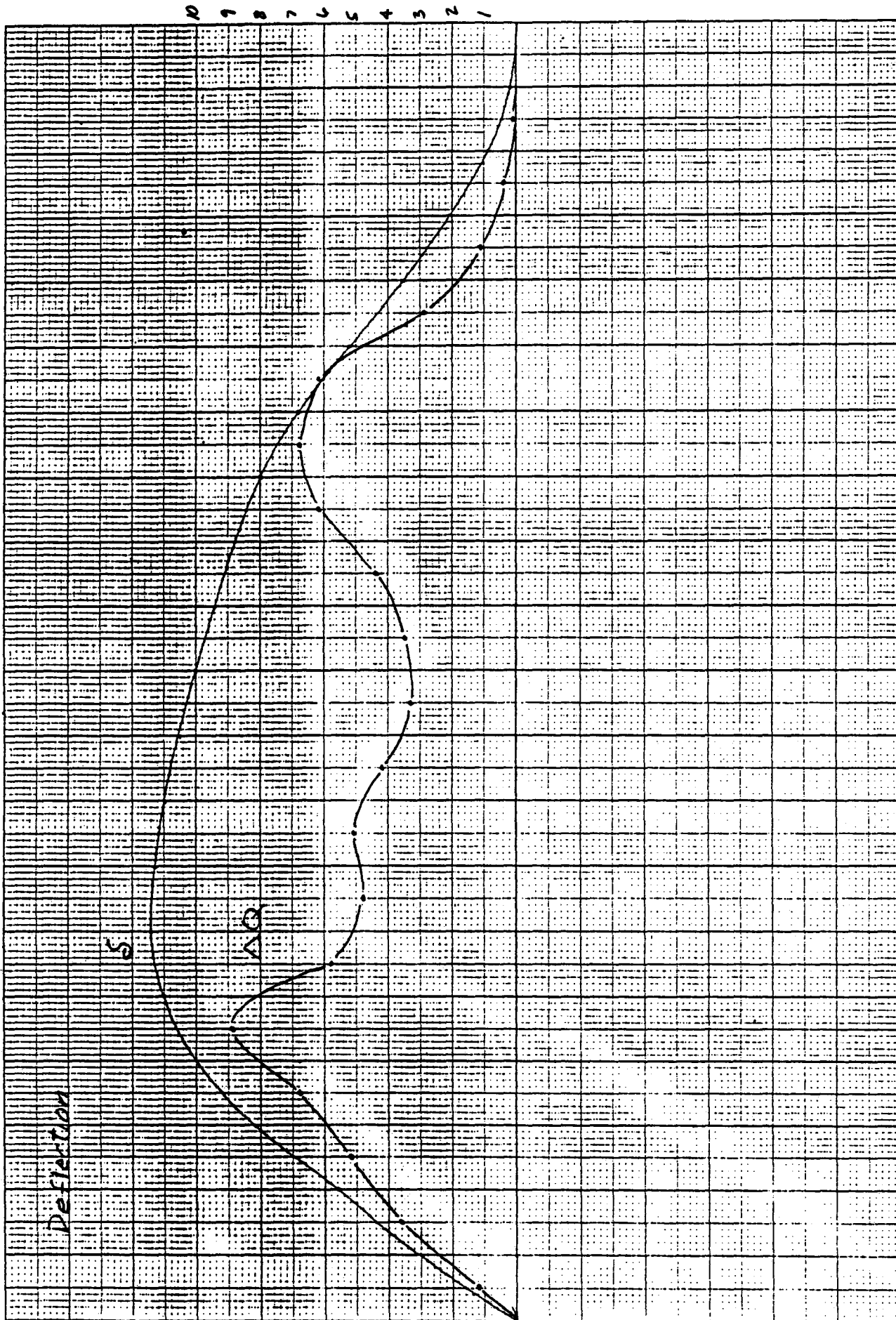
Interpreting the data is difficult, but Table 8 shows 1) Panel 7 has the highest heat flux value, from one side and from 2 sides; 2) Panel 6 has the highest imbalance at the location of maximum heat flux; 3) Panel 3 has the highest deflection; and 4) Panel 6 has the highest stress (tube and web). Further comparisons of heat flux data to axial stress levels do not indicate any predictable pattern. For example, Panel 6 with the highest heat flux has the second lowest stresses and Panel 8 with the second highest heat imbalance has the lowest stress.

### 9.1 Lateral Deflection

One sided heating of a tube causes the maximum lateral deflection of 21.5 inches (Panel 7, peak heating from North); 11.5 inches (Panel 3) is the maximum for two sided heating; maximum deflection for Panels 7 and 8 is about 6.5 inches; the maximum for Panels 5 and 6 is about 4.3" and finally Panel 7 Zone 2 is 2.9". The lateral deflection curves are presented in Figures 7; this data is repeated in Figures 10a through 10g with the heat flux imbalance curve superimposed on the same graph.

Neither maximum lateral deflection nor the deflection curve of two sided heating is easily predictable from the heat flux data given. One would expect one-sided heating to produce more bowing than two-sided heating because of the greater heat flux imbalance. However, Table 8 shows that deflection and total heat flux imbalance do not correlate.

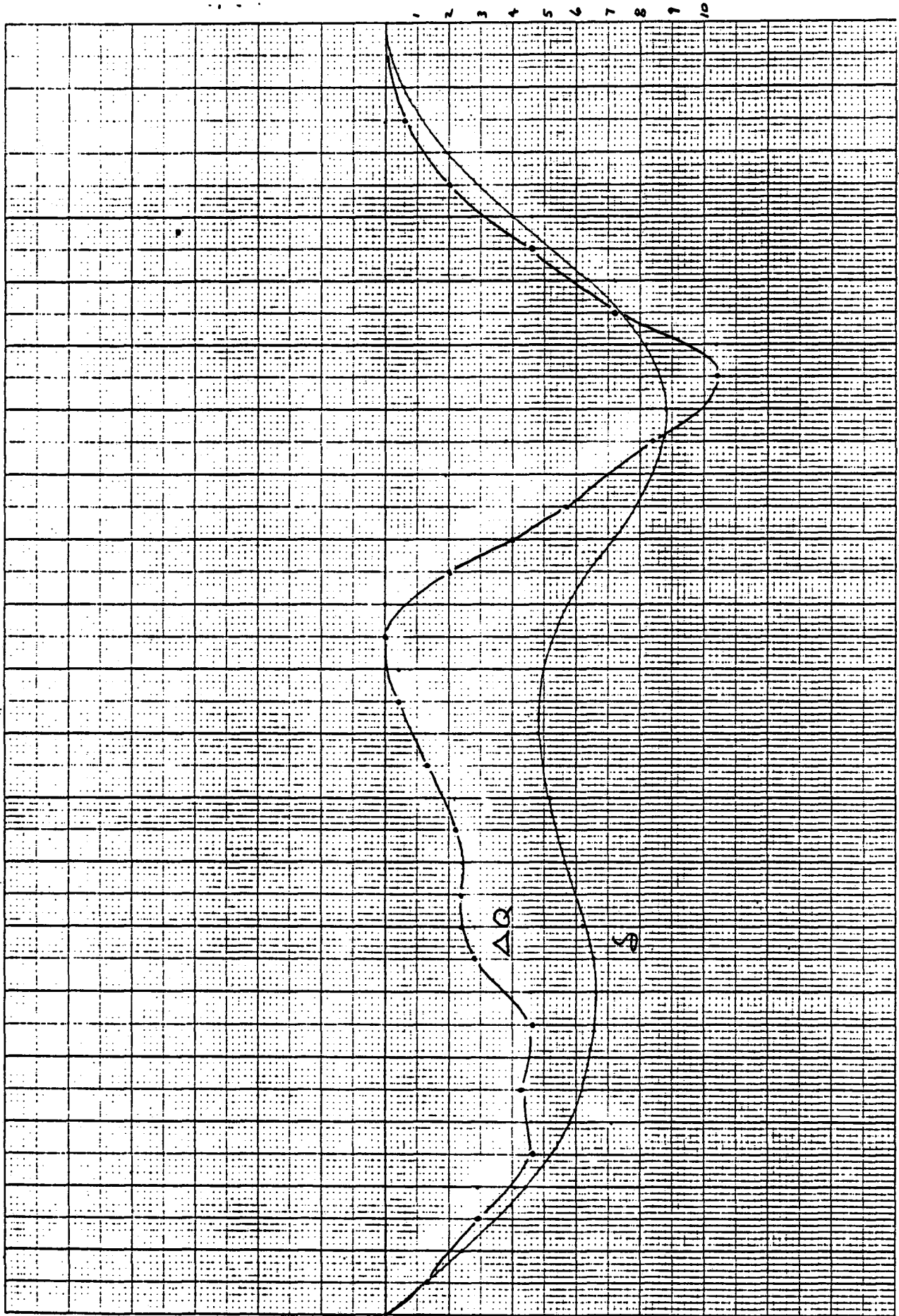
$\Delta Q (x 10,000 \text{ BTU/HR-FT}^2)$



TUBE LENGTH (PANEL 3, ZONE 1 - PEAK HEATING)

FIGURE 10a - HEAT FLUX IMBALANCE, DEFLECTION

$\Delta Q$  (X 10,000 BTU/HR-FT<sup>2</sup>)

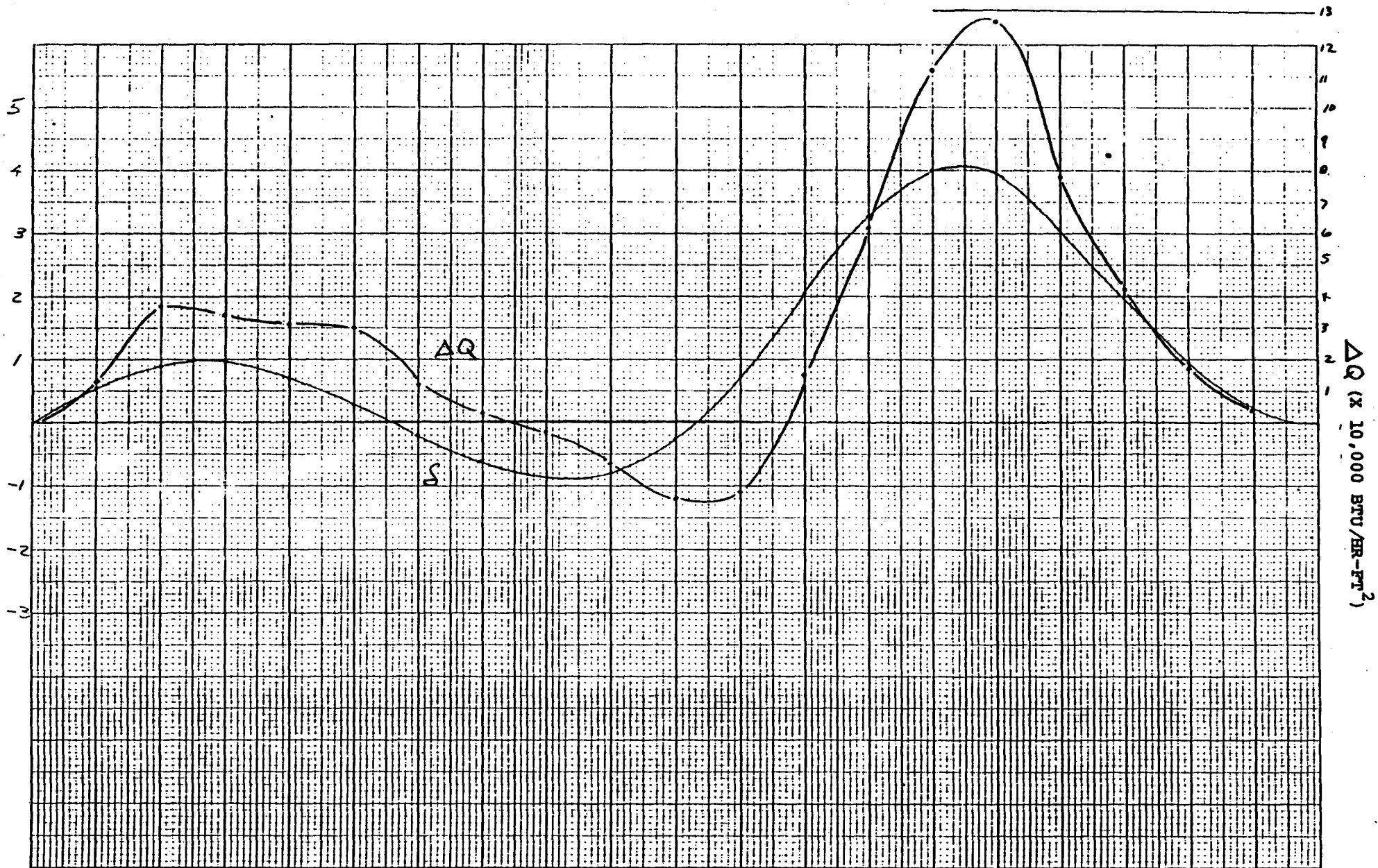


TUBE LENGTH (PANEL 5, ZONE 1 - PEAK HEATING)

FIGURE 10b - HEAT FLUX IMBALANCE, DEFLECTION

LATERAL DEFLECTION, INCHES

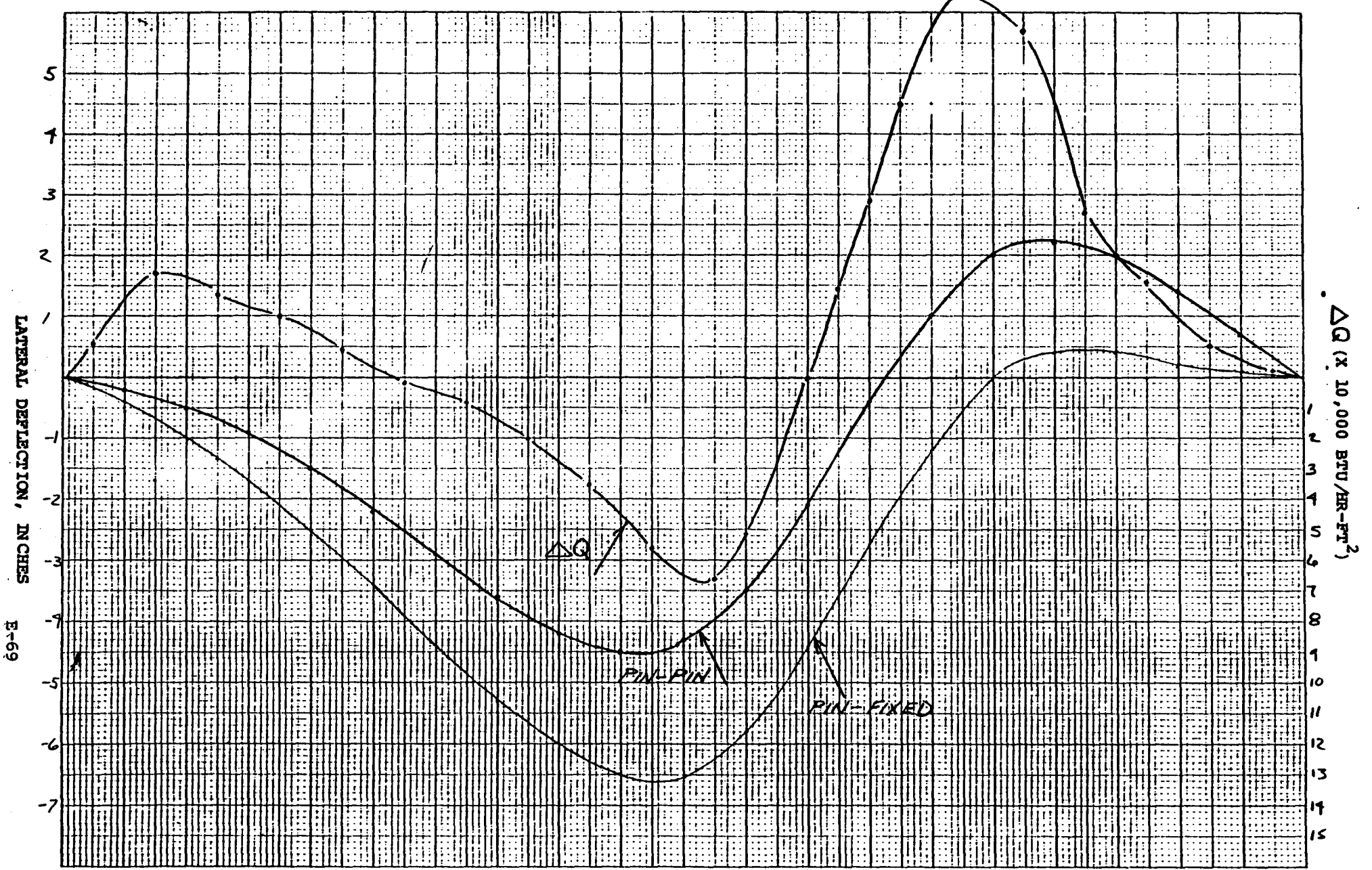
E-68  
LATERAL DEFLECTION, INCHES



TUBE LENGTH (PANEL 6, ZONE 1 - PEAK HEATING)

FIGURE 10c - HEAT FLUX IMBALANCE, DEFLECTION

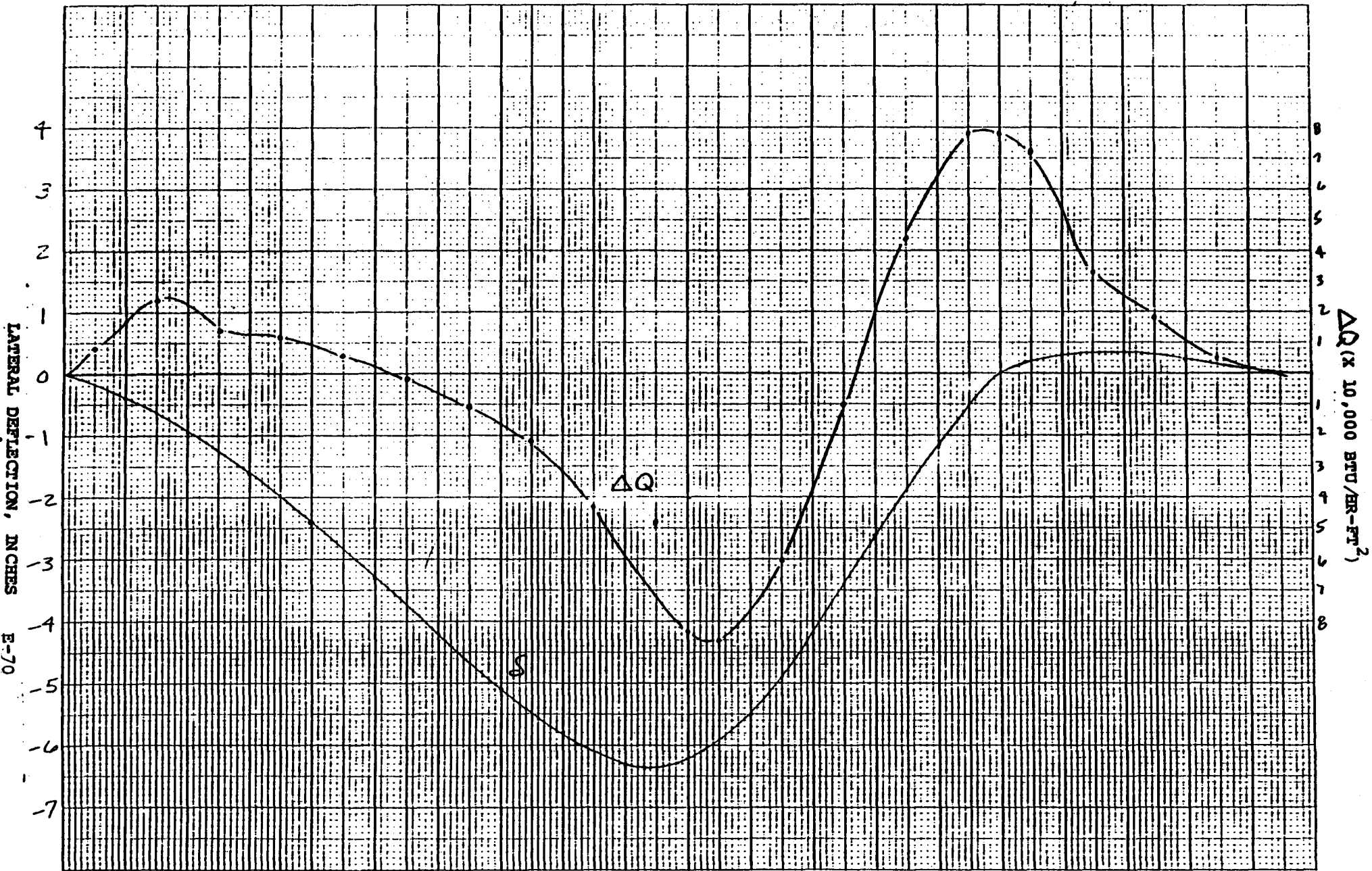
$\Delta Q$  (x 10,000 BTU/HR-FT<sup>2</sup>)



TUBE LENGTH (PANEL 7, ZONE 1 - PEAK HEATING)

FIGURE 10d - HEAT FLUX IMBALANCE, DEFLECTION

E-69

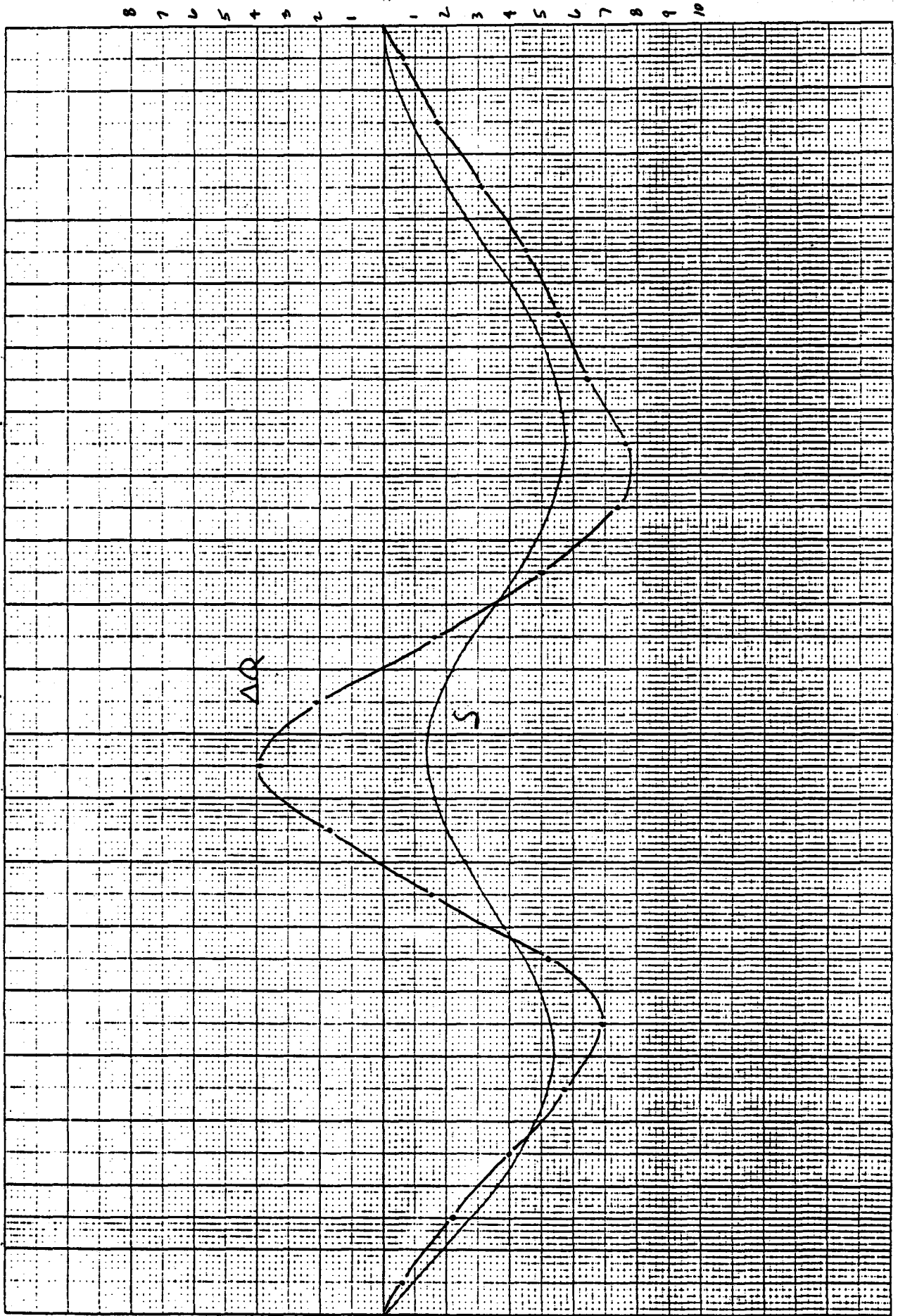


TUBE LENGTH (PANEL 8, ZONE 1 - PEAK HEATING)

FIGURE 10e - HEAT FLUX IMBALANCE, DEFLECTION



$\Delta Q$  (X 10,000 BTU/HR-FT<sup>2</sup>)

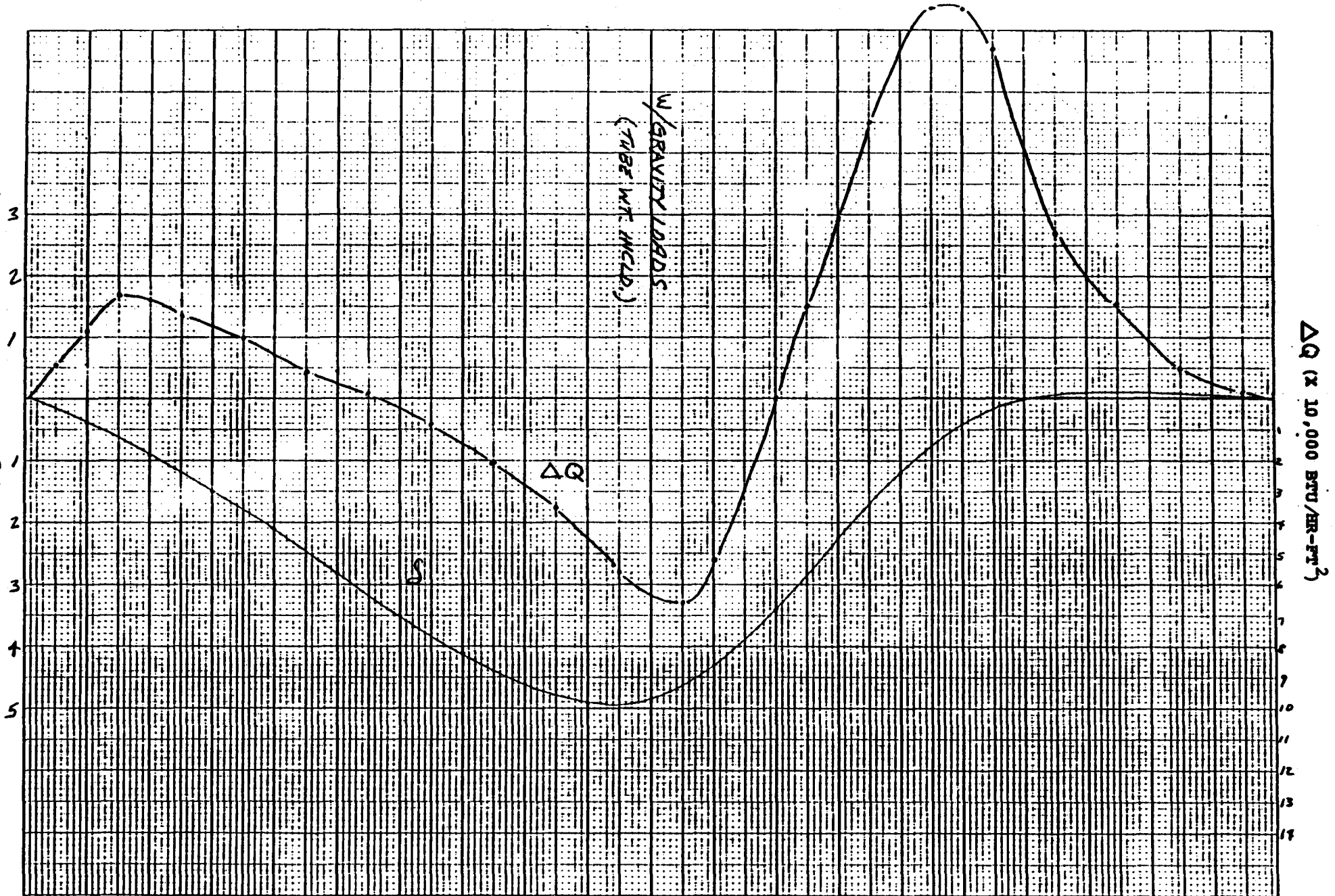


TUBE LENGTH (PANEL 7, ZONE 2 - PEAK HEATING)

FIGURE 10E - HEAT FLUX IMBALANCE, DEFLECTION

LATERAL DEFLECTION, INCHES

LATERAL DEFLECTION, X 10<sup>-1</sup> INCHES  
E-72



TUBE LENGTH, L/4 (PANEL 7, ZONE 1 - PEAK HEATING)

FIGURE 10g - HEAT FLUX IMBALANCE, DEFLECTION

At first glance, the deflection curves generated using FESAP did not exhibit any resemblance to the heating curves responsible for their shape. In an attempt to explain the dissimilarity among the deflection curves, the heat flux imbalance ( $\Delta Q$ ) was plotted as a function of tube length and superimposed on the deflection curve for each of the panels. The results (Figure 10) show a high degree of similarity. Looking at each case independent of the others, the shape of tube bowing can be attributed to the  $\Delta Q$  curve with the deflection curve being smoother than the  $\Delta Q$  curve. This is particularly noticeable in Figure 10a (Panel 3) where the "drop-off" in  $\Delta Q$  might suggest reverse bowing in the deflection curve although it does not occur.

In Figure 10b (Panel 5), the "drop-off" in  $\Delta Q$  is even greater than for Panel 3 and reverse bending does occur. The decrease in  $\Delta Q$  should cause a decrease in lateral deflection, which it does (11.4 vs 4.4). Figure 10c (Panel 6) continues the trend of reduced total  $\Delta Q$  plus has a reversal of  $\Delta Q$  from one side of the tube to the other. One might expect an appreciable decrease in lateral deflection, but it does not occur (4.4" vs 4.1"). The large local  $\Delta Q$ , which corresponds in location to the maximum deflection, could explain this.

Comparing Panel 7 to Panel 6 (Figures 10d and 10c), all correlations fall to pieces. Even though the  $\Delta Q$  curves have similar shapes and one can argue that the deflection curves follow these shapes, there is no comparison between the two deflection curves, magnitude or shape. On the other hand, Panels 7 and 8 compare very well. Panel 7, Zone 2 is somewhat of a unique curve, so comparisons are not possible. It is surprising that the shapes of the two curves are so similar.

Thus, we can conclude that the deflection curve, resulting from two sided heating closely resembles the heat flux imbalance curve but the relationship is very complex. The total heat flux imbalance curve of the north cavity Panel 3 was assumed to yield maximum lateral deflection; and it did, but entirely out of proportion to what could have been predicted.

The effects of using a combination of pinned and fixed connections for the analyses is obvious for the deflection curve of Panel 7 (Figure 10d). Releasing the fixed end reduces the maximum deflection and permits the curve to more closely follow the heat imbalance curve. Neither connection truly represents the actual end conditions, yet the error appears to be significant. In reality, the header-tube connection and header lateral support probably cause a condition closer to fixed-fixed.

The Panel 7, Zone 1 tube length was reduced to a quarter length and analyzed with the same temperature distribution, tube weight, and end load. Thus, the axial gradient was compressed to the one-quarter length. The shape of the deflection curve is unchanged but axial deflection decreases as expected (Figure 10g vs 10d). Stresses did not differ by much suggesting that the tube weight and end load has little impact on lateral deflection of a panel. The lack of convergence of stresses also remained upon reduction of model length.

## 9.2 Axial Stress

The axial stress in the tube crown results from the through-thickness gradient and the circumferential gradient. The through-tube wall gradient accounts for part of the total axial thermal stress at the tube crown but bowing of the tube does not relieve this stress. The circumferential gradient has an equivalent thermal moment across the tube cross section that causes

the bowing and relieves the stress. Thus it is reasonable to assume that the heat flux or heat flux imbalance causes the bowing. Based on the large amount of bowing as demonstrated by the deflection curves, considerable relaxation of the axial stresses would be expected.

In comparing the tube stress curves (Figure 9) to heat flux curves (Figure 4) one notices a lack of consistency, i.e., the numerous peaks and troughs characterizing the heat flux curves fail to appear in any of the corresponding stress curves. The crown stress hits a plateau or levels off; rapid increases or decreases are virtually non-existent. This suggests that much of the stress is relieved by the tube bowing and the remaining stress is a function of some through thickness gradient (Note, the through thickness gradient varies along the length.). For example, the maximum crown stress of Panel 7, Zone 1, is 21 ksi instead of 31.5 ksi for a previous analysis that assumes generalized plane strain.

No increase in tube stress was noted due to use of a fixed connection at the top, therefore, boundary conditions proved satisfactory for the analysis.

### Stress/Flux Correlations

The data collected in Table 8 contains maximum values of heat flux, tube and web stress, and lateral deflection. A careful review of Table 8 leads to the conclusion that there is no direct correlation between the maximum axial stress and the maximum heat flux or heat flux imbalance. The fact that the curve of the crown stress does not follow any pattern of the heat input curves suggests that stress is a function of the total heating, heating at any level along a tube, and the distribution of the heating. Therefore other possible correlations were calculated.

Various heat flux data were determined and are presented in Table 9. The heat flux ( $Q_N$  and  $Q_E$ ) represents area under the curve for the north and east sides, respectively. The heat flux was determined by summing the values at each of the 41 elevations (nodal layers). The total heat flux imbalance ( $\Delta Q$ ) is the difference between the two total heat fluxes ( $Q_E$  and  $Q_N$ ); it is the difference (area) between the two heat flux curves. Ratios between total heat flux and heat flux imbalance were then determined.

The significant plots arising from the data in Table 9 are Figures 11 through 15. In Figure 11, maximum crown stress is plotted against heat flux imbalance divided by the total heat from either side and then their sum. The curves are not necessarily what one might expect; however the uniformity of the curves confirm that

maximum axial tube stress is a function of the entire heating pattern and not the maximum heating at a single point. The high degree of similarity suggests that the omission of the total heat flux parameter would yield similar plots (Figures 12 and 13). Since axial crown stress consists of two components, one of which is not affected by bowing, it seems reasonable that the curve might peak at some value of total heat flux imbalance. The higher stress values above this maximum heat imbalance point presumably occur when the through-thickness gradient controls during high local heat flux conditions.

Maximum web stresses range in magnitude from 2.2 to 2.7 times respective tube crown stress values. The web stresses are not relieved by bowing; in fact, bowing may increase the web stresses. The web stresses are not a function of heat flux imbalance. Unlike the crown stress curves, web stress curves are sensitive to the total heat flux curves and the local heat flux condition. The web stress curves of Figure 13 are very similar differing in magnitude by only 6 KSI, yet the corresponding flux curves in Figure 4e show dissimilar curves with a significant  $\Delta Q$ . The total heat flux applied to any level of a tube could then be a reasonable indicator of the magnitude of web stress present in a membrane wall panel.



<b>Babcock &amp; Wilcox</b> <b>ENGINEERING CALCULATIONS</b>	REFERENCE NO.	SHEET NO.
	PREPARED BY:	OF
SUBJECT: <i>HEAT FLUX CHARACTERISTICS</i> *	CHECKED BY:	DATE:
		REVISION:

PANEL	ZONE	$Q_E$	$Q_N$	$\Delta Q$	MAX. AXIAL CROWN STRESS
3	1,4	2130	3739	1609	28 KSI
5	1,4	3242	4597	1355	30
6	1,4	3559	4683	1124	31
7	1,4	3614	4226	612	21
8	1,4	2915	2970	55	20
7	2,3	3486	$Q_S = 2250$	1236	24

PANEL	$\frac{\Delta Q}{Q_1}$	$\frac{\Delta Q}{Q_2}$	$\frac{\Delta Q}{Q_1 + Q_2}$
3	0.76	0.43	0.27
5	0.42	0.29	0.17
6	0.32	0.24	0.14
7	0.17	0.14	0.08
8	0.02	0.02	0.01
7	0.55	0.35	0.22

\* VALUES DERIVED FROM CHARTS IN APPENDIX A.

TABLE 9 - HEAT FLUX CHARACTERISTICS

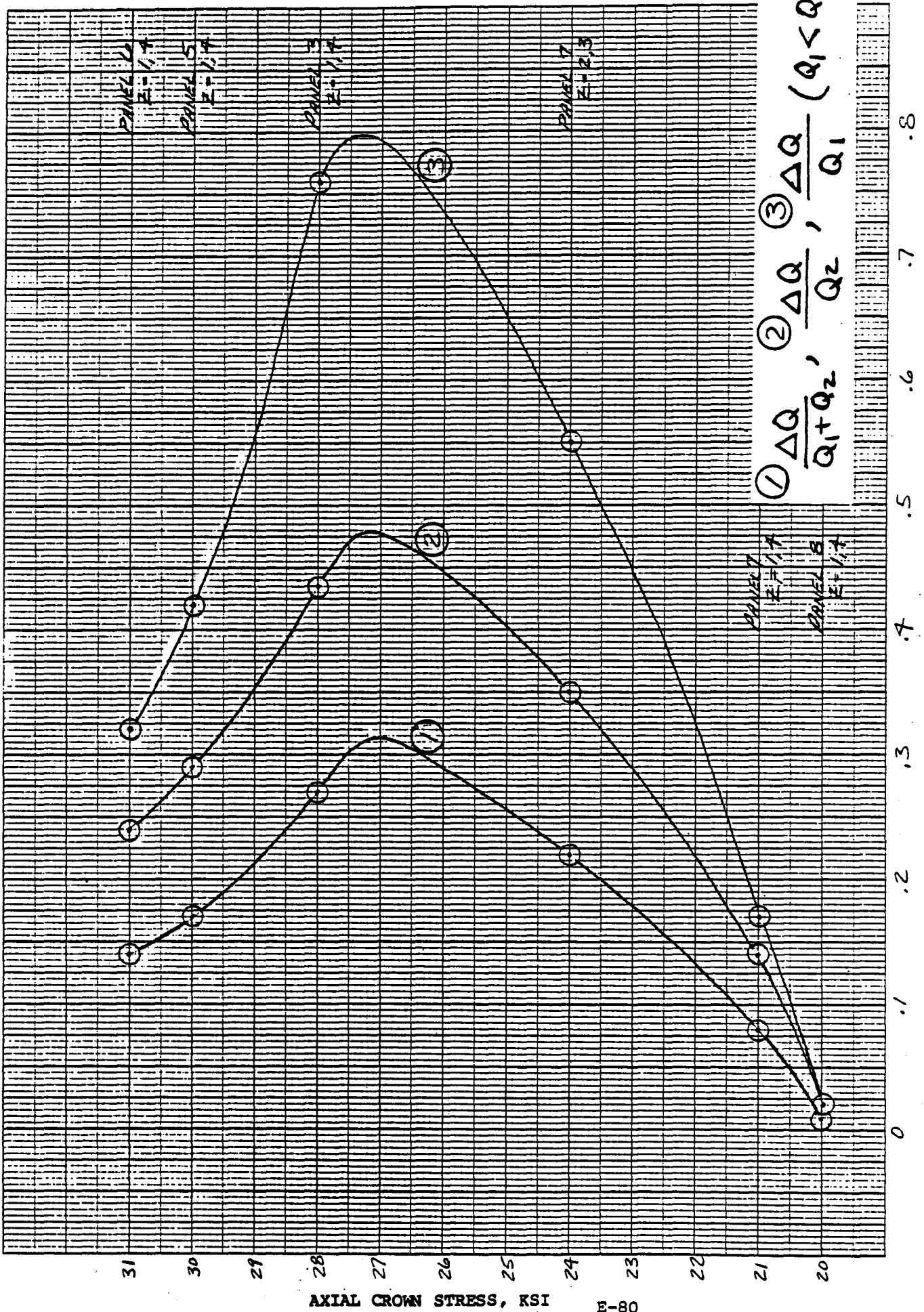
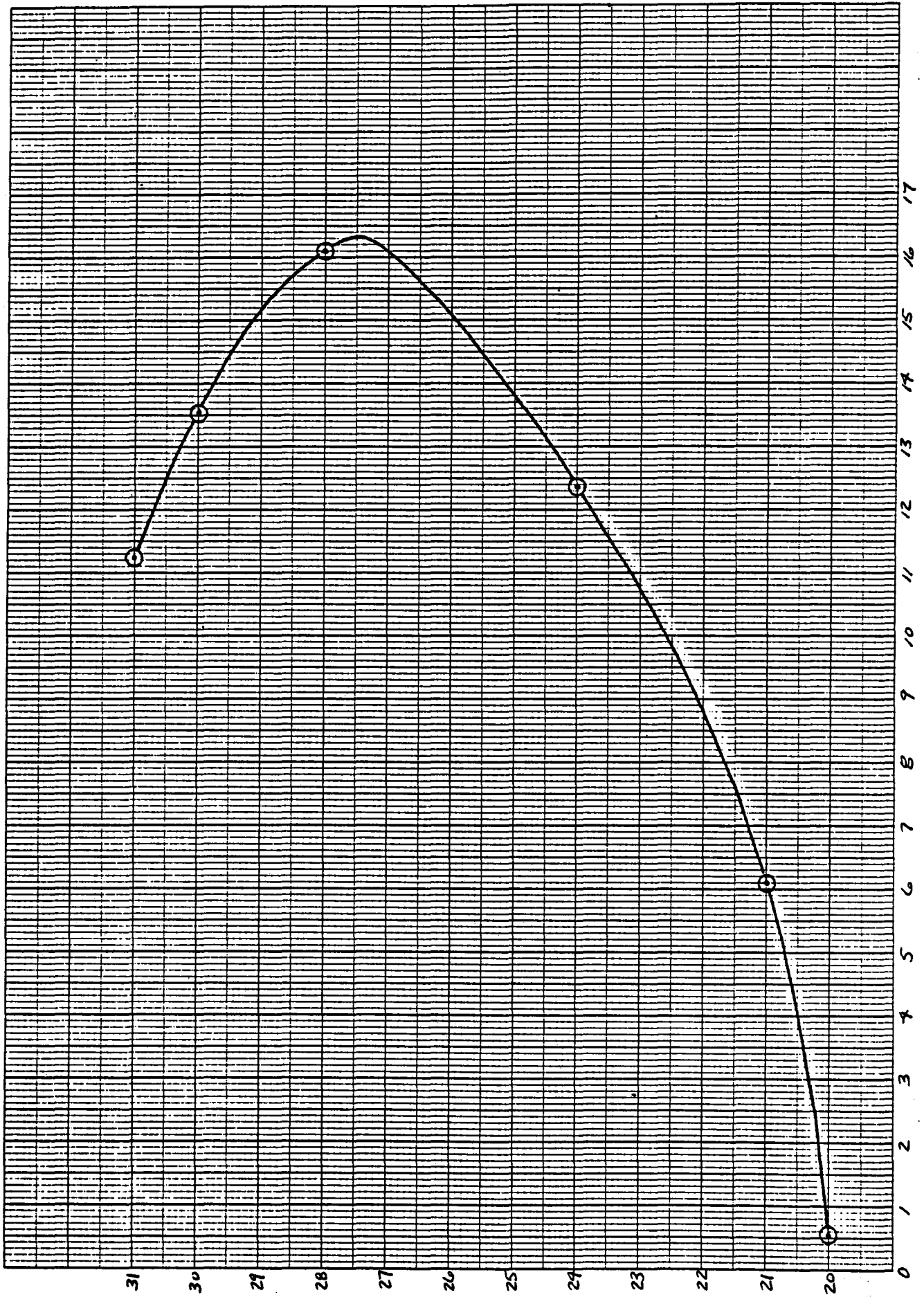


FIGURE 1

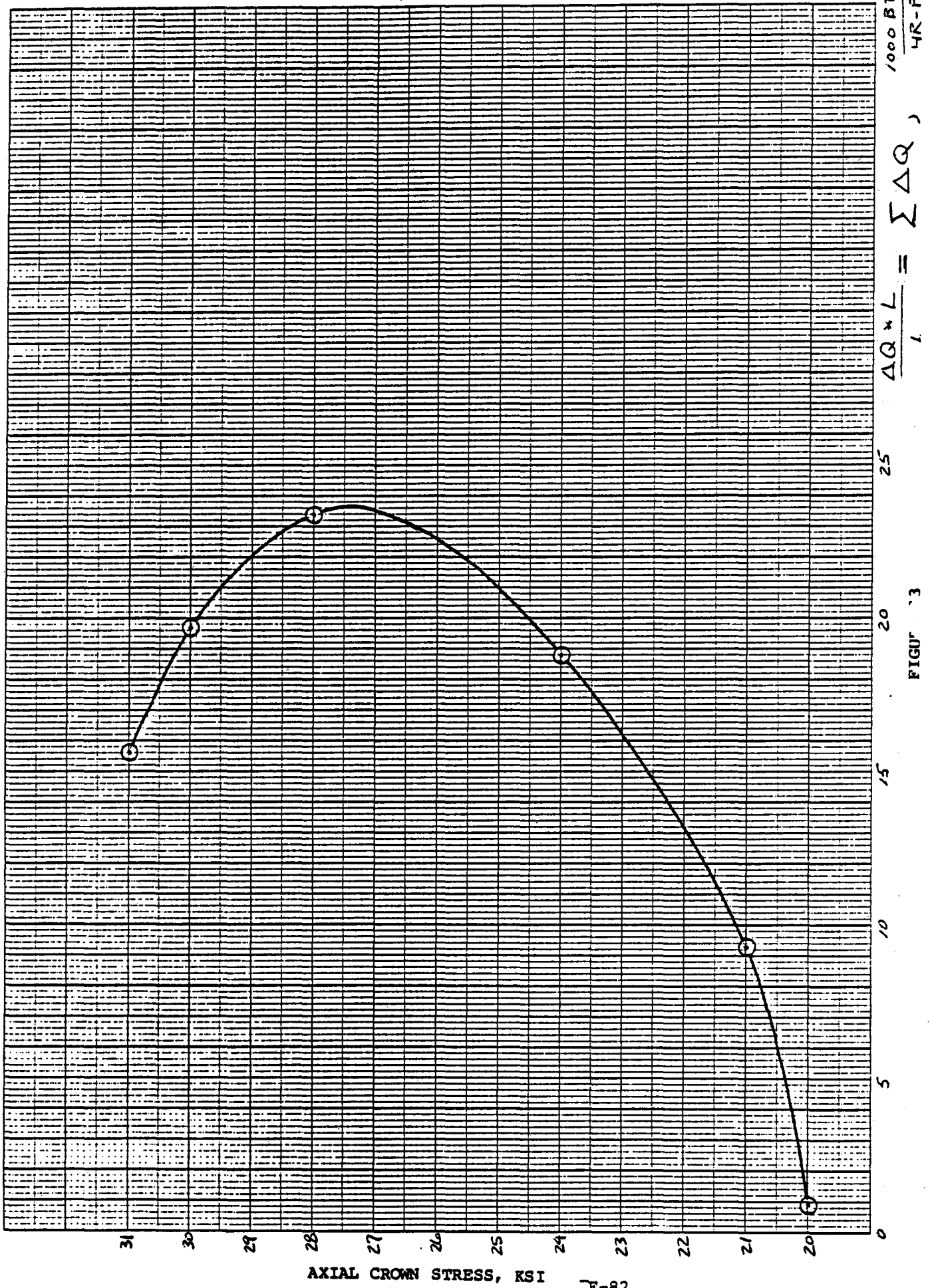


$\Delta Q * L$  (BTU \* L /  $10^5$  / HR-FT)

FIGURE 12

AXIAL CROWN STRESS, KSI

E-81



1000 BTU  
4R-FT<sup>2</sup>

FIGURE 3

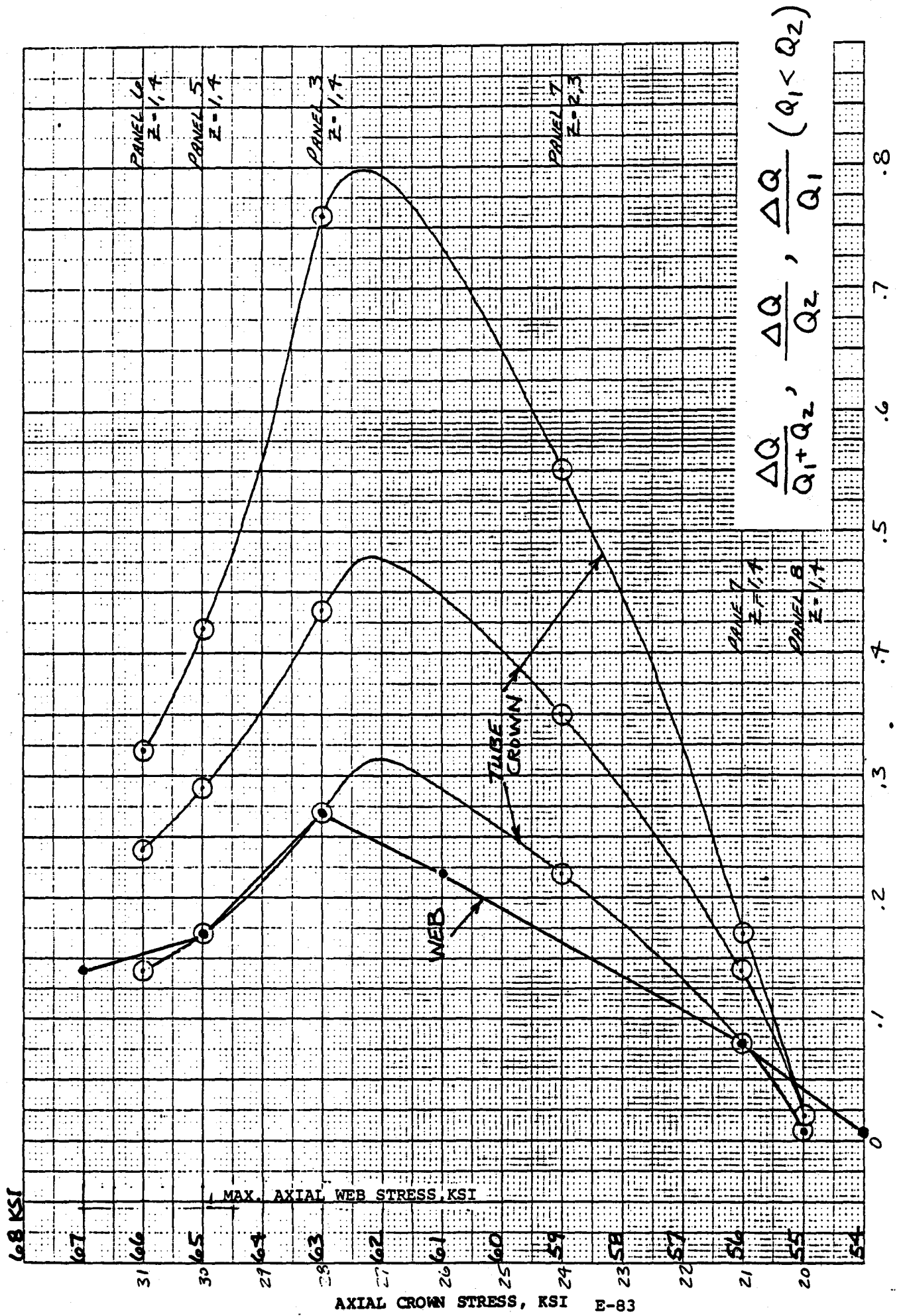
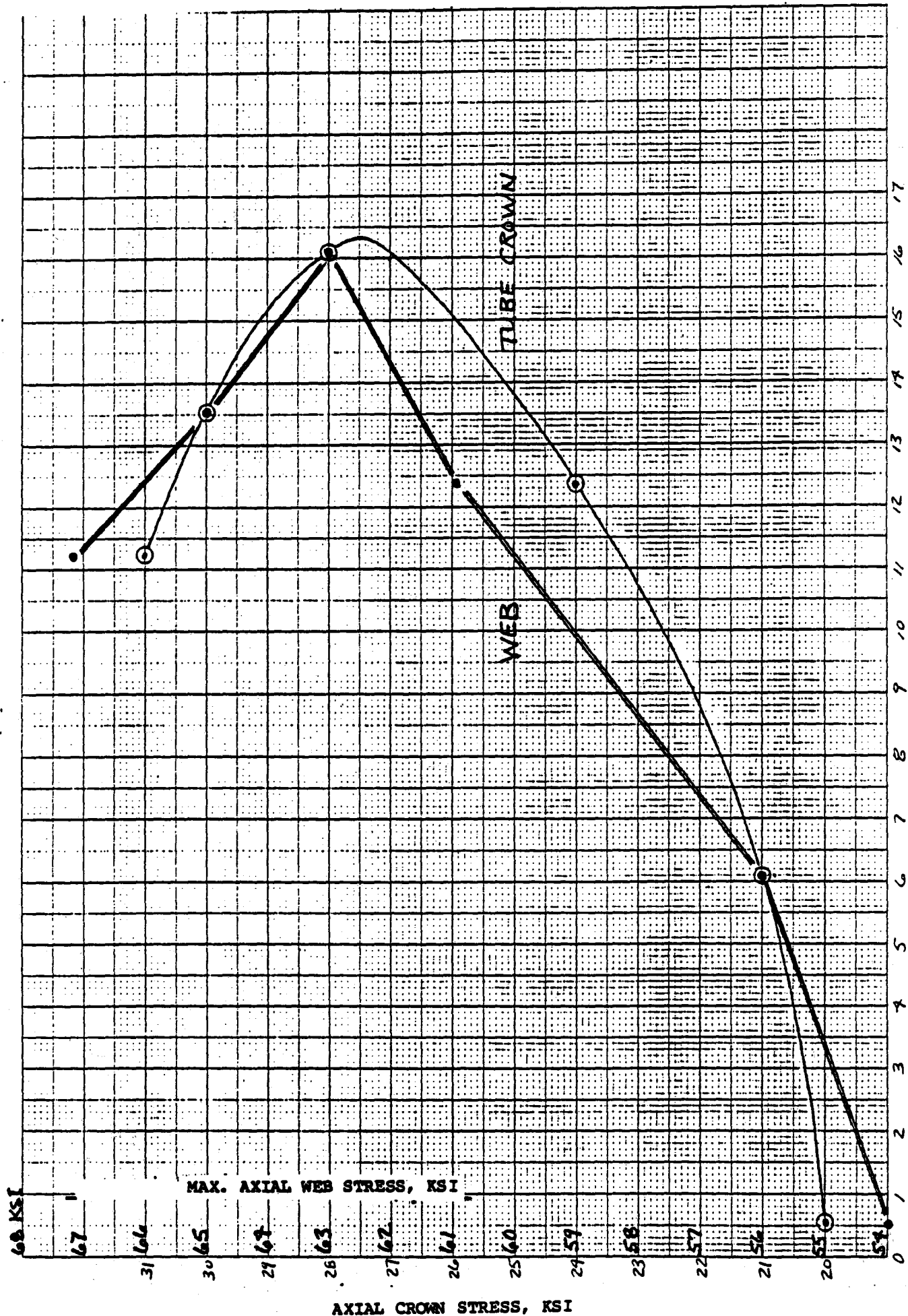


FIGURE 14



$\Delta Q * L$  (BTU X  $10^5$  / HR-FT)

FIGURE 15

### Effective Stress

Plots of effective stress for Panels 7 of Zones 1,4 and 2,3 show web stress slightly lower and tube stress to be appreciably lower than the corresponding axial stresses. Table 10 compares the maximum stresses from the plots.

Comparing the effective stress curves to axial stress and heat flux curves shows that both web and effective stress curves closely follow the heating curve associated with that side of the tube. The quarter length model serves as a check verifying the effective stress values. From the results presented, effective stress should be consistently lower than axial stress for any thermal loading.

PANEL	ZONE	$\sigma_z$ - CROWN, KSI	$\sigma_z$ - WEB, KSI
7	1,4	21 (18.5)	56 (54)
7	2,3	20 (17.5)	61 (60)

( EFFECTIVE STRESS VALUE )

$$\sigma_{\text{EFF.}} = \sqrt{\frac{(\sigma_1 - \sigma_2)^2 + (\sigma_2 - \sigma_3)^2 + (\sigma_3 - \sigma_1)^2}{2}}$$

WHERE  $\sigma_1, \sigma_2, \sigma_3$  ARE THE PRINCIPAL STRESSES.

TABLE 10 - TUBE STRESSES



## 10.0 Conclusion

FESAP results appear to be accurate for analysis of tube bowing and axial thermal stress. This is based on reasonable convergence of stresses for a node common to two elements and the general smoothness and consistency of the many plots.

Maximum lateral deflection for one-sided heating is substantially higher (21.5 inches) than for two-sided heating (maximum deflection varied from 4 inches to 11.5 inches).

Tube bowing causes the lateral deflection and results from a difference in heat flux curves. This can be demonstrated by plotting the heat flux imbalance against tube length and superimposing the resulting curve on the deflection curve ; i.e., a high degree of similarity occurs and even predicts the presence of reverse bending in several panels. The magnitude of the lateral deflection is difficult to predict, but a plot of heat flux imbalance gives a good approximation to the type of curve one might expect to develop.

For two-sided heating, maximum web stress was found to be 67 KSI and tube stress, 31 KSI. The stresses are conservative since the peak heating curves do not occur at the same time of year.

Both web and tube stresses at any location on a panel appear to be a function of the entire heating rather than the level at the location. Tube bowing does relieve axial crown stress but had little affect on web stress. Crown stress displays a somewhat constant stress level; i.e., it does not follow the heat flux curve nor the heat flux imbalance curve, it truncates the effects of any sudden peak or drop in the heat flux curve.

The web stress increases when total heating increases.

Effective stress does not exceed the values of axial stress in any of the panels although web stress differs only slightly.

#### 11.0 Recommendations

Permitting the tube to bow reduces stress levels in the tubes; however, excessive bowing can cause large deflections. Therefore, heat flux curves (two-sided heating) should be properly aligned so that the total heat flux imbalance is minimized.

Since maximum stresses are compressive and end loading causes tensile stresses, overall they reduce compressive stresses. Theoretically, increasing the end load should reduce the bowing to a point where maximum compressive stresses (plane strain) occur. However, this effect is not obtained by FESAP; presumably, it requires large deformation theory.

12.0 References

1. Creep Fatigue Analysis, Report No. 0012-9(S), by E.J. Sembroski  
August 1982.

# **Appendix F**

## **Cavity Efficiency**

## TABLE OF CONTENTS

	PAGE
Results .....	F-2
Reflection .....	F-7
Receiver Efficiency Calculations .....	F-9
Estimate of Peak Tube Temperature .....	F-10
Re-Radiation .....	F-13
Convection .....	F-16
Uncertainties .....	F-19
Conclusions .....	F-20
References .....	F-20

The accurate prediction of solar efficiency\* is of great importance in establishing the overall first cost of a complete solar central thermal power generating system. Over-prediction of the efficiency of a central receiver would result in the specification of a disproportionately smaller number of heliostats than otherwise would have been required (additional heliostats of necessity are far-field heliostats and thus of lower efficiency than average in terms of input to the receiver aperture). For example, if total heliostat costs for a 100 MWe plant were \$150M and the efficiency were underestimated by 5%, the plant would underperform. The total cost to supply the additional heliostats required to meet performance would cost as much as \$8M (if in fact they could be added). Contrarywise, overestimation could lead to an oversize plant, the cost of which may be judged uneconomic.

An evaluation of receiver efficiency requires the development of analytical techniques. In developing these techniques, thermal losses from the cavity were separated into the following mechanisms:

- . Radiation losses
  - Infrared reradiation
  - Reflection (visible)
- . Convection
- . Conduction

Methods were determined which estimate individual losses such as natural convection, reradiation, reflection, and conduction. The resulting calculated losses are found in Tables 1 and 2 and Figures 1 and 2.

---

\*The thermal efficiency of the quad-cavity receiver is defined as the ratio of the total energy retained by the working fluid (molten salt to the total energy entering the apertures.

## Results

Receiver efficiency was evaluated at design point conditions with a total absorbed power of 320 MWt ( $1.092 \times 10^9$  Btu/hr). Losses were calculated and added to the absorbed power to yield the total insolation that must enter the apertures if design thermal rating is to be achieved. Methods were determined which can estimate individual losses such as natural convection, reradiation, reflection and conduction. This section describes these methods.

The results of these calculations are found in Tables 1 and 2 and Figures 1 and 2. Radiation losses were computed by estimating the shading for each surface which radiated at an average temperature based upon the average radiative power. Reflective losses were calculated using overall view factors, assuming diffuse reflection from the tubes and a reflectivity of five percent. Convective losses were calculated for each panel using the temperature difference between the average panel temperature and the temperature of the air inside the cavity. The cavity air temperature was estimated using a convective coupling model suggested by Clausing.<sup>(1)</sup>

TABLE 1

RECEIVER LOSSES IN PERCENT OF TOTAL

	N	S	E/W	Total
<u>RADIANT</u>				
IT Reradiation	1.12	.41	1.79	3.32
Visable Reflection	.38	.11	.46	.95
<u>CONVECTION</u>				
Natural	1.5	.67	2.20	4.37
<u>CONDUCTION</u>				
Roof	.032	.017	.050	.099
Floor	.021	.011	.030	.062
Walls	.057	.016	.098	<u>.171</u>
				8.97

Receiver Efficiency = 91%

N = North Cavity

S = South Cavity

E/W = East and West Cavities



TABLE 2

RECEIVER LOSSES

Total Receiver Insolation -  $1.201 \times 10^9$

	N	S	E/W
Total Insolation Absorbed	$.4197 \times 10^9$	$.1446 \times 10^9$	$.528 \times 10^9$
Incident	$.4571 \times 10^9$	$.1594 \times 10^9$	$.5836 \times 10^9$
<b>Losses</b>			
<b>Radiant</b>			
1) Re-radiation	.0135	.00496	.0215
2) Reflection	.00457 (1%)	.00136 (.85%)	.0055 (.94%)
3) Shine Through			
<b>Convection</b>			
4) Natural	.018	.0080	.0264
5) Forced			
<b>Conduction</b>			
6) Roof	.000385	.000200	.000600
7)	.000255	.000132	.000400
8) Wall (panels)	<u>.000688</u>	<u>.000188</u>	<u>.00118</u>
Total	.0374	.0148	.0556
Percent Loss Per Cavity	8.18%	9.31%	9.53%
(cavity loss/cavity power)			

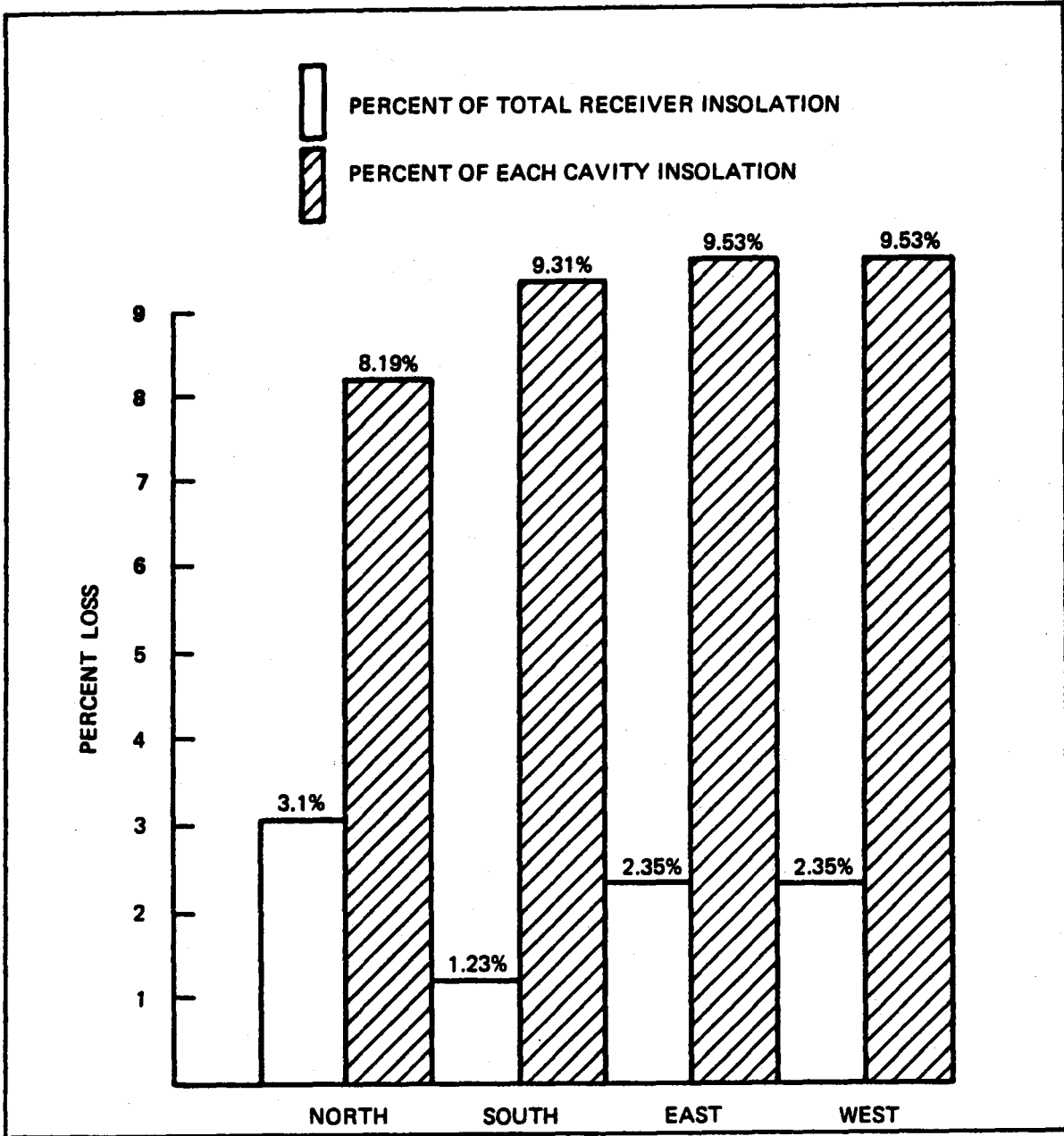
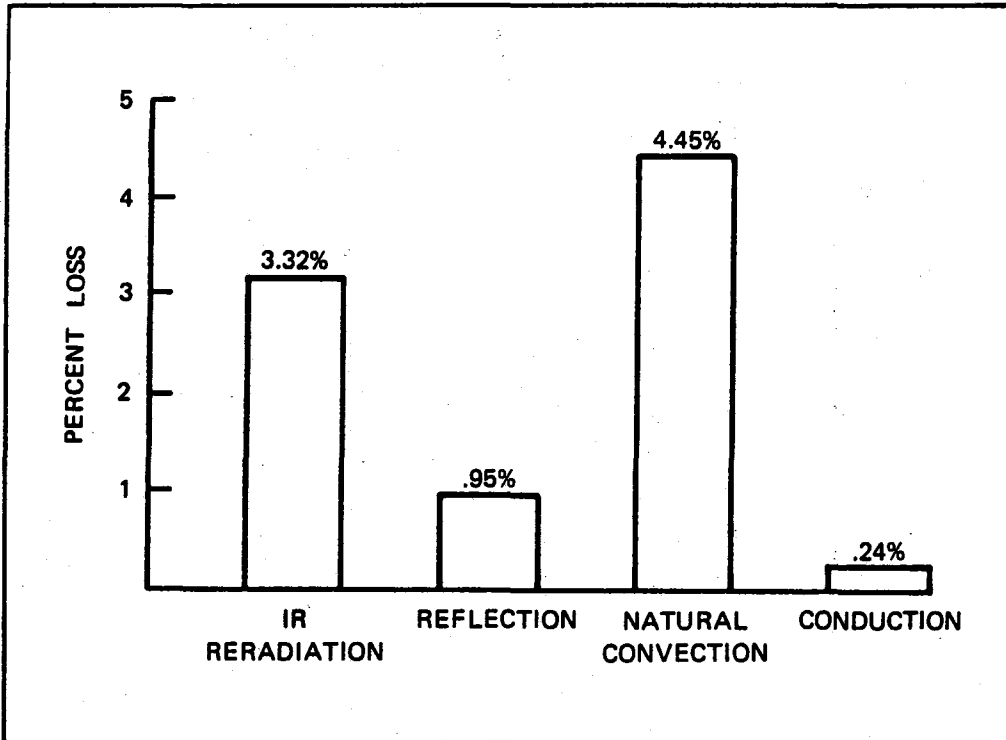


FIGURE 1 - RECEIVER LOSSES BY CAVITY



**FIGURE 2 - RECEIVER LOSSES BY TYPE**

## Reflection

Reflective heat loss is calculated by assuming diffuse reflection of five percent of the incident energy. Since most (95%) of the reflected energy is recaptured when another surface is encountered, it is necessary to use view factors to account for the rate of escape (see Figure 4). The cavity is divided into two sections by a flat plane (P1) placed at the edge of the absorbing panels as seen in Figure (1). The view factors are found for heat flow from the panels to plane P1 ( $F_{2-p1}$ ) and from plane P1 to plane P2 ( $F_{p1-p2}$ ) where P2 is the aperture. A view factor from the panels to the aperture is then calculated as  $F_{2-p2} = F_{2-p1}F_{p1-p2}$ . The total heat transport through the aperture is then calculated by equation (8).

$$Q_{\text{reflection}} = (1 - \alpha) F_{2,p2} Q_{\text{tot,incident}} \quad (8)$$

The view factor  $F_{2-p1}$  was estimated to be .8, and  $F_{p1-p2}$  varied between .3 and .4. (2)

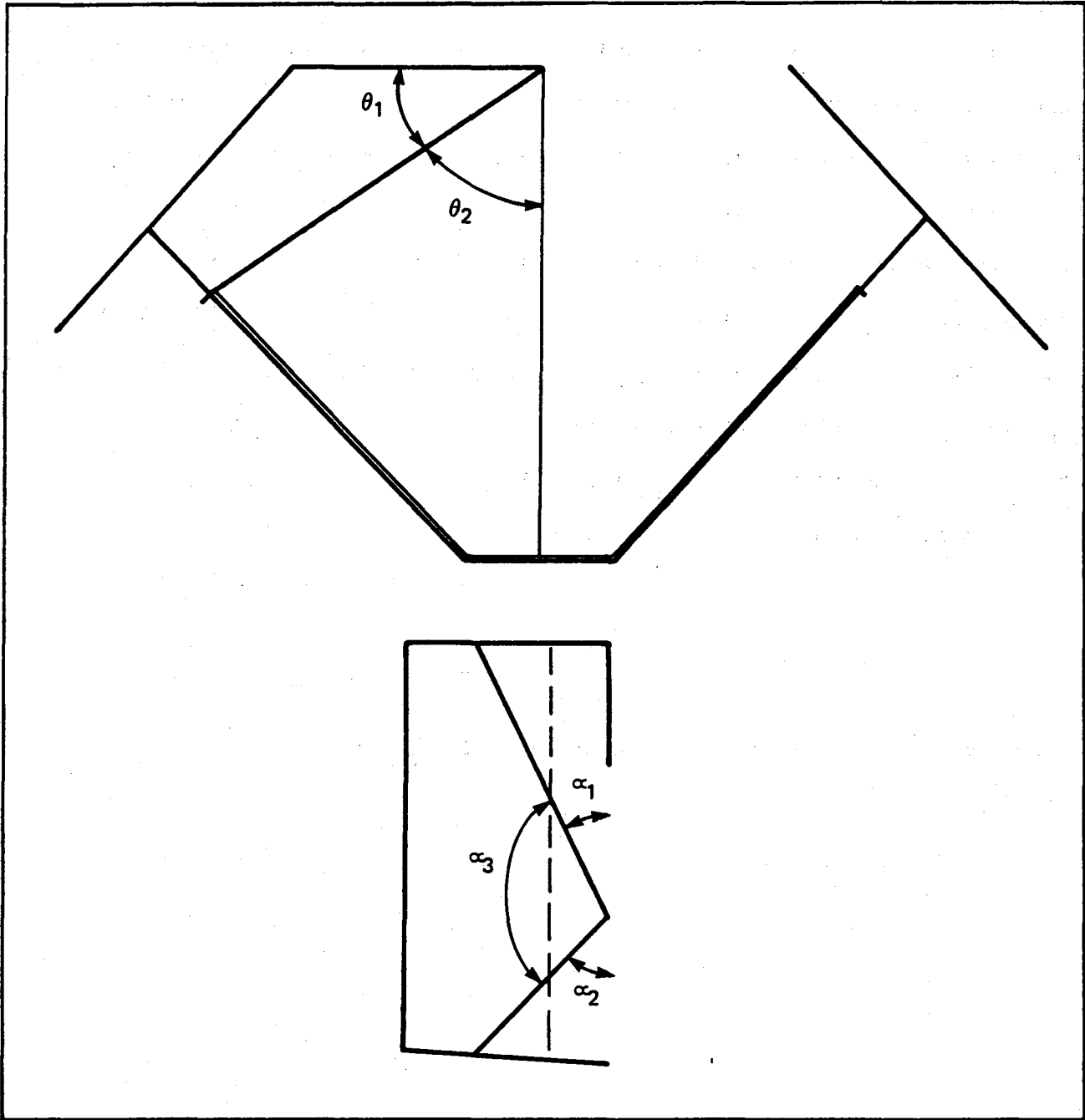


FIGURE 3 - RERADIATION APERTURE MODEL

## Receiver Efficiency Calculations

In order to calculate receiver efficiency, it is necessary to estimate the losses from convection, radiation and conduction. These losses are then added to the total power absorbed by the salt to yield the total required insolation at the apertures. Since the quad cavity receiver has three unique apertures, it is necessary to perform three independent calculations for cavity losses.

One begins with the following list of data:

- 1) Peak and average normal absorbed fluxes by panel.
- 2) All geometric data including panel height, width, tube diameter, aperture height and width.
- 3) Material properties.
- 4) Aperture temperature as seen from the panel or incoming background flux (this normally corresponds with a radiative temperature of  $400^{\circ}\text{K}$ ).
- 5) Estimates of ceiling and floor temperatures. These are estimated by assuming a nominal conduction rate through the wall and balancing the average incident and radiant flux. These surfaces are painted white having

$$\alpha_{\text{IR}} = .30 \text{ and } \epsilon_{\text{visible}} = .3$$

### Estimate of Peak Tube Temperature

Peak tube temperatures are found by assuming one-dimensional through thickness heat conduction normal to the tube surface and convection into the working fluid (molten salt). The heat transfer coefficient is calculated using equation (1) for developing turbulent flow.

$$Nu = .036Pr^{.4} Re^{.8} (D/L)^{1/18} (\mu_b/\mu_w)^{.14} \quad (1)$$

When it is assumed that the peak flux occurs at half the distance up the tube, the half of the tube length is used for L. All properties except  $\mu_b$  and  $\mu_w$  are evaluated at the film temperature corresponding to the average panel salt temperature.

Once peak temperatures and average salt temperatures have been procured for each panel, it is necessary to find an estimate for the average convective panel temperature and average radiative panel temperature. It is assumed that the temperature varies with the cosine of the angle between the point of peak temperature and the desired location. An integral average of this cosine temperature distribution around a tube yields equation (2).

$$\bar{T}_{\text{cosine}} = T_{\text{min}} + .637 (T_{\text{max}} - T_{\text{min}}) \quad (2)$$

It is assumed that the minimum temperature around the tube occurs at a location with negligible flux (i.e.  $T_{\text{min}} = T_{\text{salt}}$  at the membrane/tube interface) and that the peak temperature occurs at the point of peak flux. A vertical average of the temperature along the tube is estimated with equation (3).

$$\bar{T}_{\text{vertical}} = T_{\text{salt}} + .8 (T_{\text{peak}} - T_{\text{salt}}) \quad (3)$$

Where  $T_{\text{peak}}$  is the absolute peak temperature anywhere on the panel and  $T_{\text{salt}}$  is the salt temperature at that same location, Equations (2) and (3) are combined to yield an equation (4) for the panel convective average temperature.

$$\bar{T}_{\text{conv}} = T_{\text{salt}} + .5 (T_{\text{peak}} - T_{\text{salt}}) \quad (4)$$

The average radiative temperature is defined as the temperature that would radiate heat from a flat plane at the peaks of the tubes which would be equivalent to the total heat crossing the plane and radiated by the tubes. In order that this value be computed accurately, a computer program was developed to perform a parametric study on average radiative temperature. This program included the effects of shading by adjacent tubes. A correlation of the results was made and is seen here in equation (5).

$$\bar{T}_{\text{rad}} = T_{\text{salt}} + .788 (T_{\text{peak}} - T_{\text{salt}}) \quad (5)$$

Combining equations (5) and (3) yields the panel radiative average temperature as given in equation (6).

$$\bar{T}_{\text{rad}} = T_{\text{salt}} + .63(T_{\text{peak}} - T_{\text{salt}}) \quad (6)*$$

---

\*Although it is known that the same averaging techniques is not valid for both convection and radiation, it is felt that the error introduced is within the accuracy of this analysis.



It is also necessary to construct temperature estimates for the vertical inactive surface area such as aperture side walls since the convective losses from these areas can be large. Inactive surfaces are heated by infrared radiation emitted by absorber panels and cooled when heat is radiated by the surface to the aperture, when cold air convects heat away and when heat is conducted through the insulation. This heat balance at the panel surface provides a good estimate of surface temperatures.

Estimates are made for the view factors of panel to cavity and panel to aperture (the only radiative cooling medium). These factors together with an estimate for the average cavity temperature yield a value for the equilibrium surface temperature.

$$T_{\text{inactive}} = \sqrt[4]{\frac{T_{\text{cavity}}^4 + T_{\text{aperture}}^4 \frac{\epsilon_{F_{i,\text{aperture}}}}{F_{i,\text{cavity}}}}{1 + \frac{F_{i,\text{aperture}}}{F_{i,\text{cavity}}}}} \quad (7)$$

where,  $T_{\text{cavity}}$  = average temperature at which the cavity radiates to the inactive surface

$T_{\text{aperture}}$  = average temperature at which the aperture radiates to the inactive surface

$F_{i,\text{aperture}}$  = view factor from the inactive surface to the aperture

$F_{i,\text{cavity}}$  = view factor from the inactive surface to the cavity  
 = inactive surface emissivity

The average cavity temperature is weighted toward that of the nearest panel temperatures, the floor and ceiling temperatures, since the inactive surface sees very little of the panels at the back of the aperture.

## Re-radiation

Re-radiation heat loss is calculated on a panel by panel basis using the average radiative temperature as described earlier. Configuration factors from the aperture to the radiating surfaces are estimated such that the sum of the factors equals one. This insures conservation on energy in the model thus preventing errors that would have resulted when the panels are treated independent of the aperture.

Using figure (2), the configuration factors are found from equations (9)

- (13).

$$F_{\text{aperture, absorber}} = \frac{\alpha_3 \theta_2}{180^2} \quad (9)$$

$$F_{\text{aperture, ceiling}} = \frac{(1 - F_{\text{aperture, absorber}})^{\alpha_1}}{2(\theta_1 + \frac{\alpha_1 + \alpha_2}{2})} \quad (10)$$

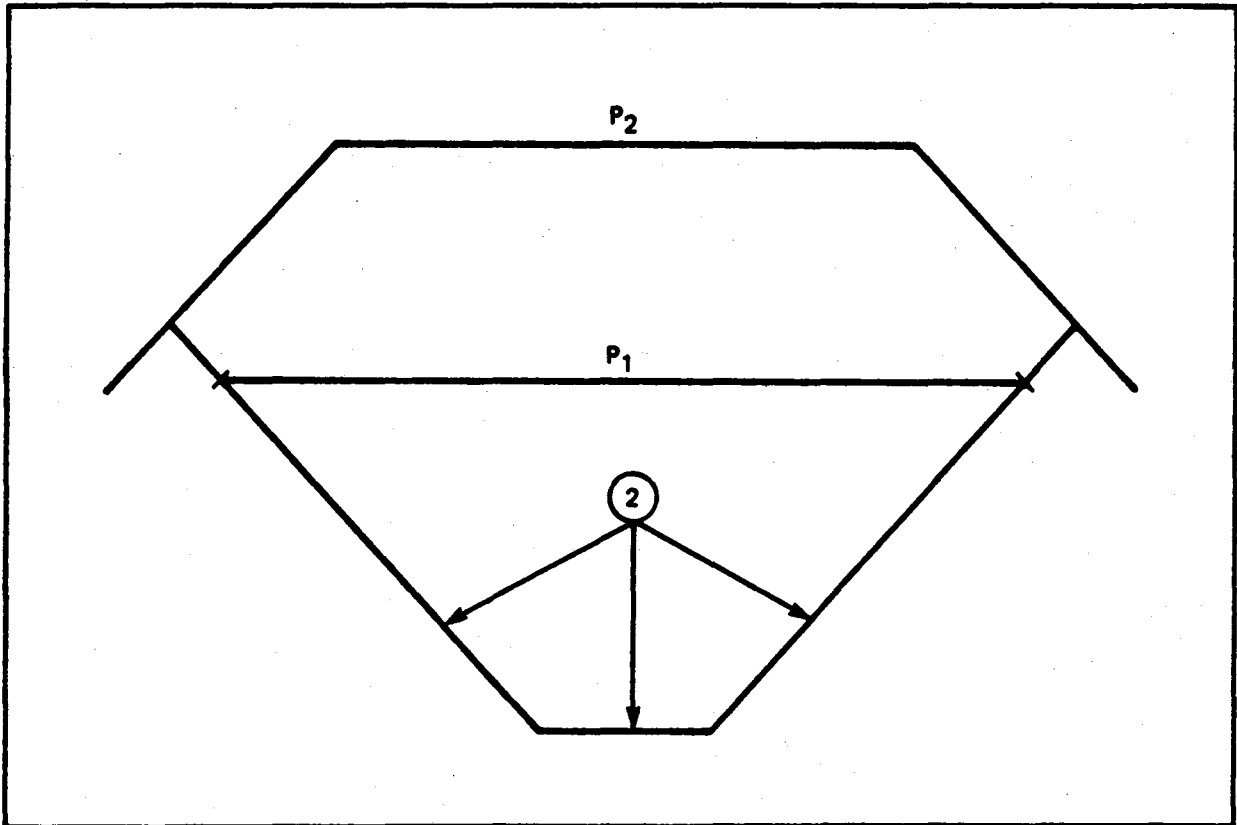
$$F_{\text{aperture, floor}} = \frac{(1 - F_{\text{aperture, absorber}})^{\alpha_2}}{2(\theta_1 + \frac{\alpha_1 + \alpha_2}{2})} \quad (11)$$

$$F_{\text{aperture, side panels}} = \frac{(1 - F_{\text{aperture, absorber}})^{\alpha_1}}{\theta_1 + \frac{\alpha_1 + \alpha_2}{2}} \quad (12)$$

$$F_{\text{aperture, panel}} = \frac{F_{\text{aperture, absorber}}}{N_{\text{panels}}} \quad (13)$$

Both black and white painted surfaces are assumed to have an infrared emissivity of .85. Since the sum of view factors equals one the heat transport is treated as emitting from a black surface at the aperture and calculated by equation (14).

$$Q_{\text{reradiation}} = A_{\text{aperture}} \sigma \sum \epsilon_i F_i (T_i^4 - T_{\text{background}}^4) \quad (14)$$



**FIGURE 4 - REFLECTIVE APERTURE MODEL**

## Convection

Convective heat loss is calculated on a panel by panel basis using the average convective temperature as described earlier. Heat transfer coefficients are calculated from a correlation derived by A. M. Clausing, Reference 3. The correlation is based upon data from his cryogenic dry nitrogen wind tunnel which simulates the high Grashof numbers and temperature differences experienced with solar receivers.

When analyzing the receiver cavity, it becomes necessary to address the question of characteristic temperatures, lengths, and areas since most correlations are derived from flat plate experimental data.

Clausing's correlation provides a correction for large temperature differences but is not suited for direct use in a cavity. It assumed that the average temperature that the panels convect to ( $T_{bulk}$ ) is inside the cavity and is at the average of that temperature exhausted from the cavity by buoyant (or chimney) force and the incoming air temperature (i.e.,  $T_b = (T_{out} + T_{in})/2$ ). In order to estimate the bulk air temperature ( $T_b$ ) a heat balance is performed on a control volume as shown in figure (3). The convective energy absorbed by the air is  $Q_{conv}$  in equation (15).

$$Q_{conv.} = \rho_a V_a C_p (T_{out} - T) \quad (15)$$

where properties are evaluated at  $T_b$  and  $A_a$  represents half of the aperture area.  $V_a$  is the average velocity of the mass influx and outflux. The convective heat transport can be found from heat transfer coefficients if the exit temperature is known. Therefore, the only unknowns are  $V_a$  and  $T_{put}$ . A linear velocity profile is assumed and is a function of  $V_{max}$ .

$$V_a = .5 V_{max} \quad (16)$$

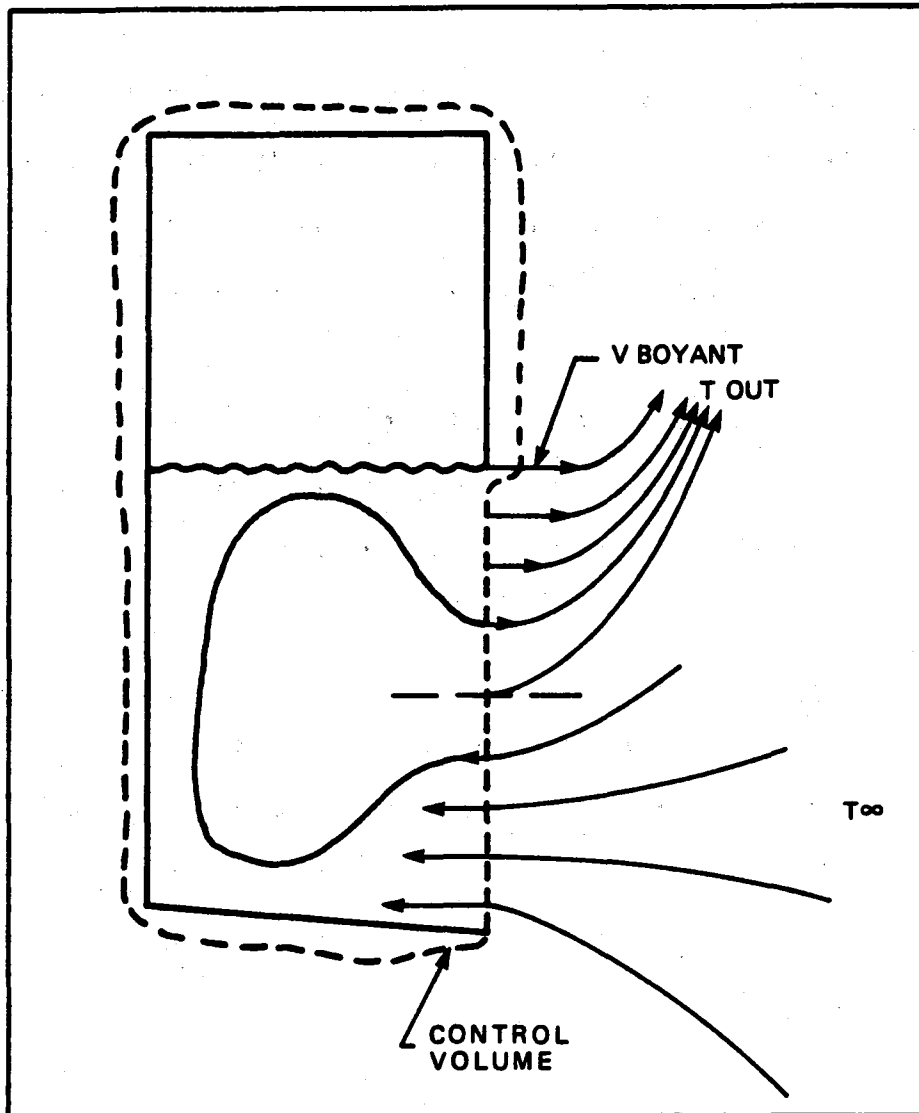


FIGURE 5 - CAVITY SCHEMATIC

Since the buoyant forces are dominant in this flow (GT is large), the maximum velocity can be estimated by modeling a frictionless fluid element accelerating along a path with a linearly increasing temperature. The buoyant velocity is given by equation (17).

$$V_{\text{boyant}} = (g\beta(T_{\text{out}} - T_{\infty})L)^{1/2} \quad (17)$$

where L is the aperture height and  $\beta$  is the isobaric compressibility.

It is assumed that this is the maximum velocity that the fluid can attain and therefore represents an upper limit to the heat transport from the cavity. However, the effect of this velocity on the overall heat transfer is small since the cavity temperature is typically within 30F of the outside temperature. This suggests that even if the velocity were 50% lower, the overall effect would be a reduction in convective loss by 5%, thereby effecting the receiver efficiency by less than .3%.

### Issues

When determining the areas over which the heat transfer takes place, the boundary layer thickness must be evaluated to determine where the major temperature drop occurs. In most cases it was found that  $Nu = 3000$ . If it is assumed that the major temperature drop occurs by conduction in the laminar sub-layer then an estimate of the layer thickness is seen in equation (18).

$$\delta \approx \frac{L}{Nu} = .01 \text{ ft} \approx 1/8 \text{ " } \quad (18)$$

where  $L_c$  is half of the average tube length. It is seen that it would be very hazardous to use the projected area for convective calculations. This area requires further study; but for the lack of a better estimate, the total tube wall area is used for membrane walls.

### Uncertainties

Despite the best efforts of all that attempt the prediction of losses, it is still hazardous to claim a tolerance better than 30% on losses. Until data can be taken from a receiver with dimensions and temperature differences on the same order of magnitude as the final design, it will be difficult to extrapolate the correlations. Therefore, it is necessary to estimate the possible errors associated with convective losses.

- 1) Boundary Layer Effects - Vertical tubes can be viewed as a flat surface with a roughness when the tube diameter is small in comparison to the laminar sub-layer. With this design, the boundary layer is less than 3/16 inch. The value of this thickness is small at the bottom of the tubes and large at the top where the flow is more fully developed. It is expected that this effect will result in a slight reduction (less than 10%) in the predicted natural convection losses.
- 2) The heat transfer correlation used in this analysis was derived from dry cryogenic nitrogen data. Under operating conditions, the actual fluid will be a mixture of air and a small percentage of water vapor. Property variations could, therefore, yield a significant error (+ 20%).



- 3) Since carbon dioxide and water vapor will be present in the air, it will be reasonable to expect that infrared radiation from the tubes will be absorbed by the air and convected out of the cavity. This effort becomes more pronounced as the cavity size increases and could reduce overall efficiency by as much as one percent.

### Conclusions

It was desired that a method be found and used to estimate cavity receiver efficiency. This work has predicted an overall receiver efficiency of 91%. The major losses were found to be natural convection with 4.45 percent of the total insolation and radiation with 4.27% of the total insolation.

It was found that these values could be as much as 30% off of the nominal predicted values and that further testing is required on units of large scale.

### References

- 1) Clausing, A. M., "Convective Losses from Cavity Solar Receivers - Comparison between Analytical Predictions and Experimental Results," Solar Engineering - 1982, Proceedings of 4th Annual ASME Solar Energy Conference, Albuquerque, NM, April, 1982, pp. 388-394.
- 2) Howell, John R., "A Catalog of Radiation Configuration Factors," McGraw-Hill, 1982.
- 3) Clausing, A. M., "Natural Convection Correlations for Vertical Surfaces Including Influences of Variable Properties," Preliminary Release.

INITIAL DISTRIBUTION  
UNLIMITED RELEASE

Department 8450 Files (2)  
Publications Division 8265, for TIC (27)  
Publications Division 8265/Technical Library Processes Division, 3141  
Technical Library Processes Division, 3141 (3)  
M. A. Pound, 8124, for Central Technical Files (3)